Copyright is owned by the Author of the thesis. Permission is given for a copy to be downloaded by an individual for the purpose of research and private study only. The thesis may not be reproduced elsewhere without the permission of the Author.

A.J.H. Clement

HOLOCENE SEA-LEVEL CHANGE IN THE NEW ZEALAND ARCHIPELAGO AND THE GEOMORPHIC EVOLUTION OF A HOLOCENE COASTAL PLAIN INCISED-VALLEY SYSTEM: THE LOWER MANAWATU VALLEY, NORTH ISLAND, NEW ZEALAND

Related publications

Clement, A.J.H., Sloss, C.R., Fuller, I.C., 2010. Late Quaternary geomorphology of the Manawatu coastal plain, North Island, New Zealand. Quaternary International 221, 36–45.

HOLOCENE SEA-LEVEL CHANGE IN THE NEW ZEALAND ARCHIPELAGO AND THE GEOMORPHIC EVOLUTION OF A HOLOCENE COASTAL PLAIN INCISED-VALLEY SYSTEM: THE LOWER MANAWATU VALLEY, NORTH ISLAND, NEW ZEALAND

A thesis presented in partial fulfilment of the requirements for the degree of

Doctor of Philosophy in Geography

at Massey University, Palmerston North, New Zealand.



MASSEY UNIVERSITY

Alastair John Hopton Clement

2011

Copyright © 2011 Alastair J.H. Clement.

Typeset with LaTeX

Supervisor:
Dr. Ian C. Fuller

Co-Supervisor:
Dr. Craig R. Sloss

Internal Examiner:
Dr. Alan Palmer

New Zealand Examiner:
Assoc. Prof. Paul S. Kench (University of Auckland)

Overseas Examiner:
Assoc. Prof. Brian G. Jones (University of Wollongong)

Abstract

The full body of work relating to Holocene sea-level histories in the New Zealand region has been integrated and critically analysed to provide context for the construction of detailed, local-scale Holocene sea-level curves for regions within the New Zealand archipelago. These local-scale sea-level reconstructions in turn provide context for an investigation of the stratigraphic and geomorphic evolution of the Manawatu coastal plain incised-valley system during the Holocene.

The state of knowledge of sea-level fluctuations in the New Zealand region during the Holocene is revealed to be poor. Holocene sea-level histories are fragmented and unreliable, with sea-level reconstructions produced for the whole of the New Zealand masking local-scale trends in Holocene sea-level fluctuations.

Local-scale Holocene sea-level curves produced for regions within the New Zealand archipelago show a north-south trend in sea-level fluctuations. In the Auckland-Northland region present mean sea-level (PMSL) was attained c. 7,700 cal. yr BP. Approximately 7,500 cal. yr BP PMSL was attained in the southwest North Island. PMSL was attained in Pegasus Bay c. 7,100–6,600 cal. yr BP, and in East Otago c. 6,900 cal. yr BP. It is also possible to discern a north-south lag in the timing of sea-level fluctuations following the attainment of PMSL between the southwest coast of the North Island and the East Otago peninsula. The degree to which the north-south lag in the timing of the attainment of PMSL is a manifest response to external driving forces is not yet clear as the local-scale sea-level histories are highly variable, quite contradictory, and appear to be responding inconsistently to different external drivers.

Vibracores and water well logs have been used to reconstruct the sedimentary infill of the lower Manawatu River valley, North Island, New Zealand, in response to Holocene sea-level change and the influx of sediment from the bordering axial ranges. Cross-sections across the incised-valley system have identified: the lowstand incision of the Manawatu River c. 22–18 ka, and associated fluvial terraces buried at depth beneath the Holocene valley fill; the extent of the Holocene estuary which occupied the lower valley at the culmination of the Holocene marine transgression (c. 7,500 cal. yr BP); the sedimentary succession which filled the valley associated with the Holocene sea-level highstand; and late Holocene to recent coastal progradation of 5–6 km. A 3D model of

the sub-surface stratigraphy of the lower valley was constructed from the borehole data and cross sections. Digital elevation models were also constructed for key palaeo-surfaces within the valley's Holocene sedimentary fill. Holocene sea-level fluctuations in the valley were reconstructed from radiocarbon dated estuarine bivalves recovered from vibracores. These radiocarbon dates also record subsidence of the valley due to a combination of sediment compaction, post-glacial water and sediment loading, the evolution of the Wanganui Basin, and neotectonics. Information from all sources was collated and used for the construction of palaeogeographic maps and a series of conceptual models of the evolution of the lower valley.

Acknowledgements

Many people contributed their expertise and gave support in many varied ways throughout my PhD research.

First and foremost I wish to thank my supervisors, Dr. Ian Fuller and Dr. Craig Sloss: hands-on supervisors who gave freely of their time, knowledge, advice, and keen and critical insight. Both are excellent mentors who provided encouragement, guidance, and support throughout the course of my research.

A great deal of this research hinged on successful fieldwork. In this respect I am extremely grateful to David Feek, whose constant optimism and innovation often meant the difference between success and failure in the field. Thanks also to those who lent a hand, always somewhere wet and often cold: John Appleby; Rob Dykes; Jane Richardson; and Gigi Woods.

Many people freely provided data, both published and unpublished, and information borne of their own expertise, which is gratefully acknowledged: Scott Nichol (GA), unpublished measurements of cores on Great Barrier Island; Christine Prior (GNS), advice about radiocarbon age determinations; Patrick Hesp (LSU), advice on Manawatu geomorphology and dune sequences; Andrew Steffert (Horizons), airborne LiDAR data and orthophotos of the Manawatu; Louise Chick (Waikato), unpublished data on tectonic movements of the Kerepehi Fault; John Ogden (Auckland), unpublished aspects of cores from Whangapaoa Estuary; Martin Hewitt and Mark Peters (Geosystems), advice on NZGeoid05 and grid files for TGO; Will Newell (Geosystems), advice on Trimble R8 use and NMEA message output; John Oldman (NIWA), advice on cores from Mahurangi Estuary; John Dymond (Landcare), subset of the ECOSAT DEM covering the Manawatu; Hisham Zarour (Horizons), bore logs from throughout the Manawatu; John Begg (GNS), data and advice for extrapolating the extent of Manawatu river terraces under the modern floodplain; Alan Hogg (Waikato Radiocarbon Laboratory), advice regarding conventional radiocarbon ages; Fiona Petchley (Waikato Radiocarbon Laboratory), advice on and a keen eye for fossil mollusc species; Dougal Townsend (GNS), preliminary data from unpublished QMAPs; and Clinton Duffy (DoC), unpublished bathymetric data for the Hauraki Gulf.

Thank-you to the many friendly farmers I met through the course of my research who gave valuable local advice and context and allowed access to and across their land: Mark Anderson; Wayne Moxham; Rachel Taylor; Denise Fraser; Des and Lyn Legg; KD Craw; Mark Craw; Bevan Claridge; Salvie;

the Malettas; Adrian Swinbank; Stuart McPhail; Justin and Sally MacLean; Colin Ryder; Ian Barnes; Chris Whittfield; Julian Marshall; Brendan; Chris Preston; Ian Eastern; Malcom Wood; and Kristian Funnell.

I am thankful to have received generous financial support in the form of: a Massey University Vice-Chancellor's Doctoral Scholarship, succeeded by a Top Achievers' Doctoral Scholarship; an IAG Travel Grant to attend the 7th International Conference on Geomorphology (ANZIAG) in Melbourne, 6–11 July 2009; an INQUA 1001 Travel Grant to attend the first joint international conference of IGCP Project 588 and the INQUA Coastal and Marine Processes Commission in Hong Kong, 30 November to 4 Decemeber 2010; the Geological Society of New Zealand Wellman Research Award 2008; as well as research grants from the School of People, Environment and Planning's Graduate Research Fund.

Last, but by no means least, I wish to thank my family who have provided constant, immeasurable support throughout the duration of my PhD research.

AJHC.

Contents

List of Figures **xiii**

List of Tables **xix**

List of Sheets **xxi**

Common abbreviations **xxiii**

A note about ages presented in this thesis **xxv**

1 Introduction **1**
1.1 Thesis aims 2
1.2 Thesis organisation 3

2 Reconstructing Holocene sea-level changes in the New Zealand archipeligo: review **5**
2.1 Introduction 5
2.2 Early investigations of strandlines as evidence of palaeo sea levels 6
2.3 Altimetric correlations with European chronologies 7
2.4 Single radiocarbon dates to inform observations of palaeo sea levels in the New Zealand region 12
2.5 Radiocarbon dating to establish sea-level chronologies in New Zealand 15
2.6 Time-depth curves of palaeo sea-level fluctuations in New Zealand 17
2.7 Modelling and mathematical analyses of Holocene sea-level fluctuations in the New Zealand region 20
2.8 Offshore investigations of palaeo sea-level fluctuations in the New Zealand archipelago 22
2.9 The de facto standard Holocene sea-level curve for New Zealand 27
2.10 Post-Gibb sea-level histories 30
2.11 Conclusions 34

3 Local-scale reconstructions of Holocene sea-level change in the New Zealand archipelago **37**
3.1 Introduction 37
3.2 Local-scale sea-level curve construction methodology 38

3.2.1 Selection of palaeo sea-level indicators 38
3.2.2 Treatment of radiocarbon ages 38
3.2.3 Sources of vertical error 43
3.2.4 Palaeo sea-level indicators 44
3.2.4.1 Formation datums 44
3.2.4.2 Maximum and minimum indicators 44
3.2.4.3 Ecological ranges of fossil shell species 44
3.2.5 Delineation of regions 51
3.2.6 Tectonic regimes of the regions 51
3.2.6.1 Auckland-Northland 51
3.2.6.2 Coromandel Peninsula and the Firth of Thames 55
3.2.6.3 South/southwest North Island 55
3.2.6.4 Christchurch and Pegasus Bay 57
3.2.6.5 East Otago Peninsula 57
3.3 Local-scale Holocene sea-level curves for the New Zealand archipelago: results and discussion 58
3.3.1 Auckland-Northland Holocene sea-level interpretation and analysis 58
3.3.2 Coromandel-Firth of Thames Holocene sea-level interpretation and analysis 61
3.3.3 South/southwest North Island Holocene sea-level interpretation and analysis 61
3.3.4 Christchurch and Pegasus Bay Holocene sea-level interpretation and analysis 64
3.3.5 East Otago Holocene sea-level curve interpretation and analysis 65
3.3.6 Comparison between the local-scale sea-level resonstructions and observations of Holocene sea levels in the New Zealand region 68
3.3.7 Sea-level fluctuations in the New Zealand region: Southwest Pacific context 70
3.4 Synthesis and conclusions 71

4 Geology and geomorphology of the lower Manawatu valley 77
4.1 Introduction 77
4.2 Geology 77
4.2.1 Geological setting 77
4.2.2 Torlesse basement 79
4.2.3 Axial ranges 79
4.2.4 Wanganui Basin 81
4.2.5 Fault structures 84
4.2.6 Poroutawhao High 86
4.3 Geomorphology 87
4.3.1 Tokomaru Marine Terrace 87
4.3.2 Manawatu River and tributaries 91

4.3.3 Manawatu River fluvial terraces 92
4.3.3.1 Forest Hill Terrace – MIS 4 92
4.3.3.2 Milson Terrace – MIS 3 94
4.3.3.3 Ashhurst Terrace – MIS 2 96
4.3.3.4 Holocene fluvial terraces 96
4.3.3.5 Fluvial terrace structure and loess coverbeds . 96
4.3.4 Manawatu floodplain 98
4.3.5 Coastal dune fields 99
4.3.5.1 Last Glacial Maximum-age dunes 99
4.3.5.2 Holocene-age dunes 102
4.3.6 Holocene evolution of the Manawatu River estuary . . . 106
4.3.7 Holocene progradation of the Manawatu coastline . . . 107
4.4 Regional tectonism 107
4.5 Climate 108
4.6 Contemporary coastal processes 110
4.7 Vegetation: past and present 110
4.7.1 Palaeovegetation 110
4.7.2 Present vegetation 111
4.8 Summary 111

5 Models of estuary and incised-valley evolution 113
5.1 Introduction 113
5.2 Background to facies and facies models, and their application to estuaries and incised-valleys 113
5.3 Background to estuarine facies models 115
5.4 Wave- and tide-dominated estuarine facies models 119
5.5 Conceptual facies model for wave-dominated estuaries 120
5.5.1 Zone 1: Marine-influenced sedimentary facies 122
5.5.2 Zone 2: Central basin mud facies 122
5.5.3 Zone 3: River-dominated sedimentary facies 123
5.6 Criticisms of the conceptual estuarine facies models 123
5.7 Wave-dominated Holocene embayments on the southeast coast of Australia: conceptual models 124
5.7.1 Wave-dominated barrier estuaries 124
5.7.2 Open-ocean embayments 124
5.7.3 Drowned-river estuaries 125
5.7.4 The position of the Manawatu valley within the context of wave-dominated estuary models from the southeast coast of Australia 126
5.8 Background to sequence stratigraphy and incised-valley facies models 127
5.9 Model for a simple incised-valley fill 129
5.9.1 Straigraphic organisation 129
5.9.2 Stratigraphic surfaces 131

5.10 Estuarine and incised-valley facies models: New Zealand context . . . 132
5.11 Summary . . . 133

6 Holocene sedimentary infill of the lower Manawatu incised-valley system reconstructed from water well logs 135
6.1 Introduction . . . 135
6.2 Previous investigations of the sub-surface geology of the Manawatu Region . . . 136
6.3 Cross-section construction methodology . . . 140
6.4 Limiting factors and sources of error . . . 145
6.4.1 Positions and elevations . . . 145
6.4.2 Well log interpretations . . . 149
6.4.3 Mismatches between surface geology and DEM topography 149
6.5 Geologic cross-sections in the Manawatu valley: results and discussion . . . 150
6.5.1 Introduction . . . 150
6.5.2 Upper Manawatu floodplain: Whakarongo through Palmerston North City to Opiki . . . 152
6.5.2.1 Sheet 1: Well logs cross-section 1 . . . 152
6.5.2.2 Sheet 2: Well logs cross-section 2 . . . 155
6.5.2.3 Sheet 3: Well logs cross-section 3 . . . 158
6.5.2.4 Sheet 4: Well logs cross-section 4 . . . 158
6.5.3 Oroua Floodplain: Feilding and Bunnythorpe to Kairanga and Opiki . . . 160
6.5.3.1 Sheet 5: Well logs cross-section 5 . . . 160
6.5.3.2 Sheet 6: Well logs cross-section 6 . . . 160
6.5.3.3 Sheet 7: Well logs cross-section 7 . . . 161
6.5.3.4 Sheet 8: Well logs cross-section 8 . . . 161
6.5.4 Manawatu-Oroua floodplain: Linton west to Rangiotu . 162
6.5.4.1 Sheet 9: Well logs cross-section 9 (eastern half) 162
6.5.5 Central Manawatu floodplain: Opiki to Shannon, Moutoa, and Marotiri . . . 162
6.5.5.1 Sheet 10: Well logs cross-section 10 . . . 162
6.5.5.2 Sheet 11: Well logs cross-section 11 . . . 164
6.5.5.3 Sheet 12: Well logs cross-section 12 . . . 164
6.5.5.4 Sheet 13: Well logs cross-section 13 . . . 165
6.5.5.5 Sheet 14: Well logs cross-section 14 . . . 165
6.5.6 Lower Manawatu floodplain: Moutoa and Marotiri through Foxton and Whirokino to Foxton Beach . . . 166
6.5.6.1 Sheet 15: Well logs cross-section 15 . . . 166
6.5.6.2 Sheet 16: Well logs cross-section 16 . . . 167
6.5.6.3 Sheet 17: Well logs cross-section 17 . . . 167
6.5.6.4 Sheet 18: Well logs cross-section 18 . . . 168
6.5.6.5 Sheet 19: Well logs cross-section 19 . . . 168

6.5.7 Lower Manawatu (south): Porotowhao and Koputaroa . 169
6.5.7.1 Sheet 20: Well logs cross-section 20 169
6.5.8 Coastal Manawatu: Himitangi 169
6.5.8.1 Sheet 9: Well logs cross-section 9 (western half) 169
6.6 Digital elevation models of key surfaces within the sedimentary fill of the lower Manawatu valley 170
6.6.1 Last Glacial Maximum fluvial aggradation surface . . . 170
6.6.1.1 Ashhurst/Ohakea LGM aggradation surface DEM construction 170
6.6.1.2 Ashhurst/Ohakea LGM aggradation surface DEM results 174
6.6.2 Digital elevation model of the estuarine-alluvial interface 176
6.6.2.1 Estuarine-alluvial interface DEM construction 176
6.6.2.2 Estuarine-alluvial DEM results 180
6.6.3 Holocene sedimentary infill volume estimation 184
6.6.4 Digital elevation models and volume estimates of incised-valley infilling: discussion 184
6.7 Summary 186

7 Holocene sedimentary stratigraphy and facies assemblages of the lower Manawatu valley reconstructed from detailed vibracores 187
7.1 Introduction 187
7.2 Vibracore collection and analysis 188
7.2.1 Vibracores 188
7.2.2 GPS surveys 192
7.2.3 Sediment analysis 193
7.2.4 Radiocarbon ages 194
7.2.5 Cross-section construction 194
7.3 Lithofacies and interpretation 198
7.3.1 Marine transgressive sands (MTS) 198
7.3.2 Highstand estuarine silts and sands (ESS) 201
7.3.3 Fluvial bay-head delta silts and sands (FBD) 201
7.3.4 Floodplain alluvium (FA) and fluvial swampy silts (FSS) 202
7.4 Vibracores cross-sections in the Manawatu valley: results and discussion 203
7.4.1 Sheet 24: Vibracores cross-section 1 203
7.4.2 Sheet 25: Vibracores cross-section 2 222
7.4.3 Sheet 26: Vibracores cross-section 3 222
7.4.4 Sheet 27: Vibracores cross-section 4 222
7.4.5 Sheet 28: Vibracores cross-section 5 223
7.4.6 Sheet 29: Vibracores cross-section 6 223
7.4.7 Sheet 30: Vibracores cross-section 7 224
7.4.8 Sheet 31: Vibracores cross-section 8 224
7.5 Summary 225

8 Discussion and synthesis **227**
8.1 Introduction . . . 227
8.2 Holocene sea-level change on the Manawatu coast . . . 227
8.2.1 Holocene sea-level fluctuations in the New Zealand archipelago . . . 227
8.2.2 Holocene sea-level changes on the south/southwest coast of the North Island . . . 228
8.2.3 Indicators of Holocene sea-level change from the lower Manawatu valley . . . 228
8.3 Subsidence in the lower Manawatu valley . . . 229
8.3.1 Sediment compaction . . . 230
8.3.2 Post-glacial water and sediment loading . . . 232
8.3.3 Evolution of the Wanganui Basin . . . 233
8.3.4 Influence of the Kairanga Trough . . . 233
8.3.5 Influence of neotectonics . . . 236
8.3.6 Subsidence in the Manawatu valley: conclusions . . . 236
8.4 Comparisons of lower Manawatu valley stratigraphy to tripartite facies models of estuary and incised-valley infilling . . . 238
8.4.1 Tripartite facies models of estuary and incised-valley infilling . . . 238
8.4.2 Comparisons of lower Manawatu valley stratigraphy with established models of incised-valley evolution . . . 239
8.5 Last Glacial Maximum and Holocene palaeogeomorphology of the lower Manawatu valley . . . 241
8.5.1 Path of the Manawatu River 18,000–15,000 years BP . . 241
8.5.2 Role of the Poroutawhao High and the Himitangi Anticline at the height of the Holocene marine transgression 242
8.5.3 Extent of the Manawatu estuary at the height of the Holocene marine transgression . . . 243
8.5.4 Manawatu coastline at the height of the Holocene marine transgression . . . 243
8.5.5 Infilling of the Manawatu estuary 8,000 cal. yr BP to present . . . 244
8.5.6 Sedimentation rates in the lower Manawatu valley following the culmination of the Holocene marine transgression . . . 248
8.6 Palaeogeographic maps and conceptual models of the Holocene evolution of the lower Manawatu incised-valley system . . . 248
8.6.1 18,000–9,000 years BP . . . 248
8.6.2 9,000–6,800 cal. yr BP . . . 250
8.6.3 5,700 cal. yr BP . . . 256
8.6.4 4,700 cal. yr BP . . . 256
8.6.5 4,700 cal. yr BP to Present . . . 256
8.7 LGM to Holocene facies evolution of the Manawatu Valley . . . 261
8.7.1 Lowstand incised-valley system . . . 261

8.7.2 Holocene marine transgression 261
8.7.3 Holocene sea-level highstand 264
8.7.4 Barrier development and coastal progradation 264

9 Conclusions **267**
9.1 Findings of this research 267
9.1.1 State of knowledge of Holocene sea-level fluctuations in the New Zealand region 267
9.1.2 Local-scale reconstructions of Holocene sea-level changes for regions within the New Zealand archipelago 268
9.1.3 Water well log reconstructions of the Holocene sedimentary fill of the lower Manawatu valley 269
9.1.4 Stratigraphy and facies assemblages reconstructed from detailed vibracores 269
9.1.5 Subsidence in the Lower Manawatu valley 270
9.1.6 Comparisons of lower Manawatu valley stratigraphy to tripartite facies models of incised-valley infill 270
9.1.7 LGM and Holocene palaeogeomorphology of the lower Manawatu valley 271
9.2 Future research 272

References **273**

A Contents of the DVD **325**

B Vibracore lithological logs **327**

C Sediment analysis results **433**

D Radiocarbon results **445**

E Other detailed bores from the lower Manawatu valley **459**

List of Figures

2.1 Conceptual diagram illustrating the provenance of several recent papers which present and/or make use of palaeo sea-level curves from the New Zealand region 6
2.2 Map of the North Island, New Zealand, showing locations utilised by studies of New Zealand palaeo sea-level fluctuations . . 8
2.3 Map of the South Island, New Zealand, showing locations utilised by studies of New Zealand palaeo sea-level fluctuations . . 9
2.4 Quaternary sea-level movements in the New Zealand region (after Brothers, 1954) 10
2.5 Summary of Holocene sea-level curves produced for the New Zealand region between 1958–1981, covering the period 20,000 years BP to present 16
2.6 Summary of Holocene sea-level curves produced for the New Zealand region between 1958–1981, covering the period 10,000 years BP to present 18
2.7 Summary of Holocene sea-level curves produced for the New Zealand region between 1979–2010, covering the period 20,000 years BP to present 25
2.8 Summary of Holocene sea-level curves produced for the New Zealand region between 1979–2010, covering the period 10,000 years BP to present 26
2.9 Holocene sea-level history for the New Zealand region presented by Clement et al. (2008a,b, 2010) 33

3.1 Locations of sites throughout the New Zealand region from which indicators of Holocene palaeo sea levels were recovered . 45
3.2 Locations of sites throughout the northern North Island, New Zealand, from which indicators of Holocene palaeo sea levels were recovered 46
3.3 Other locations mentioned in connection with the construction or analysis of the local-scale Holocene sea-level curves for the New Zealand archipelago 54
3.4 Local-scale Holocene sea-level curve for the Auckland-Northland region, New Zealand 59

3.5 Local-scale Holocene sea-level curve for the Auckland-Northland region, New Zealand, plotted with an expanded vertical axis . . . 60
3.6 Local-scale Holocene sea-level history for the Coromandel-Firth of Thames region, New Zealand . . . 62
3.7 Local-scale Holocene sea-level curve for the south/southwest North Island, New Zealand . . . 63
3.8 Local-scale Holocene sea-level curve for the Christchurch-Pegasus Bay area, New Zealand . . . 65
3.9 Local-scale Holocene sea-level curve for the East Otago Peninsula, New Zealand . . . 66
3.10 Local-scale Holocene sea-level curve for the East Otago Peninsula, New Zealand, plotted with an expanded vertical axis . . . 67
3.11 Map of the New Zealand region illustrating the north-south lag in the timing of the attainment of PMSL . . . 72
3.12 Map of the New Zealand region illustrating the position of sea levels at the 7,700 cal. yr BP time-slice . . . 73
3.13 Comparison of Holocene sea-level fluctuations on the south/southwest coast of the North Island, and around the East Otago Peninsula, illustrating the 500–1,000 year north-south lag between the two areas . . . 75

4.1 Locality map of the Manawatu region, southwest North Island, New Zealand. . . . 77
4.2 Tectonic setting of the southern North Island, New Zealand . . . 80
4.3 Schematic cross-section across the interface between the Pacific and Australian tectonic plates . . . 81
4.4 1:250,000 scale geological map of the Manawatu region . . . 82
4.5 Fold axes of the Manawatu anticlines . . . 85
4.6 Geologic cross-section across the Horowhenua coastal plain (after Aharoni, 1991) . . . 87
4.7 Correlation between climate, oxygen isotope stages, and landform development in the Manawatu region . . . 89
4.8 Conceptual model of inferred palaeoenvironmental changes in the Manawatu-Horowhenua region that formed the Tokomaru Marine Terrace (after Sewell, 1991). . . . 92
4.9 Conceptual model of inferred palaeoenvironmental changes in the Manawatu-Horowhenua region between MIS 6–2 (after Hughes, 2005a,b). . . . 94
4.10 1:75,000 scale maps of the river terraces between the Manawatu Gorge and Palmerston North City, as presented by Fair (1968), Lieffering (1990), and Lee and Begg (2002). See Figure 4.4 for regional context. . . . 96

4.11 Generalised stratigraphic collumns illustrating the typical arraignment of loess and tephra coverbeds on fluvial terraces in the lower Manawatu valley 98
4.12 Late Quaternary sea-level changes in the southwest Pacific region 101
4.13 Context map showing the locations of the Whanganui, Whangaehu, Rangitikei, and Manawatu Rivers 104
4.14 Estimates of the extent of the Manawatu River estuary at the culmination of the Holocene marine transgression 108

5.1 Classification of estuaries (after Reinson, 1992) 116
5.2 Shoreline response (transgression versus regression) to changes in sea-level and sediment supply (after Boyd et al., 1992, 2006) 118
5.3 Classification of major clastic coastal depositional environments (after Boyd et al., 1992, 2006) 118
5.4 Schematic illustrating the definitions of estuary, the physical processes operating in estuaries, and the resulting tripartite facies zonation (after Dalrymple et al., 1992) 119
5.5 Evolutionary classification of coastal environments (after Dalrymple et al., 1992) 120
5.6 Distribution of energy types, morphological components, and sedimentary facies within an idealised wave-dominated estuary (after Dalrymple et al., 1992) 121
5.7 Classification of wave-dominated estuaries on the southeast coast of Australia (after Roy et al., 1980) 125
5.8 Conceptual model of the sedimentary infilling of a drowned-river estuary (after Roy et al, 1980; Chapman et al., 1982; Roy, 1984a,b, 1994) 126
5.9 Idealised longitudinal section of a simple incised-valley system (after Zaitlin et al., 1994) 130

6.1 Locations of cross-sections and wells used for investigations of the sub-surface geology of the Manawatu region 136
6.2 Cross-section through the Holocene marine wedge south of Tangimoana (after Shepherd et al., 1986) 140
6.3 Well log correlation across part of the Tokomaru Marine Terrace (after Sewell, 1991) 142
6.4 Cross-section running northeast-southwest (line A-A') across the Horowhenua coastal plain (after Hughes 2005a, b) 142
6.5 Cross-section running southeast-northwest (line B-B') across the Horowhenua coastal plain (after Hughes 2005a, b) 142
6.6 Structural contours for the Ashhurst/Ohakea fluvial aggradation terrace extrapolated beneath the Holocene floodplain (after Begg et al., 2005) 145

6.7 Structural contours for the Milson/Rata fluvial aggradation terrace extrapolated beneath the Holocene floodplain (after Begg et al., 2005) . . . 145
6.8 Structural contours for the Tokomaru Marine Terrace extrapolated beneath the Holocene floodplain (after Begg et al., 2005) 145
6.9 Locations of geologic cross-sections constructed from well logs in the Manawatu valley . . . 150
6.10 Conceptual 3D model of the twenty geologic cross-sections constructed from well logs in the lower Manawatu valley looking southeast across the coastal plain . . . 152
6.11 Conceptual 3D model of the twenty geologic cross-sections constructed from well logs in the lower Manawatu valley looking north-northwest across the coastal plain . . . 152
6.12 Conceptual 3D model of the geologic cross-sections constructed from well logs looking east across the upper Manawatu floodplain . . . 155
6.13 Conceptual 3D model of the geologic cross-sections constructed from well logs looking south across the lower Manawatu floodplain . . . 155
6.14 Key to well logs cross-sections symbols and lithological units (Sheets 1–23) . . . 159
6.15 Stratigraphic sections from Griffin's and Barber's Farms, lower Manawatu valley (after Shepherd and Lees, 1987) . . . 163
6.16 Locations of well logs containing gravel units identified as Ashhurst/Ohakea LGM aggradation gravel . . . 171
6.17 Digital elevation model of the Ashhurst/Ohakea LGM aggradation surface reconstructed from gravel units identified in water well logs throughout the lower Manawatu valley . . . 171
6.18 Example of channel artifacts produced by the Topo to Raster algorithm . . . 175
6.19 Digital elevation model of the Ashhurst/Ohakea LGM aggradation surface reconstructed from gravel units identified in water well logs throughout the lower Manawatu valley, adjusted to remove sinks . . . 176
6.20 Comparison of the reconstructed digital elevation model of the Ashhurst/Ohakea LGM aggradation surface with the structural contours of the Ashhurst/Ohakea surface extrapolated by Begg et al. (2005) . . . 176
6.21 Comparison of the reconstructed digital elevation model of the Ashhurst/Ohakea LGM aggradation surface (adjusted to remove sinks) with the structural contours of the Ashhurst/Ohakea surface extrapolated by Begg et al. (2005) . . . 176
6.22 Locations of well logs and vibracores containing sedimentary units identified as the top of the Holocene marine/estuarine fill in the lower Manawatu valley . . . 180

6.23 Digital elevation model of the estuarine-alluvial interface reconstructed from sedimentary units identified in water well logs and vibracores througout the lower Manawatu valley 180

7.1 Locations of vibracores recovered from the lower Manawatu valley 188
7.2 Vibracoring at site Flood-8 190
7.3 Vibracoring at site LD-5 191
7.4 Logging the side of the drain at site LD-5 191
7.5 Tripod set up to extract vibracore Ran-2 192
7.6 Conceptual diagram illustrating the relationship between ellipsoidal and orthometric heights 193
7.7 Locations of vibracore cross-sections in the lower Manawatu valley 198
7.8 Representative sections of each of the five major facies identified in vibracores from the lower Manawatu valley 202
7.9 Stratigraphic log of drain section and vibracore F 203
7.10 Stratigraphic log of drain section and vibracore Kop-1 203
7.11 Stratigraphic log of drain section and vibracore Sh-1 203
7.12 Stratigraphic log of drain section and vibracore Flood-1 203
7.13 Stratigraphic log of drain section and vibracore Sh-2 203
7.14 Stratigraphic log of drain section and vibracore Cut-7 203
7.15 Stratigraphic log of drain section and vibracore Cut-4 203
7.16 Stratigraphic log of drain section and vibracore E-1 203
7.17 Stratigraphic log of drain section and vibracore Cut-2 203

8.1 Conceptual diagram of the structure of the discussion chapter in relation to previous chapters 228
8.2 Holocene sea-level curve for the south/southwest coast of the North Island, New Zealand, with index points colour-coded to indicate location 229
8.3 Graph illustrating the relationship between the elevations of sea-level index points recovered from the lower Manawatu valley and the distance up valley from the present-day coastline measured against the valley centerline 230
8.4 Graph illustrating the relationship for each palaeo sea-level indicator recovered form the lower Manawatu valley between the depth to the LGM Ashhurst/Ohakea aggradation surface (below PMSL) at the location where the indicator was recovered, and the difference between the indicator's inferred palaeo sea-level and the sea-level inferred for the Manawatu region at that time 232
8.5 Residual Bouguer anomaly map of the southern Wanganui Basin (after Rich, 1959) 234

8.6 Relationship of the Kairanga Trough to the reconstructed Ashhurst/Ohakea DEM, illustrating the depression of the LGM surface coincident with the axis of the trough 236
8.7 Positions of radiocarbon dated shell and wood samples recovered from the lower Manawatu valley 244
8.8 Locations of palaeo shorelines in the lower Manawatu valley during and following the the Holocene marine transgression . . 244
8.9 Palaeogeographic map of the lower Manawatu valley during the Last Glacial Maximum, c. 18,000–15,000 years BP 250
8.10 Conceptual model of the geomorphology of the lower Manawatu valley during the Last Glacial Maximum, c. 18,000–15,000 years BP 250
8.11 Palaeogeographic map of the lower Manawatu valley, c. 7,100–6,800 cal. yr BP 250
8.12 Conceptual model of the geomorphology of the lower Manawatu valley, c. 7,100 cal. yr BP 250
8.13 Conceptual model of the geomorphology of the lower Manawatu valley, c. 6,800 cal. yr BP 250
8.14 Palaeogeographic map of the lower Manawatu valley, c. 5,700 cal. yr BP 256
8.15 Conceptual model of the geomorphology of the lower Manawatu valley, c. 5,700 cal. yr BP 256
8.16 Palaeogeographic map of the lower Manawatu valley, c. 4,700 cal. yr BP 256
8.17 Conceptual model of the geomorphology of the lower Manawatu valley, c. 4,700 cal. yr BP 256
8.18 Conceptual summary sequence of the facies evolution of the lower Manawatu valley from the Last Glacial Maximum until present 262

List of Tables

2.1 Summary of radiocarbon ages presented by previous investigations of Holocene palaeo sea-level change in the New Zealand region 13

3.1 Details of 215 palaeo sea-level indicators from locations throughout the New Zealand region. 39
3.2 Details of known-age marine samples used to calculate a New Zealand regional marine reservoir correction ΔR value for the calibration of CRAs from fossil shells and other marine materials in sidereal years (cal yr. BP) 47
3.3 Summary of the formation datums and error ranges associated with each of the types of palaeo sea-level indicator used to reconstruct the local-scale sea-level histories in the New Zealand archipelago 48
3.4 Tidal ranges for each of the sites throughout the New Zealand region from which palaeo sea-level indicators included in the study were recovered 49
3.5 Summary of long-term and event tectonic deformation for localities and regions within the New Zealand archipelago from which indicators of Holocene palaeo sea levels were recovered . 52

4.1 Summary of radiocarbon ages obtained by previous investigations of geomorphological features of the Manawatu coastal plain 100

5.1 Morphological and sedimentalogical summary of wave-dominated estuaries (after Nichol, 1991; Marra, 1997) 122

6.1 Summary of radiocarbon ages obtained in connection with wells and bores drilled across the Manawatu coastal plain 139
6.2 Volumes of sedimentary fill estimated using digital elevation models of the LGM aggradation surface and the estuarine alluvial interface in the lower Manawatu valley 183

7.1 Vibracore location, elevation, compaction, and length details . 195
7.2 Vibracore GPS survey details 196

7.3 Summary of radiocarbon ages obtained from samples of shell and wood recovered from vibracores and auger holes in the lower Manawatu valley 197
7.4 Summary of the defining characteristics of the five facies identified in vibracores recovered from the lower Manawatu valley . 200

8.1 Details of the relationship between the elevations of sea-level index points recovered from the lower Manawatu valley and the distance up valley from the present-day coastline measured against the valley centerline 231
8.2 Details of the relationship for each palaeo sea-level indicator recovered form the lower Manawatu valley between the depth to the LGM Ashhurst/Ohakea aggradation surface (below PMSL) at the location where the indicator was recovered, and the difference between the indicator's inferred palaeo sea-level and the sea-level inferred for the Manawatu region at that time 234
8.3 Details of estuarine sedimentation rates calculated for vibracores recovered from the lower Manawatu valley 249

List of Sheets

1 Well logs cross-section 1
2 Well logs cross-section 2
3 Well logs cross-section 3
4 Well logs cross-section 4
5 Well logs cross-section 5
6 Well logs cross-section 6
7 Well logs cross-section 7
8 Well logs cross-section 8
9 Well logs cross-section 9
10 Well logs cross-section 10
11 Well logs cross-section 11
12 Well logs cross-section 12
13 Well logs cross-section 13
14 Well logs cross-section 14
15 Well logs cross-section 15
16 Well logs cross-section 16
17 Well logs cross-section 17
18 Well logs cross-section 18
19 Well logs cross-section 19
20 Well logs cross-section 20

21 Poroutawhao-Moutoa well logs
22 Himitangi-Oroua well logs
23 Rangiotu-Foxton well logs

24 Vibracores cross-section 1
25 Vibracores cross-section 2
26 Vibracores cross-section 3
27 Vibracores cross-section 4
28 Vibracores cross-section 5
29 Vibracores cross-section 6
30 Vibracores cross-section 7
31 Vibracores cross-section 8

32 Key to well logs cross-sections symbols and lithological units, and key to vibracore lithological logs

Common abbreviations

GPS Global Positioning System

LGM Last Glacial Maximum

MIS Marine isotope stage

MHT Mean high tide

MHWN Mean high water neaps

MHWS Mean high water springs

MLWN Mean low water neaps

MLWS Mean low water springs

MSL Mean sea-level

NZGD2000 New Zealand Geodetic Datum 2000

NZMG New Zealand Map Grid 1949

NZVD09 New Zealand Vertical Datum 2009

PMSL Present mean sea-level

RTK-dGPS Real-time Kinematic differential Global Positioning System

WVD53 Wellington Vertical Datum 1953

A note about ages presented in this thesis

Many of the radiocarbon ages presented by New Zealand researchers from the mid-1950s until the 1990s were not conventional radiocarbon ages (CRA) as defined by Stuiver and Polach (1977). These ages, determined at Rafter Radiocarbon Laboratory, were not determined with respect to the standards which define a CRA (C. Prior, personal communication). (All ages determined at the Waikato University Radiocarbon Laboratory are CRAs.) These "unconventional" ages are suffixed with "years BP". Broad statements about the timing of events dated by unconventional ages, such as in the interpretation of sea-level curves constructed using unconventional ages, are similarly expressed in "years BP". Conventional radiocarbon ages, where available, have been given and are suffixed "14C years". Where conventional radiocarbon ages have been calibrated to sidereal years, these dates are suffixed "cal. yr BP". Large ages of the order of millions of years are suffixed "Ma".

A note about ages presented in this thesis

Chapter 1

Introduction

Incised-valleys and the estuaries that occupy them are common features along modern transgressive coasts (e.g., Hume and Herdendorf, 1988; Roy et al., 2001; Hume, 2003; Heap et al., 2004). They are the product of fluvial incision in response to lower sea levels during glacial episodes, and subsequent inundation during marine transgressions (Zaitlin et al., 1994; Boyd et al., 2006). Estuaries and incised-valleys serve as conduits for sediment passing from the hinterland to the oceans (Blum and Tornqvist, 2000), yet they are highly efficient sediment traps (Meade, 1972; Biggs and Howell, 1984). The sediments deposited in estuaries and incised-valleys have high preservation potential (Demarest and Kraft, 1987). Consequently, the sedimentary fill of estuaries and incised-valleys is significant within the context of global environmental change as an archive of coastal responses to climate and sea-level fluctuations (Zaitlin et al., 1994; Boyd et al., 2006).

Estuaries and incised-valleys are a complex grouping of sedimentary environments reflecting the variety of formative processes responsible for their development. Internationally, a large number of studies have focused on the evolution of estuaries and incised-valleys in response to relative sea-level rise. This research has developed a unifying series of models that describe the evolution of estuaries and incised-valleys in response to different environmental conditions (e.g., Roy et al., 1980; Roy, 1984b; Dalrymple et al., 1992; Zaitlin et al., 1994). These models provide a framework for delineating the depositional fill of estuaries and incised-valleys and for interpreting their evolution. However, while the application of estuary and incised-valley facies models has been prolific overseas, comparatively few investigations have considered the evolution of New Zealand estuaries and incised-valleys within the framework of facies models. This has important implications for the understanding of the evolution of estuaries and incised-valleys in New Zealand, as the estuary and incised-valley facies models are commonly based on estuaries of extensive size (40–100 km in length) on stable coastlines, with comparatively limited sediment supplies (Wilson et al., 2007; Clement et al., 2010). In contrast, New Zealand is tectonically active (e.g., Pillans, 1986; Williams, 1991), with small estuaries (typically less than 17 km^2 in size; Hume, 2003), and comparatively

high sediment loads (e.g., Hicks and Shankar, 2003). It is therefore unclear whether the established models of incised-valley and estuary evolution can be successfully applied to estuaries and incised-valleys in a New Zealand context.

Sea-level change is a major factor in the evolution of incised-valleys and estuaries. However, knowledge of Holocene sea-level fluctuations in the New Zealand region is still in its infancy, and is highly fragmented (Hayward et al., 2010c). The current 'de facto' standard Holocene sea-level history for the New Zealand region (Gibb, 1986) indicates that present mean sea-level was attained c. 6,700 cal. yr BP, remaining largely static thereafter (Clement et al., 2008a,b). However, it has recently been suggested that composite sea-level histories such as that presented by Gibb (1986), may mask or hide local-scale sea-level fluctuations (Clement et al., 2009a,b).

The sea-level history presented by Gibb (1986) contrasts with recent research from the southeast coast of Australia which indicates an earlier culmination of the Holocene marine transgression c. 7,700 cal. yr BP, and an extended period of higher than present sea-level during the mid Holocene (e.g., Horton et al., 2007; Sloss et al., 2007). Similarly, higher than present sea levels during the mid Holocene are also indicated by recent research from some New Zealand locations (e.g., Heap and Nichol, 1997; Hicks and Nichol, 2007). The benchmark Holocene sea-level history for New Zealand (Gibb, 1986) may therefore not present an accurate picture of Holocene sea-level fluctuations in the New Zealand archipelago, making it unsuitable to contextualise investigations of the Holocene evolution of New Zealand estuaries and incised-valleys.

This thesis presents a comprehensive, critical review of the state of knowledge of Holocene sea-level fluctuations in the New Zealand region. This review provides context for local-scale reconstructions of Holocene sea-level change for regions within the New Zealand archipelago. These local-scale sea-level reconstructions inform a detailed stratigraphic and geomorphic investigation of the Holocene evolution of the lower Manawatu valley, a coastal plain incised-valley system on the southwest coast of the North Island, New Zealand. The stratigraphic and geomorphic investigation of the evolution of the lower Manawatu valley is conducted within the context of wave-dominated estuary and incised-valley facies models, providing an opportunity to examine the extent to which these facies models can be successfully applied to estuaries and incised-valleys in a New Zealand context.

1.1 Thesis aims

It is the aim of this thesis to:

1. comprehensively and critically review the state of knowledge of Holocene sea-level fluctuations in the New Zealand region;
2. construct detailed, local-scale Holocene sea-level curves for regions within the New Zealand archipelago;

3. reconstruct the stratigraphic and geomorphic evolution of the Manawatu coastal plain incised-valley system within the context of Holocene sea-level change and established models of estuary and incised-valley evolution.

1.2 Thesis organisation

This thesis is arranged into three parts. The first section considers Holocene sea-level change in the New Zealand region. The second section provides a background to incised-valleys, a geological and geomorphological framework for the lower Manawatu valley, and presents results from investigations of the stratigraphy of the valley. The final part of the thesis draws these two disparate sections together by discussing the Holocene geomorphic evolution of the lower Manawatu valley within the context of Holocene sea-level changes and incised-valley facies models.

Chapter 2 critically reviews the current state of knowledge of Holocene sea-level fluctuations in the New Zealand region. Such a review has not been completed since 1953. Chapter 3 builds on the conclusions of Chapter 2 by reviewing available palaeo sea-level indicator data in order to construct five local-scale Holocene sea-level curves for regions with the New Zealand archipelago. These curves are considered within the context of independent studies of palaeo sea levels from the New Zealand region, and recent palaeo sea-level reconstructions from the wider southwest Pacific region.

Chapter 4 reviews the geology, geomorphology, climate, vegetation, and contemporary coastal processes of the Manawatu region. Chapter 5 introduces estuary and incised-valley facies models, and reviews their use in a New Zealand context. Chapter 6 presents results of the reconstruction of the broad-scale features of the Holocene sedimentary infill of the lower Manawatu valley from water well logs. Chapter 7 presents results of facies reconstructions of the Holocene sedimentary infill of the lower Manawatu valley based on strategically positioned vibracores studied in fine detail.

Chapter 8 provides a wider context for a discussion of Holocene sea-level change and the geomorphic evolution of the Manawatu incised-valley system. The chapter discusses sea-level changes in the New Zealand region, and on the southwest coast of the North Island, to contextualise a discussion of sea-level index points from the Manawatu valley. Subsidence mechanisms at a range of spatial and temporal scales are then discussed, to provide an explanation for the variation observed in the record of Holocene sea-level changes in the Manawatu valley. This is followed by a discussion which compares the sedimentary stratigraphy preserved in the lower Manawatu valley with established models of wave-dominated estuary and incised-valley infilling. The chapter then considers various aspects of the palaeogeomorphology of the Manawatu coastal plain, before drawing this information together to construct time-series palaeogeographic maps and comceptual models of the evolution of the Manawatu extending from the Last Glacial Maximum to the mid-Holocene.

Chapter 2

Reconstructing Holocene sea-level changes in the New Zealand archipeligo: review

2.1 Introduction

This chapter integrates and critically analyses the full body of work relating to Holocene sea-level histories in the New Zealand archipelago. A comprehensive, critical review is necessary as while it is over 80 years since the first observations of palaeo sea levels in New Zealand were published (Henderson, 1924), knowledge of palaeo sea-level fluctuations in the New Zealand region is still in its infancy, and is fragmentary at best (Hayward et al., 2010b).

The last comprehensive review of New Zealand palaeo sea levels was presented nearly 60 years ago (Gage, 1953). Since then a number of annotated bibliographies of sea-level literature from around the world, including New Zealand, have been produced (e.g., Richards and Fairbridge, 1965; Richards, 1970, 1974; Richards and Shapiro, 1979; Richards et al., 1986; Pirazzoli, 1991). However, while these works offered global coverage and international scope, they were, for New Zealand at least, often incomplete and lacked critical insight. Kennedy (2008) recently forwarded what was titled a review of New Zealand sea-level research. However, only a cursory inspection of the literature was presented, restricted to a mere two works.

Analysis of several recent papers which present and/or make use of palaeo sea-level curves from the New Zealand region (e.g., Carter et al., 2002; Wilson et al., 2007; Kennedy, 2008) reveals that these curves have provenance dating back to the 1950s (Figure 2.1). For example, Carter et al. (2002) presented a sea-level curve based on the earlier work of Carter et al. (1986). This was in turn based on the work of Cullen (1967a), Herzer (1981), and Gibb (1986). Cullen (1967a) utilised observations made by Te Punga (1958), while Gibb

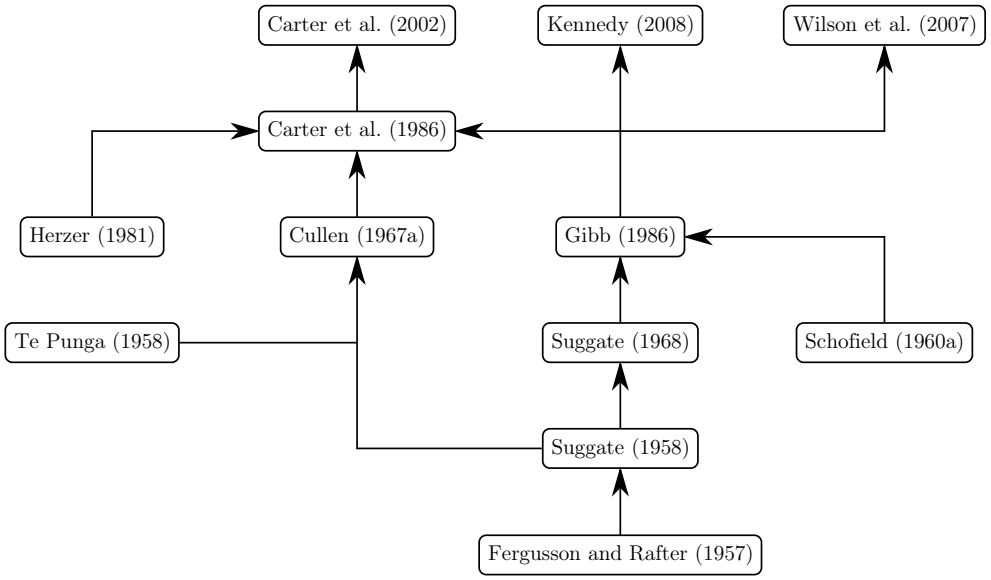

Figure 2.1: Conceptual diagram illustrating the provenance of several recent papers which present and/or make use of palaeo sea-level curves from the New Zealand region. Arrows flow upwards, indicating that the higher papers draw upon/from lower papers.

(1986), the 'de facto' New Zealand Holocene sea-level curve (Hesp et al., 1999; Kennedy, 2008), drew on work presented by Schofield (1960a) and Suggate (1968). Suggate (1968) in turn drew heavily from an earlier investigation (Suggate, 1958), which itself drew on radiocarbon age determinations first published by Fergusson and Rafter (1957) (though the age determinations were commissioned by Suggate). However, there has been no attempt to consider the accuracy or veracity of any of these papers.

Given the lack of critical attention paid to Holocene sea-level histories produced for the New Zealand region over the last 60 years there is a clear need for a detailed critical review that resolves the fragmented state of knowledge of Holocene sea-level fluctuations in New Zealand. This chapter presents such a review, which establishes the context for the Holocene sea-level reconstructions presented in Chapter 3.

2.2 Early investigations of strandlines as evidence of palaeo sea levels

Evidence of late Quaternary sea-level fluctuations in the New Zealand archipelago were first collated and reviewed by Henderson (1924), who drew together qualitative information from geological bulletins and surveys that had previously been remarked on only incidentally. Using strandlines, marine terraces, raised beaches, and shore platforms as indicators of uplift, with drowned forests and river valleys interpreted as evidence of subsidence, Henderson (1924) concluded that relative sea-level change was a uniform phenomena

throughout the New Zealand region, due either to retreat of the ocean or uplift of the entire archipelago.

The prospects for regional correlation between local palaeo sea-level indicators drew the attention of Jobberns (1926, 1928) and King (1930, 1932), who ultimately (King and Jobberns, 1934) recognised the complex nature of New Zealand's Quaternary tectonic movements. King and Jobberns (1934) concluded that there was extremely limited scope for correlation of New Zealand's marine terraces with those described internationally, and little prospect of utilising strandlines to synchronise New Zealand's Quaternary geology with that of the rest of the world. Cotton (1947) ignored these conclusions, and explicitly assumed that tectonic movements throughout the New Zealand region had no significant effect on the disposition of evidence of palaeo sea levels. In this manner Cotton (1947) presented a correlation of New Zealand strandline data with that from the wider Pacific region.

Gage (1953) summarised the state of knowledge of Quaternary strandlines in New Zealand, and condemned Cotton's (1947) work as retrograde. Gage (1953) discounted any possibility of incorporating New Zealand evidence of fluctuating sea levels with that of other regions, given the degree of New Zealand's Quaternary tectonic deformation and the qualitative nature of the majority of observations up until that time. Gage (1953) suggested that all preceding work be abandoned, and proposed that future studies of palaeo sea-level in New Zealand be centered around the relatively tectonically stable regions of Northland-Auckland and East Otago (Figures 2.2 and 2.3; cf. Cotton, 1948, 1957a; Harrington, 1958). Fleming (1953a), as part of broad discussion of methods for establishing a geochronology of New Zealand's "Recent Period", reached similar conclusions about the impact of differential earth movements on the correlation of palaeo sea-level indicators, and therefore advocated for the establishment of local-scale chronologies.

2.3 Altimetric correlations with European chronologies

Brothers (1954) correlated sea-level movements around the South Kaipara barrier (Figure 2.2) with a Pleistocene chronology from the western Mediterranean (Baulig, 1935; Zeuner, 1950), taking notice only of Gage's (1953) latter conclusion of a tectonically stable Auckland region. Brothers' (1954) sea-level history followed the then-widely held concept of progressively lower Quaternary interglacial sea levels (cf. Zeuner, 1959; Fairbridge, 1962), and recorded a series of sea-level highstands which dropped in stepwise fashion from a peak 167 m (550 feet) above present mean sea-level (PMSL) since the early Pleistocene (Figure 2.4). Leading into the Holocene (then "Recent Age"), Brothers (1954) concluded that that sea-level reached a minimum of 58 m (190 feet) below PMSL during the Last Glacial Maximum (LGM), with a maximum postglacial sea-level +2.5–+3.5 m (+8–+12 feet) above PMSL.

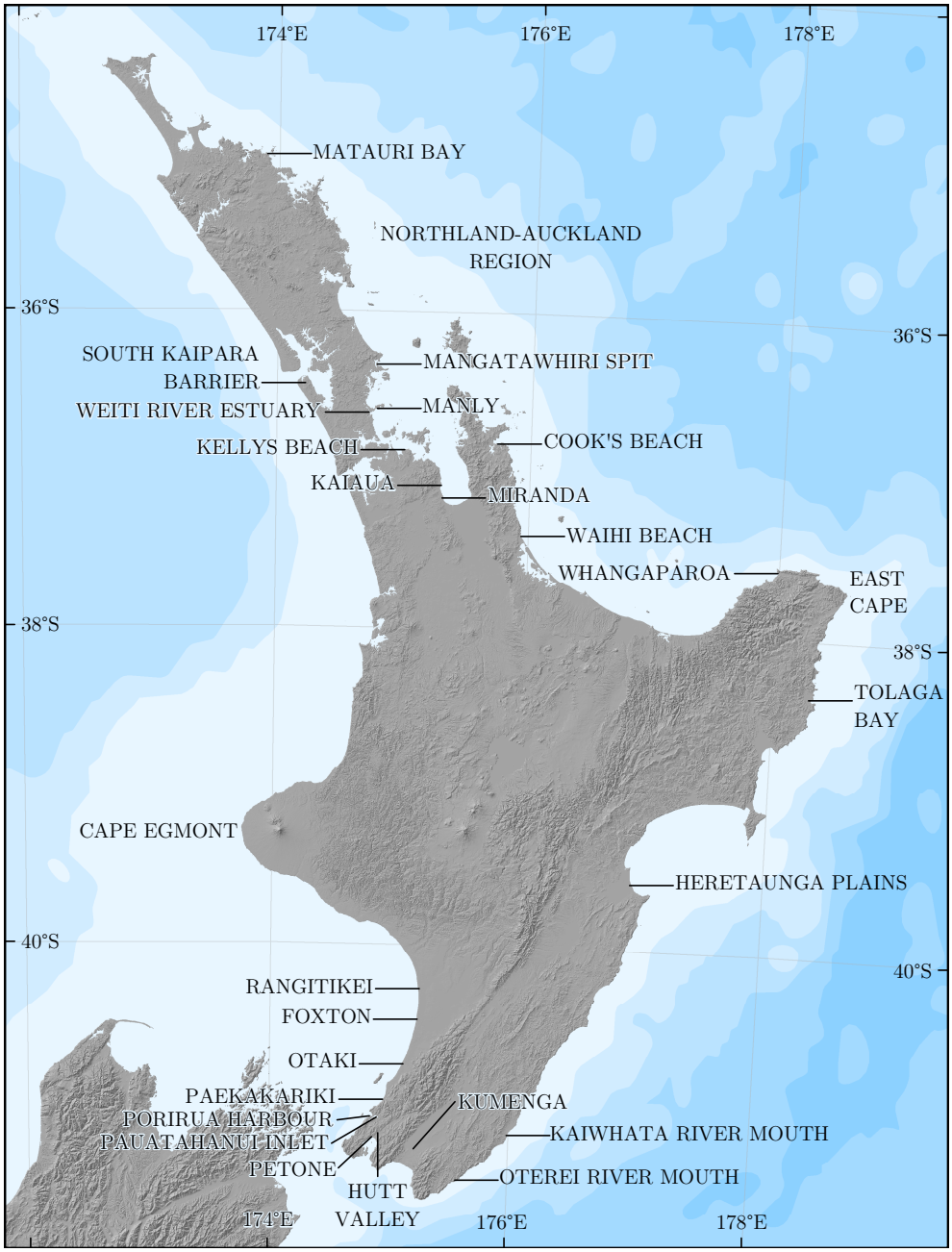

Figure 2.2: Map of the North Island, New Zealand, showing locations utilised by studies of New Zealand palaeo sea-level fluctuations.

Brothers' (1954) study led to the wide adoption of the Mediterranean sea-level terminology by New Zealand workers, as it was viewed as a useful framework with which to elucidate the formation of marine terraces (*sensu* Brothers, 1954; e.g., Searle, 1956; Kear, 1957, 1959, 1962, 1963, 1965; Schofield, 1958; Suggate, 1960; Ward, 1960, 1967; Purser, 1961; Ricketts, 1975; Glenie et al.,

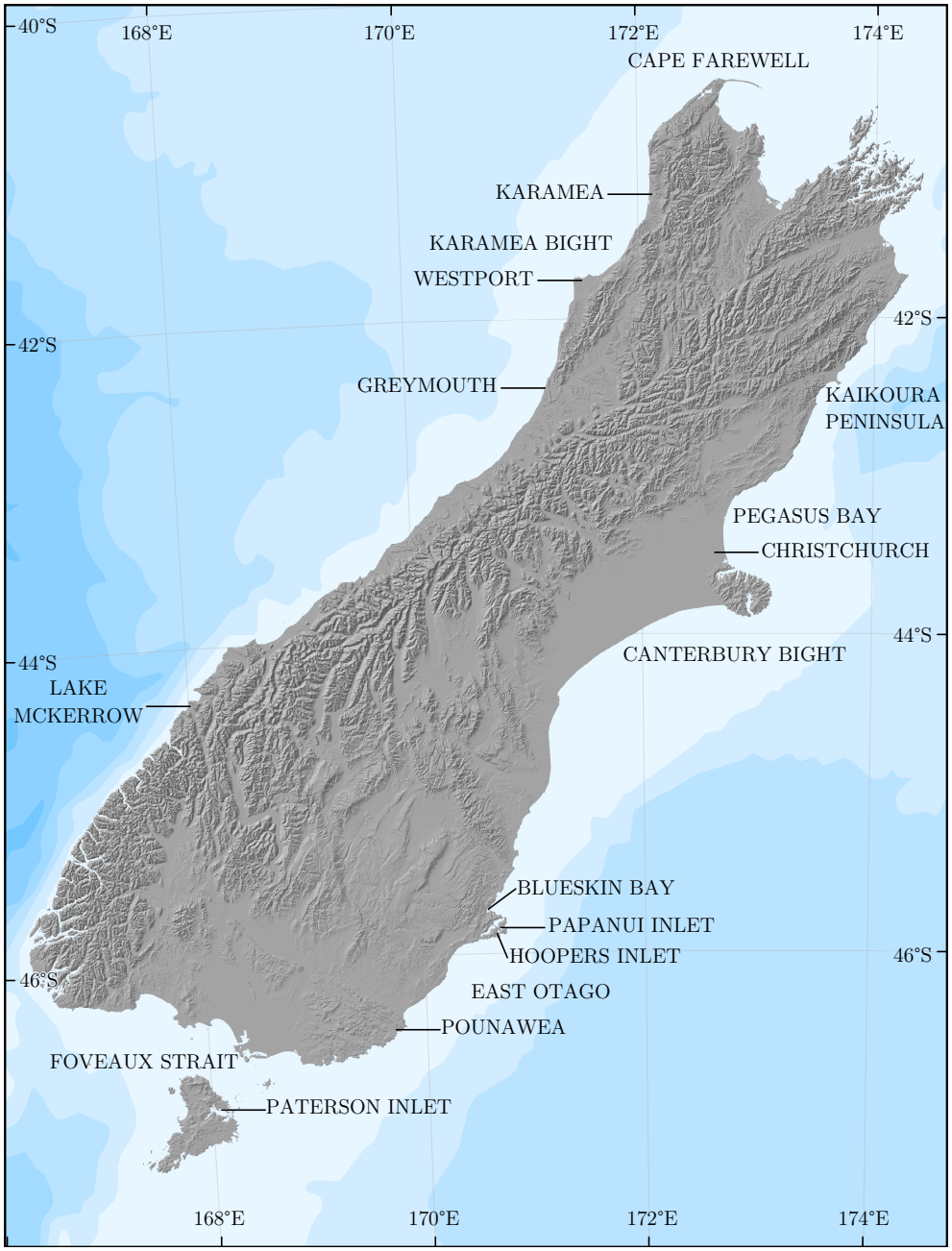

Figure 2.3: Map of the South Island, New Zealand, showing locations utilised by studies of New Zealand palaeo sea-level fluctuations.

1968; Waterhouse, 1978). Altimetric correlations between sites within New Zealand, and between New Zealand and the Northern Hemisphere were common. Unfortunately the findings by King and Jobberns (1934), Gage (1953) and Fleming (1953a) were largely overlooked, with most of the subsequent publications which drew from Brothers (1954) tending to ignore the effects

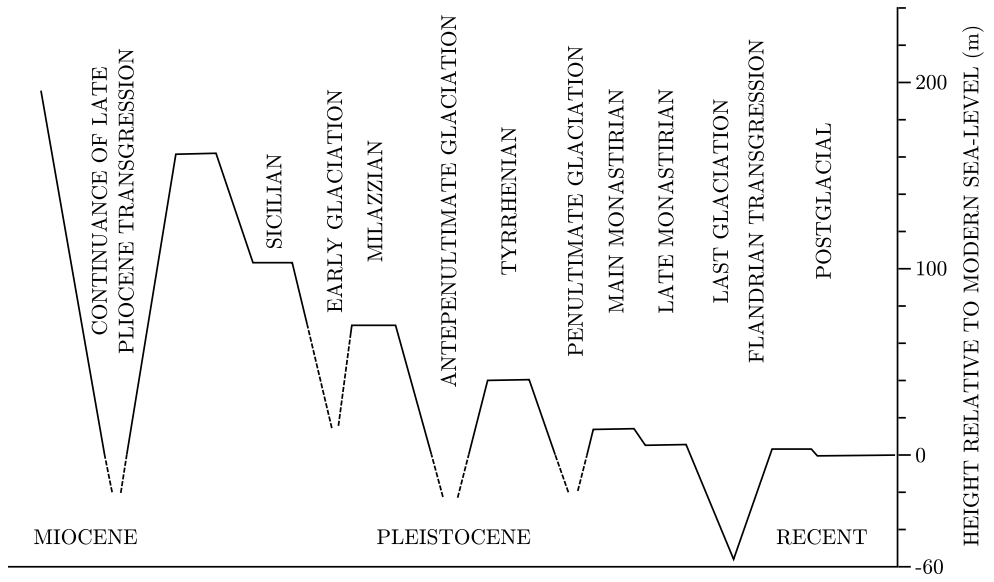

Figure 2.4: Quaternary sea-level movements in the New Zealand region presented by Brothers (1954), based on a correlation of marine terrace heights on the South Kaipara barrier with a western Mediterranean Pleistocene chronology (Baulig, 1935; Zeuner, 1950).

of tectonism on marine terraces and other indicators of palaeo sea levels. As Pillans (1990b) concluded, studies at this time appear to have commonly perceived tectonics as an unfortunate difficulty that otherwise prevented correlations with the Mediterranean scheme, and therefore the establishment of New Zealand chronologies.

Both Cotton (1957a) and Harrington (1958) attempted to correlate marine benches along the East Otago coast (Figure 2.3), with the Mediterranean Pleistocene chronology presented by Zeuner (1950), based on the elevations of the terraces. Harrington (1958) inferred close correspondence between the Otago benches, the Mediterranean chronology, and the South Kaipara terraces (Brothers, 1954). Milazzian, Tyrrhenian and Monastirian interglacial terraces were recognised (cf. Figure 2.4). Cotton (1957a), however, did not infer a close correspondence between the various sets of marine terraces, and concluded that any determination of palaeo shorelines along the Otago coast would yield little to enhance global correlations of sea-level. Elsewhere, Te Punga (1954c), and later Leamy (1958), undertook studies that attempted to correlate marine benches surrounding Porirua Harbour (Figure 2.2) with features of the Mediterranean scheme (Zeuner, 1945), despite the latter's awareness of the conclusions of both Gage (1953) and Fleming (1953a). Leamy (1958) suggested, on the basis of height, that terraces around Porirua Harbour corresponded with Late and Main Monastirian, Tyrrhenian, Milazzian, and Sicilian shorelines (cf. Figure 2.4). Te Punga (1954c) made tentative correlations with the Tyrrhenian higher shoreline.

Cotton (1963) reviewed the Mediterranean Pleistocene high shoreline chronology presented by Zeuner (1945) and others, in response to the attention paid to Brothers (1954) in the form of the wide adoption of the Mediterranean sea-level terminology by New Zealand researchers. Cotton (1963) noted that both the Calabrian (not recognised by Brothers, 1954) and Sicilian levels (cf. Figure 2.4) were named after marine formations which contained cold water faunas, with the Sicilian formation containing fossil indicators of deposition in deep water. Aside from the likelihood that the Calabrian and Sicilian sequences represented glacial rather than interglacial conditions, Cotton (1963) observed that due to tectonic deformation the altitudes of the Calabrian and Sicilian strandlines could not be accurately determined. Of the lower surfaces (see Figure 2.4), Cotton (1963) noted that due to tectonic uplift the Milazzian level was in fact a warped Tyrrhenian surface, while the Tyrrhenian levels originally identified in the Mediterranean were part of only a single sequence which had been locally uplifted. Cotton (1963) therefore concluded that the theory of a global correlation of Pleistocene marine stages formed by gradual lowering of sea levels (e.g., Zeuner, 1945, 1950, 1954, 1959) was in no way supported. Like Gage (1953) and Fleming (1953a), Cotton's (1963) conclusions were generally ignored.

Kear and Waterhouse (1961, 1971) adopted the Mediterranean chronology for their study of marine terraces at Waihi Beach (Figure 2.2), and presented a direct correlation between the benches there and the work of Brothers (1954) (Figure 2.4). Selby et al. (1971) later revisited this work, relating the Waihi terrace surfaces and covering ash beds to a global sea-level curve presented by Morner (1971). Selby et al. (1971) recognised a series of MIS 5 marine terraces, and one post-glacial sea-level highstand terrace.

Chapman-Smith and Grant-Mackie (1971) described two marine terraces at Whangaparoa (Figure 2.2), considered to have formed either during periods of tectonic stability during a general lowering of sea-level, or by spasmodic uplift of the Whangaparoa Peninsula. Chapman-Smith and Grant-Mackie (1971) concluded that the terraces were formed by the spasmodic lowering of sea levels, and suggested that any similarity between the elevations of terraces at Whangaparoa and South Kaipara (Brothers, 1954), may be a coincidence resulting from tectonic disturbances, given Whangaparoa's evidence of long-term tectonic instability.

Ward (1965, 1966) related sedimentary sequences near Adelaide, South Australia, to Brothers (1954) sea-level chronology from South Kaipara, which was modified, based on South Australian observations, to produce a single composite sea-level history for the two regions. Using this chronology, Ward (1965, 1966) forwarded a correlation with Northern Hemisphere glacial stages presented by Zeuner (1959) and Fairbridge (1961). Later, Ward et al. (1971) presented a simple model which attempted to correlate marine terraces, as a proxy for high sea levels, between any two localities regardless of the age of the palaeo sea-level or the degree of tilting or warping of the terrace. This model was initially used to correlate marine terraces in Gippsland, Australia, with

features in South Carolina, USA, before it was expanded to include strandlines between Greymouth and Westport on the west coast of the South Island, New Zealand (Figure 2.3; Suggate, 1965). Ward (1972) subsequently employed this model and these correlations to infer ages for marine terraces from northern New Zealand previously documented by Brothers (1954), Ward (1960) and Chappell (1964, 1970). Notably, Ward's (1972) modelled correlations assume long-term (750,000 years) tectonic stability, based on the supposed identification and correlation of a +3 m sea-level c. 30,000 years BP in northern New Zealand and south and eastern Australia (see criticisms by Chappell, 1975).

Chappell (1964, 1970) correlated marine terraces of the western and northern North Island with Brothers' (1954) sequence from South Kaipara on the basis of elevation and supporting stratigraphy. Chappell later (1975) expressed significant dissatisfaction with altitude-based correlations of coastal terraces, and attempted to end the practice of making national and international altimetric correlations by New Zealand researchers. Chappell (1975) noted that the practice was particularly detrimental to the development of a New Zealand national time stratigraphy. Therefore, Chappell (1975) eschewed altimetry, instead making correlations using tephra stratigraphy. In this manner Chappell (1975) revisited the observations of Kear and Waterhouse (1961, 1971), Chapman-Smith and Grant-Mackie (1971), and Selby et al. (1971), presenting a correlation of coastal terrace sequences around the Bay of Plenty, from Waihi Beach to East Cape (Figure 2.2), elucidated solely on the basis of covering tephras. Thereafter, only a few workers persisted in making altitude-based correlations (e.g., Goldie, 1975; Ricketts, 1975; Waterhouse, 1978; Heine, 1982).

2.4 Single radiocarbon dates to inform observations of palaeo sea levels in the New Zealand region

The advent of radiocarbon dating generated new interest in New Zealand's record of Quaternary sea-level change (Kidson, 1982, offers an international perspective). Stevens (1956a,b, 1957), working in the Hutt Valley (Figure 2.2), obtained two radiocarbon ages from a fossil forest underlying an aggradational river terrace (the Melling) considered to be formed in response to higher sea levels at the end of the Holocene marine transgression (cf. Fleming, 1957). Stevens (1956a,b, 1957) suggested that the terrace, rising approximately +3 m (+10 feet) above PMSL, was built up to the elevation of the highest sea-level during the Holocene marine transgression. The radiocarbon ages, at $4{,}350 \pm 100$ and $4{,}275 \pm 100$ years BP (Table 2.1), led Stevens (1956a,b, 1957) to correlate the terrace with elevated shorelines and other evidence of mid-Holocene higher sea levels from the Pacific, North Africa, Australia, Europe and North America. While a fluvial aggradational response to base-level rise is certainly not unreasonable, it is unclear why Stevens (1956a,b, 1957) interpreted the Melling terrace as a surface formed directly by and at higher sea-level, as opposed to a simple aggradational river terrace.

Table 2.1: Summary of radiocarbon ages presented by previous investigations of Holocene palaeo sea-level change in the New Zealand region. Wood and peat CRAs calibrated using the the non-marine calibration curve for the Southern Hemisphere (SHCal04; McCormac et al. 2004). Shell CRAs calibrated using the marine model calibration curve Marine04 (Hughen et al., 2004) with a ΔR value of -7 ± 45 to correct for the marine reservoir effect (see Sections 3.2.2 and 7.2.4).

Source	Locality	Indicator	Radiocarbon laboratory code	Reported age (years BP)	Conventional radiocarbon age (14C years)	Sidereal age range (cal. yr BP)
Te Punga (1953b)	Rangitikei Valley	Wood	NZ5	3050±200	–[a]	–
Stevens (1956b, 1957)	Hutt Valley	Wood	NZ30	4350±100	4468±83	4850–5291
	Hutt Valley	Wood	NZ31	4275±100	4365±83	4585–5277
Te Punga (1958)	Foxton	Wood	NZ81	9900±150	9919±76	–[b]
Suggate (1958)	Christchurch	Wood	NZ118	9400±120	9439±72	10378–10789
	Christchurch	Shells	NZ120	6100±120	6096±69	6339–6724
Schofield (1960a)	Miranda	Shells	NZ272	3900±90	4274±48	4188–4582
Fleming (1965)	Paekakariki	Wood	NZ519	5140±90	5136±86	5641–5992
Cullen (1967a)	Paterson Inlet	Peat	NZ674	9300±80	9303±77	10239–10591
Herzer (1977, 1981)	Offshore, Canterbury Bight	Shells	NZ3898	15100±200	15440±101	18021–18668
Woodroffe et al. (1983)	Miranda	Shells	WK341	→	3980±60	3793–4226
	Miranda	Shells	Wk408	→	1590±50	996–1282
Hull (1985)	Whangaparoa	Wood	NZ6284	1985±70	1930±61	1690–1950
Carter et al. (1986)	Offshore, Canterbury Bight	Shells	NZ3897	11750±250	12098±219	13143–14008
	Offshore, Canterbury Bight	Shells	NZ4619	11800±250	12141±217	13185–14055

[a] No CRA recorded in Rafter Radiocarbon Laboratory database.
[b] CRA is just beyond the range suitable for dating. Sidereal age is approximately 11,000 cal. yr BP.

An investigation by Te Punga (1958) of a bore from onshore Foxton (Figure 2.2) received wide attention, and was incorporated into a number of sea-level histories (e.g., Godwin et al., 1958; Schofield, 1962, 1964; Jelgersma, 1966; Cullen, 1967a; Suggate, 1968; Norris, 1972). From a log recovered from −46 m below PMSL Te Punga (1958) obtained a radiocarbon age of $9{,}900 \pm 150$ years BP (Table 2.1, Figures 2.5 and 2.6), and tentatively inferred that the log was driftwood deposited at that time. Whether this assumption is correct is unclear. The log rests within a 21 m (70 feet) thick unit of clay and sand which Te Punga (1958) assumed was either estuarine or shallow marine sediments. However, if this is the case, it does not follow that the log was necessarily deposited at mean sea-level. Further, the clay and sand unit directly overlies a unit of fluvial gravels which can be reasonably assumed to be of LGM age (e.g., Fair, 1968; Litchfield, 2003; Clement and Fuller, 2007; Clement et al., 2010). Therefore, it is most likely that the clay and sand unit is either a fluvial or transgressive facies. Again, it does not necessarily hold that the log was deposited at mean sea-level. Te Punga (1958) acknowledged a lack of evidence to characterise the tectonic regime of the region, and tempered any conclusion of 46 m of sea-level rise through the Holocene. However, these limitations were not considered by many of the subsequent studies that incorporated Te Punga's (1958) observations.

South of Foxton, on the Otaki coast (Figure 2.2), Te Punga (1954c, 1962) studied a marine-cut cliff 3.6–21 m (12–70 feet) high, with a base +3–+14 m (+10–+45 feet) above PMSL. Te Punga (1953b) had previously observed dunes overlying a Rangitikei River terrace (Figure 2.2), and had obtained a radiocarbon date from wood within the terrace of $3{,}050 \pm 200$ years BP (Table 2.1). At Otaki, Te Punga (1954c, 1962) noted similar dunes had drifted across the marine-cut cliff, and therefore concluded that the lower age limit of the marine cutting was slightly older than 3,000 years BP. To constrain the upper age Te Punga (1954c, 1962) observed that the cliff truncated solifluction deposits supposed to have ceased forming c. 8,000 years BP (Cotton and Te Punga, 1955). However, this date is unreliable, as it was arrived at by assuming that the periglacial conditions under which the solifluction deposit formed were synchronous with the Late Wisconsin glacial episode (MIS 2) in North America. Te Punga (1954c, 1962) therefore concluded that the cliff was cut by sea levels +3 m (+10 feet) higher than present during the most recent post-glacial marine transgression. Hesp (1975) revisited the Otaki cliff, confirmed that the cliff was marine cut (later affirmed by Palmer et al., 1988 and Hawke and McConchie, 2005, 2006), and surveyed the modern beach and beach ridges. Hesp (1975) drilled the latter to determine the height of former storm ridges in order to ascertain if the height of the cliff-foot deposits was related to higher sea levels. Hesp (1975) noted that the oldest gravel beach at the base of the cliff, as well as all the subsequent gravel beach ridges, were lower than the present-day storm beach (see also Hesp and Shepherd, 1978). Hesp (1975) therefore concluded that there was no evidence for higher than present Holocene sea levels.

Building on the research by Te Punga (1962), Fleming (1965) studied a marine cliff at Paekakariki (Figure 2.2), considered to be an extension of the cliff at Otaki in the north. Fleming (1965) obtained a radiocarbon age of $5{,}140 \pm 90$ years BP (Table 2.1) from a sample of wood debris lying at mean high water level within beach deposits at the base of the cliff. Fleming (1965) concluded that post-glacial higher Holocene sea levels post-dated the beach deposit. However because of the coseismic vertical earth movements that characterised the area, no correlation between the age and elevation of the deposit was made.

2.5 Radiocarbon dating to establish sea-level chronologies in New Zealand

The first New Zealand study to utilise multiple radiocarbon dates to establish a chronology for late Quaternary sea-level change was completed by Suggate (1958), as part of an investigation of the stratigraphy of post-glacial deposits in the Christchurch metropolitan area (Figure 2.3). Suggate (1958) found that sea-level rose rapidly from -22 m (73 feet) below PMSL c. $9{,}400 \pm 120$ years BP to -3.6 m (10 feet) below PMSL c. $6{,}200 \pm 120$ years BP (Table 2.1). Present mean sea-level was inferred to have been reached c. 5,000 years BP, and was correlated by Suggate (1958) with the findings of Stevens (1956a,b, 1957). Suggate (1958) considered the implications of subsidence of the Christchurch area on the chronology within the context of Zeuner's (1954) Northern Hemisphere Pleistocene sea-level history.

A number of workers subsequently utilised Suggate's (1958) Christchurch data in prominent studies of global eustatic sea-level change (e.g., Godwin et al., 1958; Fairbridge, 1961; Schofield, 1964; Morner, 1971, 1976). Notably, Fairbridge (1961) significantly misinterpreted a number of Suggate's (1958) indicator points, incorrectly utilising several dated fluvial and alluvial deposits which do not mark a former sea-level. Fairbridge (1961) also misrepresented the elevation of a sample of wood which Suggate (1958) recovered from an estuarine sequence -1 m (-3 feet) below sea-level, using it to indicate a $+3$ m ($+10$ feet) sea-level. Suggate (1968) therefore expressed a lack of confidence in the accuracy of Fairbridge's (1961) sea-level curve.

Godwin et al. (1958) incorporated several of Suggate's (1958) dates into a dataset used to construct a global eustatic sea-level change history. In addition, Godwin et al. (1958) also included Te Punga's (1958) observation from Foxton, as well as indicators from Western Europe, the Persian Gulf, and the Gulf coast of the United States. Godwin et al. (1958) found that global sea-level had risen steadily at the rate of 1 m (3 feet) per century since 14,000 years BP, stabilising at the present level approximately 5,500 years BP. Importantly, in addition to the erroneous assumption of globally equable sea-level change and the error introduced from using such a spatially distributed composite dataset, Godwin et al. (1958) also seemingly ignored the concerns of both

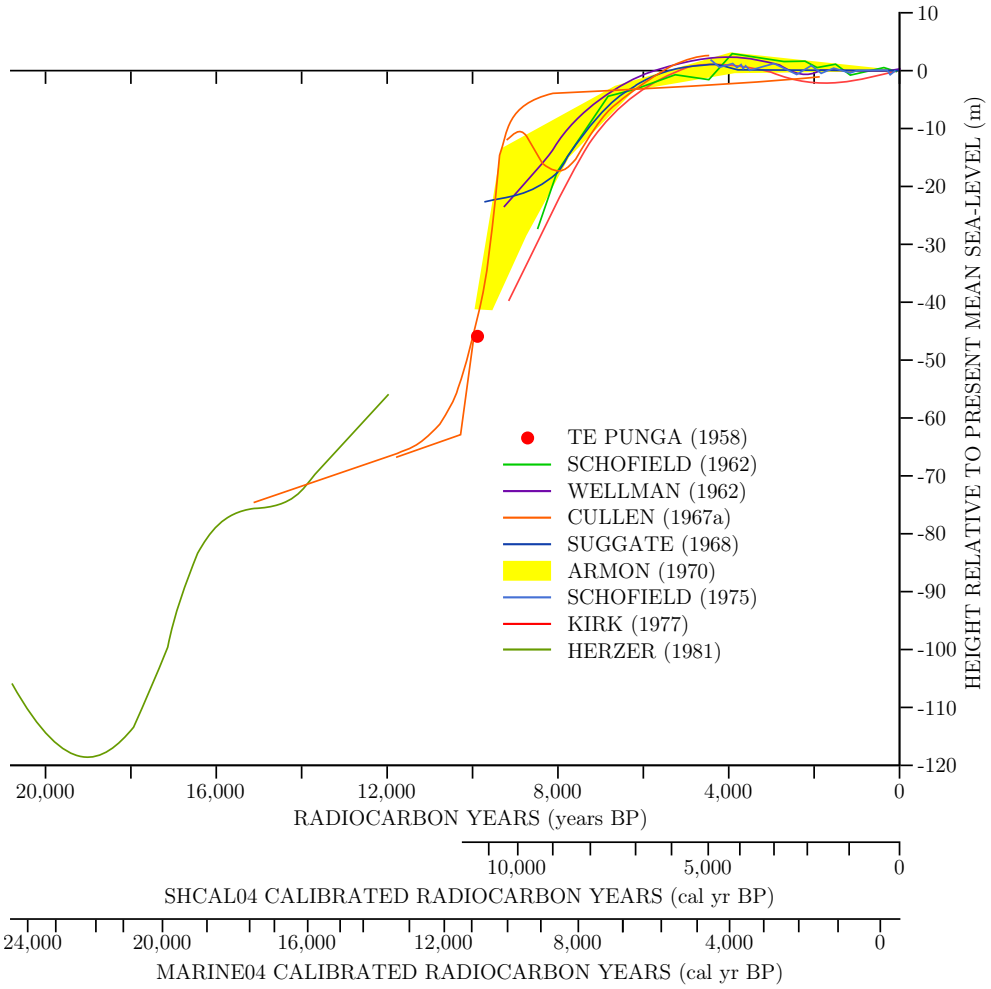

Figure 2.5: Summary of Holocene sea-level curves produced for the New Zealand region between 1958–1981 (not including Gibb, 1979: see Figures 2.7 and 2.8), covering the period 20,000 years BP to present. Greater detail of the period 10,000 years BP to present is shown in Figure 2.6.

Te Punga (1958) and Suggate (1958) about the effects of tectonic deformation on the observed elevations of their palaeo sea-level indicators.

Wellman (1962) subsequently employed the findings made by Godwin et al. (1958) to construct a New Zealand Holocene sea-level history, by supplementing the international dataset with observations of a large number of coastal sections around the North Island, correlated using tephra and pumice deposits. Following Godwin et al. (1958), Wellman (1962) described steadily rising sea levels through the early Holocene, with PMSL attained about 5,500 years BP. Using the Waimihia Tephra as a marker, Wellman (1962) concluded that sea-level reached a maximum of +3 m (+10 feet) above PMSL c. 3,900 years BP (cf. Waimahia Ash: $3{,}230 \pm 20$ 14C years, Lowe et al., 1999), dropping to just below PMSL coincident with the emplacement of the Taupo Pumice (1,850 14C

years: Froggatt and Lowe, 1990). By 1,500 years BP, when Wellman (1962) suggested the Loisels Pumice was emplaced (cf. Loisels Pumice: 610 ± 20 and/or 1250 ± 40 years BP, Lowe et al., 2000), sea-level had rebounded to present levels. Wellman (1962) suggested that sea-level remained static from then on, and projected future higher sea levels based on the (then unspecified) rate of modern sea-level rise. Given the composite nature of the dataset Wellman (1962) acknowledged that the sea-level history has a tectonic component that was otherwise unrecognised.

2.6 Time-depth curves of palaeo sea-level fluctuations in New Zealand

The first New Zealand study to construct a regional time-depth curve of Holocene sea-level changes was completed by Schofield (1960a), and was subsequently refined and re-presented thereafter (e.g., Schofield, 1960b, 1968, 1975). To construct this curve Schofield (1960a) surveyed and dated cheniers on the Miranda coastal plain (Figure 2.2), using the height of the cheniers as a proxy for sea-level. Schofield's (1960a) curve extends to $3{,}900 \pm 90$ years BP (Table 2.1), when sea level was inferred to have been c. +2.1 m (+7 feet) higher than present (Figures 2.5 and 2.6). This was based on a radiocarbon age from shells in the oldest Miranda chenier. Schofield (1960a) suggested that sea-level then went through five fluctuations between 3,900–1,000 years BP, ultimately descending to close to PMSL (Figures 2.5 and 2.6).

Woodroffe et al. (1983) also investigated the development of the Miranda cheniers. Woodroffe et al. (1983) concluded that sea-level lay only +0.7–+0.9 m above present c. $3{,}980 \pm 60$ 14C years, thereafter falling smoothly to reach PMSL by c. 1590 ± 50 14C years (Table 2.1). Woodroffe et al. (1983) noted that the shell layer which formed the cheniers was continuous, and suggested that the episodic creation of the shell ridges related not to sea-level fluctuations, but progradation of the coastal plain during gradually falling sea levels.

Schofield later extended the Miranda late Holocene sea-level history (1962; 1964; the latter paper is sometimes cited as Schofield and Thompson, 1964) by incorporating dates from the studies by Stevens (1956a), Suggate (1958), and Te Punga (1958) (Figures 2.5 and 2.6). However, despite the suggestions by both Suggate (1958) and Te Punga (1958), Schofield (1962, 1964) made no attempt to consider the effects of tectonic movement on the elevations of their samples. Following Fergusson and Rafter (1959), Schofield (1962, 1964) added 100 years to the ages of the shell samples taken from Suggate (1958), to account for the Seuss effect (the change in atmospheric carbon concentrations by the addition of large amounts of carbon dioxide derived from the burning of fossil fuels; e.g., Suess, 1955; Tans et al., 1979). It was not stated whether this age adjustment was undertaken on the shell samples included from Miranda. Schofield (1962, 1964) also incorporated 11 radiocarbon dated palaeo sea-level indicators from Christchurch presented by Grant-Taylor and Rafter (1962).

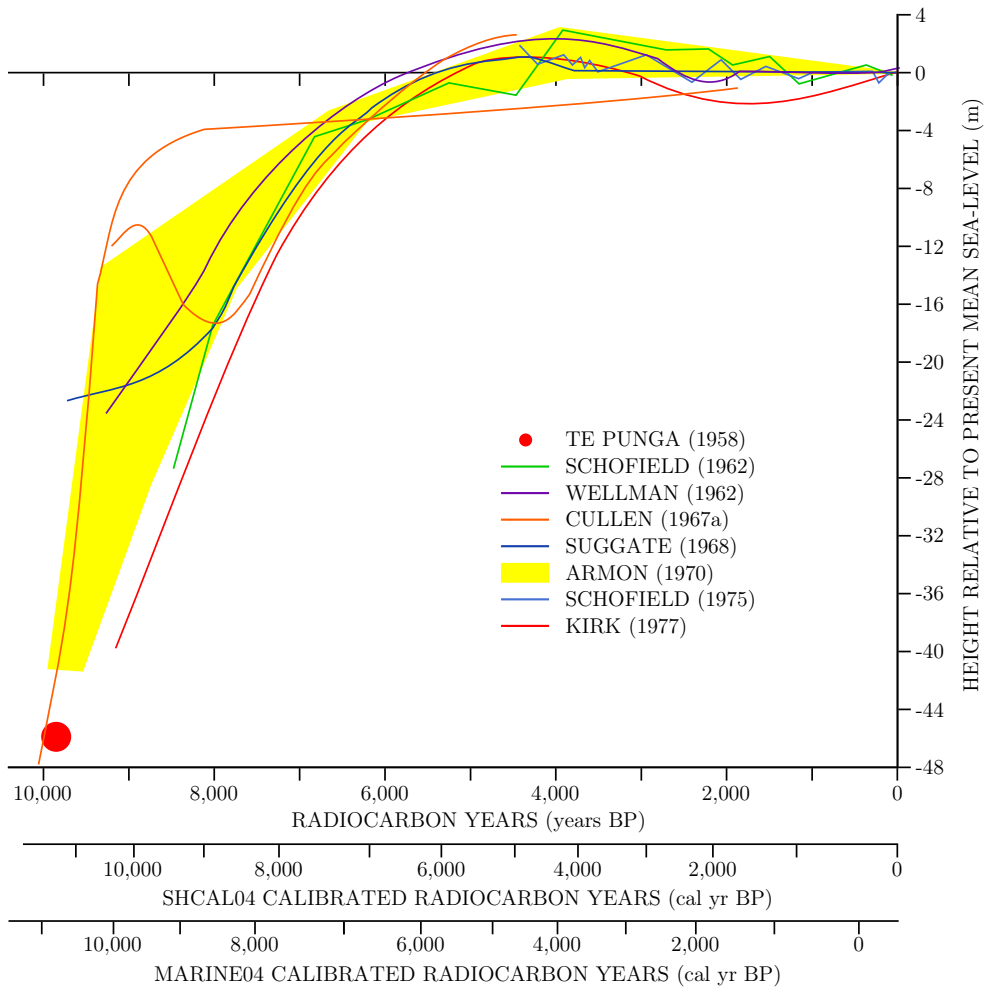

Figure 2.6: Summary of Holocene sea-level curves produced for the New Zealand region between 1958–1981 (not including Gibb, 1979: see Figures 2.7 and 2.8), covering the period 10,000 years BP to present. The curve presented by Herzer (1981) is not shown, as it falls outside the age and depth bounds of the figure.

These are dates originally collected by Suggate, and are presented in Suggate (1968). Three of these dates were from shells, the balance from samples of peat and wood. Of the peat and wood samples, only one peat sample is described as having a direct relationship to sea-level, being overlain by what is assumed to be estuarine mud. The remainder were related to fluvial aggradation deposits.

Schofield's (1962; 1964) extended sea-level record indicated that sea-level rose rapidly from −28 m below PMSL c. 9,500 years BP to −4 m below PMSL by 6,900 years BP (Figures 2.5 and 2.6). However, the sea-level at −28 m is based on a peat sample which Suggate (1968) later dismissed as unreliable (see discussion below). From −4 m Schofield (1962, 1964) suggested that the rate of sea-level rise slowed, reaching −1 m below PMSL by 5,200 years BP. Schofield (1962, 1964) indicated that sea-level then fell to approximately −2 m

below PMSL c. 4,500 years BP, followed by a rapid rise to PMSL c. 4,300 years BP. Sea levels reached a post-glacial peak of +2 m above present c. 4,000 years BP. From 4,000 years BP, Schofield (1962, 1964) suggested, following previous observations from Miranda (Schofield, 1960a,b), that sea-level fell in a series of fluctuations, reaching present mean sea-level approximately 1,000 years BP (Figures 2.5 and 2.6).

Later, in an effort to assess whether the palaeo sea-level history recorded at Miranda was local or regional, Schofield (1973) undertook a survey of beach ridges at Matauri Bay, Mangatawhiri Spit, Manly, and Cook's Beach (Figure 2.2). At all four locations Schofield (1973) recognised several beach ridges, and inferred that the highest ridge at each locality was the equivalent of the highest Miranda chenier dated at $3{,}900 \pm 90$ years BP (Table 2.1; Schofield, 1960a). Schofield (1973) concluded that apparent post-glacial sea-level changes had been consistent throughout the Auckland-Northland region, such that either epeirogenic movement, without tilting, had occurred, or that eustatic sea-level had risen to a post-glacial maximum of +2 m across the region. Having been satisfied with the regional applicability of the Miranda sea-level history, Schofield (1975) subsequently attempted a detailed assessment of the results of this sea-level fall. To this end, Schofield (1975) examined the post-glacial progradation and development of the South Kaipara barrier (Figure 2.2) within the context of the Miranda sea-level curve (Schofield, 1960a), and correlated five separate periods of progradation on the barrier with the five sea-level fluctuations detailed at Miranda (Figures 2.5 and 2.6).

Suggate (1968) reinvestigated evidence of sea-level change in the Christchurch area (Figure 2.3), and obtained an additional 21 dates to supplement the original 1958 dataset. Suggate (1968) debated evidence of the tectonic regime of the region, and concluded that long-term subsidence was more likely than short-term uplift (cf. Wellman, 1979; Gibb, 1986; Lambeck et al., 2002). However, for the purposes of constructing the sea-level curve, Suggate (1968) regarded the area as tectonically stable. Suggate's (1968) sea-level history (Figures 2.5 and 2.6) indicated that sea levels rose from −22 m below PMSL $9{,}400 \pm 120$ years BP (Table 2.1), to reach PMSL c. 5,000 years BP (a 'Shepard'-style curve, cf. Shepard, 1963, 1964). The sea-level index points were joined by fitting a simple curve, which Suggate (1968) regarded as improbably smooth. However, the position of the individual points was considered acceptable, with the exception of a 9,400 year BP peat sample from −22 m below PMSL, which was held to be unreliable. Suggate (1968) noted that the sand facies overlying the peat was only assumed to be marine or estuarine based on the inferred development of the coast, rather than from any intrinsic property of the sand. Further, because the stratigraphic log was poorly detailed, Suggate (1968) questioned whether the thickness of the peat indicated its accumulation over a considerable period of time prior to its inundation by rising sea levels.

Armon (1970) was the first to propose an envelope to constrain the Holocene sea-level history of the New Zealand region. The envelope (Figures 2.5

and 2.6) was constructed as a means of resolving the considerable differences between previously presented sea-level curves (Shepard, 1963; Schofield, 1964; Curray, 1965; Cullen, 1967a; Suggate, 1968), which Armon (1970) variously attributed to tectonic movements, misinterpreted sea-level indicators and poor age control due to sample contamination. Armon (1970) therefore delineated an envelope to constrain the spread of sea-level index points presented by Schofield (1964), Cullen (1967a, see discussion below), and Suggate (1968). Armon (1970) suggested that sea level had been within (above or below) 4.5 m (15 feet) of the present level for the past 7,000 years BP, although the envelope indicated that PMSL was attained at the earliest c. 5,000 years BP. Within the last 5,000 years BP Armon (1970) considered the variations in sea-level recorded by the envelope to be too great as to allow for reliable or useful determinations of palaeo sea-level. However, this caveat should be applied to Armon's (1970) envelope as a whole, comprised as it is from a composite of curves sourced from different regions of New Zealand.

2.7 Modelling and mathematical analyses of Holocene sea-level fluctuations in the New Zealand region

Through the 1970s and 1980s a number of sea-level curves were forwarded based on modeling and mathematical analyses of sea-level data. Chappell (1974), as part of a study of isostatic responses of the Earth through the Quaternary, presented a sea-level curve for the Australia-New Zealand region. The curve was constructed by averaging Suggate's (1968) record from Christchurch with a sea-level history produced by Thom and Chappell (1975) for the south-east coast of Australia. Notably, Chappell (1974) assumed that Christchurch was tectonically stable (cf. Wellman, 1979; Herzer, 1981; Gibb, 1986; Williams, 1991; Barnes, 1995; Lambeck et al., 2002). The curve presented by Chappell (1974) indicated that sea-level rose steadily from −22 m below PMSL c. 8,500 years BP, to reach −5 m below PMSL shortly before 7,000 years BP. From 7,000 years BP the rate of sea-level rise gradually slowed, reaching PMSL c. 5,900 cal. yr BP, and remaining stable from then on.

Kirk (1977) constructed a eustatic sea-level curve for New Zealand as part of a study investigating the effects of sea-level change and tectonic uplift on shore platform development on the Kaikoura Peninsula (Figure 2.3). Kirk (1977) derived the curve (Figures 2.5 and 2.6) by fitting polynomial regressions to 44 radiocarbon dated palaeo sea-level indicators recovered from the marginal marine environment throughout the New Zealand archipelago. None of the sea-level indicators used were documented or referenced. The sea-level history indicated that sea-level rose from −40 m below PMSL c. 9,200 years BP at a steady rate to reach −16 m below PMSL c. 8,500 years BP. Thereafter the rate of sea-level rise declined, with PMSL being attained c. 5,000 years BP. After 5,000 years BP, Kirk (1977) suggested that sea-level continued to

rise, reaching +1 m above PMSL c. 4,300 years BP. From this high sea-level fell to PMSL by c. 3,200 years BP, before a low of −2 m below PMSL was reached c. 1,700 years BP. Kirk (1977) then proposed that sea-level rose once again, reaching PMSL c. 100 years BP. Kirk (1977) stated satisfaction with the fit of the curve to the distribution of sea-level index points. However, Kirk (1977) acknowledged that it was a best-fit curve that did not take into account variables such as tectonics, as well as sampling and dating errors. Indeed, Kirk (1977) suggested that the pattern of changes presented for the past 5,000 years was most likely exaggerated, and that the curve was unlikely to precisely reflect the pattern of palaeo sea-level changes anywhere in the New Zealand region. As Pirazzoli (1991) concluded, composite curves such as that by Kirk (1977) cannot be viewed with any confidence, given that they are constituted from palaeo sea-level indicators from areas with differing tectonic regimes.

Clark and Lingle (1979) presented several late Quaternary sea-level histories for New Zealand based on modelled predictions of sea-level changes caused by the late-glacial retreat of the Antarctic ice sheets. Broadly, assuming a linear model of ice sheet shrinkage yielded a sea-level history that rose steadily from −28 m below PMSL c. 17,000 years BP, to reach PMSL shortly after 6,000 years BP. Sea levels were then slightly higher than present for the remainder of the Holocene. In contrast, when Clark and Lingle (1979) used exponential and fluctuating exponential models of ice sheet shrinkage, New Zealand sea levels were predicted to rise from c. −23 m below PMSL c. 17,000 years BP, to reach −2 m below PMSL c. 10,000 years BP. During this period of sea-level rise the latter model predicted two fluctuations from 15,000–10,000 years BP, while the former predicted a smoothly rising sea-level. From 10,000 years BP sea-level was modelled as rising gradually, with PMSL reached c. 200 years BP. Clark and Lingle (1979) also combined the predictions of the fluctuating exponential model of Antarctic ice melt with predicted sea-level changes based on a model of Northern Hemisphere ice disintegration, which was compared with the palaeo sea-level observations made by Schofield (1964). Under the combined influence of ice melt in both Antarctica and the Northern Hemisphere, Clark and Lingle (1979) modelled New Zealand sea levels rising steadily from −90 m below PMSL c. 14,000 years BP to c. −8 m below PMSL c. 7,000 years BP. The rate of sea-level rise then slowed, with PMSL being attained c. 5,000 years BP, rising to +1.5 m PMSL by c. 4,800 years BP. From this point, Clark and Lingle (1979) modelled sea levels dropping at a uniform rate to reach PMSL c. 1,000 years BP. The latter stages of this model, from 8,000 years onward, showed broad agreement with Schofield's (1964) observations and sea-level curve.

Peltier (1988) modified the model employed by Clark and Lingle (1979), in order to rectify discrepancies between the modelled predictions of late Quaternary sea-level change and actual palaeo sea-level observations from throughout the Southern Hemisphere. To achieve closer agreement between the actual and modelled observations, Peltier (1988) delayed and otherwise altered the timing

of Antarctic ice sheet melting, and altered the thickness of the Earth's lithosphere used by the model. For New Zealand, Peltier (1988) constructed plots of observed and predicted sea-level change for Kaipara Harbour, Wairau Valley, and Christchurch (Figures 2.2 and 2.3), providing constraints on the nature of the sea-level change in response to the deglaciation history. Peltier (1988) presumably sourced observations of Holocene sea-level change for Christchurch from one or other of the papers by Suggate (1958, 1968). The source of the observed palaeo sea-level data for the Kaipara Harbour and Wairau Valley is not stated. For all three sites the model developed by Peltier (1988) suggested that PMSL was attained sometime between 9,000–7,000 years BP. Peltier (1988) suggested that whatever the model conditions, this was followed by a period of higher than present sea levels ranging from <1 to 5 m above PMSL.

Nakada and Lambeck (1989) also examined New Zealand sea-level histories, seeking, like Peltier (1988), to constrain models of the melting history of Last Glacial ice sheets and the Earth's rheological responses. Nakada and Lambeck (1989) presented a range of sea-level curves for Christchurch and Auckland (Figures 2.2 and 2.3), and considered both to have been tectonically stable through the Holocene. Broadly, Christchurch was modelled as having experienced either lower than present sea levels leading up to the present day, or some degree of higher than present sea-level which gradually declined to the present level through the mid-Holocene. Modelled sea levels at Auckland followed either the latter pattern, or were modelled to reach the present level and thereafter remain stable.

2.8 Offshore investigations of palaeo sea-level fluctuations in the New Zealand archipelago

Cullen (1967a) presented one of earliest studies of evidence of late Quaternary sea-level change preserved offshore on New Zealand's continental shelf. Working in Foveaux Strait (Figure 2.3), Cullen (1967a) utilised earlier surveys of the Strait's geology and bathymetry (Cullen, 1964, 1967b) to identify a submerged shoreline −64 m below PMSL. Cullen (1967a) correlated the Foveaux submerged shoreline with a sea-level regression c. 11,000 years BP at the same depth on Curray's (1961, 1965) curve of late Quaternary sea-level fluctuations. Cullen (1967a) reinforced this conclusion by also correlating the Foveaux shoreline with submarine platforms at the same depth off the Australian coast (Fairbridge, 1950; Carrigy and Fairbridge, 1954), considered by Fairbridge (1961) to have been formed during the LGM (then Wurm-Wisconsin glacial stage). Cullen (1967a) also presumed time-depth agreement between the Foveaux shoreline and an 11,000 year BP radiocarbon dated sample of salt-marsh peat recovered by Emery et al. (1965) from 59 m water depth at Georges Bank in the North Atlantic. Carter et al. (1986) later obtained two radiocarbon ages of c. 12,000 years BP (Table 2.1) for a submarine shoreline at similar depth off the northeastern South Island (see discussion below), which they correlated with Cullen's (1967a) submerged shoreline. However,

this finding makes Cullen's (1967a) submerged shoreline correlations no less speculative.

In addition to observations of the Foveaux Strait submarine shoreline, Cullen (1967a) reported a radiocarbon age determination of a peat horizon recovered in a core taken in 11 m of water from Paterson Inlet on the periphery of the Strait (Figure 2.3). The peat yielded a radiocarbon age of 9300 ± 80 years BP (Table 2.1), and contained remnants of a sedge-like plant, leading Cullen (1967a) to assume that it represented a tidal marsh. 3 m of muddy-sand and marine muds overlaid the peat layer, which indicated to Cullen (1967a) that sedimentation since the inundation of the peat had been continuous. No periods of non-deposition or erosion that might indicate a stillstand or regression sequence were noted. Cullen (1967a) therefore suggested that sea-level had risen continuously at the rate of 1.5 m every 1,000 years between 9,000 years BP and the present. By further assuming continuous sea-level rise in the interval between the submergence of the Foveaux submarine shoreline and formation of the Paterson Inlet peat, Cullen (1967a) concluded that sea-level rose the intervening 50 m at an average rate of 30 m per 1,000 years. Cullen (1967a) did speculate that the initial rate of sea-level rise immediately after the submergence of the Foveaux shoreline may have been much higher, though this was within the context of observations made by Fairbridge (1961) from Northern Europe.

Cullen (1967a) combined the dates and depths of the peat and shoreline with selected sea-level indicators presented by Suggate (1958) and Te Punga (1958) in order to construct a New Zealand sea-level curve (Figures 2.5 and 2.6). However, Cullen (1967a) made no attempt to address the concerns by Suggate (1958) and Te Punga (1958) regarding tectonic uncertainties in their datasets, and offered no reason for only including three of the dates from Suggate's (1958) dataset. One of these dates, a peat sample from -22 m below PMSL that yielded a radiocarbon age of 9400 ± 120 years BP (Table 2.1), was later discounted by Suggate (1968) as unreliable (see discussion above). The remaining two dates were used by Cullen (1967a) to constrain the shape of the curve through the period after 9,000 years BP. Cullen (1967a) suggested that this period was marked either by a 4 m drop in sea-level c. 8,000 years BP, or by a dramatic decrease in the rate of sea-level rise after 9,200 years BP (Figures 2.5 and 2.6). However, both these propositions contradict the conclusion of steady sea-level rise following the inundation of the Paterson Inlet peat.

Following Cullen (1967a) there appeared a number of other studies of offshore evidence of late Quaternary sea-level change. McKnight (1968) recovered relict shell assemblages from offshore Cape Farewell (Figure 2.3) at a depth of -126 m below PMSL. Based on the contemporary environmental requirements of the nine mollusc species encountered (shallow coastal situations on sandy substrates), and the LGM coastline reconstructions of Te Punga (1953a) and Fleming (1962), McKnight (1968) tentatively inferred that the fossil shells indicated Last Glacial sea levels 100–120 m lower than present.

Norris (1972) obtained radiocarbon age determinations on a number of shell layers identified in cores collected on the western continental shelf between Cape Egmont (Figure 2.2) and Karamea (Figure 2.3). Norris (1972) attempted a correlation with the sea-level curve constructed by Curray (1965). However, Norris (1972) was only able to broadly conclude that the shell layers had been deposited on the continental shelf between −25 to −100 m below PMSL, during the late Pleistocene and Holocene marine transgression. Van der Linden and Norris (1974) reached much the same conclusions, determining that sea levels within the Karamea Bight (Figure 2.3) lay approximately 110 m lower than present between 16,000–17,000 years BP.

Herzer (1977, 1981), working on the Canterbury continental shelf (Figure 2.3), presented a sea-level curve for the New Zealand region covering the period 28,000–12,000 years BP (Figure 2.5). The sea-level curve was constructed using radiocarbon dated fossil molluscs recovered in sediment cores collected offshore from depths of 53–87 m,[1] and by comparing these dates to the sea-level histories of Curray (1965) and Shackleton and Opdyke (1973). The curve presented by Herzer (1977, 1981) indicated that sea-level fell from c. −86 m below PMSL c. 24,500 years BP, to a low of −120 m below PMSL c. 19,000 years BP (Figure 2.3). This region of the curve is clearly influenced by Curray (1965) and Shackleton and Opdyke (1973), as Herzer (1977, 1981) had no dates to support a sea-level minimum at this time. Following the −120 m minimum, Herzer (1977, 1981) suggested that sea levels rose rapidly, reaching −76 m below present c. 15,000 years BP, before the curve terminates at c. −55 m approximately 12,000 years BP. Herzer (1977, 1981) didn't extend the curve further, despite having dated a number of fossil molluscs to between 12,000–6,000 years BP, presumably due to the poor depth control offered by these younger samples, which have living depth ranges of 0–90 m (*Scalpomactra scalpellum*) and 0–120 m (*Tawera spissa*) below PMSL.

Carter et al. (1986) built upon a number of previous observations of offshore and onshore evidence of palaeo sea-level fluctuations (e.g., for New Zealand: Cullen, 1967a; Gibb, 1979, 1983; Herzer, 1981; Carter et al., 1982, 1985), to construct a sea-level envelope for New Zealand (Figures 2.7 and 2.8), and a regional curve for the southwest Pacific, encompassing both New Zealand and Australia. Carter et al. (1986) utilised high resolution seismic profiles and regional stratigraphic data to identify 10 submerged shorelines on the East Otago continental shelf (Figure 2.3). Fossil molluscs recovered from five shorelines (S1, S2, S3a, S5, S6) were radiocarbon dated to provide a chronology; the ages of the five undated shorelines (S3, S4, S4a, S7, S8) were inferred. Carter et al. (1986) suggested that the post-glacial marine transgression in the Australia-New Zealand region was episodic, comprising shoreline-forming stillstands interspersed with periods of rapid sea-level rise. The oldest shoreline (S8) at −118 m below PMSL was inferred to been formed during the LGM, c. 18,000 years BP. Carter et al. (1986) did not present in-

[1]The depth of one of Herzer's (1981) cores, H790, is misreported as 63 m, when it should read 53 m. This is corrected by Pocknall et al. (1989).

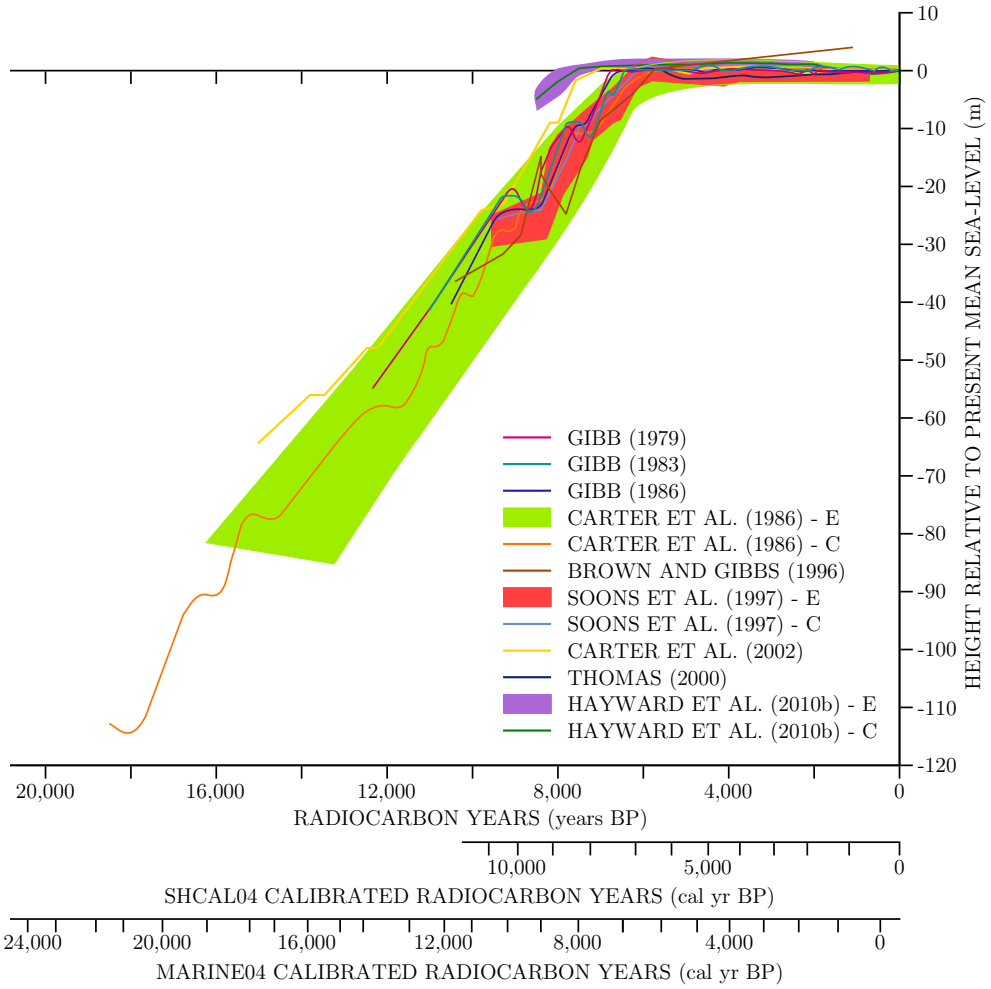

Figure 2.7: Summary of Holocene sea-level curves produced for the New Zealand region between 1979–2010 (not including Herzer, 1981: see Figure 2.5), covering the period 20,000 years BP to present. Greater detail of the period 10,000 years BP to present is shown in Figure 2.8. C = sea-level history as a curve; E = sea-level history as an envelope.

dependent age control for this low sea-level. Presumably this age was adopted from the sea-level curves of Milliman and Emery (1968) and Shackleton and Opdyke (1973), to which Carter et al. (1986) attributed the timing of the LGM sea-level lowstand.

By 17,000 years BP, Carter et al. (1986) suggested that sea-level rose to −88 m below PMSL, where another shoreline (S7) was formed. This was followed by another rise and a stillstand forming shoreline S6 at −75 m below PMSL, which Carter et al. (1986) correlated with a submerged spit-lagoon complex at similar depths off Banks Peninsula, described and dated by Herzer (1981) at 15,100 ± 200 years BP (Table 2.1). Radiocarbon age determinations on fossil *Zethalia zelandica* and *Austrovenus stutchburyi* of 11,750 ± 250 years

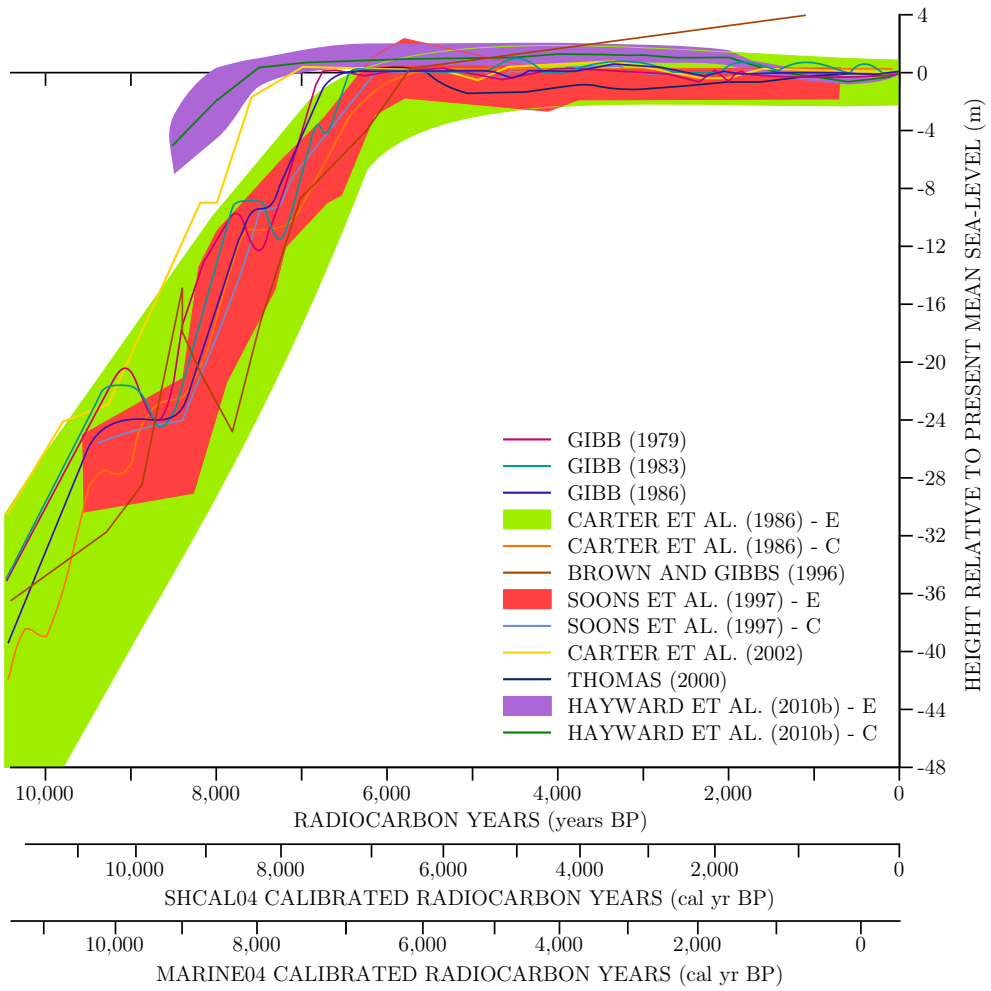

Figure 2.8: Summary of Holocene sea-level curves produced for the New Zealand region between 1979–2010 (not including Herzer, 1981: see Figure 2.5), covering the period 10,000 years BP to present. C = sea-level history as a curve; E = sea-level history as an envelope.

BP and 11,800 ± 250 years BP respectively (Table 2.1), provided age control for the timing of sea-level rise to and stabilisation at c. −56 m below PMSL (shoreline S5). However, Carter et al. (1986) admitted that adoption of this depth was arbitrary: the −56 m level represents a grouping of submerged shorelines lying at mid-shelf depths of −55 to −68 m below PMSL. Despite this considerable depth variation, the exact reasoning behind the adoption of the −56 m level is unclear, though Carter et al. (1986) did acknowledge that the true elevation of sea-level at this time may be significantly lower. Shoreline S4, lying −46 m below PMSL, was inferred to have been formed by a sea-level stillstand c. 11,000 years BP, based on its intermediate position between shorelines S5 and S3. Carter et al. (1986) also recognised shoreline

S4a at −39 m, which was correlated with features at similar depths on central Great Barrier Reef shelf, Queensland (Carter and Johnson, 1986).

By c. 9,000 years BP the curve presented by Carter et al. (1986) indicated that sea levels had risen to c. −28 to −24 m below PMSL, forming two shorelines, S3 and S3a, at those levels respectively. The age of the S3(a) shoreline was based on radiocarbon dates presented by Suggate (1968) and Gibb (1986) from onshore Christchurch, 400 km to the northeast (Figure 2.3). Importantly, Suggate's (1968) only radiocarbon age from this depth is of wood from a peat deposit, which was considered to be an unreliable indicator of palaeo sea-level (see discussion above). The radiocarbon dates reported by Gibb (1986), which corresponded to this age and depth, were also derived from wood and peat. From −24 m, Carter et al. (1986) suggested that sea-level rose to −9 m below PMSL, forming shoreline S2 during a stillstand c. 7,600 years BP. This shoreline was not identified by Carter et al. (1986), but was presumed to exist, following Gibb (1979, 1983, 1986) whose sea-level histories suggested a stillstand occurred at this level and time. Similarly, the timing of formation of the S1 shoreline, at PMSL c. 6,500 years BP, was presumably based on Gibb's (1979, 1983, 1986) timing of the attainment of PMSL, though this was unstated.

2.9 The de facto standard Holocene sea-level curve for New Zealand

Gibb variously refined and revised a sea-level curve for the New Zealand region, presenting three iterations (Gibb, 1979, 1983, 1986), of which the latter became the (de facto) benchmark or standard reconstruction of Holocene eustatic[2] sea-level change for New Zealand (Hesp et al., 1999; Kennedy, 2008). A key feature of the three curves is the method by which the effects of tectonism on the elevation of palaeo sea-level indicators was separated from eustatic effects, in order to isolate the eustatic component of each indicator's elevation from any post-emplacement tectonic deformation. To achieve this Gibb (1979, 1983, 1986) used the palaeo sea-level indicators from Blueskin Bay (Figure 2.3) and Weiti River Estuary[3] (Figure 2.2) as a 'zero datum', predicated on the assumption that sea-level had been stable about the present level over the past 6,500 years BP. The data from each of the other locations were fitted to this datum, allowing Gibb (1979, 1983, 1986) to estimate long-term (10^4 years) rates of tectonic deformation for each of the sites considered tectonically unstable. These rates were then used to correct the observed levels of the indicators for tectonic movement, yielding eustatic levels. This is a somewhat circular determination, as the assumption about stable sea-level is used to correct for tectonics, which in turn is used to reinforce the original assumption

[2]Eustatic in the sense of 'ice-equivalent' (cf. Lambeck and Chappell, 2001), rather than a measure of global sea levels

[3]Not used as a zero datum by Gibb (1979).

regarding sea-level. Essentially, the perceived accuracy of any of the curves presented by Gibb (1979, 1983, 1986) depends on whether the assumption of a stable sea-level at the present level since 6,500 years BP is reasonable. In addition, the accuracy of the curves is dependant upon the degree to which the tectonic-eustatic separation technique yields reasonable results.

Gibb's initial (1979) sea-level curve for the New Zealand region was plotted from 56 radiocarbon ages sourced from eleven localities: Kelly's Beach, Kaiaua, Miranda, the Heretangua Plains, Pauatahanui Inlet, Petone, Kaiwhata River mouth, and Oterei River mouth (Figure 2.2); and Christchurch, offshore in the Canterbury Bight, and Blueskin Bay Estuary (Figure 2.3). For this early curve Gibb (1979) took Blueskin Bay as the sole zero-datum, adjusting the remaining 10 locations to fit. The resulting sea-level history (Figures 2.7 and 2.8) indicated that sea-level rose from −135 m below PMSL c. 20,000 years BP, reaching −31 m below PMSL c. 10,300 years BP. There were no sea-level index points covering the intervening period. Gibb (1979) suggested that sea levels then rose to c. −21 m below PMSL by c. 8,700 years BP, before undergoing a regression to −24 m below PMSL c. 8,500 years BP. The curve indicates that sea-level then rose swiftly, reaching c −9.5 m below PMSL by 7,500 years BP, before experiencing another regression falling to −13 m below PMSL by c. 7,300 years BP (Figures 2.7 and 2.8). Sea-level then rose to attain the present level 6,500 years BP. Gibb (1979) suggested that sea-level then remained largely static for the remainder of the Holocene. From 5,000–4,500 years BP Gibb (1979) indicated that sea-level dropped slowly to c. −1 m below PMSL, rising back to the present level by 4,000 years BP. Between 2,500–2,000 years BP it was suggested that sea-level made some minor negative fluctuations to c. −1 m below present. Sea-level was inferred to drop to c. −0.5 m below PMSL c. 1,700 years BP, gradually rising back to the present level by c. 100 years BP (Figures 2.7 and 2.8).

For Gibb's intermediate (1983) revision, 64 dates from eight localities were used to reconstruct New Zealand's palaeo sea-level record. Gibb (1983) omitted samples from the Oterei River mouth, Heretangua Plains, the Canterbury Bight and Petone that had been used to construct the 1979 curve, and introduced new samples from Weiti River Estuary (Figure 2.2). No reason for the omissions is given. The indicator points from Weiti River estuary were used in conjunction with the samples from Blueskin Bay Estuary to separate tectonic and eustatic effects at the other locations. Having set aside the sample from offshore in the Canterbury Bight which indicated a sea-level of −135 m below present c. 20,000 years BP, the sea-level curve presented by Gibb (1983) indicated that sea-level rose from c. −41 m below PMSL c. 10,800 years BP, reaching −22 m below PMSL c. 9,100 years BP (Figures 2.7 and 2.8). The early part of this rise is only assumed, as the earliest index point indicates a sea-level of only −29 m below PMSL c. 9,700 years BP. Upon reaching the −22 m level, Gibb (1983) suggested that sea levels stabilised for a period of 400–500 years. Again, this was an unsupported assumption, as Gibb (1983) only had a single radiocarbon dated indicator at this level. The details of

this indicator are not presented, so the suitability of this indicator for this assumption is unclear. From the −22 m stillstand sea-level fell to −25 m below PMSL c. 8,600 years BP, before it rose to −9 m below PMSL by 7,800 years BP. It was inferred that sea-level stabilised at this level for 400–500 years, this time with the support of multiple (unspecified) radiocarbon ages. Gibb (1983) suggested that sea-level then regressed once again, falling to −11.5 m below PMSL by c. 7,300 years BP, before rising again to reach −4 m below PMSL c. 6,800 years BP. Another regression of c. −1 m is identified, before PMSL is finally attained c. 6,500 years BP (Figures 2.7 and 2.8). As in the 1979 curve, Gibb (1983) suggested that once PMSL was reached, sea levels oscillated about this level by no more than several decimetres. A sea-level high of +0.7 m above PMSL c. 4,600 years BP was identified, with smaller peaks suggested at 3,400 years BP, 2,000 years BP, 1,400 years BP and 600 years BP. Possible minor negative oscillations in sea-level were recognised at 5,100 years BP, 4,200 years BP, 2,500 years BP, 1,600 years BP, and 800 years BP (Figures 2.7 and 2.8).

Gibb's final (1986) revision of New Zealand's Holocene eustatic sea-level history utilised 82 radiocarbon dated palaeo sea-level indicators from eight sites. Kumenga in the Wairarapa (Figure 2.2) was introduced at the expense of the Kaiwhata River mouth. Again, no specific explanation was offered for the omission of the Kaiwhata River mouth. As in the 1983 revision, Gibb (1986) adopted Blueskin Bay Estuary and Weiti River mouth as zero-datums to separate tectonic and eustatic effects at the remaining six sites. The curve presented by Gibb (1986) indicated that sea levels rose from −40 m below PMSL c. 10,500 years BP, though as in the 1983 revision this is clearly only assumed, as the earliest, lowest point in the palaeo sea-level dataset indicates a sea-level of c. −32 m about 9,800 years BP (Figures 2.7 and 2.8). Above this point Gibb (1986) recognised a sea-level stillstand at −24 m below PMSL (cf. the S3a shoreline of Carter et al., 1986), lasting from c. 9,300 to c. 8,500 years BP. Following this stillstand sea-level rose steadily, reaching −9 m below PMSL c. 7,500 years BP, where sea levels stabilised for c. 200 years (cf. the S2 shoreline of Carter et al., 1986). Gibb (1986) inferred that sea-level then rose to PMSL, which was attained c. 6,500 years BP. Sea-level remained here until c. 5,000 years BP, when a minor regression of c. −0.4 m took place, lasting until c. 4,500 years BP. This was immediately followed by a small rise to +0.6–+0.9 m above PMSL from 4,500–3,500 years BP. Following this, Gibb (1986) suggested that sea-level fell back to the present level by c. 2,000 years BP, where it stabilised for the remainder of the Holocene (Figures 2.7 and 2.8).

Where Gibb's 1983 revision showed three stillstands followed by sea-level regressions through the early part of the Holocene, prior to 6,500 years BP, the 1986 iteration shows no regressions and only two stillstands. Gibb (1986) offered no explanation for these changes, which makes it difficult to accept the 1986 sea-level interpretation over the 1983 record, particularly when the vast majority of the index points are relatively unchanged between each history. As

an example, in the 1983 interpretation Gibb suggested that a short stillstand occurred at −22 m below PMSL from c. 9,300–8,900 years BP, followed by a regression to −25 m below PMSL by c. 8,700 years BP. In contrast, in the 1986 interpretation the sea-level index points in this region of the record remain in the same relative positions, yet Gibb inexplicably extended the length of the suggested stillstand, eliminating the regression, and seemingly ignoring those index points which had previously served as indicators of a drop in sea-level. As Pirazzoli (1991) noted, the unstated changes between the two iterations leaves the impression that the range of effective vertical uncertainty may be larger than Gibb (1986) infers. This has important implications, given the practice by some workers of reproducing Gibb's (1986) sea-level curve as a single line, without error bars or an envelope (e.g., Thomas, 1998, 2000; Heap, 1995; Ota et al., 1995; Heap and Nichol, 1997; Carter et al., 2002).

2.10 Post-Gibb sea-level histories

Hull (1985) reviewed radiocarbon ages from throughout New Zealand that indicated some degree of Holocene eustatic sea-level fluctuation within the context of the sea-level history presented by Gibb (1986). Hull (1985) suggested that the culmination of the most recent post-glacial marine transgression, at PMSL c. 6,500 years BP (Gibb, 1986), was followed by a lowering of eustatic sea-level, with a subsequent peak in sea-level from c. 4,500 years BP until c. 2,000 years BP. However, Holocene uplift at many of the sites reviewed prevented Hull (1985) from making a determination of the magnitude of the sea-level changes. Hull's (1985) interpretation of sea-level movements was based on stratigraphic sections at Whangaparoa (Figure 2.2) and Lake McKerrow (Figure 2.3) which showed changes from fluvial/brackish conditions to estuarine to terrestrial/fluvial conditions within the last 4,500 years BP. Also considered was a section from Tolaga Bay (Figure 2.2), which showed a transition from estuarine to beach to terrestrial facies from 4,500 years BP, though Hull (1985) conceded that the transition there may have been due to tectonic uplift. In addition, Hull (1985) considered selected dates presented by Schofield (1960a) and Woodroffe et al. (1983) from Miranda (Figure 2.2), and identified Stevens' (1956a) dates from the Hutt Valley as indirect evidence supporting a higher mid-Holocene sea-level. Notably, a single piece of wood within a sequence of estuarine muds at Whangaparoa provided the only basis for Hull's (1985) suggestion that mid-Holocene higher sea levels persisted until c. 1985 ± 70 years BP (Table 2.1). Further, the environmental transition at Lake McKerrow, in the South Island, appears to begin c. 4,100 years BP, at least 400 years later than at any of the North Island locations presented, suggesting a degree of age uncertainty for the inferred sea-level fluctuations much greater than Hull (1985) otherwise implied. Hull (1985) observed that the inferred eustatic sea-level rise c. 4,500 years BP coincided with a period of glacial expansion in the South Island (Burrows, 1979), and concluded that minor climatic changes were probably not responsible for regional sea-level

fluctuations. Ultimately, Hull (1985) suggested that the inferred eustatic sea-level fluctuations may be linked to the isostatic response of the New Zealand landmass to volumetric changes of the ocean caused by inputs of meltwater from the Antarctic and Northern Hemisphere ice sheets.

Brown and Gibbs (1996) presented a sea-level curve for the Heretaunga Plains (Figure 2.2) constructed using radiocarbon dated wood and shell samples recovered from a groundwater bore (Figures 2.7 and 2.8). The majority of the indicator points used to construct the curve (8 out of eleven) came from samples of fossil wood, while only three of the dated palaeo sea-level indicators were fossil shells. At least one of these shell assemblages was suggested to indicate a palaeo water depth of 5–10 m. The degree to which the wood samples were suggested to accurately represent palaeo sea-level is unclear. Brown and Gibbs (1996) suggested that both subsidence and sediment compaction may have affected the recovered elevations of the palaeo sea-level indicators. However, no attempt was made to account for the effects of either. No age or height errors were acknowledged; the curve was presented as a single line. The implied accuracy of the sea-level history is therefore misleading as the nature of the source data precludes such an accurate reconstruction.

Soons et al. (1997) constructed a relative sea-level envelope and curve for Canterbury (Figures 2.7 and 2.8) utilising Gibb's (1986) dated sea-level indicators from Christchurch, together with dates compiled by Shulmeister and Kirk (1993, 1997) from northern Pegasus Bay (Figure 2.3). While Gibb (1979, 1983, 1986) considered the Christchurch area to have undergone long-term uniform subsidence (cf. Wellman, 1979; Herzer, 1981; Williams, 1991; Barnes, 1995; Lambeck et al., 2002), Soons et al. (1997) regarded the Canterbury coast as tectonically stable, as Gibb's (1986) dates were presented without tectonic correction. As a result of this, and the use of only a subset of Gibb's index points, Gibb's (1986) New Zealand sea-level record, as reproduced by Soons et al. (1997), shows significant deviations from the original (Figures 2.7 and 2.8). In fact, the reproduction should be seen as a local-scale interpretation of Gibb's (1986) sea-level history, within the context of the index points utilised by Soons et al. (1997). The major differences between the sea-level histories presented by Soons et al. (1997) and Gibb (1986) show in the last 7,000 years; prior to 7,500 years BP both reconstructions are in reasonably close agreement (Figures 2.7 and 2.8). Where Gibb (1986) inferred that PMSL for the New Zealand region was attained c. 6,500 years BP, Soons et al. (1997) suggested that on the Canterbury coast this occurred as late as 6,000 years BP. Soons et al. (1997) further proposed that at the post-glacial peak c. 5,800 years BP, sea levels on the Canterbury coast were potentially as much as 1.5 m higher than those in the New Zealand region as a whole. For the past 4,000 years BP, Soons et al. (1997) suggested that sea levels lay between +0.2 m and −2 m about PMSL, on average c. 1 m lower than proposed by Gibb (1986). However, this difference may be accounted for by the latter's use of tectonic correction.

Thomas (1998, 2000) made assessments of local-scale sea-level fluctuations at East Otago and Weiti River Estuary (the tectonically stable 'zero datum' sites of Gibb, 1979, 1983, 1986), in direct comparison to the New Zealand regional sea-level record presented by Gibb (1986). Notably, Thomas (1998, 2000) presented both the regional and local-scale sea-level histories as single lines, seemingly ignoring the inherent errors. For East Otago (Figure 2.3), Thomas (1998, 2000) constructed a sea-level curve (Figures 2.7 and 2.8) using data from Ensor (1986) (from Blueskin Bay; Figure 2.3) and Rayns (1985) (from Hoopers and Papanui Inlets; Figure 2.3).[4] This curve suggested that sea levels in the East Otago area followed Gibb's (1986) New Zealand regional determination prior to 5,600 years BP. From 5,500 years BP Thomas (1998, 2000) inferred that sea levels fell from PMSL to c. −1.5 m below PMSL, remaining here until c. 3,700 years BP. From this low it was suggested that sea-level rose steadily, reaching PMSL c. 500 years BP. For the reconstruction of sea-level change at Weiti River estuary (Figure 2.2) Thomas (1998, 2000) considered radiocarbon dated sea-level indicators recovered by Heap and Nichol (1997). Thomas (1998, 2000) inexplicably included a radiocarbon date from a mangrove root presented by Heap and Nichol (1997), without apparent regard for the root's relationship to the other index points or its context. Heap and Nichol (1997) clearly state that the root is considered rafted material. As a result, Thomas (1998, 2000) concluded that sea levels at Weiti River estuary dropped from PMSL c. 8,000 years BP (this being the age and elevation of the dated mangrove root), to c. −5.2 m below PMSL by c. 7,700 years BP. It is from here Thomas (1998, 2000) suggested that the final rise to PMSL. Thomas (1998, 2000) therefore erroneously concluded, given this apparent pattern of sea-level regression and transgression from 8,000–6,500 years BP, that Weiti River Estuary should be reevaluated as a reference locality for eustatic sea-level determinations.

Carter et al. (2002) combined the sea-level curves presented by Gibb (1986) and Carter et al. (1986), into a single sea-level history for the New Zealand region (Figures 2.7 and 2.8). While no recalculation or calibration of the radiocarbon ages used in the earlier studies is stated, Carter et al. (2002) have, without explanation, "aged" parts of the curves by up to 1500 years. As a result, the newer combined history indicates that PMSL was first attained c. 7,000 years BP (cf. S1 stillstand of 6,500 years BP, Carter et al., 1986; Gibb, 1986). Similarly, the S4 and S5 stillstands originally dated by Carter et al. (1986) to c. 11,000 years BP and c. 12,000 years BP, respectively, are shown by Carter et al. (2002) to occur at approximately 12,500 years BP and 13,600 years BP. In addition, no height or age errors are acknowledged; the history is presented as a single line. The implied accuracy of the sea-level history is therefore misleading.

[4]Thomas (1998, 2000) also presented dates from Blueskin Bay attributed to Witman (1974). These dates were not given by Witman (1974), and are in fact dates first presented by Gibb (1986).

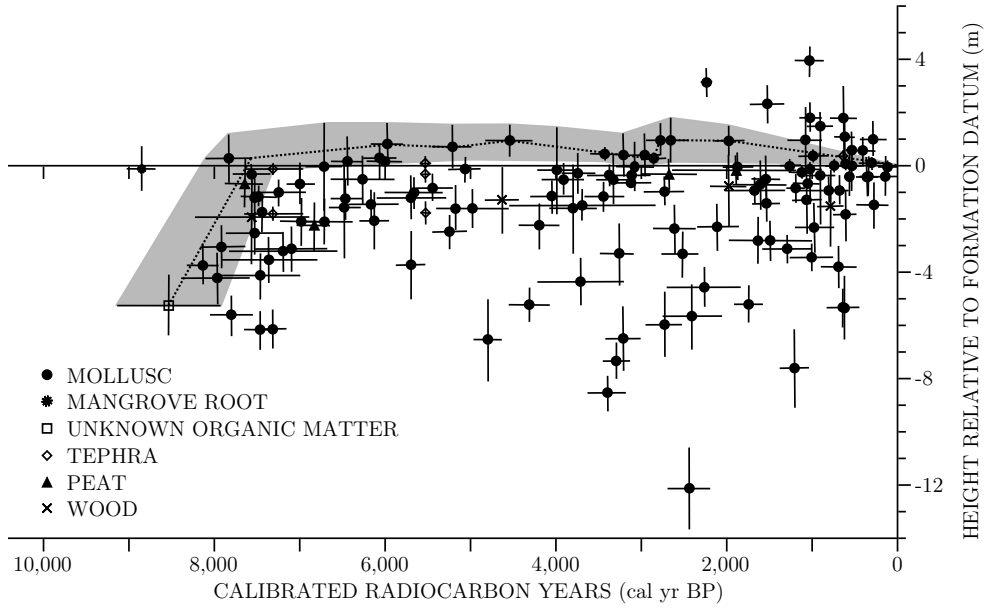

Figure 2.9: Holocene sea-level history for the New Zealand region presented by Clement et al. (2008a,b, 2010).

Wilson et al. (2007) presented an interpretation of Gibb's (1986) Holocene sea-level curve for New Zealand, constructed by calibrating the original dataset to sidereal years. Unfortunately, as the ΔR value used to correct for the marine reservoir effect was not reported, the calibrated history is of limited usefulness for comparisons with other records. In addition, it is unclear whether Wilson et al. (2007) utilised the dates as originally reported by Gibb (1986), many of which are not conventional radiocarbon ages (cf. Stuiver and Polach, 1977). The calibration is therefore inaccurate, although the degree of inaccuracy is unclear. As the elevations and vertical errors of the samples remained unchanged, the overall trend of the calibrated sea-level history is largely coincident with Gibb's (1986) original record. Otherwise, Wilson et al. (2007) suggested that PMSL in the New Zealand region was attained c. 7,100 cal. yr BP, remaining within c. 1 m above or below present levels since that time.

Gehrels et al. (2008) used foraminiferal analyses on salt marsh cores to construct a proxy sea-level history for Pounawea (Figure 2.3) covering the past 500 years. This record showed sea-level c. -0.38 m below PMSL at AD 1500, rising at the rate of 0.3 ± 0.3 mm yr^{-1} to reach c. -0.28 m below PMSL by AD 1900. For the 20th Century Gehrels et al. (2008) estimated that the rate of sea-level rise increased to 2.8 ± 0.5 mm yr^{-1}, with PMSL being attained c. AD 1950.

Clement et al. (2008a,b, 2010) presented a sea-level history for the New Zealand region constructed using sea-level indicators compiled from a number of published and unpublished reports, papers and theses (Figure 2.9). Clement et al. (2008a,b, 2010) attempted to calibrate the dated indicators to sidereal

years; however, many of the radiocarbon ages used were not conventional radiocarbon ages. As with the curve by Wilson et al. (2007), the calibrated ages presented are inaccurate. Clement et al. (2008a,b, 2010) suggested that PMSL was attained c. 7,550 cal. yr BP, with sea levels rising to +0.8 m above PMSL by 5,800 cal. yr BP. The record indicated that sea levels then fluctuated by ±0.2 m until c. 4,500 cal. yr BP, when a peak of c. 1 m above PMSL was reached. From 4,500–3,000 cal. yr BP sea-level fell to c. +0.2 m above present levels. This was followed by a rapid rise from 3,000–2,700 cal. yr BP where sea-level rose again to +1 m above present. Sea-level remained stable at this level until c. 2,000 cal. yr BP, when it fell to PMSL (Figure 2.9).

Hayward et al. (2010a,b,c) produced a generalised, composite Holocene sea-level envelope and curve for New Zealand (Figures 2.7 and 2.8), based on the findings of Clement et al. (2008a,b), as well as observations by Schofield (1960a), Hayward et al. (2007), Hicks and Nichol (2007), and Gehrels et al. (2008). Hayward et al. (2010a,b,c) suggested that PMSL was attained c. 7,500 years BP, rising slowly to a peak of c. +1 m above PMSL by 4,000 years BP. From this high, Hayward et al. (2010a,b,c) inferred that sea-level fluctuated slightly about PMSL until c. 2,000 years BP, when sea-level began to fall. Sea levels fell to c. −0.4 m below PMSL c. 500 years BP, before rising back to PMSL by the present day.

2.11 Conclusions

By reviewing the entire body of work relating to palaeo sea-level histories for the New Zealand region it becomes clear that even sea-level reconstructions made very recently have provenance to research conducted over 60 years ago (Figure 2.1). This is not in and of itself a problem; however, the errors and/or limitations of earlier studies have often been ignored or overlooked. The problems with these earlier studies are therefore not widely recognised or understood. This is typified by the large number of studies which represent sea-level fluctuations as single lines, with no age or height errors (Figures 2.5, 2.6, 2.7, and 2.8). The product is a series of fragmented sea-level histories that are ultimately unreliable records of Holocene sea-level fluctuations. There is therefore a clear need to re-evaluate the data presented by these older sea-level curves, to understand the weaknesses and limitations of this data, and to produce a new, refined reconstruction of Holocene sea-level changes in the New Zealand region.

Clement et al. (2009a,b, 2010) have suggested that the wide geographic range from which regional studies have drawn and integrated proxy sea-level indicators (e.g., Carter et al., 1986, 2002; Gibb, 1986; Wilson et al., 2007; Clement et al., 2008a,b, 2010; Hayward et al., 2010a,b,c) did not take into account local-scale sea-level histories (e.g., Soons et al., 1997; Thomas, 1998, 2000; Gehrels et al., 2008). This echoes the findings by Gage (1953) and Fleming (1953a). Regional sea-level datasets may therefore hide or mask local trends in sea-level fluctuations while blending together an unrealistic picture

of regional sea-level movements. Therefore, moving forward, it is necessary to produce local-scale sea-level histories for regions within the New Zealand archipelago, from sea-level index points which have been fully assessed for errors and limitations.

Chapter 3

Local-scale reconstructions of Holocene sea-level change in the New Zealand archipelago

3.1 Introduction

The benchmark research into the Holocene sea-level history of New Zealand presented by Gibb (1979, 1983, 1986) indicated that present mean sea-level (PMSL) was attained c. 6700 cal. yr BP, thereafter remaining largely static (Clement et al., 2008a,b, 2009a,b). While this record has become the 'de facto standard Holocene sea-level curve' for New Zealand (Hesp et al., 1999; Kennedy, 2008), the wide geographic range from which Gibb (1979, 1983, 1986) drew and integrated proxy sea-level indicators did not take into account local-scale sea-level histories. This is a problem shared with other, more recent palaeo sea-level reconstructions (e.g., Carter et al., 2002; Wilson et al., 2007; Clement et al., 2008a,b, 2010). All these Holocene sea-level curves may therefore mask or hide local trends in sea-level fluctuations within the New Zealand region.

Recent research has focused on Holocene depositional environments within the context of Gibb's (1986) curve (e.g., Heap and Nichol, 1997; Abrahim, 2005; Abrahim et al., 2008). However, there has been no effort to utilise this data to refine regional Holocene sea-level histories. As Chapter 2 concluded, there is therefore a clear need to re-evaluate the data presented by previous Holocene sea-level reconstructions, to understand its weaknesses and limitations, and to produce a new, refined reconstruction of Holocene sea-level changes in the New Zealand region. Moving forward, such a reconstruction must focus on local-scale sea-level histories for regions within the New Zealand archipelago, constructed using sea-level index points which have been fully assessed for errors and limitations. This chapter does just that, by reviewing published and unpublished Holocene palaeo sea-level indicators from through-

out the New Zealand region in order to construct detailed, local-scale Holocene sea-level histories for the New Zealand archipelago.

3.2 Local-scale sea-level curve construction methodology

3.2.1 Selection of palaeo sea-level indicators

A total of 215 radiocarbon dated palaeo sea-level indicators were compiled from 38 published and unpublished papers, reports and theses (Table 3.1). The locations of sites from which sea-level indicators were recovered are shown on Figures 3.1 and 3.2. Selected indicators were restricted to studies which presented both an accurate description of the facies association and related dated material to an established vertical datum. Only fossil mollusc species with well constrained ecological ranges were utilised. Palaeo sea-level indicators from the east coast of the North Island were not included, as this region has been subject to considerable tectonic movements during the Holocene. It is therefore difficult to isolate an ice-equivalent sea-level signal (cf. Lambeck and Chappell, 2001) from palaeo sea-level indicators along this coast. Table 3.1 is therefore not a comprehensive list of all radiocarbon dated palaeo sea-level indicators recovered in the New Zealand region. Compilation of such a list in the context of this thesis was viewed as prohibitively time consuming.

3.2.2 Treatment of radiocarbon ages

Many of the selected palaeo sea-level indicators were fossil shells radiocarbon dated by Rafter Radiocarbon Laboratory using a 'modern standard New Zealand marine shell' for the age calculations, rather than NBS oxalic acid as the modern standard (C. Prior, personal communication). As a result, these ages, as originally reported, were not conventional radiocarbon ages (CRA; cf. Stuiver and Polach, 1977). Where this was the case these ages have been recalculated as conventional radiocarbon ages by Rafter Radiocarbon Laboratory. Both the originally reported radiocarbon age and the recalculated CRA are presented (Table 3.1).

Conventional radiocarbon ages were calibrated to sidereal years (expressed as cal. yr BP) using the radiocarbon calibration program CALIB REV 5.0.1 (Stuiver and Braziunas, 1993; Stuiver and Reimer, 1993). Palaeo sea-level indicators with CRAs outside the range suitable for calibration to sidereal years have been omitted from the dataset. Calibration of fossil molluscs utilised the marine model calibration curve Marine04 Hughen et al. (2004) with a ΔR value of -7 ± 45 to correct for the marine reservoir effect (Table 3.2; Clement et al., 2010). This is a weighted mean value for the New Zealand region based on Rafter et al. (1972), McFadgen and Manning (1990), Higham and Hogg (1995), and Kalish (1993). For wood, peat and other materials that derive their carbon from terrestrial sources the non-marine calibration curve

Table 3.1: Details of 215 palaeo sea-level indicators from locations throughout the New Zealand region.

Source	Locality	Indicator	Radiocarbon laboratory code	Environment / Facies	Elevation	L (m)	D (m)	B (m)	Tectonic correction	V (m)	Inferred eustatic sea-level (m)	Vertical error (m)	Reported age (years BP)	Conventional radiocarbon age (14C years)	Sidereal age range (cal yr BP)
Northland / Auckland															
Osborne et al. (1991)	Matai Bay	Mixed shells	NZ7658	Loisels Pumice	0·40[h]	0·20	1·05	0·02	–	–	0·40	1·07	762±74	725±90	138–529
	Tokerau Beach	*P. subtriangulata*	NZ7613	Shell bank	1·65[h]	0·20	0·90	0·02	–	–	1·65	0·92	1441±34	1441±42	879–1159
	Tokerau Beach	*A. stutchburyi*	NZ7560	Shell bank	1·83[h]	0·20	0·53	0·02	–	–	1·83	0·56	1360±45	1373±50	760–1078
	Tokerau Beach	*P. subtriangulata*	NZ7649	Loisels Pumice	3·80[h]	0·20	0·90	0·02	–	–	3·80	0·92	1449±52	1450±69	826–1206
	Tokerau Beach	*P. subtriangulata*	NZ7648	Loisels Pumice	3·00[h]	0·20	0·90	0·02	–	–	3·00	0·92	2383±54	2186±74	1562–1990
Osborne (1983)	Bream Bay	Mixed shells	GX3840	Estuary/open beach	−2·50	0·20	1·30	0·02	–	–	−2·50	1·32	→	1440±110	753–1248
	Bream Bay	Mixed shells	GX4005	Estuary/open beach	−2·20	0·20	1·30	0·02	–	–	−2·20	1·32	→	1735±120	1006–1566
	Bream Bay	Mixed shells	GX3701	Estuary/open beach	0·00	0·20	1·30	0·02	–	–	0·00	1·32	→	2080±150	1311–2022
	Bream Bay	Mixed shells	NZ6376	Estuary/open beach	−0·50	0·20	1·30	0·02	–	–	−0·50	1·32	5750±140	3779±64	3523–3947
	Bream Bay	Mixed shells	NZ6377	Low energy estuary	1·00	0·20	1·30	0·02	–	–	1·00	1·32	2330±50	2663±35	2184–2572
Millener (1981)	Tokerau Beach	Shell	NZ4614	Beach ridge	0·80	0·20	1·05	0·15	–	–	0·80	1·08	2970±50	3311±37	2993–3329
	Tokerau Beach	*Paphies spp.*	NZ4726	Shell bank	0·85	0·20	0·90	0·30	–	–	0·85	0·97	636±43	973±40	489–658
	Tokerau Beach	*Paphies spp.*	NZ4727	Shell bank	0·45	0·20	0·90	0·30	–	–	0·45	0·97	897±44	1233±28	678–899
	Tokerau Beach	Mixed shells	NZ5063	Shell bank	−0·10	0·20	1·05	0·20	–	–	−0·10	1·09	3170±80	3510±66	3212–3603
	Tokerau Beach	Shell	NZ5064	Beach ridge	−0·10	0·20	1·05	0·20	–	–	−0·10	1·09	2920±50	3257±36	2918–3266
	Tokerau Beach	Shell	NZ4610	Beach ridge	0·80	0·20	1·05	0·15	–	–	0·80	1·08	4360±60	4692±40	4801–5136
Brook (1999)	Tokerau Beach	Shell	NZ7291	Prograding beach face	0·90[i]	0·20	1·05	0·20	–	–	0·90	1·09	1030±60	1366±68	730–1102
Hutcheon (2006)	Tapora Flats	Valve	WK17480	Sub-tidal	−2·26	0·20	1·65	0·02	–	–	−2·26	1·66	→	2449±93	1858–2335
Horrocks et al. (2000a)	Northern Kaitoke	*M. ovata*	WK5557	Tidal flat	−5·63	0·20	0·45	0·02	–	–	−5·63	0·49	→	6800±70	7163–7472
Horrocks et al. (2000b)	Southern Kaitoke	*M. liliana*	WK7381	Tidal flat	−1·57	0·20	0·90	0·10	–	–	−1·57	0·93	→	4710±150	4553–5389
	Southern Kaitoke	*A. stutchburyi*	WK6397	Tidal flat	−5·67	0·20	0·45	0·08	–	–	−5·67	0·50	→	6960±100	7264–7654
Hicks and Nichol (2007)	Kowhai Beach	Peaty sand	WK17125	Tidal wetland	−0·63[h]	0·20	0·90	0·02	–	–	−0·63	0·92	→	6860±134	7101–7642
Horrocks et al. (1999)	Awana	Peat	WK5561	Estuarine salt marsh	−2·22	0·20	0·90	0·02	–	–	−2·22	0·92	→	6050±80	6639–7027
Hume and McGlone (1986)	Waitamata Harbour	*A. stutchburyi*	WK251	Tidal flat	−1·28[h]	0·20	0·75	0·14	–	–	−1·28	0·79	→	5730±60	5954–6292
Heap and Nichol (1997)	Weiti River Estuary	*A. stutchburyi*[a]	WK3810	Transgressive open bay	−1·95	0·20	0·55	0·02	–	–	−1·95	0·59	→	7020±170	7192–7861
	Weiti River Estuary	*A. marina* roots	WK3811	Vegetated tidal point-bar	−0·55	0·20	0·48	0·02	–	–	−0·55	0·52	→	8050±50	8692–9009
	Weiti River Estuary	*M. lilianna*[a]	WK3812	Transgressive open bay	−2·45	0·20	1·10	0·02	–	–	−2·45	1·12	→	7440±120	7649–8170
	Weiti River Estuary	*A. stutchburyi*[a]	WK3814	Transgressive open bay	−3·15	0·20	0·55	0·02	–	–	−3·15	0·59	→	7660±80	7948–8323
	Weiti River Estuary	Organic matter	WK3815	Fluvial terrace	−4·65	0·20	1·10	0·02	–	–	−4·65	1·12	→	7700±270	7932–9135
Abrahim et al. (2008)	Tamaki Estuary	*A. stutchburyi*	WK6372	Shallow, subtidal marine	−3·44[i]	0·20	0·71	0·02	–	–	−3·44	0·74	→	7490±200	7575–8359
	Tamaki Estuary	*A. stutchburyi*	WK7826	Shallow, subtidal marine	0·23[i]	0·20	0·71	0·02	–	–	0·23	0·74	→	5830±160	5893–6622
	Tamaki Estuary	*A. stutchburyi*	WK7827	Channel fill	0·02[i]	0·20	0·71	0·02	–	–	0·02	0·74	→	2030±130	1304–1912
	Tamaki Estuary	*A. stutchburyi*	WK7943	Shallow, subtidal marine	0·41[i]	0·20	0·71	0·02	–	–	0·41	0·74	→	7350±130	7564–8103
	Tamaki Estuary	*A. stutchburyi*	WK9557	Shallow, subtidal marine	−1·35[i]	0·20	0·71	0·02	–	–	−1·35	0·74	→	6494±114	6707–7266
	Tamaki Estuary	Tuhua Tephra	–	Shallow, subtidal marine	−1·04[i]	0·20	1·42	0·05	–	–	−1·04	1·43	→	→	6970–7650
	Tamaki Estuary	Tuhua Tephra	–	Shallow, subtidal marine	0·63[i]	0·20	1·42	0·02	–	–	0·63	1·43	→	→	6970–7650
Mather (2004)	Christian Bay	*A. stutchburyi*	WK15130	Back-barrier	−0·13	0·20	0·53	0·02	–	–	−0·13	0·56	→	6477±41	6826–7152
Johnston (1984)	Mahurangi Estuary	*A. stutchburyi*	WK350	Estuarine shell bed	1·05[j]	0·20	0·75	0·02	–	–	1·05	0·78	→	5640±80	5869–6262
	Mahurangi Estuary	*A. stutchburyi*	WK401	Tidal flat	−0·95[j]	0·20	0·75	0·02	–	–	−0·95	0·78	→	6940±40	7335–7562
Wratt (1999)	Puhoi River Estuary	*A. stutchburyi*	WK7570	Tidal flat	−0·60	0·20	0·55	0·02	–	–	−0·60	0·59	→	7020±70	7378–7667
	Puhoi River Estuary	*A. stutchburyi*	WK7571	Tidal channel	−0·61	0·20	0·55	0·02	–	–	−0·61	0·59	→	5300±170	5291–6088
Swales et al. (1997)	Mahurangi Estuary	Shell	–[d]	Tidal flat	−2·43	0·20	1·50	0·02	–	–	−2·43	1·51	→	6735±302	6557–7827
	Mahurangi Estuary	Shell	–[d]	Tidal flat	−2·03	0·20	1·50	0·02	–	–	−2·03	1·51	→	1904±217	1000–1979
	Mahurangi Estuary	Shell	–[d]	Tidal flat	−3·76	0·20	1·50	0·02	–	–	−3·76	1·51	→	2549±168	1833–2690
	Mahurangi Estuary	Shell	–[d]	Tidal flat	−3·02	0·20	1·50	0·02	–	–	−3·02	1·51	→	1085±110	488–892
	Mahurangi Estuary	Shell	–[d]	Tidal flat	−4·56	0·20	1·50	0·02	–	–	−4·56	1·51	→	1031±100	448–823
	Mahurangi Estuary	Shell	–[d]	Tidal flat	−4·83	0·20	1·50	0·02	–	–	−4·83	1·51	→	7323±122	7549–8049
Richardson (1985)	Ru Point	Wood	NZ3871	Estuary	−0·68	0·50	1·65	0·15	–	–	−0·68	1·73	7050±90	6179±88	6787–7247
Nichol et al. (2009)	Tauhara	*A. stutchburyi*[a]	WK9631	Tidal flat	0·16[h]	0·20	0·83	0·02	–	–	0·16	0·85	→	3956±114	3631–4310
Schofield (1973)	Mangatawhiri Spit	Mixed shells	NZ833	Intertidal or shallow estuary	2·23[k]	0·20	1·25	0·02	–	–	2·23	1·27	6460±60	6768±60	7154–7429
	Matauri Bay	Mixed shells	NZ731	Beach ridge	0·90	0·20	1·05	0·02	–	–	0·90	1·07	1990±63	2297±70	1710–2126
Grant-Taylor and Rafter (1971)	Okahu Bay	Shell	NZ441	Estuary	1·20	0·20	1·42	0·02	–	–	1·20	1·43	4205±67	4581±50	4583–4971
	Okahu Bay	Wood	NZ494	Estuary	0·00	0·20	1·42	0·02	–	–	0·00	1·43	4485±85	4476±76	4856–5289
Goff et al. (2010)	Kaituna Bay	*A. stutchburyi*	WK19433	Estuary	−0·26	0·20	0·48	0·02	–	–	−0·26	0·52	→	6570±36	6947–7235
Gibb (1986)	Weiti River Estuary	Shell	NZ6519	Chenier	−0·46	0·24[t]	–	–	–	–	−0·46	0·24	395±34	732±32	280–478
	Weiti River Estuary	Shell	NZ6462	Beach ridge	−0·23	0·22[t]	–	–	–	–	−0·23	0·22	365±30	701±28	263–461

Continued over page

Table 3.1: (continued)

Source	Locality	Indicator	Radiocarbon laboratory code	Environment / Facies	Elevation	L (m)	D (m)	B (m)	Tectonic correction	V (m)	Inferred eustatic sea-level (m)	Vertical error (m)	Reported age (years BP)	Conventional radiocarbon age (14C years)	Sidereal age range (cal yr BP)
	Weiti River Estuary	Shell	NZ1965	Chenier	0·00	0·24[t]	–	–	–	–	0·00	0·24	470±50	791±40	302–516
	Weiti River Estuary	Shell	NZ1962	Chenier	0·12	0·23[t]	–	–	–	–	0·12	0·23	670±50	984±41	493–663
	Weiti River Estuary	Shell	NZ6509	Beach ridge	0·03	0·23[t]	–	–	–	–	0·03	0·23	1150±30	1486±27	924–1167
	Weiti River Estuary	Shell	NZ1966	Chenier	0·11	0·22[t]	–	–	–	–	0·11	0·22	1020±50	1341±42	748–1034
	Weiti River Estuary	Shell	NZ1770	Chenier	0·39	0·22[t]	–	–	–	–	0·39	0·22	1420±60	1703±61	1079–1411
	Weiti River Estuary	Shell	NZ6487	Chenier	−0·08	0·24[t]	–	–	–	–	−0·08	0·24	1445±35	1783±29	1243–1474
	Weiti River Estuary	Shell	NZ6493	Chenier	−0·21	0·23[t]	–	–	–	–	−0·21	0·23	1570±50	1907±42	1314–1608
	Weiti River Estuary	Shell	NZ1971	Chenier	0·31	0·22[t]	–	–	–	–	0·31	0·22	3050±50	3371±47	3056–3397
	Weiti River Estuary	Shell	NZ6479	Chenier	0·47	0·24[t]	–	–	–	–	0·47	0·24	3530±50	3866±38	3664–4014
	Weiti River Estuary	Shell	NZ6475	Tidal flat	0·42	0·80[t]	–	–	–	–	0·42	0·80	3140±50	3482±31	3234–3516
	Weiti River Estuary	Shell	NZ6488	Tidal flat	0·42	0·80[t]	–	–	–	–	0·42	0·80	3360±50	3701±37	3469–3802
	Weiti River Estuary	Shell	NZ1970	Tidal flat	−0·14	1·61[t]	–	–	–	–	−0·14	1·61	3970±60	4282±50	4206–4609
	Weiti River Estuary	Shell	NZ6510	Tidal flat	0·77	0·80[t]	–	–	–	–	0·77	0·80	4900±60	5241±41	5466–5740
	Weiti River Estuary	Shell	NZ6461	Tidal flat	0·83	0·80[t]	–	–	–	–	0·83	0·80	5560±50	5896±34	6202–6438
	Weiti River Estuary	Shell	NZ1968	Tidal flat	−0·01	1·63[t]	–	–	–	–	−0·01	1·63	6260±70	6597±59	6935–7283
	Kelly's Beach	*A. stutchburyi*	NZ4423	Beach ridge	0·46	0·24[t]	–	–	–	–	0·46	0·24	2170±60	2502±44	2005–2318
	Kelly's Beach	*A. stutchburyi*	NZ4424	Beach ridge	−0·28	0·24[t]	–	–	–	–	−0·28	0·24	2300±50	2640±45	2140–2540
	Kelly's Beach	*A. stutchburyi*	NZ4425	Beach	0·05	0·24[t]	–	–	–	–	0·05	0·24	4550±60	4888±52	4993–5418
Coromandel / Firth of Thames															
Gibb and Aburn (1986)	Pauanui Beach	Shell	NZ6500	Beach	−0·93	0·20	0·90	0·02	−0·25[v]	0·04	−1·41	0·92	1960±40	2295±35	1776–2080
	Pauanui Beach	Shell	NZ6501	Nearshore	−4·63	0·20	0·90	0·02	−0·25[v]	0·04	−5·17	0·92	2150±50	2491±35	2004–2305
	Pauanui Beach	Shell	NZ6502	Nearshore	−6·43	0·20	0·90	0·02	−0·25[v]	0·04	−7·35	0·92	3410±40	3747±27	3545–3836
	Pauanui Beach	Shell	NZ6514	Nearshore	−7·63	0·20	0·90	0·02	−0·25[v]	0·05	−8·58	0·92	3500±80	3837±65	3584–4020
	Pauanui Beach	Shell	NZ6467	Beach	−0·12	0·20	0·90	0·02	−0·25[v]	0·05	−1·25	0·92	4010±70	4344±53	4286–4718
	Pauanui Beach	Shell	NZ6521	Nearshore	−4·12	0·20	0·90	0·02	−0·25[v]	0·05	−5·24	0·92	4220±70	4321±50	4254–4679
	Pauanui Beach	Shell	NZ6522	Beach	−1·22	0·20	0·90	0·02	−0·25[v]	0·03	−2·62	0·92	4920±50	5258±30	5488–5746
Hume and Dahm (1991)	Coromandel Harbour	Shell	WK1466	Tidal flat	−0·26[l]	0·20	1·15	0·02	−0·25[v]	0·04	−0·53	1·17	1330±60	1505±60	916–1232
	Coromandel Harbour	Shell	WK1376	Tidal flat	−0·37[l]	0·20	1·15	0·02	−0·25[v]	0·07	−1·66	1·17	4680±80	4869±80	4912–5432
	Coromandel Harbour	Shell	WK1377	Tidal flat	−0·49[l]	0·20	1·15	0·02	−0·25[v]	0·08	−2·17	1·17	6090±130	6239±130	6379–7043
	Coromandel Harbour	Shell	WK1467	Tidal flat	−3·39[l]	0·20	1·15	0·02	−0·25[v]	0·13	−4·32	1·17	3510±190	3732±190	3207–4212
	Coromandel Harbour	Shell	WK1468	Tidal flat	−1·30[l]	0·20	1·15	0·02	−0·25[v]	0·04	−1·37	1·17	320±50	632±50	106–445
	Coromandel Harbour	Shell	WK1378	Tidal flat	−1·56[l]	0·20	1·15	0·02	−0·25[v]	0·03	−1·71	1·17	720±60	1020±60	494–718
	Coromandel Harbour	Shell	WK1379	Tidal flat	−1·94[l]	0·20	1·15	0·02	−0·25[v]	0·06	−2·18	1·17	1120±100	1409±100	732–1205
	Coromandel Harbour	Shell	WK1380	Tidal flat	−2·27[l]	0·20	1·15	0·02	−0·25[v]	0·05	−2·68	1·17	1790±70	2060±70	1434–1846
	Coromandel Harbour	Shell	WK1381	Tidal flat	−2·59[l]	0·20	1·15	0·02	−0·25[v]	0·05	−3·22	1·17	2540±80	2789±80	2320–2733
	Firth of Thames	Shell	WK1469	Tidal flat	−3·28[m]	0·20	1·35	0·02	–	0·50	−3·28	1·45	3170±60	3401±60	3066–3450
	Firth of Thames	Shell	WK1470	Tidal flat	−7·57[m]	0·20	1·35	0·02	–	–	−7·57	1·36	1380±60	1661±60	1051–1363
	Firth of Thames	Shell	WK1471	Tidal flat	−5·31[m]	0·20	1·35	0·02	–	–	−5·31	1·36	730±60	1030±60	498–726
	Firth of Thames	Shell	WK1382	Tidal flat	−5·60[m]	0·20	1·35	0·02	–	0·50	−5·60	1·45	2440±130	2692±130	2073–2738
	Firth of Thames	*A. stutchburyi*	WK1383	Tidal flat	−5·26[m]	0·20	0·68	0·02	–	0·50	−5·26	0·86	2720±60	2964±60	2526–2931
	Firth of Thames	Shell	WK1384	Tidal flat	−6·45[m]	0·20	1·35	0·02	–	0·50	−6·45	1·45	3130±60	3362±60	3011–3405
	Whangapoua Estuary	Shell	WK1235	Tidal flat	0·00[n]	0·85	0·85	0·02	−0·25[v]	0·05	−1·62	1·20	5890±70	6045±70	6291–6657
	Whangapoua Estuary	Shell	WK1237	Tidal flat	0·00[n]	0·85	0·85	0·02	−0·25[v]	0·04	−0·22	1·20	1060±65	1351±65	720–1074
Naish (1990)	Firth of Thames	*A. stutchburyi*	WK1280	Estuary	−11·43[o]	0·50	0·68	0·02	–	1·00	−11·43	1·31	→	2700±80	2191–2690
	Firth of Thames	Wood	WK1283	Estuary	−0·73[o]	0·50	1·35	0·02	–	–	−0·73	1·44	→	2080±90	1776–2180
	Firth of Thames	Wood	WK1284	Estuary	−1·50[o]	0·50	1·35	0·02	–	–	−1·50	1·44	→	870±115	626–938
	Firth of Thames	*A. stutchburyi*	WK1285	Estuary	−3·03[o]	0·50	0·68	0·02	–	0·50	−3·03	0·98	→	5290±54	5527–5859
	Firth of Thames	*A. stutchburyi*	WK1448	Estuary	−5·83[o]	0·50	0·68	0·02	–	1·00	−5·83	1·31	→	4590±28	4642–4956
	Firth of Thames	*A. stutchburyi*	WK1664	Estuary	1·68[o]	0·50	0·68	0·02	–	–	1·68	0·84	→	1500±90	863–1274
	Firth of Thames	*A. stutchburyi*	WK1665	Estuary	2·48[o]	0·50	0·68	0·02	–	–	2·48	0·84	→	1060±70	502–778
Hutcheon (2006)	Mirada	Valve	WK17479	Beach face	0·38	0·20	1·35	0·02	–	–	0·38	1·36	→	4786±51	4869–5265
Gibb (1986)	Kaiaua	Shell	NZ4427	Beach ridge	−0·28	0·24[t]	–	–	–	–	−0·28	0·24	450±50	784±40	299–511
	Kaiaua	Shell	NZ4426	Beach ridge	−0·17	0·24[t]	–	–	–	–	−0·17	0·24	1130±50	1464±42	900–1168
	Kaiaua	Shell	NZ4428	Beach ridge	0·59	0·24[t]	–	–	–	–	0·59	0·24	1840±50	2179±43	1612–1931
	Kaiaua	Shell	NZ4429	Beach ridge	−0·15	0·24[t]	–	–	–	–	−0·15	0·24	2210±50	2549±44	2044–2353
	Kaiaua	Shell	NZ4430	Beach ridge	0·33	0·24[t]	–	–	–	–	0·33	0·24	3070±60	3406±52	3093–3445
	Kaiaua	Shell	NZ4431	Beach ridge	0·83	0·24[t]	–	–	–	–	0·83	0·24	3450±60	3786±48	3558–3912

Continued over page

Table 3.1: (continued)

Source	Locality	Indicator	Radiocarbon laboratory code	Environment / Facies	Elevation	L (m)	D (m)	B (m)	Tectonic correction	V (m)	Inferred eustatic sea-level (m)	Vertical error (m)	Reported age (years BP)	Conventional radiocarbon age (14C years)	Sidereal age range (cal yr BP)
	Kaiaua	Shell	NZ4432	Beach ridge	0·61	0·24[t]	–	–	–	–	0·61	0·24	3660±50	3998±38	3844–4191
	Miranda	Shell	WK408	Tidal flat	0·09	0·70[t]	–	–	–	–	0·09	0·70	→	1260±50	674–933
	Miranda	Shell	WK341	Tidal flat	0·85	0·70[t]	–	–	–	–	0·85	0·70	→	3650±60	3376–3766
	Miranda	Shell	WK357	Tidal flat	−0·30	0·70[t]	–	–	–	–	−0·30	0·70	→	4510±70	4471–4902
	Miranda	Shell	NZ265	Chenier	−0·03	0·24[t]	–	–	–	–	−0·03	0·24	980±60	1341±41	749–1033
	Miranda	Shell	NZ267	Chenier	0·00	0·24[t]	–	–	–	–	0·00	0·24	1540±60	1909±42	1316–1610
	Miranda	Shell	NZ268	Chenier	0·49	0·24[t]	–	–	–	–	0·49	0·24	1960±70	2352±43	1826–2141
	Miranda	Shell	NZ270	Chenier	1·22	0·24[t]	–	–	–	–	1·22	0·24	2730±70	3104±45	2742–3065
	Miranda	Shell	NZ272	Chenier	2·16	0·24[t]	–	–	–	–	2·16	0·24	3900±90	4274±48	4188–4582
South / Southwest North Island															
Swales et al. (2005)	Karehana Bay	*A. stutchburyi*	NZ7379	Tidal flat	0·63[p]	0·10	0·33	0·20	0·20[v]	0·05	0·01	0·40	2950±70	3290±78	2889–3355
	Pauatahanui Inlet	*A. stutchburyi*	NZ7381	Tidal flat	0·18	0·20	0·33	0·04	–	–	0·18	0·39	6650±95	6985±106	7267–7683
	Pauatahanui Inlet	*A. stutchburyi*	NZ7383	Tidal flat	0·99[q]	0·20	0·33	0·04	–	–	0·99	0·39	6720±95	7058±107	7341–7779
	Pauatahanui Inlet	Shell[b]	NZ7387	Tidal flat	0·15	0·15	0·66	0·30	–	–	0·15	0·74	5079±90	5079±90	5208–5661
	Pauatahanui Inlet	Shell[b]	NZ7393	Tidal flat	0·60	0·20	0·66	0·04	–	–	0·60	0·69	3258±78	3285±78	2884–3350
	Pauatahanui Inlet	Shell[b]	NZ7421	Tidal flat	0·60	0·20	0·66	0·04	–	–	0·60	0·69	3487±88	3487±88	3128–3628
AJH Clement et al. (unpublished)	Manawatu valley	*A. stutchburyi*	WK22171	Tidal flat	−1·58[r]	0·05	0·55	0·04	–	–	−1·58	0·55	→	7605±105	7853–8320
	Manawatu valley	*A. stutchburyi*	WK22172	Tidal flat	−2·99[r]	0·05	0·55	0·04	–	–	−2·99	0·55	→	7850±140	7986–8634
	Manawatu valley	*A. stutchburyi*	WK22173	Tidal flat	0·70[r]	0·05	0·55	0·04	–	–	0·70	0·55	→	6335±125	6501–7144
	Manawatu valley	*A. stutchburyi*[a]	WK26357	Tidal flat	−1·46[r]	0·05	0·55	0·04	–	–	−1·46	0·55	→	5588±30	5883–6153
	Manawatu valley	*A. stutchburyi*[a]	WK26360	Tidal flat	−0·87[r]	0·05	0·55	0·04	–	–	−0·87	0·55	→	6260±30	6588–6874
	Manawatu valley	*A. stutchburyi*[c]	WK26359	Tidal flat	−0·93[r]	0·05	0·55	0·04	–	–	−0·93	0·55	→	6365±30	6699–6988
	Manawatu valley	*A. stutchburyi*[a]	WK26361	Tidal flat	−1·17[r]	0·05	0·55	0·04	–	–	−1·17	0·55	→	6733±30	7160–7388
	Manawatu valley	*A. stutchburyi*[a]	WK26364	Tidal flat	−3·27[r]	0·05	0·55	0·04	–	–	−3·27	0·55	→	5661±30	5927–6202
	Manawatu valley	*A. stutchburyi*[c]	WK26358	Tidal flat	−3·55[r]	0·05	0·55	0·04	–	–	−3·55	0·55	→	5343±30	5594–5857
	Manawatu valley	*A. stutchburyi*[a]	WK26362	Tidal flat	−2·26[r]	0·05	0·55	0·04	–	–	−2·26	0·55	→	5920±30	6237–6468
	Manawatu valley	*A. stutchburyi*[a]	WK26363	Tidal flat	−3·13[r]	0·05	0·55	0·04	–	–	−3·13	0·55	→	5320±30	5581–5840
	Manawatu valley	*A. stutchburyi*[a]	WK28289	Tidal flat	−2·29[r]	0·05	0·55	0·04	–	–	−2·29	0·55	→	5717±30	5989–6262
	Manawatu valley	*A. stutchburyi*[a]	WK28299	Tidal flat	−0·39[r]	0·05	0·55	0·04	–	–	−0·39	0·55	→	6386±32	6713–7019
Shepherd and Lees (1987)	Manawatu valley	*A. stutchburyi*	NZ5218[e]	Tidal flat	−5·05	0·20	0·55	0·04	–	–	−5·05	0·59	6280±220	6613±181	6699–7484
Hesp and Shepherd (1978)	Manawatu valley	*A. stutchburyi*	NZ3085	Tidal flat	1·65	0·20	0·55	0·04	−0·06[v]	0·01	1·23	0·59	6630±70	6475±45	6814–7154
MJ Shepherd (unpublished)	Manawatu valley	*A. stutchburyi*[a]	NZ7911	Tidal flat	0·57	0·20	0·55	0·04	–	–	0·57	0·59	→	4525±43	4533–4857
	Rangitikei valley	Shell	NZ4606	Beach ridge	1·75	0·25	1·10	0·04	–	–	1·75	1·13	5480±60	5831±42	6120–6393
	Rangitikei valley	Shell	NZ4719	Beach ridge	1·75	0·25	1·10	0·04	–	–	1·75	1·13	5770±50	6105±34	6398–6673
Goff et al. (2000)	Okupe Lagoon	*A. stutchburyi*	WK6351	Estuary/open embayment	0·36[h]	0·25	0·33	0·05	−2·25[w]	0·75	−1·90	0·86	→	4010±100	3735–4355
	Okupe Lagoon	*A. stutchburyi*	WK6352	Estuary/open embayment	0·10[h]	0·25	0·33	0·13	−2·25[w]	0·75	−2·16	0·86	→	4510±140	4293–5123
Gibb (1986)	Taupo Swamp	*A. stutchburyi*	NZ4866	Tidal flat	1·90	0·80[t]	–	–	−0·50[v]	0·09	−0·20	0·80	3780±50	4121±32	4018–4376
	Pauatahanui Inlet	*A. stutchburyi*	NZ3118	Upper tidal flat	1·90	0·50[t]	–	–	–	–	1·90	0·50	6230±60	6566±41	6938–7236
	Pauatahanui Inlet	Carbonaceous Mud	NZ4392	Estuary	−11·22	0·40[t]	–	–	–	–	−11·22	0·40	7310±160	7517±143	7684–8299
	Pauatahanui Inlet	Carbonaceous Mud	NZ4391	Estuary	−11·33	0·30[t]	–	–	–	–	−11·33	0·30	7480±110	7480±91	7731–8164
	Pauatahanui Inlet	Carbonaceous Mud	NZ4400[f]	Estuary	−9·35	0·30[t]	–	–	–	–	−9·35	0·30	7750±110	7931±99	8159–8645
	Pauatahanui Inlet	Carbonaceous Mud	NZ4390	Estuary	−12·63	0·30[t]	–	–	–	–	−12·63	0·30	7870±160	8072±145	8257–8987
	Pauatahanui Inlet	Carbonaceous Mud	NZ4389	Estuary	−13·75	0·30[t]	–	–	–	–	−13·75	0·30	7970±130	8194±114	8406–9019
	Pauatahanui Inlet	Carbonaceous Mud	NZ4388	Estuary	−16·04	0·30[t]	–	–	–	–	−16·04	0·30	8360±130	8360±115	8584–9277
	Kumenga	Shell	NZ1634	Estuary	0·00	0·73[t]	–	–	–	0·25	0·00	0·77	3470±50	3786±55	3547–3930
	Kumenga	Shell	NZ1635	Estuary	−0·10	0·73[t]	–	–	–	0·25	−0·10	0·77	4120±50	4437±58	4427–4807
	Kumenga	*M. ovata*	NZ3106	Estuary	−0·35	0·73[t]	–	–	–	0·25	−0·35	0·77	4510±90	4827±77	4846–5326
	Kumenga	Shell	NZ3107	Estuary	−0·60	0·73[t]	–	–	–	0·25	−0·60	0·77	4600±60	4895±59	5033–5327
Christchurch / Pegasus Bay															
Shulmeister and Kirk (1993)	Pegasus Bay	Wood	NZ7954	Back-barrier estuary	−2·10[i]	0·30	1·07	0·20	0·20[v]	0·04	−1·17	1·13	→	4154±74	4434–4826
	Pegasus Bay	Shell	NZ7955	Marine sand	−3·05[i]	0·50	1·07	0·04	0·20[v]	0·05	−2·21	1·18	→	4138±71	3963–4431
Shulmeister and Kirk (1997)	Pegasus Bay	Shell	NZ7953	Gravel beach/nearshore	1·95[i]	0·20	1·07	0·04	0·20[v]	0·04	2·25	1·09	→	1958±70	1325–1717
	Pegasus Bay	Shell	NZ7956	Gravel beach/nearshore	−2·90[i]	0·20	1·07	0·04	0·20[v]	0·05	−2·38	1·09	→	2895±88	2356–2862
	Pegasus Bay	Shell	NZA2606	Gravel beach/nearshore	−2·35[i]	0·20	1·07	0·04	0·20[v]	0·05	−1·59	1·09	→	3810±83	3526–4043
Soons et al. (1997)	Kaitorete Barrier	Shell	NZ7929[g]	Not reported	−36·08	0·20	1·07	0·04	0·20[v]	0·03	−34·01	1·09	→	9483±59	10196–10508
	Kaitorete Barrier	Shell	NZ7928	Not reported	−27·08	0·20	1·07	0·04	0·20[v]	0·04	−25·24	1·09	→	8530±43	9005–9355
Gibb (1986)	Christchurch	Wood	NZ312	Estuary	−0·60	1·00[t]	–	–	0·20[v]	0·01	−0·46	1·00	735±55	753±40	630–723

Continued over page

Table 3.1: (continued)

Source	Locality	Indicator	Radiocarbon laboratory code	Environment / Facies	Elevation	L (m)	D (m)	B (m)	Tectonic correction	V (m)	Inferred eustatic sea-level (m)	Vertical error (m)	Reported age (years BP)	Conventional radiocarbon age (14C years)	Sidereal age range (cal yr BP)
	Christchurch	Wood	NZ122	Estuary	−0·90	1·00[t]	–	–	0·20[v]	0·02	−0·06	1·00	3810±70	3852±48	4073–4318
	Christchurch	Shell	NZ1816	Estuary	0·30	2·03[t]	–	–	0·20[v]	0·04	1·62	2·03	5830±90	6151±59	6410–6767
	Christchurch	Shell	NZ4711	Estuary	−6·00	2·47[t]	–	–	0·20[v]	0·05	−4·51	2·47	6600±140	6936±130	7177–7681
	Christchurch	Shell	NZ117	Estuary	−6·00	3·05[t]	–	–	0·20[v]	0·04	−4·56	3·05	6750±90	6679±58	7029–7379
	Christchurch	Shell	NZ1245	Estuary	−10·00	2·83[t]	–	–	0·20[v]	0·06	−8·38	2·83	7350±130	7655±144	7819–8415
	Christchurch	Shell	NZ1244	Estuary	−12·00	2·83[t]	–	–	0·20[v]	0·06	−10·37	2·83	7370±110	7678±140	7845–8428
	Christchurch	Shell	NZ4851	Estuary	−9·60	2·24[t]	–	–	0·20[v]	0·04	−7·96	2·24	7470±120	7777±97	8003–8447
	Christchurch	Shell	NZ4045	Beach	−10·40	2·83[t]	–	–	0·20[v]	0·06	−8·74	2·83	7490±150	7823±143	7962–8599
	Christchurch	*A. stutchburyi*	NZ1817	Estuary	−16·20	2·26[t]	–	–	0·20[v]	0·04	−14·52	2·26	7670±110	7939±84	8189–8608
	Christchurch	Shell	NZ691	Estuary	−15·70	2·29[t]	–	–	0·20[v]	0·04	−13·97	2·29	7820±70	8129±48	8432–8855
	Christchurch	Shell	NZ4524	Estuary	−19·00	2·43[t]	–	–	0·20[v]	0·05	−17·24	2·43	7940±90	8274±73	8569–9036
	Christchurch	Shell	NZ4712	Estuary	−13·30	2·24[t]	–	–	0·20[v]	0·08	−11·51	2·24	8030±170	8367±149	8545–9365
	Christchurch	Shell	NZ4319	Estuary	−16·30	2·24[t]	–	–	0·20[v]	0·08	−14·48	2·24	8180±70	8514±163	8671–9507
	Christchurch	*A. stutchburyi*	NZ4318	Estuary	−27·00	2·24[t]	–	–	0·20[v]	0·04	−25·16	2·24	8280±70	8617±51	9093–9448
	Christchurch	Shell	NZ4713	Estuary	−24·10	2·90[t]	–	–	0·20[v]	0·08	−22·22	2·90	8410±70	8744±154	9001–9835
	Christchurch	Shell	NZ276	Beach	−26·50	2·24[t]	–	–	0·20[v]	0·04	−24·58	2·24	8530±100	8872±66	9389–9783
	Christchurch	Peat	NZ1819	Estuary	−25·10	1·25[t]	–	–	0·20[v]	0·07	−23·05	1·25	9180±140	9173±118	9912–10585
	Christchurch	Wood	NZ118	Estuary	−25·80	1·00[t]	–	–	0·20[v]	0·04	−23·68	1·00	9400±120	9439±72	10378–10789
	Christchurch	Peat	NZ4485	Estuary	−29·20	1·14[t]	–	–	0·20[v]	0·05	−27·05	1·14	9520±140	9518±116	10477–11000
East Otago Peninsula															
Rayns (1985)	Hoopers Inlet	*A. stutchburyi*	NZ6634	Estuarine shell bed	−0·97[s]	0·50	0·15	0·10	–	–	−0·97	0·53	3530±80	3565±37	3335–3613
	Hoopers Inlet	*A. stutchburyi*	NZ6635	Estuarine shell bed	−0·67[s]	0·50	0·15	0·10	–	–	−0·67	0·53	1645±35	1936±29	1350–1632
	Hoopers Inlet	*A. stutchburyi*	NZ6750	Estuarine shell bed	−0·72[s]	0·50	0·15	0·10	–	–	−0·72	0·53	1250±65	1571±58	968–1274
	Hoopers Inlet	*A. stutchburyi*	NZ6783	Estuarine shell bed	−0·72[s]	0·50	0·15	0·10	–	–	−0·72	0·53	1105±40	1404±33	819–1098
	Hoopers Inlet	*A. stutchburyi*	NZ6780	Estuarine shell bed	−0·72[s]	0·50	0·15	0·10	–	–	−0·72	0·53	1450±35	1745±34	1174–1415
	Hoopers Inlet	*A. stutchburyi*	NZ6638	Estuarine shell bed	−0·77[s]	0·50	0·15	0·08	–	–	−0·77	0·53	2970±70	3122±36	2756–3074
	Papanui Inlet	*A. stutchburyi*	NZ6637	Estuarine shell bed	−0·81[s]	0·50	0·39	0·15	–	–	−0·81	0·65	6020±70	5499±41	5718–6045
	Papanui Inlet	*A. stutchburyi*	NZ6636	Estuarine shell bed	0·14[s]	0·50	0·39	0·04	–	–	0·14	0·63	3780±60	3777±37	3565–3880
	Papanui Inlet	*A. stutchburyi*	NZ6775	Estuarine shell bed	0·04[s]	0·50	0·39	0·10	–	–	0·04	0·64	505±63	827±58	297–566
	Papanui Inlet	*A. stutchburyi*	NZ6749	Estuarine shell bed	0·04[s]	0·50	0·39	0·10	–	–	0·04	0·64	945±62	1272±57	673–955
	Papanui Inlet	*A. stutchburyi*	NZ6786	Estuarine shell bed	0·04[s]	0·50	0·39	0·10	–	–	0·04	0·64	683±59	1000±55	487–691
	Papanui Inlet	*A. stutchburyi*	NZ6789	Estuarine shell bed	0·04[s]	0·50	0·39	0·10	–	–	0·04	0·64	673±36	990±33	501–660
Thomas (2000)	Blueskin Bay	*A. stutchburyi*[a]	NZ3547	Estuarine shell bed	−0·88	1·00[u]	–	–	–	–	−0·88	1·00	4400±140	4572±30	4615–4935
	Blueskin Bay Estuary	Wood	WK6389	Transgressive sand	−1·89	1·40[u]	–	–	–	–	−1·89	1·40	→	6800±330	6900–8211
Ensor (1986)	Blueskin Bay Estuary	*A. stutchburyi*	NZ6853	Estuary	0·05[h]	0·20	0·53	0·05	–	–	0·05	0·56	4010±20	3925±72	3677–4153
	Blueskin Bay Estuary	*A. stutchburyi*	NZ6866	Estuary	−0·46[h]	0·20	0·53	0·05	–	–	−0·46	0·56	5880±230	5316±142	5323–6000
	Blueskin Bay Estuary	*A. stutchburyi*	NZ6867	Estuary	−0·91[h]	0·20	0·53	0·05	–	–	−0·91	0·56	3760±430	3728±331	2835–4541
	Blueskin Bay Estuary	Peat	NZ6953	Deltaic channel deposits	−0·13[h]	0·20	1·05	0·05	–	–	−0·13	1·07	2850±150	1907±352	1166–2618
	Blueskin Bay Estuary	Peat	NZ6952	Deltaic channel deposits	−0·28[h]	0·20	1·05	0·02	–	–	−0·28	1·07	2410±510	2661±137	2342–3005
Gibb (1986)	Blueskin Bay	*P. subtriangulata*	NZ5270	Beach	0·00	0·50[t]	–	–	–	–	0·00	0·50	413±30	751±28	292–487
	Blueskin Bay	Shell	NZ6485	Tidal flat	0·02	0·90[t]	–	–	–	–	0·02	0·90	907±62	1243±59	659–930
	Blueskin Bay	*A. stutchburyi*	NZ1973	Tidal flat	−0·50	0·90[t]	–	–	–	–	−0·50	0·90	1970±50	2290±44	1752–2086
	Blueskin Bay	*P. subtriangulata*	NZ5269	Beach	0·00	0·50[t]	–	–	–	–	0·00	0·50	2250±50	2591±35	2116–2423
	Blueskin Bay	*A. stutchburyi*	NZ1975	Tidal flat	0·00	0·90[t]	–	–	–	–	0·00	0·90	3240±60	3556±47	3315–3624
	Blueskin Bay	*M. liliana*	NZ1974	Tidal flat	−0·50	0·90[t]	–	–	–	–	−0·50	0·90	3440±60	3754±48	3517–3876
	Blueskin Bay	Shell	NZ1978	Tidal flat	0·20	0·90[t]	–	–	–	–	0·20	0·90	5600±70	5913±56	6188–6489
	Blueskin Bay	Shell	NZ1976	Beach ridge	0·30	0·50[t]	–	–	–	–	0·30	0·50	5640±70	5956±56	6239–6556
	Blueskin Bay	*A. stutchburyi*	NZ1977	Tidal flat	0·20	0·90[t]	–	–	–	–	0·20	0·90	6000±70	6338±57	6634–6996
	Blueskin Bay	Shell	NZ6484	Tidal flat	−0·97	0·50[t]	–	–	–	–	−0·97	0·50	6750±150	7084±117	7356–7829

Table 3.1: (continued)

a	Articulated.
b	Estuarine.
c	Disarticulated.
d	Not reported (dated by Waikato University Radiocarbon Laboratory).
e	Given incorrectly as NZ5128.
f	Given incorrectly as NZ4399.
g	Given incorrectly as NZ7994.
h	Inferred from log in source.
i	Inferred from fence diagram in source.
j	Elevation converted from chart datum (Chart NZ5321) to MSL.
k	Converted from MHT to MSL using tides for Whangateau Harbour.
l	Converted from MLWS to MSL using tides for Coromandel Harbour.
m	Converted from MLWS to MSL using tides for Thames (Rocky Point).
n	Elevation is given as being "above MLWS" — therefore elevation error is spring tidal range of 1.7 m (after Thrush et al., 2000).
o	Inferred from NIWA bathymetry (Morrison et al., 2003) with 1 m contour interval.
p	Gibb and Cox (2009) give the elevation for this date as 0.96 m.
q	Gibb and Cox (2009) give the elevation for this date as −0.66 m.
r	RTK-dGPS determination; height relative to WVD1953.
s	Inferred from bathymetry given in source with 1 m contour interval.
t	Includes vertical error components D and B (see Gibb, 1986).
u	Includes vertical error components D and B (see Gibb, 1986; Thomas, 2000).
v	Long-term, mm yr^{-1}.
w	Event.
x	Originally reported using new half-life (Godwin, 1962), and with a secular correction of 330 years subtracted.
y	Originally reported as a calibrated age with a secular correction of 336 ± 30 years subtracted.

for the Southern Hemisphere was used (SHCal04; McCormac et al., 2004). The sidereal age range for the Tuhua Tephra is taken as 6970–7650 cal. yr BP. This is the maximum range from the calibrated ages for the tephra given by Carter et al. (2002) and Manighetti et al. (2003). All calibrated radiocarbon ages are presented using the 2-sigma uncertainty term (95 per cent degree of confidence).

3.2.3 Sources of vertical error

Following Gibb (1986), total sample elevation errors are calculated as the root-sum-square of the component errors:

$$(\text{Elevation error})^2 = L^2 + D^2 + B^2 + V^2$$

where

L is the accuracy of the measurement of the indicators elevation (Table 3.1). The elevation of some indicators was determined using bathymetric contours. For these samples L is taken as half the bathymetric contour interval. Where no measurement error is specified, ±0.2 m has been adopted.

D is the present day living range of the dated indicator (Table 3.1). For fossil shells this is species specific (Table 3.3). The ecological ranges of fossil

shell species are discussed in detail below. Tidal ranges as they relate to the ecological ranges of shell species are site specific (Table 3.4).

B is the vertical range of the dated sample (Table 3.1). Where the thickness of the indicator deposit was not specified by the collector, ±0.02 m has been adopted.

V is the potential long-term or event tectonic deformation (Table 3.1). Long-term tectonic deformation is calculated as half the age error of the sample, multiplied by the rate of long-term tectonic deformation for the site (Table 3.5). The tectonic regimes of all the sites from which palaeo sea-level indicators were recovered are discussed below.

The component errors for each of the palaeo sea-level indicators are presented in Table 3.1.

3.2.4 Palaeo sea-level indicators

3.2.4.1 Formation datums

The formation datums and potential error ranges of palaeo sea-level indicators are summarised in Table 3.3. Elevations of palaeo sea-level indicators presented in Table 3.1 are relative to these formation datums. For wood and tephra samples recovered from tidal flat or estuarine sequences the assumed datum is MSL, with half the spring tidal range as error. Following Gibb (1986), the elevations of samples presented by Millener (1981), Osborne (1983), and Osborne et al. (1991) from shell bank deposits are given relative to mean high water springs (MHWS). Both Gibb (1986) and Thomas (2000) presented samples with respect to formation heights; these heights are retained.

3.2.4.2 Maximum and minimum indicators

The vast majority of wood, peat, root, and shell samples were recovered from sedimentary facies indicative of estuarine environments. These samples serve as minimum indicators of palaeo sea-level as they indicate that sea-level cannot have been lower than the level that they indicate. Shells recovered from beach ridge, shell bank, and chenier deposits serve as maximum indicators of palaeo sea-level, as they indicate that sea-level cannot have been above the level indicated by these geomorphic features.

3.2.4.3 Ecological ranges of fossil shell species

Gibb (1979) presented a compilation of studies which recorded the living depth ranges of a number of shell species used as palaeo sea-level indicators. Gibb (1979) noted that records were often inconsistent, and concluded that many were unreliable because of insufficient observations. Numerous other studies comment on the lack of information on the ecology of shell species in New Zealand (e.g., Blackwell, 1984; Roper et al., 1992; Grant, 1994; Hooker and

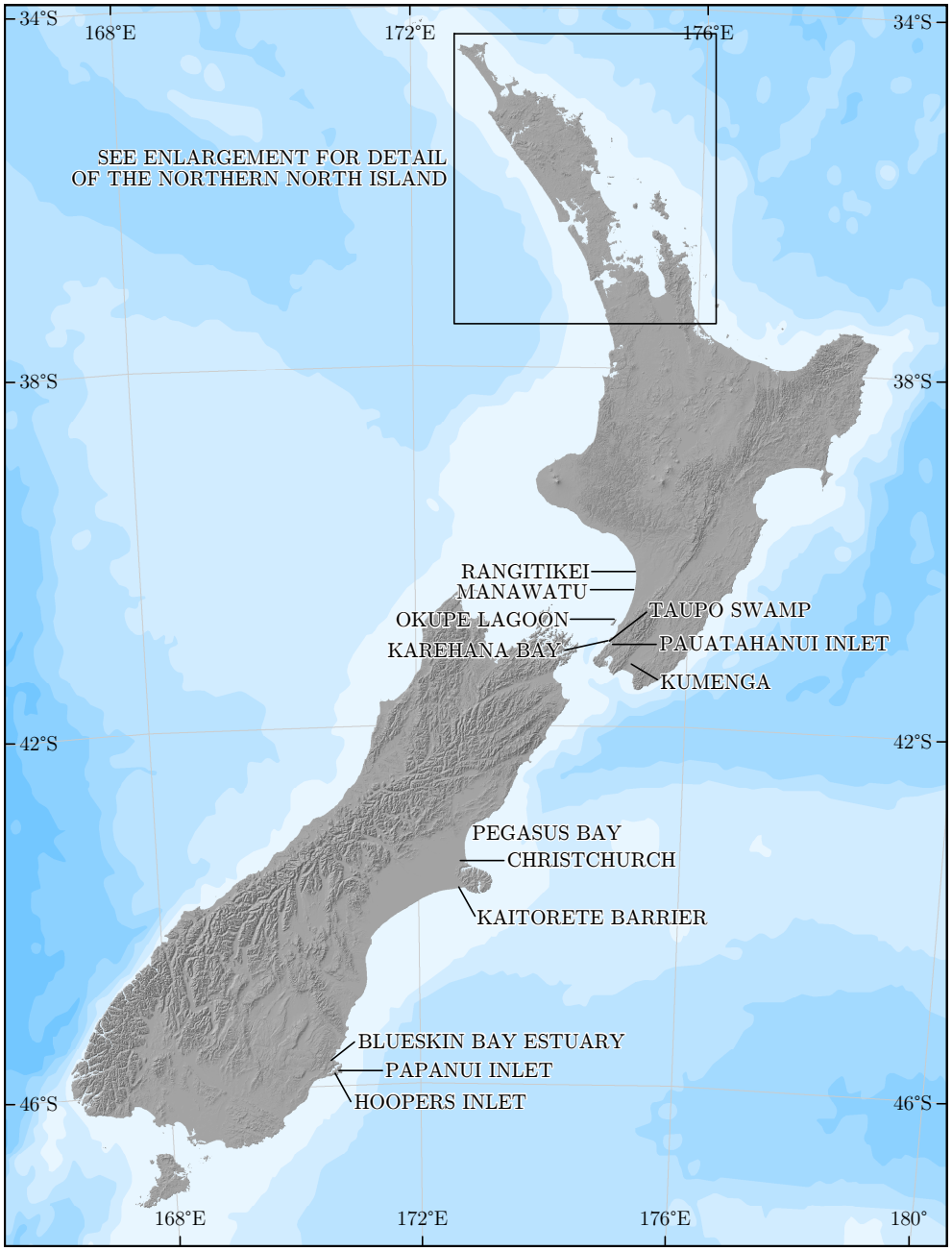

Figure 3.1: Locations of sites throughout the New Zealand region from which indicators of Holocene palaeo sea levels were recovered. For detail of the Auckland-Northland region refer to Figure 3.2.

Creese, 1995; Norkko et al., 2001). Gibb (1979) therefore suggested that the true ecological ranges of such shell species may not be definitively recognised.

Radiocarbon dated fossil shell species utilised as indicators of palaeo sea-level include *A. stutchburyi*, *Macomona liliana*, *Mactra ovata*, *Paphies aus-*

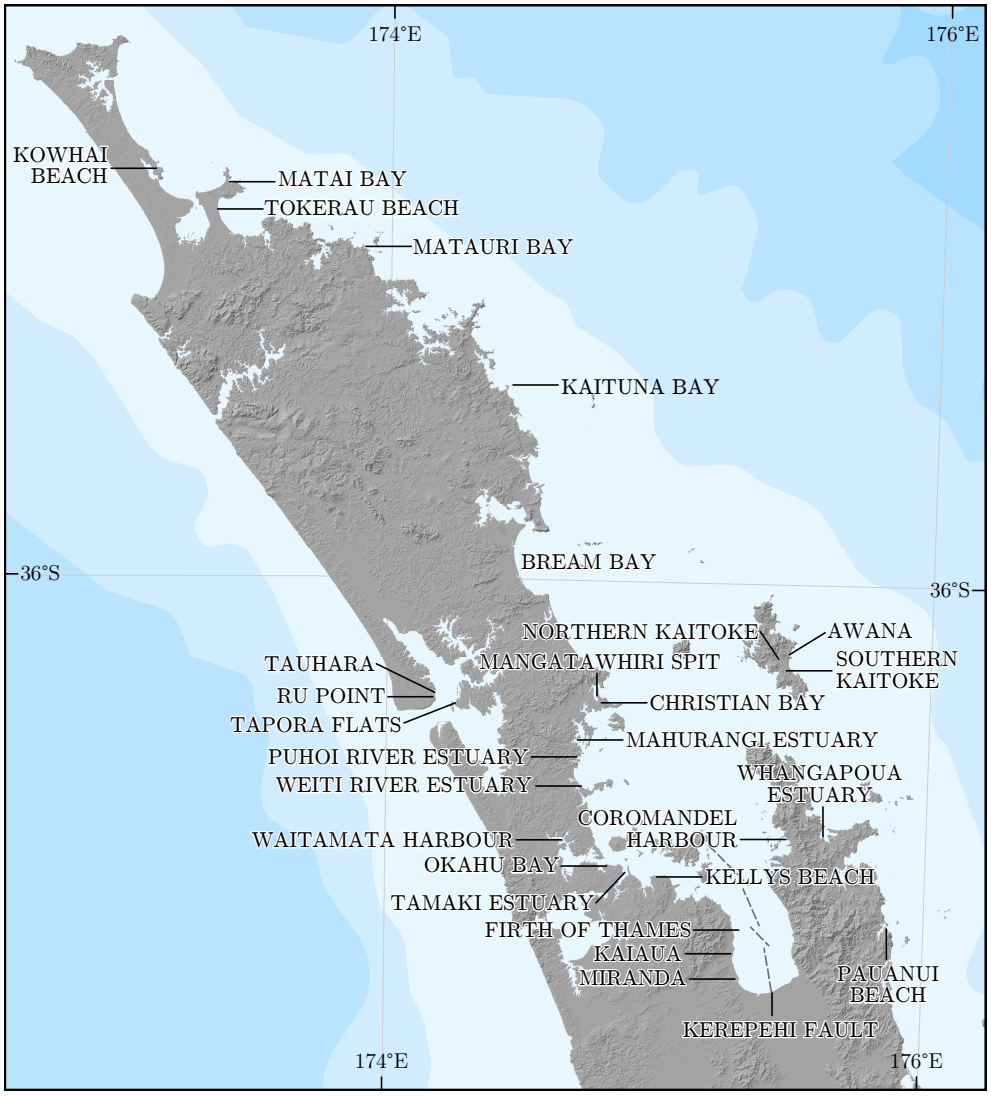

Figure 3.2: Locations of sites throughout the northern North Island, New Zealand, from which indicators of Holocene palaeo sea levels were recovered. The extent of this map is shown on Figure 3.1.

tralis, and *Paphies subtriangulata*, all of which are commonly found in lower energy intertidal settings. Species such as *Mactra ordinaria*, *Maoricolpus roseus*, *Mactra discors* and *Volutidae* spp. that were dated by some studies from which the indicators were drawn have been specifically omitted, as they have extremely broad ecological ranges (e.g., McKnight, 1969; Allmon et al., 1994; Cranfield et al., 1994; Haddon et al., 1996; Cranfield and Michael, 2001a,b; Bax et al., 2003; Handley, 2006; Probst and Crawford, 2008) which make them unsuitable indicators of palaeo sea-level.

A. stutchburyi (formerly *Chione stutchburyi*; Jones, 1979) is perhaps the most common shell species used as an indicator of palaeo sea levels in the

Table 3.2: Details of known-age marine samples used to calculate a New Zealand regional marine reservoir correction ΔR value for the calibration of CRAs from fossil shells and other marine materials into sidereal years (cal. yr BP). Data sourced from the Marine Reservoir Correction Database (`http://www.calib.qub.ac.uk/marine/`).

Reference	Chrono database sample number	Collection year	Reservoir age	Radiocarbon age	Radiocarbon laboratory code	Sample
Rafter et al. (1972)	462	1955	250±42	427±39	NZ2439	*Protothaca crassitesta*
McFadgen and Manning (1990),	463	1923	268±47	410±46	NZ1799	*Dosinia anus*
Higham and Hogg (1995)	464	1949	273±48	432±46	NZ1813	*Austrovenus stutchburyi*
	465	1953	329±42	506±39	NZ114	*Paphies ventricosum*
	466	1954	317±38	494±35	NZ1481	*Paphies subtriangulatum*
	467	1954	274±35	451±32	NZ4698	*Alcithoe arabica*
	468	1954	245±64	422±62	NZ2421	*Haliotes*
	469	1954	287±64	464±62	NZ2433	*Cellana*
	470	1954	213±46	390±44	NZ2431	*Austrovenus stutchburyi*
Kalish (1993), Higham and Hogg (1995)	471	1918	299±58	429±57	NZA2740	*Pagrus auratus*
	472	1928	195±62	345±61	NZA2799	*Pagrus auratus*
	473	1932	348±59	501±58	NZA2741	*Pagrus auratus*
	474	1943	276±60	427±59	NZA2721	*Pagrus auratus*
	475	1943	310±66	461±65	NZA2797	*Pagrus auratus*
	476	1950	385±58	546±57	NZA2742	*Pagrus auratus*
Sikes et al. (2000)	477	1924	344±33	490±31	–	Bivalve

Weighted mean ΔR: −7
Standard deviation: 45
Weighted mean measurement error: 11
ΔR uncertainty is the larger of the standard deviation or weighted mean measurement error

Table 3.3: Summary of the formation datums and error ranges associated with each of the types of palaeo sea-level indicator used to reconstruct the local-scale sea-level histories in the New Zealand archipelago. See Sections 3.2.4.1 and 3.2.4.3 for greater detail.

Indicator	Formation height	Error range
A. stutchburyi	MSL − 1/2 Spring tide range	1/2 Spring tidal range
M. liliana	MSL	1/2 Mean tidal range
M. ovata	MSL − 1/2 Spring tide range	1/2 Spring tidal range
P. australis	MSL	1/2 Mean tidal range
P. subtriangulata	MSL	1/2 Mean tidal range
Wood	MSL	1/2 Spring tidal range
Tephra	MSL	1/2 Spring tidal range
Mangrove	MSL + 1/2 MHW	1/2 Mean tidal range
Beach ridge	MHWS	1/4 Spring − neep range
Peat	MSL	1/2 Spring tidal range

New Zealand archipelago. *A. stutchburyi* is most commonly described in very broad terms as an intertidal bivalve found in sheltered environments (e.g., Morton and Miller, 1968; Larcombe, 1971; Powell, 1979; Purchase and Fergusson, 1986; Hewitt et al., 1996; Hayward et al., 1997, 2002; Hogg et al., 1998; Thrush et al., 1999; Norkko et al., 2001; Lelieveld et al., 2004; Lundquist et al., 2004; Tallis et al., 2004). Hayward and Stilwell (1995) noted that *A. stutchburyi* valves may float to exposed coasts. However the indicative value of the valves is derived from more than the species assemblage alone, and involves factors such as valve position and sedimentological context. Morton and Miller (1968) suggested that *A. stutchburyi* inhabits the neap tide flat, while Gibb (1986) suggested that the bivalve was most common between MSL and mean low water springs (MLWS). Wilson et al. (2007) therefore suggested that the elevation of fossil *A. stutchburyi* be measured relative to PMSL less half the spring tidal range, with an error of half the spring tidal range. This accounts for shells living half-way between mid- and low-tide, with a 95 per cent uncertainty spanning the mid-low tide range (Table 3.3).

M. liliana is variously described as inhabiting either the intertidal (e.g., Nipper and Roper, 1995; Hogg et al., 1998; Thrush et al., 1999; Norkko et al., 2001; Cummings and Thrush, 2004; Lelieveld et al., 2004; Lundquist et al., 2004) or subtidal zone (e.g., Grange, 1979; Roper, 1990; Roper et al., 1992). Gibb (1979) posited that *M. liliana* occupied the intertidal lower foreshore, although later (Gibb, 1986) suggested that the valves occurred across the entire tidal flat.

Few studies have documented the ecological range of *M. ovata*. Morton and Miller (1968) suggested that the bivalve inhabited sheltered harbours, being found from high water to the lower beach. Powell (1979) described the habitat as estuaries and tidal flats, while Leach and Anderson (1974) suggested that *M. ovata* was common to estuaries from the mid tide level to low water.

P. australis inhabits partially sheltered waters (Powell, 1979; Carroll and Wells, 1995). Some studies propose that the valve is found from the intertidal to subtidal range (e.g., Gibb, 1979, 1986; Hooker and Creese, 1995), while

Table 3.4: Tidal ranges for each of the sites throughout the New Zealand region from which palaeo sea-level indicators included in the study were recovered. Tide gauge levels are taken from the New Zealand Nautical Almanac.

Locality	Tide data source	Mean spring tide variation (± m)	Mean neep tide variation (± m)	Proximity of tide data source to sample location (km)
Awana	Typhena tidal gauge	0·90	0·65	7
Blueskin Bay Estuary	Ensor (1986)	1·05	0·50	–
Bream Bay	Nichol (2002)	1·30	0·55	13
Christian Bay	Mansion House Bay tidal gauge	1·05	0·75	6
Coromandel Harbour	Coromandel Harbour tidal gauge	1·15	0·85	–
Firth of Thames	Thames (Rocky Point) tidal gauge	1·35	1·05	–
Hoopers Inlet	Albrecht and Vennell (2007)	0·30	0·17	–
Kaitorete Barrier	Lyttelton tidal gauge	1·07	0·69	28
Kaituna Bay	Russell tidal gauge	1·05	0·60	32
Karehana Bay	Gibb and Cox (2009)	0·66	0·11	–
Kowhai Beach	Hicks and Nichol (2007)	0·90	0·60	–
Mahurangi Estuary	Oldman et al. (2003)	1·50	1·00	–
Manawatu	Manawatu River Entrance tidal gauge	1·10	0·45	–
Mangatawhiri Spit	Whangateau Harbour tidal gauge	1·25	0·85	8
Matai Bay	Rangaunu Harbour tidal gauge	1·05	0·75	12
Matauri Bay	Russell tidal gauge	1·05	0·60	27
Mirada	Thames (Rocky Point) tidal gauge	1·35	1·05	–
Northern Kaitoke	Typhena tidal gauge	0·90	0·65	7

Continued over page

Table 3.4: (continued)

Locality	Tide data source	Mean spring tide variation (± m)	Mean neep tide variation (± m)	Proximity of tide data source to sample location (km)
Okahu Bay	Auckland tidal gauge	1·42	0·88	8
Okupe Lagoon	Waiorua Bay (Kapiti Island) tidal gauge	0·65	0·15	1
Papanui Inlet	Albrecht and Vennell (2007)	0·78	0·43	–
Pauanui Beach	Tairua tidal gauge	0·90	0·60	–
Pauatahanui Inlet	Gibb and Cox (2009)	0·66	0·12	–
Pegasus Bay	Lyttelton tidal gauge	1·07	0·69	45
Puhoi River Estuary	Weiti River Mouth tidal gauge	1·10	0·80	13
Rangitikei	Manawatu River Entrance tidal gauge	1·10	0·45	20
Ru Point	Tinopai tidal gauge	1·65	0·85	8
Southern Kaitoke	Typhena tidal gauge	0·90	0·65	7
Tamaki Estuary	Auckland tidal gauge	1·42	0·88	8
Tapora Flats	Tinopai tidal gauge	1·65	0·85	14
Tauhara	Tinopai tidal gauge	1·65	0·85	11
Tokerau Beach	Rangaunu Harbour tidal gauge	1·05	0·75	4
Waitamata Harbour	Hume and McGlone (1986)	1·50	1·00	–
Weiti River Estuary	Weiti River Mouth tidal gauge	1·10	0·80	–
Whangapoua Estuary	Thrush et al. (2000)	0·85	0·65	–

others suggest that the bivalve is found only intertidally (e.g., Hogg et al., 1998; Cummings and Thrush, 2004). Both Herzer (1981) and Carter et al. (1986) declare that the species is strictly intertidal.

P. subtriangulata (previously *Amphidesma subtriangulatum*; Grant and Hay, 2003) is described as a common beachface intertidal species (Powell, 1979; Pillans and Huber, 1995), with a habitat possibly extending into the surfzone (McLachlan et al., 1995). As with *P. australis*, both Herzer (1981) and Carter et al. (1986) declare that the species is strictly intertidal.

One sample indicator is a fragment of a root presumed to have come from the mangrove *Avicennia marina*. *A. marina* grows in swamps, tidal estuaries and on coastal shallow water mudflats (Mildenhall and Brown, 1987), and thrives where high water is no more than 0.6 m (2 feet) deep (Morton and Miller, 1968). Morrisey et al. (2007) suggest that the mangrove is confined to the area between MSL and mean high-water (MHW) (see also Sloss et al., 2007).

3.2.5 Delineation of regions

Indicator sites were grouped together into local regions. Groupings attempted to balance the proximity of the sites to one another, whether sites formed a contiguous region, the differing tectonic regimes throughout New Zealand, and the need to have sufficient indicator points within a region to construct a sea-level history. Broadly, the regions delineated were Auckland-Northland (Kowhai Beach south to Kelly's Beach, including Northern and Southern Kaitoke and Awana on Great Barrier Island: Figure 3.2), Coromandel Peninsula and the Firth of Thames (including Coromandel Harbour, Miranda, Kaiaua, Pauanui Beach and Whangaparoa Estuary: Figure 3.2), the south/southwest coast of the North Island (Rangitikei south to Kumenga: Figure 3.1), Pegasus Bay (including Christchurch, Banks Penninsula, and the Kaitorete Barrier: Figure 3.1), and the East Otago Peninsula (including Blueskin Bay estuary, Papanui Inlet, and Hoopers Inlet: Figure 3.1).

3.2.6 Tectonic regimes of the regions

In order to isolate the ice-equivalent sea-level signal (cf. Lambeck and Chappell, 2001), adjustments for long-term and event-specific tectonic movements were made (Table 3.1). Adjustments for tectonic deformation are summarised in Table 3.5.

3.2.6.1 Auckland-Northland

The Auckland-Northland region (Figure 3.2) is widely considered to have been tectonically stable through the Quaternary (e.g., Brothers, 1954; Cotton, 1957a; Ward, 1972; Gibb, 1983, 1986; Pillans, 1986; Kershaw and Strickland, 1988; Brook and Thrasher, 1991; Heap and Nichol, 1997; Brook, 1999; Berryman and Hull, 2003; Marra et al., 2006; Dougherty and Nichol, 2007;

Table 3.5: Summary of long-term and event tectonic deformation for localities and regions within the New Zealand archipelago from which indicators of Holocene palaeo sea levels were recovered. See Sections 3.2.6.1–3.2.6.5 for greater detail.

Region / Site	Analysis of tectonic regime	Tectonic correction rate (TCR)	Long-term / event deformation	Potential error
Northland / Auckland	Tectonically stable	–	–	–
Coromandel Peninsula	Tectonic uplift	0.25 mm/yr	Long-term	14C age error × TCR
Firth of Thames — proximal to Kerepehi Fault	Fault rupture c. 2,500 years BP	–	Event	1.00 m
Firth of Thames — distal from Kerepehi Fault	Fault rupture c. 2,500 years BP	–	Event	0.50 m
Miranda / Kaiaua	Tectonically stable	–	–	–
Manawatu — proximal to MIS 5e marine terrace	Tectonic uplift	0.06 mm/yr	Long-term	14C age error × TCR
Manawatu — distal from MIS 5e marine terrace	Tectonically stable	–	–	–
Rangitikei coastal plain	Tectonically stable	–	–	–
Pauatahanui Inlet — east	Tectonically stable	–	–	–
Taupo Swamp	Tectonic uplift	0.50 mm/yr	Long-term	14C age error × TCR
Karehana Bay	Tectonic uplift	0.20 mm/yr	Long-term	14C age error × TCR
Okupe Lagoon	Tectonic uplift	2.50 m	Event	0.75 m
Kumenga	Ambiguous	–	Event?	0.25 m
Christchurch / Pegasus Bay	Tectonic subsidence	0.20 mm/yr	Long-term	14C age error × TCR
East Otago Peninsula	Tectonically stable	–	–	–

Hicks and Nichol, 2007; Horrocks et al., 2007). Some studies suggest tectonic stability since at least the Miocene (e.g., Marwick, 1948; Gage, 1953; Eiby, 1955; Schofield, 1958, 1960a; Glenie et al., 1968; Lensen, 1975). Auckland and Northland are distant from areas of high seismicity, and are two of the lowest earthquake activity regions in New Zealand (Hull et al., 1995). No active faults (displaced within the last 125,000 years) are recognised in Northland (Beetham et al., 2004), while there is only one known and one possibly active fault recognised in the Auckland region (Edbrooke et al., 2003). Auckland and Northland are therefore inferred to have been tectonically stable through the Quaternary (Table 3.5).

However, some studies have recognised possible tectonic movements in the Northland and Auckland regions. Claessens et al. (2009) calculated uplift rates for the Waitakeri Ranges (Figure 3.3) using marine terrace elevations. Age control was provided by deposits of the Potaka (1 Ma; Shane, 1994; Shane et al., 1996), Rangitawa (formerly named Mt Curl Tephra; c. 345,000 years BP; Froggatt et al., 1986; Pillans et al., 1996; Shane, 2000) and Rotoehu tephras (43,000–55,000 years BP; Shane and Sandiford, 2003; Newnham et al., 2004; Litchfield and Berryman, 2005; Claessens et al., 2009 appear to use 50,000 years BP for their calculations) preserved in the terrace coverbeds. Claessens et al. (2009) calculated that from 1 Ma to 345,000 years BP the time averaged uplift rate for the Waitakeri Ranges was 0.072 mm yr^{-1}, rising to 0.278 mm yr^{-1} from 345,000–50,000 years BP, and to 0.42 mm yr^{-1} for the past 50,000 years BP. However, these rates are questionable. Claessens et al. (2009) report the elevation of the Rotoehu Tephra as 44 m; however, the calculated uplift rates use an elevation of 21 m. Also, Claessens et al. (2009) calculated the uplift rates between terrace levels by dividing the altitude difference between successive tephras by the age difference of the tephras. This appears to erroneously assume that the tephras were deposited at sea-level. However, this cannot be the case. At best the tephras may indicate the timing of erosion of the wave cut platform of the terrace immediately below the lowest terrace on which the tephra is found. This implies that a significant amount of uplift may have occurred prior to the emplacement of the tephra. Therefore the uplift rates calculated by Claessens et al. (2009) should be viewed as maximum rates. In addition, the rates are only applicable to the Waitakere Ranges 'tectonic block' (L. Claessens, personal communication).

D'Costa et al. (2009) presented a multi-proxy study of two cores recovered near Dargaville in Northland (Figure 3.3). D'Costa et al. (2009) utilised diatom analysis to identify the marine-freshwater transition in each core, which was dated to 6,405–7,274 cal. yr BP. In one core the transition was suggested to occur between +5.72–+6.01 m above PMSL, while in the other core the transition was estimated to occur at +4.94 m above PMSL. D'Costa et al. (2009) therefore inferred uplift rates at both sites of the order of 0.8–1.0 mm yr^{-1}. However, D'Costa et al. (2009) levelled the cores using spot heights, which may have extremely poor vertical precision, rather than geodetic marks which have been accurately levelled. A recent analysis of the core sites suggests

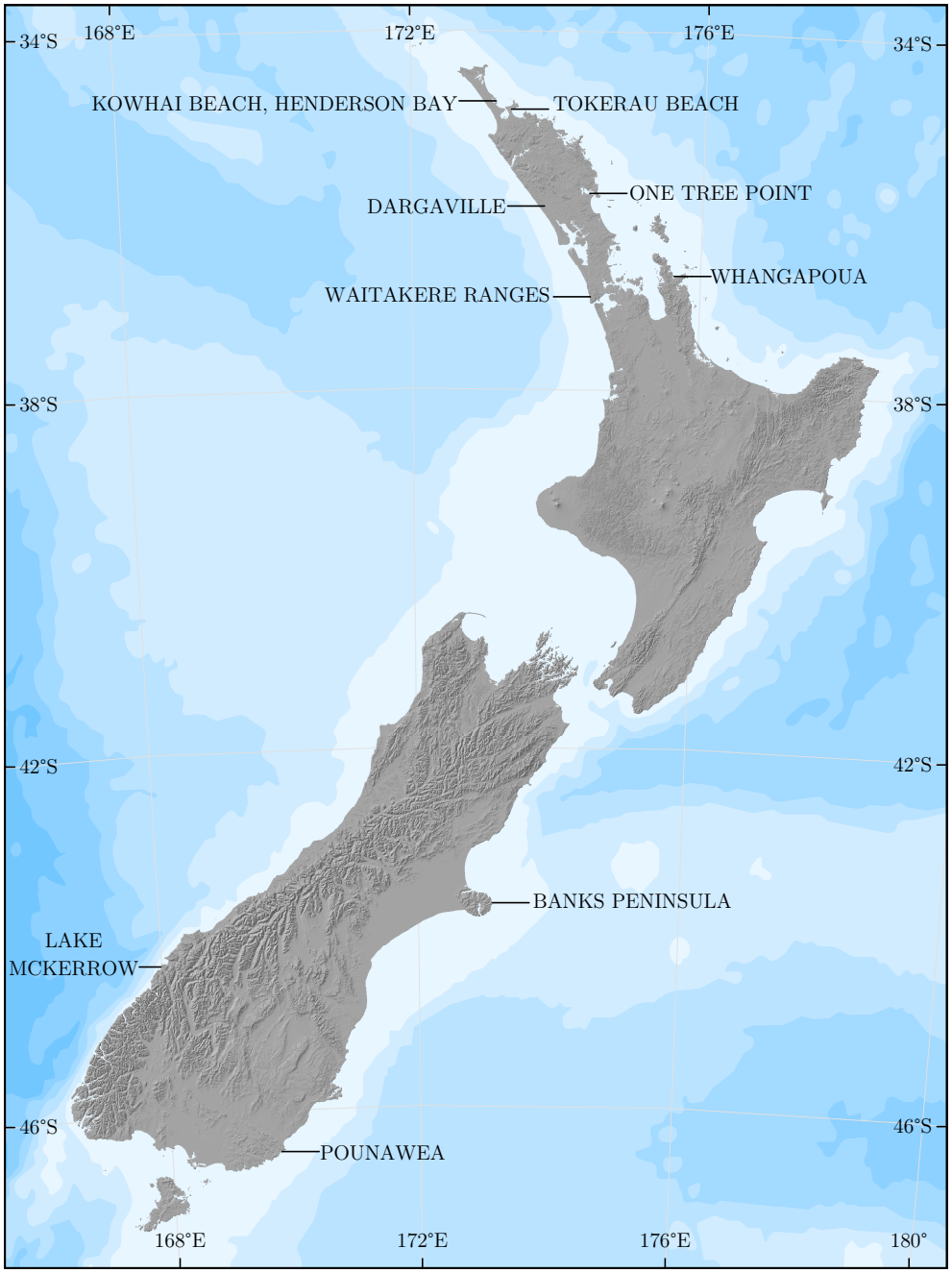

Figure 3.3: Other locations mentioned in connection with the construction or analysis of the local-scale Holocene sea-level curves for the New Zealand archipelago.

that D'Costa et al. (2009) may have significantly overestimated the elevation of the cores (J. Richardson, personal communication). In addition, the proposed uplift rates are significant within a New Zealand context (cf. Wellman, 1979; Pillans, 1986; Williams, 1991), but do not appear to have generated the

uplifted fluvial or marine terraces that would otherwise be expected to be seen in the area (N. Litchfield, personal communication).

3.2.6.2 Coromandel Peninsula and the Firth of Thames

For the Coromandel Peninsula (Figure 3.2) Pillans (1986) suggested Quaternary uplift rates of 0.25–0.3 mm yr^{-1}. Abrahamson (1987) calculated a rate of 0.3 mm yr^{-1} for the eastern Coromandel Peninsula. A long-term uplift rate of 0.25 mm yr^{-1} has been adopted for the Coromandel Peninsula (Table 3.5).

Chick (1999) used seismic sub-bottom profile data to analyse vertical movement along the Kerepehi Fault in the Firth of Thames (Figure 3.2), and suggested that at least 4.2 m of vertical movement had taken place along the three southernmost segments of the fault during last 6,500 years BP. de Lange and Lowe (1990) used tephra layers and radiocarbon dated peat horizons to analyse the vertical displacement of the northernmost terrestrial segment of the fault. Step function analysis of the progressive offset of the peat horizons and tephras with time indicated a mean recurrence interval of 2,500 years. Chick (1999) assumed that the recurrence intervals along the submarine sections of the fault were similar to the terrestrial segments, and so concluded that the 4.2 m of estimated displacement had probably occurred during two displacement events. Therefore, palaeo sea-level indicators dated to between c. 2,500–5000 years BP and recovered in the proximity of the Kerepehi Fault have an added error of ±1 m (cores 31 and 40 from Naish, 1990; Table 3.5). Samples older than 2,500 years BP and from the periphery of the Firth of Thames have an added error of ±0.5 m (cores T1A and T4 from Hume and Dahm, 1991; cores 21 and 33 from Naish, 1990; Table 3.5).

For Miranda and Kaiaua (Figure 3.2), Pillans (1986) applied Gibb's (1983) method of tectonic separation to the sea-level data presented by Schofield (1960a) and Woodroffe et al. (1983). Pillans (1986) suggested that uplift rates of the order of 0.2–0.9 mm yr^{-1} were indicated. Gibb (1986) suggested a Holocene uplift rate of 0.1 mm yr^{-1}. However, both Schofield (1960a) and Woodroffe et al. (1983) considered the area to be relatively stable and likely to have undergone little or no tectonic movement. No tectonic adjustment has been applied to palaeo sea-level indicators from Miranda and Kaiaua (Table 3.5).

3.2.6.3 South/southwest North Island

Hesp and Shepherd (1978) averaged the elevation of a Last Interglacial marine terrace on the periphery of the Manawatu coastal plain (Figure 3.1), inferring a long-term uplift rate for the area of 0.35 mm yr^{-1} over the past 120,000 years BP. Hesp and Shepherd (1978) assumed an average elevation for the marine terrace of 55 m, including 8 m of cover beds, and assumed Last Interglacial sea levels c. 5 m higher than PMSL. However, the terrace is tilted along its length, and rises from a low of c. +30 m to over +90 m above PMSL. In addition, the terrace is also tilted laterally towards the Manawatu coastal

plain, implying lower rates of uplift on the plain than at the rear of the terrace, which lies adjacent to the Tararua Ranges. The marine terrace in the vicinity of the location on the coastal plain where Hesp and Shepherd (1978) recovered estuarine shells (Table 3.1) is only 10–20 m above PMSL, implying uplift rates of 0–0.06 mm yr^{-1} since the Last Interglacial (Table 3.5).

Litchfield and Berryman (2007) used LGM-age river terraces in the Manawatu valley above the coastal plain to estimate rates of fluvial incision as a proxy for rock uplift. Litchfield and Berryman (2007) inferred an average uplift rate for the upper valley of 0.5 mm yr^{-1} over the last 18,000 years BP. For the lower Rangitikei valley (Figure 3.1), above the coastal plain, Litchfield and Berryman (2007) suggested an average uplift rate of 0.2 mm yr^{-1} over the last 18,000 years BP. However, it is unclear whether these rates would extend onto the coastal plains. Pillans (1986) and Williams (1991) note that the coastal plains lie in a zone of subsidence, though both suggest zero rates of tectonic movement through the late Quaternary (Table 3.5).

Tectonic deformation of the area surrounding Pauatahanui Inlet (Figure 3.1) has been variously attributed to the magnitude ∼8.1 Wairarapa earthquake of 1855, as well as movements along the Ohariu Fault, which bisects the inlet. Adkin (1921) reported that a long-time resident of the area estimated that the earthquake uplifted the tidal flats in the inlet by at least 1 m (3 feet). This contrasted with the reports of Roberts (1855) and Lyell (1868), who considered uplift of the area to have been 'very slight,' of the order of 0.3 m (1 foot) (Grapes and Downes, 1997). Eiby (1990), Wynne (1981), and Healy (1980) all concluded that the area was not uplifted during the 1855 Wairarapa earthquake.

Gibb (1986) estimated an average rate of tectonic uplift for Pauatahanui Inlet of 0.3 mm yr^{-1} for the last 6,500 years BP. Swales et al. (2005) analysed radiocarbon dated shells recovered from the inlet, and concluded that rates of tectonic uplift in the inlet over the last several thousand years were very low, with Gibb's (1986) rate of 0.3 mm yr^{-1} regarded as a maximum value. Gibb and Cox (2009) reviewed evidence of tectonic deformation from the Pauatahanui Inlet area, within the context of the active Oharui fault. From observation of shoreline sites around the inlet Gibb and Cox (2009) concluded that Pauatahanui Inlet east of the Oharui fault had been tectonically stable over the last 7,500 years (Table 3.5). West of the fault Gibb and Cox (2009) suggested that uplift was indicated, and proposed a rate of 0.5 mm yr^{-1} for Porirua Harbour and the Plimmerton coast, including Taupo Swamp (Figure 3.1), trending to 0.2 mm yr^{-1} at Karehana Bay (Figure 3.1, Table 3.5).

Goff et al. (2000) used micropaleontological evidence from cores recovered from Okupe Lagoon (Figure 3.1), together with surveys of beach ridges surrounding the lagoon, to recognise an uplift event presumed to have been caused by rupture of a local fault. Goff et al. (2000) dated the event to c. 3360 ± 140 14C years, and suggested that 1.5–3.0 m of uplift was indicated (Table 3.5).

Gibb (1986) suggested that Kumenga (Figure 3.1) had been either unaffected by tectonics, or affected by only a very slight rate of tectonic downdrop.

Gibb (1986) inferred a long-term downdrop rate of 0.05 mm yr^{-1}, for an average total of 0.21 m since the early to mid Holocene. In contrast, Leach and Anderson (1974) suggested that the area underwent 0.2–0.3 m of uplift associated with the 1855 Wairarapa earthquake. Grapes and Downes (1997) also considered any tectonic movement due to the earthquake to have been minor, and suggested that the area was uplifted by no more than 0.3 m. As the tectonic regime is difficult to define an error of ±0.25 m has been adopted (Table 3.5).

3.2.6.4 Christchurch and Pegasus Bay

While Chappell (1974) and Nakada and Lambeck (1989) both suggested that Christchurch (Figure 3.1) was tectonically stable, most studies suggest that the region is uniformly subsiding (e.g., Suggate, 1958, 1968; Williams, 1991). Various rates of subsidence have been proposed. Wellman (1979) suggested a rate of 0.1–0.2 mm yr^{-1}, while Lensen (1975) proposed a rate of 0.3 mm yr^{-1} for much of the eastern South Island. For the continental shelf east of Banks Peninsula (Figure 3.3) Herzer (1981) calculated subsidence rates of 0.05–0.09 mm yr^{-1} since the lower Miocene. Barnes (1995) suggested a rate of about 0.4 mm yr^{-1} over the last 0.5 Ma for offshore Pegasus Bay (Figure 3.1). Gibb (1979) calculated a subsidence rate of 0.3 mm yr^{-1} for the Christchurch area (Figure 3.1), but later (Gibb, 1983, 1986) revised this to 0.1 mm yr^{-1}. Lambeck et al. (2002) followed Wellman's (1979) assessment, and used a subsidence rate of 0.2 mm yr^{-1}. A subsidence rate of 0.2 mm yr^{-1} has been adopted for Christchurch and Pegasus Bay, as it represents an average of all suggested rates (Table 3.5).

3.2.6.5 East Otago Peninsula

The East Otago Peninsula (Figure 3.1) is a Miocene volcanic complex widely considered to have been tectonically stable through the late Quaternary (e.g., Cotton, 1948, 1957a; Harrington, 1958; Gibb, 1979, 1983, 1986; Wellman, 1979; Landis, 1988; Pillans, 1990b; Williams, 1991; Bishop and Turnbull, 1996; Thomas, 2000). Litchfield and Lian (2004) examined a section of the northeast trending Waitati Fault, which bisects Blueskin Bay (Figure 3.1), but found no evidence for Quaternary activity. However, Litchfield and Lian (2004) did note that the marine terrace which surrounds that bay, presumed by Gibb (1986) to be Last Interglacial in age, was slightly deformed, being tilted to the northeast, and was offset 1 m by a small northwest striking fault. The East Otago peninsula is therefore inferred to have been tectonically stable through the late Quaternary (Table 3.5).

3.3 Local-scale Holocene sea-level curves for the New Zealand archipelago: results and discussion

The distribution of sea-level index points for each of the five regions within the New Zealand archipelago have been plotted on common axes, with envelopes delineating sea-level changes fitted to the point distributions (Figures 3.4, 3.6, 3.7, 3.8, and 3.9). Because of the smaller vertical distributions of index points from Auckland-Northland and East Otago, the sea-level plots for these two regions have been plotted with expanded vertical axes (Figures 3.5 and 3.10).

The sea-level envelopes for each of the regions were constructed with reference to the relative indicative value (e.g., Petersen, 1986) of the palaeo sea-level indicators in each region, perceived indicative value being based on the collective evaluation of elevation errors, the indicator material (shell, wood, peat, tephra), and the stratigraphic context of each indicator. Indicators with perceived high indicative value are typically articulated valves recovered in growth position from estuarine sediments. Wood, peat or tephra samples recovered from similar sediments have comparatively lower indicative value as these are not intrinsically tied to sea-level. Mixed shell assemblages are perceived to have comparatively low indicative value as the constituent shell species may indicate a variety of environmental conditions. Further, indicators that are well constrained, for example by having their elevations reported by the source, have relatively higher perceived indicative value compared with indicators where the elevation has been interpolated from bathymetric contours, logs, or fence diagrams. These assessments of indicative value are relative, and apply within the context of the delineation of the sea-level envelopes and the index points surrounding them, rather than being absolute assessments within the context of the entire population of index points from all the locations. For this reason the relative indicative values used in the delineation of the sea-level envelopes are discussed within that context (Sections 3.3.1–3.3.5), rather than presenting an assessment of the indicative value of every point in Table 3.1, lest the scope of the indicative values be misrepresented.

3.3.1 Auckland-Northland Holocene sea-level interpretation and analysis

Sea-level in the Auckland-Northland region had risen to c. −3 m below PMSL by c. 8,000 cal. yr BP. This is suggested by the grouping of three radiocarbon ages at this depth (A on Figure 3.5, cf. Figure 3.4; WK6372, WK3812, WK3814; Table 3.1), two from Heap and Nichol (1997) and one from Abrahim et al. (2008). The two ages presented by Heap and Nichol (1997) have high indicative value (e.g., Petersen, 1986), as they were obtained from articulated bivalves in growth position. The organic material index point previously used by Clement et al. (2008a,b) is ignored, as it was recovered from a fluvial terrace (WK3815, Heap and Nichol, 1997; Table 3.1), and therefore has no indicative

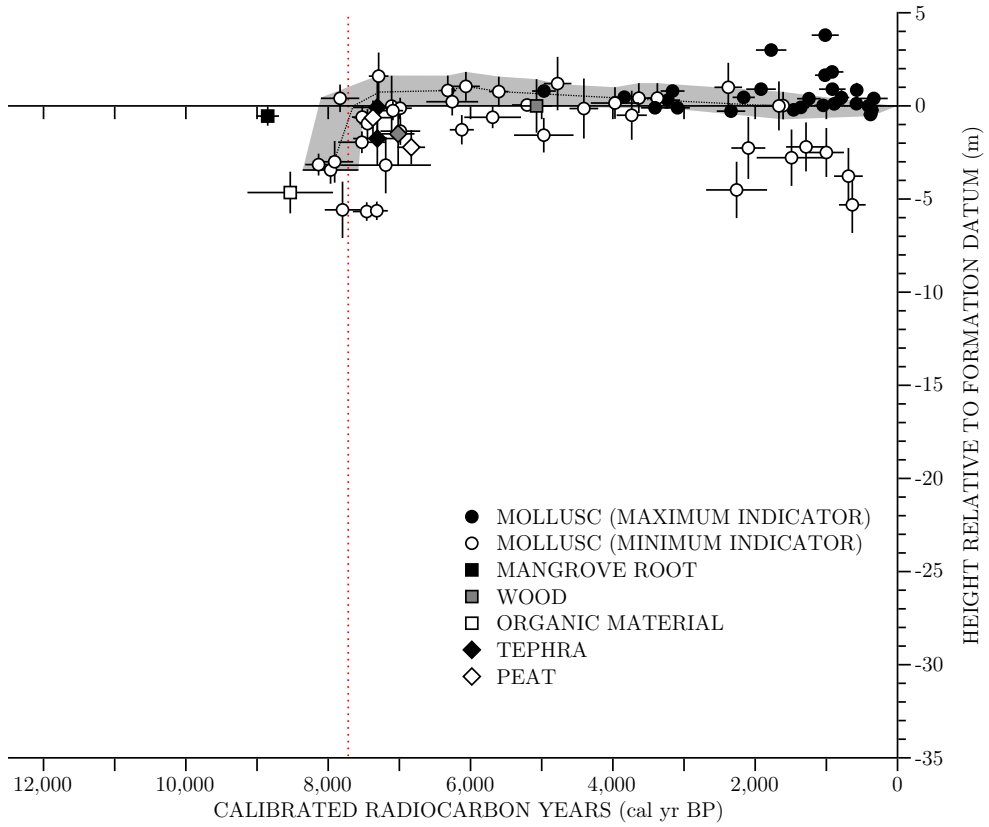

Figure 3.4: Local-scale Holocene sea-level curve for the Auckland-Northland region, New Zealand. This curve has also been plotted with an expanded vertical axis (Figure 3.5). The vertical red dotted line indicates 7,700 cal. yr BP, the approximate time PMSL was attained in the Auckland-Northland region.

value of palaeo sea-level. Similarly, the *A. marina* roots dated by Heap and Nichol (1997) are ignored, as they are rafted material, and are therefore not reliable except as an indicator of the maximum age of the onset of marine-influenced conditions in the Auckland-Northland region.

The cluster of mollusc, peat and tephra ages that delineates the lower limb of the rising envelope c. 7,500 cal. yr BP (B on Figure 3.5, cf. Figure 3.4), suggests that sea-level rose quickly from the −3 m level after 8,000 cal. yr BP. A single radiocarbon age from an *A. stutchburyi* valve within a buried shell layer in Tamaki Estuary (C on Figure 3.5, cf. Figure 3.4; WK7943, Abrahim et al., 2008; Table 3.1), indicates that PMSL was probably attained earlier than 7,500 cal. yr BP, perhaps c. 7,700 cal. yr BP.

A continued rise in sea-level in the Auckland-Northland region is indicated by a mixed shell assemblage from Mangatawhiri Spit radiocarbon dated by Schofield (1973) (D on Figure 3.5, cf. Figure 3.4; NZ833; Table 3.1). Schofield (1973) suggested that the shell assemblage indicated sea levels of +1.1 to +2.3 m above PMSL. However, the shell assemblage is described as being mixed from a variety of environments, including lagoonal and offshore. It

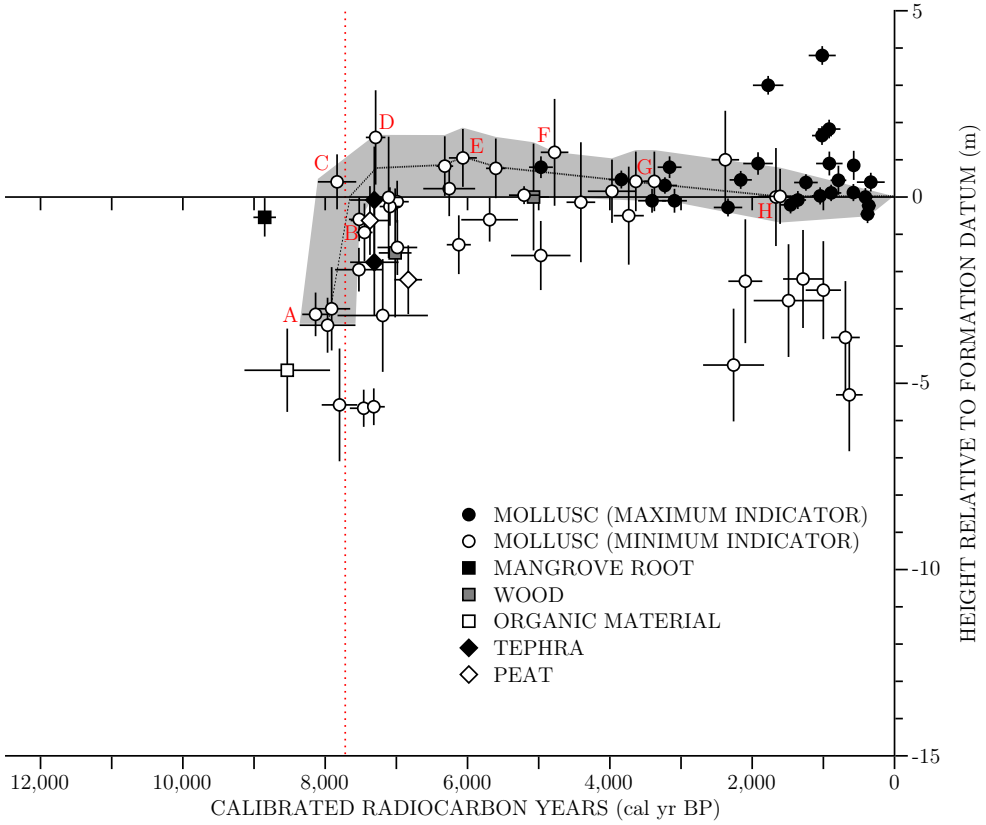

Figure 3.5: Local-scale Holocene sea-level curve for the Auckland-Northland region, New Zealand, plotted with an expanded vertical axis. This curve has also been plotted with standard axes (Figure 3.4). The vertical red dotted line indicates 7,700 cal. yr BP, the approximate time PMSL was attained in the Auckland-Northland region. Letters A–H indicate elements of the reconstruction referred to in the text.

therefore has a poor indicative value. Consequently, it may be more correct for the sea-level trend-line to rise directly from PMSL c. 7,700 call yr BP to the sea-level high suggested by the indicator points at E (Figure 3.5, cf. Figure 3.4).

A sea-level maxima of c. +0.9 m above PMSL from 6,300–5,600 cal. yr BP is suggested by the cluster of three indicator molluscs at E (Figure 3.5, cf. Figure 3.4). Two of these shells were recovered from an upper tidal flat environment by Gibb (1986) (NZ6461, NZ6510, species unidentified; however, over 90 per cent of the indicators presented by Gibb, 1986, were *A. stutchburyi*; Table 3.1), while the third shell is an *A. stutchburyi* valve from a shell bed (WK350, Johnston, 1984; Table 3.1).

The minimum indicator mollusc at F (Figure 3.5, cf. Figure 3.4) is a radiocarbon dated shell presented by Grant-Taylor and Rafter (1971). The shell was recovered from Okahu Bay from an 'incoherent' blue-grey silt which constituted a widespread terrace up to 3 m (10 feet) above PMSL. As the

precise significance of the terrace and shell (species and position) is unclear, the shell is considered to have poor indicative value.

A gradual decline in sea-level from +0.9 m above PMSL c. 5,600 cal. yr BP to c. +0.4 m above PMSL c. 3,500 cal. yr BP is indicated by the cluster of indicators at G (Figure 3.5, cf. Figure 3.4). The two minimum sea-level indicators come from fossil shells recovered from an upper tidal flat environment (NZ6488, NZ6475, Gibb, 1986; Table 3.1), while the two outer maximum indicators both come from the same chenier in Weiti River Estuary (NZ6479, NZ1971, Gibb, 1986; Table 3.1). All four indicators are well constrained by Gibb (1986), and therefore have moderate to high indicative value. The gentle step-down by each of these points from c. 3,850–3,200 cal. yr BP confirms the slow rate of sea-level decline after 5,600 cal. yr BP.

Sea levels in the Auckland-Northland region had most probably dropped back to PMSL by c. 1,600 cal. yr BP. This is suggested by the cluster of minimum and maximum sea-level indicators at H (Figure 3.5, cf. Figure 3.4). Of the two minimum sea-level indicators, one (GX3701; Table 3.1) is a mixed shell assemblage reported by Osborne (1983) from Bream Bay. The species dated is unclear; this indicator therefore has low indicative value. The other minimum indicator is an *A. stutchburyi* valve (WK7827; Table 3.1) recovered by Abrahim et al. (2008) from Tamaki Estuary. As this indicator is better constrained, it has much greater indicative value.

The maximum sea-level indicators distributed within ±0.25 m of PMSL for the last 1,600 cal. yr BP come entirely from the dataset compiled by Gibb (1986). These indicators come from beach ridges and cheniers in Weiti River estuary, and are well constrained with moderate indicative values (NZ6493, NZ6487, NZ6509, NZ1966, NZ1962, NZ1965; Table 3.1). They suggest that sea levels in the Auckland-Northland region have remained within ±0.25 m of PMSL since c. 1,600 cal. yr BP.

3.3.2 Coromandel-Firth of Thames Holocene sea-level interpretation and analysis

The extreme variation among the sea-level index points compiled for the Coromandel Peninsula and the Firth of Thames (Figure 3.6) makes it difficult to definitively elucidate sea-level trends through the Holocene. The maximum index points, all from Miranda and Kaiaua (Gibb, 1986) appear to suggest that sea levels may have broadly dropped towards PMSL since the mid-Holocene. The rate of decline would appear to be broadly synchronous with the rate of sea-level fall in the Auckland-Northland region.

3.3.3 South/southwest North Island Holocene sea-level interpretation and analysis

Sea levels on the south/southwest coast of the North Island rose swiftly from c. −16 m below PMSL c. 9,000 cal. yr BP, to c. −9.3 m below PMSL c. 8,400 cal. yr BP (Figure 3.7). This is indicated by radiocarbon dated carbonaceous

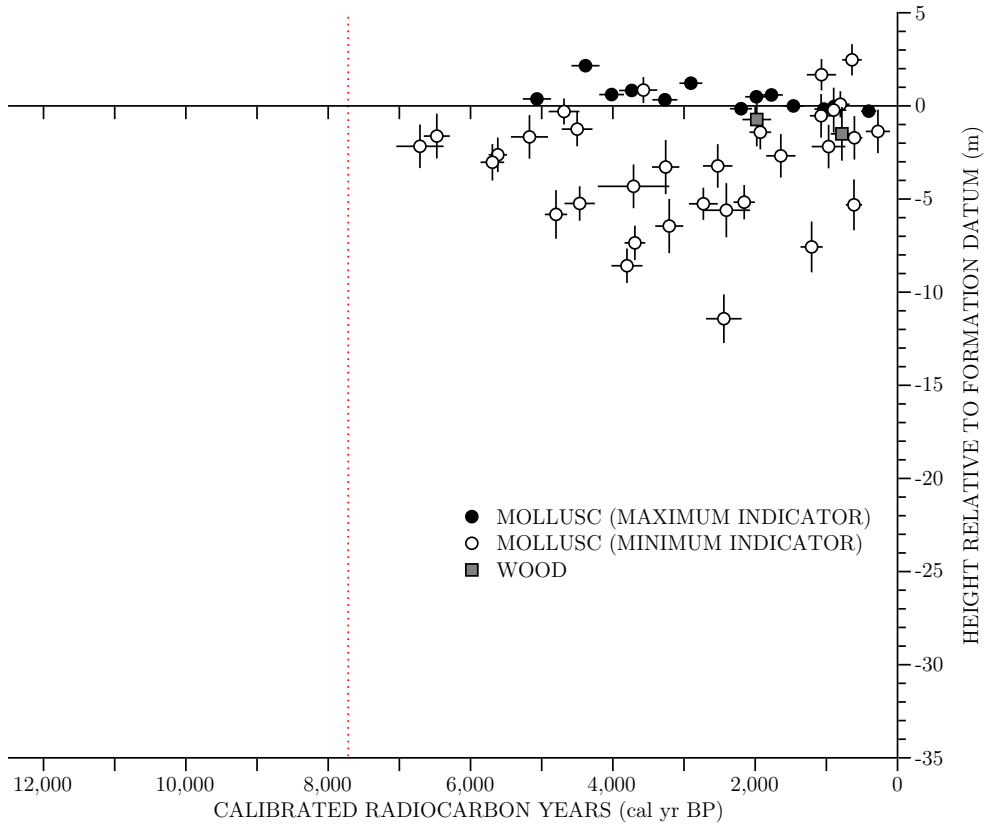

Figure 3.6: Local-scale Holocene sea-level history for the Coromandel-Firth of Thames region, New Zealand. The vertical red dotted line indicates 7,700 cal. yr BP, the approximate time PMSL was attained in the Auckland-Northland region.

muds presented by Gibb (1986). However, Gibb and Cox (2009) suggested that these marine silt layers have no indicative value of palaeo sea-level. Certainly, the ascribed vertical errors (less than ±0.4 m for all the marine mud samples) suggest a degree of precision that may not be warranted.

It is strongly indicated that sea levels in the south/southwest North Island region had reached c. −3 m below PMSL by c. 8,300 cal. yr BP, rising to −1.5 m below PMSL c. 8,100 cal. yr BP. This is indicated by two disarticulated radiocarbon dated *A. stutchburyi* valves recovered from the same core in the lower Manawatu valley (I on Figure 3.7; WK22172, WK22171, see Chapter 7 for details; Table 3.1). The valves are well constrained, and therefore have moderate indicative value.

Two *A. stutchburyi* dates reported by Swales et al. (2005) from Pauatahanui Inlet (J on Figure 3.7; NZ7383, NZ7381; Table 3.1) strongly indicate that PMSL was attained c. 7,500 cal. yr BP, if not shortly before. A sea-level maxima of c. +1.2 m above PMSL c. 6,800 cal. yr BP is suggested by the cluster of three mollusc indicators at K (Figure 3.7). The highest of these is an *A. stutchburyi* valve recovered from an upper tidal flat environment (NZ3118, Gibb, 1986; Table 3.1), while the lower two index points are *A. stutchburyi*

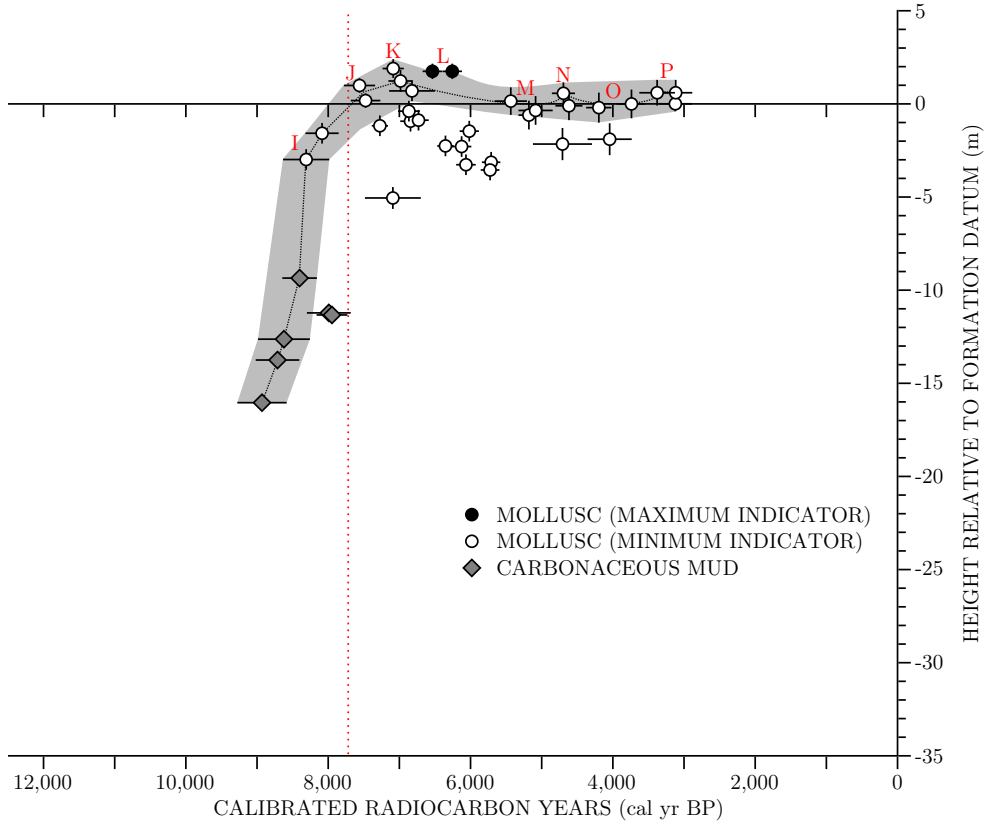

Figure 3.7: Local-scale Holocene sea-level curve for the south/southwest North Island, New Zealand. The vertical red dotted line indicates 7,700 cal. yr BP, the approximate time PMSL was attained in the Auckland-Northland region. Letters I–P indicate elements of the reconstruction referred to in the text.

valves recovered from the lower Manawatu valley (NZ3085, Hesp and Shepherd, 1978; WK22173, see Chapter 7 for details; Table 3.1). All have high indicative value.

The two maximum sea-level indicators at L (Figure 3.7) come from beach ridges at Rangitikei (NZ4606, NZ4719, M.J. Shepherd, unpublished data; Table 3.1). They are of moderate indicative value, and suggest that sea levels on the south/southwest coast of the North Island had not peaked higher than +1.75 m above PMSL in the last 6,500 cal. yr BP.

A gradual decline in sea-level from +1.2 m above PMSL c. 6,800 cal. yr BP to PMSL c. 5,400 cal. yr BP is suggested by the cluster of indicators at M (Figure 3.7). These shells are all estuarine species with moderately high indicative value. The lower two were recovered from an estuarine sequence at Kumenga (NZ3106, NZ3107, Gibb, 1986; Table 3.1). The upper valve is from an estuarine sequence in Pauatahanui Inlet (NZ7387, Swales et al., 2005; Table 3.1).

It is strongly indicated that sea levels rose to c. +0.6 m above PMSL c. 4,700 cal. yr BP (N on Figure 3.7). This is suggested by an articulated *A.*

stutchburyi valve recovered from an estuarine sequence in the lower Manawatu valley (NZ7911, M.J. Shepherd, unpublished data; Table 3.1). The fossil mollusc indicators at O (Figure 3.7) suggest that sea-level did not remain elevated for any great length of time, and had fallen back to PMSL by c. 4,200 cal. yr BP.

Sea levels on the south/southwest coast of the North Island probably remained at PMSL until c. 3,700 cal. yr BP, before rising to +0.6 m above PMSL c. 3,350 cal. yr BP. This rise is suggested by a cluster of fossil mollusc indicators (P on Figure 3.7). These indicators are estuarine shells recovered from estuarine sequences (NZ7421, NZ7393, NZ7397, Swales et al., 2005; Table 3.1), and so have moderately high indicative value. The absence of any palaeo sea-level indicators for the past 3,000 cal. yr BP makes it impossible to comment on the length of this sea-level high.

3.3.4 Christchurch and Pegasus Bay Holocene sea-level interpretation and analysis

Early Holocene sea-level in Christchurch and Pegasus Bay may have reached c. −34 m below PMSL c. 10,350 cal. yr BP. This is suggested by a single radiocarbon age from an unidentified shell (Q on Figure 3.8; NZ7929; Table 3.1) presented by Soons et al. (1997). The facies association of the shell is not reported; the shell therefore has poor indicative value. The vertical error of this indicator may potentially be much greater than is assumed.

The majority of the palaeo sea-level indicators used to construct the palaeo sea-level envelope for Christchurch and Pegasus Bay were presented by Gibb (1986). It is therefore possible to only make broad inferences about the indicative values of these palaeo sea-level indicators. In the case of the cluster of index points at R (Figure 3.8), it is assumed that the radiocarbon dated fossil molluscs have much greater indicative value than the peat and wood deposits. These fossil molluscs indicate that sea-level at Christchurch and Pegasus Bay had risen to c. -23 m below PMSL by c. 9,500 cal. yr BP.

All of the cluster of fossil mollusc indicators at S (Figure 3.8) were presented by Gibb (1986). Delineation of one particular sea-level trend over another is therefore quite arbitrary.

Mid-Holocene sea-level at Christchurch and Pegasus Bay had reached c. −8.4 m below PMSL c. 8,200 cal. yr BP (T on Figure 3.8). This is strongly suggested by the cluster of three indicator molluscs at this depth (NZ4851, NZ1245, NZ4045, Gibb, 1986; Table 3.1). From −8.4 m below PMSL, the cluster of two indicator molluscs at U (Figure 3.8) strongly suggests that sea-level in the Christchurch-Pegasus Bay area had risen to c. −4.5 m below PMSL by c. 7,300 cal. yr BP.

The single fossil mollusc indicator at V (Figure 3.8) suggests that sea-level had risen to c. +1.6 m by 6,600 cal. yr BP. However, this is not definitive. PMSL may have been attained any time between 7,100–6,600 cal. yr BP. There

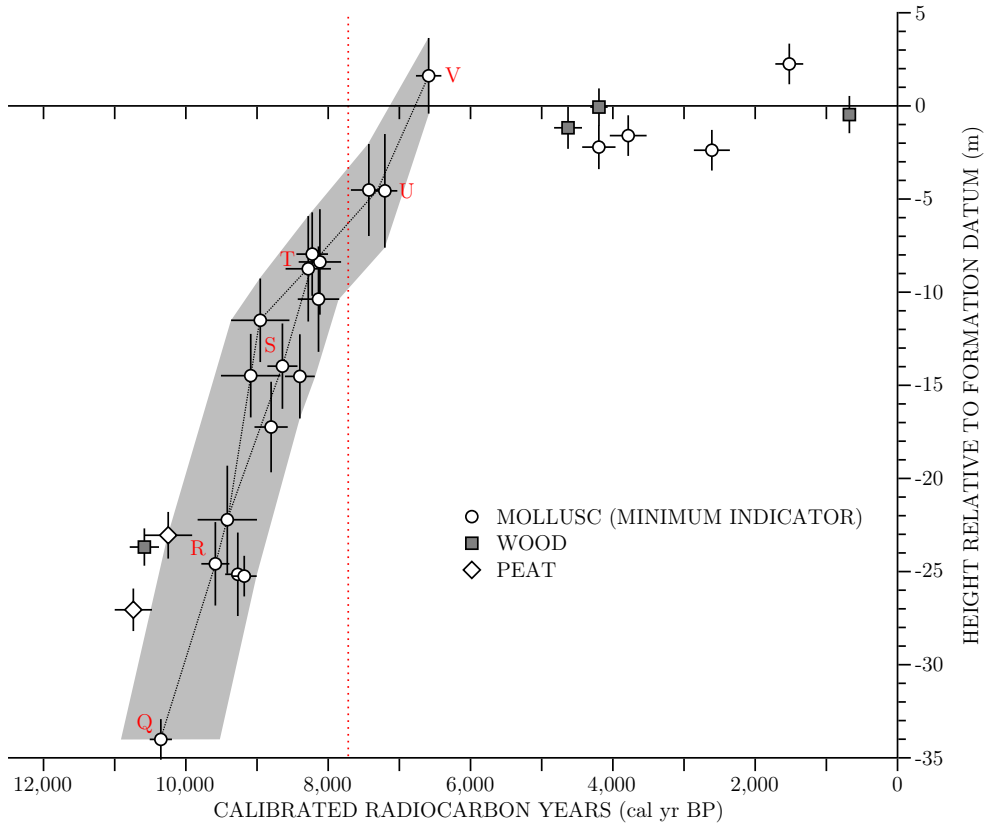

Figure 3.8: Local-scale Holocene sea-level curve for the Christchurch-Pegasus Bay area, New Zealand. The vertical red dotted line indicates 7,700 cal. yr BP, the approximate time PMSL was attained in the Auckland-Northland region. Letters Q–V indicate elements of the reconstruction referred to in the text.

are not sufficient indicators to enable a sea-level envelope to be delineated for the Christchurch and Pegasus Bay region for the remainder of the Holocene.

3.3.5 East Otago Holocene sea-level curve interpretation and analysis

Sea levels at the East Otago Peninsula had reached c. −1 m below PMSL by c. 7,600 cal. yr BP (W on Figure 3.10, cf. Figure 3.9). This is suggested by a single radiocarbon dated mollusc presented by Gibb (1986). Thomas (2000) presented a radiocarbon date from a wood fragment recovered from a transgressive sand unit in Blueskin Bay, which indicated that sea-level may have been c. −1.9 m below PMSL at this time. However, comparatively the wood fragment has a much lower indicative value. The fossil mollusc has therefore been used to delineate the sea-level curve.

Sea levels around the East Otago Peninsula rose to +0.2 m by c. 6,800 cal. yr BP, and remained at this level until at least 6,300 cal. yr BP. This is indicated by three fossil mollusc indicators at this level (X on Figure 3.10,

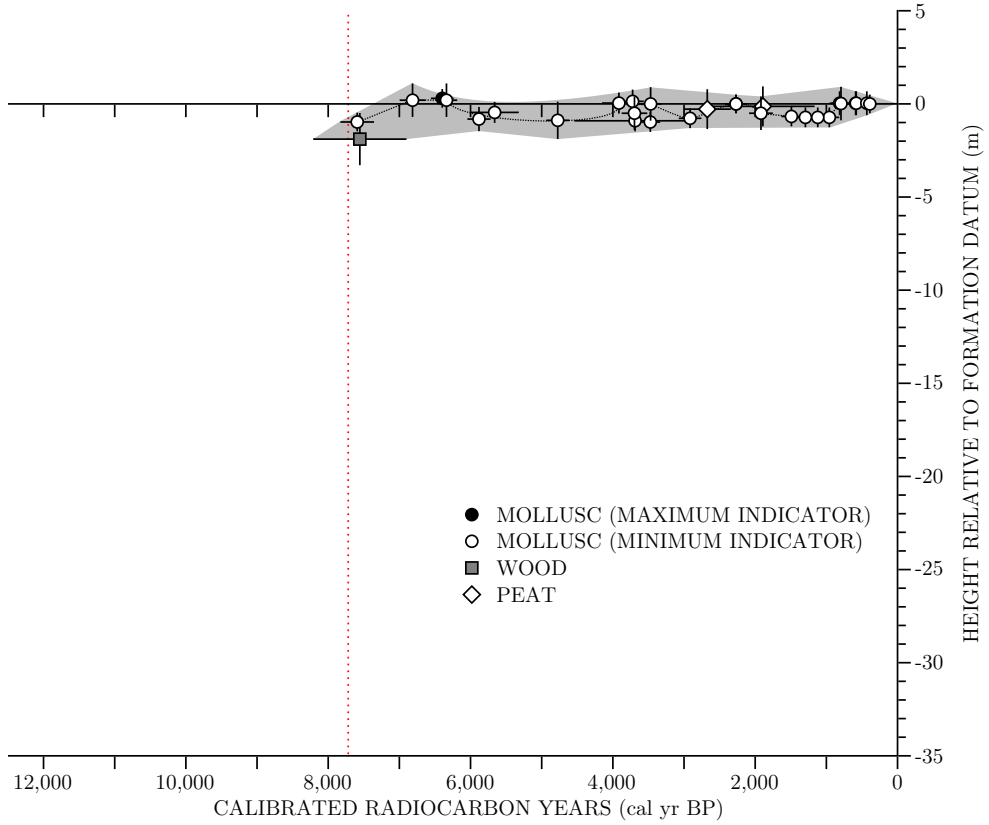

Figure 3.9: Local-scale Holocene sea-level curve for the East Otago Peninsula, New Zealand. This curve has also been plotted with an expanded vertical axis (Figure 3.10). The vertical red dotted line indicates 7,700 cal. yr BP, the approximate time PMSL was attained in the Auckland-Northland region.

cf. Figure 3.9): two minimum indicators, and a maximum indicator (NZ1977, NZ1976, NZ1978, Gibb, 1986; Table 3.1). These fossil molluscs have moderately high indicative value. From this high stillstand two minimum sea-level indicator molluscs (Y on Figure 3.10, cf. Figure 3.9) suggest that sea-level fell to c. −0.6 m below PMSL by 5,700 cal. yr BP. These indicators are both well constrained *A. stutchburyi* valves with high indicative value (NZ6866, Ensor, 1986; NZ6637, Rayns, 1985; Table 3.1).

An articulated *A. stutchburyi* valve recovered from Blueskin Bay Estuary (Z on Figure 3.10, cf. Figure 3.9) strongly indicates that sea levels around the East Otago Peninsula fell to a low of −0.9 m below PMSL c. 4,800 cal. yr BP (NZ3547, Thomas, 2000; Table 3.1). The cluster of mollusc ages at PMSL from 4,000–3,500 cal. yr BP (1 on Figure 3.10, cf. Figure 3.9) suggests that sea-level did not remain at this level for a great length of time.

From PMSL c. 3,500 cal. yr BP, sea levels around the East Otago Peninsula fell again, reaching c. −0.8 m below PMSL c. 2,900 cal. yr BP (2 on Figure 3.10, cf. Figure 3.9). This drop in sea-level is indicated by a well constrained *A.*

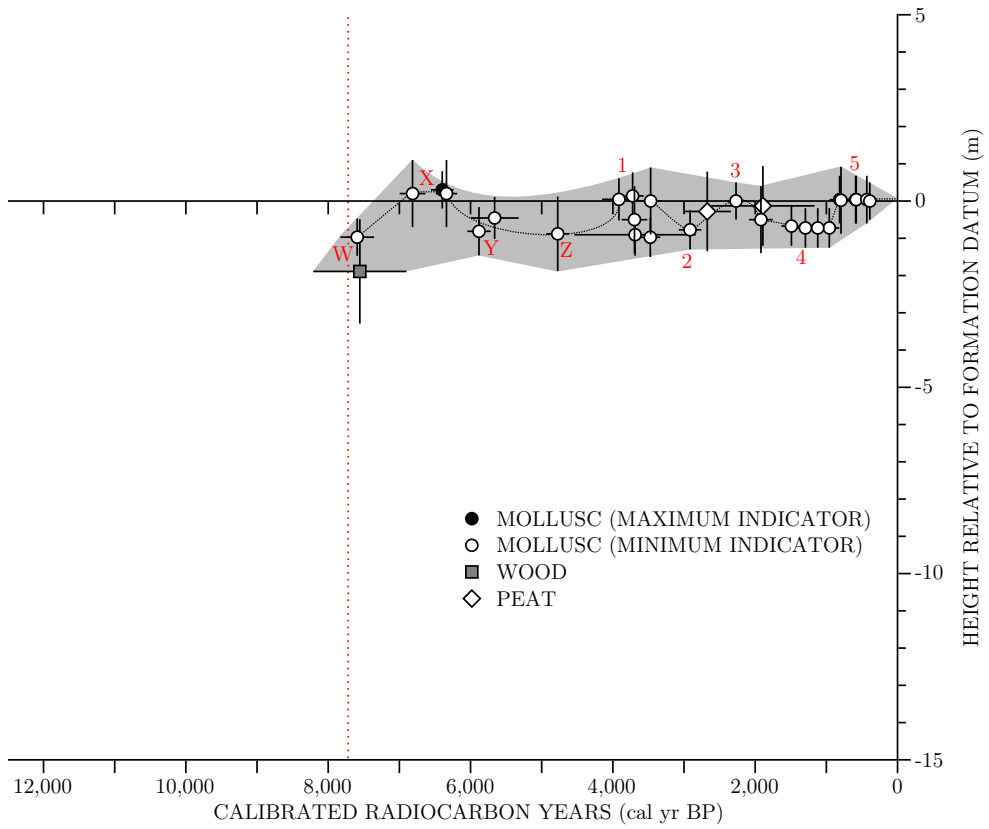

Figure 3.10: Local-scale Holocene sea-level curve for the East Otago Peninsula, New Zealand, plotted with an expanded vertical axis. This curve has also been plotted with standard axes (Figure 3.9). The vertical red dotted line indicates 7,700 cal. yr BP, the approximate time PMSL was attained in the Auckland-Northland region. Letters W–Z and numbers 1–5 indicate elements of the reconstruction referred to in the text.

stutchburyi valve recovered by Rayns (1985) from Hoopers Inlet (NZ6638; Table 3.1).

Sea levels again rose back to PMSL for a short period c. 2,270 cal. yr BP (3 on Figure 3.10, cf. Figure 3.9), before dropping to c. −0.7 m below PMSL (4 on Figure 3.10, cf. Figure 3.9). Sea-level remained stable at this lower level from c. 1900–900 cal. yr BP. This is suggested by four radiocarbon dated fossil *A. stutchburyi* valves (NZ6635, NZ6780, NZ6750, NZ6783; Table 3.1) recovered by Rayns (1985) from Hoopers Inlet. These valves are well constrained, and have high indicative value.

Two fossil mollusc indicators at PMSL c. 800 cal. yr BP (5 on Figure 3.10, cf. Figure 3.9) indicate that sea-level rose very rapidly back to PMSL (c. 0.7 m rise in c. 100 years). The remaining indicators suggest that sea-level around the East Otago Peninsula stabilised at approximately the present level for the remainder of the Holocene.

3.3.6 Comparison between the local-scale sea-level resonstructions and observations of Holocene sea levels in the New Zealand region

Both Clement et al. (2008a,b) and Kennedy (2008) have noted that little attempt has been made in the last 30 years to integrate the growing body of local evidence of Holocene sea-level fluctuations in New Zealand. Post-Gibb (1986) only a small number of investigations have presented new observations of palaeo sea-level changes. Consequently, there are few independent studies of palaeo sea-level fluctuations with which to compare the local-scale Holocene sea-level reconstructions.

Heap and Nichol (1997) studied the geomorphic evolution of Weiti River Estuary (Figure 3.1) in response to Holocene sea-level change, and noted that formation of the earliest beach ridge at the river mouth was delayed until c. 3,200 cal. yr BP (NZ1971; Table 3.1), at least 3,500 years after the attainment of PMSL in the Auckland-Northland region. Heap and Nichol (1997) hypothesised that a temporary sea-level high may have controlled the formation of beach ridges in the estuary. A sea-level highstand would have precluded significant wave reworking of bay-floor deposits. The formation of beach ridges would therefore have been delayed until either the bay floor accreted or sea-level dropped sufficiently to allow wave reworking. Heap and Nichol (1997) lacked unequivocal evidence of higher mid-Holocene sea levels at Weiti River Estuary, and therefore considered the lag in beach ridge formation to be unexplained.

Formation of the earliest beach ridge at Weiti River estuary (NZ1971; Gibb, 1986; Heap and Nichol, 1997; Table 3.1) took place mid-way (G on Figure 3.5, cf. Figure 3.4) through the drop in sea-level from 5,600–1,600 cal. yr BP inferred for the Auckland-Northland region (E to H on Figure 3.5, cf. Figure 3.4). Heap and Nichol's (1997) original hypothesis could therefore be correct. Following the attainment of PMSL in the Auckland-Northland region c. 7,700 cal. yr BP, sea-level rose to +0.9 m above PMSL until c. 5,600 cal. yr BP, too high to allow wave reworking of bay-floor deposits in the estuary. Wave reworking could only take place after sea-level fell to c. +0.2 m above PMSL.

Hicks and Nichol (2007) used diatoms to examine sedimentary successions in a wetland at Kowhai Beach in Northland (Figure 3.3). Hicks and Nichol (2007) analysed diatom salinity zones in a core recovered from the wetland, and inferred that the mid-Holocene tidal range at Kowhai Beach c. 3,350 cal. yr BP was up to 1.2 m above the modern tidal range. This confirms the suggestion that sea-level in the Auckland-Northland region was higher than present during the mid-Holocene. However, the assessment by Hicks and Nichol (2007) places sea-level c. 0.8 m higher than indicated for the Auckland region at this time (G on Figure 3.5, cf. Figure 3.4). Significantly higher sea levels c. 3,300 cal. yr BP appears contrary to the indications for Weiti River Estuary. It may be that Hicks and Nichol (2007) overestimated the degree of sea-level elevation. Kennedy (2008) recently suggested that more studies

from Northland were required, as differing wave climates and sediment supply regimes may have affected observations of palaeo sea-level.

Elsewhere in Northland at sites such as Henderson Bay, One Tree Point and Tokerau Beach (Figure 3.3; e.g., Millener, 1981; Hicks, 1983; Nichol, 2002; Osborne and Nichol, 2006) Holocene dune ridges show significant seaward progradation and decreases in height. These dune sequences may record coastal responses to higher mid-Holocene sea levels (Kennedy, 2008), as well as falling sea levels through the late Holocene. Marks and Nelson (1979) made a similar observation of dune ridge heights on the Omaro Spit in Whangapoua Estuary on the Coromandel Peninsula (Figure 3.3). An overall seaward decrease in the height of successive dune ridges and swales of 2–3 m was noted, which was suggested to reflect a first-order lowering of sea-level during progradation of the barrier. Marks and Nelson (1979) inferred that sea levels in Whangapoua Estuary where at least 2 m higher than present 4,000—5,000 years BP. However, they did not consider the effects of tectonic uplift, which could account for c. 1 m of this elevated sea-level (cf. Table 3.5). Nevertheless, the suggestion of gradually falling sea levels since the mid-Holocene supports the inferred apparent sea-level trend for the Coromandel Peninsula (Figure 3.6).

Hull (1985) suggested that an estuarine sequence described by Hull and Berryman (1986) at Lake McKerrow, on the west coast of the South Island (Figure 3.3), recorded a rise in sea-level c. 4,400 cal. yr BP (from calibration of NZ5398, NZ6369, and NZ6367; originally reported as 4,100 years BP). Hull and Berryman (1986) recovered articulated bivalves from shellbeds within a 3 m thick deposit of well sorted silty sand and sandy silt, inferred to be an estuarine sequence. Bivalves at the base of the sequence were dated at 4413 ± 71 cal. yr BP (NZ6367) and 4448 ± 81 cal. yr BP (NZ6369), ages statistically similar to a bivalve 2 m above which was dated at 4468 ± 39 cal. yr BP (NZ5398). Hull (1985) inferred that this sequence indicated relative sea-level rise, and suggested that as the Lake McKerrow area had been subject to tectonic uplift through the Holocene, the rise was most probably eustatic rather than apparent. Although the Lake McKerrow area is spatially removed from East Otago, Hull's (1985) hypothesised sea-level rise c. 4,400 cal. yr BP appears to coincide with a period of sea-level rise around the Otago Peninsula (Z to 1 on Figure 3.10, cf. Figure 3.9). As there are scant palaeo sea-level indicators for the period Z to 1 (Figure 3.10, cf. Figure 3.9), it is possible that the c. 1 m of sea-level rise inferred for the Otago Peninsula from 4,800 cal. yr BP was considerably more rapid that is supposed.

Gehrels et al. (2008) used foraminiferal analyses on salt marsh cores to construct a proxy sea-level history for Pounawea (Figure 3.3) covering the past 500 years. Gehrels et al. (2008) suggested that sea-level at Pounawea, approximately 100 km southwest of the Otago Peninsula, lay c. -0.38 m below PMSL c. 500 years BP, rising to PMSL by AD 1950. While all the sea-level indicators from the past 900 years BP from the East Otago area lie within ± 0.03 m of PMSL, the error range is considerably greater, up to the order of ± 0.9 m (5 on Figure 3.10, cf. Figure 3.9). The sea-level changes suggested

by Gehrels et al. (2008) therefore fall completely within the sea-level envelope suggested for the Otago Peninsula for the past 500 years BP. The sea-level reconstruction presented by Gehrels et al. (2008) has vertical errors of the order of ±0.05 m, an order of magnitude smaller than the fossil mollusc indicators from the Otago Peninsula, and consequently could be seen to have higher indicative value. Therefore, it is not unreasonable to suggest that sea levels from the East Otago Peninsula south to Pounawea did lie below PMSL for the past 500 years BP, beneath the threshold of detection of fossil mollusc indicators.

3.3.7 Sea-level fluctuations in the New Zealand region: Southwest Pacific context

While the sea-level history presented by Gibb (1986) has become the (de facto) benchmark or standard reconstruction of Holocene sea-level change for New Zealand, it contrasts with much recent research from the wider southwest Pacific region (Clement et al., 2008a,b; Hicks and Nichol, 2007). For example, while many studies from the southwest Pacific have documented higher than present mid-Holocene sea levels (e.g., Nunn, 1995, 1998; Woodroffe et al., 1995; Baker and Haworth, 1997, 2000a,b; Baker et al., 2001a,b; Horton et al., 2007; Sloss et al., 2007; Woodroffe, 2009), New Zealand workers have been noticeably reticent on the subject (Hicks and Nichol, 2007). Kennedy (2008) noted that sea-level histories from southeast Australia and the Tasman Sea in particular may be significant in the New Zealand context, as these records come from within the same oceanic region as New Zealand (e.g., Clark and Lingle, 1979; Pirazzoli, 1991), and so may be expected to yield similar histories of Holocene sea-level fluctuations.

Baker and Haworth (1997, 2000a,b) and Baker et al. (2001a,b) undertook comprehensive studies of late Holocene sea levels along the southeast Australian coast (28–36°S) using fixed biological indicators as a proxy to discern sea-level fluctuations. Baker et al. (2001b) considered the biostratigraphical implications of various fixed biological indicators, and presented an oscillating, or stepped, model of late Holocene sea-level fluctuations. This model indicated that the Holocene marine transgression culminated with sea levels +2 m above PMSL, before falling to +1–+1.4 m above PMSL between 5,460–5,000 cal. yr BP (Baker and Haworth, 2000a,b; Baker et al., 2001a,b). Between 4,000–3,200 cal. yr BP the model suggested that sea levels rose to +1.5–+1.7 m above PMSL (see Baker and Haworth, 2000a). This rise was followed by a marked fall in sea-level to +1.1 m above PMSL c. 3,000 cal. yr BP. Sea levels stayed at this level until c. 2,000 cal. yr BP (Baker and Haworth, 2000b; Baker et al., 2001a,b), before rising to +1.4 m above PMSL for a short period (Baker and Haworth, 2000b; Baker et al., 2001a). Following this rise the model suggested that sea levels fell to PSML.

Sloss et al. (2007) presented a revised Holocene sea-level curve for the southeast coast of Australia (34–36°S), based on a review of previously pub-

lished geochronological results for fossil molluscs, organic-rich mud, mangrove roots, and fixed biological indicators such as wormtubes and barnacles. Sloss et al. (2007) concluded that sea-level on the southeast Australian coast had risen to at least −5 m below PMSL by 8,500 cal. yr BP. PMSL was attained between 7,900–7,700 cal. yr BP. Following the attainment of PMSL sea levels continued to rise, reaching +1.5 above PMSL by 7,400 cal. yr BP. Sloss et al. (2007) indicated that this higher sea-level was sustained until c. 2,000 cal. yr BP, and that a series of minor oscillations may have occurred during the highstand. From 2,000 cal. yr BP Sloss et al. (2007) posited that sea-level fell slowly and smoothly back to PMSL. They also noted that the oscillating models of sea-level change on the southeast Australian coast assumed that wave climate and tidal range had not changed throughout the late Holocene (e.g., Baker et al., 2001a). Sloss et al. (2007) therefore suggested that the sea-level oscillations noted during the mid-late Holocene highstand most likely represented the adjustment of intertidal species to variations in coastal exposure and/or variable wave and climatic conditions during the Holocene.

Horton et al. (2007) utilised subtidal foraminifera recovered in cores collected on the continental shelf near Townsville to reconstruct Holocene sea-level fluctuations for the central Great Barrier Reef. Horton et al. (2007) developed a model capable of inferring the water depths of sediment samples based on their foraminiferal content. These sediment samples were used to produce ten sea-level index points. The index points suggested that sea-level in the central Great Barrier Reef area had reached -8.8 ± 4.5 m below PMSL between 9,300–8,600 cal. yr BP. A mid-Holocene sea-level highstand of $+1.7 \pm 3.9$ m above PMSL was inferred for the period 6,900–6,400 cal. yr BP, before sea-level fell steadily back to PMSL by the present day.

Woodroffe (2009) also presented a sea-level history for the Great Barrier Reef coastline of northern Australia using a foraminifera-based transfer function in conjunction with a review of other palaeo sea-level indicators from the area. Woodroffe (2009) suggested that sea levels rose above PMSL between 8,000–6,200 cal. yr BP, with the peak of the sea-level highstand c. +2.8 above PMSL c. 5,000 cal. yr BP. Woodroffe (2009) posited that sea-level remained relatively stable above +1.5 m above PMSL from 6,200–2,300 cal. yr BP, before falling to PMSL during the past 1,000 cal. yr BP.

3.4 Synthesis and conclusions

Local-scale histories of the Holocene marine transgression in the New Zealand region show an apparent north-south trend in sea-level fluctuations (Figures 3.11 and 3.12). The timing of the attainment of PMSL appears to lag from north to south. In the Auckland-Northland region, PMSL was attained c. 7,700 cal. yr BP, c. 1,000 cal. yrs earlier than has been suggested for the New Zealand region as a whole (cf. Gibb, 1986). Approximately 200 cal. yrs later c. 7,500 cal. yr BP PMSL was attained in the southwest North Island.

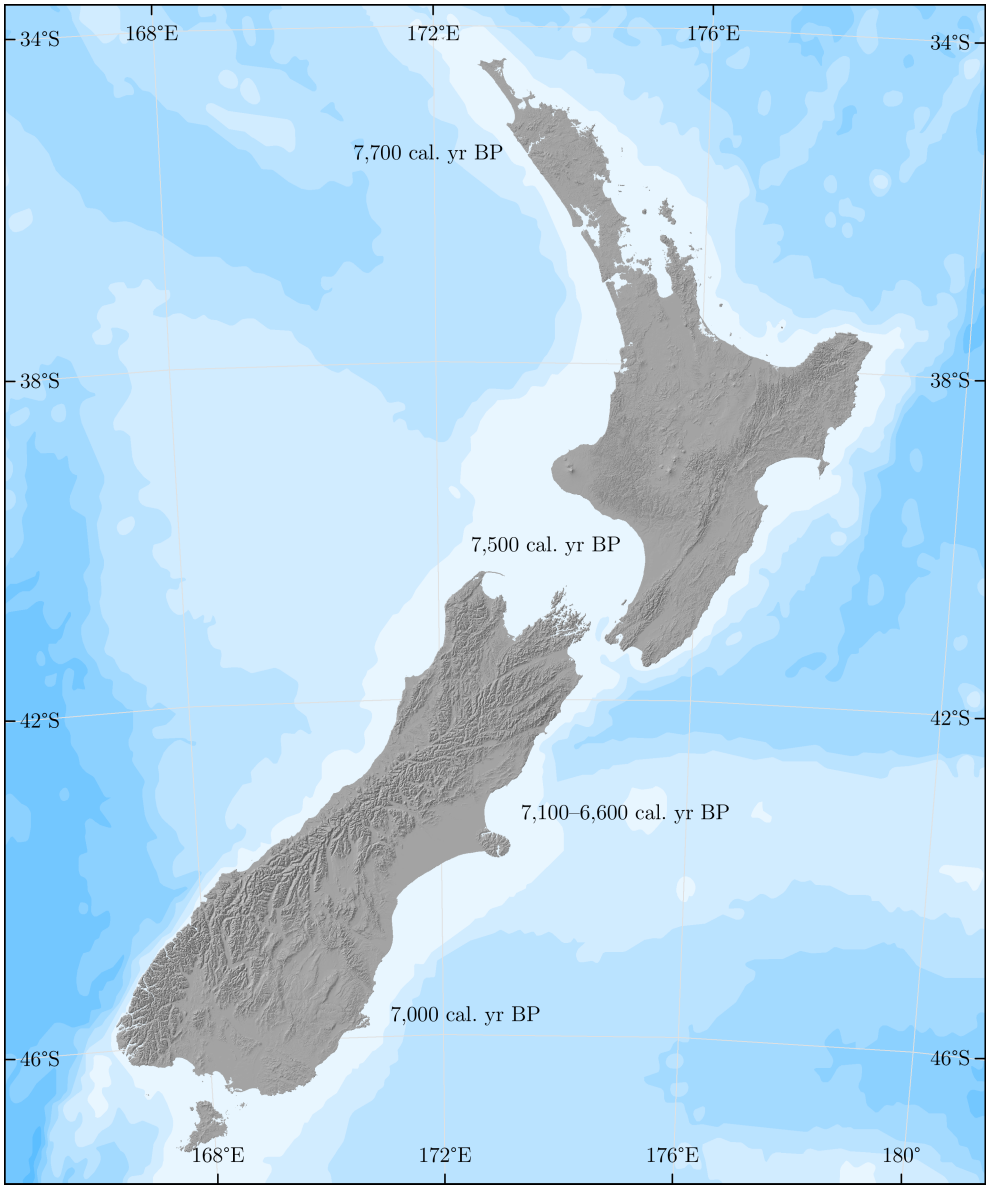

Figure 3.11: Map of the New Zealand region illustrating the north-south lag in the timing of the attainment of PMSL.

PMSL was attained in Pegasus Bay c. 7,100–6,600 cal. yr BP, and in East Otago c. 6,900 cal. yr BP (Figure 3.11).

The same effect is revealed if the phenomenon is looked at from the point of view of a time-slice, c. 7,700 cal. yr BP (Figure 3.12). In the Auckland-Northland region PMSL has been attained at this time. On the south/southwest coast of the North Island sea-level is c. −0.5 to −1.0 m below PMSL, while in Pegasus Bay sea-level is c. −4.5 m below PMSL. In the far south, in East Otago, sea-level is c. −1.0 to −1.5 m below PMSL c. 7,700 cal. yr BP (Fig-

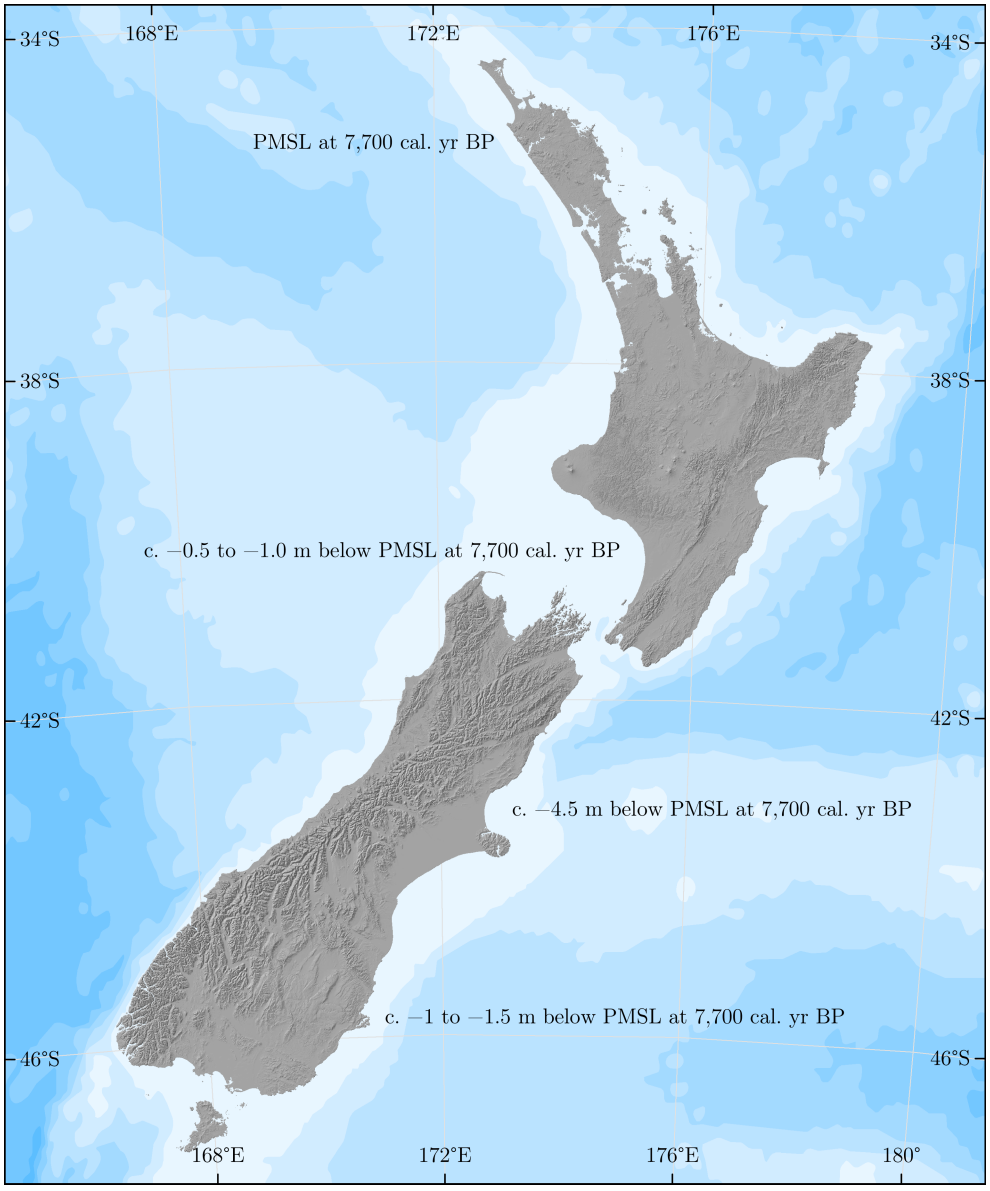

Figure 3.12: Map of the New Zealand region illustrating the position of sea levels at the 7,700 cal. yr BP time-slice.

ure 3.12). The much lower sea-level in Pegasus Bay in the 7,700 cal. yr BP time-slice possibly reflects the error associated with the lack of sea-level indicators from that area which record the final stages of the culmination of the Holocene marine transgression (Figure 3.8). Alternatively, this much lower sea-level may be the product of underestimating the rate of subsidence in Pegasus Bay during the Holocene. While this investigation utilised a value of 0.20 mm yr^{-1} for the rate of subsidence, as it represented an average of all suggested rates, it may be that the true rate of subsidence in Pegasus Bay is

close to (or even greater than) the higher rate of 0.4 mm yr^{-1} proposed by Barnes (1995).

It is also possible to discern a north-south lag in the timing of sea-level fluctuations following the attainment of PMSL between the south/southwest coast of the North Island and the East Otago Peninsula (Figure 3.13). Between c. 7,500–2,500 cal. yr BP sea-level rises and falls on the North Island's southwest coast are followed approximately 500–1,000 years later by similar fluctuations at East Otago. However, it is unclear why this effect is not manifest in the Auckland-Northland region. The lack of mid-to-late Holocene sea-level indicators from Pegasus Bay precludes any conclusions for that area.

Thom and Chappell (1975) suggested that major differences between Holocene sea-level histories from different areas may be explained in the context of global isostatic processes. The hydro-isostatic model presented by Nakada and Lambeck (1989) predicted that during the Holocene marine transgression sea levels around the Australian continent would increase northwards with increasing distance from Antarctica. However, Bryant (1992) and Haworth et al. (2002) tested the implied suggestion of southern latitude downwarping during the Holocene, and found that there was sufficient evidence to indicate that north-south differences in Holocene sea levels due to hydro-isostatic influences were either limited or non-existent. Regardless, the trend identified for New Zealand would appear to suggest downwarping, or some other external driver, north, rather than south of New Zealand.

While the Auckland-Northland regional sea-level record suggests a slow, steady decline in sea-level following a maxima of +0.9 m above PMSL c. 6,300–5,600 cal. yr BP, the sea-level histories of the southwest North Island and the East Otago Peninsula show sea-level fluctuations of c. ±1 m about PMSL through the Holocene. Baker and Haworth (1997, 2000a) and Lewis et al. (2008) have suggested that sea levels in far-field locations oscillated during the mid- to late-Holocene in response to fluctuations of climate or ice-sheet mass. Such oscillations have been documented for the southeast coast of Australia (e.g., Baker and Haworth, 1997, 2000a,b; Baker et al., 2001a,b). However, Woodroffe (2009) suggested that there was no evidence in northern Australia for sea-level oscillations, although they were not ruled out entirely. Woodroffe (2009) further noted that geophysical models of sea-level changes for the region predict a smooth decline in sea-level from the peak of the mid-Holocene high-stand. Sloss et al. (2007) noted potential oscillations on the southeast coast of Australia, but concluded that they were due to the adjustment of fixed biological indicator species to changing wave and climatic conditions, rather than external driving by climatic or ice sheet mass fluctuations. If these external forces were driving the sea-level fluctuations inferred for the southwest North Island and the Otago Peninsula, it is unclear why these oscillations are not recorded in the Auckland-Northland region.

In New Zealand there are few independent observations which uphold the suggestion of an earlier attainment of PMSL; however, there are a number of recent studies from Australia which do support this. The study by Sloss et al.

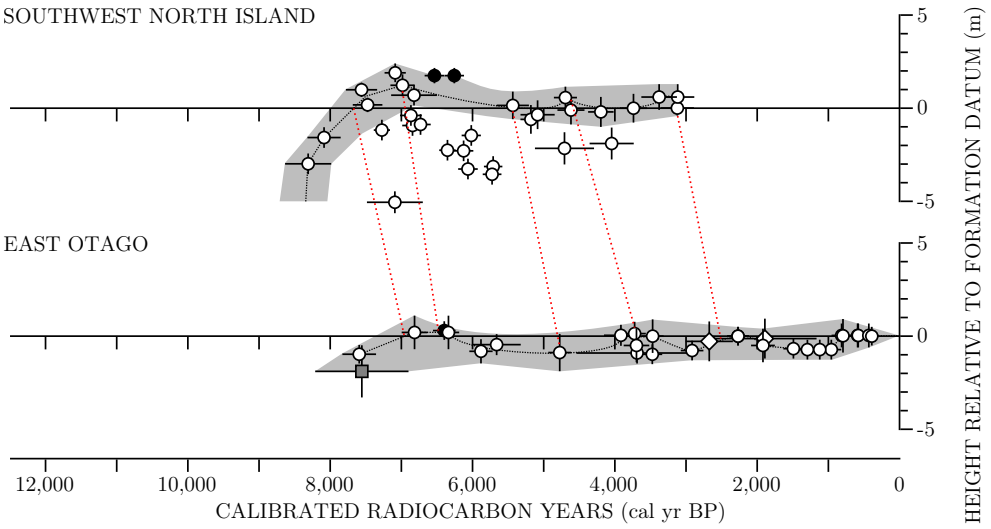

Figure 3.13: Comparison of Holocene sea-level fluctuations on the south/southwest coast of the North Island, and around the East Otago Peninsula, illustrating the 500–1,000 year north-south lag between the two areas.

(2007) is perhaps the most relevant as it covers the length of the east Australian coast between 34–36°S, while the Auckland-Northland region lies between 35–37°S. The attainment of PMSL on both the southeast Australian coast and in the Auckland-Northland region appears to have occurred synchronously.

Taken altogether the local-scale Holocene sea-level histories for regions within the New Zealand archipelago are highly variable, quite contradictory, and appear to be responding inconsistently to different external drivers. However, the histories are compiled from review data, and therefore the sea-level interpretations may be less accurate than is implied by the sea-level envelopes. Indeed, some variables such as sediment compaction, which is suggested to have occurred in some of localities from which sea-level indicators were recovered (e.g., Swales et al., 2005), cannot be easily quantified or assessed. In terms of the apparent north-south trend in the timing of the attainment of PMSL, it must therefore be considered that this may be an artifact of the sea-level review data, rather than a recorded response to an external driver. However, this is not a question that can necessarily be answered at this point in time, given both the quality and quantity of the review data, and the current state of knowledge of sea-level changes in the New Zealand region.

Regardless, this study represents the most up-to-date assessment of Holocene sea-level changes in the New Zealand region. The assertion by Clement et al. (2009a,b) that New Zealand regional sea-level datasets may hide or mask local trends in sea-level is confirmed. There is clearly scope for studies to target the recovery of palaeo sea-level indicators of high indicative value to fill gaps and deficiencies in the current state of knowledge of palaeo sea-level changes. These gaps are most evident in the Christchurch-Pegasus Bay region through the last 6,700 cal. yrs BP, and the southwest North Island

through the last 3,000 cal. yrs BP. There is also a deficiency in the Otago Peninsula area through the early Holocene leading up to the attainment of PMSL. The choice of indicators to fill these gaps and deficiencies is crucial. Studies such as Gehrels et al. (2008) illustrate that palaeo sea-level histories, such as the local-record presented for the East Otago Peninsula, assembled using indicators such as fossil molluscs may only reconstruct coarse fluctuations in sea-level. This is a caveat that extends to all the local-scale sea-level records presented.

Chapter 4

Geology and geomorphology of the lower Manawatu valley

4.1 Introduction

This chapter introduces the setting of the Manawatu coastal plain, and reviews the area's geology, geomorphology, tectonic regime, climate, vegetation, and contemporary coastal environment to provide context for the chapters that follow. The Manawatu region encompasses a low lying, undulating coastal plain on the southwest coast of the North Island, New Zealand (Figure 4.1). The Manawatu is bounded to the south and east by the Tararua and Ruahine Ranges, and to the west by the Tasman Sea. The main municipality is Palmerston North City, and there are a large number of satellite towns spread across the coastal plain. Administratively the Manawatu region is bordered to the north by the Rangitikei District (north of Bulls), and in the south by the Horowhenua District (Levin south).

4.2 Geology

4.2.1 Geological setting

The Manawatu region of the southern North Island, New Zealand (Figure 4.1), lies 200 km northwest of the Hikurangi Trough, at the southern end of the Tonga-Kermadec subduction zone which forms the boundary between the Australian and Pacific lithospheric plates (Figures 4.2 and 4.3). The North Island is positioned on the Australian Plate, which is being obliquely underthrust from the east by the subducting Pacific Plate at the rate of 40–50 mm yr^{-1} (Walcott, 1978; Lamb and Vella, 1987; DeMets et al., 1990; Cashman et al., 1992; Begg and Johnston, 2000). Much of the strain of the plate collision is

Figure 4.1 *(following page)*: Locality map of the Manawatu region, southwest North Island, New Zealand. Base landcover raster image by Geographx.

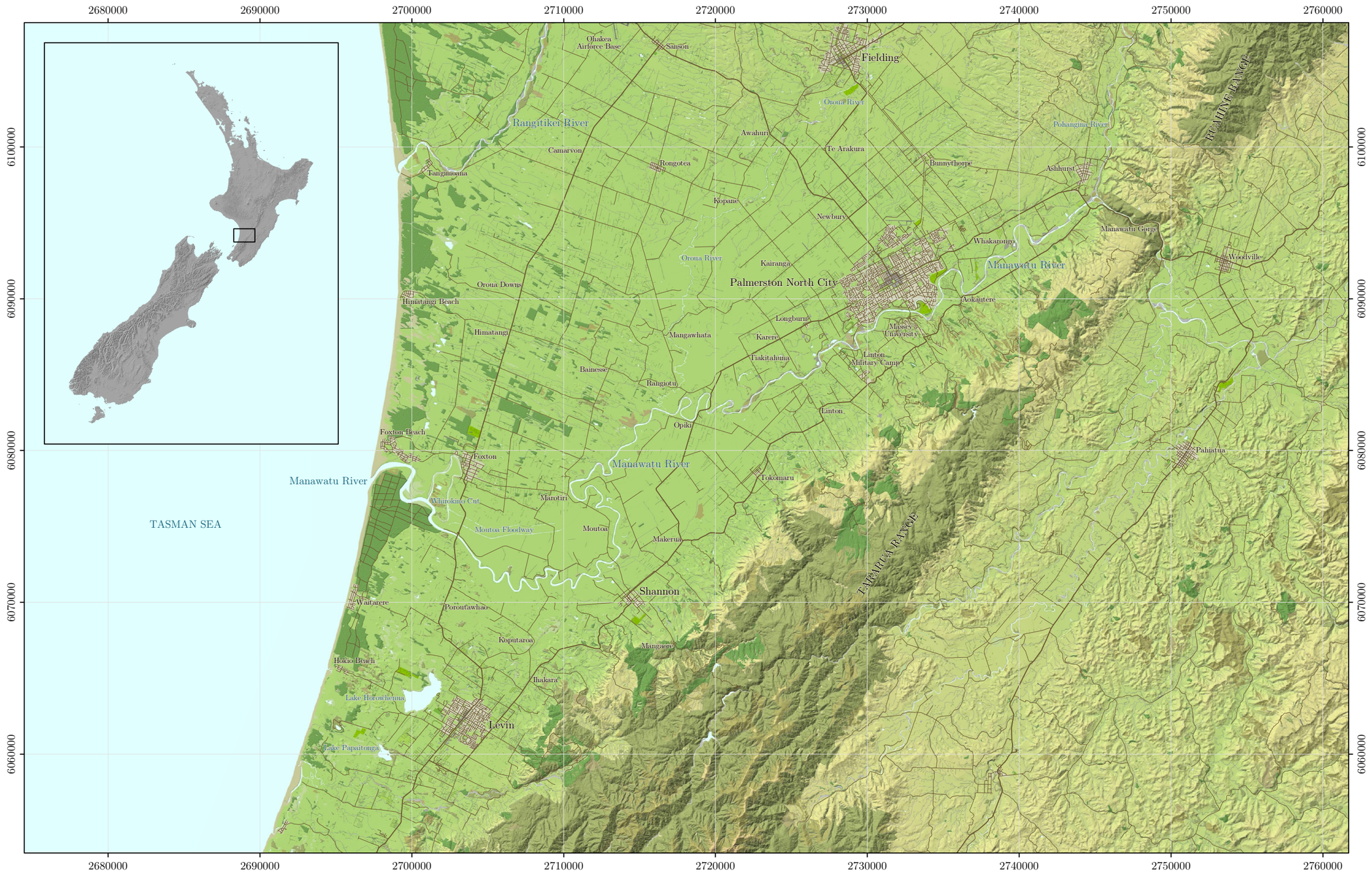
2680000
2690000
2700000
2710000
2720000
2730000
2740000
2750000
2760000
6100000
6090000
6080000
6070000
6060000
Ohakea Airforce Base
Sanson
Fielding
Oroua River
Rangitikei River
Awahuri
Pohangina River
RUAHINE RANGE
Canarvon
Te Arakura
Rongotea
Bunnythorpe
Ashhurst
Tangimoana
Kopane
Newbury
Manawatu Gorge
Whakarongo
Oroua River
Kairanga
Woodville
Manawatu River
Oroua Downs
Palmerston North City
Himatangi Beach
Aokautere
Longburn
Himatangi
Massey University
Mangawhata
Karere
Linton Military Camp
Tiakitahuna
Bainesse
Rangiotu
Linton
Opiki
Foxton Beach
Foxton
Manawatu River
Manawatu River
Pahiatua
Tokomaru
TASMAN SEA
Whirokino Cut
Marotiri
Moutoa Floodway
Moutoa
Makerua
TARARUA RANGE
Shannon
Waitarere
Poroutawhao
Koputaroa
Mangaore
Hokio Beach
Ihakara
Lake Horowhenua
Levin
Lake Papaitonga

being transferred to the leading edge of the Australian plate. As a result the North Island landmass, which is formed by the leading edge of the Australian Plate, is undergoing crustal shortening and is actively deforming (Cole and Lewis, 1981; Begg and Johnston, 2000; Begg et al., 2005). The over-ridden Pacific Plate dips to approximately 30 km depth beneath the southern North Island, where the plate interface, or subduction thrust, is locked due to high frictional sheer stresses (Figure 4.3; e.g., Walcott, 1984, 1987; Robinson, 1987; Smith et al., 1989; Stern et al., 1992, 1993).

4.2.2 Torlesse basement

The Manawatu is underlain at depth by indurated quartzofeldspathic and lithic sandstone (greywacke) and mudstone (argillite) basement rocks (Lillie, 1953; Kingma, 1957, 1962, 1967), which form part of the Torlesse lithostratigraphic composite terrane (e.g., Campbell and Coombs, 1966; Coombs et al., 1976; Mortimer, 1994; Lee and Begg, 2002). The rocks of the greywacke basement were laid down in the New Zealand Geosyncline from sediment eroded from Gondwanaland. The few fossils preserved within the greywacke have shown that it ranges in age from Permian to Late Jurassic, though the rocks are mostly Triassic in age (Begg et al., 2005). The Torlesse greywackes were elevated from the New Zealand Geosyncline during the Rangitata Orogeny. A period of tectonic quiescence during the Tertiary allowed the landscape to be denuded, forming a peneplain of the New Zealand continent (e.g., Cotton, 1957b; Stevens, 1957; Kingma, 1958). Subsequent movement of the New Zealand continental block associated with sea-floor spreading and the formation of the Tasman Sea led to a marine transgression which submerged most of the continent by the Oligocene. Collision of the Australia and Pacific Plates began approximately 25 Ma, compressing the New Zealand continental crust and initiating the Kaikoura Orogeny, which heavily compressed, folded and faulted the Torlesse terrane, with inter-fault blocks being elevated to form the axial ranges of the North and South Islands.

4.2.3 Axial ranges

The Tararua and Ruahine Ranges form the southern part of the axial range of mountains which extend throughout the North Island (Figures 4.1 and 4.2). The ranges bound the Manawatu region to the south and east, and are composed of well dissected Torlesse basement greywacke blocks mantled with marine cover beds (Figure 4.4). The Wellington, Ruahine, and Mohaka faults border the ranges to the southeast, while numerous other faults intersect the ranges (Figure 4.4). The uplift of ranges was probably initiated during the Pliocene by upwarping of the greywacke basement into a broad geanticlinal dome (Heerdegen, 1972). However, the major phase of uplifting was only initiated c. 1–2 Ma (Lamb and Vella, 1987; Heerdegen and Shepherd, 1992), when reverse faults on either side of the ranges led to uplift of the mountains as a horst block (Marden, 1984). Uplift varies spatially along the ranges from

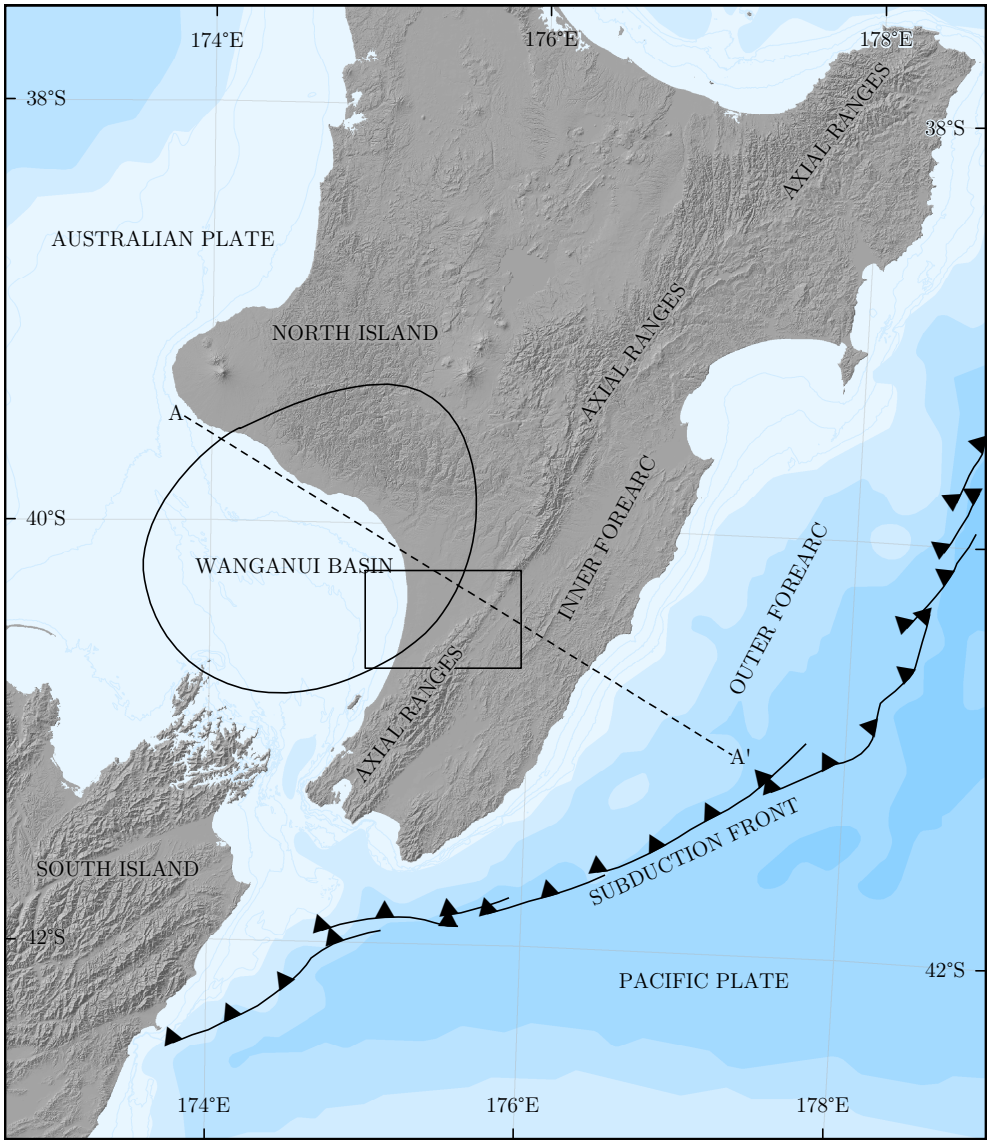

Figure 4.2: Tectonic setting of the southern North Island, New Zealand (after Walcott, 1978; Cole and Lewis, 1981; Lewis and Pettinga, 1993; Beanland, 1995; Beanland and Haines, 1998; Beanland et al., 1998). Line A–A' is the approximate position of the schematic cross-section shown in Figure 4.3. The black rectangle shows the extent of the detailed 1:250,000 scale locality and geological maps of the Manawatu region (Figures 4.1 and 4.4).

1–4 mm yr^{-1} (e.g., Wellman, 1972; Ghani, 1978; Pillans, 1986; Whitehouse and Pearce, 1992), due to the varying deformational histories of the individual fault blocks which make up the ranges (e.g., Heerdegen and Shepherd, 1992; Kamp, 1992a,b). The Ruahine Ranges, in the north, are separated from the Tararua Ranges, in the south, by the Manawatu Gorge, an antecedent cutting maintained by the Manawatu River (Figure 4.1). (Lillie (1953) has

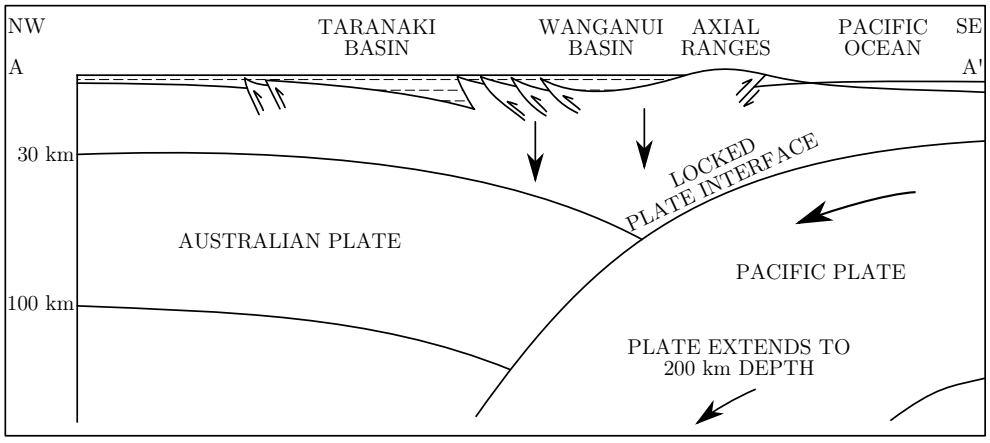

Figure 4.3: Schematic cross-section across the interface between the Pacific and Australian tectonic plates in the vicinity of the Wanganui Basin, southern North Island, New Zealand (after Stern et al., 1992, 1993). The approximate line of the cross-section is shown on Figure 4.2.

summarised the literature discussing the origins of the gorge.) In the vicinity of the gorge the ranges achieve elevations of 350–400 m. South of the gorge the Tararua Ranges increase in height to c. 1500 m, while north of the gorge the Ruahine Ranges reach elevations in excess of 1700 m.

4.2.4 Wanganui Basin

West of the axial ranges lies the South Wanganui Basin, a 200 by 200 km ovoid back-arc subsiding sedimentary basin extending from the central volcanic region in the north to the Marlborough Sounds in the south (Figure 4.2; Katz, 1968; Anderton, 1981; Katz and Leask, 1990). The South Wanganui Basin is the surface manifestation of a progressive, southward-travelling, lithospheric-scale downwarp resulting from high friction at the subduction interface between the Australian and Pacific Plates (e.g., Walcott, 1970; Stern and Davey, 1989; Stern et al., 1992, 1993; Wilson and McGuire, 1995). Subsidence of the basin was initiated during the Pliocene when the mass of the leading edge of the subducting Pacific Plate began to exert a net downward pull on the overlying lithosphere in locations where the plate is locked with the Australian Plate (Stern et al., 1992, 1993). Sedimentation within the South Wanganui Basin broadly matched the rate of subsidence for much of its history (Naish, 1997; Naish and Kamp, 1997b; Carter and Naish, 1998; Naish et al., 2005). As a result at least 4–5 km of largely shallow marine Plio-Pleistocene sediment has accumulated within the basin (e.g., Feldmeyer et al., 1943; Fleming, 1953b; Rich, 1959; Cope and Reed, 1967; Katz, 1968; Anderton, 1981). The basin fill comprises numerous cycles of deep and shallow marine sedimentary successions related to glacio-eustatic sea-level cycles and represents one of the most complete and undeformed shelf and shallow marine Plio-Pleistocene records in the world (Pillans, 1983; Abbott and Carter, 1994; Naish and Kamp, 1995,

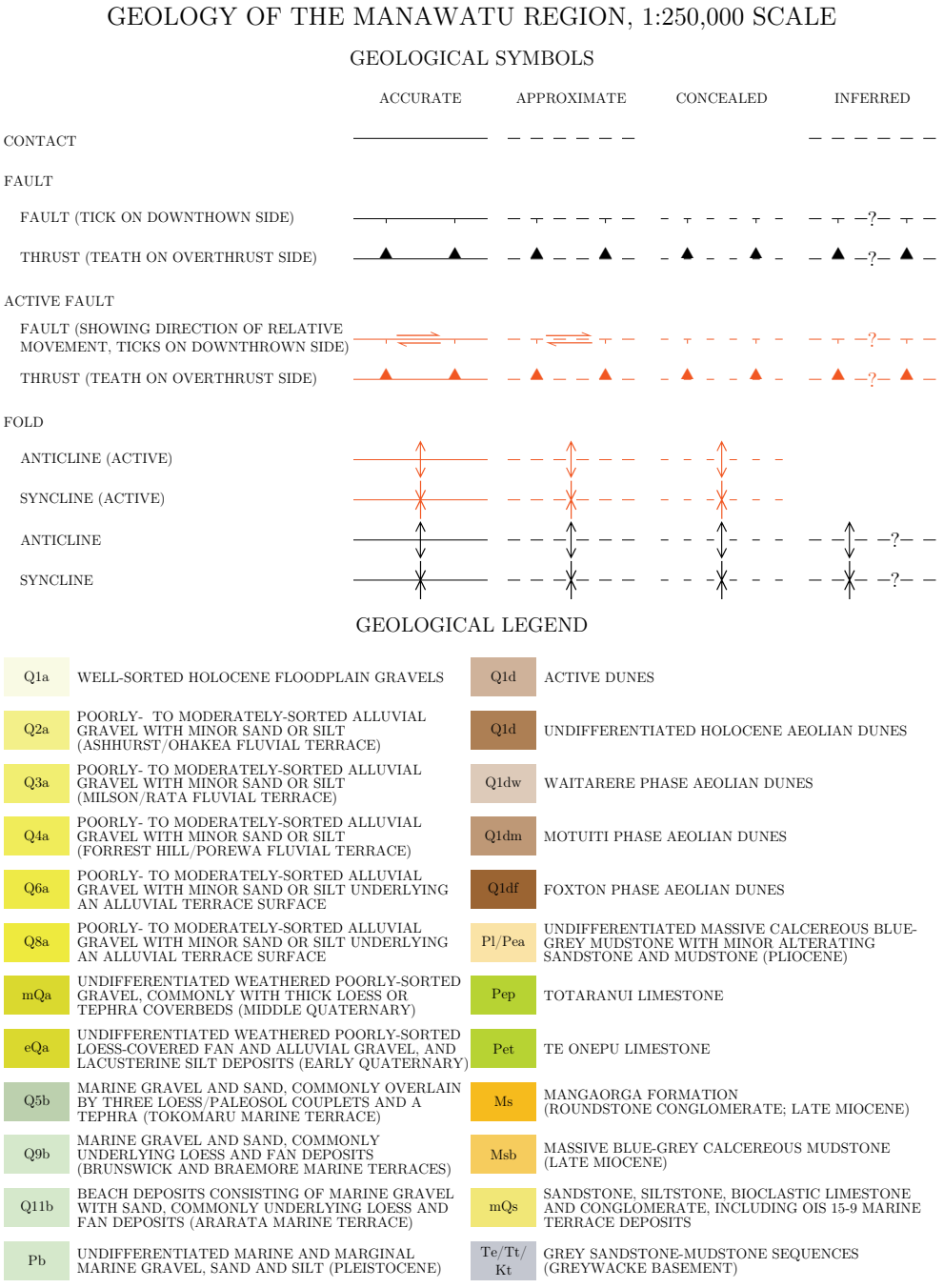

Figure 4.4 *(above and facing page)*: 1:250,000 scale geological map of the Manawatu region (after Kingma (1962), Cowie et al. (1967), Pillans (1990a), Begg and Johnston (2000), Lee and Begg (2002), Townsend et al. (2008), and unpublished data from the QMAP project made available by D. Townsend). The black outline marks extent of the large-scale maps of the Manawatu River terraces (Figure 4.10).

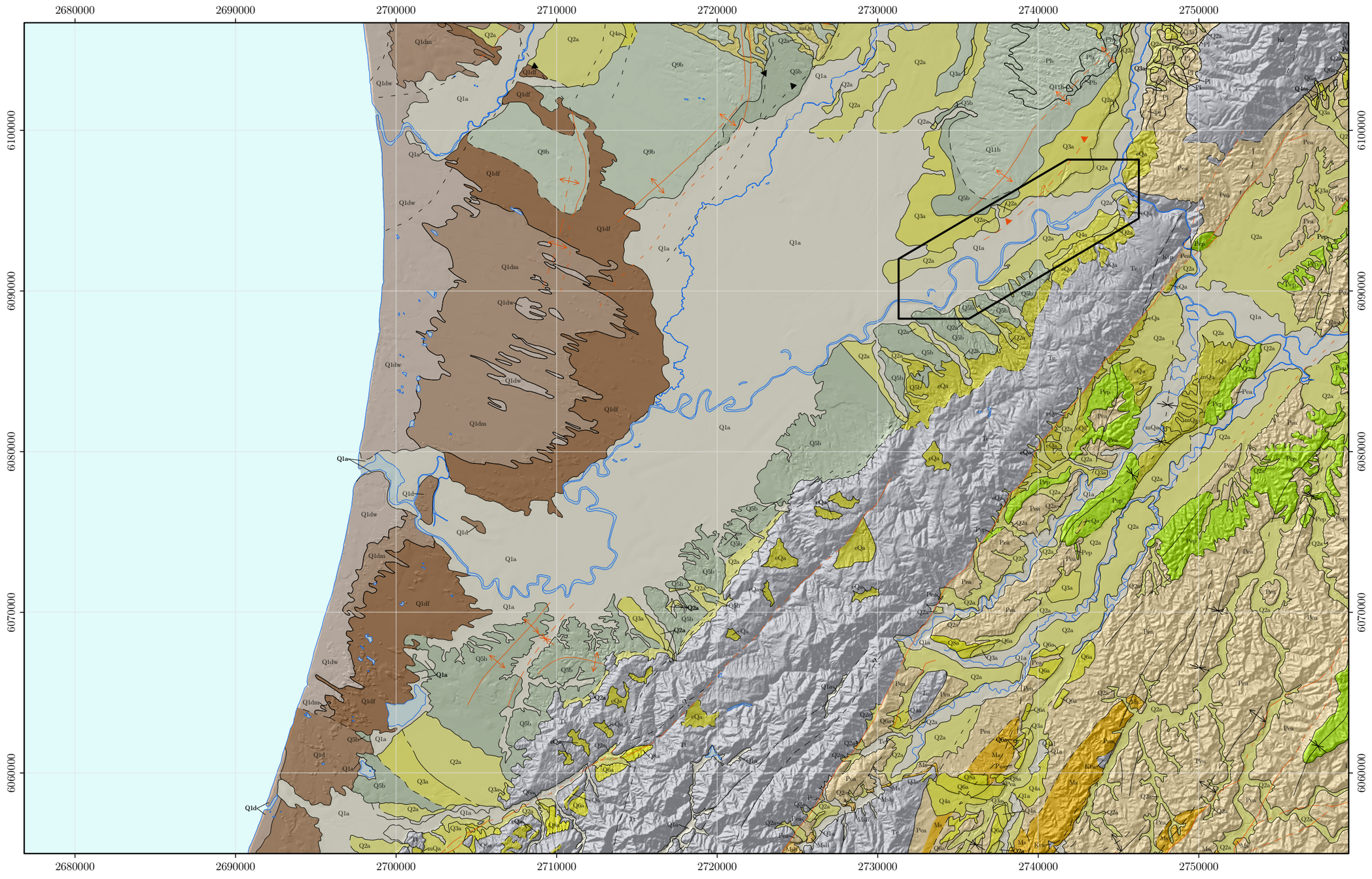
2680000
2690000
2700000
2710000
2720000
2730000
2740000
2750000
6100000
6090000
6080000
6070000
6060000

1997a,b; Journeaux et al., 1996; Naish et al., 1998; Saul et al., 1999). Through the Plio-Pleistocene gradual movement of the basin depocenter to the south and west caused emergence of the basin in the north, and produced a regional 4.5 degree southward tilt of the strata within the basin.

4.2.5 Fault structures

Continental shortening across the Wanganui Basin has resulted in the formation of a number of northeast to north-northeast striking active faults (Figure 4.4). These faults are long-lived, and are believed to have been active since the early Pleistocene (Begg et al., 2005). Yeats (1986) suggested that they may be oblique-slip faults. However, seismic reflection studies indicate that they are reverse faults, dipping either westward or eastward (e.g., Anderton, 1981; Melhuish et al., 1996; Lamarche et al., 2005). Many of the faults are buried, and fail to penetrate to the surface.

Where the faults are buried at depth they manifest anticlinal folds in the landscape (Figure 4.5). Early geological and seismic reflection surveys by Feldmeyer et al. (1943) and Te Punga (1957) outlined a series of folds thought to be fault controlled, though the faults did not appear to reach the surface. Both Feldmeyer et al. (1943) and Te Punga (1957) inferred that basement 'highs' or 'ridges' of rock formed the core of the anticlines.

Te Punga (1957) described five anticlines of 'prominent geomorphic expression' across the Manawatu coastal plain: the Marton; Mt Stewart-Halcombe; Feilding; Oroua; and Pohangina (Figure 4.5). Rich (1959) subsequently identified the Himitangi anticline, and noted the presence of an elongate depression, the Kairanga trough, that extends from Feilding township to Lake Horowhenua (Figure 4.5). A further anticline, the Shannon, was described by Hesp (1975) in the vicinity of Shannon township (Figure 4.5).

The five northernmost anticlines (Marton, Mt Stewart-Halcombe, Himitangi, Fielding and Pohangina) share a number of common morphological characteristics (Jackson et al., 1998; Clement and Brook, 2008):

1. Steep eastern limbs (<60 degrees), compared with gentle western limbs (2–4 degrees),
2. A drainage divide close to the eastern limb of each anticline, apparently coincident with the anticlinal axis,
3. Parallel streams draining the shallow western limbs of the folds,
4. A fold axis that plunges to the south,
5. And, as a consequence of the southward tilting, the capture of northern, upslope low-relief streams by southern, downslope main (trunk) streams.

Similarly, the Shannon anticline is described by Hesp (1975) as an asymmetrical fold with a shallow western limb (1–2 degrees), the axis of which tilts strongly to the south.

A seismic reflection survey undertaken by Bounty Oil in 1970 delineated the anticlinal structures. However, only a superficial interpretation of the

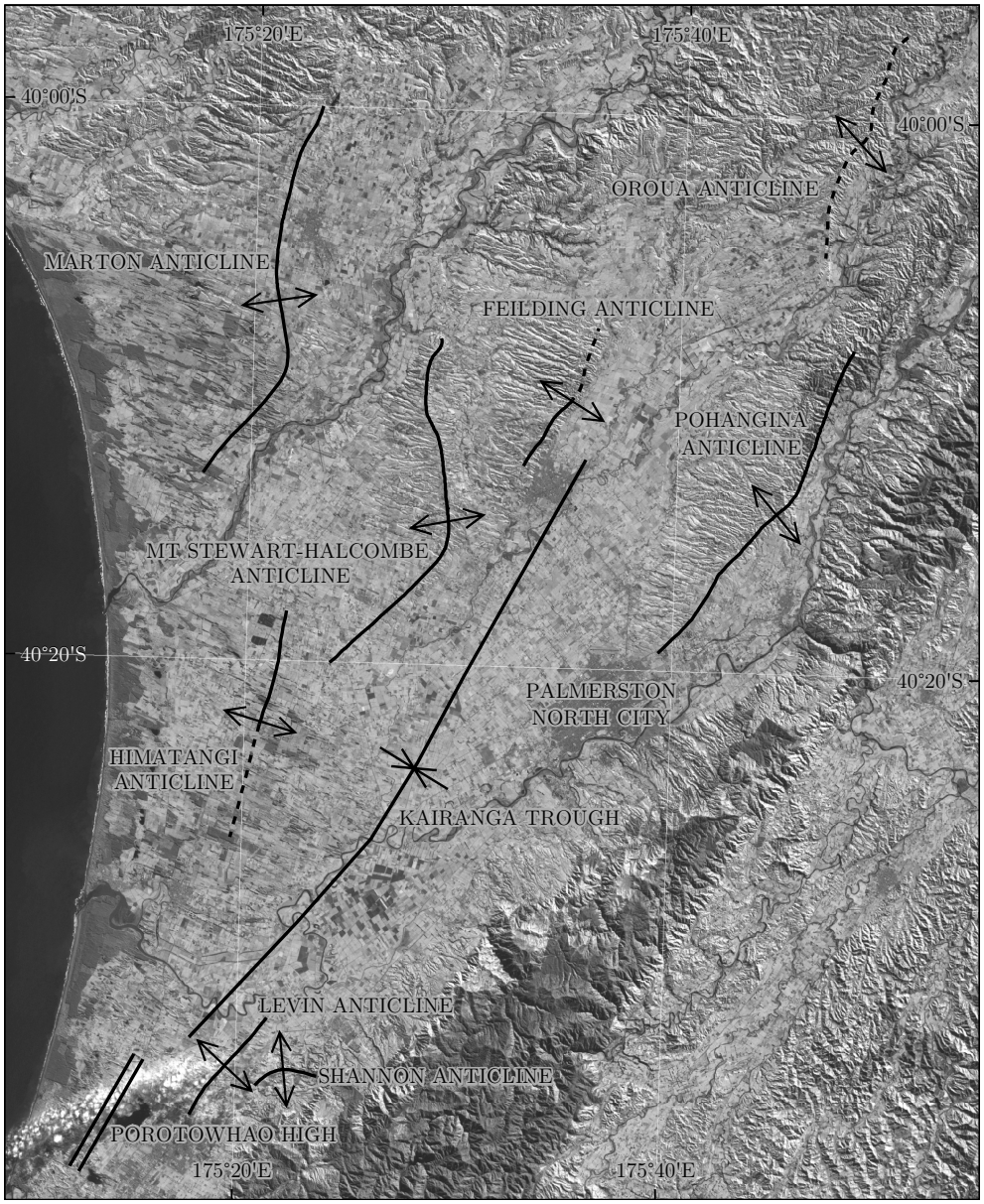

Figure 4.5: Fold axes of the Manawatu anticlines overlaid on an Enhanced Thematic Mapper satellite image of the Wanganui Basin (after Jackson et al., 1998; Clement and Brook, 2008; Clement et al., 2010).

data was made, with no attempt to identify geological horizons or correlate them across the numerous faults (Oil, 1970). Anderton (1981), as part of a description of the structure and evolution of the Wanganui Basin, reinterpreted the Bounty Oil survey data, and concluded that the anticlines were formed by growth faulting. Subsequently, the high resolution seismic reflection survey undertaken by Melhuish et al. (1996) showed that the Mt Stewart-Halcombe anticline was controlled by two reverse faults. Both Melhuish et al. (1996) and

Jackson et al. (1998) considered the structure of the Mt Stewart-Halcombe anticline to be broadly analogous to that of the other active folds deforming the Manawatu landscape.

Te Punga (1957) considered the anticlines to be very young features, uplifted at the rate of 8 mm yr^{-1} over approximately the past 20,000 years. This age was based on Te Punga's (1957) contention that the beds at the summit of the Mt Stewart-Halcombe anticline were Halcombe conglomerates, which had previously been assigned an age of 20,000–50,000 years BP (Te Punga, 1953a). Te Punga (1953a) assumed that the Halcombe conglomerates were deposited shortly before the formation of the highest fluvial terrace in the Rangitikei River valley, which was suggested to be no older than 15,000 years BP. However, this age assessment was highly speculative, and was based on a radiocarbon age of 3,000 years BP obtained from a log preserved within a lower terrace fill (Te Punga, 1953b). Later workers (Lensen, 1959; Kingma, 1962; Hesp, 1975) suggested that the summit beds were instead part of the much older Rapanui Formation (cf. Rapanui Terrace, MIS 5e; Fleming, 1953b; Pillans, 1990a).

While Anderton (1981) considered that the faults underlying the anticlines were mostly active during the Pleistocene, Melhuish et al. (1996) showed that the growth of the Mt Stewart-Halcombe anticline had been ongoing since c. 3.1 Ma. However, only one of the two faults underlying the Mt Stewart-Halcombe anticline has been active since c. 400,000 years BP (Jackson et al., 1998). Jackson et al. (1998) observed that a prominent geomorphological characteristic of the four northernmost anticlines was the preservation of a mid-Quaternary (c. 300,000 years BP) marine horizon across the folds, and concluded that folding had been ongoing since at least this time.

4.2.6 Poroutawhao High

The Poroutawhao High is a north-northeast trending elongate basement greywacke fault block uplifted to the west of the Levin Fault in the vicinity of Poroutawhao (Figure 4.5). The high is approximately 2–2.5 km wide, and the upper surface of the block is tilted gently to the west. Gravity and seismic surveys also suggest that the fault block dips slightly to the southwest. The Poroutawhao High is sometimes referred to as an anticline (e.g., Brown, 1978, 1984), or bedrock dome (e.g., Stevens, 1990).

Te Punga (1953a) first reported the presence of a bedrock high at Poroutawhao, following the drilling of a bore which struck solid rock about +1.5 m (+5 feet) above mean sea-level. Te Punga (1953a) suggested that the high may have prevented the southward movement of the course of the lower Manawatu River during glacial periods. Hesp (1975) reviewed a number of bore logs drilled in the Poroutawhao area which supported Te Punga's (1953a) initial observations. Hesp (1975) noted that bedrock was struck anywhere between +8 m above mean sea-level, to −60 m below mean sea-level. Hesp (1975) suggested that the Poroutawhao High may have prevented major direct marine

incursions into the southern Manawatu during interglacials (see also: Hesp and Shepherd, 1978; Brown, 1984; Heerdegen and Shepherd, 1992; Clement et al., 2010).

Farther south, Bekesi (1989) conducted resistivity and gravity surveys across the Poroutawhao High in the vicinity of Lake Horowhenua. Bekesi's (1989) resistivity survey suggested that the high was comprised of two layers of greywacke: an upper shattered and fractured layer overlying a deeper massive, cohesive body. The gravity survey suggested for the first time the breadth of the bedrock high, and showed that it was bounded by the high-angle Levin Fault to the east. Bekesi (1989) further noted that in the vicinity of Lake Horowhenua the high was overlain by c. 100 m of Cenozoic sediment. Aharoni (1991) conducted seismic reflection and gravity surveys immediately south of Bekesi's (1989) survey area. The seismic reflection survey revealed the structure of the Poroutawhao High, and confirmed that the block was bounded by faults on the western side (Figure 4.6). Aharoni's (1991) seismic reflection survey also suggested that the high was tilted gently to the west, and that in the area beneath Lake Papaitonga was overlain by c. 200 m of sediment.

4.3 Geomorphology

4.3.1 Tokomaru Marine Terrace

The Tokomaru Marine Terrace (Cowie, 1961; cf. Tiritea Formation: Rich, 1959; Otaki Formation: Oliver, 1948, Sewell, 1991; Horowhenua Sandstone: Adkin, 1910) is a Last Interglacial (MIS 5e; Figure 4.7) marine terrace preserved along the western flanks of the Tararua Ranges, immediately adjacent to the Manawatu coastal plain (Figure 4.4). The terrace surface rises from +30 m above PMSL near Shannon, to over +90 m above PMSL near Palmerston North, reflecting a northerly increase in uplift rates along the flanks of the Tararua Ranges (Heerdegen and Shepherd, 1992; Uemura and Shepherd, 2006). The terrace is also tilted laterally towards the coastal plain, implying lower rates of uplift on the plain than at the rear of the terrace. The Tokomaru Marine Terrace is underlain by soft sandstones, as well as greywacke conglomerates, dune sands, beach sands, and lagoonal and swamp deposits (Oliver, 1948). The terrace features a surface cover of loess, Kawakawa Tephra, and in places late Pleistocene (Koputaroa Phase) dunesands. The Tokomaru Marine Terrace is dissected by a large number of box-shaped valleys filled with Holocene marine and alluvial sediments. Cotton (1918), Adkin (1919) and Te Punga (1962) all suggested that the cliffed margin of the terrace indicated that it had faced the open ocean at the height of the most recent post-glacial

Figure 4.6 *(following page)*: Geologic cross-section across the Horowhenua coastal plain interpreted from seismic reflection survey data (after Aharoni, 1991). The location of this cross-section is shown on Figure 6.1.

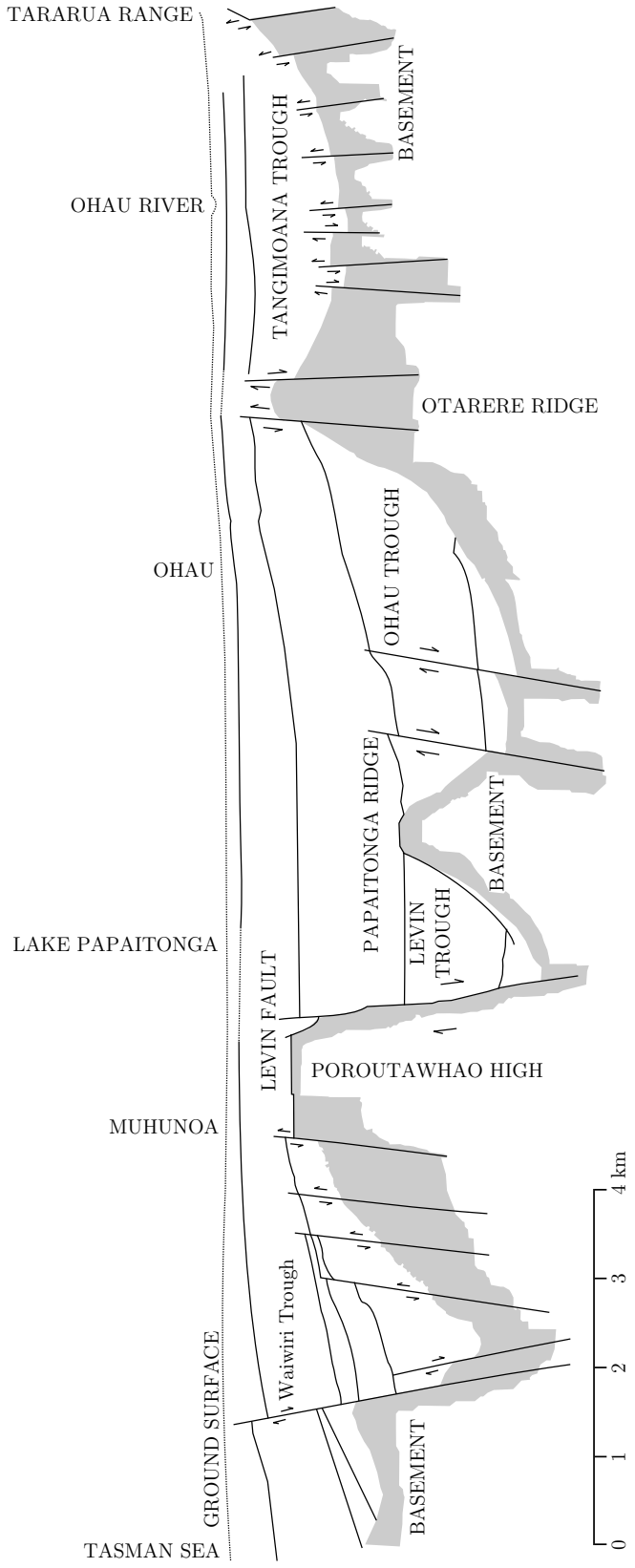
TARARUA RANGE
OHAU RIVER
OHAU
LAKE PAPAITONGA
MUHUNOA
GROUND SURFACE
TASMAN SEA
TANGIMOANA TROUGH
BASEMENT
OTARERE RIDGE
OHAU TROUGH
PAPAITONGA RIDGE
LEVIN TROUGH
BASEMENT
LEVIN FAULT
POROUTAWHAO HIGH
Waiwiri Trough
BASEMENT
0
1
2
3
4 km

marine transgression. This was disputed by Hesp (1975) and Hesp and Shepherd (1978), who noted that the elevation of the terrace foot increased sufficiently towards Tokomaru to preclude wave cutting by Holocene sea levels. Near Shannon, Hesp and Shepherd (1978) suggested that the presence of soft inliers of terrace material rising from the floodplain at the base of the terrace, as well as the presence of Holocene estuarine beds at the base of the cliff, indicated that the cliff developed in a relatively low wave-energy environment.

Sewell (1991) reconstructed the stratigraphy, distribution, environment of deposition, and post-depositional history of the Tokomaru Marine Terrace in the Levin area, and related this to the late Quaternary history of the Wanganui Basin. Based on well log data Sewell (1991) concluded that much of the Manawatu was occupied by a low relief coastal plain immediately prior to the culmination of the Last Interglacial marine transgression (Figure 4.8A). When sea-level rose in response to global climatic warming c. 140,000 years BP, the Himitangi Anticline and Poroutawhao High formed barriers to the encroaching sea, initially resulting in the formation of an embayment in the area of the Kairanga Trough (Figure 4.8B; Sewell, 1991). At the height of the marine transgression the barriers were overtopped, and more extensive marine conditions prevailed (Figure 4.8C; Sewell, 1991). During this time tidal processes dominated north of Shannon. Here, sedimentation patterns were primarily controlled by the deepening Kairanga Trough which was receiving most of its sediment from the Manawatu River (Sewell, 1991). South of Shannon mixed wave-tide processes operated with wave-induced longshore currents which provided abundant sediment from the northwest. (Sewell, 1991) suggested that the period of maximum sediment deposition of the Otaki Formation occurred after the culmination of the marine transgression, when sea levels appear to have remained stable for some time prior to the regression. As sea-level receded the top of the Tokomaru Marine Terrace was bevelled, producing the characteristic flat terrace surface. The terrace was later deformed by localized basement block faulting (Sewell, 1991). Subsequently, two minor marine transgressions, probably during MIS substages 5c and 5a, cut treads on the outer edge of the marine terrace (Figure 4.8D; Sewell, 1991).

Hughes (2005a,b, see also Hughes and Kennedy, 2009) presented a late Pleistocene palaeoenvironmental reconstruction of the lower Manawatu-Horowhenuna region from analysis of a borehole drilled near Levin. During MIS 6 (c. 186,000 years BP) the Manawatu coastal plain was quite extensive due to much lower sea-level. At this time the Kairanga Trough was receiving considerable amounts of fluvial sediment (Figure 4.9A; Hughes, 2005a,b). Based on sediment characteristics and foraminifera analysis Hughes (2005a,b) determined that at the height of the Last Interglacial marine transgression (MIS 5e)

Figure 4.7 *(following page)*: Correlation of loess deposition, floodplain development, and coastal plain development with inferred late Quaternary climate and oxygen isotope stages (after Pillans, 1985; Heerdegen and Shepherd, 1992)

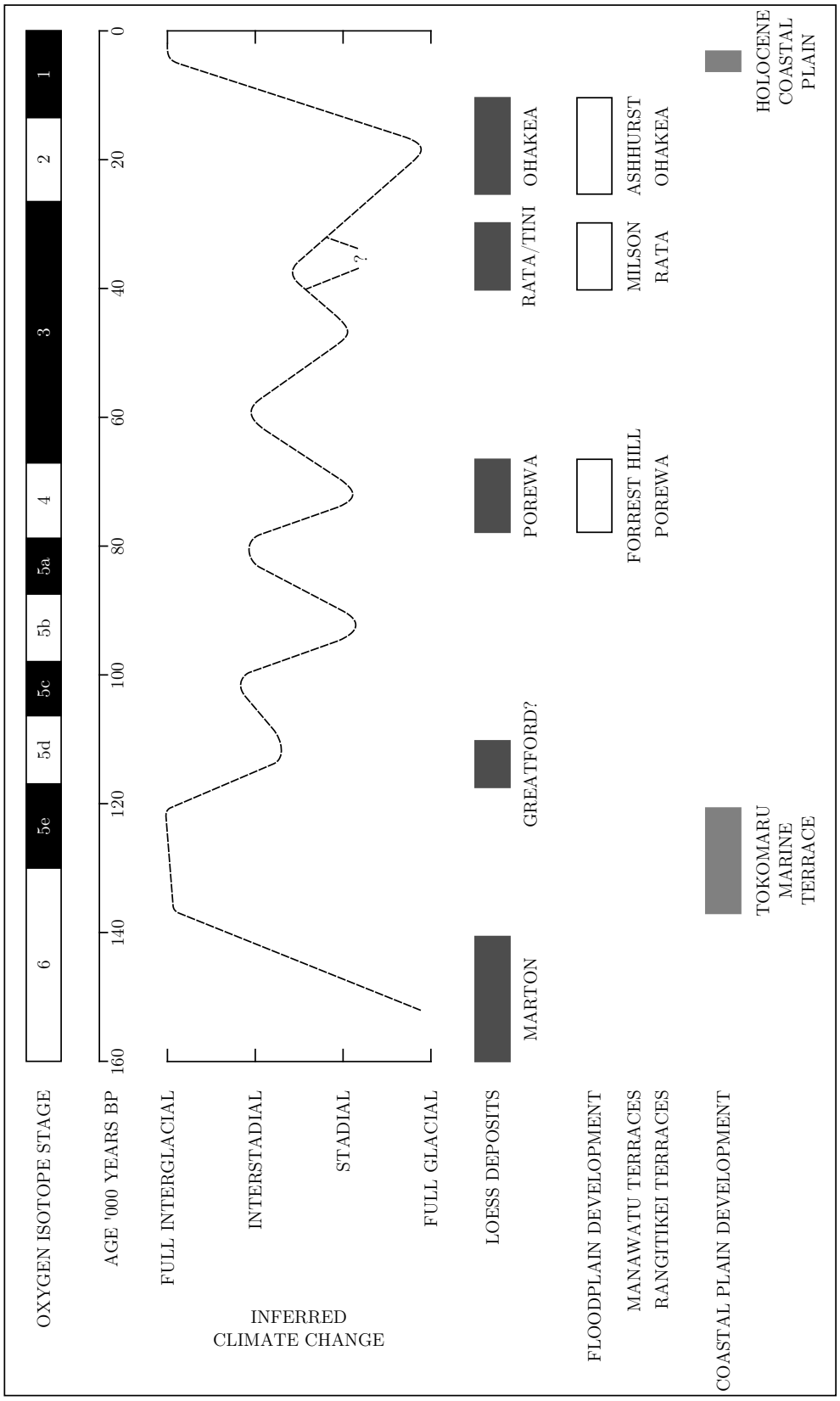
OXYGEN ISOTOPE STAGE
6
5e
5d
5c
5b
5a
4
3
2
1
AGE '000 YEARS BP
160
140
120
100
80
60
40
20
0
INFERRED CLIMATE CHANGE
FULL INTERGLACIAL
INTERSTADIAL
STADIAL
FULL GLACIAL
?
LOESS DEPOSITS
MARTON
GREATFORD?
POREWA
RATA/TINI
OHAKEA
FLOODPLAIN DEVELOPMENT
MANAWATU TERRACES
RANGITIKEI TERRACES
FORREST HILL
POREWA
MILSON
RATA
ASHHURST
OHAKEA
COASTAL PLAIN DEVELOPMENT
TOKOMARU MARINE TERRACE
HOLOCENE COASTAL PLAIN

estuarine conditions prevailed in the lower Manawatu-Horowhenua area. The estuary was expansive, extending from Horowhenua to the northern Manawatu (Figure 4.9B; Hughes, 2005a,b). Hughes (2005a,b) suggested that the estuary was infilled during the latter stages of the Last Interglacial, forming a flat, low lying strandplain (Figure 4.9C). With the lowering of sea-level during the Last Glaciation, much of this strandplain was removed or buried by fluvial aggradation (Figure 4.9D). However, while there is some evidence of the removal or burial of the Tokomaru Marine Terrace, predominantly south of Levin (Figure 4.4), there is little evidence to suggest that the Otaki Formation was initially as extensive as Hughes (2005a,b) proposed, particularly north of Poroutawhao and Koputaroa. Hughes (2005a,b) appears to have ignored the findings of Sewell (1991), who suggested a much more conservative formative extent for the Otaki Formation (Figure 4.8).

4.3.2 Manawatu River and tributaries

The Manawatu River catchment has an area of 5950 km^2, and is divided into two distinct areas by the Tararua and Ruahine Ranges (Figure 4.1). The Manawatu River rises in the eastern slopes of the Ruahine Ranges north of the township of Dannevirke, and flows in a southwesterly direction to the Manawatu Gorge, an antecedent cutting through the axial ranges (Figure 4.1). Above the gorge the river is known as the upper Manawatu. Before flowing through the gorge, the Manawatu River is joined by several major north-flowing tributaries, the Mangatainoka and Mangahao Rivers, which rise in the northeastern Tararua Ranges. Annual precipitation in these catchments is high at 2,000–3,200 mm yr^{-1} (Burgess, 1985). Immediately downstream of the gorge is the confluence of the Manawatu and Pohangina Rivers (Figure 4.1). The Pohangina River rises on the western side of the Ruahines and its catchment receives up to 5,000 mm of rain annually (Hannigan and Barnes, 1982). From the Manawatu Gorge to its mouth at Foxton Beach the river is known as the lower Manawatu. The lower Manawatu River has a mean annual discharge of 102 m^3 sec^{-1}, and a mean annual flood of 1450 m^3 sec^{-1} (Duncan, 1992). Floods of up to 4,500 m^3 sec^{-1} have been recorded (Clement et al., 2010). The current annual sediment yield carried by the lower Manawatu is estimated at 3.4 Mt yr^{-1} (Hicks and Shankar, 2003).

The course of the lower Manawatu River across the Holocene coastal plain has been influenced by the Himatangi anticline and Poroutawhao High, which have anchored the mouth of the river at Foxton Beach and forced the course of the river below Rangiotu in a curve south, then east (Figure 4.5; Hesp, 1975; Stevens, 1990; Heerdegen and Shepherd, 1992). At Ashhurst, the presence of the Pohangina anticline has caused the Manawatu River to be directed to the southwest, while the courses of the Oroua and Pohangina Rivers are similarly controlled by the Pohangina, Feilding and Mt Stewart-Halcombe anticlines (Figure 4.5).

4.3.3 Manawatu River fluvial terraces

A flight of four well-defined late-Pleistocene fluvial aggradation terraces are preserved between the Manawatu Gorge and Palmerston North City (Figure 4.10). In the valley below Palmerston North, the late-Pleistocene fluvial terraces are buried beneath the Holocene coastal plain (e.g., Hesp and Shepherd, 1978; Heerdegen and Shepherd, 1992). Begg et al. (2005) have presented a simple extrapolation of the path of the late-Pleistocene fluvial terraces beneath the Holocene floodplain (see Chapter 6). The Manawatu River terraces in the vicinity of Palmerston North City were first recognised and mapped by Fair (1968), who attempted to correlate the formation of the terraces with (then) known ice advances of the Otiran Glaciation (MIS 4–2). Lieffering (1990) attempted to re-map the terraces, made addition observations of their stratigraphy, and correlated them with late-Pleistocene fluvial aggradation terraces in the Rangitikei valley (Figure 4.7; cf. Milne, 1973). The most recent mapping of the fluvial terraces was completed by Begg and Johnston (2000) and Lee and Begg (2002). Given the discrepancies between the various terrace mappings (Figure 4.10; see discussion below), Begg and Johnston (2000) and Lee and Begg (2002), as the most recent mappers, are taken as the authorities on the spatial extent of the terraces. A number of studies have presented age estimates for the fluvial terraces in the Manawatu River catchment, largely on the basis of loess stratigraphy and the presence of the Kawakawa Tephra in loess on pre-LGM age terraces (e.g., Milne and Smalley, 1979; Hubbard and Neall, 1980; Grant, 1985; Stevens and Palmer, 1986; Vella et al., 1988; Marden and Neall, 1990; Litchfield and Berryman, 2005; Litchfield and Reiser, 2005). Age control data for the Manawatu terraces was coallated, correlated, and converted to a common timescale by Litchfield (2003) and Clement and Fuller (2007). Within the wider Manawatu catchment fluvial terraces are also preserved on the eastern side of the ranges (e.g., Rhea, 1968; Kaewyana, 1980; Vella et al., 1988; Begg and Johnston, 2000; Lee and Begg, 2002; Litchfield, 2003; Clement and Fuller, 2007), and in the Oroua and Pohangina valleys (e.g., Milne, 1968; Challands, 1976).

4.3.3.1 Forest Hill Terrace – MIS 4

The oldest and highest late Pleistocene fluvial aggradation surface preserved in the Manawatu valley between the Manawatu Gorge and Palmerston North City was mapped by Fair (1968) as the Forest Hill Terrace (Figures 4.7 and 4.10). The Forest Hill Terrace is preserved only on the southern side of the river, between the Manawatu Gorge and the township of Aokautere (Lee and Begg, 2002). This is approximately the same extent mapped by Fair (1968)

Figure 4.8 *(facing page)*: Conceptual model of inferred palaeoenvironmental changes in the Manawatu-Horowhenua region that formed the Tokomaru Marine Terrace (after Sewell, 1991).

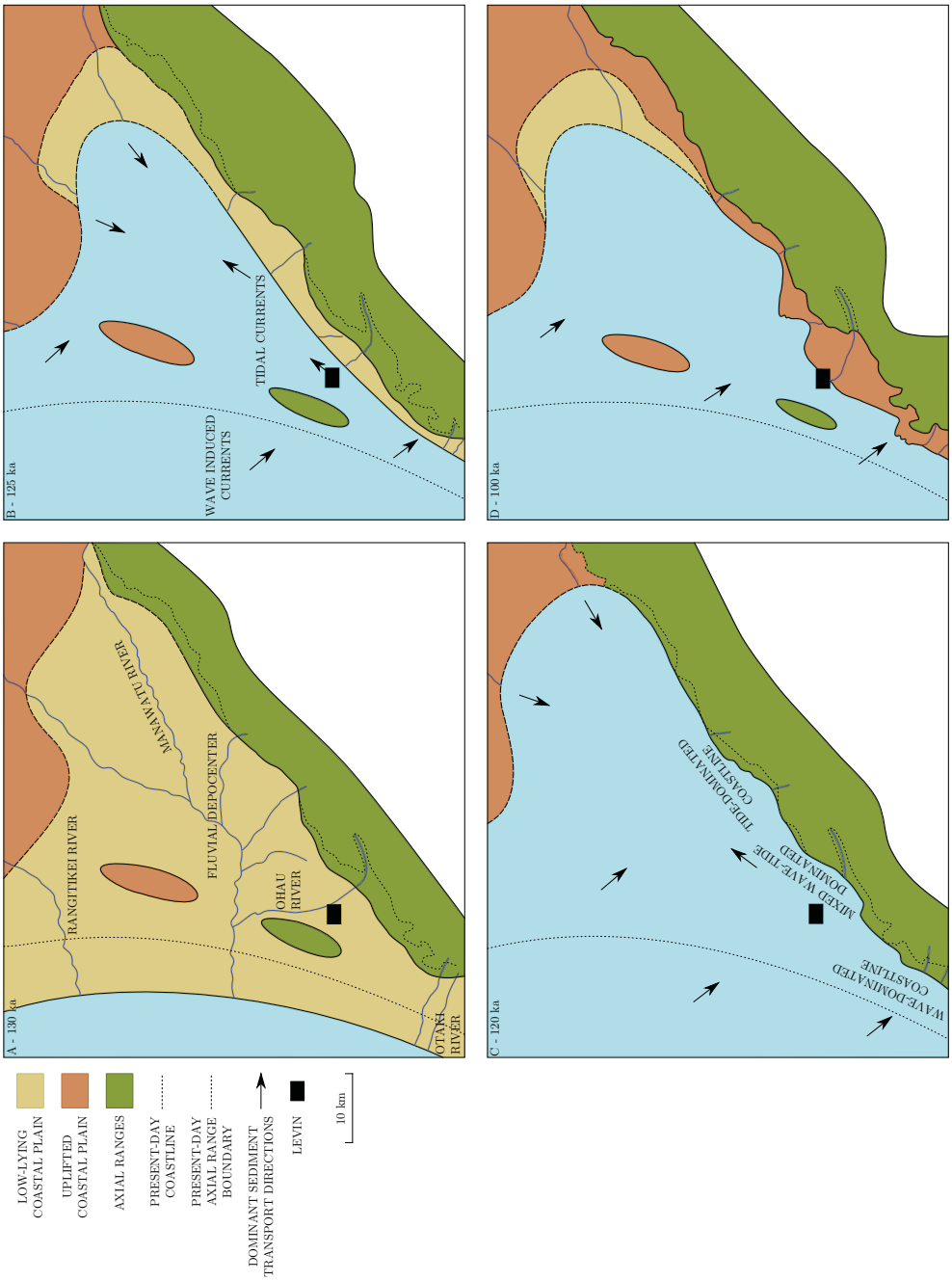
A - 130 ka
RANGITIKEI RIVER
MANAWATU RIVER
FLUVIAL DEPOCENTER
OHAU RIVER
OTAKI RIVER
B - 125 ka
WAVE INDUCED CURRENTS
TIDAL CURRENTS
C - 120 ka
WAVE-DOMINATED COASTLINE
MIXED WAVE-TIDE DOMINATED
TIDE-DOMINATED COASTLINE
D - 100 ka
LOW-LYING COASTAL PLAIN
UPLIFTED COASTAL PLAIN
AXIAL RANGES
PRESENT-DAY COASTLINE
PRESENT-DAY AXIAL RANGE BOUNDARY
DOMINANT SEDIMENT TRANSPORT DIRECTIONS
LEVIN
10 km

(Figure 4.10). Lieffering (1990) suggested that there was confusion over the extent of the Forest Hill Terrace on the northern side of the river (although no mention is made of who Lieffering (1990) considered to be confused, or what the nature of the confusion was), and mapped sections of the Forest Hill Terrace in the vicinity of the township of Ashhurst and to the north-east of Palmerston North City. However, it appears that Lieffering (1990) miss-identified sections of younger aggradation surfaces as Forest Hill Terrace (Figure 4.10).

Fair (1968) suggested that the Forest Hill Terrace was formed during the later part of the Last (then Oturian) Interglacial (MIS 5), at the same time that the Tokomaru Marine Terrace was formed. This was based on the presence of "buckshot gravels" in the upper part of the terrace sequence, which Te Punga (1954b,c) had suggested were formed under periods of uninterrupted soil formation and warm climate. However, the Forest Hill Terrace is inset below the Tokomaru Marine Terrace, and is therefore younger. In fact, the Forest Hill Terrace was likely formed during MIS 4, the first advance of the Otiran Glaciation (cf. Milson Terrace theory of formation by Fair (1968), below), and is equivalent to the Porewa terrace in the Rangitikei (Figure 4.7; Lieffering, 1990; Heerdegen and Shepherd, 1992; Litchfield, 2003; Clement and Fuller, 2007).

4.3.3.2 Milson Terrace – MIS 3

Below the Forest Hill aggradation surface lies the Milson Terrace, which is preserved only on the northern side of the river in two large extents: one at the northeastern boundary of Palmerston North City, the other in the vicinity of Ashhurst township (Figure 4.10; Lee and Begg, 2002). This is much the same as the extent of Milson Terrace mapped by Fair (1968) on the northern side of the river, who suggested that the surface ran continuously from Palmerston North to Ashhurst. Fair (1968) also mapped the Milson Terrace on the southern side of the river, beneath the Forest Hill surface (Figure 4.10). Lieffering (1990) mapped the same extent as Fair (1968) on the southern side of the river, but suggested that on the northern side the Milson Terrace was restricted to a small remnant near Ashhurst, and a larger, disconnected remnant near the northeastern side of Palmerston North. It appears that both Fair (1968) and Lieffering (1990) misidentified younger aggradation surfaces as Milson Terrace on the southern side of the river (Figure 4.10).

Fair (1968) suggested that the Manawatu River degraded its bed during the first advance of the Otiran Glaciation (MIS 4–2) in response to lower sea levels, eroding most of the Forest Hill Terrace. With the onset of warmer conditions during a subsequent interstadial Fair (1968) suggested the Manawatu River became overwhelmed with greywacke detritus. Fair (1968) therefore

Figure 4.9 *(facing page)*: Conceptual model of inferred palaeoenvironmental changes in the Manawatu-Horowhenua region between MIS 6–2 (after Hughes, 2005a,b).

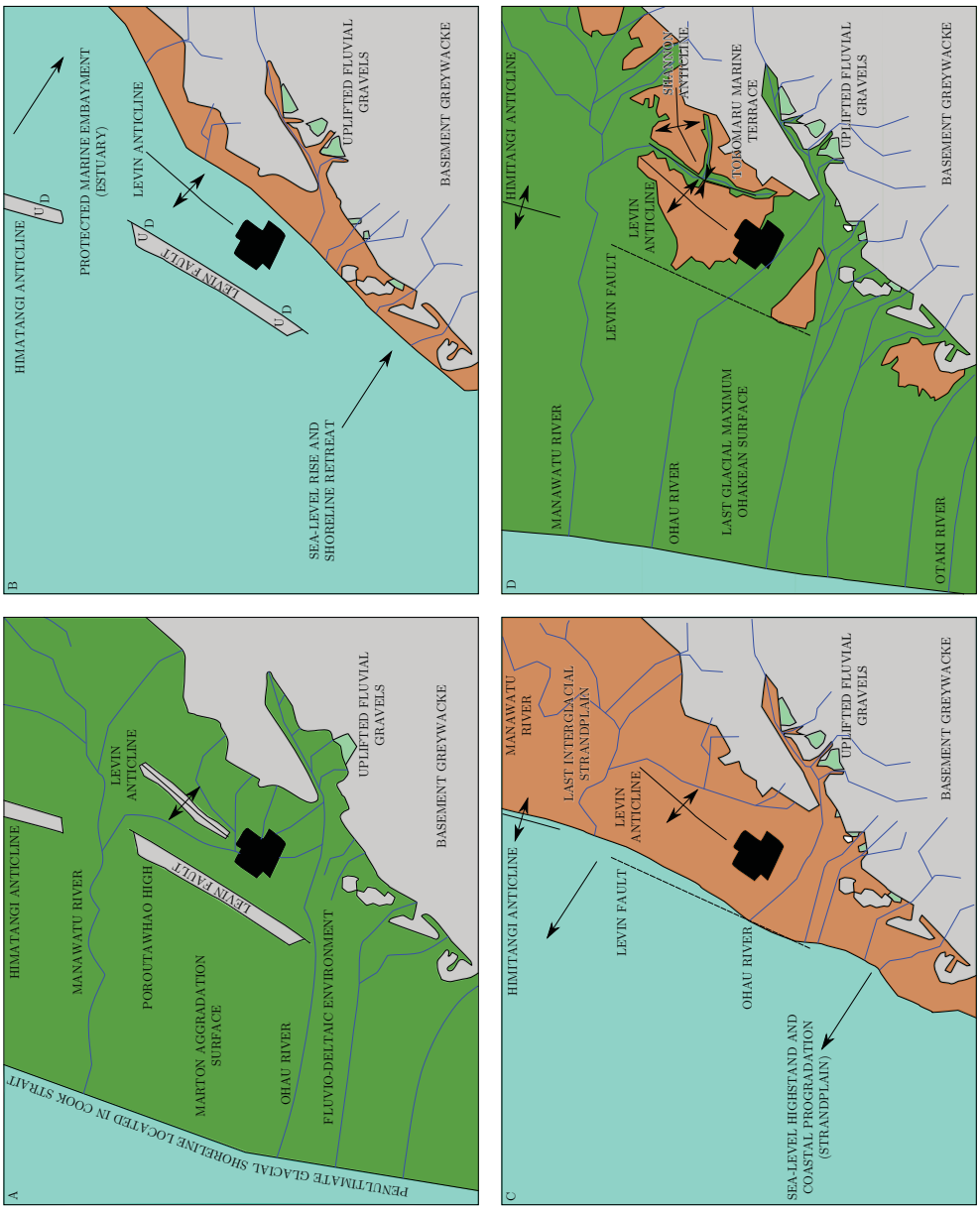
A
PENULTIMATE GLACIAL SHORELINE LOCATED IN COOK STRAIT
HIMATANGI ANTICLINE
MANAWATU RIVER
LEVIN ANTICLINE
LEVIN FAULT
POROUTAWHAO HIGH
MARTON AGGRADATION SURFACE
OHAU RIVER
FLUVIO-DELTAIC ENVIRONMENT
UPLIFTED FLUVIAL GRAVELS
BASEMENT GREYWACKE
B
HIMATANGI ANTICLINE
PROTECTED MARINE EMBAYMENT (ESTUARY)
LEVIN ANTICLINE
LEVIN FAULT
U
D
SEA-LEVEL RISE AND SHORELINE RETREAT
UPLIFTED FLUVIAL GRAVELS
BASEMENT GREYWACKE
C
HIMITANGI ANTICLINE
MANAWATU RIVER
LAST INTERGLACIAL STRANDPLAIN
LEVIN ANTICLINE
LEVIN FAULT
OHAU RIVER
SEA-LEVEL HIGHSTAND AND COASTAL PROGRADATION (STRANDPLAIN)
UPLIFTED FLUVIAL GRAVELS
BASEMENT GREYWACKE
D
HIMITANGI ANTICLINE
MANAWATU RIVER
LEVIN FAULT
LEVIN ANTICLINE
SHANNON ANTICLINE
TOKOMARU MARINE TERRACE
OHAU RIVER
LAST GLACIAL MAXIMUM OHAKEAN SURFACE
UPLIFTED FLUVIAL GRAVELS
BASEMENT GREYWACKE
OTAKI RIVER

proposed that rising sea levels and the increased sediment load of the river resulted in the aggradation of the Milson Terrace. Lieffering (1990) disputed this interpretation, and suggested that it was the Forest Hill Terrace, rather the Milson, that was formed during the first advance of the Otiran Glaciation. Subsequent workers have confirmed that the Milson Terrace was formed by aggradation of the Manawatu River during MIS 3, and is the equivalent of the Rata Terrace in the Rangitikei (Figure 4.7; Heerdegen and Shepherd, 1992; Litchfield, 2003; Clement and Fuller, 2007).

4.3.3.3 Ashhurst Terrace – MIS 2

Preserved below the Milson aggradation surface is the Ashhurst Terrace, which is present on both sides of the Manawatu River, although lateral corrasion has eroded much of its former extent (Figure 4.10). Fair (1968), Lieffering (1990) and Lee and Begg (2002) all mapped broadly similar extents of the Ashhurst Terrace (Figure 4.10). Fair (1968) posited that the Ashhurst Terrace was formed in broadly similar fashion to the Milson terrace above. Fair (1968) suggested that a second advance during the Otiran Glaciation caused the Manawatu River to downcut into the Milson Terrace, before a subsequent interglacial formed the Ashhurst aggradation surface. As with Fair's (1968) assessment of the formation of the Milson surface, this explanation is climatically out of phase with the accepted mode of formation of the Ashhurst Terrace. Rather, the Ashhurst Terrace is considered to have formed during MIS 2, and is regarded as the equivalent of the Ohakea Terrace in the Rangitikei (Figure 4.7; Lieffering, 1990; Heerdegen and Shepherd, 1992; Litchfield, 2003; Clement and Fuller, 2007).

4.3.3.4 Holocene fluvial terraces

The lowest and most recent terrace mapped by Fair (1968), the Raukawa Terrace, consists of laterally extensive alluvial surfaces +4–+6 m above the present level of the Manawatu River (Figure 4.10). This terrace is not explicitly mapped or defined by other workers, who map the extents generically as Holocene alluvium. This surface is probably a degradation terrace equivalent of the Rewa terrace in the Rangitikei valley (cf. Milne, 1973; Litchfield, 2003; Clement and Fuller, 2007), and is possibly the equivalent of Cowie's (1978) Karapoti and Te Arakura series.

4.3.3.5 Fluvial terrace structure and loess coverbeds

In terms of structure the Ashhurst, Milson and Forest Hill terraces comprise predominantly pebble- to cobble-sized greywacke gravel, with relatively minor

Figure 4.10 *(facing page)*: 1:75,000 scale maps of the river terraces between the Manawatu Gorge and Palmerston North City, as presented by Fair (1968), Lieffering (1990), and Lee and Begg (2002). See Figure 4.4 for regional context.

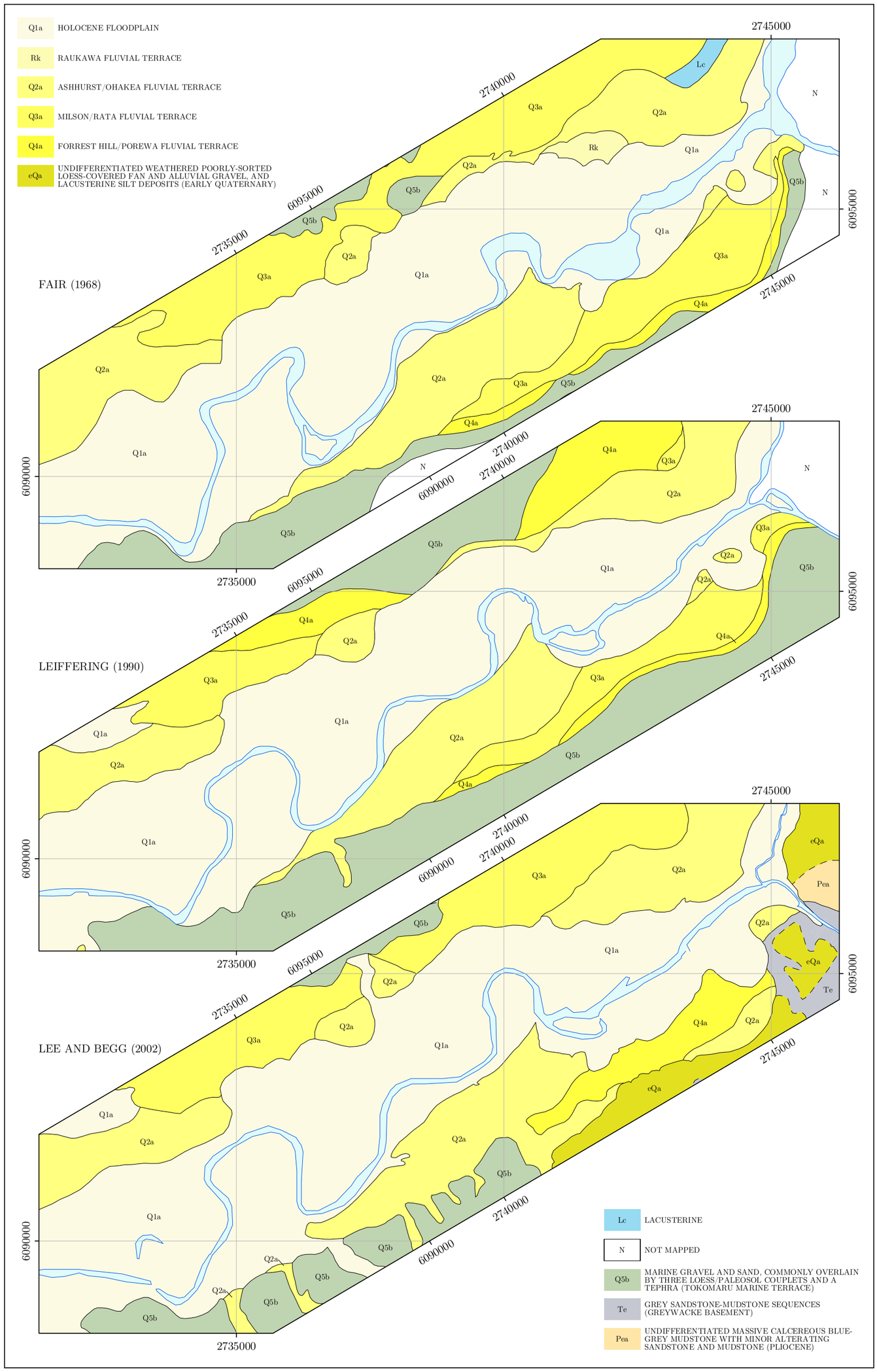
Q1a HOLOCENE FLOODPLAIN
Rk RAUKAWA FLUVIAL TERRACE
Q2a ASHHURST/OHAKEA FLUVIAL TERRACE
Q3a MILSON/RATA FLUVIAL TERRACE
Q4a FORREST HILL/POREWA FLUVIAL TERRACE
eQa UNDIFFERENTIATED WEATHERED POORLY-SORTED LOESS-COVERED FAN AND ALLUVIAL GRAVEL, AND LACUSTERINE SILT DEPOSITS (EARLY QUATERNARY)
FAIR (1968)
LEIFFERING (1990)
LEE AND BEGG (2002)
2735000
2740000
2745000
6090000
6095000
Lc LACUSTERINE
N NOT MAPPED
Q5b MARINE GRAVEL AND SAND, COMMONLY OVERLAIN BY THREE LOESS/PALEOSOL COUPLETS AND A TEPHRA (TOKOMARU MARINE TERRACE)
Te GREY SANDSTONE-MUDSTONE SEQUENCES (GREYWACKE BASEMENT)
Pea UNDIFFERENTIATED MASSIVE CALCEREOUS BLUE-GREY MUDSTONE WITH MINOR ALTERATING SANDSTONE AND MUDSTONE (PLIOCENE)

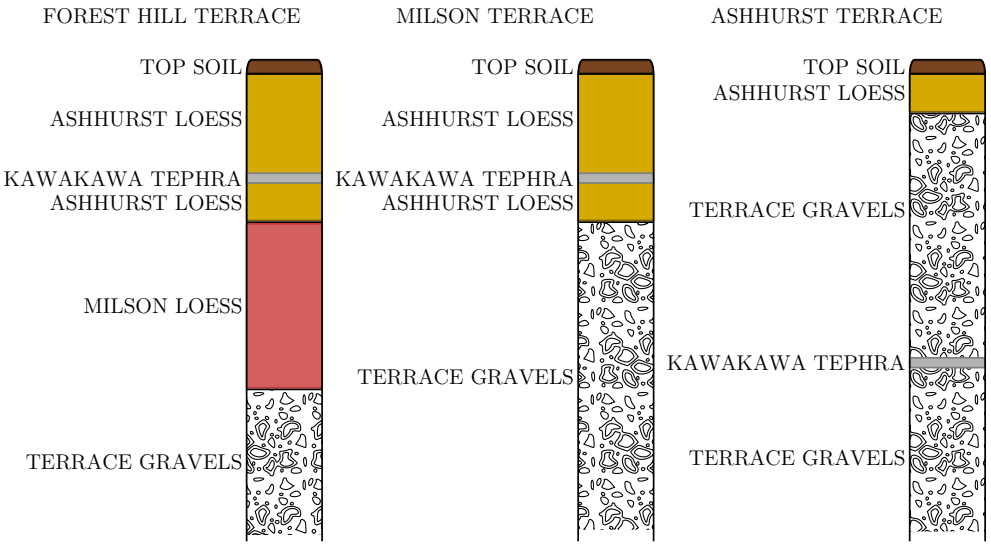

Figure 4.11: Generalised stratigraphic collumns illustrating the typical arrangement of loess and tephra coverbeds on fluvial terraces in the lower Manawatu valley (after Heerdegen, 1972; Litchfield, 2003).

amounts of silt and sand (Litchfield, 2003). All are mantled by loess coverbeds. In the Manawatu region loess deposition occurred during glacial periods when dry silts on the floodplain were entrained by the prevailing northwesterly winds (e.g., Cowie, 1964b). Given the predominant wind direction the greatest thickness of loess has accumulated on the terraces on the southern side of the river. As each glacial phase was marked by a period of loess deposition, the river terraces each possess a unique coverbed stratigraphy (Figure 4.11). The Forest Hill surface, as the highest and oldest terrace in the valley, is mantled by loess blown onto the terrace during the Milson and Ashhurst aggradational phases (Figure 4.11). The Milson loess is a red friable loess, often with a palaeosol developed in the upper third, while the Ashhurst loess is straw-coloured (Begg et al., 2005). The Kawakawa Tephra (first identified by Cowie, 1964a; dated at $22{,}590 \pm 230$ 14C years, calibrated to 26,300–26,900 cal. yr BP: Froggatt and Lowe, 1990; Litchfield and Berryman, 2005) is commonly interbedded within the Ashhurst loess. The Milson terrace is covered by a single loess layer, the Ashhurst, with interbedded Kawakawa Tephra. The lowest aggradation surface, the Ashhurst terrace, may in some locations be overlain by a small layer of straw-coloured loess (Begg et al., 2005), but does not feature Kawakawa Tephra deposits (Figure 4.11). Heerdegen (1972) erroneously identified a Raukawa loess (cf. Raukawa terrace), which appears to be misidentified Ashhurst loess.

4.3.4 Manawatu floodplain

The lower Manawatu River is characterised by two discrete channel phases. In the upper floodplain between the Manawatu Gorge and Opiki (Figure 4.1)

the channel has a relatively steep slope (0.0012), is gravel-bedded and has a sinuosity of 1.4 (Page and Heerdegen, 1985). The floodplain here comprises gravels, sands and silts, and is inset beneath a flight of aggradation terraces (see Section above). Clement et al. (2010) suggested that the upper floodplain fitted the classification of a medium energy non cohesive wandering (B2) or lateral migration (B3) floodplain (Nanson and Croke, 1992). The Holocene and modern alluvium of the upper floodplain displays a series of palaeomeanders, indicating that the sinuosity of the reach has recently changed (Page and Heerdegen, 1985).

From Opiki to the coast (Figure 4.1) the Manawatu River is no longer competent to transport gravel and becomes sand-bedded, with a sinuosity of 2.4 and a low gradient (0.0002; Page and Heerdegen, 1985). The modern floodplain in this lower reach reflects this lower energy, muddy-silty-sandy phase. However, in some bends lateral migration is evident, with well developed scroll patterns observed. Clement et al. (2010) therefore classified the lower floodplain as a medium energy, lateral migration, scrolled/backswamp floodplain (B3b/c; Nanson and Croke, 1992). River terraces are not evident in this part of the floodplain. Hesp and Shepherd (1978) noted that the floodplain was underlain at depth by gravels, and obtained a radiocarbon age of c. 41,500 14C years (Table 4.1), possibly correlative with the Milson Terrace. This suggests the terraces plunge beneath the increasing thickness of fine-grained alluvium and estuarine deposits in the lowermost part of the valley as the river graded to a lower sea-level (Litchfield and Berryman, 2005; Begg et al., 2005).

4.3.5 Coastal dune fields

4.3.5.1 Last Glacial Maximum-age dunes

Aeolian activity through the LGM resulted in the formation of a parabolic dune field at Koputaroa (the Koputaroa dune building phase: Cowie, 1963), partially overlying the Tokomaru Marine Terrace (MIS 5e) and adjacent Ashhurst/Ohakean-age fluvial aggradation surface (MIS 2; Figure 4.4). Koputaroa Phase dunes are regionally expansive, extending southwards in the vicinity of Otaki. Cowie (1963) suggested that the Koputaroa dune building phase took place between 20,000–10,000 years BP, based on the stratigraphic relationship with the Ashhurst/Ohakea surface, the presence of the Kawakawa Tephra interbedded within the dune sands (Cowie, 1964a), and palynological examination of peat from within the dunes which indicated that peat accumulation occurred under a much cooler climate than present. Both Cowie (1963), and later Fleming (1972), who presented a radiocarbon date of $34{,}950 \pm 1{,}680$ 14C years from peat at the base of a Koputaroa dune (Table 4.1), considered it unlikely that the dunes were derived from a marine source, as they noted that sea-level would have been much lower than present during the period of active dune formation. Instead, Cowie (1963) and Fleming (1972) suggested that the Koputaroa dune building phase was supplied locally from the beds and bars of braided rivers.

Table 4.1: Summary of radiocarbon ages obtained by previous investigations of geomorphological features of the Manawatu coastal plain. *Coriaria* stump CRA calibrated using the the non-marine calibration curve for the Southern Hemisphere (SHCal04; McCormac et al. 2004). *A. stutchburyi* CRAs calibrated using the marine model calibration curve Marine04 (Hughen et al., 2004) with a ΔR value of -7 ± 45 to correct for the marine reservoir effect (see Sections 3.2.2 and 7.2.4).

Source	Locality	Material	Radiocarbon laboratory code	Reported age (years BP)	Conventional radiocarbon age (14C years)	Sidereal age range (cal yr BP)
Te Punga (1958)	Foxton	*Podocarpus* log	NZ81	9900±150	9919±76	–[a]
Cowie (1963)	Oroua Downs	*Coriaria* spp. stump	NZ293	855±50	898±40	679–813
Fleming (1972)	Koputaroa	Peat	NZ522	35000±1700	34948±1684	–
Hesp and Shepherd (1978)	Opiki	Totara log	NZ3938	42700±7650	41509±4895	–
	Shannon-Buckley	*A. stutchburyi*	NZ3085	6630±70	6475±45	6814–7154
Shepherd and Lees (1987)	Murray's Farm	*A. stutchburyi*	NZ5218[b]	6280±220	6613±181	6699–7484
Froggatt and Lowe (1990), Litchfield and Berryman (2005)	–	Kawakawa Tephra	–	–	22590±230	26300–26900

[a] CRA is just beyond the range suitable for dating. Sidereal age is approximately 11,000 cal. yr BP.
[b] Shepherd and Lees (1987) mistakenly give the lab number as NZ5128; the correct number is NZ5218.

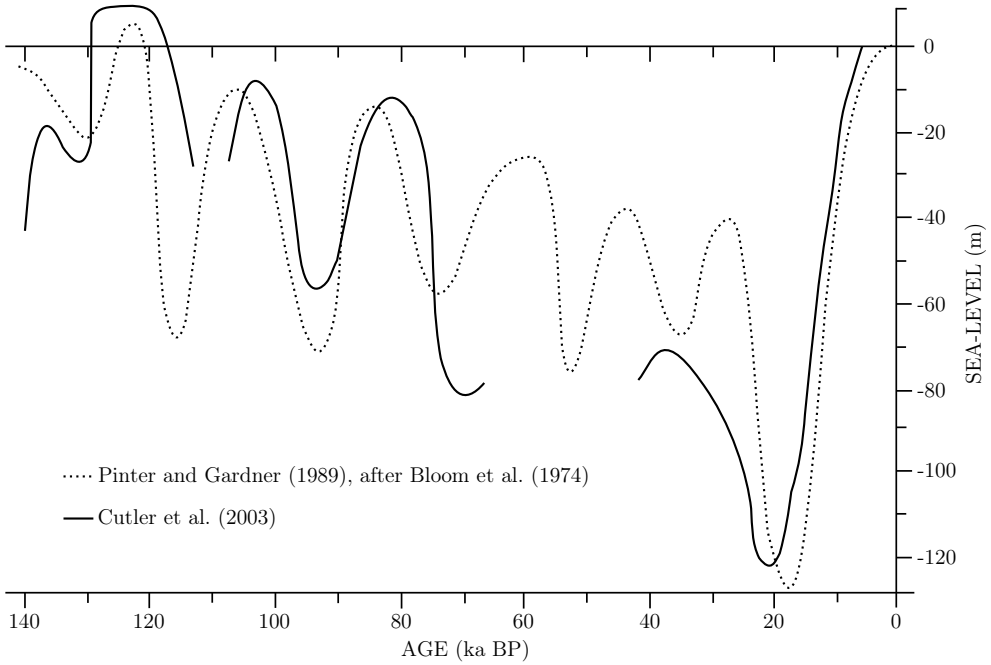

Figure 4.12: Late Quaternary sea-level changes in the southwest Pacific region surrounding New Zealand as documented by records from the Huon Peninsula (after Clement et al., 2010).

Shepherd (1985) analysed the heavy mineral content and roundness of Koputaroa dune sand, modern fluvial sand, and Holocene coastal dune sand, and concluded that the Koputaroa dune sand was derived from a marine source. This conclusion was based primarily on the heavy mineral content of the Koputaroa dune sand, which comprised hornblende, hypersthene and augite. Shepherd (1985) considered that these minerals were originally sourced from the Taranaki and Central Volcanic regions to the north and subsequently transported to the coast by rivers before being carried southwards to the Manawatu by littoral drift. In contrast, the sediment load of the rivers in the region of the Koputaroa Phase dunes consisted of quartzo-feldspathic sediment derived from the Mesozoic greywacke which forms the axial Tararua-Ruahine Ranges. Based on these sedimentological characteristics Shepherd (1985) therefore suggested that the most likely source of the Koputaroa dunes was the mobilisation of transgressive and regressive deposits on the inner continental shelf that were deposited during relative higher sea levels associated with interstadials of the last glacial cycle (MIS 5a, 5c and MIS 3) when sea-level rose to within 30 m of PMSL (Figure 4.12; e.g., Bloom et al., 1974; Chappell et al., 1996; Cann et al., 2000; Murray-Wallace, 2002; Cutler et al., 2003). Shepherd (1985) posited that during interstadials marine sands would have been deposited only 15–20 km west of the location of the Koputaroa dunes, providing sandy material that was subsequently reworked and transported landward during the cooler and windier conditions through the LGM.

However, while acknowledging the remoteness of the Koputaroa dune field to the LGM shoreline (approximately 30 km to the west), Shepherd (1985) ignored results which showed a high degree of similarity between Koputaroa Phase dune sand and sand eroded from the Tokomaru Marine Terrace (Clement et al., 2010). Clement et al. (2010) therefore stressed the importance of distinguishing between the marine origin of the dune sands, as determined by Shepherd (1985), and the source of the dunes. This supported the assertions of Cowie (1963) and Fleming (1972) that the Koputaroa dunes are source-bordering dunes derived from sand bars of the Manawatu River during this cold, dry, windy period (e.g., Nott and Price, 1991; Page et al., 1996; Bullard and McTainsh, 2003; Hesse et al., 2004), with the bars being formed from sediment eroded from the Tokomaru Marine Terrace.

More recently, Duller (1992a,b, 1994, 1996) obtained nine infrared stimulated luminescence dates from Koputaroa dunes at Koputaroa, while Hawke and McConchie (2005) obtained three thermoluminescence dates from Koputaroa dunes in the vicinity of Otaki. All these ages ranged from 46,000–10,000 years BP. The synthesis of geochronological data indicated that there were two phases of dune activity separated by a hiatus in aeolian transport most likely associated with the stabilisation of the Koputaroa dunes (Shepherd, 1985; Shepherd and Price, 1990; Duller, 1996; Hawke and McConchie, 2005). Results from these studies showed that the initial phase of deposition occurred between 50,000–40,000 years BP when sea levels oscillated between 40 and 50 m below present levels (Figure 4.12). At this time the dunes would have been only 5–10 km from the coast, which supplied sediment for this initial phase of development. At 50,000–40,000 years BP, these ages are significantly older than the radiocarbon age from the basal peat presented by Fleming (1972). Duller (1996) postulated that this discrepancy may be the result of the peat sample being contaminated by modern carbon.

Following the initial phase of dune development from 50,000–40,000 years BP active dune migration ceased until the dunes were re-mobilised leading into and during the LGM. It was at this time that the Kawakawa Tephra was incorporated into the dune successions. This second phase of Kopotuaroa dune activity continued through the LGM until c. 11,000 years BP (Muckersie and Shepherd, 1995; Duller, 1996; Hawke and McConchie, 2005). Dune activity during the period from 22,000–11,000 years BP most likely reflected an increase in the intensity of westerly winds and a decrease in vegetation associated with drier and colder climate (Pillans et al., 1993). Through the LGM the water table would also have been substantially lower than present, resulting in less moisture at the surface to inhibit aeolian transport (Clement et al., 2010).

4.3.5.2 Holocene-age dunes

During the late Holocene, following the culmination of the Holocene marine transgression, sand which had migrated landward with rising sea levels was transported to the nearshore, beach and back-beach environment by the dominant westerly swell, and farther inland by the prevailing west-north-westerly

winds to form the most extensive transgressive dune field in New Zealand. The dune field covers c. 900 km^2 and consists largely of stabilised parabolic dunes aligned almost exactly parallel with the dominant onshore west-north-westerly winds. The dunes have migrated inland between the Rangitikei and Manawatu Rivers over the inner margins of the relatively flat Holocene coastal plain to reach the floodplains of the Manawatu (Figure 4.4). The dune field also extends south into the Otaki-Te Horo area (south of Levin; Figure 4.1), however there the dunes are much more subdued and restricted in their landward progradation.

The Manawatu coast is particularly suited for aeolian transport of fine sand and the mobilisation of large parabolic and transgressive dunes for several reasons:

1. The favourable onshore wind and wave regime. The Manawatu coast is dominated by onshore west-north-west winds strong enough to initiate sand transport approximately 33 per cent of the time (Figure 4.13; Shepherd and Lees, 1987; Muckersie and Shepherd, 1995).
2. The dominant onshore wave-approach maintained on the Manawatu coast by the dominant west-north-west wind direction.
3. A large supply of sandy sediment from the Whanganui, Whangaehu, Rangitikei, and Manawatu Rivers (Figure 4.13; Gibb, 1977). Together, these four rivers supply over 10 million tonnes of sediment to the Manawatu coast every year (Hicks and Shankar, 2003).
4. Manawatu beaches typically feature modally dissipative profiles dominated by fine-grained sand with wide gently sloping foreshores, resulting in a large surface area with the potential for sediment mobilisation and aeolian transport (Clement et al., 2010).

Pedological studies by Cowie (1963) identified three Holocene dune building phases: the Foxton; Motuiti; and Waitarere (Figure 4.4). Recent research based on radiocarbon and luminescence dating from deposits associated with the dunes has supported the concept of dune phases (e.g., Shepherd and Lees, 1987; Muckersie and Shepherd, 1993, 1995; Hawke and McConchie, 2006). However, these later studies have indicated that the phases were less distinct than originally proposed. McFadgen (1985) correlated the latter two phases with depositional episodes from throughout the North and South Islands, and subdivided the Waitarere dunes into early and late phases.

Foxton Phase dunes

The Foxton Phase of Holocene dune migration is the most extensive with dunes extending up to c. 16 km inland and rising to a maximum elevation of c. 30 m above the surrounding alluvial plain (Figure 4.4). Cowie (1963) estimated, based on the degree of soil development, that the Foxton Phase of dune development was initiated c. 4,000 years BP, continuing until c. 2,000 years BP. Foxton Phase dunes are characterised by having a moderately well

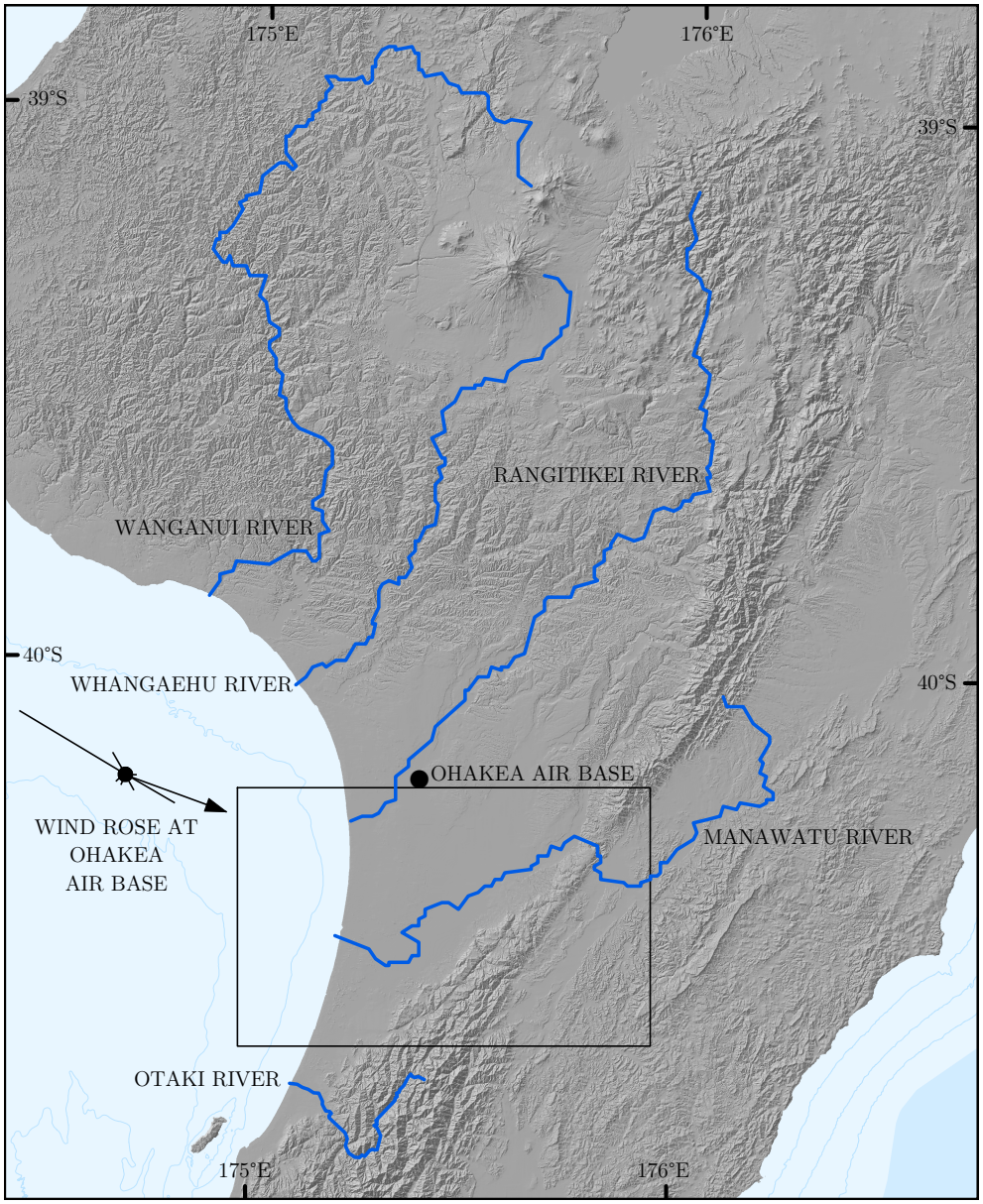

Figure 4.13: Context map of the southwestern North Island showing the locations of the Whanganui, Whangaehu, Rangitikei, and Manawatu Rivers. Also shown is the wind rose from Ohakea Air Base which depicts the Manawatu region's dominant west-north-west wind. The black rectangle shows the extent of the detailed 1:250,000 scale locality and geological maps of the Manawatu region (Figures 4.1 and 4.4).

developed soil profile with a c. 0.3 m thick organic rich "A" horizon and a distinct dark brown "B" horizon of variable depth.

More recent research has suggested that the Foxton Phase of active dune migration was initiated soon after the culmination of the Holocene marine transgression, and continued until c. 1,600 years BP (Shepherd and Lees, 1987;

Shepherd and Price, 1990; Muckersie and Shepherd, 1993, 1995; Hawke and McConchie, 2005). During the early stages of the Holocene marine transgression sediment stored on the continental shelf would have been moved shoreward by rising sea levels, providing a sediment source for the formation of foredunes in the back beach environment (Shepherd and Lees, 1987). At this time the Manawatu coastline was approximately 4 km landwards of its current position (McFadgen, 1974; Muckersie and Shepherd, 1995; Hawke and McConchie, 2006).

By 2,300 years BP Foxton Phase dunes had prograded over the Himitangi Anticline, reaching the lower Manawatu floodplain near the junction of the Manawatu and Oroua Rivers (Figure 4.4). The dunes left in their wake a thin aeolian veneer over the floodplain. The Foxton Phase dunes reached their maximum extent c. 16 km from the present day coastline, stabilising c. 1,600 years BP (Shepherd and Lees, 1987). Muckersie and Shepherd (1993, 1995) have suggested that there was a possible hiatus of active dune formation at the coast that lasted until c. 3,500 years BP, while the already mobilised dunes continued to migrate inland. Following this hiatus active dune migration resumed, during which time the Taupo Pumice (1,717 cal. yr BP: Lowe et al., 2008) was incorporated into the dunes (Muckersie and Shepherd, 1995).

Based on sedimentological analysis and eight optically stimulated luminescence (OSL) ages obtained from Foxton Phase dunes at Otaki-Te Horo, Hawke and McConchie (2006) named the earlier advancement of the Foxton Phase the Swamp Road dunes. This distinction is based on differing sedimentary characteristics: Swamp Road dunes feature more poorly sorted sediments with a higher magnetic content than Foxton Phase dunes, due to the higher energy conditions of the gravel beaches and gravel-bedded Otaki River.

The OSL ages obtained from Swamp Road led Hawke and McConchie (2006) to conclude that while the Swamp Road dunes were of similar age to the Foxton Phase dunes (c. 4,000 years BP in the Otaki-Te Horo area), Swamp Road represented the leading edge of the Foxton Phase, and was locally influenced by sediment supply from the Otaki River and the beach (Figure 4.13). Additional OSL ages from Foxton dunes in this area ranged from 1830 ± 540 years BP to 2980 ± 1070 years BP, consistent with the age of landward Foxton Dunes in the region of the Manawatu River (Muckersie and Shepherd, 1995).

Motuiti Phase dunes

The dunes and sand plains of the Motuiti Phase extend up to 11 km from the present day coast (Figure 4.4). North of the Manawatu River a line of small lakes mark the contact between the Motuiti dunes and the younger Waitarere Phase dunes (Figure 4.4; Cowie, 1963). Dunes of the Motuiti Phase are characterised by a shallow c. 0.15 m dark grey/black organic stained sandy "A" horizon and a c. 0.18 m pale yellowish-brown "B" horizon which overlies grey sand. The Motuiti Phase of active dune migration is believed to have been initiated c. 1,000 years BP. This is based on a radiocarbon age determination of 898 ± 40 14C years (Table 4.1) of an *in situ* tutu (*Coriaria* spp.) stump

rooted in the underlying (preceding) Foxton Phase, which is overlain by 22 m of Motuiti Phase dune sand (Cowie, 1963). Based on its stratigraphic position Cowie (1963) suggested that the tutu was killed by advancing sand. A similar chronology for the Motuiti Phase dunes was also reported from the Otaki area, where an OSL age of 670 ± 140 years BP was obtained from dune sands (Hawke and McConchie, 2006). Based on the timing of active dune formation this phase of dune mobilisation has been attributed to de-vegetation of previously stabilised dunes associated with Maori occupation, which began in the Manawatu region 650–700 years BP (e.g., McGlone, 1983; McGlone and Wilmshurst, 1999).

Waitarere Phase dunes

The Waitarere Phase dunes form a coastal belt of active and stabilised dunes that extend inland between 0.5–4 km from the coastline (Figure 4.4; Cowie, 1963). These dunes lack soil development apart from a slight darkening of the upper few centimetres by organic matter and are relatively unweathered. Cowie (1963) suggested that the Waitarere Phase of active dune mobilisation was less than 120 years old, as in places Waitarere Phase dunes have prograded over European artefacts and introduced plants. This phase of dune activity was therefore partly attributed to overgrazing and the burning of vegetation on previously stabilised dunes (Cowie, 1963). Vegetated dunes of the Waitarere Phase are extensively covered with *Scirpus nodosus* (Pingao), *Spinifex hirsutus* (Spinifex) and *Ammophila arenarua* (Marram). However, there are large areas that are occupied by active foredune blowouts and parabolic dunes. Since active dune progradation continues today despite significant human intervention in the form of planting, dune re-shaping, and fertilising, it may be that early human activity merely aided natural processes in the development of this most recent phase of dune activity. An OSL age of 470 ± 130 years BP from Waitarere Phase dunes in the Otaki-Te Horo area (Hawke and McConchie, 2006) supports the assertion that active dune migration was dominantly a natural process, as this age predates the arrival of Europeans in New Zealand.

4.3.6 Holocene evolution of the Manawatu River estuary

The latter stages of the Holocene marine transgression inundated the lower Manawatu valley, resulting in an estuary that extended east to Shannon and north to Opiki (Hesp and Shepherd, 1978; Heerdegen and Shepherd, 1992). Rich (1959) and Fair (1968) both suggested that the estuary may have extended inland to Shannon and Opiki, while Hesp (1975) speculated that the estuary possibly extended from Rongotea south to Palmerston North City (Figure 4.14). Today, the Manawatu River estuary covers an area of approximately 2 km^2. It has been widely suggested that during the later stages of the Holocene marine transgression the Himatangi and Marton anticlines, together with the Poroutawhao High (Figure 4.5), had attained altitudes sufficient to

prevent or restrict major marine incursions into the incised-valley, allowing a low-energy estuary to form (e.g., Te Punga, 1953a; Rich, 1959; Hesp, 1975; Hesp and Shepherd, 1978; Heerdegen and Shepherd, 1992; Clement et al., 2010). However, there has been little research to confirm this hypothesis.

Shells recovered by Shepherd and Lees (1987) place the upper limit of the Holocene estuary in the vicinity of Murray's Farm (Figure 4.14). Here, shells from the top of the estuarine facies suggest that estuarine infill was succeeded by fluvial progradation c. 7091 ± 392 cal. yr BP (Table 4.1). The southeastern margin of the palaeo estuary features a number of box-shaped valleys in the vicinity of Shannon township, formed when small river valleys incised into the Tokomaru Marine Terrace during the LGM were filled with estuarine sediment. Here, the date of succession from estuarine to fluvial deposition is placed at 6984 ± 170 cal. yr BP (Bore H26: Figure 4.14; Table 4.1; Hesp and Shepherd, 1978). This suggests that sea level was close to present levels well before 7,000 cal. yr BP, to allow for the development of a low energy estuarine environment within the incised valley close to present sea level by 6,800 cal. yr BP (Clement et al., 2010).

4.3.7 Holocene progradation of the Manawatu coastline

Since the culmination of the Holocene marine transgression large quantities of sediment sourced from rivers to the north have been delivered to the Manawatu by southward-dominant littoral drift (Figure 4.13; e.g., Fleming, 1965, 1972; Gibb, 1977, 1979; Muckersie and Shepherd, 1995) enabling progradation of the coast. North of the Manawatu at Tangimoana (Figure 4.1), Shepherd et al. (1986) and Heerdegen and Shepherd (1992) suggested that the coast had prograded c. 4 km in the time since PMSL was attained. South of Levin it has been widely posited that the coast has prograded c. 2–3 km (e.g., Te Punga, 1962; Fleming, 1965, 1972; Gibb, 1978; Barnett, 1984; Palmer et al., 1988; Hawke and McConchie, 2005, 2006). In the Manawatu Muckersie and Shepherd (1995) and Heerdegen and Shepherd (1992) have suggested that c. 4 km of coastal progradation occurred following the culmination of the Holocene marine transgression. This is less than the amount suggested by Hesp (1975) and Rich (1959), who inferred that the amount was closer to 5–6 km.

4.4 Regional tectonism

The Manawatu coastal plain occupies the margin between the Wanganui Basin and the Tararua and Ruahine Ranges. Broadly, the former is subsiding, while in contrast the latter are being uplifted. As a result regional tectonism is not simple to characterise.

Hesp and Shepherd (1978) averaged the elevation of the Last Interglacial Tokomaru Marine Terrace on the periphery of the Manawatu coastal plain, inferring a long-term uplift rate for the area of 0.35 mm yr^{-1} over the past 120,000 years BP. Hesp and Shepherd (1978) assumed an average elevation

for the marine terrace of 55 m, including 8 m of cover beds, and assumed Last Interglacial sea levels c. +5 m higher than PMSL. However, the terrace is tilted along its length, and rises from a low of c. +30 m to over +90 m above PMSL (Heerdegen and Shepherd, 1992; Uemura and Shepherd, 2006). In addition, the terrace is also tilted laterally towards the Manawatu coastal plain, implying lower rates of uplift on the plain than at the rear of the terrace, which lies adjacent to the Tararua Ranges. The marine terrace in the vicinity of the location on the coastal plain where Hesp and Shepherd (1978) recovered estuarine shells (Bore H26: Figure 4.14) is only 10–20 m above PMSL, implying uplift rates of 0–0.06 mm yr^{-1} since the Last Interglacial.

Litchfield and Berryman (2007) used the elevation of the Ashhurst/Ohakea fluvial terraces in the Manawatu valley above the coastal plain (Figures 4.4 and 4.10) to estimate rates of fluvial incision as a proxy for rock uplift. Litchfield and Berryman (2007) inferred an average uplift rate for the upper valley of 0.5 mm yr^{-1} over the last 18,000 years BP. However, it is unclear whether this rate would extend onto the coastal plain. Gibb (1983), Pillans (1986), and Williams (1991) have all noted that the coastal plain lies in a zone of subsidence, although the latter two studies have both suggested zero rates of tectonic movement for the Manawatu through the late Quaternary.

4.5 Climate

The Manawatu region is characterised by a maritime climate, with rainfall increasing from 800 mm yr^{-1} at the coast, to more than 5,000 mm yr^{-1} along the inland ranges (Heerdegen and Shepherd, 1992). There is no marked seasonality, with rainfall being evenly spread through the year (Saunders, 1964). Heavy rain is uncommon on the coastal plain, but is typical in the foothills and along the ranges (Heerdegen and Shepherd, 1992). Summers are warm and frosts are frequent in most places during the winter (Burgess, 1985). The Manawatu does not experience extremes of temperature, with temperatures differing by approximately 10°C between summer and winter. The diurnal range is of similar magnitude (Heerdegen and Shepherd, 1992). The Manawatu is windy, although the winds are characterised more by persistence than strength (Heerdegen and Shepherd, 1992). The prevailing surface winds are westerly to northwesterly, and occur 30–50 per cent of the time (Figure 4.13; Burgess, 1985).

Figure 4.14 *(facing page)*: Estimates of the extent of the Manawatu River estuary at the culmination of the Holocene marine transgression by Rich (1959), Fair (1968), and Hesp (1975), and the locations of radiocarbon dated fossil shells used to deliniate the history of the palaeo estuary. Base geological map constructed using data from Kingma (1962), Cowie et al. (1967), Pillans (1990a), Begg and Johnston (2000), Lee and Begg (2002), Townsend et al. (2008), and unpublished data from the QMAP project made available by D. Townsend.

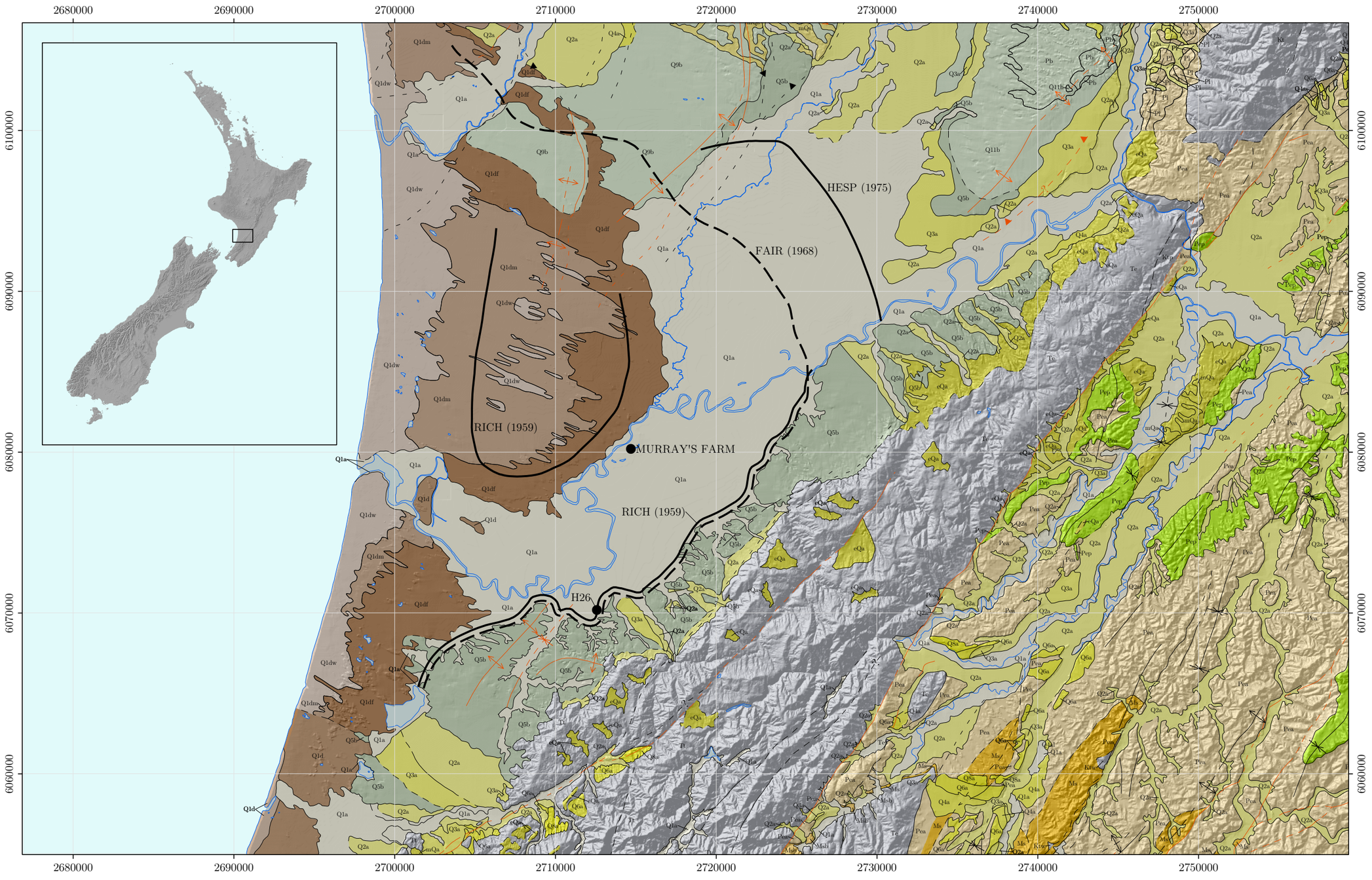
2680000
2690000
2700000
2710000
2720000
2730000
2740000
2750000
6100000
6090000
6080000
6070000
6060000
HESP (1975)
FAIR (1968)
RICH (1959)
MURRAY'S FARM
H26

4.6 Contemporary coastal processes

The Manawatu coast is wave-dominated (Clement et al., 2010) and microtidal, with a spring tidal range of 1.1 m, and a neep tidal range of c. 0.45 m (New Zealand Nauitical Almanac tide levels at the Manawatu River mouth). At the coast, waves approach the Manawatu from either the southwest or west. From the southwest, waves generated in the northern Cook Strait have a maximum fetch of 100 km, resulting in moderate wave energy. Waves approaching from the west (Tasman Sea) have a much greater fetch, resulting in a dominant westerly swell (Clement et al., 2010). Mean significant wave height along the coast is 1.4 m, with a 5 per cent exceedance value of 2.6 m. Comparative deepwater wave climate statistics are 1.3 m and 2.5 m, respectively. The average wave period is 10.3 s (Shand et al., 2001). North of the Manawatu region the westerly swell approaches the coast at an oblique angle resulting in a southward moving longshore drift. Accordingly, waves in the nearshore not only transport large quantities of sand-sized sediment shoreward from the northwest, but also southwards due to longshore drift (Muckersie and Shepherd, 1995; Gibb, 1979).

The Manawatu coastline is dominated by fine-grained sandy sediment derived from Plio-Pleistocene Wanganui Basin sediments and the greywacke axial ranges to the east. The coast is characterised by low gradients due to the fine-grained nature of the sediment, the relatively low tidal range, and moderate wave energy (Shand et al., 2001). The beaches themselves tend to have modally intermediate (ripped) to dissipative (uniform) configurations with lower cross-shore slopes, and are typically backed by a foredune which in places reaches several metres in height. The morphology of the foredune varies alongshore from well-vegetated, stabilised incipient and established foredunes to poorly-vegetated, blown-out, and hummocky (Hesp, 2001).

4.7 Vegetation: past and present

4.7.1 Palaeovegetation

At the time of European settlement of the Manawatu in the mid 1800s most of the region was forested, with portions of scrub, grassland, dune vegetation, and swamp (Esler, 1962, 1964, 1978). Forest covered parts of the dune country, most of the Manawatu-Oroua lowland floodplain, the Pleistocene fluvial terraces, and the flanks of the Tararua and Ruahine Ranges. Esler (1964, 1978) therefore broadly divided the forests:

1. Semi-swamp forest dominated kahikatea and pukatea. Found on the lowland floodplain and in the dune country in low lying areas adjacent to rivers.
2. Totara forests, often with matai. Totara forest occupied free draining strips along the river margins in low rainfall areas.

3. Mixed podocarp forest composed of rimu, matai, totara, and kahikatea. Found on the Manawatu plains and fluvial terraces. The forest on the terraces was much older than the forest on the plains. As a result larger quantities of northern rata occupied the terraces.
4. Tawa forest occupying low hills adjacent to the Tararua and Ruahine Ranges. Found predominantly in the Manawatu Gorge and in the upper Turitea valley. Tawa forest was also found in small stands on the Manawatu plains.
5. Black beech forest, occupying pockets in the courses of the Manawatu and Pohangina Rivers.
6. Rimu and northern rata forest. Found on most of the hill country, except where tawa forest was present. Rimu and northern rata dominated the western flanks of the Tararua Ranges above 300 m. Above 700 m the forest was dominated by kamahi.
7. Forests of the dune country. Infrequent, isolated patches of kahikatea, pukatea and totara.

Of the other vegetation types, scrub and shrubland developed in patches across the lowlands where fire or drainage conditions prevented woody vegetation from completing the full succession to forest (Esler, 1964, 1978). Grassland was extensive on the lowlands, particularly in the sand country. Prior to the introduction of marram grass, the dunes were occupied by spinifex and pingao. Some scrubs were present in the dune country, typically growing on the sheleterd lee side of dunes (Esler, 1964, 1978). Swamps were common on the lowlands, particularly where water ponded between the levees of confluent rivers. The swamplands were typically occupied by flax, raupo and toetoe (Esler, 1964, 1978).

4.7.2 Present vegetation

The present-day vegetation of the Manawatu is characterised by intensive agricultural and pastoral land use (Warr, 1964; Christensen, 2000). The lowlands have been almost entirely cleared of forest and the swamps drained for conversion into pasture for beef, sheep, and dairy farming (Mayo, 1964; Roche, 2000). Much of the dune country has also been converted to pasture. Forest is restricted to the flanks of the Tararua and Ruahine Ranges, and isolated stands of preserved native bush on the plains (Esler, 1962, 1964).

4.8 Summary

The Manawatu region of the southern North Island, New Zealand, lies within the Wanganui Basin, 200 km northwest of the subduction zone between the Pacific and Australian lithospheric plates. The Manawatu coastal plain is bounded to the south and east by axial mountain ranges composed of well dissected Torlesse basement greywacke rocks mantled with marine cover beds. A

remnant Last Interglacial marine terrace is preserved along the western flanks of the ranges, adjacent to the coastal plain. The coastal plain features a number of anticlines, formed by buried reverse faults associated with continental shortening across the Wanganui Basin. A bedrock high is present at Poroutawhao, where an elongate basement greywacke fault block has been uplifted to the west of the Levin Fault. A flight of four well-defined late-Pleistocene fluvial aggradation terraces are preserved in the upper valley. These terraces plunge beneath the Holocene alluvial and estuarine deposits in the lower valley. The coastal plain features the largest transgressive dune field in New Zealand, covering c. 900 km^2. The dune field consists largely of stabilised parabolic dunes, formed in three dune-building phases coincident with progradation of the coast. The lower valley was inundated during the Holocene marine transgression, forming an estuary that extended east to Shannon and north to Opiki. It has been widely suggested that during the latter stages of the Holocene marine transgression the Himitangi Anticline and Poroutawhao High restricted major marine incursions into the lower valley, allowing a low-energy estuary to form. However, there has been little research to confirm this hypothesis.

Chapter 5

Models of estuary and incised-valley evolution

5.1 Introduction

Estuaries and incised-valleys feature a variety of morphologic, hydrodynamic and sedimentological features formed by the interplay of numerous complex processes that interact with varying intensities and over different time scales. A large number of studies have focused on the evolution of estuaries and incised-valleys in response to relative sea-level rise. This research has developed a unifying series of models that describe the evolution of estuaries and incised-valleys in response to different environmental conditions and provide necessary perspective for understanding facies variations between estuaries and incised-valleys. At the core of the models is a predictable spatial and temporal arrangement of depositional environments that evolves in response to changing environmental conditions. The models therefore provide a framework for delineating the depositional fill of estuaries and incised-valleys and for interpreting their evolution. This chapter reviews these estuarine and incised-valley facies models to provide context for the well log investigation (Chapter 6) and facies reconstruction (Chapter 7) of the Manawatu valley which follow. These models also provide a framework for understanding the evolution of the lower Manawatu valley during and following the Holocene marine transgression (Chapter 8).

5.2 Background to facies and facies models, and their application to estuaries and incised-valleys

A facies is a body of rock or sediment which has specific characteristics of lithology and biological and physical structure that distinguish it from other proximal sedimentary bodies. These characteristics are dependant on the physical and chemical parameters of the depositional environment and the processes which controlled deposition. For example: hydrodynamics, sedi-

ment supply, and biological components. The analysis of facies and facies associations is therefore used to reconstruct depositional environments. Such analysis fundamentally relies on the combination of observations of the internal characteristics of, and the spatial relationships between, facies (Middleton, 1978).

Individual facies have variable interpretive value, and a single facies, taken in isolation, may have many ambiguous environmental interpretations (e.g., see the discussion by Boyd et al. (2006) of the tide-dominated delta versus estuary controversy). Individual facies should therefore be grouped together into facies associations that are either genetically or environmentally related (Collinson, 1969). A facies association therefore provides context beyond that of an individual facies, facilitating the elimination of alternative environmental interpretations. Allen (1983) referred to these larger scale facies associations as architectural elements, implying that they constituted the building blocks of the various depositional systems (see also Fisher and McGowen, 1967; Posamentier et al., 1988; Galloway, 1989; Van Wagoner, 1995). This concept emphasises the three dimensional geometry of facies associations (Walker, 1992).

Facies associations can be incorporated into the broader scheme of facies successions (cf. facies sequence; Walker, 1990, 1992; Reading and Levell, 1996). In some sedimentary sequences facies may lie in some semblance of order, with vertical transitions from one facies to another occurring more often or more regularly than would be expected if the facies lay randomly. There is therefore a degree of predictability which allows for the grouping of such succeeding facies into facies successions. Facies successions emphasise the spatial characteristics of facies highlighted by facies associations, while accenting the temporal nature of depositional systems. This concept is epitomised by Walther's Law of Facies (1894; see also Middleton, 1973). Walther's Law suggests that a gradual transition between two facies implies that the environments indicated by the facies were once laterally adjacent. However, where a contact between facies is sharp and/or erosional, then it cannot be inferred that the adjacent facies represent formerly adjacent environments.

A facies model is a three-dimensional representation of a depositional system produced through the correlation of vertical and lateral facies successions. A facies model provides a broad summary of a depositional system expressed in terms that allow it to serve four main functions (Walker, 1984):

1. As a norm for comparison,
2. As a framework and guide for future observations,
3. As a predictor in new geological situations,
4. And as an integrated basis for interpretation for the system it represents.

This is achieved through the process of "distillation" (Walker, 1984), in which local variability is replaced with a simplified model based on a summary of representative facies and geomorphology. This is often translated into "idealistic" facies successions that supposedly represent the "essence" of the environment (Boyd et al., 2006).

However, it can be difficult to appreciate this ideal view of a depositional environment when attempting to confront the contrasts between specific examples. Boyd et al. (2006) noted that the search for geomorphological simplicity may have diverted attention from the fundamental basis for the development of models: characterising the processes that control sedimentation in depositional settings. Boyd et al. (2006) therefore suggested that the key to understanding depositional environments is to characterise the controlling processes in each one and then determine the sedimentary response or combination of responses. The ideal facies model then becomes one that covers the environmental range while simultaneously recognising the most probable combination of process controls and sedimentary responses.

Characterisation of the process controls in a depositional environment takes place at two scales: the local, autocyclic scale; and the regional to global allocyclic scale. For the former the controlling variables are things such as fluid shear, salinity, density, and sediment size. The manifest response is the production of distinctive sedimentary bodies (facies, facies successions, and architectural elements) that reflect the genetic process. For the latter the controlling variables are accommodation space (*sensu* Jervey, 1988) and the amount and character of the incoming sediment. Both are determined by tectonics, climate, and sea-level fluctuations. The response is the production of stratigraphic units and distinct bounding surfaces.

These principles of process control can be explicitly applied to facies models of the sedimentary infill of estuarine and incised-valley systems (Boyd et al., 2006). At the autocyclic scale estuaries and incised-valleys are characterised by a combination of fluvial, wave and tidal processes supplemented by local processes such as organic production (e.g., peat and shells), wind, and density stratification. The interplay between wave and tidal processes produces a spectrum of depositional settings in estuarine systems, from the macrotidal, tide-dominated to microtidal, wave-dominated. The interaction between all the processes operating in the estuarine and incised-valley settings produces many characteristic geomorphic forms, including river channels, floodplains, bay-head deltas, estuarine central basins, barriers, tidal deltas, and sand flats (Boyd et al., 2006). The allocyclic controls result in fluvial incision during periods of reduced sediment input, increased fluvial activity or lower relative sea-level. Increases in relative sea-level result in fluvial deposition, followed by estuarine deposition and the migration landward of marine, estuarine and fluvial facies.

5.3 Background to estuarine facies models

Estuarine facies models are complex due to the occurrence of and interplay between multiple dominant processes (fluvial, wave, and tidal), and specific varied responses elicited by a continuous range of relative sea-level and sediment flux parameters (Boyd et al., 2006). The widely-used "tripartite" facies model for wave-dominated estuaries was popularised by Roy et al. (1980) and

Roy (1984b), and was the first to encompass the entire length of an estuarine system. These two papers built upon prior work by Oomkens and Terwindt (1960), Bird (1967), Klum and Byrne (1967), Allen et al. (1970), Nelson and Bray (1970), and Reinson (1977).

Through the 1980s and into the early 1990s a number of studies began to discuss and apply the tripartite facies model to a range of estuarine settings, both ancient (e.g., Zaitlin and Shultz, 1984, 1990; Demarest and Kraft, 1987; Rahmani, 1988; Wood and Hopkins, 1989) and modern (e.g., Allen, 1991; Dalrymple et al., 1990; Nichols et al., 1991; Nichol, 1991). Reviews by Reinson (1992) and Dalrymple (1992) synthesised much of this earlier work on estuarine facies concepts and began to consider the role of tides in shaping the tripartite facies model in more detail. Reinson (1992) presented an estuarine classification scheme (Figure 5.1), identified diagnostic sedimentary structures, and provided summary facies successions. At the same time Boyd et al. (1992) presented a classification scheme for coasts which summarised shoreline responses to changes in sea-level and sediment supply (Figure 5.2), and organised the major clastic coastal depositional environments based on shoreline translation direction (progradation or transgression), and the relative power of waves and tidal and river currents (Figure 5.3).

Dalrymple et al. (1992) integrated many of these ideas into a conceptual facies model for estuarine systems that has become a keystone of such research. Within a geological context Dalrymple et al. (1992) defined an estuary as:

> "... the seaward portion of a drowned valley system which receives sediment from both fluvial and marine sources and which contains facies influenced by tide, wave and fluvial processes. The estuary is considered to extend from the landward limit of tidal facies at its head to the seaward limit of coastal facies at its mouth." (Dalrymple et al., 1992, p. 1132; Figure 5.4).

It is implicit in this definition that estuaries are formed only under transgressive conditions. This was important, as the then widely-used oceanographic definition of an estuary (Pritchard, 1967) applied to both transgressive and regressive coastal settings. In addition, Pritchard's (1967) definition (Figure 5.4), which was based on salinity, could not be applied to the distribution of ancient estuarine deposits, which is determined primarily by physical processes rather than salinity.

Figure 5.1 *(facing page)*: Classification of estuaries (based on the volume of the tidal prisim) illustrating morphological, oceanographic, and sedimentological characteristics of each estuary type (after Reinson, 1992).

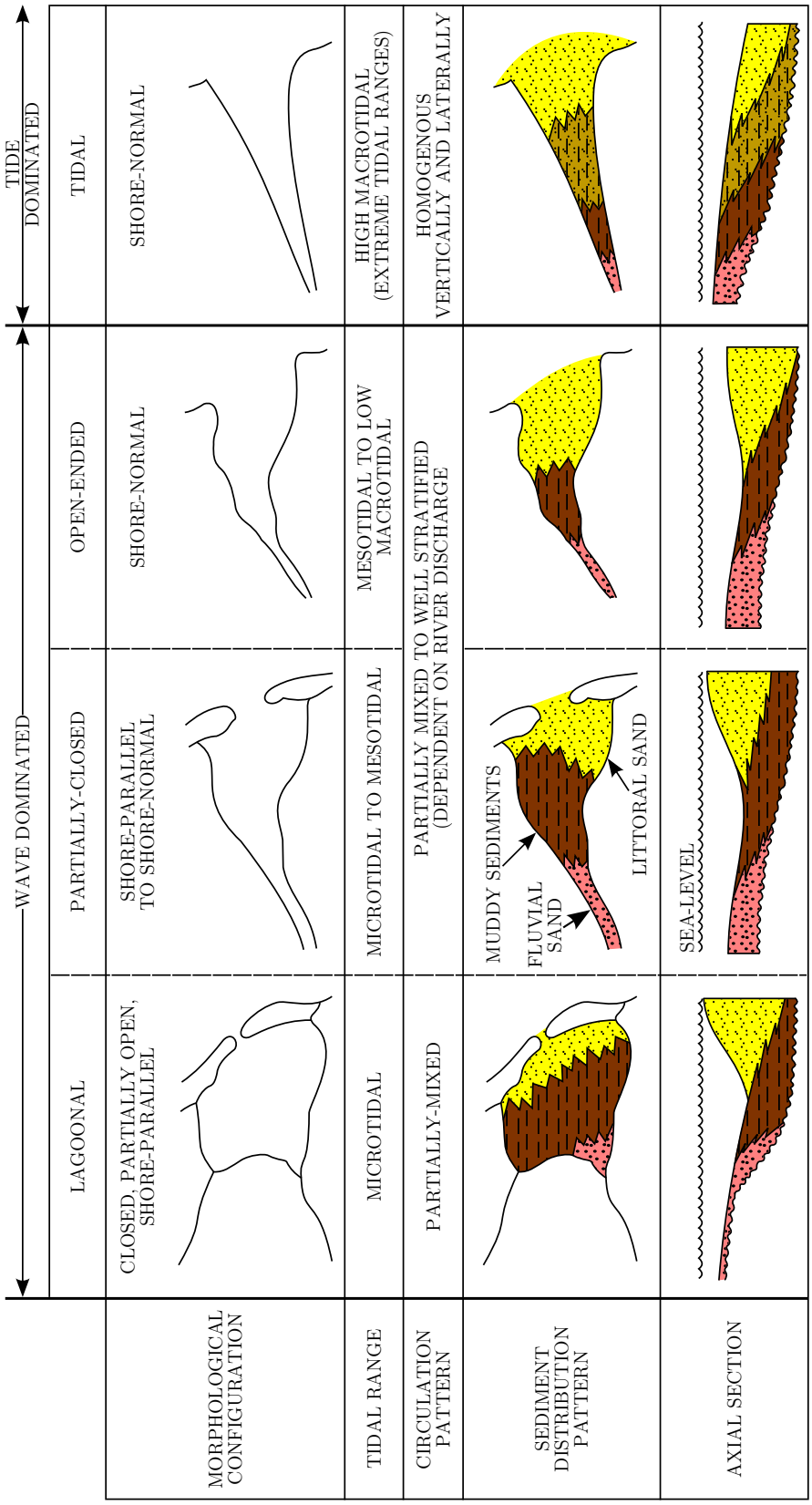
WAVE DOMINATED
TIDE DOMINATED
LAGOONAL
PARTIALLY-CLOSED
OPEN-ENDED
TIDAL
MORPHOLOGICAL CONFIGURATION
CLOSED, PARTIALLY OPEN, SHORE-PARALLEL
SHORE-PARALLEL TO SHORE-NORMAL
SHORE-NORMAL
SHORE-NORMAL
TIDAL RANGE
MICROTIDAL
MICROTIDAL TO MESOTIDAL
MESOTIDAL TO LOW MACROTIDAL
HIGH MACROTIDAL (EXTREME TIDAL RANGES)
CIRCULATION PATTERN
PARTIALLY-MIXED
PARTIALLY MIXED TO WELL STRATIFIED (DEPENDENT ON RIVER DISCHARGE
HOMOGENOUS VERTICALLY AND LATERALLY
SEDIMENT DISTRIBUTION PATTERN
MUDDY SEDIMENTS
FLUVIAL SAND
LITTORAL SAND
AXIAL SECTION
SEA-LEVEL
EXAMPLE
GREAT SOUND, NEW JERSEY
MIRAMICHI, NEW BRUNSWICK
GIRONDE, FRANCE
BROAD SOUND, AUSTRALIA

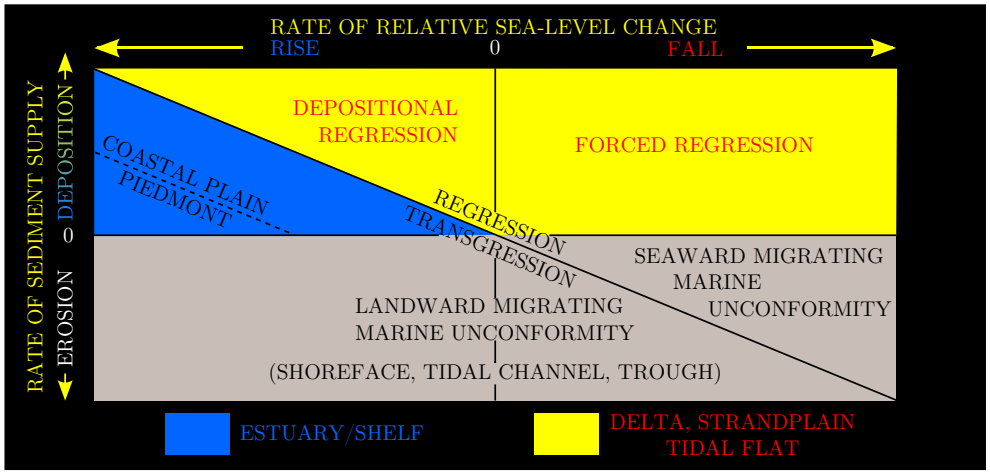

Figure 5.2: Shoreline response (transgression versus regression) to changes in sea-level and sediment supply (after Boyd et al., 1992, 2006).

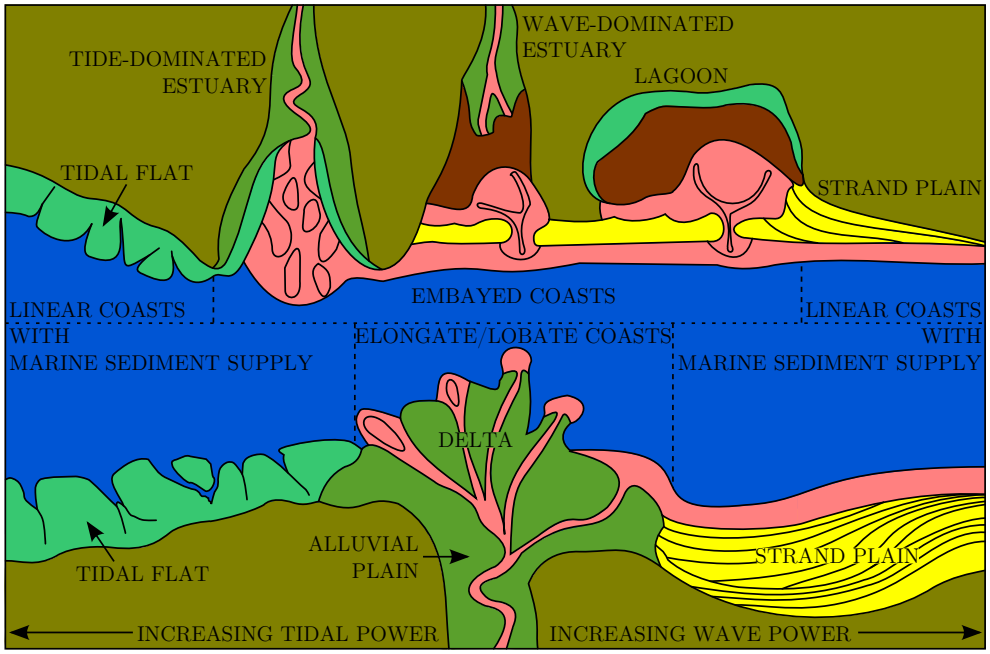

Figure 5.3: Classification after Boyd et al. (1992, 2006), illustrating the organisation of all major clastic coastal depositonal environments based on shoreline translation direction (progradation or transgression), and the relative power of waves, tidal currents, and river currents. The upper coastline is transgressive, the lower coastline regressive. The influence of tides relative to wave power increases from right to left.

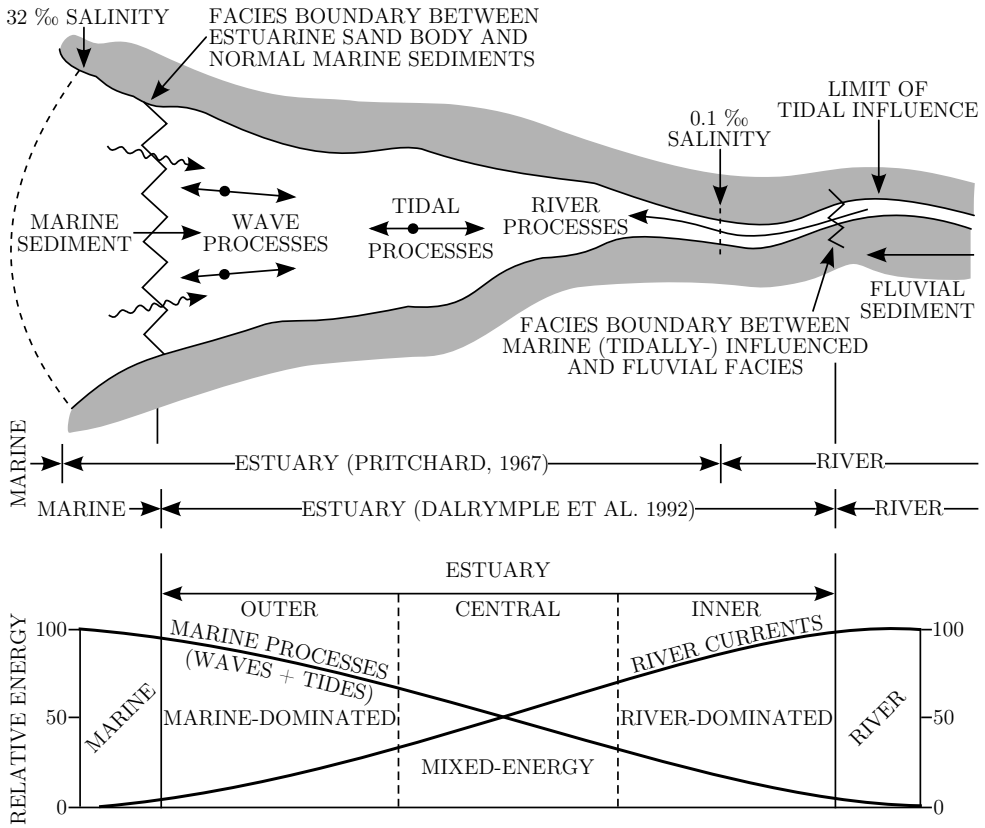

Figure 5.4: (A) Schematic representation of the definitions of estuary according to Pritchard (1967) and Dalrymple et al. (1992), and the generalised pattern of net, bed-material transport. The facies boundary marking the landward end of the estuary as defined here almost lies landward of the 0.1 ‰ salinity value, but the facies boundary at the outer end may lie either landward (as shown here) or seaward of the limit of normal marine salinities (∼32 ‰). (B) Schematic distribution of the physical processes operating within estuaries, and the resulting tripartite facies zonation. (After Dalrymple et al., 1992.)

5.4 Wave- and tide-dominated estuarine facies models

Dalrymple et al. (1992) considered the relationship of estuaries to other coastal systems, with reference to the relative importance of the physical processes operating at the coast (tidal, wave, and fluvial), as well as temporal changes driven by relative sea-level fluctuations and changes in sediment supply (Figure 5.5). Following the coastal classification schemes of Hayes (1979) and Davis and Hayes (1984), Dalrymple et al. (1992) subdivided estuaries into two distinct but intergradational end-member types, wave- and tide-dominated, with the degree of river influence varying from weak to strong in each category.

Dalrymple et al. (1992) presented a generalised process-based tripartite division of wave- and tide-dominated estuaries, based on the interaction between

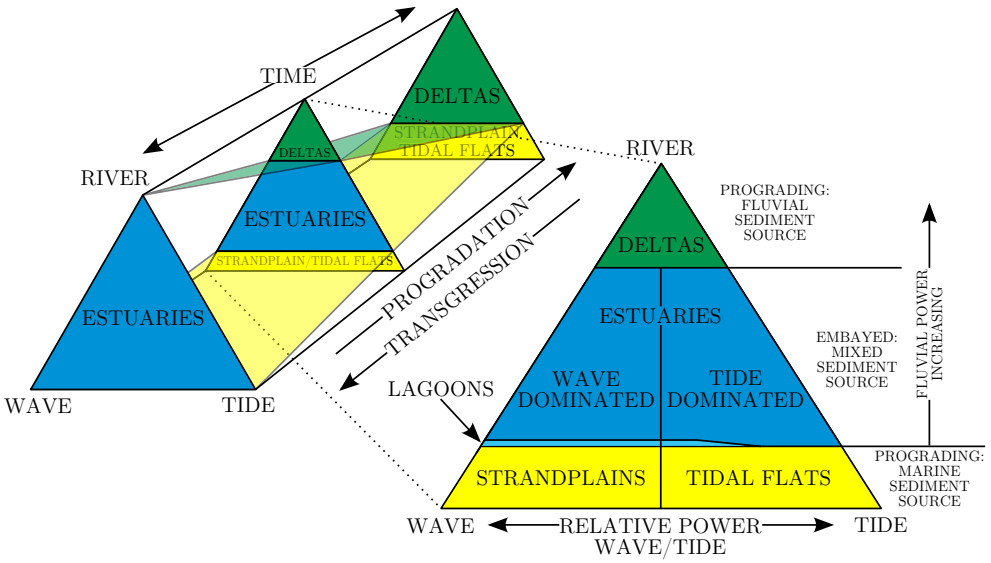

Figure 5.5: Evolutionary classification of coastal environments (after Dalrymple et al., 1992). The long axis of the three-dimensional prism (left) represents relative time with reference to changes in relative sea level and sediment supply (i.e., transgression and progradation). The three edges of the prism correspond to conditions dominated by fluvial, wave and tidal processes. The enlargement of the center of the prisim (right) shows the position of representative modem systems. Systems which are at different stages of infilling and are thus spread out along the length of the prism have been projected into the plane of the enlargment.

fluvial and marine processes (Figure 5.4). Fluvial energy typically decreases towards the mouth of an estuary, while marine energy generally decreases towards the estuary head. Dalrymple et al. (1992) therefore divided both wave- and tide-dominated estuaries into three idealised zones (Figure 5.4):

1. An outer zone dominated by marine processes (waves and/or tidal currents),
2. A relatively low energy central zone where marine energy (generally tidal currents) and river currents are approximately equal in strength through the long term,
3. And an inner, river-dominated zone.

5.5 Conceptual facies model for wave-dominated estuaries

Following the models presented by Dalrymple et al. (1992) the Manawatu valley would be classified as a wave-dominated estuary (Clement et al., 2010). The Manawatu coast is wave-dominated, being subject to waves from both the southwest and west (see Section 4.6). From the southwest, waves generated in the northern Cook Strait have a maximum fetch of 100 km, resulting in

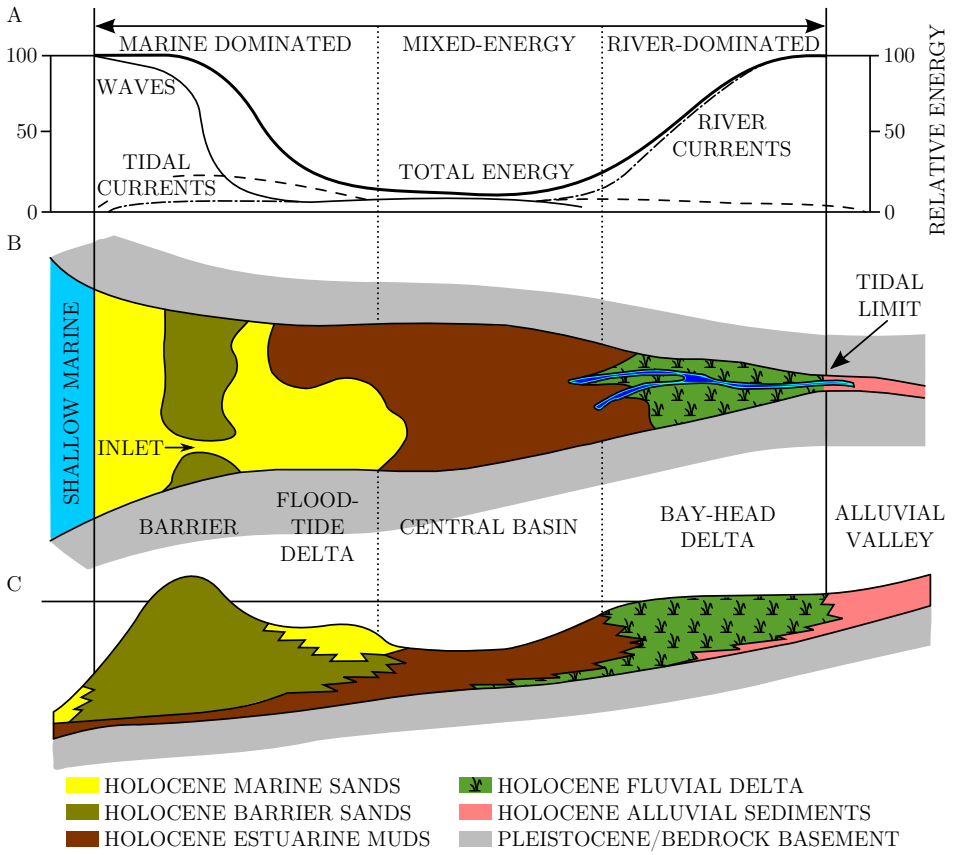

Figure 5.6: Distribution of (A) energy types, (B) morphological components in plan view, and (C) sedimentary facies in longitudinal section within an idealised wave-dominated estuary (after Dalrymple et al., 1992). For simplicity the complete transgressive succession that would be formed by landward migration of the estuary is not shown.

moderate wave energy. Waves approaching from the west (Tasman Sea) have a much greater fetch, resulting in a dominant westerly swell (Clement et al., 2010). In contrast, the Manawatu coast is barely mesotidal, with a spring tidal range of ±1.1 m, and a neep tidal range of c. ±0.45 m (New Zealand Nauitical Almanac tide levels at the Manawatu River entrance). This discussion will therefore focus on the conceptual facies model for wave-dominated estuaries.

The longitudinal profile of total energy (that is, the sum of all energy from all sources: waves and tidal and river currents) for an idealised wave-dominated estuary displays two maxima: one at the estuary mouth produced by wave energy, and one at the head generated by river currents (Figure 5.6A). This distribution of total energy creates a clearly defined "tripartite" distribution of lithofacies (coarse-fine-coarse) within most wave-dominated estuaries (Figure 5.6B and C; e.g., Bird, 1967; Klum and Byrne, 1967; Reinson, 1977; Roy et al., 1980; Zaitlin and Shultz, 1984, 1990; Rahmani, 1988; Reinson et al., 1988; Allen, 1991; Nichol, 1991; Nichols et al., 1991; Pattison, 1992; Marra,

Table 5.1: Morphological and sedimentalogical summary of wave-dominated estuaries (after Nichol, 1991; Marra, 1997).

Facies zone	Morphostratigraphic units/ depositional environments	Lithofacies
Zone 1: Marine-influenced	Barrier spit Back barrier tidal flats Flood-tide delta Tidal channel Beach ridge	Medium- to coarse-grained well-sorted quartz-dominated sand, sourced mainly from the nearshore and upper shoreface. Low organic content with burrowing organisms limit to areas of weak tidal action. Bi-directional and planar bedforms in tidal channels and distal portion of the flood tide delta.
Zone 2: Estuarine central basin	Central basin Supratidal beach Intertidal beach Tidal flats Salt marsh	Fine-grained organic and shell-rich mud. Sands introduced by fluvial flooding. Bedforms absent. Fine laminae and minor sand-mud interbedding.
Zone 3: River-dominated	Supratidal fluvial delta Intertidal fluvial delta Fluvial channel Point bar Floodplain	Fluvial gravels, sands, silts and muds. High organic content and biogenic activity. Poorly developed bedforms.

1997; Glover, 1997). As the estuary infills the energy minimum at the centre becomes less pronounced.

5.5.1 Zone 1: Marine-influenced sedimentary facies

Ideally a marine sand-body of well sorted, mineralogically mature sediment accumulates in the area of high wave energy at the mouth of the estuary (Figure 5.6B and C). This sediment is generally marine quartzose sand sourced from the nearshore and upper shoreface and moved into the mouth of the estuary by longshore drift. River sediment is not usually transported into the marine-dominated zone unless the estuary is at an advanced stage of infilling, providing the river with a direct connection to the ocean. Morphologically the marine sand body is controlled by barrier complex and tidal inlet processes which may manifest barrier spits, back-barrier sand flats, washover fans, flood- and ebb-tide deltas and tidal inlet channels (Figure 5.6B and C; Table 5.1; Roy et al., 1980; Nichol, 1991; Boyd et al., 1992; Dalrymple et al., 1992; Reinson, 1992; Roy, 1994; Glover, 1997; Heap and Nichol, 1997; Marra, 1997; Heap et al., 2004; Sloss et al., 2004a,b, 2005, 2006a,b, 2007, 2010; Skuja, 2006; Wilson et al., 2007).

5.5.2 Zone 2: Central basin mud facies

The central portion of a wave-dominated estuary is a low-energy, back barrier environment in which fine-grained organic rich mud accumulates (Figure 5.6B and C; Table 5.1; e.g., Biggs, 1967; Donaldson et al., 1970; Roy et al., 1980; Chapman et al., 1982; Reinson, 1992; Sloss et al., 2004a,b, 2005, 2006a,b, 2007, 2010). This mud is made up of fine river sediment, supplied mainly during

floods; they are the estuarine equivalent of pro-delta lithofacies (e.g., Dalrymple et al., 1992; Roy, 1994; Boyd et al., 2006). In partially filled estuaries the low-energy central mud basin is typically replaced by extensive salt marshes, mud flats, tidal channels and mangrove swamps (e.g., Dorjes and Howard, 1975; Roy et al., 1980, 2001; Chapman et al., 1982; Clifton, 1983; Dalrymple et al., 1992; Roy, 1994; Heap, 1995; Heap et al., 2004).

5.5.3 Zone 3: River-dominated sedimentary facies

The head of a wave-dominated estuary is ideally dominated by tidally-influenced fluvial processes. Sand and/or gravel are deposited in this region by the inflowing river, forming a bay-head delta (Figure 5.6B and C; Table 5.1; e.g., Roy et al., 1980; Chapman et al., 1982; Roy, 1984a,b; Nichol, 1991; Boyd et al., 1992; Dalrymple et al., 1992; Broger et al., 1997; Sloss et al., 2004a,b). The extent and morphology of the bay-head delta is controlled by the catchment size, amount of rainfall, consequent river discharge, the supply of fluvial sediment, and the wave and wind regime of the estuary (Sloss, 2005). In estuaries with a broad central basin the delta typically develops a fluvially-dominated, birdsfoot morphology, though this is generally not exhibited in more confined estuaries (Dalrymple et al., 1992).

5.6 Criticisms of the conceptual estuarine facies models

Washington and Chisick (1994) suggested that the estuary model presented by Dalrymple et al. (1992) was too simplistic, and should have included factors such as the production and accumulation of autochthonous biogenic sediment, the rate of sea-level rise relative to the rate of marine sediment input, and differing climatic regimes. In reply, Dalrymple et al. (1994) noted that no generalised model could include the full range of factors that may be present in a depositional environment. Dalrymple et al. (1994) stated that while the three factors identified by Washington and Chisick (1994) may be important in local examples, they were excluded from the original model (Dalrymple et al., 1992) as part of the distillation process (e.g., Walker, 1992). More specifically, Dalrymple et al. (1994) noted that the factors did not control the basic geomorphic organisation of estuarine facies, that it was the interaction of fluvial and marine processes that fundamentally characterised estuarine deposits, and that the factors identified by Washington and Chisick (1994) were secondary to the fluvial-marine process interaction. This position was reaffirmed by Boyd et al. (2006).

5.7 Wave-dominated Holocene embayments on the southeast coast of Australia: conceptual models

Roy et al. (1980), from an examination of embayments on the southeast coast of Australia, developed evolutionary models for three broad classes of wave-dominated estuary (Figure 5.7): wave-dominated barrier estuaries; open ocean embayments; and drowned-river estuaries. These three basic types of estuary classification have provided a framework upon which subsequent investigations of estuarine sedimentation and the geomorphological evolution of the southeast Australian coast have been based (e.g., Nichol, 1991; Bradshaw, 1993; Roy, 1994; Roy et al., 1994, 2001; Yassini and Jones, 1995; Roy and Boyd, 1996; Masatomo et al., 2001; Heap et al., 2004; Sloss et al., 2004a,b, 2005, 2006a,b, 2007, 2010).

5.7.1 Wave-dominated barrier estuaries

Wave-dominated barrier estuaries feature estuarine lakes impounded behind Holocene coastal barrier systems that fill the mouths of valleys incised during the Last Glacial sea-level lowstand (Figure 5.7). Broad back-barrier sand-flats and extensive central mud basins are characteristic features (Roy et al., 1980; Roy, 1984a,b; Roy and Boyd, 1996; Heap et al., 2004; Sloss et al., 2004a,b, 2005, 2006a,b, 2007, 2010). The mouth of the estuary receives considerable wave energy, while the back-barrier lagoon has a small tidal influence. The combination of wave and tidal energy causes sediment to move along and onshore into the estuary mouth forming the barrier which prevents waves from entering the estuary (Roy et al., 1980; Roy, 1984a,b; Heap et al., 2004).

Stratigraphic studies suggest that in the intial stages of infilling wave-dominated barrier estuaries feature a tripartite facies division (Roy et al., 1980; Roy, 1984a,b, 1994; Chapman et al., 1982; Dalrymple et al., 1992). Landward, the antecedent Pleistocene land surface is directly overlain by fluvial deposits, while the central basin is filled with fine-grained estuarine mud. Seaward lies a transgressive sand body (e.g., Roy et al., 1980, 2001; Chapman et al., 1982; Roy, 1984a,b, 1994; Dalrymple et al., 1992). Recent research by Sloss et al. (2005, 2006a,b, 2007, 2010) has shown that the Holocene transgressive facies is more extensive than previously anticipated, being preserved as a basal, near basin-wide shell-rich sandsheet that overlies the antecedent Pleistocene valley floor.

5.7.2 Open-ocean embayments

On the southeast Australian coast open-ocean embayments are large open bay mouths typically formed between rocky headlands and dominated by ocean swell and wind waves (Figure 5.7). The influence of fluvial and estuarine processes is negligible (e.g., Roy et al., 1980; Chapman et al., 1982; Yassini and Jones, 1995). In contrast to the other estuary typed identified by Roy et al. (1980), open-ocean embayments do not feature a characteristic tripartite facies

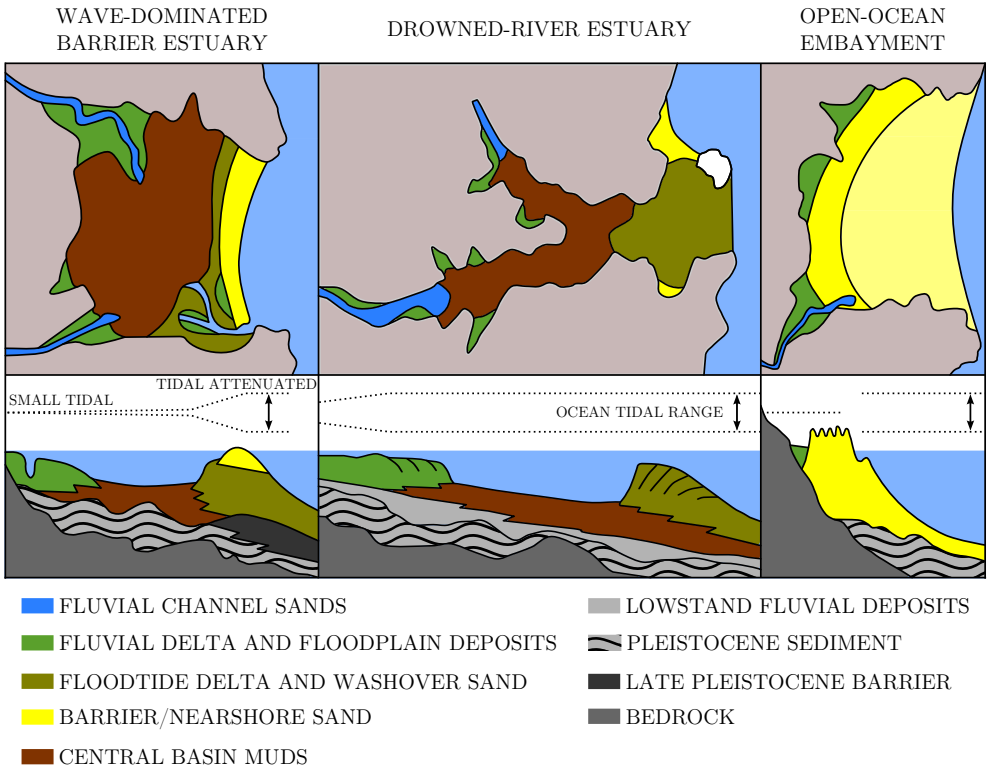

Figure 5.7: Classification of wave-dominated estuaries on the southeast coast of Australia (after Roy et al., 1980; Chapman et al., 1982).

division. Instead, open-ocean embayments are characterised by four distinct depositional environments controlled by ocean swells and wind waves (Roy et al., 1980; Chapman et al., 1982; Yassini and Jones, 1995):

1. Nearshore, medium- to coarse-grained beach and barrier dune facies, extending to depths of up to 30 m below PMSL.
2. Fine-grained sand lining the rest of the embayment, at depths of less than 30 m below PMSL.
3. Fine silty mud deposited in water depths greater than 30 m below PMLS.
4. Low-energy back-barrier facies spatially restricted to small depressions landward of the barrier/beach facies.

5.7.3 Drowned-river estuaries

In the southeast Australian context, drowned-river estuaries form in deeply-incised (>80 m) valleys with deep-water entrances (Figures 5.7 and 5.8; Roy et al., 1980; Chapman et al., 1982; Roy, 1984a,b). The entrances of drowned-river estuaries are exposed to direct ocean influences, and are therefore dominated by marine-influenced processes. This typically produces large, subaqueous flood-tide deltas which extend from the estuary mouth into the lower estuary (Figure 5.8). At the landward end, drowned-river estuaries are char-

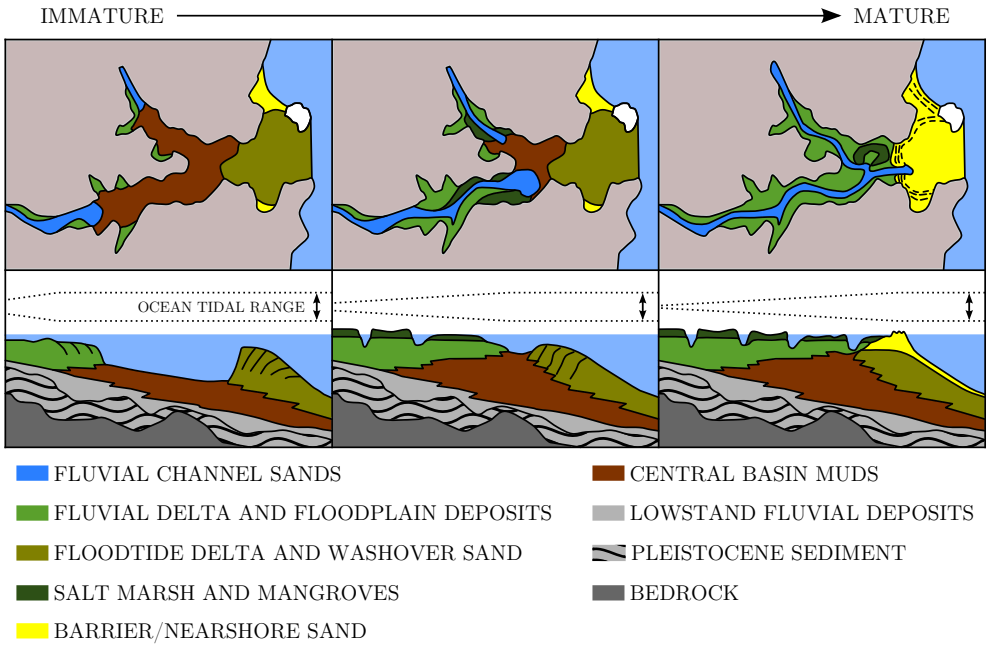

Figure 5.8: Conceptual model of the sedimentary infilling of a drowned-river estuary (after Roy et al., 1980; Chapman et al., 1982; Roy, 1984a,b, 1994).

acterised by fluvial deltas which prograde into low energy central mud basins (Roy et al., 1980; Chapman et al., 1982; Roy, 1984a,b, 1994).

Roy et al. (1980) characterised the Holocene evolution of drowned-river estuaries in three stages from immature to mature (Figure 5.8). At an early stage of infilling during the Holocene marine transgression, tidal delta sills or proto-barriers protected the central basin from direct marine influences. Once sea levels had stabilised, transgressive marine sediments would have continued to prograde into the estuary mouth, typically producing a landward-migrating flood-tide delta. At the same time, the fluvial delta at the head of the estuary would be prograding, constricting the central basin (Figure 5.8; Roy et al., 1980, 1994; Chapman et al., 1982; Roy, 1984a,b, 1994; Roy and Boyd, 1996). In the late stages of infilling of a drowned-river estuary, fluvial processes would have dominated due to a decrease in accommodation. Fluvial deposits would therefore eventually fill the valley and prograde seaward over the tidal delta.

5.7.4 The position of the Manawatu valley within the context of wave-dominated estuary models from the southeast coast of Australia

Under the three broad classes of wave-dominated estuary identified by Roy et al. (1980), the lower Manawatu valley would be considered a drowned-river estuary (Clement et al., 2010). The Manawatu was formerly a deeply incised-valley. Given the present geomorphology of the lower Manawatu, it can be

presumed that the entrance to this valley would have been exposed to direct marine influences.

In considering the other two estuary types, it can be seen that the lower Manawatu valley is clearly not an open-ocean embayment. It does not feature an open bay mouth. Nor is the Manawatu a wave-dominated barrier estuary. While the Manawatu is suggested to have featured barriers in the form of the Porotawhao High and Himitangi Anticline (Hesp, 1975; Hesp and Shepherd, 1978; Heerdegen and Shepherd, 1992), these are not barriers in the sense of a wave-dominated barrier estuary.

5.8 Background to sequence stratigraphy and incised-valley facies models

Through the late 1970s and into the 1980s a series of papers were presented that developed the paradigm of seismic stratigraphy (e.g., Vail, 1975, 1987; Mitchum, 1977; Payton, 1977; Vail et al., 1977, 1980), which sought to provide geological context to the stratigraphic interpretation of seismic data. Vail and co-workers recognised that convergences or truncations of seismic reflectors corresponded to unconformities in the stratigraphic record, assumed to be the product of eustatic sea-level fluctuations. Seismic stratigraphy therefore presented a means of elucidating the chronostratigraphic depositional and structural patterns recorded by seismic sections (Vail and Mitchum, 1977). Jervey (1988) revolutionised seismic stratigraphy with accommodation models which considered the interplay between eustasy, tectonics, and sedimentation, and the impact these factors had on the space available for potential sediment accumulation. This work led to the realisation that sequences could be subdivided into systems tracts (e.g., Brown and Fisher, 1977; Baum and Vail, 1988; Donovan et al., 1988; Loutit et al., 1988).

Seismic stratigraphy subsequently developed into the more geologically-oriented concept of sequence stratigraphy (e.g., Posamentier et al., 1988; Posamentier and Vail, 1988; Van Wagoner et al., 1988; Wilgus et al., 1988; Haq, 1991), which incorporated lithological data, in the form of well logs, cores, and outcrops, and the concept of facies successions (Van Wagoner et al., 1988, 1990; Catuneanu, 2006). This enabled facies and time-transgressive lithostratigraphy to be analysed within the chronostratigraphic framework of systems tracts, sequences, and sequence boundaries (Van Wagoner et al., 1990).

The emphasis placed by sequence stratigraphy on subaerial unconformities in the subdivision of the stratigraphic record brought attention to incised-valleys and their fill (Dalrymple, 2006), particularly with the realisation that incised-valley systems represented the major component of sequences formed during periods of lower relative sea-level (Van Wagoner et al., 1990), and recognition that incised-valleys were important identifying features overlying sequence boundaries (e.g., Belknap et al., 1994; Zaitlin et al., 1994). In order to elucidate the fill of incised-valleys in a range of coastal settings a number of workers integrated the concept of estuarine facies models (Dalrymple et al.,

1992) with the principles of sequence stratigraphy (e.g., Allen and Posamentier, 1993, 1994; Ashley and Sheridan, 1994; Nichol et al., 1994). This approach was formalised by Zaitlin et al. (1994) in the form of the first integrated facies model for an incised-valley system.

Zaitlin et al. (1994) restricted consideration to incised-valley systems developed as a result of relative sea-level fall (either eustatically, or tectonically driven). Within this context an incised-valley system was defined as:

> "[a] fluvially-eroded, elongate topographic low that is typically larger than a single channel form, and is characterised by an abrupt seaward shift of depositional facies across a regionally mappable sequence boundary at its base. The fill typically begins to accumulate during the next base-level rise, and may contain deposits of the following highstand and subsequent sea-level cycles." (Zaitlin et al., 1994, p. 47).

Estuaries, following the definition presented by Dalrymple et al. (1992), are therefore transgressive, tidally influenced environments that constitute an important and distinctive component of incised-valleys in their seaward parts (Boyd et al., 2006).

Zaitlin et al. (1994) identified four fundamental characteristics of incised valley systems that may be used to aid their recognition (see also Boyd et al., 2006):

1. The valley is a negative (i.e. erosional) palaeotopographic feature, the base of which truncates underlying strata, including any regional markers that may be present.
2. The base and walls of the incised-valley system represent a sequence boundary that correlates with an erosional (or hiatal) surface outside the valley.
3. The base of the incised-valley fill exhibits an erosional juxtaposition of more proximal (landward) facies over more distal (seaward) deposits (i.e., a "basinward shift in facies," *sensu* Van Wagoner et al., 1990).
4. Depositional markers within the deposits of the incised-valley fill will onlap the valley walls, but do not occur outside the valley.

Zaitlin et al. (1994) recognised two different types of incised-valley systems: piedmont and coastal plain. The former have their headwaters rising in a (mountainous) hinterland, and cross a "fall line" where there is a significant reduction in gradient. The latter are confined to low-gradient coastal plains and do not cross a "fall line." Zaitlin et al. (1994) also distinguished two classes of incised-valley fill, simple or compound, depending on the absence or presence, respectively, of multiple, internal, high-frequency sequence boundaries. Thus, if an incised-valley is filled completely during one incision-deposition cycle, the fill is simple. A compound fill consists of multiple depositional sequences produced by multiple fluctuations in base level, and is therefore

punctuated by one or more sequence boundaries above the main, lower-order sequence boundary at the base of the incised-valley.

5.9 Model for a simple incised-valley fill

5.9.1 Straigraphic organisation

The idealised fill of a wave-dominated incised-valley is subdivided longitudinally into three segments (distinct from the tripartite estuarine zonation discussed above) (Figure 5.9). This subdivision arises from the unique depositional and stratigraphic organisation of the fill, produced by the sequence of lowstand erosion, transgressive deposition, and highstand progradation (Zaitlin et al., 1994; Boyd et al., 2006). The relative length of each of the three segments may be quite variable (Boyd et al., 2006). In the case of an extensive transgression the outer incised-valley is likely to be long, and may extend across most of the width of the formerly exposed continental shelf. The length of the centre and inner segments of an incised-valley is related to the depth of valley incision and the valley gradient above the highstand shoreline (e.g., Thomas and Anderson, 1994; Blum and Tornqvist, 2000).

The outer incised-valley (segment 1) extends from the most seaward point of valley incision, near the mouth of the valley, landward, to the position where the shoreline stabilises at the beginning of highstand progradation (Figure 5.9; Zaitlin et al., 1994; Boyd et al., 2006). A lowstand delta may form or shoreline progradation may take place via the deposition of sediment which is bypassed to the mouth of the valley. As sea-level rises at the beginning of the transgression, the lower reaches of the valley cease to be a conduit for fluvially-eroded sediment, and become the site of fluvial (and subsequently estuarine) deposition. Through the early stages of the transgression fluvial deposition continues in the outer incised-valley, with the locus of deposition shifting landward as relative sea-level rises and the shoreline transgresses (Westcott, 1993; Wright and Marriott, 1993). The transition from fluvial conduit to fluvial deposition migrates landward as the transgression progresses. As a result, in the outer segment of the incised-valley the boundary between the lowstand and transgressive systems tracts may lie within the fluvial deposits, rather than at their top.

The depositional gradient and capacity of the fluvial system decreases as the shoreline approaches, resulting in a vertical succession of lowstand to transgressive fluvial sediments at the river mouth. The thickness of the fluvial succession may vary along the length of the outer segment of the incised-valley, and is ultimately controlled by the accommodation developed during the sea-level rise (Jervey, 1988). Accommodation is in turn controlled by the difference between the rate of sediment input and the rate of sea-level rise (e.g., Curray, 1964; Posamentier and Allen, 1999; Coe et al., 2003; Catuneanu, 2002, 2006). Therefore, where rapid sea-level rise outpaces fluvial deposition the thickness of the deposits is less than occurs when abundant sediment input occurs during

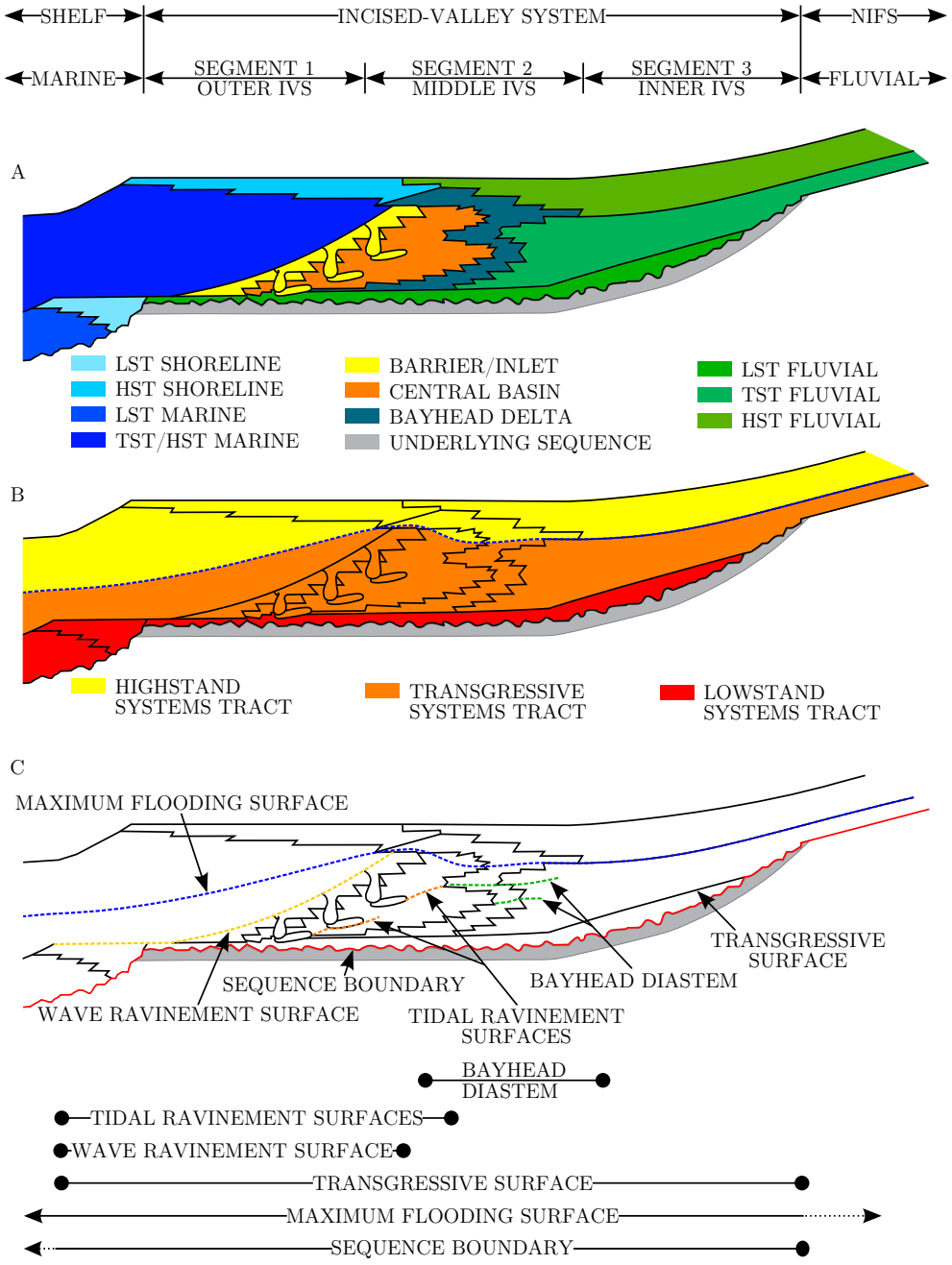

Figure 5.9: Idealised longitudinal section of a simple incised-valley system showing the distribution of: (A) depositional environments; (B) system tracts; and (C) key stratigraphic surfaces. Segments 1 and 3 are typically much longer than segment 2, and are compressed here for ease of presentation. LST - lowstand systems tract; TST = transgressive systems tract; HST highstand systems tract; NIFS = non-incised fluvial system. (After Zaitlin et al., 1994.)

a slow rise in sea-level. In all cases, the thickness of the fluvial succession that is preserved may be affected by erosion association with the transgression.

As sea levels continue to rise the estuarine conditions established at the mouth migrate up the valley. In wave-dominated estuarine settings tidally influenced fluvial and bay-head delta deposits are the first estuarine sequences to be laid down. These deposits are overlain by central-basin deposits as the transgressions progresses. The central-basin deposits are subsequently overlain by estuarine flood-tide-delta and other barrier deposits (cf. Boyd et al., 1992; Dalrymple et al., 1992).

The central segment of an idealised incised-valley system extends from the initial highstand shoreline (i.e., the inner end of segment 1) to the estuarine limit at the time of maximum flooding (Figure 5.9; Zaitlin et al., 1994; Boyd et al., 2006). Segment 2 therefore represents the area occupied by the drowned-valley estuary at the end of the transgression, with the landward limit of tidal influence in segment corresponding to the inner boundary of the wave-dominated estuary as defined by Dalrymple et al. (1992).

In the central segment the sequence boundary at the base is immediately overlain by lowstand to early-transgressive fluvial deposits similar to those in segment 1. These are in turn overlain by transgressive estuarine facies. At the seaward end of the central segment the facies succession is broadly similar to that in segment 1, with fluvial and bayhead delta deposits overlain by central basin sediments. These are capped with estuary-mouth-barrier sands. Because open marine conditions do not extend this far into the valley, these barrier sands are overlain by highstand fluvial deposits, unless a fall in sea-level occurs before the estuary is completely infilled, in which case the barrier sediments are overlain by the next sequence boundary. In the middle portion of segment 2 barrier sands are absent, while the central-basin deposits present a coarsening upward succession. These central-basin sediments are overlain by bay-head delta and fluvial deposits provided that the sea-level highstand is of sufficient duration to allow the estuary to be completely filled. At the upper end of segment 2 central-basin deposits are absent, with the bayhead-delta deposits being directly overlain by highstand fluvial sediments.

Segment 3 of an idealised incised-valley lies landward of the transgressive marine-estuarine limit, but is still influenced by changes in relative sea-level. Segment 3 contains exclusively fluvial sediments preserved between the transgressive limit and the landward limit of fluvial incision (Zaitlin et al., 1994; Boyd et al., 2006), and may extend inland for tens to hundreds of kilometres (Shanley et al., 1992; Schumm, 1993; Levy and Christie-Blick, 1994).

5.9.2 Stratigraphic surfaces

A number of stratigraphically-significant surfaces characterise the infill of incised-valley systems (Zaitlin et al., 1994). The surface which defines the valley form is the sequence boundary, which is developed through fluvial incision within the valley. In the idealised case, the sequence boundary is immedi-

ately overlain by lowstand fluvial deposits (see above) which constitute the lowstand systems tract. These lowstand deposits are in turn overlain by sediments of the transgressive systems tract, which are deposited in response to rising sea-level. The transgressive surface separates the lowstand and transgressive systems tracts, and ideally occurs low in the valley fill. Another important horizon low in the valley fill is the contact between estuarine and fluvial facies, which commonly represents the initial flooding surface. Additional flooding surfaces may be produced by progradational episodes controlled by variations in the rate of sea-level rise or sediment supply. The outer and middle segments of an idealised incised-valley feature a tidal ravinement surface (Figure 5.9), which is produced by erosion at the base of the deepest tidal inlet or other tidal channel. This surface is diachronous, becoming younger up the valley. As sea levels continue to rise a wave ravinement surface develops as the shoreface migrates up-valley, eroding pre-existing barrier sediments (e.g., Swift, 1968), and, depending upon the depth of the wave base, potentially central-basin, bayhead-delta and fluvial deposits (e.g., Allen and Posamentier, 1994; Ashley and Sheridan, 1994; Belknap et al., 1994). The wave ravinement surface is regionally significant, extending across the incised-valley and interfluves (Figure 5.9). The maximum flooding surface (MFS) corresponds to the time of maximum transgression. In the outer segment of the incised-valley the MFS lies within the marine sediments which overlie the wave ravinement surface and passes through the sands of the estuary-mouth barrier and initial highstand shoreline. In the central segment the MFS lies within the central basin deposits where they are sandwiched between underlying transgressive and overlying regressive bayhead-delta deposits. Within the upper segment of an incised-valley, the MFS may be hard to recognise, but may be associated with the most finely-grained fluvial sediments.

5.10 Estuarine and incised-valley facies models: New Zealand context

There are relatively few studies which have applied models of estuarine and incised-valley infilling to New Zealand localities. Investigations by Marra (1997) in Waitotahi estuary, Skuja (2006) in Tairua estuary, and Wratt (1999) in Puhoi River estuary, all documented infill sequences which showed broad agreement with the models presented by Dalrymple et al. (1992) and Zaitlin et al. (1994). However, there are a number of other studies which have outlined significant deviations from the model infill sequences (e.g., Heap and Nichol, 1997; Wilson et al., 2007; Abrahim et al., 2008; Kennedy et al., 2008; Clement et al., 2010).

Wilson et al. (2007) utilised the estuarine and incised-valley facies models presented by Dalrymple et al. (1992) and Zaitlin et al. (1994) as a base from which to elucidate the fill of the Pakarae River incised-valley, which experienced coseismic uplift throughout the Holocene. Wilson et al. (2007) noted that the case studies of Holocene incised-valley infill upon which the tripartite

facies models are based commonly come from estuaries of extensive size (40–100 km in length) on stable coastlines, with comparatively limited sediment supplies (e.g., Allen and Posamentier, 1993, 1994) and low river discharges (e.g., Dalrymple et al., 1992). Wilson et al. (2007) therefore suggested that it was unclear whether the models would scale to New Zealand conditions (estuaries an order of magnitude smaller, actively uplifted coastlines, high river discharges). At Pakarae, Wilson et al. (2007) identified a basal fluvial sediment package immediately overlain by estuary-head delta deposits, all capped with barrier sands, which it was suggested correlated well with models of incised-valley infill. However, the central section of the Pakarae stratigraphy displayed complex alternations of estuarine and fluvial environments, rather than the typical estuarine central mud basin. Wilson et al. (2007) attributed this difference to incision by the fluvial system due to base level fall driven by coseismic uplift events, coupled with the rapid delivery of large volumes of earthquake-generated sediment into the valley following uplift.

Other studies of incised-valley fill in New Zealand have demonstrated that the development and preservation of the central basin facies is affected by the combined effects of the allocentric controls of accommodation space, tectonism, sedimentation rate and sea-level behaviour (e.g., Heap and Nichol, 1997; Abrahim et al., 2008; Kennedy et al., 2008). In Tamaki Estuary, Auckland, Abrahim et al. (2008) reported the absence of a central basin facies in a sequence that is otherwise broadly consistent with the idealised case of a wave-dominated incised-valley system. Elsewhere, Heap and Nichol (1997) and Kennedy et al. (2008), working in Weiti River Estuary and Whanganui Inlet respectively, have reported stratigraphic records where high sedimentation rates, shallow valley form and lack of a seaward barrier have limited the development of a low-energy central basin.

5.11 Summary

Estuarine and incised-valley facies models provide a framework to delineate the infilling of these systems following their inundation during Holocene marine transgression. The sedimentary fill of wave-dominated estuaries such as the lower Manawatu valley is characterised by a tripartite facies division: a marine sand body comprised of barrier, washover, tidal inlet, and tidal delta deposits; a fine-grained low-energy central basin; and a prograding bay-head delta complex at the head of the estuary. Similarly, a three stage evolutionary model has been proposed for wave-dominated drowned-river valleys like the Manawatu: deeply-incised valleys with deep water entrances which feature a large central basin protected by a proto-barrier.

The development of sequence stratigraphy enabled facies and time-transgressive lithostratigraphy to be analysed within the chronostratigraphic framework of systems tracts, sequences, and sequence boundaries. In order to elucidate the fill of incised-valleys a number of researchers therefore integrated the concept of estuarine facies models with the principles of sequence stratig-

raphy. The result was a model for a simple incised-valley fill which described the unique depositional and stratigraphic organisation of an incised-valley produced by the sequence of lowstand erosion, transgressive deposition, and highstand progradation.

These models provide a framework for the interpretation of the evolution of the lower Manawatu valley during and following the Holocene marine transgression. The following chapter utilises water well logs to identify and delineate features of the sedimentary infill of the lower Manawatu valley, within the context of the simple model of incised-valley infilling. After this, Chapter 7 utilises detailed vibracores to produce accurate facies reconstructions and models for the lower Manawatu valley's Holocene fill. Chapter 8 then uses the estuarine and incised-valley facies models as a framework for understanding the evolution of the lower Manawatu valley following the Holocene marine transgression.

Chapter 6

Holocene sedimentary infill of the lower Manawatu incised-valley system reconstructed from water well logs

6.1 Introduction

Stratigraphic data obtained from water wells drilled across the Manawatu region represents a major source of information for the delineation of the subsurface geology of the Manawatu valley (Taylor et al., 2001; Begg et al., 2005). A number of studies have attempted to analyse aspects of the subsurface stratigraphy of the wider Manawatu using well logs (e.g., Te Punga, 1954a; Hesp, 1975; Brown, 1978, 1984; Kampman and Caldwell, 1985; Shepherd et al., 1986; Lieffering, 1990; Sewell, 1991; Schumacher, 1999; Martley, 2001; Hughes, 2005a,b). However, no single study has yet sought to piece together a comprehensive picture of the sedimentary sequences beneath the entire Manawatu valley.

This chapter utilises lithological data from over 400 water well logs from across the Manawatu region to identify and delineate features of the Holocene sedimentary infill of the Manawatu valley. This is accomplished within the context of previous investigations. The primary aim is to reconstruct the path of the Ashhurst/Ohakea Last Glacial Maximum fluvial aggradation surface beneath the Holocene floodplain. This surface is important to understanding the sedimentary infill of the valley as it represents the top of the Lowstand Systems Tract (LST), and therefore forms the Transgressive Surface (TS) at the base of the Holocene sedimentary fill. Secondary to this is the identification of broad-scale depositional environments, namely shallow marine/estuarine, aeolian, and Holocene alluvium, rather than the subdivision into specific sys-

tems tracts. This broad-scale approach is necessary as despite being a major source of information on the subsurface stratigraphy of the Manawatu region, the well logs accumulated by Horizons Regional Council are of limited usefulness. As water well drillers are not geologists their lithological descriptions do not follow a standard nomenclature. This effectively precludes the use of the water well logs for analysis of small-scale sedimentary structures. However, the potential exists to reconstruct broader features of the Holocene sedimentary infill.

6.2 Previous investigations of the sub-surface geology of the Manawatu Region

A number of workers have utilised well logs and other sources of information to elucidate aspects of the sub-surface geology of the Manawatu and surrounding areas. Hydrogeological studies by Kampman and Caldwell (1985) (Otaki area, south of Levin), Lieffering (1990) (Manawatu Gorge to Palmerston North City), Schumacher (1999) (Palmerston North City) and Martley (2001) (Feilding District) utilised well logs to construct geologic cross-sections to aid in the identification of aquifers. Kampman and Caldwell (1985) made a tentative interpretation of the subsurface strata penetrated by water wells in the Otaki area (south of Levin) within the context of Quaternary glacial and interglacial stages. Lieffering (1990) constructed two geologic cross-sections using bore data from the Horizons Regional Council water bores database: one from Ashhurst to Palmerston North City along the Manawatu River; the other from Bunnythorpe to the confluence of the Manawatu and Oroua Rivers. However, Lieffering (1990) considered correlation between borelogs to be extremely difficult due to "the meandering history [of the Manawatu River, which] resulted in a complex sequence of lithologies being deposited with limited spatial extent" (p. 32). Lieffering (1990) also used bore logs in an attempt to construct palaeogeographic maps showing the course of the Manawatu River from the Manawatu Gorge to Palmerston North City. These maps were compiled in the context of height, rather than by attempting to correlate units between bores. Their accuracy is therefore difficult to ascertain.

Te Punga (1954a) described and discussed the sediments in a 135 m deep well drilled at Awahuri (Figure 6.1). Based on the sediment characteristics and

Figure 6.1 *(facing page)*: Locations of cross-sections and wells used for investigations of the sub-surface geology of the Manawatu region. Also shown is the extent of the 1:100,000 scale maps of the DEM of the estuarine-alluvial interface in the lower Manawatu valley (solid black line; Figures 6.22 and 6.23), and the extent of the map showing an example of channel artifacts produced by the Topo to Raster algorithm (dashed black line; Figure 6.18). Base geological map constructed using data from Kingma (1962), Cowie et al. (1967), Pillans (1990a), Begg and Johnston (2000), Lee and Begg (2002), Townsend et al. (2008), and unpublished data from the QMAP project made available by D. Townsend.

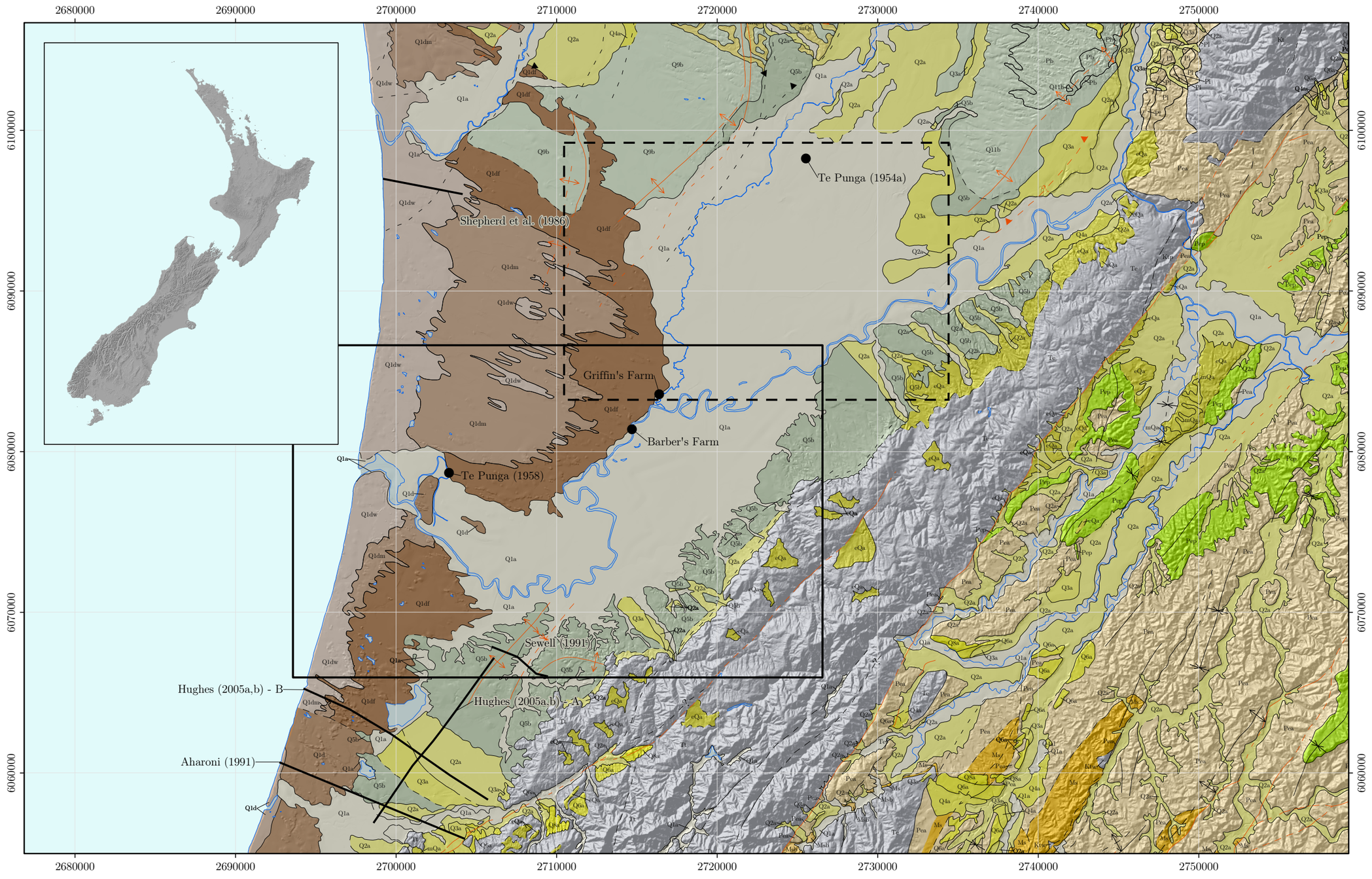
2680000
2690000
2700000
2710000
2720000
2730000
2740000
2750000
6100000
6090000
6080000
6070000
6060000
Te Punga (1954a)
Shepherd et al. (1986)
Griffin's Farm
Barber's Farm
Te Punga (1958)
Sewell (1991)
Hughes (2005a,b) - B
Hughes (2005a,b) - A
Aharoni (1991)

fossil shells recovered from the well Te Punga (1954a) inferred a change from marine through estuarine to fluvitile conditions since the Last Interglacial. It was on this basis that Hesp (1975) inferred that the Manawatu estuary at the height of the Holocene marine transgression extended inland to Palmerston North (see Chapter 4).

Te Punga (1958) also documented and discussed the sediments in a 66 m deep well drilled near Foxton (Figure 6.1). The well penetrated silts, sands with shells, and gravels with shells down to a depth of 47 m. From 47–47.8 m the well penetrated a *Podocarpus* log, which was radiocarbon dated to 9,900 cal. yr BP (Table 6.1). Beneath the log lay 7.6 m of clay and sand, underlain by 11 m of well rounded gravel. Te Punga (1958) tentatively assumed that the log was drift wood stranded in the intertidal zone and later buried beneath estuarine and/or shallow marine sediments. The log was utilised by Te Punga (1958) as a palaeo sea-level indicator; however, its utility in this context is questionable (see Section 2.4). The gravels that underlie the log can reasonably be assumed to be of LGM age (e.g., Fair, 1968; Litchfield, 2003; Clement and Fuller, 2007; Clement et al., 2010).

Hesp (1975) presented a basic map which plotted the position of water bores in the valley above Shannon, with annotations giving the depth below the land surface to the upper boundary of river gravel deposits. This was used to produce a long profile of the Ashhurst/Ohakea terrace from Palmerston North City to Tokomaru, which estimated the dip of the terrace at approximately 0.17 degrees to the southwest. Hesp (1975) also inspected the logs of water bores drilled in the vicinity of Foxton and Foxton Beach, and identified alluvial gravels at depths of up to −60 m below PMSL.

Brown (1978) presented a geologic cross-section constructed using water bore data that extended from Shannon southwest to Waitarere. The cross-section identifies the greywacke 'high' at Poroutawhao (although it is named the Levin Anticline), and Holocene and late Pleistocene sedimentary units dipping to the west. However, Brown (1978) suggested that these units pass through, or are otherwise unaffected by the presence of the Poroutawhao High. In addition the accuracy of the surface profile is questionable, and the lithological symbols of the bores used to construct the cross-section are unreadable.

Shepherd et al. (1986) presented a cross-section constructed from boreholes drilled across the coastal plain south of Tangimoana (Figures 6.1 and 6.2). The cross-section shows a prograded wedge of marine sediments overlying Ohakea LGM aggradation gravels. Shepherd et al. (1986) suggested rates and/or phases of progradation of the coast (Figure 6.2). However, the accuracy of this chronology is unclear as many of the radiocarbon ages were obtained from disarticulated valves within marine gravels. The shells are therefore likely to have been subject to reworking.

Sewell (1991) utilised water bore logs from the Horizons Regional Council database to inform a palaeoenvironmental investigation of the Otaki Formation which makes up the Tokomaru Marine Terrace. Sewell (1991) constructed a series of geologic cross-sections across the terrace from Forest Lakes (south of

Table 6.1: Summary of radiocarbon ages obtained in connection with wells and bores drilled across the Manawatu coastal plain. Wood and peat CRAs calibrated using the the non-marine calibration curve for the Southern Hemisphere (SHCal04; McCormac et al. 2004). *A. stutchburyi* CRA calibrated using the marine model calibration curve Marine04 (Hughen et al., 2004) with a ΔR value of -7 ± 45 to correct for the marine reservoir effect (see Sections 3.2.2 and 7.2.4).

Source	Locality	Material	Radiocarbon laboratory code	Reported age (years BP)	Conventional radiocarbon age (14C years)	Sidereal age range (cal yr BP)
Te Punga (1958)	Foxton	*Podocarpus* log	NZ81	9900±150	9919±76	–[a]
Hesp and Shepherd (1978)	Opiki	Totara log	NZ3938	42700±7650	41509±4895	–
Shepherd et al. (1986)	Tangimoana	Mixed shells	NZ5225	–	495±144	Modern
	Tangimoana	Mixed shells	NZ5226	–	2880±139	2419–2801
	Tangimoana	Mixed shells	NZ5227	–	4548±172	4508–4970
	Tangimoana	Mixed shells	NZ5228	–	4929±150	5027–5460
	Tangimoana	Mixed shells	NZ5229	–	4116±175	3929–4414
	Tangimoana	Mixed shells	NZ5224	–	12821±238	14064–14962
	Tangimoana	Mixed shells	NZ5223	–	4904±147	5003–5438
	Tangimoana	Mixed shells	NZ5222	–	4736±142	4829–5230
	Tangimoana	Mixed shells	NZ4606	–	5831±123	6120–6393
Shepherd and Lees (1987)	Griffin's Farm	Wood	NZ4820	1800±65	1799±60	1530–1819
	Griffin's Farm	Peat	NZ5215	1595±65	1596±60	1310–1544
	Griffin's Farm	Peat	NZ5216	1950±65	1952±62	1696–1991
	Griffin's Farm	Peat	NZ5217	1775±65	1774±61	1515–1817
	Barber's Farm	Wood	NZ5219	3419±80	3372±65	3390–3697
	Barber's Farm	Wood	NZ5220	2270±60	2272±49	2113–2344
	Barber's Farm	Wood	NZ5221	1875±60	1874±61	1595–1885
	Murray's Farm	*A. stutchburyi* valve	NZ5218[b]	6280±220	6613±181	6699–7484
Lieffering (1990)	Kairanga	Tree trunk	NZ7693	25900±410	25953±879	–

[a] CRA is just beyond the range suitable for dating. Sidereal age is approximately 11,000 cal. yr BP.
[b] Shepherd and Lees (1987) mistakenly give the lab number as NZ5128; the correct number is NZ5218.

Levin) to Koputaroa. The northern-most cross-section at Koputaroa crosses the Shannon and Levin anticlines approximately 4 km south of the Manawatu River (Figures 6.1 and 6.3).

Hughes (2005a,b) constructed two geologic cross-sections across the Horowhenua coastal plain near Levin using water bore logs from the Horizons Regional Council database (Figures 6.1, 6.4, and 6.5). The purpose of the cross-sections was to provide context for a deep borehole drilled at the intersection of the profiles. The geologic cross-sections identify Holocene and late Pleistocene alluvium overlying the Otaki Formation. Notably, while Hughes (2005a,b) cross-section A (Figure 6.4) runs across both Ashhurst/Ohakea and Milson/Rata aggradation surfaces (Figure 6.1), on the cross-section Hughes (2005a,b) labels all the alluvial fill as Ashhurst/Ohakea alluvium. The reason for the omission of the Milson/Rata fill is unclear.

Begg et al. (2005) presented a series of contour maps detailing extrapolated sub-surface elevations of the Ashhurst/Ohakea and Milson/Rata aggradation terraces, and the Tokomaru Marine Terrace (Figures 6.6, 6.7, and 6.8). This first-order subsurface extrapolation was based on the assumption that terrace surfaces identified in the contemporary landscape were more or less planar, and that the dip of the surfaces was constant over small-to-medium distances down-dip. Therefore, the topographic contours across each surface are structure contours, the spacing of which should remain relatively constant up-dip and down-dip as long as the surface remains planar. Begg et al. (2005) were therefore able to extrapolate subsurface contours for each of the three terraces. However, the extrapolation makes no account for lateral or down-dip complexity, and active tectonism along the flanks of the Tararua-Ruahine Ranges lessens the certainty of surface continuity over moderate distances (J. Begg, personal communication).

6.3 Cross-section construction methodology

Cross-sections at 1:50,000 scale were constructed in ArcMap 9.2 using the eXacto cross-section tool (Carrell, 2009). Additional detailing was performed in Inkscape 0.47. The surface profile for each of the cross-sections was generated using a subset of the ECOSAT 15 m digital elevation model (DEM) of New Zealand. This DEM was constructed using spot heights and 20 m contours from the 1:50,000 topographic map series produced by Land Information New Zealand (LINZ), and digital stream data produced by the National Institute of Water and Atmospheric Research (NIWA). Surface elevations were sampled at 10 m intervals along each profile. Elevations were exaggerated by a factor of 60. Surface geological data was sourced from the QMAPs for

Figure 6.2 *(facing page)*: Cross-section through the Holocene marine wedge south of Tangimoana (after Shepherd et al., 1986). The location of this cross-section is shown on Figure 6.1.

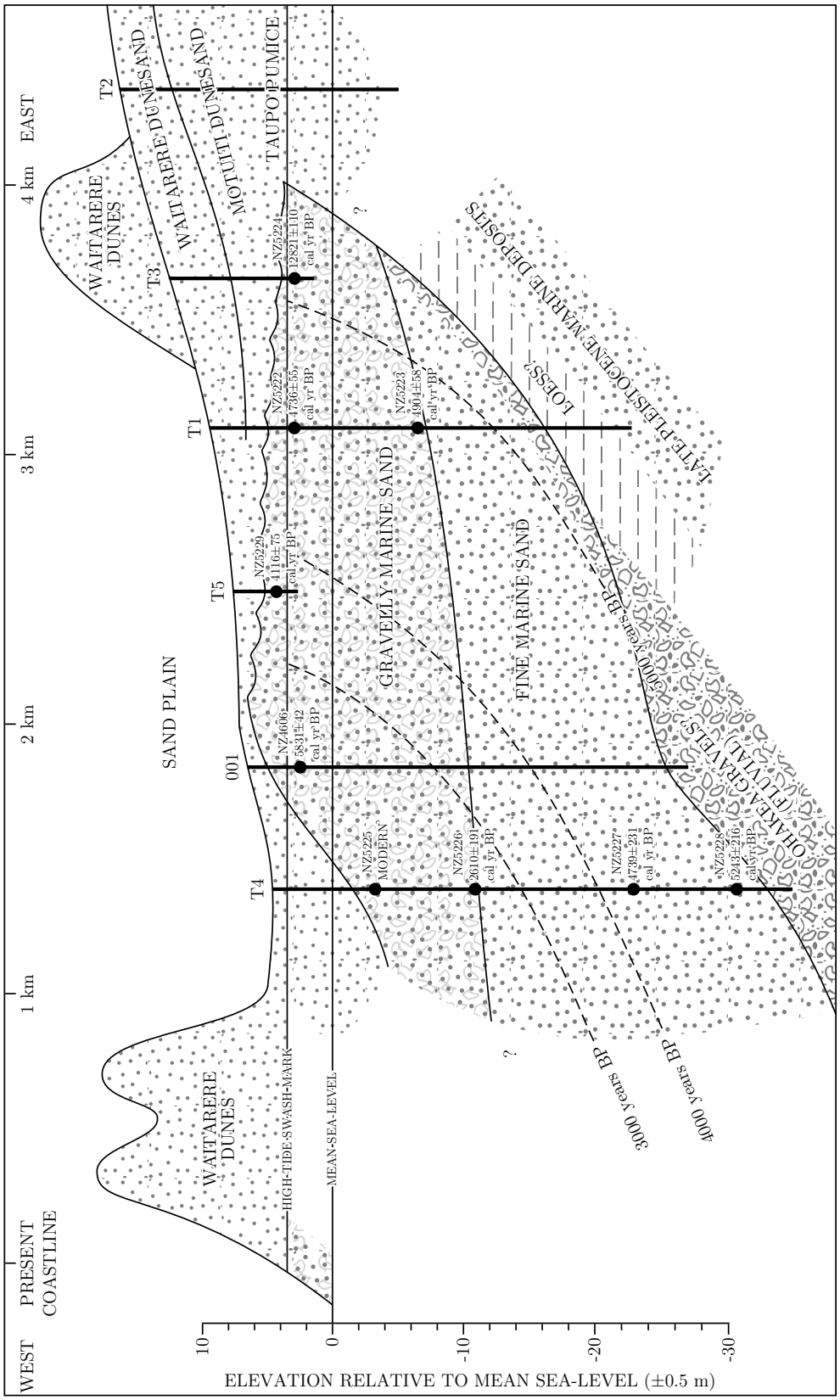
WEST
PRESENT COASTLINE
1 km
2 km
3 km
4 km
EAST
WAITARERE DUNES
WAITARERE DUNES
SAND PLAIN
T1
T2
T3
T4
T5
001
WAITARERE DUNESAND
MOTUTIL DUNESAND
TAUPO PUMICE
NZ5224 12821±110 cal yr BP
NZ5222 1736±55 cal yr BP
NZ5223 1904±58 cal yr BP
NZ5220 4116±75 cal yr BP
NZ4606 5831±42 cal yr BP
NZ5225 MODERN
NZ5226 2610±191 cal yr BP
NZ5227 4739±231 cal yr BP
NZ5228 5243±216 cal yr BP
GRAVELLY MARINE SAND
FINE MARINE SAND
LOESS?
LATE PLEISTOCENE MARINE DEPOSITS
OHAKEA GRAVELS (FLUVIAL)
3000 years BP
4000 years BP
6000 years BP
HIGH-TIDE SWASH-MARK
MEAN-SEA-LEVEL
10
0
-10
-20
-30
ELEVATION RELATIVE TO MEAN SEA-LEVEL (±0.5 m)

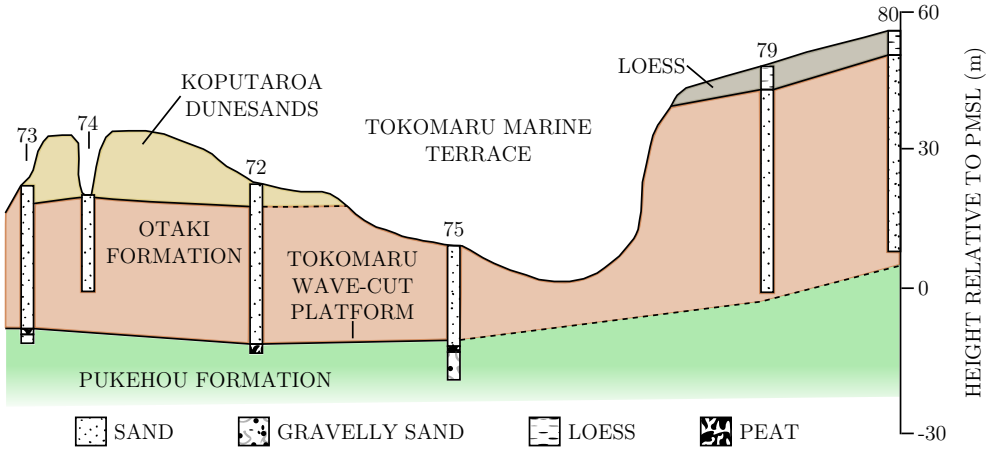

Figure 6.3: Well log correlation across part of the Tokomaru Marine Terrace near Koputaroa (after Sewell, 1991). Well numbers as given by Sewell (1991). The location of the cross-section is shown on Figure 6.1.

Wellington, Wairarapa and Taranaki (Begg and Johnston, 2000; Lee and Begg, 2002; Townsend et al., 2008). D. Townsend (GNS Science) provided access to unpublished QMAP data from Taranaki and Hawke's Bay.

Well log data was sourced primarily from the water well log database maintained by Horizons Regional Council. Additional well logs were sourced from Te Punga (1953a, 1954a, 1958), Hesp (1975), Hesp and Shepherd (1978), and Shepherd and Lees (1987). Also utilised were unpublished well logs obtained by P.A. Hesp (personal communication to M.J. Shepherd, 1979) directly from well drillers. The published and unpublished logs were compared to the Horizons Regional Council database and screened for duplicates. In total over 400 well logs were utilised. Details of the well logs used for each cross-section are presented as ESRI shapefiles on the DVD that accompanies this thesis (see Appendix A).

Well positions were mapped, with cross-section paths fitted to the distribution of wells. Each cross-section was run twice using the eXacto tool. The first run used ECOSAT DEM elevations for the heights of the wells. These elevations were then compared to the elevation of the surface profile at the location of each well. In the second run, the well surface elevations were adjusted to

Figure 6.4 *(facing page)*: Cross-section running northeast-southwest across the Horowhenua coastal plain (after Hughes, 2005a,b). The location of the cross-section is shown on Figure 6.1. Well numbers correspond to the Horizons Regional Council water wells database.

Figure 6.5 *(page 144)*: Cross-section running southeast-northwest (line B-B') across the Horowhenua coastal plain (after Hughes, 2005a,b). The location of the cross-section is shown on Figure 6.1. Well numbers correspond to the Horizons Regional Council water wells database.

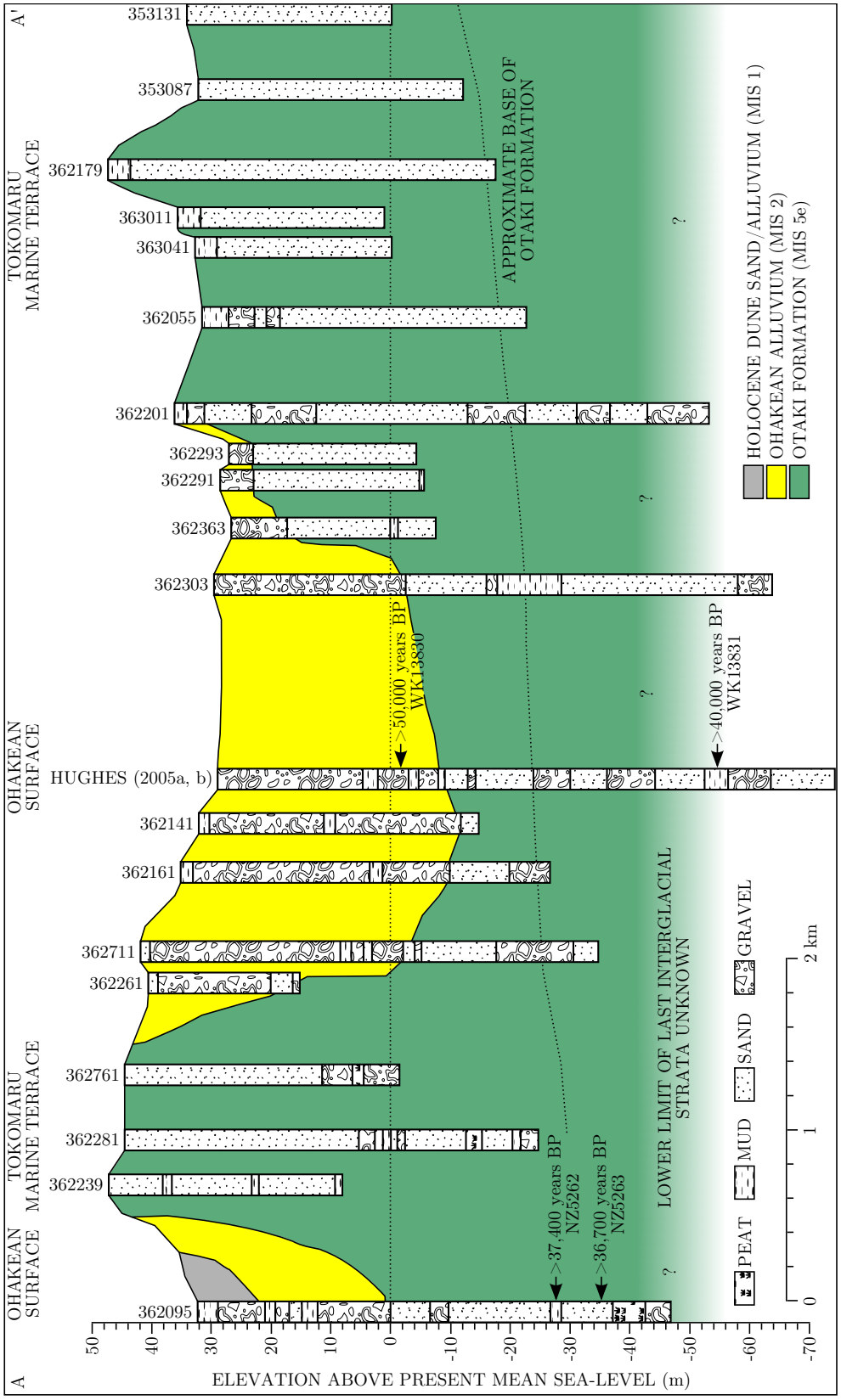
A
A'
353131
353087
362179
363011
363041
362055
362201
362293
362291
362363
362303
HUGHES (2005a, b)
362141
362161
362711
362261
362761
362281
362239
362095
TOKOMARU MARINE TERRACE
OHAKEAN SURFACE
APPROXIMATE BASE OF OTAKI FORMATION
>50,000 years BP WK13830
>40,000 years BP WK13831
>37,400 years BP NZ5262
>36,700 years BP NZ5263
LOWER LIMIT OF LAST INTERGLACIAL STRATA UNKNOWN
HOLOCENE DUNE SAND/ALLUVIUM (MIS 1)
OHAKEAN ALLUVIUM (MIS 2)
OTAKI FORMATION (MIS 5e)
PEAT
MUD
SAND
GRAVEL
0
1
2 km
50
40
30
20
10
0
-10
-20
-30
-40
-50
-60
-70
ELEVATION ABOVE PRESENT MEAN SEA-LEVEL (m)

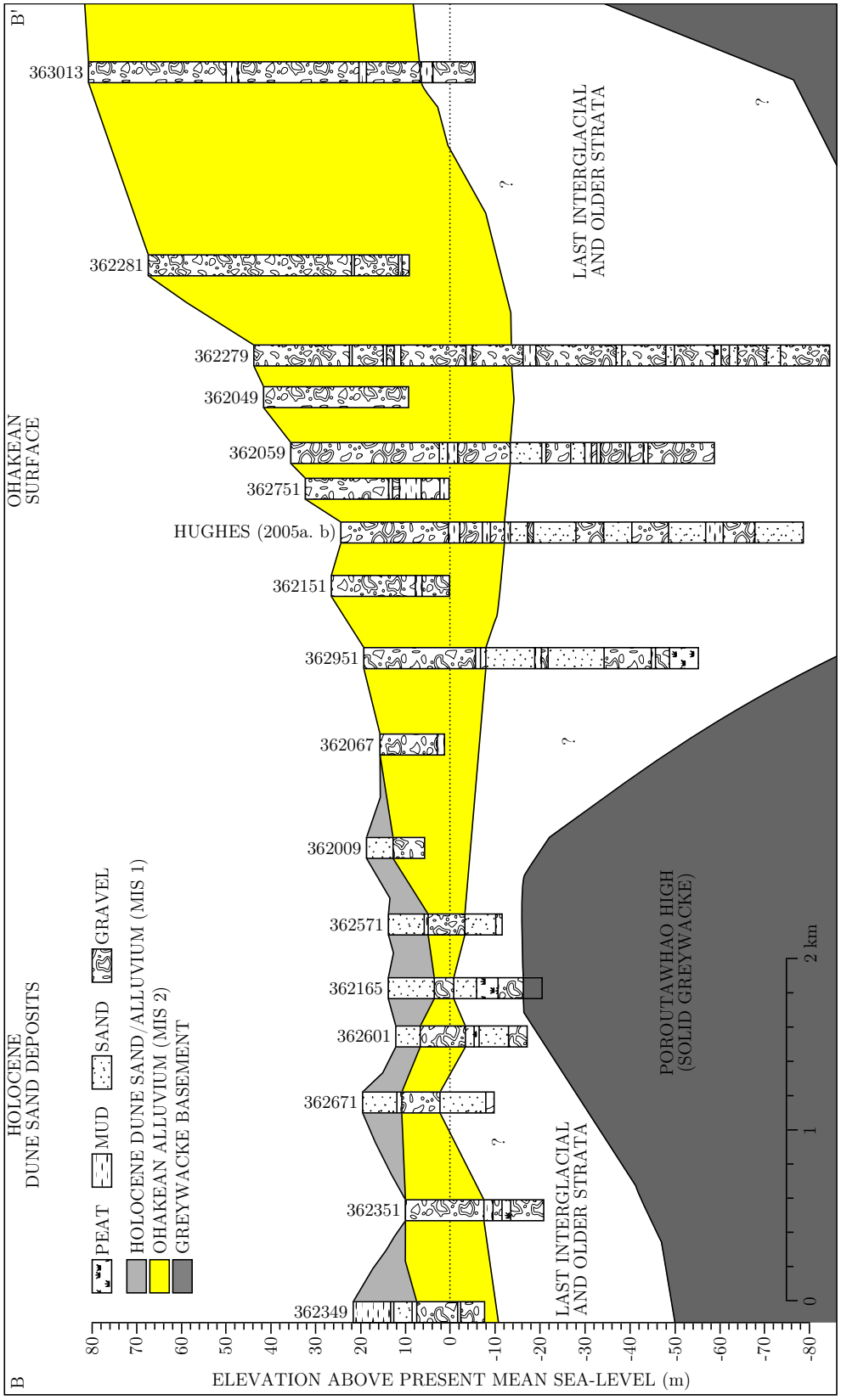
B
B'
363013
362281
362279
362049
362059
362751
HUGHES (2005a. b)
362151
362951
362067
362009
362571
362165
362601
362671
362351
362349
OHAKEAN SURFACE
LAST INTERGLACIAL AND OLDER STRATA
LAST INTERGLACIAL AND OLDER STRATA
POROUTAWHAO HIGH (SOLID GREYWACKE)
HOLOCENE DUNE SAND DEPOSITS
PEAT
MUD
SAND
GRAVEL
HOLOCENE DUNE SAND/ALLUVIUM (MIS 1)
OHAKEAN ALLUVIUM (MIS 2)
GREYWACKE BASEMENT
0
1
2 km
80
70
60
50
40
30
20
10
0
-10
-20
-30
-40
-50
-60
-70
-80
ELEVATION ABOVE PRESENT MEAN SEA-LEVEL (m)

coincide with the profile surface elevations. Wells located some distance from each cross-section, typically in areas between cross-sections, were sometimes plotted to provide wider context. These additional wells were located on average up to 780 m from the cross-section line. The context wells were not adjusted to fit the surface profile, given their distance away from the cross-section line.

Interpretations were made using the original driller's descriptions. No standardisation of the driller's descriptions was attempted (cf., Schumacher, 1999). Pictorial logs were created following the interpretations.

6.4 Limiting factors and sources of error

6.4.1 Positions and elevations

While all of the wells detailed in the Horizons Regional Council database have positions recorded, the majority of these positions are listed as estimates. No indication of the degree of error that may accompany these estimates is given. Many of the well logs have well head elevations, which are also stated to be estimates. Again, the degree of uncertainty of these elevations is unclear. Some wells have well head elevations derived from GPS observations. It is unclear whether such observations are of ellipsoidal or orthometric heights. Well head and cross-profile elevations have therefore been derived from the ECOSAT 15 m DEM. The ECOSAT 15 m DEM has an estimated vertical accuracy of ±7 m (Barringer and Newsome, 2006). A LiDAR-derived DEM with sub-decimetre vertical accuracy (A. Steffert, personal communication) is available; however, it offers only partial coverage of the study area. It

Figure 6.6 *(following page)*: Structural contours for the Ashhurst/Ohakea fluvial aggradation terrace extrapolated beneath the Holocene floodplain (after Begg et al., 2005). Contour elevations are relative to PMSL. Base geological map constructed using data from Kingma (1962), Cowie et al. (1967), Pillans (1990a), Begg and Johnston (2000), Lee and Begg (2002), Townsend et al. (2008), and unpublished data from the QMAP project made available by D. Townsend.

Figure 6.7 *(page 147)*: Structural contours for the Milson/Rata fluvial aggradation terrace extrapolated beneath the Holocene floodplain (after Begg et al., 2005). Contour elevations are relative to PMSL. Base geological map constructed using data from Kingma (1962), Cowie et al. (1967), Pillans (1990a), Begg and Johnston (2000), Lee and Begg (2002), Townsend et al. (2008), and unpublished data from the QMAP project made available by D. Townsend.

Figure 6.8 *(page 148)*: Structure contours for the Tokomaru Marine Terrace extrapolated beneath the Holocene floodplain (after Begg et al., 2005). Contour elevations are relative to PMSL. Base geological map constructed using data from Kingma (1962), Cowie et al. (1967), Pillans (1990a), Begg and Johnston (2000), Lee and Begg (2002), Townsend et al. (2008), and unpublished data from the QMAP project made available by D. Townsend.

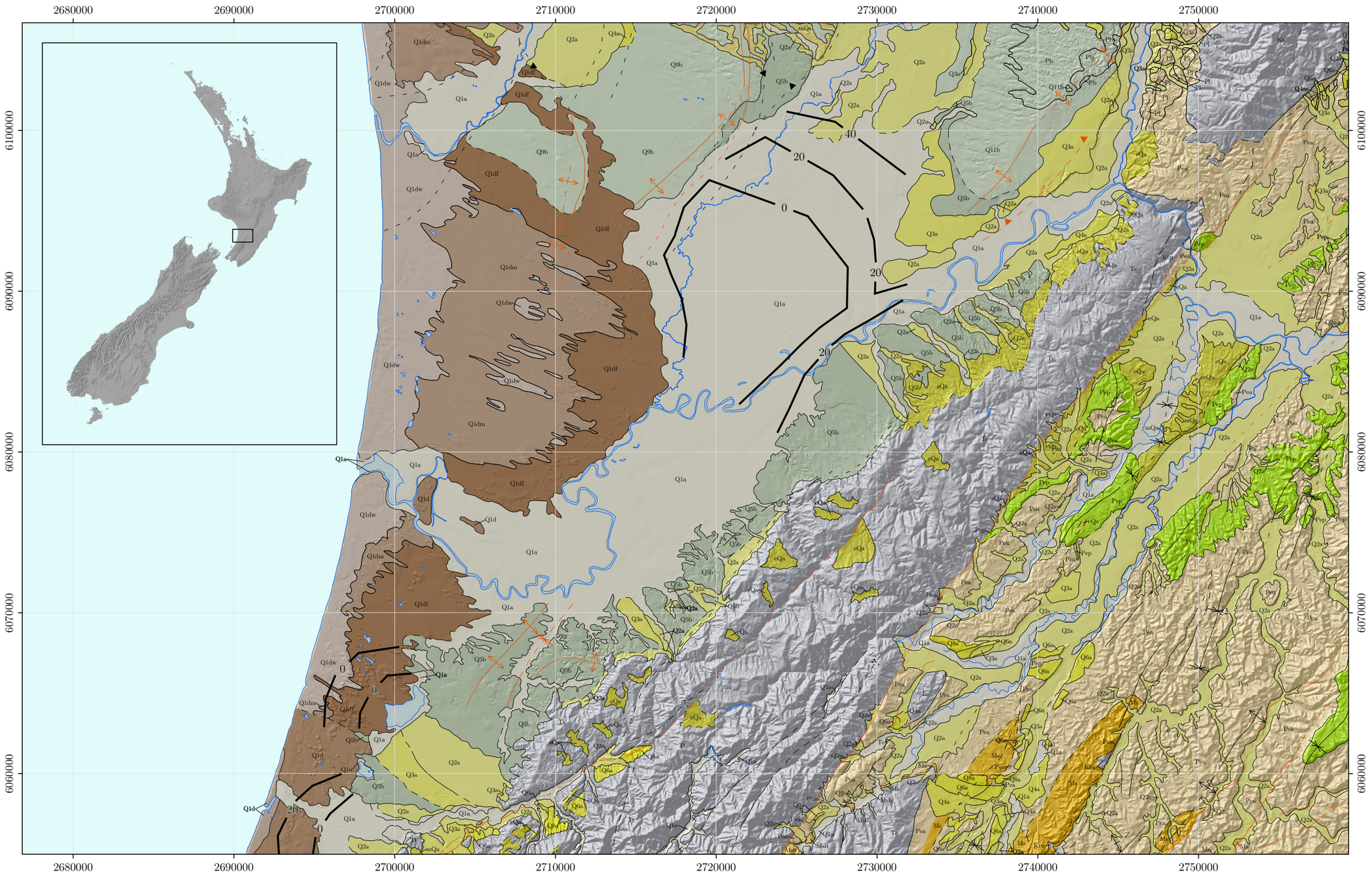
2680000
2690000
2700000
2710000
2720000
2730000
2740000
2750000
6100000
6090000
6080000
6070000
6060000
40
20
0
20
20
0
0
-20
0

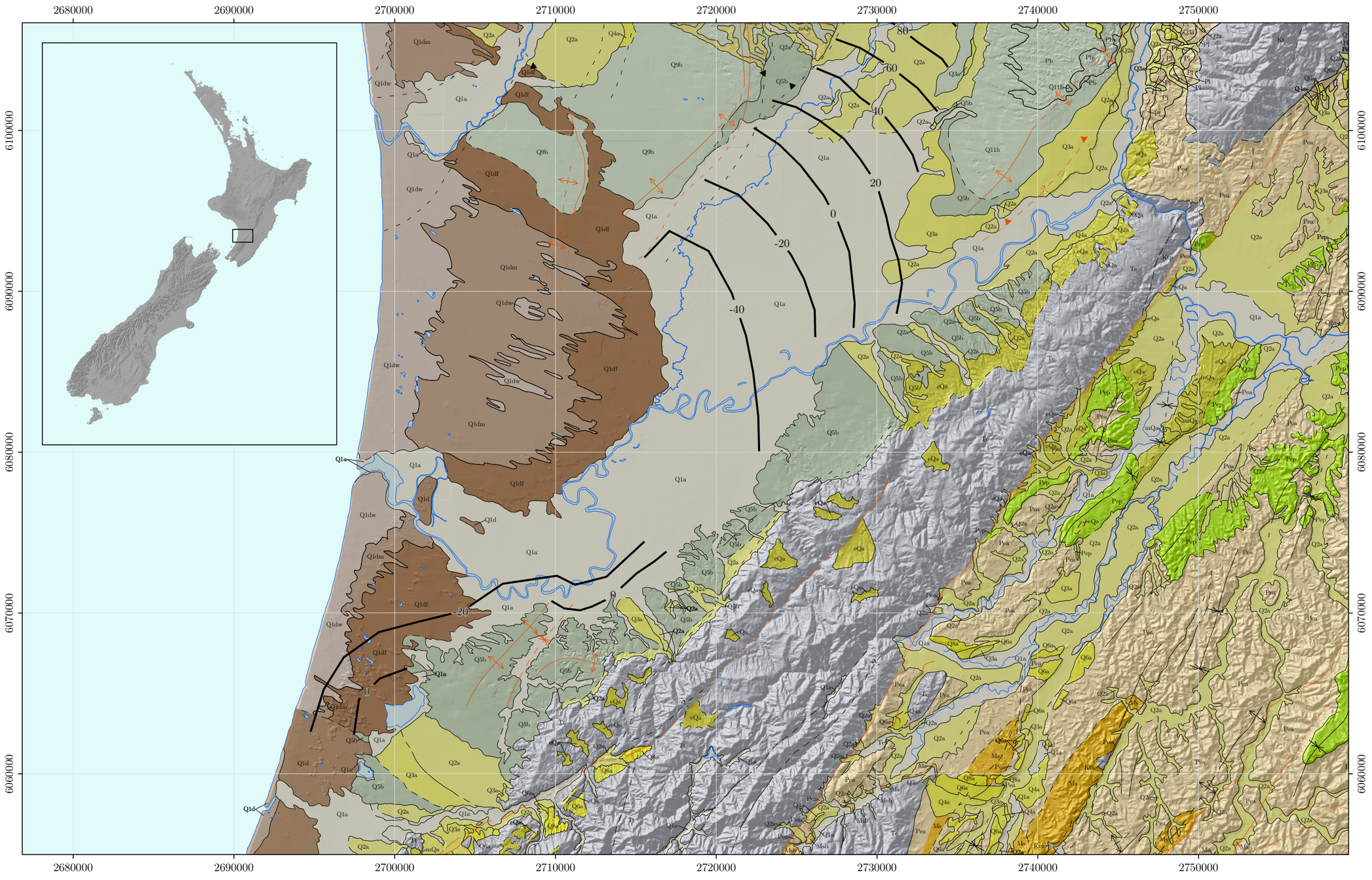
2680000
2690000
2700000
2710000
2720000
2730000
2740000
2750000
6100000
6090000
6080000
6070000
6060000
80
60
40
20
0
-20
-40

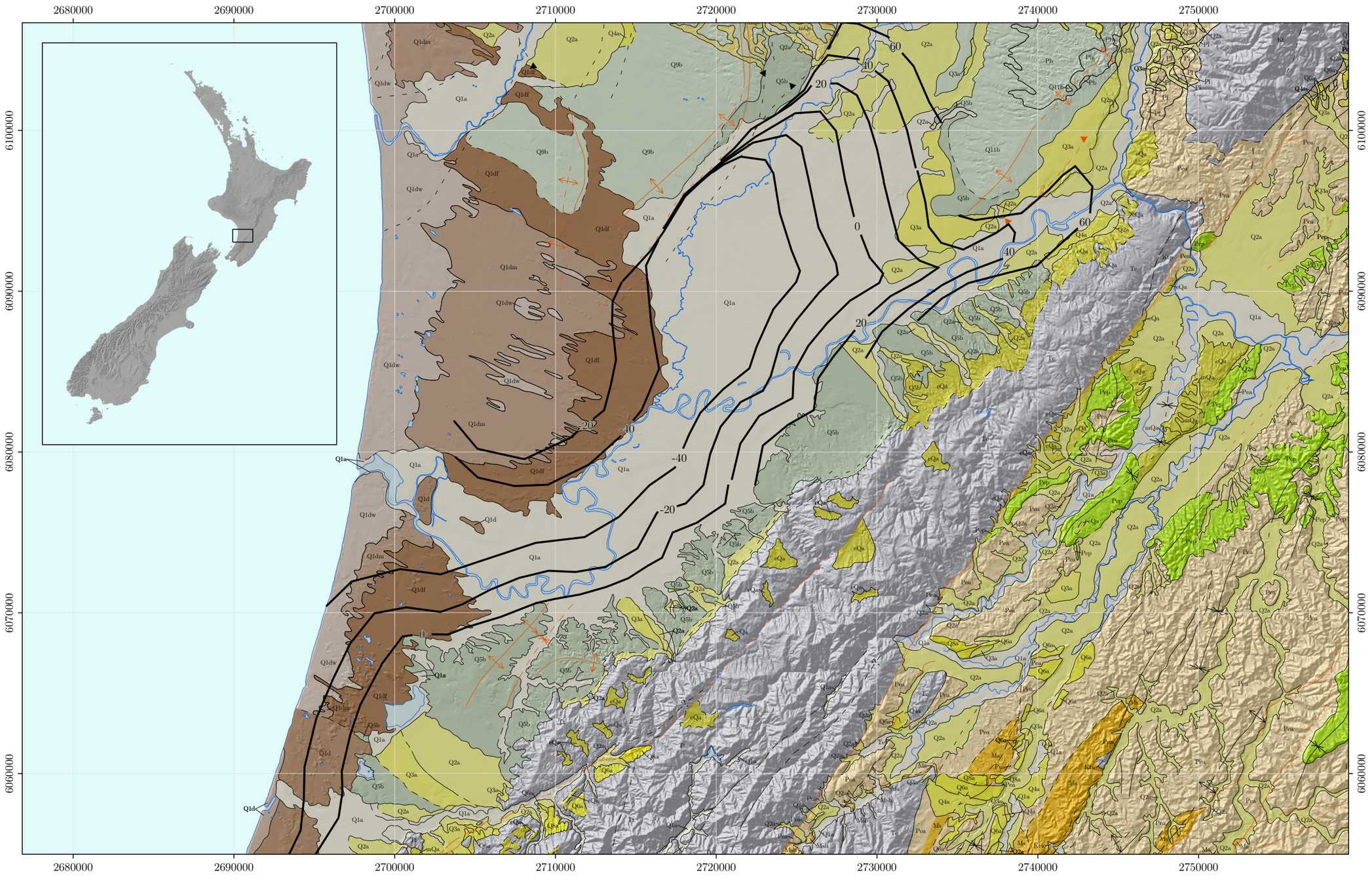
2680000
2690000
2700000
2710000
2720000
2730000
2740000
2750000
6100000
6090000
6080000
6070000
6060000
60
40
20
0
-20
-40

was considered unreasonable to construct some of the geologic cross-sections using the LiDAR-derived DEM (where coverage was afforded), and some using the ECOSAT DEM. Therefore, all elevations were derived from the ECOSAT DEM, which offered complete coverage of the study area.

The elevations of individual wells, and by extension the elevation of the interpreted sub-surface geology, are therefore subject to variable vertical errors. The extent of such errors is illustrated for each well on the geologic cross-sections.

6.4.2 Well log interpretations

The degree of detail in driller's descriptions may be highly variable as there is no standard or uniform scheme for lithological descriptions to which water well drillers must adhere. Typically, the descriptions recorded by well drillers are minimal statements of observed lithology intended to meet the logging requirements of the regional council or other statutory authority. Generic statements such as "sand" or "gravel" are common. Colours, such as "blue sand" or "brown gravel" are frequently mentioned. Seemingly separate lithological units are frequently compressed into a single description, such as "sand and clay". The intent of such descriptions (sandy clay, clayey sand, or interbedded sands and clays) is often unclear. Brown's (1990) guide for well drillers logging water wells has been consulted to aid in the interpretation of driller's descriptions. The degree of consistency between drillers in their descriptions of water wells is unclear, although both Lieffering (1990) and Schumacher (1999) have suggested that there is considerable variability. Based on driller's descriptions it is not necessarily possible to distinguish between genetically similar lithological units, for example: transgressive sand sheets, barrier sands, dune sands, sand flats and fluvial sands. However, it is possible to assess the broader significance of genetically different sedimentary units.

Driller's descriptions also contain no information on the nature of the contacts between sedimentary units. This is obviously more of an issue with respect to unconformities. The abiding assumption where surfaces have been reconstructed is that the top of the unit(s) used for the reconstruction is not an unconformity, such that the reconstructed surface is an accurate representation. However, as information about erosional contacts is lacking, it is always the case that the surfaces reconstructed may not be accurate representations. Unfortunately, it is generally not possible to assess the degree to which a reconstructed surface is deemed to be accurate.

6.4.3 Mismatches between surface geology and DEM topography

On a number of the cross-sections there are mismatches between the topography as expressed by the ECOSAT 15 m DEM, and the surface geology from the QMAPs. These mismatches are most apparent wherever a cross-section crosses the course of the Manawatu River. This is not an issue of different map

projections, as both the ECOSAT DEM and the QMAP geological data are projected using New Zealand Map Grid. Rather, it is an issue of the different scales at which each was produced and the different scales of the source data used to construct each of the products. Therefore, when viewing the profiles it is necessary to bear in mind that neither the surface geology nor topography is absolutely correct.

6.5 Geologic cross-sections in the Manawatu valley: results and discussion

6.5.1 Introduction

Twenty geologic cross-sections were constructed using lithological data from water well logs across the lower Manawatu region (Figures 6.9, 6.10, 6.11, 6.12, and 6.13). These cross-sections reconstruct the Last Glacial Maximum and Holocene sedimentary fill of the Manawatu valley. The cross-sections are discussed individually, in detail, below. The discussion groups the cross-sections by area, into: the upper Manawatu floodplain (cross-sections 1–4); the Oroua floodplain (cross-sections 5–8); the Manawatu-Oroua floodplain (cross-section 9, eastern half); the central Manawatu floodplain (cross-sections 10–14); the lower Manawatu floodplain (cross-sections 15–19); the lower Manawatu (south) (cross-section 20); and coastal Manawatu (cross-section 9, western half). Where the discussion focuses on specific parts of a cross-section (a 'point of interest,' POI) this is indicated as such in the text (e.g., Sheet 6, POI 3). Such points of interest are indicated on the cross-sections by a number (corresponding to the appropriate in-text remark) in red, surrounded by a red circle. The well log cross-sections themselves are included as loose sheets in the rear of the thesis. Each sheet presents (from top to bottom):

1. A planform map showing the line of the cross-section and the locations of wells used to construct it (these planform maps are summarised in Figure 6.9). Wells proximal to the cross-section line are plotted in black. Context wells are plotted either in red (wells south of the cross-section line) or blue (wells north of the cross-section line).
2. The geologic cross-section itself.

Figure 6.9 *(facing page)*: Locations of geologic cross-sections constructed from well logs in the Manawatu valley. These cross-sections are presented as loose sheets in the rear of the thesis. The points of view presented by the conceptual 3D models of the cross-sections (Figures 6.10–6.13) are indicated by arrows. Base geological map constructed using data from Kingma (1962), Cowie et al. (1967), Pillans (1990a), Begg and Johnston (2000), Lee and Begg (2002), Townsend et al. (2008), and unpublished data from the QMAP project made available by D. Townsend.

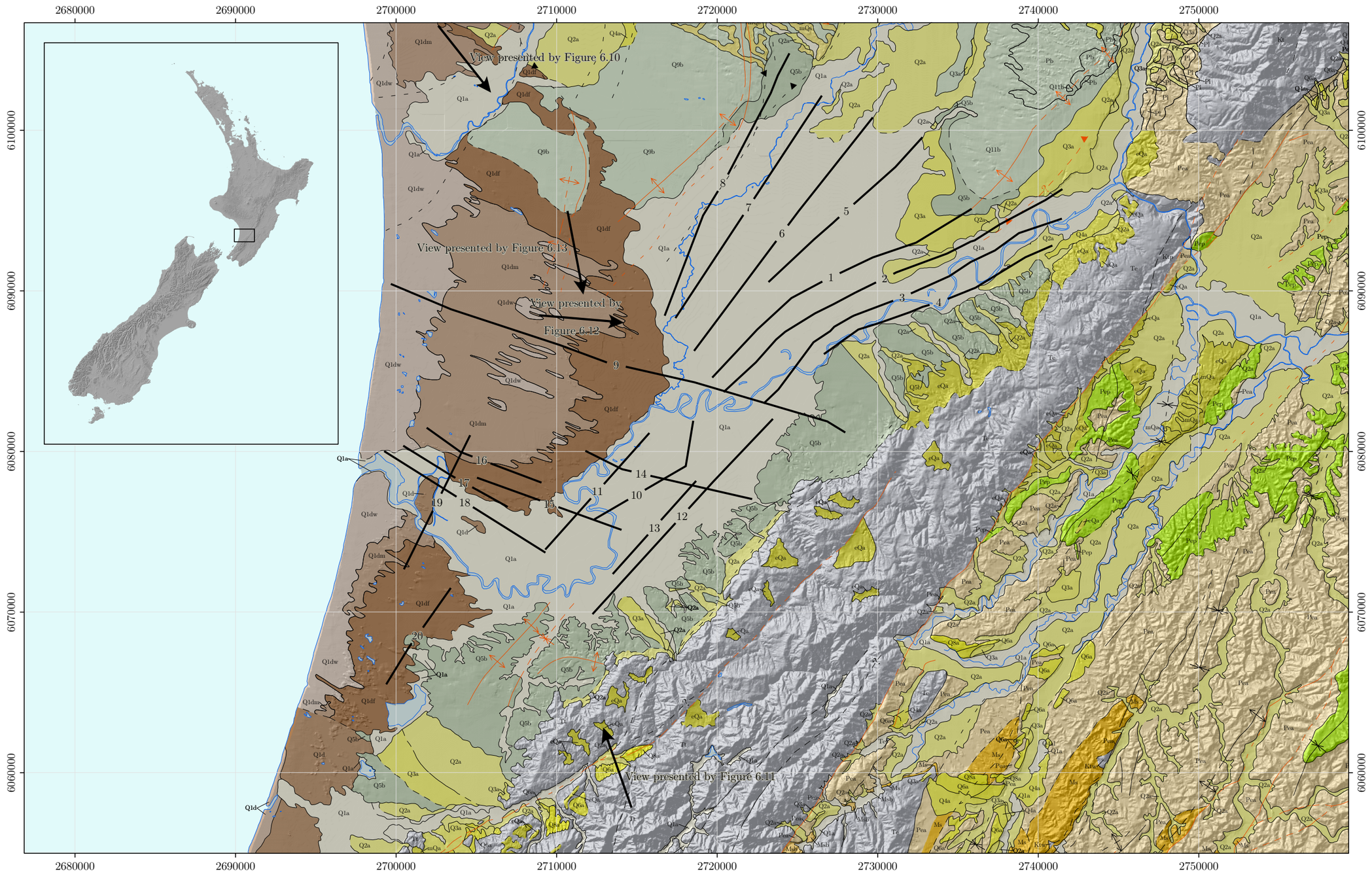
2680000
2690000
2700000
2710000
2720000
2730000
2740000
2750000
6100000
6090000
6080000
6070000
6060000
View presented by Figure 6.10
View presented by Figure 6.13
View presented by Figure 6.12
View presented by Figure 6.11
1
2
3
4
5
6
7
8
9
10
11
12
13
14
15
16
17
18
19
20

3. A diagram illustrating the surface profile extracted from the ECOSAT DEM, the surface profile extracted from available LiDAR data, and the adjusted and unadjusted surface elevations of the wells.

A key to the well logs cross-sections is presented in Figure 6.14 (Page 159). This key is also presented on a seperate sheet in the rear of the thesis (Sheet 32). PDF copies of all the sheets are presented on the DVD that accompanies this thesis. Also included on the DVD are all the raw GIS files used/generated in the course of the construction of the cross-sections (see Appendix A).

6.5.2 Upper Manawatu floodplain: Whakarongo through Palmerston North City to Opiki

6.5.2.1 Sheet 1: Well logs cross-section 1

Beneath the Holocene floodplain the Ashhurst/Ohakea aggradation surface can be traced as the top of the uppermost gravel unit in many wells. Equivalent LGM aggradational surfaces have been indentified plunging beneath Holocene fill in many locations throughout New Zealand (e.g., Suggate, 1968; Shepherd et al., 1986; Brown, 1995; Bal, 1996; Dravid and Brown, 1997; Berryman et al., 2000; Litchfield, 2003; Litchfield and Berryman, 2005, 2007). However, determination of the base of the Ashhurst/Ohakea gravels is less definite, as this presumes precise differentiation between the Ashhurst/Ohakea unit and the underlying Milson/Rata gravels. This is outside the scope of this research.

Ashhurst/Ohakea gravel can be traced westward from well 336201 (Sheet 1, POI 1) dipping at an average angle of approximately 0.17 degrees. This is a much shallower degree of dip than was estimated by Begg et al. (2005) (see Figure 6.6). At well 147 the depth to the uppermost gravel unit suddenly increases by c. 22.5 m (Sheet 1, POI 2). This phenomena is not localised to well 147, and can also be observed in well 335151 on well logs cross-section 2 (Sheet 2, POI 5), and is therefore interpreted as post-LGM cutting by the Manawatu River (Figures 6.10 and 6.12). Approximately 600 m to the northeast Lieffering (1990) reported a radiocarbon age of 25953 ± 879 14C years (NZ7693) from

Figure 6.10 *(facing page)*: Conceptual 3D model of the twenty geologic cross-sections constructed from well logs in the lower Manawatu valley looking southeast across the coastal plain. Also shown are the positions of the over 400 well logs used in the cross-section construction. The "point of view" of the model shown here is indicated on Figure 6.9. Detailed 3D models of the cross-sections through the upper and lower floodplain are presented in Figures 6.12 and 6.13.

Figure 6.11 *(page 154)*: Conceptual 3D model of the twenty geologic cross-sections constructed from well logs in the lower Manawatu valley looking north-northwest across the coastal plain. Also shown are the positions of the over 400 well logs used in the cross-section construction. The "point of view" of the model shown here is indicated on Figure 6.9. Detailed 3D models of the cross-sections through the upper and lower floodplain are presented in Figures 6.12 and 6.13.

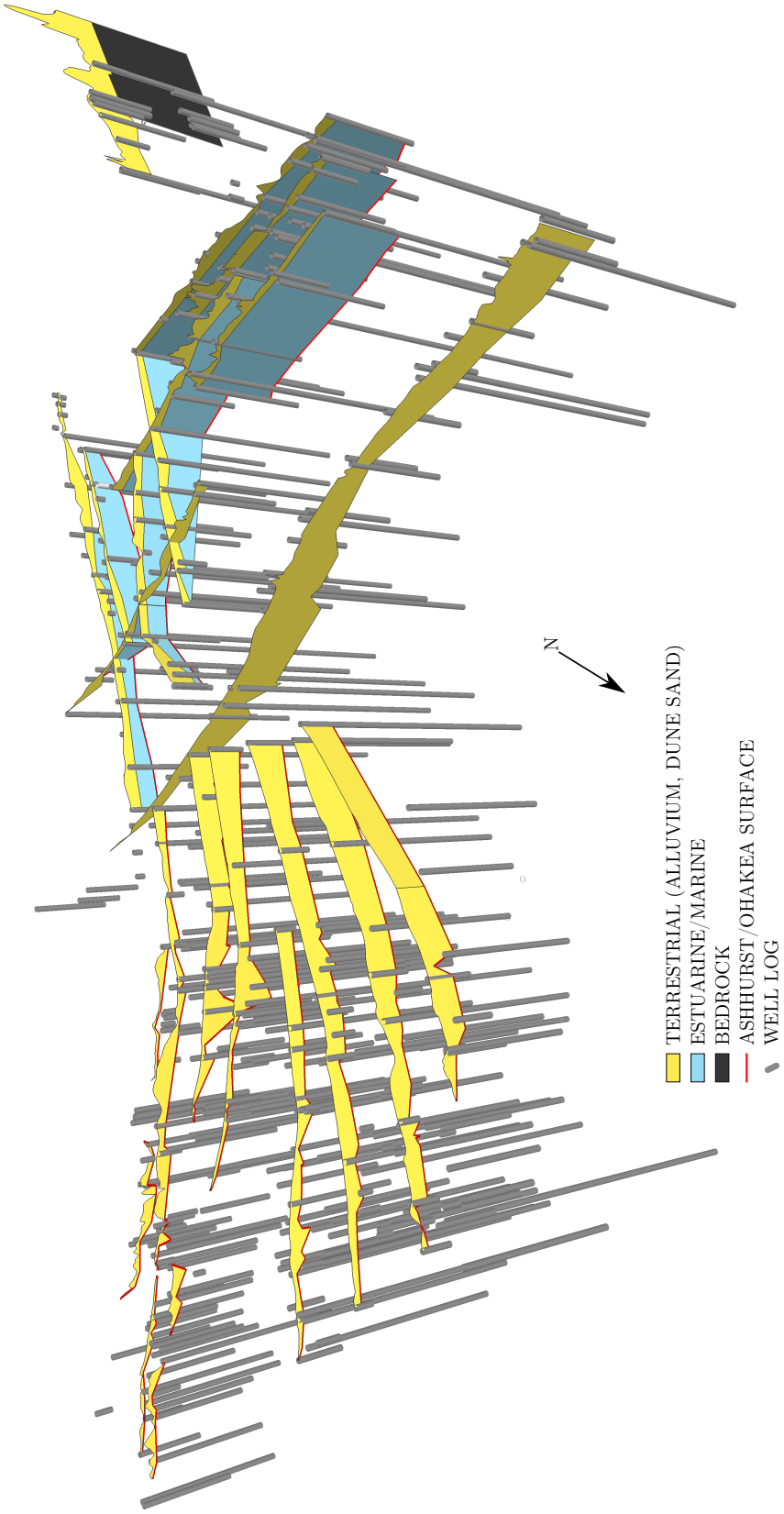
N
TERRESTRIAL (ALLUVIUM, DUNE SAND)
ESTUARINE/MARINE
BEDROCK
ASHHURST/OHAKEA SURFACE
WELL LOG

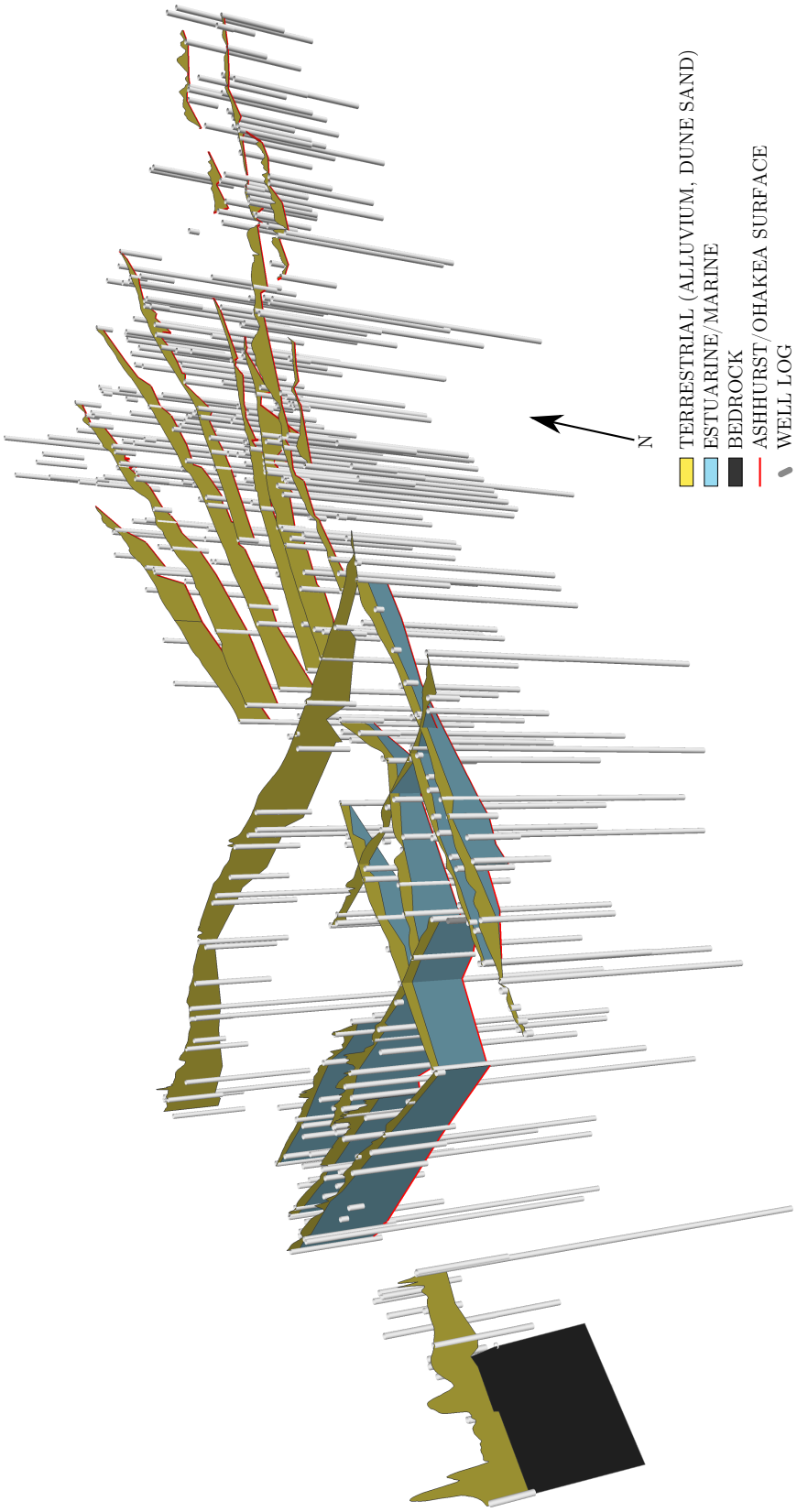
N
TERRESTRIAL (ALLUVIUM, DUNE SAND)
ESTUARINE/MARINE
BEDROCK
ASHHURST/OHAKEA SURFACE
WELL LOG

a tree trunk encountered at 22 m depth in well 335421 (Sheet 1, POI 3; Table 6.1). Lieffering (1990) therefore inferred that the blue gravel unit below the log was the Milson/Rata aggradation surface. It is likely that the blue gravel unit at the base of the inferred palaeochannel in well 147 is Milson/Rata gravel. West of well 147 the Ashhurst/Ohakea aggradation surface continues to dip at approximately 1.5 degrees to the west, reaching a depth of c. −13 m below PMSL in the vicinity of Opiki.

6.5.2.2 Sheet 2: Well logs cross-section 2

East of Palmerston North City (east of well 336261; Sheet 2, POI 1) lateral erosion by the Manawatu River during the Holocene has removed extensive tracts of the Ashhurst/Ohakea aggradation surface (e.g., Fair, 1968; Lieffering, 1990; Heerdegen and Shepherd, 1992). Holocene alluvium, in the form of sands, silts and clays have been deposited in place of the gravels. The base of the Holocene alluvium is therefore relatively easy to discern. At most 8–10 m of Ashhurst/Ohakea gravel appears to have been removed during the Holocene (cf. wells 336025 and 337003; Sheet 2, POIs 2 and 3). It is therefore not unreasonable to suggest that it is unlikely that the full depth of Ashhurst/Ohakea gravel has been removed. Therefore, the Holocene alluvium east of Palmerston North City most likely rests directly on the base of the Ashhurst/Ohakea fill, rather than on the underlying Milson/Rata gravels. However, the true depth of the Ashhurst/Ohakea fill is impossible to discern.

West of well 336681 (Sheet 2, POI 4) the Ashhurst/Ohakean aggradation surface can be traced under the Holocene floodplain dipping westward at an average angle of approximately 0.17 degrees. As for well logs cross-section 1 (Sheet 1) this is accomplished by assuming that the uppermost gravel unit in the wells across the floodplain is Ashhurst/Ohakea gravel. At well 335151 (Sheet 2, POI 5) the depth to the uppermost layer of gravel increases dramatically (Figures 6.10 and 6.12). As at well 147 on well logs cross-section 1 (Sheet 1, POI 2), this is interpreted as post-LGM cutting by the Manawatu River. The gravel at the base of this palaeochannel is most likely from the Milson/Rata aggradation terrace. This is consistent with the estimate made

Figure 6.12 *(following page)*: Conceptual 3D model of the geologic cross-sections constructed from well logs looking east across the upper Manawatu floodplain (well logs cross-sections 1–8). Also shown are the positions of the well logs used in the cross-section construction. The "point of view" of the model shown here is indicated on Figure 6.9.

Figure 6.13 *(page 157)*: Conceptual 3D model of the geologic cross-sections constructed from well logs looking south across the lower Manawatu floodplain (well logs cross-sections 9–20). Also shown are the positions of the well logs used in the cross-section construction. The "point of view" of the model shown here is indicated on Figure 6.9.

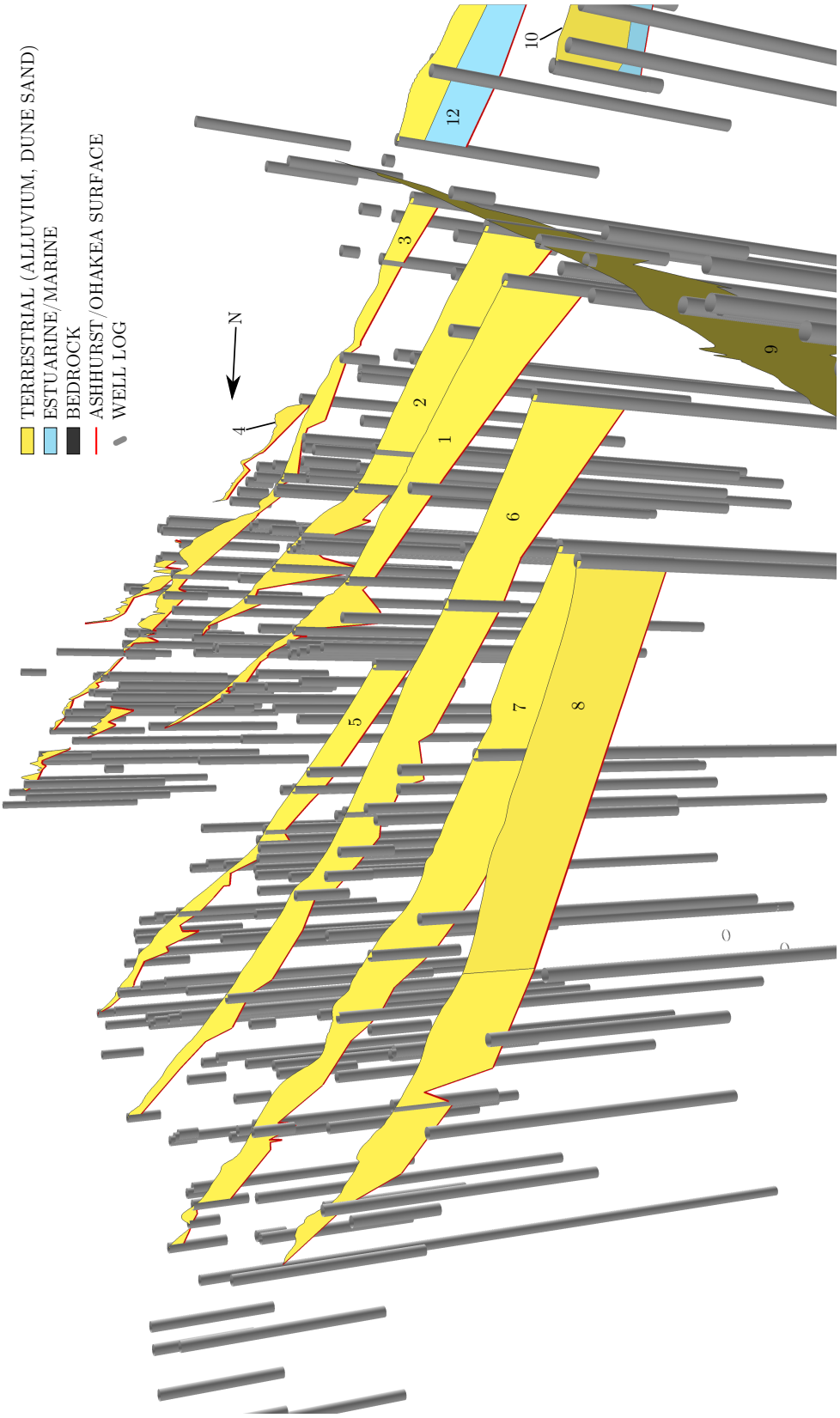
TERRESTRIAL (ALLUVIUM, DUNE SAND)
ESTUARINE/MARINE
BEDROCK
ASHHURST/OHAKEA SURFACE
WELL LOG
N
1
2
3
4
5
6
7
8
9
10
12

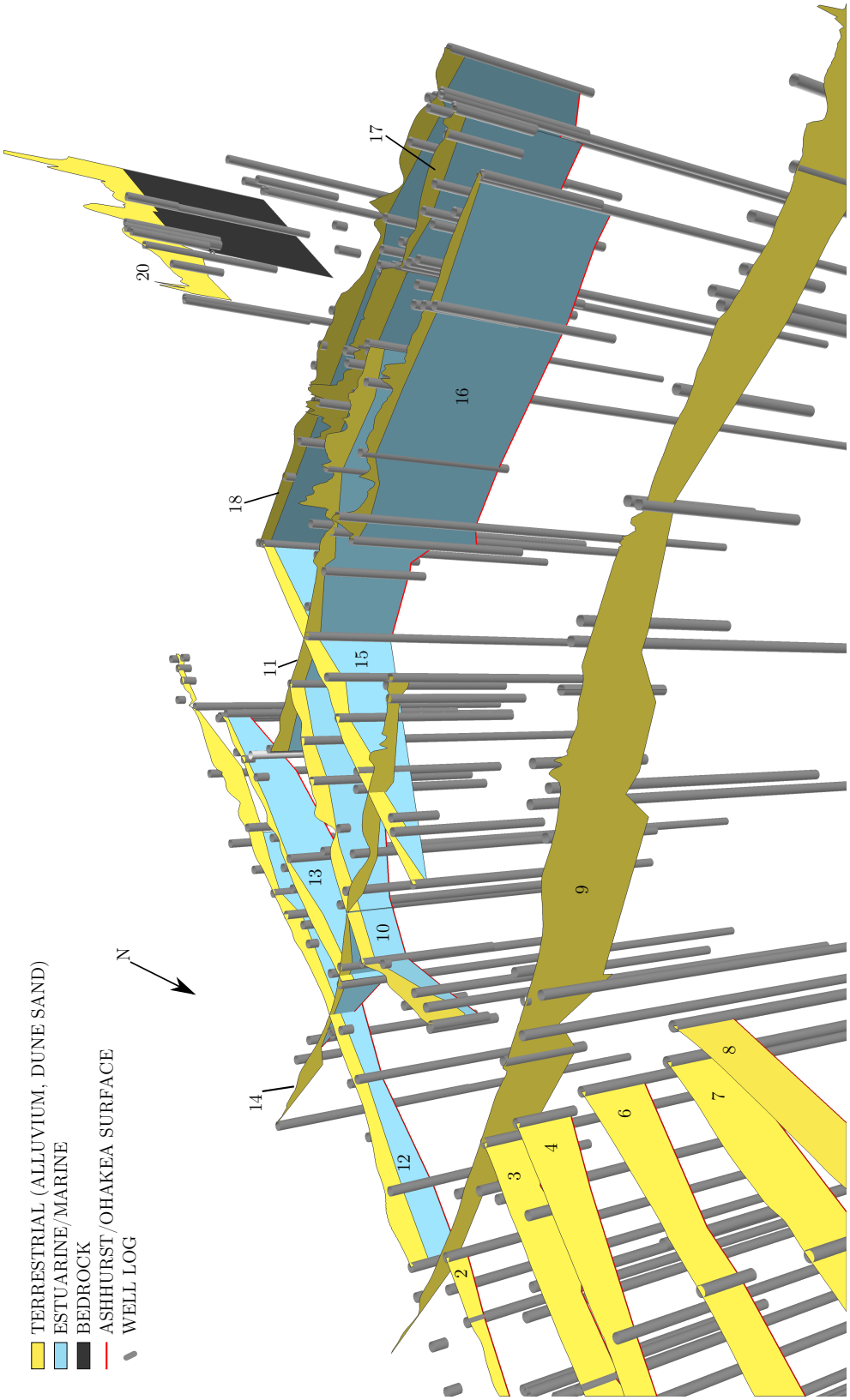
TERRESTRIAL (ALLUVIUM, DUNE SAND)
ESTUARINE/MARINE
BEDROCK
ASHHURST/OHAKEA SURFACE
WELL LOG
N
2
3
4
6
7
8
9
10
11
12
13
14
15
16
17
18
20

by Begg et al. (2005) of the depth of the Milson/Rata surface at this location (Figure 6.7).

West of well 335151 (Sheet 2, POI 5) the Ashhurst/Ohakea surface continues to dip at approximately 0.13 degrees (Figures 6.10, 6.11, and 6.12). There are two further post-LGM palaeochannels cut into the top of the Ashhurst/Ohakea terrace at wells 335461 and 335051 (Sheet 2, POIs 6 and 7; Figure 6.12). The Ashhurst/Ohakea surface passes through PMSL in the vicinity of wells 23 and 335101 (Sheet 2, POI 8), reaching a depth of approximately −11.5 m below PMSL northeast of Opiki.

6.5.2.3 Sheet 3: Well logs cross-section 3

The Ashhurst/Ohakea aggradation surface is easy to identify beneath the modern floodplain along the length of well logs cross-section 3 (Sheet 3) as the top of the highest gravel unit penetrated by the water wells. East of Palmerston North City (east of well 336187; Sheet 3, POI 1) the depth of Holocene alluvium overlying the Ashhurst/Ohakea gravels is typically 0.5–2.5 m (Figures 6.10, 6.11, and 6.12). Immediately west of Palmerston North City, within a meander loop, well 336481 penetrates c. 10 m of river silt before encountering Ashhurst/Ohakea gravel (Sheet 3, POI 2). As in well logs cross-sections 1 and 2 (Sheets 1 and 2) this is interpreted as a palaeochannel. This corresponds with the surface expression of a palaeochannel recorded by a LiDAR scan of the meander loop (see LiDAR image insert on Sheet 3).

Through the southern suburbs of Palmerston North City (well 336187 west to well 335411; Sheet 3, POIs 1 and 3) the thickness of Holocene alluvium, and corresponding depth to the Ashhurst/Ohakea aggradation surface, increases to between c. 4.5–12.5 m. This is possibly an artefact of the undulating surface topography and the sparser number of wells between which the alluvium-gravel interface can be traced. Below Palmerston North City (west of well 335411; Sheet 3, POI 3) the Ashhurst/Ohakea gravel is overlaid by 2.5–5.5 m of Holocene alluvium in the form of loams, silts, sands, and clays. The cross-section turns to the south-southwest at well 335185 (Sheet 3, POI 4), whereupon the Ashhurst/Ohakea aggradation surface begins to dip at c. 0.05 degrees to the southwest.

6.5.2.4 Sheet 4: Well logs cross-section 4

Well logs cross-section 4 (Sheet 4) passes across a spur of the Tokomaru Marine Terrace in the vicinity of Massey University (Figure 6.9). However, due to the mismatch between the QMAP surface geology and the ECOSAT DEM this is mapped as Holocene alluvium (Sheet 4, POI 1).

The base of the Holocene alluvium can be followed from the downstream edge of the remnant of Ashhurst/Ohakea aggradation terrace (Sheet 4, POI 2) to the upstream side of the Tokomaru Marine Terrace spur (well 336191; Sheet 4, POI 3). This is accomplished, as was done on the preceding well logs cross-sections, by tracing the uppermost gravel layer in wells sited on

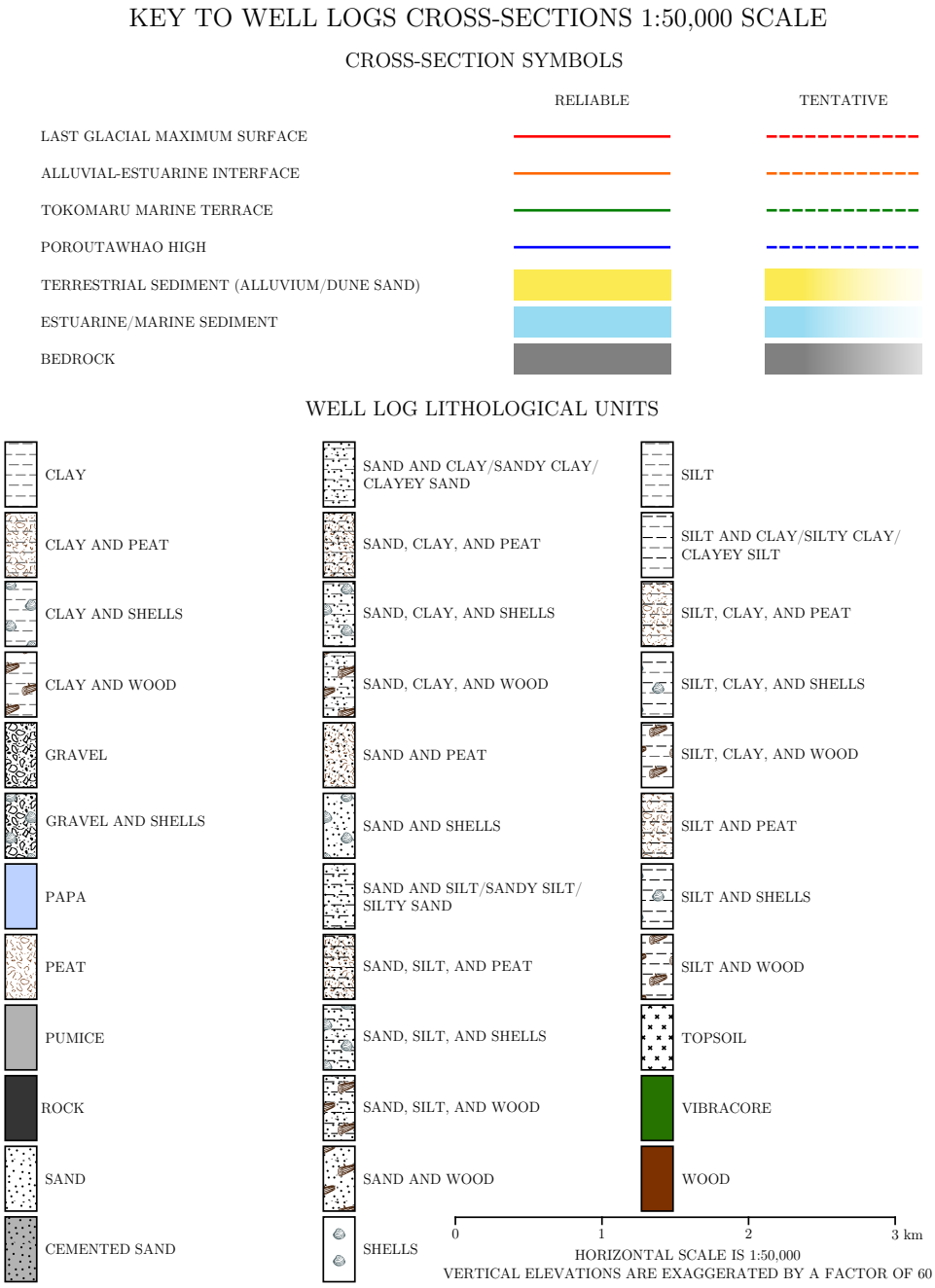

Figure 6.14: Key to well logs cross-sections symbols and lithological units (Sheets 1–23). This key is also presented as a separate sheet in the rear of the thesis (Sheet 32).

the Holocene floodplain. It is unclear whether the uppermost brown sandy gravel unit penetrated by well 336191 (Sheet 4, POI 3) on the eastern side of the Tokomaru Marine Terrace spur is Ashhurst/Ohakea gravel or part of the Otaki Formation (cf. Oliver, 1948; Rich, 1959; Sewell, 1991). Within the spur, above +20 m above PMSL the sands and gravels of the Otaki Formation are

easily identified, although the lower limit of the Last Interglacial strata is not (cf. Hughes, 2005a,b, Figures 6.4, 6.5). Downstream of the Tokomaru Marine Terrace remnant (Sheet 4, POI 1) Holocene alluvium is easily recognisable as a thin veneer over gravels of the Ashhurst/Ohakea aggradation surface (Figure 6.11). The cemented sands and gravels at the base of well 335025 possibly represent an outcrop of the Otaki Formation (Sheet 4, POI 4). This suggests that in this area the Ashhurst/Ohakea gravels are approximately 9–14 m thick.

6.5.3 Oroua Floodplain: Feilding and Bunnythorpe to Kairanga and Opiki

6.5.3.1 Sheet 5: Well logs cross-section 5

The Ashhurst/Ohakea aggradation surface can be traced underneath the Holocene floodplain along the length of well logs cross-section 5 (Sheet 5). The LGM surface descends from c. +45 m above PMSL in the vicinity of Bunnythorpe (well 326221; Sheet 5, POI 1) in a stepwise fashion, reaching c. +1.2 m above PMSL southwest of Kairanga (well 335451; Sheet 5, POI 2; Figures 6.10 and 6.12). This is at a broadly shallower gradient than was estimated for the surface by Begg et al. (2005) (see Figure 6.6).

Along most of the length of the cross-section the base of the Ashhurst/Ohakea gravel is not readily identifiable, with the possible exception of the area around well 335441, immediately northeast of Kairanga (Sheet 5, POI 3). Here, two gravel units are separated by a sand and clay unit at c. −5 m below PMSL. This sand and clay unit may correspond to the silt and clay units in well 335421, 1.1 km to the southeast, from which Lieffering (1990) reported a radiocarbon age from a log of 25953 ± 879 14C years (Sheet 1, POI 3; Table 6.1). The sand and clay unit in well 335441 may therefore approximate the base of the Ashhurst/Ohakea gravel, and the top of the Milson/Rata surface. This elevation is approximately 7 m higher than was estimated by Begg et al. (2005) for the Milson/Rata surface in this area (see Figure 6.6).

6.5.3.2 Sheet 6: Well logs cross-section 6

Similar to well logs cross-section 5 (Sheet 5), the base of the Holocene alluvium (top of the Ashhurst/Ohakea aggradation surface) is easily recognised along the length of well logs cross-section 6 (Sheet 6) as the level at which the water wells have penetrated the uppermost gravel layer beneath the floodplain (Figures 6.10 and 6.12). The gradient of the Ashhurst/Ohakea surface appears to decrease at well 335491 (Sheet 6, POI 1) from c. 0.3 degrees to an average of c. 0.02 degrees. There are a number of papa units (soft grey mudstone; well 335489 west to well 335501; Sheet 6, POIs 2 and 3) which suggest that the subsurface geology of the eastern half of the cross-section may be more complex than is indicated by the simple reconstruction of the Ashhurst/Ohakea surface.

6.5.3.3 Sheet 7: Well logs cross-section 7

The buried surface of the Ashhurst/Ohakea aggradation terrace is easily traced between water wells along the length of well logs cross-section 7 (Sheet 7). The Ashhurst/Ohakea surface descends from c. +45 m above PMSL at Te Arakura (well 325151; Sheet 7, POI 1), reaching PMSL in the vicinity of Kopane (well 334181; Sheet 7, POI 2). At Kopane the dip of the Ashhurst/Ohakea surface lessens from c. 0.32 degrees (well 325111 southwest to well 334181) to c. 0.07 degrees (well 334181 southwest to well 334191; see Sheet 7, POI 2). A similar effect is observed in well logs cross-section 6 (Sheet 6, POI 1; Figures 6.10, 6.11, and 6.12). Northeast of Kopane the dip of 0.32 degrees, while high, is less than the dip estimated by Begg et al. (2005), which is approximately 0.38 degrees. There is a thin unit of gravel and timber in well 335002 (Sheet 7, POI 3) well above the reconstructed LGM surface. This gravel unit is interpreted as a Holocene palaeochannel deposit from the Oroua River. Over the last 3.8 km of the cross-section the Ashhurst/Ohakea surface appears to flatten into a plain approximately −11 m below PMSL. It is unclear whether this is a real observation, or an artefact due to the absence of wells through this segment of the cross-section. Notably, the papa penetrated by water wells on well logs cross-section 6 (Sheet 6) does not appear (or was not recognised by drillers) on this cross-section.

6.5.3.4 Sheet 8: Well logs cross-section 8

The steeply dipping remnant of Tokomaru Marine Terrace at the northern end of well logs cross-section 8 (Sheet 8) can be traced for a short distance underneath the Holocene floodplain as cemented blue sands and loose black sands in wells 324007 and 324045 (Sheet 8, POI 1). Units with similar drillers descriptions feature in a number of the wells which penetrate the Tokomaru Marine Terrace remnant (e.g., wells 325023, 325005, 325381; Sheet 8, POIs 2, 3 and 4). The black sand units are presumed to be beach sands (cf. Duller, 1992a,b).

The top of the Ashhurst/Ohakea surface can be followed as thick gravel units at c. +20 m above PMSL in wells 324007 and 324045 (Sheet 8, POI 1), south to well 334081 (Sheet 8, POI 5) at c. −4 m below PMSL. Northeast of wells 324007 and 324045 (Sheet 8, POI 1) Ashhurst/Ohakea gravels are assumed to pinch-out between the overlying Holocene alluvium and the beds of the Tokomaru Marine Terrace remnant. There are several thin gravel units c. 1 m thick above the reconstructed Ashhurst/Ohakea surface in wells 334061 and 334283 (Sheet 8, POIs 6 and 7; cf. Sheet 7, POI 3). These thin gravel units are interpreted as Holocene palaeochannel deposits from the Oroua River. Between well 334081 (Sheet 8, POI 5) and the southern end of the well logs cross-section 8 (Sheet 8) there are no wells within close proximity to the line of the cross-section — the precise level of the Ashhurst/Ohakea surface is therefore not determinable under this part of the floodplain. The Ashhurst/ Ohakea surface can be found in both wells at the southern end of the cross-

section (wells 334161 and 334111; Sheet 8 POI 8) at c. −10 m below PMSL. This is at the same elevation as in well 334031 (Sheet 7, POI 4) at the southern end of well logs cross-section 7, 600 m east (Figures 6.10 and 6.12).

6.5.4 Manawatu-Oroua floodplain: Linton west to Rangiotu

6.5.4.1 Sheet 9: Well logs cross-section 9 (eastern half)

The Holocene alluvium penetrated by wells along the eastern half of well logs cross-section 9 (Sheet 9) varies in thickness from c. 6–31 m (Figures 6.10, 6.11, and 6.13). In the vicinity of Rangiotu the Holocene alluvium is overridden by encroaching Foxton Phase dune sands (Sheet 9, POI 1). This floodplain to dunefield succession corresponds with the stratigraphic sections from Griffin's Farm (0.5 km south, see Figure 6.1) and Barbers Farm (4 km south, see Figure 6.1) presented by Shepherd and Lees (1987) (Figure 6.15).

The Ashhurst/Ohakea aggradation surface can be traced west from well 344055 (Sheet 9, POI 2) underneath the floodplain as gravels and coarse sands. From well 344055 (Sheet 9, POI 2) to well 344021 (Sheet 9, POI 3) the Ashhurst/Ohakea surface lies between +6.1–+1.3 m above PMSL. This possibly represents a higher surface as part of a set of two or more Ashhurst/Ohakea terraces (cf. Milne, 1973). The Ashhurst/Ohakea surface drops to c. −8.5 m below PMSL in the vicinity of well 344011 (Sheet 9, POI 4), and reaches −20 m below PMSL at well 344071 (Sheet 9, POI 5). This is approximately 8 m lower than might be expected, given the reconstruction along well logs cross-section 1 (Sheet 1). This is interpreted as post-LGM incision by the Manawatu River. The elevation of the Ashhurst/Ohakea gravels increases in well 344193 (Sheet 9, POI 6) to c. −8 m below PMSL, before dropping again to c. −20 m below PMSL in the vicinity of wells 344179 and 344081 (Sheet 9, POI 7). This is the farthest west that the Ashhurst/Ohakea gravels can be traced. It is presumed that they pinch out in the area around Rangiotu.

6.5.5 Central Manawatu floodplain: Opiki to Shannon, Moutoa, and Marotiri

6.5.5.1 Sheet 10: Well logs cross-section 10

The Holocene alluvium along well logs cross-section 10 (Sheet 10) is almost uniformly described by well drillers as clay with some silt content, and varies in thickness from 8–18 m. Beneath the Holocene alluvium is a wedge of estuarine sediment which tapers up-valley (Figures 6.10, 6.11, and 6.13). The estuarine sequence consists of interbedded sands, silts, and clays, with shells, peat, and frequent logs or timber.

The base of the estuarine sequence corresponds with the Ashhurst/Ohakea aggradation surface, which can be followed from the northern end of the cross-section south to well 344177 (Sheet 10, POI 1) at depths of between −11 to −15 m below PMSL. This is supported by a radiocarbon age of 41,500 ± 4,900

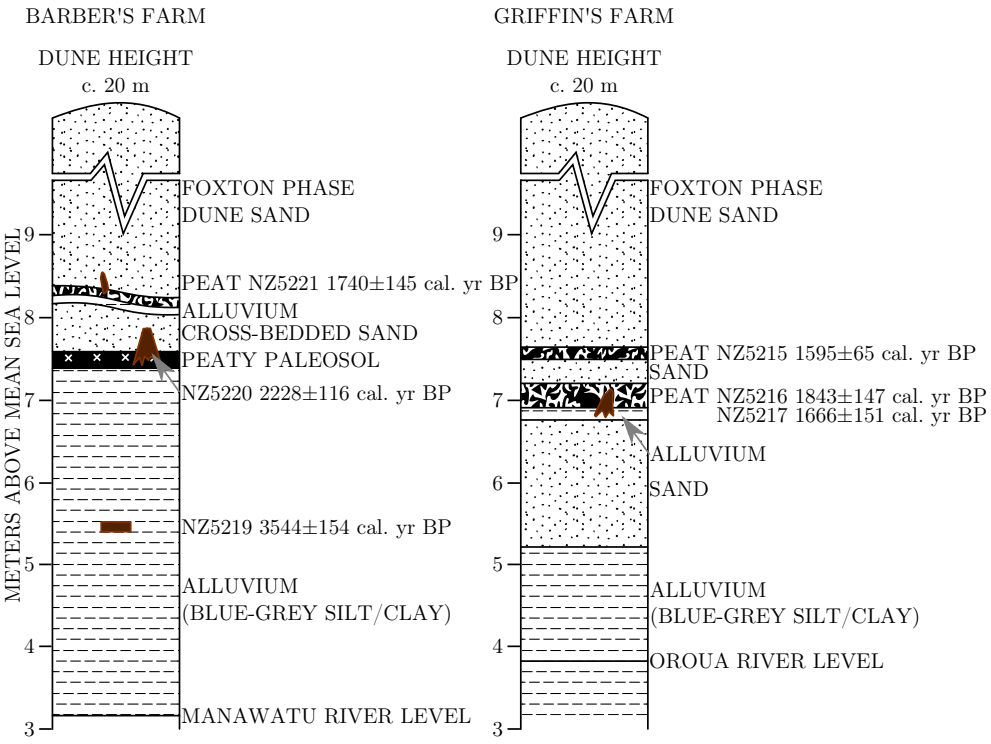

Figure 6.15: Stratigraphic sections from Griffin's and Barber's Farms, lower Manawatu valley (after Shepherd and Lees, 1987). For the locations of Griffin's and Barber's farms see Figure 6.1.

14C years (NZ3938; Table 6.1) from a totara log at the bottom of the uppermost gravel unit in well 1 reported by Hesp and Shepherd (1978) (Sheet 10, POI 2). Southwest of well 344177 gravels are located at depths beyond −40 m below PMSL in wells 344101 and 344201 (Sheet 10, POIs 3 and 4). These may be Ashhurst/Ohakea gravels; however, it is extremely unlikely that the top of these gravel units corresponds with the Ashhurst/Ohakea surface. These may in fact be Milson/Rata or older gravel, with the overlying Ashhurst/Ohakea gravel having been entirely removed. Alternatively, it may be that overbank flood sands, rather than Ashhurst/Ohakea gravels were deposited in this locality during the LGM, suggesting that the main course of the Manawatu River at this time was some distance away. However, the gravels at −33 m below PMSL in well 353051 (Sheet 10, POI 5), at the southern-most end of the cross-section, are presumed to be Ashhurst/Ohakea gravels. This unit is considerably higher than the gravels in wells 344101 and 344201 (Sheet 10, POIs 3 and 4), and corresponds with Ashhurst/Ohakea gravels recognised at similar elevations in adjacent wells (−34 m below PMSL in well 343006, Sheet 11, POI 2, 1.2 km northwest, and −35 m below PMSL in well 354069, Sheet 15, POI 5, 1.8 km southeast).

6.5.5.2 Sheet 11: Well logs cross-section 11

The Holocene alluvium penetrated by wells along well logs cross-section 11 (Sheet 11) consists of blue clays and occasional silts, similar to well logs cross-section 10 (Sheet 10). The alluvium varies in thickness from 4.5–8.5 m (Figures 6.10, 6.11, and 6.13). Underlying the Holocene alluvium are estuarine sands, silts, and clays. Shells such as *A. stutchburyi* are sometimes reported, as is unspecified vegetation and peat (e.g., well 344015; Sheet 11, POI 1). Shepherd and Lees (1987) recovered an articulated *A. stutchburyi* valve from a bore at Murray's Farm, which was radiocarbon dated at 7091 ± 392 cal. yr BP (NZ5218; Table 6.1).

The base of the estuarine sequence is difficult to delineate as the Ashhurst/Ohakea aggradation surface can only be reliably traced between well 343006 (Sheet 11, POI 2) south to well 353031 (Sheet 11, POI 3). There, the Ashhurst/Ohakea surface lies at approximately −34 m below PMSL. North of well 343006 gravels are penetrated below −40 m below PMSL (e.g., wells 344091, 344041, and 344015; Sheet 11 POIs 4, 5 and 6). However, given the depth, these are unlikely to be Ashhurst/Ohakea gravels. As in well logs cross-section 10 (Sheet 10), Ashhurst/Ohakea gravels may have been removed in this area. Alternatively, the Manawatu River may not have flowed through this area during the LGM, and therefore may have deposited only unrecognised fluvial sands.

6.5.5.3 Sheet 12: Well logs cross-section 12

Along well logs cross-section 12 (Sheet 12) the Ashhurst/Ohakea aggradation surface can be traced from well 345021 (Sheet 12, POI 1) southwest to well 354013 (Sheet 12, POI 2). Near Linton the Ashhurst/Ohakea surface lies at approximately −9 m below PMSL (Sheet 12, POI 3). The relatively high elevation of the Ashhurst/Ohakea surface here most likely represents a terrace/fan complex built by a river, such as the Turitea, Kahuterawa, or Tokomaru, flowing out of the Tararua Ranges into the Manawatu valley to meet the base level of the Manawatu River. From well 344061 (Sheet 12, POI 4) the elevation of the Ashhurst/Ohakea surface drops with increasing distance to the southwest, reaching −23 to −27 m below PMSL in the area around well 354013 (Sheet 12, POI 2). At well 354061 gravels are penetrated at around −6 m below PMSL (Sheet 12, POI 5). This is comparable with the height of the Ashhurst/Ohakea gravels near Linton. These gravels most likely represent an Ashhurst/Ohakea alluvial fan/terrace complex built by a stream flowing from the Tararua Ranges across the Tokomaru Marine Terrace and out into the Manawatu valley (see inset figure on Sheet 12).

The Ashhurst/Ohakea aggradation surface is overlain by estuarine sediments in the form of interbedded sands and clays (Figures 6.11 and 6.13). Shells are only observed in well 354075 (Sheet 12, POI 6). As in well logs cross-sections 10 and 11 (Sheets 10 and 11), the estuarine sequence is overlain by Holocene alluvium in the form of blue clays. At well 354005 at the southern

end of the cross-section brown and blue cemented sands of the Otaki Formation outcrop almost to the present level of the floodplain (Sheet 12, POI 7). This is unsurprising, as the Tokomaru Marine Terrace lies less than 100 m to the east.

6.5.5.4 Sheet 13: Well logs cross-section 13

The Ashhurst/Ohakea aggradation surface can be followed horizontally along well logs cross-section 13 (Sheet 13) at approximately −19 m below PMSL from well 344181 (Sheet 13, POI 1) southwest to well 354065 (Sheet 13, POI 2) as clean blue gravels. To the southwest gravel is penetrated at two levels by well 354011 (Sheet 13, POI 3). Neither gravel unit appears to be sufficiently thick to be definitively identified as Ashhurst/Ohakea gravel. However, it may be that the drillers were stopped by the lower gravel unit, which may be much thicker than actually drilled. The lower unit may therefore mark the Ashhurst/Ohakea surface, while the upper gravel unit may be an alluvial fan/terrace complex constructed by a river flowing out of the ranges into the lower valley (cf. Sheet 12, POI 5). Alternatively, the upper gravel unit may be Holocene palaeochannel deposits of the type observed in well logs cross-sections 7 and 8 (Sheets 7 and 8).

At the southwestern end of the cross-section brown gravels and sands are penetrated by water wells at −10 to −15 m below PMSL (Sheet 13, POI 4). These units are most likely Ashhurst/Okakea gravels outwashed from the Tararua Ranges by the Tokomaru River. The sands and gravels of the Ashhurst/Ohakea aggradation surface are overlain by approximately 18 m of sands and clays which are presumed to be estuarine (Figure 6.13). While no shells are reported, it is not unreasonable to assume that these units are estuarine, given the estuarine sequences in the adjacent cross-sections. As in well logs cross-sections 10, 11 and 12 (Sheets 10, 11 and 12), Holocene alluvium overlies the estuarine sequence in the form of clays and silts. The Holocene alluvium varies in thickness from 1.2–6.5 m (Figure 6.13).

6.5.5.5 Sheet 14: Well logs cross-section 14

Well logs cross-section 14 intersects, from east to west, with well logs cross-sections 12, 13, 10, and 11 (Figures 6.9, 6.10, 6.11, and 6.13). Holocene alluvium is easily traced across well logs cross-section 14 between the intersecting cross-sections as blue and brown silts and clays. The base of the Holocene alluvium is generally at or around PMSL. At the eastern end of the cross-section, near the township of Tokomaru, there is only a thin veneer of Holocene alluvium which caps Ashhurst/Ohakea gravels deposited by the proximal Tokomaru Stream (Figure 6.13).

Immediately adjacent to the Otaki Formation wells 344013 and 344175 penetrate 5–6 m of blue clay and gravels (Sheet 14, POI 1). Their blue colour suggests that they are younger and 'fresher' than the brown gravels of the Otaki Formation (cf. 'buckshot' gravels: Fair, 1968; Te Punga, 1954b). They

are therefore interpreted as LGM-age gravel, most likely as part of an alluvial fan/terrace complex constructed by a river flowing out of the Tararua Ranges onto the lower Manawatu floodplain (cf. Sheet 12, POI 5).

The main Ashhurst/Ohakea aggradation surface can be traced from the intersection with well logs cross-section 12 (Sheet 12) west to the intersection with well logs cross-section 10 (Sheet 10). The surface drops from approximately −13 m below PMSL in the vicinity of the intersection with well logs cross-section 10 to c. −19 m below PMSL at the intersection with well logs cross-section 12 (wells 344181 and 344005; Sheet 14, POI 2; Figure 6.13). As the surface continues west, it rises back to c. −13 m below PMSL at the intersection with well logs cross-section 12 (wells 344177 and 344183; Sheet 14, POI 3). It is unclear whether this rise from well logs cross-section 13 to cross-section 10 represents two surfaces within a set of Ashhurst/Ohakea terraces (cf. Milne, 1973).

The Ashhurst/Ohakea aggradation surface is overlain by estuarine sands, silts and clays. West of the intersection with well logs cross-section 10 to the intersection with well logs cross-section 11, the base of the Holocene estuarine sequence is difficult to definitively reconstruct (Figure 6.13). At the western end of the cross-section, beneath the brown and grey sands of the dune country, there are a number of sand and silt units with shells between 0–20 m below PMSL that may be Holocene estuarine sediments. However, drillers have noted the presence of papa and cemented sands. These may therefore be Pleistocene-age units.

6.5.6 Lower Manawatu floodplain: Moutoa and Marotiri through Foxton and Whirokino to Foxton Beach

6.5.6.1 Sheet 15: Well logs cross-section 15

The Ashhurst/Ohakea aggradation surface is readily traced along well logs cross-section 15 (Sheet 15) from Moutoa to Foxton as blue and grey gravels at depths of −26 to −48 m below PMSL (Figures 6.11 and 6.13). Between wells 343131 and 343021 it appears that a large amount of Ashhurst/Ohakea gravel may have been removed (Sheet 15, POI 1). Some of what appears to be eroded gravel can be explained by the vertical adjustment of well 343021 to fit the surface profile. However, it still appears that a considerable volume of Ashhurst/Ohakea gravel has possibly been removed, perhaps due to extensive lateral reworking by the Manawatu River prior to the flooding of the lower valley during the Holocene marine transgression.

Above the Ashhurst/Ohakea aggradation surface lies 35–40 m of marine/estuarine clays, sands and gravels (Figures 6.11 and 6.13). A number of wells at the western end of the cross-section, in the vicinity of Foxton township, penetrate what are probably marine gravel/sand units containing shells (e.g., wells 343167, 343151, 343011; Sheet 15, POIs 2, 3, and 4). Similar units were described by Shepherd et al. (1986) at Tangimoana 20 km to the north (Figure 6.2). From Moutoa to Marotiri the marine/estuarine sequence is overlain

by approximately 7 m of alluvium in the form of brown and blue clays. From Marotiri to Foxton the cross-section crosses into the dune country. Here, the marine estuarine sequence is overlain by up to 17 m of Holocene dune sands (Figures 6.11 and 6.13).

6.5.6.2 Sheet 16: Well logs cross-section 16

Along the length of well logs cross-section 16 (Sheet 16) the Ashhurst/Ohakea aggradation surface can be followed as blue and grey gravels at depths of −42 to −54 m below PMSL. This is broadly agreeable with the Ashhurst/ Ohakea surface reconstructed along well logs cross-section 15 (Sheet 15), approximately 1 km to the south (Figures 6.10 and 6.13). The Ashhurst/Ohakea aggradation surface is overlain by 50–60 m of marine/estuarine clays, sands, and gravels, similar to those penetrated along cross-section 15 (Sheet 15). Notably, well 342141 penetrates a 42 m thick unit of black/grey sands with shells and small gravels (Sheet 16, POI 1) which possibly constitutes a prograded marine wedge (cf. Shepherd et al., 1986; Figure 6.2). The marine/estuarine sequences are overlain by dune sands from each of the three main dune building phases, with age decreasing towards the northwest. With the exception of some peat beds all of the sedimentary units above PMSL along the length of well logs cross-section 16 (Sheet 16) are described by drillers as sands of various colours. It is therefore difficult to definitively identify particular bodies of sand as dune sand. The demarcation line between the marine/estuarine sequence and the dune field may therefore be erroneous in places.

6.5.6.3 Sheet 17: Well logs cross-section 17

Wells along well logs cross-section 17 (Sheet 17) penetrate the blue gravels of the Ashhurst/Ohakea LGM aggradation surface at between −55 to −63 m below PMSL. However, it should be noted that well 343013 (Sheet 17, POI 1) at the southeastern end of the cross-section is vertically adjusted by c. 9 m to fit the surface profile. Therefore, the Ashhurst/Ohakea surface may lie at approximately −45 m below PMSL in this area. As in well logs cross-sections 15 and 16 (Sheets 15 and 16), the Ashhurst/Ohakea surface is overlain by approximately 50 m of marine/estuarine sands, silts, and gravels (Figures 6.10 and 6.13). Shells are frequently reported. Close to the base of the marine/ estuarine sequence, at c. −45 m below PMSL, lies a *Podocarpus* log within a clay and sand unit that was radiocarbon dated by Te Punga (1958) at 9,919 ± 76 14C years (>11,000 cal. yr BP; Table 6.1). Te Punga (1958) tentatively inferred that the log was stranded in the intertidal zone and later buried beneath estuarine and/or shallow marine sediments (see Section 2.4). Southeast of Foxton the marine/estuarine sequence is overlain by the brown sands of the Foxton Phase dunes. At well 343013, these possibly encroach over blue silty clays of the Holocene floodplain (Sheet 17, POI 1). Northeast of Foxton the opposite occurs, as the Holocene floodplain cuts northward into

the dunefield. Sands, rather than silts and clays present at the surface (Sheet 17, POI 2).

6.5.6.4 Sheet 18: Well logs cross-section 18

Along well logs cross-section 18 (Sheet 18) the level of the Ashhurst/Ohakea aggradation surface drops from c. −34 m below PMSL in well 353031 (Sheet 18, POI 1), to approximately −40 m below PMSL in the vicinity of wells 353001 and 342085 (Sheet 18, POI 2). In between these wells the level of the surface can only be estimated. Ashhurst/Ohakea gravels are encountered at depths of −45 to −50 m below PMSL beneath Foxton Beach township at the western end of the cross-section. A relatively uniformly dipping Ashhurst/ Ohakea aggradation surface can therefore be estimated for the full length of well logs cross-section 18 (Sheet 18; Figures 6.11 and 6.13).

The Ashhurst/Ohakea aggradation surface is overlain by approximately 35–55 m of marine/estuarine sediment, consistent with other cross-sections from the lower Manawatu. Beneath the floodplain west from Moutoa to Whirokino (well 353031 west to well 342031; Sheet 18, POIs 1 and 3) interbedded sands and clays are prevalent, while in the vicinity of Foxton Beach sand and gravel units with shells are common (cf. the marine wedge of Shepherd et al., 1986). The marine/estuarine sequence is overlaid with a veneer of Holocene alluvial sands. At Whirokino the cross-section crosses relict dunes isolated by the Manawatu River (Sheet 18, POI 3), while west of Whirokino the marine/estuarine sequence is topped by late Holocene beach sands (Sheet 18, POI 4).

6.5.6.5 Sheet 19: Well logs cross-section 19

Well logs cross-section 19 (Sheet 19) intersects, from south to north, with well logs cross-sections 18, 17, and 16. The gravels of the Ashhurst/Ohakea aggradation surface are only penetrated where well logs cross-section 19 intersects with cross-sections 17 and 16, at approximately −53 to −55 m below PMSL (Sheet 19, POI 1). Gravels are penetrated at −60 m below PMSL in well 352180, at the southern end of the cross-section (Sheet 19, POI 2); however, it is not possible to discern if these are from the Ashhurst/Ohakea surface.

Above −55 m PMSL the sand, stilt, and gravel units penetrated by the water wells along the length of well logs cross-section 19 (Sheet 19) are presumed to be Holocene shallow marine/estuarine sediments; however, this is not possible to definitely ascertain. The base of the Holocene dune sequence and floodplain can be broadly defined. However, as was the case with well logs cross-section 16 (Sheet 16), it is difficult to definitively distinguish individual sand units identified by well drillers as marine/estuarine or aeolian or floodplain sands.

6.5.7 Lower Manawatu (south): Porotowhao and Koputaroa

6.5.7.1 Sheet 20: Well logs cross-section 20

Greywacke bedrock of the Poroutawhao High is encountered at between +3 and +5 m above PMSL between Lake Horowhenua and Poroutawhao. The bedrock high ends abruptly between well 10 (Hesp and Shepherd, 1978) and well 352281 (Sheet 20, POI 1; Figures 6.10, 6.11, and 6.13). The northern end of the Poroutawhao High is overlain by a spur of the Tokomaru Marine Terrace, which is itself overlain in places by Holocene dune sands. South of the Tokomaru Marine Terrace spur the bedrock high is overlain by blue gravels. It is difficult to identify the provenance of the gravels. They may be LGM-age gravels deposited by the Ohau River, or beach gravels deposited on top of the high at the height of the Holocene marine transgression.

The gravels on top of the Poroutawhao High are in turn overlain by blue and brown sands. The blue sands may be beach sands which accompany the gravels, while the brown sands are most likely dune sands. However, this differentiation is done on the basis of colour alone, and may therefore be incorrect. North of the Poroutawhao High dune sands form the uppermost sedimentary unit. Again, however, definitively delineating the base of the dunes is difficult given the well drillers minimal descriptions. Beneath these dunes lie interbedded sands, gravels and clays that are most likely Holocene marine/estuarine sediments. The base of these marine/estuarine sediments is difficult to define.

6.5.8 Coastal Manawatu: Himitangi

6.5.8.1 Sheet 9: Well logs cross-section 9 (western half)

Hesp (1975) presented a cross-section along much the same line as the western half of well logs cross-section 9 (Sheet 9). Hesp (1975) noted that wells at the coast appeared to penetrate a sedimentary sequence described as typical of a prograding coastline. Hesp (1975) also noted the absence of LGM alluvial gravels, and suggested that this indicated that the Himitangi Anticline may have had expression sufficient to control the path of the Manawatu River. Hesp (1975) further suggested that sand units appeared to arc upwards across the path of the Himitangi Anticline, indicating the presence of either that structural barrier, or the existence of a Pleistocene sand barrier/bar complex (Figures 6.10, 6.11, and 6.13).

At the coast beneath Himitangi Beach there does appear to be a wedge of sand, clay, silt, and gravel layers with frequent shells and peat overlying cemented sand and papa units (Sheet 9, POI 8). A similar wedge of marine sediment has been described by Shepherd et al. (1986) at Tangimoana (Figure 6.2). It is tentatively suggested that the apparent wedge of progradational marine sediment discerned at Himitangi Beach is much the same as that observed at Tangimoana, comprising Holocene shallow marine sediment deposited as the coast prograded following the Holocene marine transgression.

The Holocene progradational wedge is overlain by up to 20 m of Holocene dune sand. The base of the dune sequence may be different than defined, as most of the wells penetrate sands which are distinguished only by colour in the driller's descriptions. As Hesp (1975) suggested, there may be an arc or core of sands rising above PMSL (Figures 6.10, 6.11, and 6.13). However, it is impossible to discern whether this is due to structural control by the Himitangi Anticline. The suggestion of a core of Pleistocene sands is not unreasonable.

6.6 Digital elevation models of key surfaces within the sedimentary fill of the lower Manawatu valley

6.6.1 Last Glacial Maximum fluvial aggradation surface

The discrete observations of the LGM aggradation surface presented by the well log cross-sections can be interpolated and extrapolated to reconstruct the buried Ashhurst/Ohakea terrace as a continuous digital elevation model (DEM). The Ashhurst/Ohakea LGM surface represents the top of the Low-stand Systems Tract (LST), and therefore forms the Transgressive Surface (TS) at the base of the Manawatu incised-valley's Holocene fill. A DEM of this surface therefore allows estimates to be made of the accommodation space made available to infilling sediment due to the Holocene marine transgression, and the total volume of Holocene sediment deposited in the lower valley. Reconstruction of the valley's morphology prior to its inundation during the Holocene marine transgression also provides valuable context to assist with understanding the effects that post-glacial sediment loading and sediment compaction may have had on the sedimentary fill of the valley (see Section 8.3), and aspects of the palaeogeographic reconstruction of the valley's Holocene evolution, such as the extent of the estuary (see Section 8.5.3).

6.6.1.1 Ashhurst/Ohakea LGM aggradation surface DEM construction

The lithological units which represent the Ashhurst/Ohakea aggradation surface were extracted from the well log cross-sections (Sheets 1–20) as a series of points (Figure 6.16). The location of each point corresponded with the location of the well log from which the lithological unit was sourced. The elevation of each point was calculated as the elevation of the modern land surface at that point, as represented by the ECOSAT DEM, less the depth to the top of the lithological unit. Between Poroutawhao and the Moutoa floodway, where there are no cross-sections, well logs were examined (Figure 6.16; Sheet 21: Poroutawhao-Moutoa well logs) for the gravel signature which marks the presence of the Ashhurst/Ohakea aggradation surface (see Sheets 1–20). However, Ashhurst/Ohakea gravels were not located.

A barrier or margin was delineated (Figure 6.16) to limit the extent of the interpolated DEM to the probable extent of the Ashhurst/Ohakea aggradation surface. The barrier also ensured that elevation observations from different, disparate parts of the valley did not unduly influence each other. For example, it was desirable that elevations in the area immediately southwest of the Manawatu Gorge did not influence interpolation of the DEM near the Oroua River.

From Palmerston North City southwest to Koputaroa the southern extent of the Ashhurst/Ohakea surface was defined as the northern edge of the Tokomaru Marine Terrace (Figure 6.16). West of Koputaroa the maximum southern extent of the LGM surface would have been limited by the presence of the Poroutawhao High (see Sheet 20: well logs cross-section 20). The northern limit of the reconstructed Ashhurst/Ohakea surface, from Ashhurst northwest to Feilding, conforms to the margin of preserved Ashhurst/Ohakea and Milson/Rata fluvial terraces. Southwest from Feilding to Rongotea the possible extent of the Ashhurst/Ohakea surface is confined by Pleistocene marine terraces (Figure 6.16).

From Rongotea south to Rangiotu, in the vicinity of the border between the Holocene transgressive dunefield and the floodplain of the Oroua River, the possible extent of the Ashhurst/Ohakea surface is not clearly limited by morphological barriers. Well logs from this area (Figure 6.16) were examined (Sheet 22: Himitangi-Oroua well logs) for signature gravels marking the presence of the Ashhurst/Ohakea aggradation surface. Signature gravels were only identified in five wells (334101, 334121, 165, 344167, and 344185), all relatively proximal to the Oroua floodplain. The limit of the Ashhurst/Ohakea aggradation surface was therefore placed along the dunefield-floodplain margin to include these wells. The same approach was taken to delineate the

Figure 6.16 *(facing page)*: Locations of well logs containing gravel units identified as Ashhurst/Ohakea LGM aggradation gravel (black points) (1:200,000 scale). Also shown is the margin/barrier used to confine the Spline with Barriers DEM interpolation algorithm when constructing the DEM of the Ashhurst/Ohakea LGM aggradation surface (black line). The locations of well logs examined in the Porotouwhao-Moutoa area (Sheet 21) are shown in red. The locations of well logs examined in the Himitangi-Oroua area (Sheet 22) are shown in green. The locations of well logs examined in the Rangiotu-Foxton area (Sheet 23) are shown in blue. Base geological map constructed using data from Kingma (1962), Cowie et al. (1967), Pillans (1990a), Begg and Johnston (2000), Lee and Begg (2002), Townsend et al. (2008), and unpublished data from the QMAP project made available by D. Townsend.

Figure 6.17 *(page 173)*: Digital elevation model of the Ashhurst/Ohakea LGM aggradation surface reconstructed from gravel units identified in water well logs throughout the lower Manawatu valley (1:200,000 scale). Vertical contour interval is 5 m. Base geological map constructed using data from Kingma (1962), Cowie et al. (1967), Pillans (1990a), Begg and Johnston (2000), Lee and Begg (2002), Townsend et al. (2008), and unpublished data from the QMAP project made available by D. Townsend.

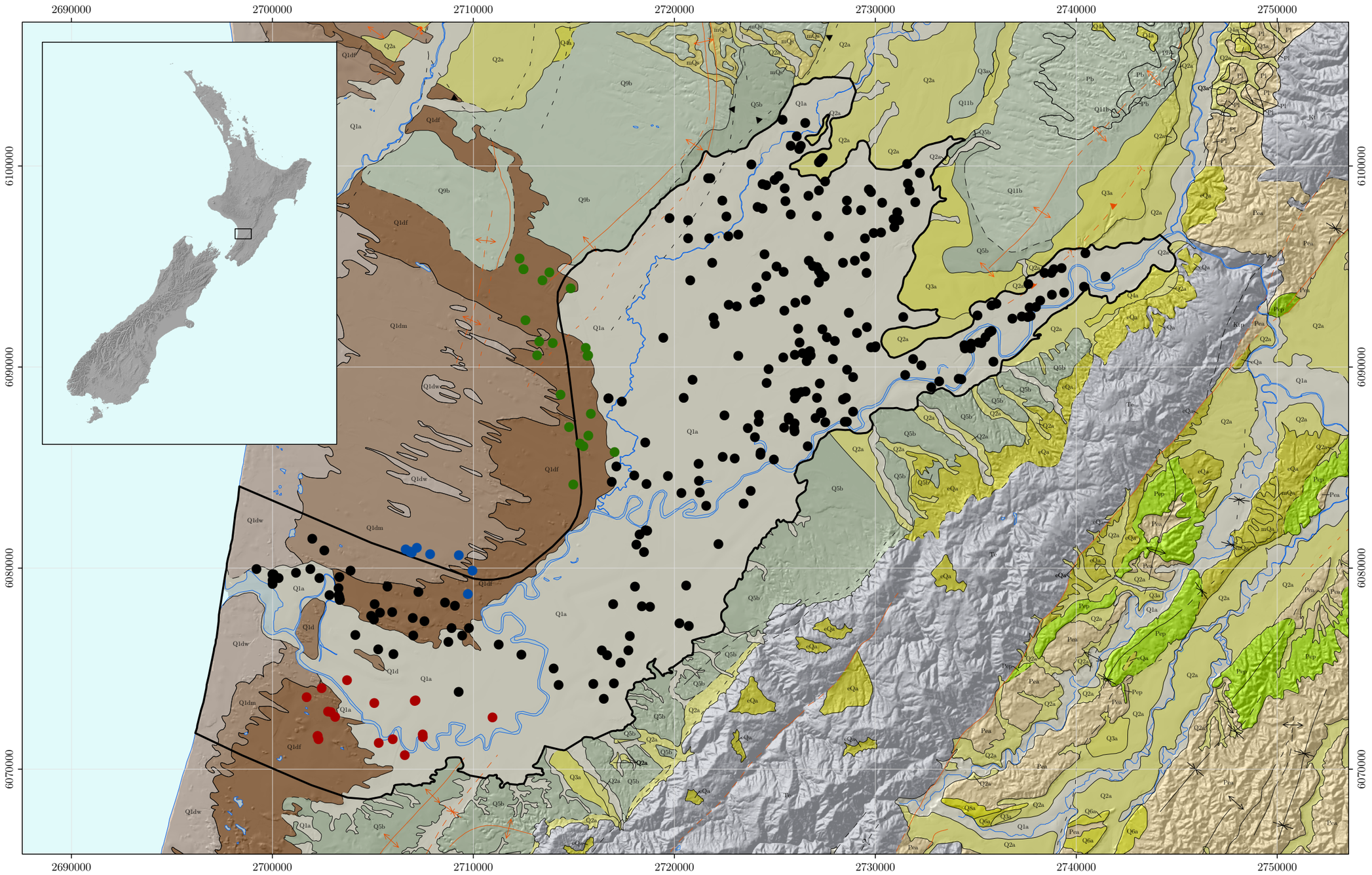
2690000
2700000
2710000
2720000
2730000
2740000
2750000
6100000
6090000
6080000
6070000

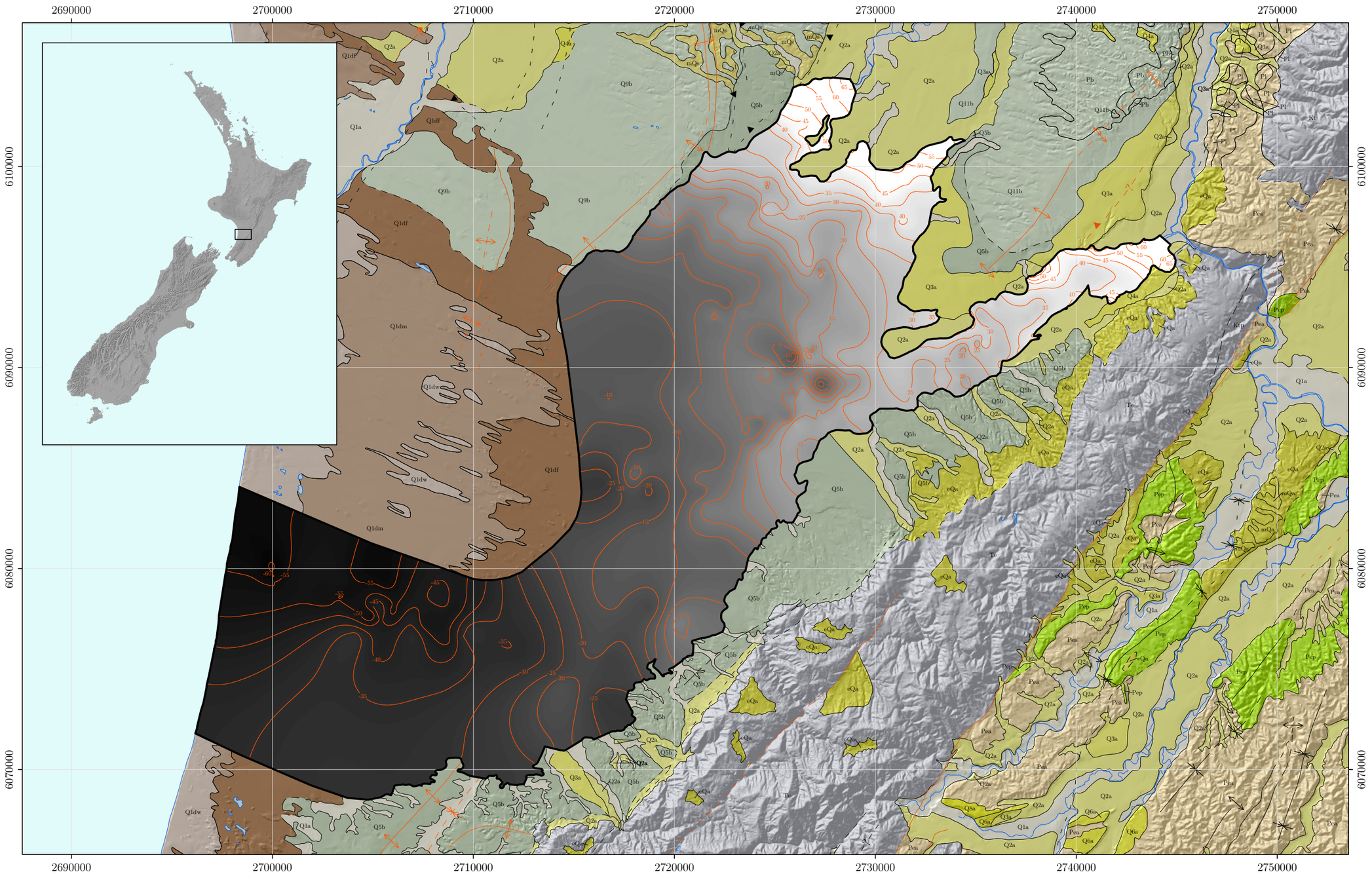
2690000
2700000
2710000
2720000
2730000
2740000
2750000
6100000
6090000
6080000
6070000

limit of the Ashhurst/Ohakea surface between Rangiotu and Foxton (Sheet 23: Rangiotu-Foxton well logs). However, none of the wells examined featured identifiable Ashhurst/Ohakea gravel units. The probable margin of the LGM surface therefore excludes these wells (Figure 6.16).

The DEM of the Ashhurst/Ohakea LGM fluvial aggradation surface (Figure 6.17) was constructed using the point observations of the gravel surface and the surface's probable extent boundary in ArcGIS 9.2 using the Spline with Barriers algorithm. This interpolates a minimum curvature smooth surface that passes exactly through the input points (e.g., Briggs, 1974; Terzopoulos, 1988; Smith and Wessel, 1990; Zoraster, 2003). The surface produced is therefore a reliable reflection of the input points. The effect is the same as when the Topo to Raster algorithm is used with drainage enforcement not applied.

Other possible interpolation methods such as IDW (inverse distance weighted), kriging, and Topo to Raster were rejected as unsuitable. IDW was rejected as it assumes that the influence of the variable being interpolated decreases with distance from its sampled location. The variable being interpolated is therefore a locationally dependant. However, the distribution of well log observations is entirely random. Kriging was discounted for the same reason as it assumes that the there is a spatial correlation in the distance or direction between sample points that can be used to explain variation in the surface. Topo to Raster with drainage enforcement applied was not used as it attempts to produce a hydrologically correct surface. Tests showed that DEMs of the LGM surface produced with Topo to Raster with drainage enforcement applied typically contained channel artefacts (Figure 6.18). The validity of these artefacts is impossible to ascertain as the sample points of the Ashhurst/Ohakea surface obtained from the well logs are random, subject to elevation errors (see Section 6.4.1), and are not necessarily representative of a hydrologically correct surface.

6.6.1.2 Ashhurst/Ohakea LGM aggradation surface DEM results

The DEM of the Ashhurst/Ohakea fluvial aggradation terrace (Figure 6.17) reveals that the LGM surface is generally higher on the true left of the valley, proximal to the Tokomaru Marine Terrace. In contrast, on the true right of valley from Kopane southwest to Rangiotu, and from Marotiri west to Foxton Beach, the reconstructed surface is markedly depressed. It is unclear whether this trend is entirely due to the distribution of input data points from which the DEM was constructed (cf. Figure 6.16). The depression in the vicinity of Foxton and Foxton Beach appears reliable, given the large number of observations in the area. However, the rise in the LGM surface south from the Whirokino Cut towards Poroutawhao, where there are no observations of the depth of the Ashhurst/Ohakea surface, should be taken as a by-product of this lack of input data, rather than as a result of tectonic uplift along the Tararua Ranges (cf. Section 4.4).

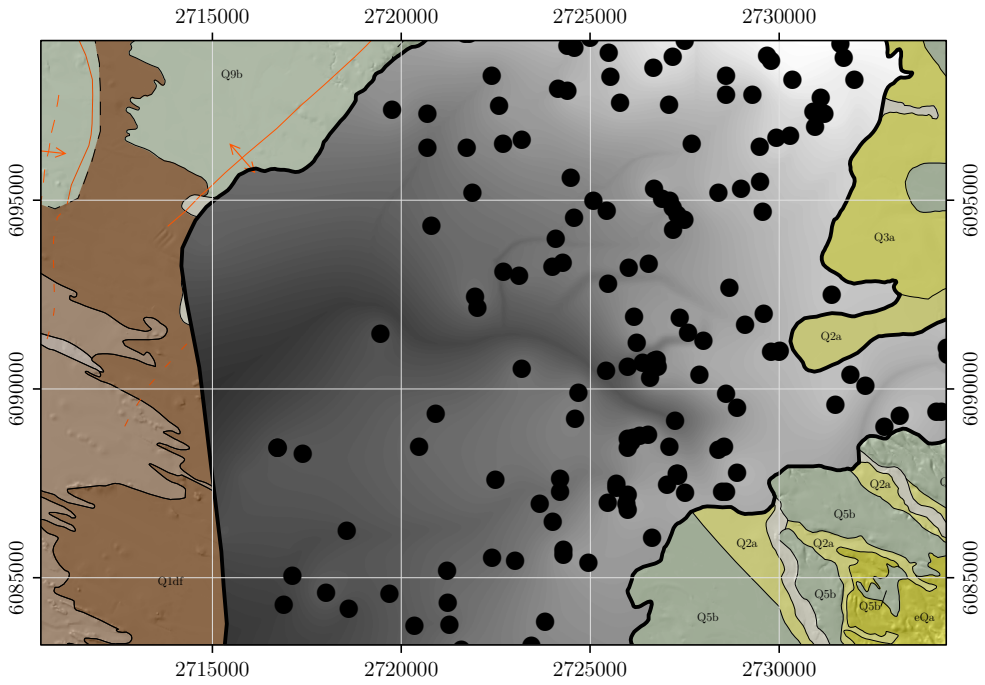

Figure 6.18: Example of channel artifacts produced by the Topo to Raster algorithm (1:200,000 scale). These channels are not defined by any of the gravel units from the water well logs (black points). The extent of this map is shown on Figure 6.1. Base geological map constructed using data from Kingma (1962), Cowie et al. (1967), Pillans (1990a), Begg and Johnston (2000), Lee and Begg (2002), Townsend et al. (2008), and unpublished data from the QMAP project made available by D. Townsend.

There are several sinks obvious in the surface in the vicinity of Palmerston North City. These sink features are unlikely to be representative of the surface, as sinks are generally rare in natural landscapes (Goodchild and Mark, 1987), and are broadly irreconcilable with fluvially derived surfaces. Most likely these sinks are the result of either elevation errors, or errors in logging by the original well drillers. A subjectively or intuitively 'corrected' version of the DEM was produced to eliminate the sinks by altering the elevations of the sink-producing points to 'fill in the holes' (Figure 6.19).

Contours generated for the reconstructed LGM surfaces (Figures 6.20 and 6.21) show that they are broadly coincident with the extrapolated 20 m contours presented by Begg et al. (2005). In the vicinity of Kopane the 0 m contour of the reconstructed surfaces is somewhat coincident with the 0 m contour extrapolated by Begg et al. (2005). However, near Palmerston North City the reconstructed Ashhusrt/Ohakea DEMs are generally higher (c. +20 m; excluding sinks) than suggested by Begg et al. (2005) (c. 0 m; Figures 6.20 and 6.21). Given the errors inherent in both the extrapolated contours (Begg et al., 2005) and the reconstructed DEMs, they are not considered to be definitively contradictory.

6.6.2 Digital elevation model of the estuarine-alluvial interface

The well log cross-sections constructed across the lower Manawatu valley also reveal the interface between overlying alluvial and dune sediments and underlying estuarine/marine sediments. In the same manner in which observations of the LGM aggradation surface were interpolated and extrapolated to create a digital elevation model, observations of the alluvial-estuarine interface can also be interpolated to form a DEM. Such a DEM would allow specific volume estimates of the alluvial and estuarine sedimentary infill of the incised-valley.

6.6.2.1 Estuarine-alluvial interface DEM construction

The lithological units which represent the top of the Holocene estuarine fill were extracted from the well log cross-sections (Sheets 1–20) as a series of points (Figure 6.22). Distinguishing the estuarine fill from the overlying alluvium was sometimes difficult, due to the general descriptions provided by the well drillers (see Section 6.4.2). The location of each point corresponded with the location of the well log from which the lithological unit was sourced. The elevation of each point was calculated as the elevation of the modern land surface at that point, as represented by the ECOSAT DEM, less the depth to the top of the lithological unit. Between Poroutawhao and the Moutoa floodway, where there are no cross-sections, well logs were examined to identify the

Figure 6.19 *(facing page)*: Digital elevation model of the Ashhurst/Ohakea LGM aggradation surface reconstructed from gravel units identified in water well logs throughout the lower Manawatu valley, adjusted to remove sinks (1:200,000 scale). Vertical contour interval is 5 m. Base geological map constructed using data from Kingma (1962), Cowie et al. (1967), Pillans (1990a), Begg and Johnston (2000), Lee and Begg (2002), Townsend et al. (2008), and unpublished data from the QMAP project made available by D. Townsend.

Figure 6.20 *(page 178)*: Comparison of the reconstructed digital elevation model of the Ashhurst/Ohakea LGM aggradation surface with the structural contours of the Ashhurst/Ohakea surface extrapolated by Begg et al. (2005) (Figure 6.6; 1:200,000 scale). Vertical contour interval for the DEM is 5 m (orange); for the structural contours the interval is 20 m (black). Base geological map constructed using data from Kingma (1962), Cowie et al. (1967), Pillans (1990a), Begg and Johnston (2000), Lee and Begg (2002), Townsend et al. (2008), and unpublished data from the QMAP project made available by D. Townsend.

Figure 6.21 *(page 179)*: Comparison of the reconstructed digital elevation model of the Ashhurst/Ohakea LGM aggradation surface (adjusted to remove sinks) with the structural contours of the Ashhurst/Ohakea surface extrapolated by Begg et al. (2005) (Figure 6.6; 1:200,000 scale). Vertical contour interval for the DEM is 5 m (orange); for the structural contours the interval is 20 m (black). Base geological map constructed using data from Kingma (1962), Cowie et al. (1967), Pillans (1990a), Begg and Johnston (2000), Lee and Begg (2002), Townsend et al. (2008), and unpublished data from the QMAP project made available by D. Townsend.

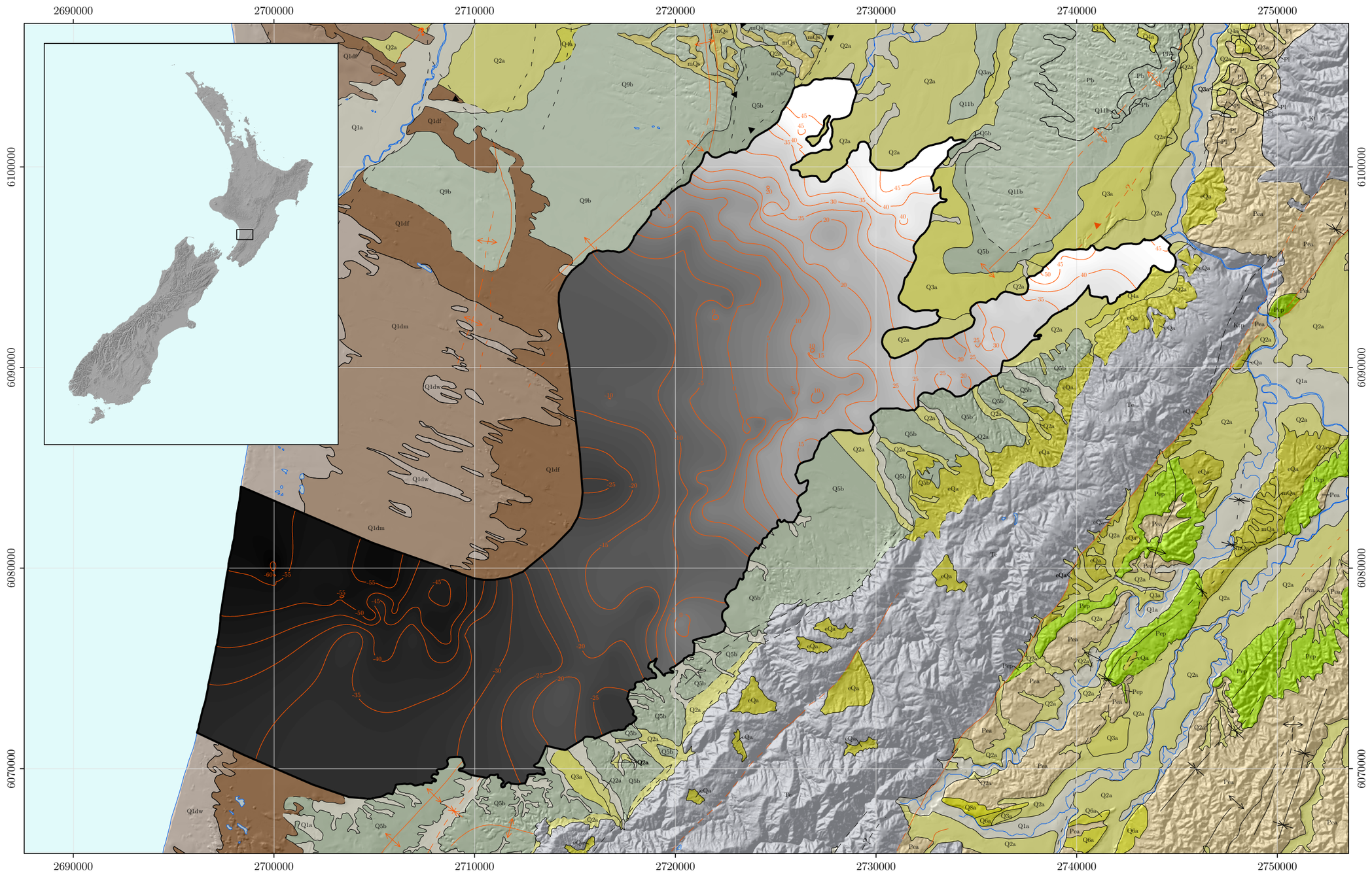
2690000
2700000
2710000
2720000
2730000
2740000
2750000
6100000
6090000
6080000
6070000

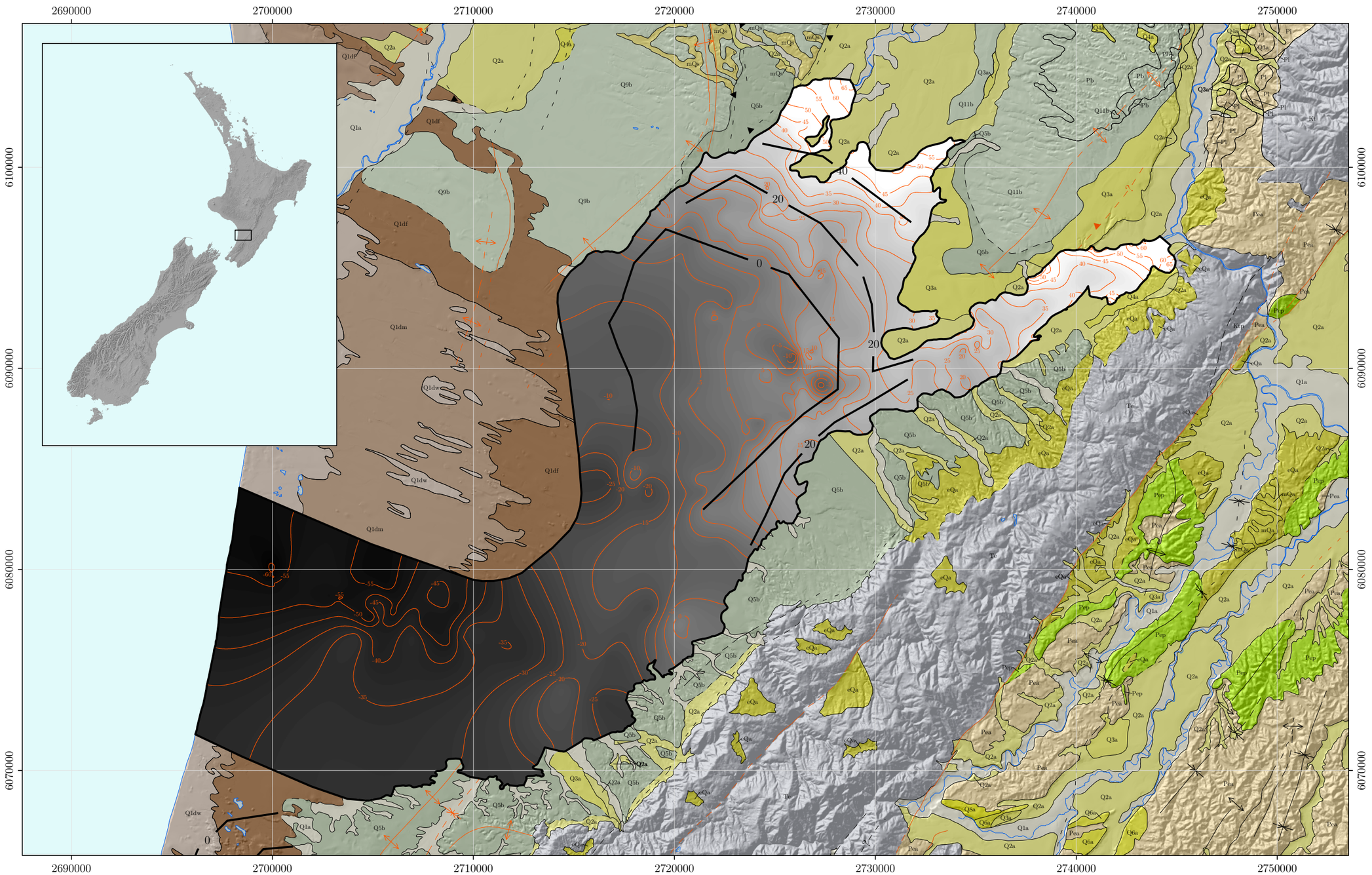
2690000
2700000
2710000
2720000
2730000
2740000
2750000
6100000
6090000
6080000
6070000

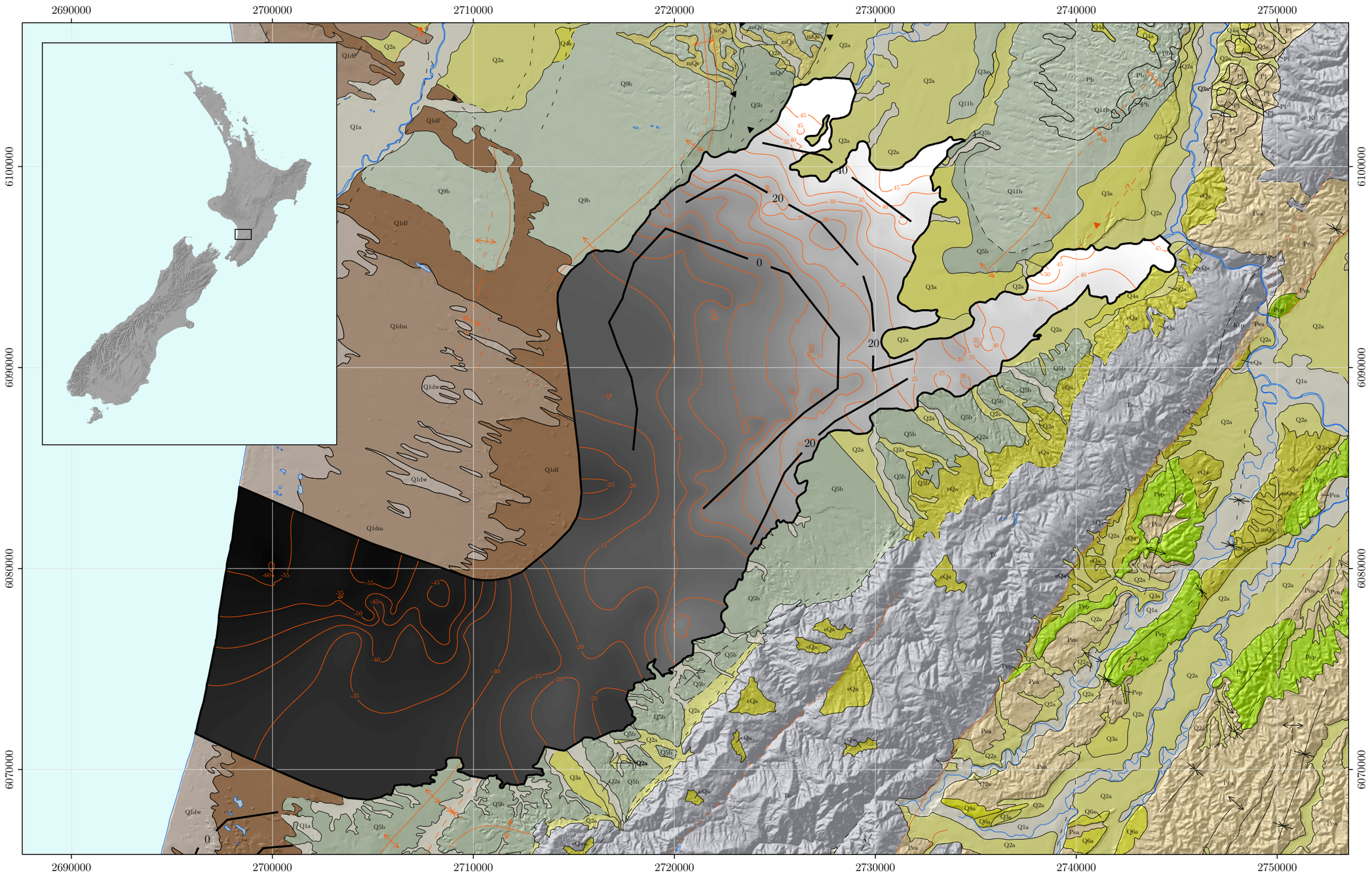
2690000
2700000
2710000
2720000
2730000
2740000
2750000
6100000
6090000
6080000
6070000

estuarine-alluvial transition (Figure 6.22; Sheet 21: Poroutawhao-Moutoa well logs). The interface was identified in eleven of the 21 well logs. Observations of the top of the highstand estuarine sand and silt facies identified in vibracores recovered from the lower valley (Chapter 7) were also included. Elevations of the top of the estuarine sands and silts were taken relative to the Wellington Vertical Datum elevations for the surveyed vibracores.

A barrier or margin was delineated to ensure that the estuarine surface model corresponded with the DEM of the Ashhurst/Ohakea aggradation surface (Figure 6.22). The estuarine surface barrier therefore coincides with the Ashhurst/Ohakea barrier along its southern, western, and northern margins. The northeastern margin of the estuarine surface barrier simply encloses the population of points which represent the top of the estuarine infill.

The digital elevation model of the estuarine-alluvial interface (Figure 6.23) was constructed using the point observations of the interface and the estuary's probable extent boundary in ArcGIS 9.2 using the Spline with Barriers algorithm.

6.6.2.2 Estuarine-alluvial DEM results

The DEM of the estuarine-alluvial interface (Figure 6.23) shows considerable variability, and ranges in elevation from −8.39 m to +13.96 m. However the mean elevation is 0 m, with a standard deviation of ±3.30 m. Some of this variability possibly reflects the difficulty encountered distinguishing between estuarine and alluvial sediments based solely on the limited descriptions given by well drillers. However, much of the higher elevations of the estuarine-alluvial interface DEM are located at the southern end of the Himitangi Anticline (Figure 6.23; e.g., Sheet 16, Sheet 18, POI 4). Therefore, it may be that the estuarine-alluvial interface proximal to the anticline may have been uplifted or otherwise deformed by the anticline through the Holocene. A maximum

Figure 6.22 *(facing page)*: Locations of well logs and vibraocres containing sedimentary units identified as the top of the Holocene marine/estuarine fill in the lower Manawatu valley (1:100,000 scale). Also shown is the margin/barrier used to confine the Spline with Barriers DEM interpolation algorithm when constructing the estuarine-alluvial interface DEM. The extent of this map is shown on Figure 6.1. Base geological map constructed using data from Kingma (1962), Cowie et al. (1967), Pillans (1990a), Begg and Johnston (2000), Lee and Begg (2002), Townsend et al. (2008), and unpublished data from the QMAP project made available by D. Townsend.

Figure 6.23 *(page 182)*: Digital elevation model of the estuarine-alluvial interface reconstructed from sedimentary units identified in water well logs and vibracores througout the lower Manawatu valley (1:100,000 scale). Vertical contour interval is 2 m. The extent of this map is shown on Figure 6.1. Base geological map constructed using data from Kingma (1962), Cowie et al. (1967), Pillans (1990a), Begg and Johnston (2000), Lee and Begg (2002), Townsend et al. (2008), and unpublished data from the QMAP project made available by D. Townsend.

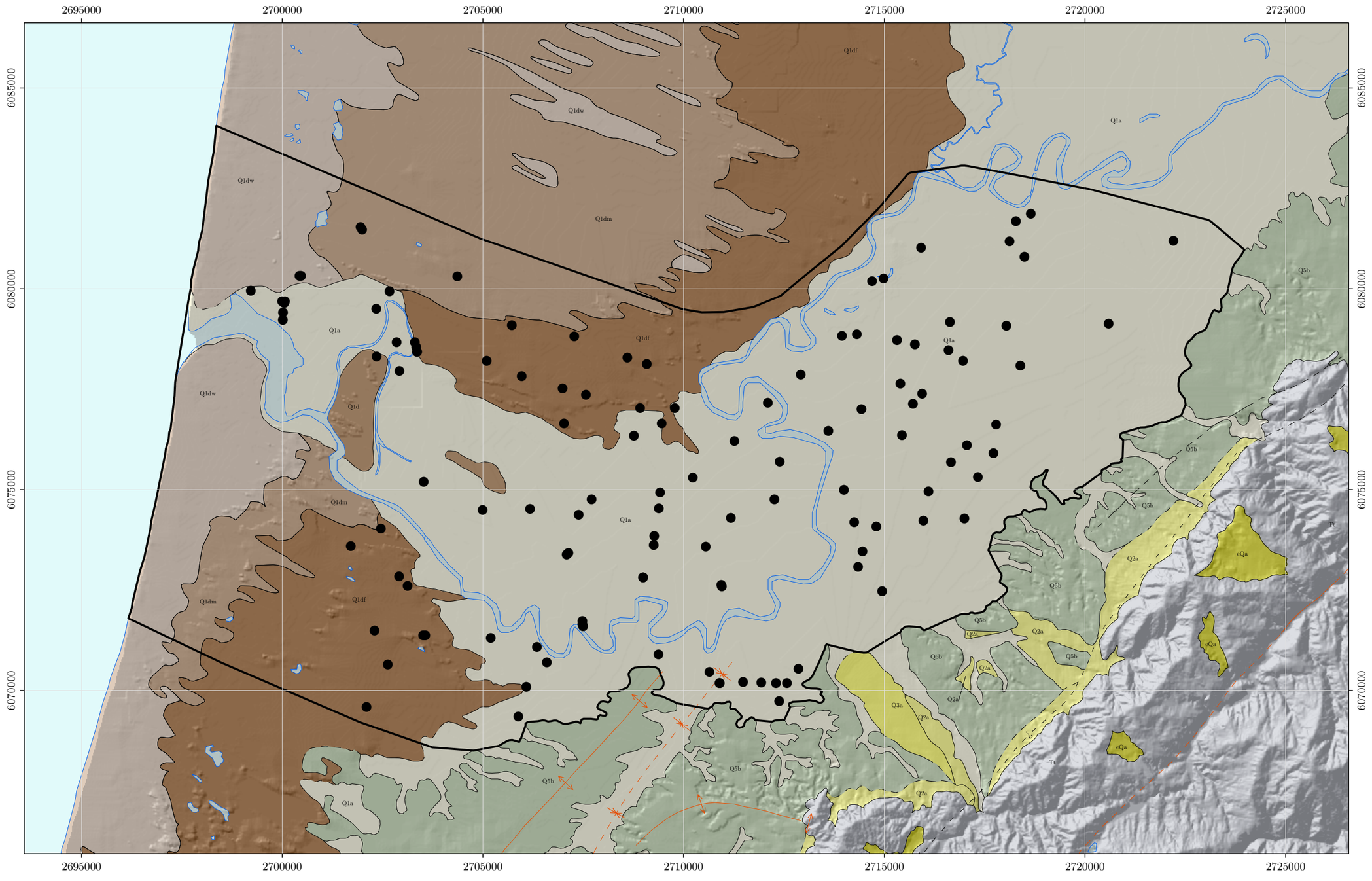
2695000
2700000
2705000
2710000
2715000
2720000
2725000
6085000
6080000
6075000
6070000
Q1df
Q1dw
Q1dm
Q1a
Q1d
Q5b
Q2a
Q3a
eQa
Tt

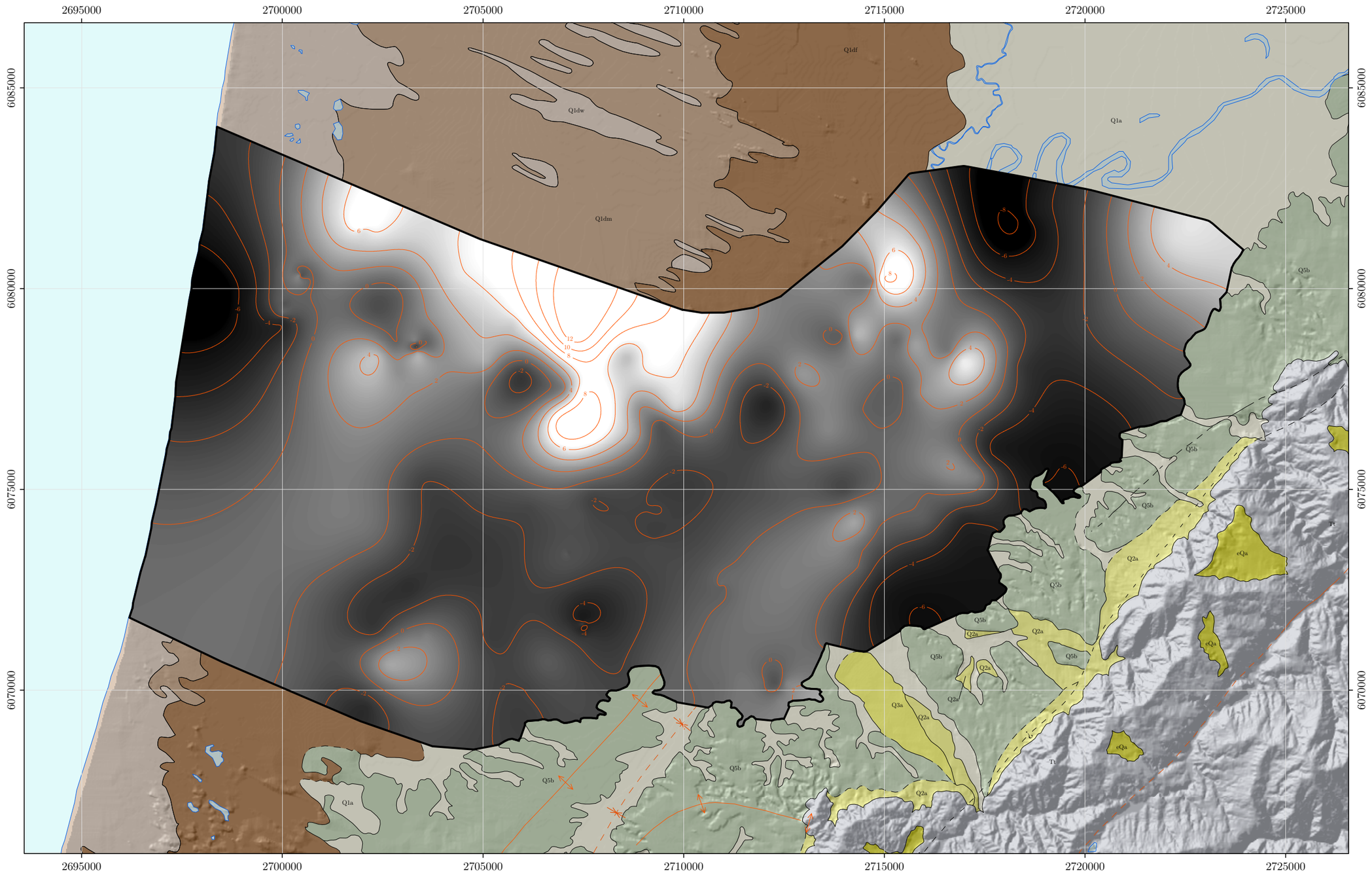
2695000
2700000
2705000
2710000
2715000
2720000
2725000
6085000
6080000
6075000
6070000
Q1df
Q1dw
Q1dm
Q1a
Q5b
Q2a
Q3a
eQa
Tr

Table 6.2: Volumes of sedimentary fill estimated using digital elevation models of the LGM aggradation surface and the estuarine alluvial interface in the lower Manawatu valley.

Volume estimated	Before surface	After surface	Fill (m^3)	Cut (m^3)	Fill (km^3)	Cut (km^3)
Total Holocene fill	Reconstructed LGM surface	ECOSAT modern DEM	14632330091	36951592	14·63	0·03
	Reconstructed LGM surface (adjusted)	ECOSAT modern DEM	14691990082	8899676	14·69	0·01
Marine/estuarine fill	Reconstructed LGM surface	Reconstructed estuarine surface	8770405500	12116445	8·77	0·01
	Reconstructed LGM surface (adjusted)	Reconstructed estuarine surface	8685663300	12118999	8·68	0·01
Alluvial fill	Reconstructed LGM surface	Total Holocene fill	5861924591	–	5·86	–
	Reconstructed LGM surface (adjusted)	Total Holocene fill	6006326782	–	6·00	–
Accomodation space	Reconstructed LGM surface	PMSL	9791355600	–	9·79	–
with sea-level at PMSL	Reconstructed LGM surface (adjusted)	PMSL	9767418300	–	9·76	–
Accomodation space with	Reconstructed LGM surface	+1.2 m PMSL	10272277800	–	10·27	–
sea-level at +1.2 m PMSL	Reconstructed LGM surface (adjusted)	+1.2 m PMSL	10229445900	–	10·22	–

elevation of the interface of +13.96 m suggests a possible uplift rate of 2–2.8 mm yr^{-1}, assuming the estuarine-alluvial transition took place c. 7,000–5,000 cal. yr BP (Chapter 7).

6.6.3 Holocene sedimentary infill volume estimation

Cut/fill analysis of reconstructed surfaces within the lower Manawatu incised-valley sedimentary fill reveals the sheer volume of sediment deposited in the lower valley since the Holocene marine transgression (Table 6.2). These volumes can be used to estimate time and area averaged sedimentation rates for the lower Manawatu valley (Section 8.5.6).

6.6.4 Digital elevation models and volume estimates of incised-valley infilling: discussion

Assessments of the volume of incised-valley fill have been undertaken relatively infrequently. A number of Chinese researchers have presented volume estimates of the sedimentary facies deposted in the Qiantangjiang estuary incised-valley in eastern China since the Last Glaciation (e.g., Zhang and Li, 1998; Li et al., 2003, 2006; Lin et al., 2004, 2005). These volume estimates were derived by generating isopath maps of each of the sediment facies based on data from approximately 100 bores, with each facies' volume being calculated by the area it occupied by its average thickness. This is a comparatively simple, straight forward approach. However, it is unclear precisely how the thicknesses are averaged, and therefore the accuracy of the calculated volumes may be harmed if this is too generalised. The total volume of Holocene sediments deposited in the Qiantangjiang estuary was estimated at c. 386 km^3. This appears very large by comparison with the Manawatu (Table 6.2); however the present Qiantangjiang estuary is approximately 270 km long with a mouth 100 km wide. The surrounding coastal plain has an area of approximately 20,000 km^2 (Lin et al., 2005).

Rodriguez et al. (2008) constructed an 'exposure surface' that represented the anticendant topography that was flooded to create the modern Mobile Bay estuary in the Gulf of Mexico. This exposure surface was used to calculate a time series of accommodation space available to infilling sediment during the Holocene marine transgression. The surface was reconstructed by interpolating between two cross-sections approximately 30 km apart. Additional information was provided by a rotary drill core and a small grid of seismic data collected within the bay. The use of cross-sections spaced so widely apart calls into question the accuracy of the reconstructed exposure surface, and the consequent volume estimation. Cross-sections have been widely criticized at the decimetre scale for not accurately representing morphology away from the cross-section line (e.g., Naden and Brayshaw, 1987; Lane et al., 1994; Fuller et al., 2002, 2003). Cross-sections spaced 30 km apart may therefore not represent the exposure surface accurately at all. The total volume of Holocene sediments is estimated at between 15-20 km^3, on a similar scale to the

Manawatu. In comparison to the Manawatu valley, Mobile Bay is 20–40 km wide, but the exposure surface, equivilaent to the Manawatu LGM surface, is much shallower, with a maximum depth of −15 below sea-level.

Wolinsky et al. (2010) used borelogs and present day bathymetric data to reconstruct the palaeo-bathymetry of Poverty Bay, East Coast, North Island, which represents the lower boundary of the regressive sediment fill deposited in the bay during the last 7,000 years. The palaeo-bathymetric model was used to constrain sediment volumes in the Poverty Bay Flats, to inform a model of bulk sediment storage and sediment flux out onto the continental shelf. The reconstructed palaeo bathymetry for Poverty Bay is in many ways similar to the reconstructed Manawatu LGM surface. The palaeo Poverty Bay surface is approximately 8 km wide and 16 km long, with a maximum depth of 25 m below sea-level. The volume of the surface below PMSL is approximately 1.8 km^3, with an area of approximately 142 km^2.

Duchesne et al. (2010) used high resolution seismic data to produce a 3D seismic stratigraphic model of the St Lawrence Estuary, eastern Canada. Digital elevation models of key seismic units were extracted from the seismic stratigraphic model and used to calculate a volume model of the estuary. This model estimated the volume of 11,520 km^3. This is extremely large compared to the Manawatu; however, the St Lawrence study was undertaken at a greater spatial and temporal scale. The estuary itself is one of the world's largest estuarine basins with dimensions of 200 by 40 km, with the fill being comprised of sediments from MIS 2–4, and possibly older.

Broad comparisons can be made between the volumes estimated by different researchers for different incised-valleys. For example, the volume of the Poverty Bay palaeobathymetric model (Wolinsky et al., 2010) at 1.8 km^3 is over five times smaller than the comparative volume from the Manawatu (c. 9.8 km^3). However, the Manawatu volume model covers twice the area of the Poverty Bay model (c. 272 km^2 compared to c. 142 km^2, while the Manawatu model has a maximum depth of over −60 m below PMSL, compared with the Poverty Bay model of c. −30 m below PMSL. Despite all this context such comparisons are not necessarily meaningful or useful. While the DEM reconstruction of the Manawatu LGM surface provides valuable context to this investigation of the geomorphic evolution of the Manawatu valley around accommodation space and rates of sediment infilling, in a wider context the DEM can be leveraged to provide a foundation for analysis of sediment flux through the valley during the Holocene (*sensu* Wolinsky et al., 2010), or to quantify the creation of sediment accomodation space in response to sea-level changes (*sensu* Rodriguez et al., 2008). It is in these works, beyond the scope of this thesis, that real value could be derived from direct comparisons.

It can be seen then that the approach taken in the Manawatu for reconstructing the LGM surface as a digital elevation model from which to estimate volumes of sedimentary infill is comparatively novel. While a number of other researchers have presented volume estimates of Holocene incised-valley infilling, the methods they have employed (e.g., thickness averaging, widely spaced

cross-sections) may not yield particularly accurate results. The use of well logs to construct a continuous surface in the form of a DEM, rather than discrete observations such as for cross-sections, represents the best opportunity for accurately reconstructing the palaeo volume of incised-valleys. This has future application with respect to reconstructing accommodation space by viewing palaeo DEMs within the context of detailed sea-level curves (e.g., Rodriguez et al., 2008), or estimating sediment storage and sediment flux in source-to-sink studies (e.g., Wolinsky et al., 2010).

6.7 Summary

Broad-scale features of the Holocene sedimentary infill of the lower Manawatu valley have been reconstructed from cross-sections constructed from water well logs. The cross-sections show the path of the LGM Ashhurst/Ohakea aggradation surface beneath the Holocene fill of the lower valley. This surface is significant as it represents the top of the Lowstand Systems Tract, and therefore forms the Transgressive Surface at the base of the Holocene sedimentary fill. The cross-sections also identify broad-scale Holocene depositional environments in the form of marine/estuarine sediments and alluvium. The discrete observations of the LGM aggradation surface presented by the well log cross-section can be interpolated and extrapolated to reconstruct the buried Ashhurst/Ohakea aggradation surface as a DEM. This surface allows estimates to be made of the accommodation space available to infilling sediments due to the Holocene marine transgression, and the total volume of Holocene sediment deposited in the lower valley.

Chapter 7

Holocene sedimentary stratigraphy and facies assemblages of the lower Manawatu valley reconstructed from detailed vibracores

7.1 Introduction

Water well logs provide useful stratigraphic information about the Holocene sedimentary infilling of the Manawatu valley. However, the well logs lack fine detail required to interpret facies associations and chronological information. This chapter presents data from sixty vibracores recovered from the middle and lower Manawatu valley. The vibracores were strategically positioned, and studied in fine detail, to provide information required to produce accurate facies descriptions and models. The vibracores also importantly provide wood and shell samples which have been radiocarbon dated for the purpose of delineating a chronology for the infilling of the valley. The trade-off for this higher level of detail is reduced depth. The longest vibracore section is only 9 m; the deepest penetrates to just below −4 m PMSL relative to Wellington Vertical Datum 1953 (WVD1953). Depending on the location this is sufficient to penetrate sediments deposited c. 8,100 cal. yr BP. In contrast the water well logs reached depths of up to −280 m below PMSL, penetrating sediments of late-Pleistocene age.

7.2 Vibracore collection and analysis

7.2.1 Vibracores

Sixty semi-undisturbed cores of unconsolidated sediment were recovered from the middle and lower Manawatu valley using a vibracorer driven by an electric concrete vibrator (Figure 7.1). The concrete vibrator was attached to a length of aluminium barrel which was held in a vertical position and vibrated down into the sediment (Figure 7.2). The vibrations cause a thin layer of material to mobilise along the inner and outer barrel wall, reducing friction and easing penetration into the substrate, while liquid spaces in the matrix allow sediment grains to be displaced by the vibrating tube. As a result recovered sedimentary sequences are more representative, due to minimal compaction (compared to techniques such as percussion coring), and individual sedimentary layers are preserved (compared to techniques such as hand augering).

Vibracores were collected using either 5 m long, 50 mm diameter aluminium barrels, or 6.5 m long, 75 mm diameter aluminium barrels, depending on the anticipated lithological characteristics of the sediments being cored (silts and coarse sands typically retard penetration), and the desired depth of penetration (the larger the barrel diameter, the larger the friction force both during emplacement and recovery: this affects penetrable depth).

Almost all the vibracores were recovered from the bottom of open drains (Figures 7.2 and 7.3). The majority of the drains were excavated during the late nineteenth and early twentieth centuries by settlers in order to convert swamps, which occupied much of the lower valley, into arable land (e.g., Akers, 1978; Hannigan and Barnes, 1982; Dreaver, 1984; Law, 1987). The drains vary in width from 2–8 m, and in depth from 3–5 m. Vibracoring in the drains was advantageous as it ensured that the substrate being cored was fully saturated, and meant that with the logging and sampling of the drain sides (Figure 7.4) longer sedimentary sections could be analysed than would have been possible if cores had been taken from the surface of the floodplain.

The vibracores were recovered from the drains by a winch and tripod/quadpod (Figure 7.5). The retrieved vibracores were opened and visually logged for colour, sediment texture, lithological composition, the presence of macrofossils, and significant facies changes. In selected vibracores approximately 50 g (wet weight) of sediment was collected every 10 cm, as well as at locations of significant facies changes, for sediment analysis. The vibracores were adjusted for compaction or expansion (measured versus recovered length). Most vibra-

Figure 7.1 *(facing page)*: Locations of vibracores recovered from the lower Manawatu valley (black) (1:50,000 scale). Also shown are the locations of detailed cores recovered by Hesp (1975) and Shepherd and Lees (1987) (red). The extent of this map is shown on Figure 6.1. Base geological map constructed using data from Kingma (1962), Cowie et al. (1967), Pillans (1990a), Begg and Johnston (2000), Lee and Begg (2002), Townsend et al. (2008), and unpublished data from the QMAP project made available by D. Townsend.

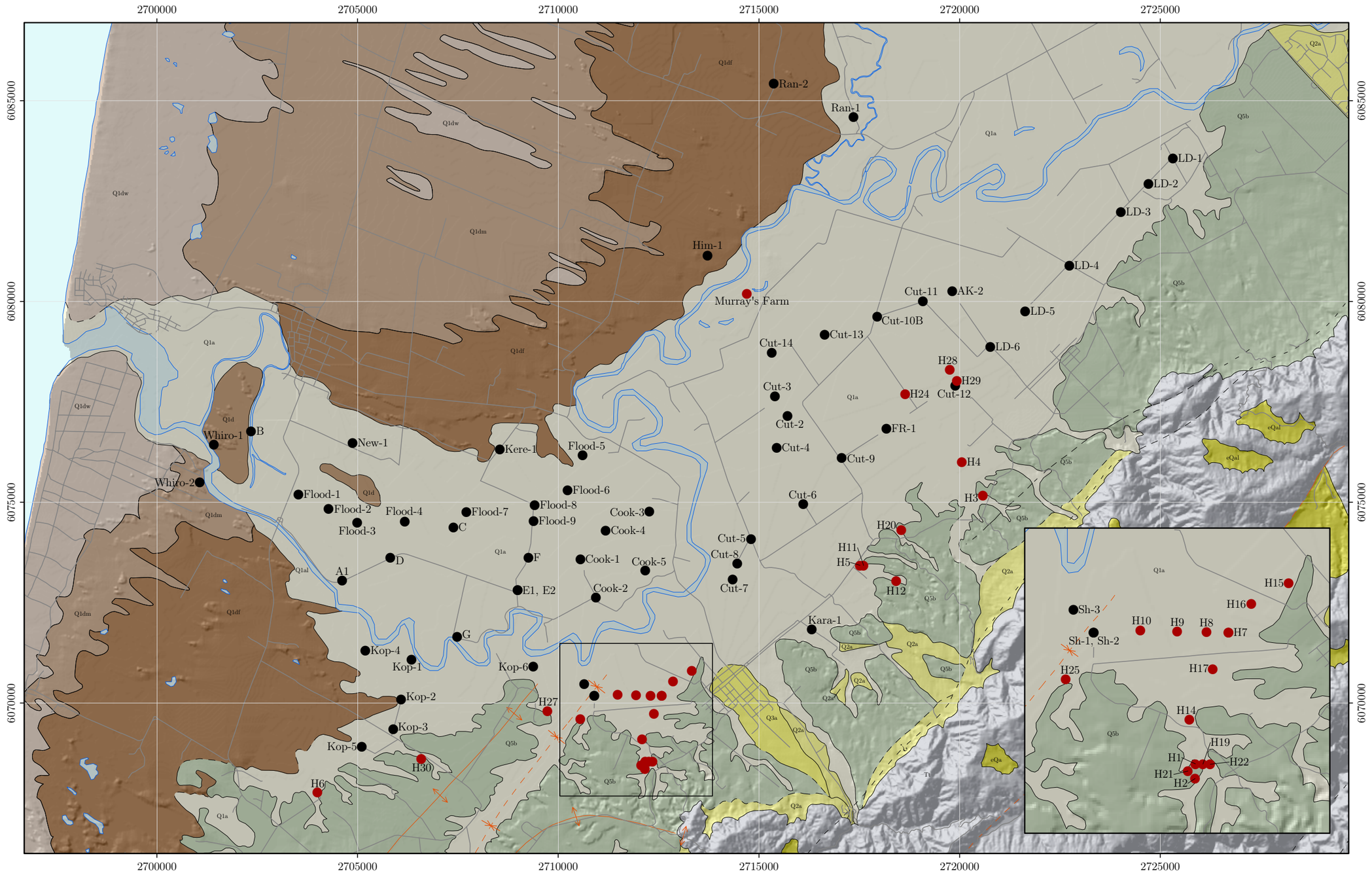
2700000
2705000
2710000
2715000
2720000
2725000
6085000
6080000
6075000
6070000
Ran-2
Ran-1
Him-1
Murray's Farm
LD-1
LD-2
LD-3
LD-4
LD-5
LD-6
Cut-11
AK-2
Cut-10B
Cut-13
Cut-14
H28
H29
H24
Cut-12
Cut-3
Cut-2
FR-1
Cut-4
Cut-9
H4
H3
Cut-6
H20
H11
H5
H12
Cut-5
Cut-8
Cut-7
Kara-1
Whiro-1
B
New-1
Kere-1
Flood-5
Flood-6
Whiro-2
Flood-1
Flood-2
Flood-3
Flood-4
C
Flood-7
Flood-8
Flood-9
Cook-3
Cook-4
D
F
Cook-1
Cook-5
A1
E1, E2
Cook-2
G
Kop-4
Kop-1
Kop-6
Kop-2
Kop-3
Kop-5
H27
H30
H6
Sh-3
Sh-1, Sh-2
H15
H16
H10
H9
H8
H7
H25
H17
H14
H19
H1
H22
H21
H2
Q1dw
Q1dm
Q1df
Q1a
Q1d
Q1al
Q2a
Q3a
Q5b
eQal
eQa
Tv



Figure 7.2: Vibracoring at site Flood-8, within the Moutoa Floodway, with a 6.5 m long, 75 mm diameter barrel. The concrete vibrator attachment at the top of the barrel is driven by the flexible shaft leading off to the right of the photograph.



Figure 7.3: Vibracoring at site LD-5, in Linton Drain, adjacent to Linton Drain Road.



Figure 7.4: Logging the side of the drain at site LD-5.



Figure 7.5: Tripod set up to extract vibracore Ran-2. A quadpod was sometimes employed (see Fig. 7.3). The endcap at the top of the barrel was used to seal it prior to winching out of the drain. Sometimes the vibracores presented a lot of resistance during extraction; the board underneath the tripod is there to provide support.

cores were compacted to some degree; however some expanded. Expansion is indicated by a negative compaction value (Table 7.1). Logs of the complete sections (vibracore and overlying drain section) were plotted using Inkscape 0.47. Logs not presented in this chapter are given in Appendix B. Full details of the vibracores and sections are presented in Table 7.1.

7.2.2 GPS surveys

The position and elevation of the vibracores was determined through a number of RTK-dGPS surveys. For a typical survey the GPS base station was erected on a topographic high, often a river stopbank. Core positions (latitude and longitude, in NZGD2000) and elevations (relative to the NZGD2000 ellipsoid) were determined with the rover GPS unit. Positions were measured to be accurate to within ±0.001 m, and with a precision of a hundred-thousandth of an arc-second (∼sub-millimetre). Elevations were measured to be accurate to within ±0.001 m, and with a precision of a thousandth of a metre. The locations of geodetic marks were also surveyed (also in NZGD2000). This ensured that following correction (see Tables 7.1 and 7.2) the locations and elevations of the surveyed vibracores were accurate relative to the New Zealand geodetic

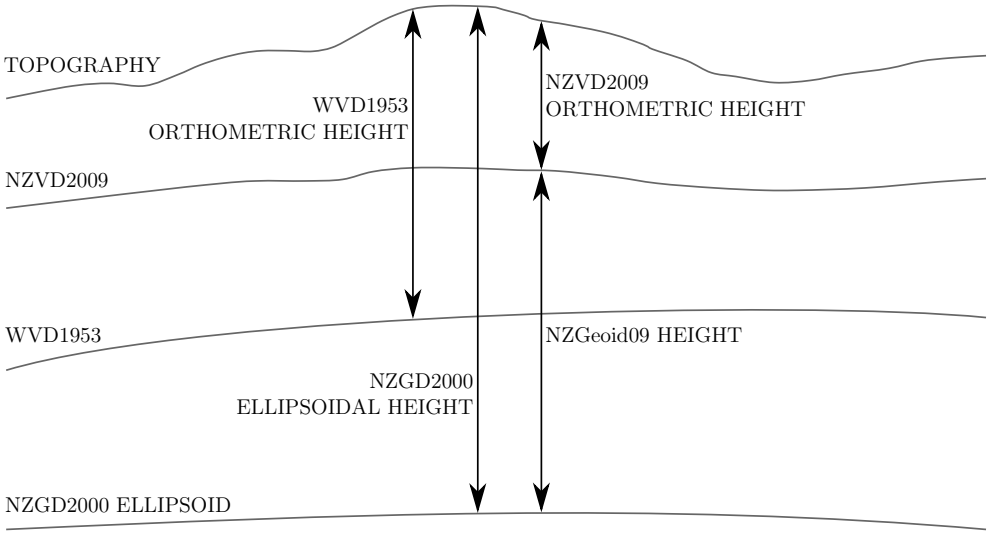

Figure 7.6: Conceptual diagram illustrating the relationship between the NZGD2000 ellipsoid, the NZVD2009 geoid, the WVD1953 geoid, the consequent differences between ellipsoidal and orthometric heights, and how the different elevations or heights of the vibracores were derived.

network. The elevation of the New Zealand Quasigeoid 2009 (NZGeoid09) was calculated for each vibracore location. NZGeoid09 is a surface related to the Earth's gravitational field that approximates the level of the ocean across the New Zealand landmass. NZGeoid09 is also a reference surface for the New Zealand Vertical Datum 2009 (NZVD2009), the official vertical datum for New Zealand and its offshore islands. The elevation of the NZGeoid09 at each vibracore location therefore allowed the GPS-surveyed ellipsoidal heights for each vibracore (which is not relative to any sea-level datum) to be converted to normal-orthometric heights (relative to sea-level) (Figure 7.6). The NZVD2009 orthometric height was converted to Wellington Vertical Datum 1953 (WVD53) using a datum offset of 0.44 m. Position and elevation information for the vibracores is presented in Table 7.1. Details of the GPS surveys and the geodetic corrections are given in Table 7.2.

7.2.3 Sediment analysis

Sediment analysis was conducted on selected cores to determine sediment constituents, textural characteristics, and to distinguish between sediments from different depositional environments. Given financial and time constraints sediment analysis was only performed on sediment samples from locations where radiocarbon ages had been obtained. Samples from vibracores Sh-1, Sh-2, Sh-3 and LD-5 were analysed using a Malvern Mastersizer 2000 laser particle size analyser at the University of Wollongong. Samples from vibracores Cut-2, Cut-4, Cut-7, E1, Flood-1, G, and Kop-1 were analysed using a Horiba Partica LA-950V2 laser particle size analyser at the Institute of Natural Resources,

Massey University. The Malvern Mastersizer 2000 was used initially for sediment analysis, prior to the Institute of Natural Resources acquiring the Horiba Partica LA-950V2, at which time financial considerations precluded returning to Wollongong to complete the analyses. The Horiba Partica LA-950V2 requires that the refractive index of the suspension medium and sample material be specified at the time of measurement. Measurements were taken using refractive index values of 1.33 for the deionised water suspension medium and 1.56 for the sample material. The latter value is valid for quartz, clay minerals and feldspars (e.g., Loizeau et al., 1994; Buurman et al., 2001; Trentesaux et al., 2001; Sperazza et al., 2004). Such settings are not required for the operation of the Malvern Mastersizer 2000. Results for mean grain size and sorting were recorded (Appendix C). Unfortunately the sediment size results from each analyser differ such that they are not directly comparable, but are useful as relative measures of sediment constituents and textural characteristics.

7.2.4 Radiocarbon ages

Wood and shell samples recovered from the vibracores were radiocarbon dated using accelerator mass spectrometry (AMS) at the Waikato Radiocarbon Dating Laboratory, Waikato University. One sample of fossil wood and 13 fossil *Austrovenus stutchburyi* valves were radiocarbon dated (Table 7.3). *A. stutchburyi* is most commonly described in broad terms as an intertidal bivalve found in sheltered environments (e.g., Morton and Miller, 1968; Larcombe, 1971; Powell, 1979; Purchase and Fergusson, 1986; Hewitt et al., 1996; Hayward et al., 1997, 2002; Hogg et al., 1998; Thrush et al., 1999; Norkko et al., 2001; Lelieveld et al., 2004; Lundquist et al., 2004; Tallis et al., 2004).

All conventional radiocarbon ages were calibrated to sidereal (calendar) years (expressed as cal. yr BP) using the radiocarbon calibration program CALIB REV 5.0.1 (Stuiver and Braziunas, 1993; Stuiver and Reimer, 1993). The age of the single wood sample was calibrated using the non-marine calibration curve for the Southern Hemisphere (SHCal04; McCormac et al., 2004). The ages of the *A. stutchburyi* valves were calibrated using marine model calibration curve Marine04 (Hughen et al., 2004) with a ΔR value of -7 ± 45 to correct for the marine reservoir effect (Table 3.2; Clement et al., 2010). This is a weighted mean value for the New Zealand region based on Rafter et al. (1972), McFadgen and Manning (1990), Kalish (1993), Higham and Hogg (1995), and Sikes et al. (2000). All calibrated radiocarbon ages are presented using the 2-sigma uncertainty term (95 per cent degree of confidence). The results sheets returned by the Waikato Radiocarbon Dating Laboratory are presented in Appendix D.

7.2.5 Cross-section construction

Cross-sections at 1:50,000 scale were constructed in ArcMap 9.2 using the eXacto cross-section tool (Carrell, 2009). Additional detailing was performed in Inkscape 0.47. The surface profile for each of the cross-sections was generated

Table 7.1: Location, elevation, compaction, and length details for all vibracores/drain sections recovered/logged in the lower Manawatu valley.

Core	Length recovered (m)	Compaction (m)	Drain logged above core (m)	GPS Survey	Surveyed latitude (NZGD2000)	Surveyed longitude (NZGD2000)	Surveyed ellipsoidal height (m)	Corrected latitude (NZGD2000)	Corrected longitude (NZGD2000)	Corrected ellipsoidal height (m)	NZMG northing (corrected)	NZMG easting (corrected)	NZGeoid09 height at corrected location (m)	NZVD2009 orthometric height (m)	WVD1953 orthometric height (m)
LD-1	2.02	0.32	3.00	Linton	40° 25′ 34.07291″	175° 32′ 16.99276″	32.538	40° 25′ 34.03360″	175° 32′ 17.00389″	28.344	6083559.52	2725319.17	13.2964	15.0476	15.4876
LD-2	0.81	0.13	4.80	Linton	40° 25′ 55.09715″	175° 31′ 51.97016″	30.960	40° 25′ 55.05784″	175° 31′ 51.98129″	26.766	6082928.31	2724710.99	13.2820	13.4840	13.9240
LD-3	0.28	0.00	2.50	Linton	40° 26′ 18.37490″	175° 31′ 23.74226″	26.760	40° 26′ 18.33559″	175° 31′ 23.75339″	22.566	6082229.74	2724025.40	13.2683	9.2977	9.7377
LD-4	1.47	0.23	3.30	Linton	40° 27′ 02.81683″	175° 30′ 30.81893″	24.989	40° 27′ 02.77752″	175° 30′ 30.83006″	20.795	6080895.21	2722739.66	13.2438	7.5512	7.9912
LD-5	2.26	0.48	2.20	Linton	40° 27′ 40.44518″	175° 29′ 45.54863″	21.973	40° 27′ 40.40587″	175° 29′ 45.55976″	17.779	6079765.42	2721640.54	13.2261	4.5529	4.9929
LD-6	4.32	0.20	3.30	Linton	40° 28′ 10.33935″	175° 29′ 09.57819″	22.451	40° 28′ 10.30004″	175° 29′ 09.58932″	18.257	6078867.74	2720767.44	13.2119	5.0451	5.4851
AK-2	1.30	0.51	2.30	Linton	40° 27′ 26.09769″	175° 28′ 27.70864″	23.520	40° 27′ 26.05838″	175° 28′ 27.71977″	19.326	6080259.52	2719819.92	13.0238	6.3022	6.7422
Cut-2	2.39	0.00	2.87	Cut	40° 29′ 10.59534″	175° 25′ 37.40164″	17.842	40° 29′ 10.62749″	175° 25′ 37.36446″	16.179	6077147.26	2715719.05	12.8923	3.2867	3.7267
Cut-3	2.02	−0.10	2.62	Cut	40° 28′ 54.71649″	175° 25′ 23.48707″	17.455	40° 28′ 54.74864″	175° 25′ 23.44989″	15.792	6077645.86	2715404.98	12.8310	2.9610	3.4010
Cut-4	1.95	0.10	3.27	Salvie	40° 29′ 36.45096″	175° 25′ 26.79280″	17.964	40° 29′ 36.47708″	175° 25′ 26.76616″	16.378	6076357.17	2715447.60	12.9270	3.4510	3.8910
Cut-5	1.27	−0.06	4.37	Cut	40° 30′ 50.45728″	175° 25′ 02.24222″	18.962	40° 30′ 50.48943″	175° 25′ 02.20504″	17.299	6074091.16	2714806.80	13.0437	4.2553	4.6953
Cut-6	1.60	0.00	3.28	Cut	40° 30′ 21.13640″	175° 25′ 56.45808″	17.944	40° 30′ 21.16855″	175° 25′ 56.42090″	16.281	6074960.00	2716107.53	13.0897	3.1913	3.6313
Cut-7	2.33	0.01	4.31	Cut	40° 31′ 23.73206″	175° 24′ 44.08291″	18.622	40° 31′ 23.76421″	175° 24′ 44.04573″	16.959	6073076.98	2714351.37	13.0860	3.8730	4.3130
Cut-8	1.51	0.00	3.42	Cut	40° 31′ 10.80732″	175° 24′ 48.48345″	17.788	40° 31′ 10.83947″	175° 24′ 48.44627″	16.125	6073472.63	2714465.83	13.0637	3.0613	3.5013
Cut-9	2.85	−0.13	1.87	Cut	40° 29′ 42.82694″	175° 26′ 35.70405″	17.712	40° 29′ 42.85909″	175° 26′ 35.66687″	16.049	6076115.54	2717063.93	13.0855	2.9635	3.4035
Cut-10B	1.67	0.00	1.19	Salvie	40° 27′ 48.37092″	175° 27′ 09.33287″	18.364	40° 27′ 48.39704″	175° 27′ 09.30623″	16.778	6079622.49	2717954.06	12.9063	3.8717	4.3117
Cut-11	1.19	0.10	1.34	Salvie	40° 27′ 34.78510″	175° 27′ 57.21693″	18.399	40° 27′ 34.81122″	175° 27′ 57.19029″	16.813	6080009.84	2719093.38	12.9772	3.8358	4.2758
Cut-12	3.05	0.24	2.59	Salvie	40° 28′ 42.19916″	175° 28′ 33.86372″	19.648	40° 28′ 42.22528″	175° 28′ 33.83708″	18.062	6077907.19	2719897.93	13.2055	4.8565	5.2965
Cut-13	2.69	0.06	2.32	Salvie	40° 28′ 04.03090″	175° 26′ 14.13801″	18.431	40° 28′ 04.05702″	175° 26′ 14.11137″	16.845	6079175.79	2716640.94	12.8267	4.0183	4.4583
Cut-14	1.31	0.03	2.89	Salvie	40° 28′ 19.78908″	175° 25′ 18.81706″	18.465	40° 28′ 19.81520″	175° 25′ 18.79042″	16.879	6078725.92	2715324.93	12.7516	4.1274	4.5674
Kop-1	3.55	−0.20	2.74	Koputaroa	40° 32′ 35.12993″	175° 19′ 06.36949″	15.676	40° 32′ 35.12684″	175° 19′ 06.42072″	14.007	6071090.38	2706349.72	12.6059	1.4011	1.8411
Kop-2	1.17	0.00	2.17	Koputaroa	40° 33′ 07.71698″	175° 18′ 56.27157″	14.890	40° 33′ 07.71389″	175° 18′ 56.32280″	13.221	6070091.90	2706085.75	12.6542	0.5668	1.0068
Kop-3	1.69	0.00	1.60	Koputaroa	40° 33′ 32.03588″	175° 18′ 48.73681″	14.823	40° 33′ 32.03279″	175° 18′ 48.78804″	13.154	6069346.75	2705888.81	12.6923	0.4617	0.9017
Kop-4	2.13	−0.17	1.68	Koputaroa	40° 32′ 29.14497″	175° 18′ 17.16391″	14.490	40° 32′ 29.14188″	175° 18′ 17.21514″	12.821	6071305.35	2705197.18	12.5170	0.3040	0.7440
Kop-5	2.42	0.50	1.88	Koputaroa	40° 33′ 46.52287″	175° 18′ 15.99206″	15.463	40° 33′ 46.51978″	175° 18′ 16.04329″	13.794	6068920.31	2705107.08	12.6662	1.1278	1.5678
Kop-6	2.53	−0.13	3.90	Koputaroa	40° 32′ 38.53925″	175° 21′ 15.23430″	18.476	40° 32′ 38.53616″	175° 21′ 15.28553″	16.807	6070904.71	2709377.97	12.8429	3.9641	4.4041
A1	2.34	0.00	3.02	Motua B	40° 31′ 33.01521″	175° 17′ 50.64809″	16.406	40° 31′ 32.97181″	175° 17′ 50.67604″	12.777	6073053.55	2704618.17	12.3752	0.4018	0.8418
B	3.72	1.14	0.00	Whirokino A	40° 29′ 34.51965″	175° 16′ 10.23256″	11.170	40° 29′ 34.47890″	175° 16′ 10.19728″	10.809	6076768.38	2702348.47	12.0246	−1.2156	−0.7756
C	2.75	0.10	1.36	Motua C	40° 30′ 47.71795″	175° 19′ 46.89699″	12.889	40° 30′ 47.70942″	175° 19′ 46.89695″	12.582	6074377.12	2707389.50	12.4651	0.1169	0.5569
D	2.70	0.03	2.46	Motua B	40° 31′ 13.52225″	175° 18′ 40.92760″	16.120	40° 31′ 13.47885″	175° 18′ 40.95555″	12.491	6073623.55	2705816.91	12.4131	0.0779	0.5179
E1	1.50	0.10	2.96	Motua B	40° 31′ 36.92084″	175° 20′ 56.73423″	18.263	40° 31′ 36.87744″	175° 20′ 56.76218″	14.634	6072817.43	2708993.06	12.6756	1.9584	2.3984
E2	2.89	0.17	2.96	Motua B	40° 31′ 36.92084″	175° 20′ 56.73423″	18.263	40° 31′ 36.87744″	175° 20′ 56.76218″	14.634	6072817.43	2708993.06	12.6756	1.9584	2.3984
F	2.83	0.14	2.06	Motua B	40° 31′ 10.38946″	175° 21′ 07.24761″	17.161	40° 31′ 10.34606″	175° 21′ 07.27556″	13.532	6073628.84	2709262.28	12.6392	0.8928	1.3328
G	3.26	0.08	3.34	Motua B	40° 32′ 16.00900″	175° 19′ 53.96165″	17.769	40° 32′ 15.96560″	175° 19′ 53.98960″	14.140	6071651.57	2707484.27	12.6470	1.4930	1.9330
Flood-1	3.20	0.30	1.35	Motua C	40° 30′ 24.53358″	175° 17′ 02.02265″	12.769	40° 30′ 24.52505″	175° 17′ 02.02261″	12.462	6075193.75	2703528.30	12.1868	0.2752	0.7152
Flood-2	2.41	0.20	0.35	Motua C	40° 30′ 35.33991″	175° 17′ 34.32507″	12.492	40° 30′ 35.33138″	175° 17′ 34.32503″	12.185	6074840.78	2704279.81	12.2516	−0.0666	0.3734
Flood-3	2.34	0.00	1.43	Motua C	40° 30′ 45.71472″	175° 18′ 05.00197″	12.767	40° 30′ 45.70619″	175° 18′ 05.00193″	12.460	6074502.04	2704993.36	12.3129	0.1471	0.5871
Flood-4	1.61	0.02	1.52	Motua C	40° 30′ 43.85661″	175° 18′ 55.24045″	12.954	40° 30′ 43.84808″	175° 18′ 55.24041″	12.647	6074528.29	2706177.07	12.3815	0.2655	0.7055
Flood-5	1.02	0.10	3.22	Motua C	40° 29′ 46.51253″	175° 22′ 01.71212″	16.121	40° 29′ 46.50400″	175° 22′ 01.71208″	15.814	6076179.47	2710612.68	12.5660	3.2480	3.6880
Flood-6	2.60	−0.10	2.36	Motua C	40° 30′ 15.19788″	175° 21′ 46.69323″	14.873	40° 30′ 15.18935″	175° 21′ 46.69319″	14.566	6075304.56	2710235.42	12.5969	1.9691	2.4091
Flood-7	2.43	−0.12	1.90	Motua C	40° 30′ 35.08802″	175° 20′ 00.10396″	13.557	40° 30′ 35.07949″	175° 20′ 00.10392″	13.250	6074758.29	2707710.61	12.4619	0.7881	1.2281
Flood-8	1.87	0.00	2.78	Motua B	40° 30′ 27.95819″	175° 21′ 12.29061″	17.437	40° 30′ 27.91479″	175° 21′ 12.31856″	13.808	6074933.90	2709415.93	12.5647	1.2433	1.6833
Flood-9	2.45	0.00	1.60	Motua B	40° 30′ 41.02239″	175° 21′ 11.60624″	16.531	40° 30′ 40.97899″	175° 21′ 11.63419″	12.902	6074531.54	2709389.05	12.5887	0.3133	0.7533
Cook-1	3.21	−0.12	2.06	Motua B	40° 31′ 10.61979″	175° 22′ 02.25696″	17.642	40° 31′ 10.57639″	175° 22′ 02.28491″	14.013	6073587.00	2710556.42	12.7373	1.2757	1.7157
Cook-2	3.65	−0.40	2.03	Motua B	40° 31′ 41.20883″	175° 22′ 19.77738″	18.359	40° 31′ 41.16543″	175° 22′ 19.80533″	14.730	6072632.78	2710943.23	12.8378	1.8922	2.3322
Cook-3	2.80	−0.10	1.60	Motua B	40° 30′ 30.81853″	175° 23′ 13.63344″	18.040	40° 30′ 30.77513″	175° 23′ 13.66139″	14.411	6074768.75	2712269.14	12.7845	1.6265	2.0665
Cook-4	3.18	−0.10	1.35	Motua B	40° 30′ 46.89650″	175° 22′ 28.12471″	17.074	40° 30′ 46.85310″	175° 22′ 28.15266″	13.445	6074302.03	2711184.81	12.7347	0.7103	1.1503
Cook-5	2.89	0.40	0.90	Motua B	40° 31′ 18.42955″	175° 23′ 11.02311″	18.626	40° 31′ 18.38615″	175° 23′ 11.05106″	14.997	6073302.48	2712167.90	12.8847	2.1123	2.5523
Kere-1	1.08	0.32	0.00	Motua B	40° 29′ 43.75545″	175° 20′ 33.84630″	18.879	40° 29′ 43.71205″	175° 20′ 33.87425″	15.250	6076320.91	2708547.50	12.4221	2.8279	3.2679
New-1	1.45	0.00	0.90	Whirokino A	40° 29′ 41.71029″	175° 17′ 58.00965″	15.170	40° 29′ 41.66954″	175° 17′ 57.97437″	14.809	6076480.75	2704879.61	12.1952	2.6138	3.0538
Kara-1	4.09	0.10	1.72	Cut	40° 32′ 01.99596″	175° 26′ 09.33476″	19.536	40° 32′ 02.02811″	175° 26′ 09.29758″	17.873	6071841.96	2716324.50	13.3662	4.5068	4.9468
Sh-1	4.75	0.00	3.10	Motua A	40° 33′ 00.57737″	175° 22′ 20.91062″	16.999	40° 33′ 00.56384″	175° 22′ 20.93263″	16.109	6070184.04	2710903.72	13.0243	3.0847	3.5247
Sh-2	4.64	0.15	2.16	Motua A	40° 33′ 00.56057″	175° 22′ 20.67001″	15.824	40° 33′ 00.54704″	175° 22′ 20.69202″	14.934	6070184.71	2710898.08	13.0237	1.9103	2.3503

Continued over page

Table 7.1: (continued)

Core	Length recovered (m)	Compaction (m)	Drain logged above core (m)	GPS Survey	Surveyed latitude (NZGD2000)	Surveyed longitude (NZGD2000)	Surveyed ellipsoidal height (m)	Corrected latitude (NZGD2000)	Corrected longitude (NZGD2000)	Corrected ellipsoidal height (m)	NZMG northing (corrected)	NZMG easting (corrected)	NZGeoid09 height at corrected location (m)	NZVD2009 orthometric height (m)	WVD1953 orthometric height (m)
Sh-3	4.62	−0.20	4.56	Motua A	40° 32′ 51.50820″	175° 22′ 09.73378″	18.269	40° 32′ 51.49467″	175° 22′ 09.75579″	17.379	6070470.75	2710648.39	12.9801	4.3989	4.8389
Him-1	3.36	0.22	1.39	Himatangi	40° 27′ 02.71742″	175° 24′ 07.94628″	16.120	40° 27′ 02.71481″	175° 24′ 07.95903″	19.634	6081148.74	2713722.07	12.4878	7.1462	7.5862
Ran-1	1.92	0.00	0.00	Rangiotu	40° 25′ 07.79291″	175° 26′ 38.16586″	20.016	40° 25′ 07.79279″	175° 26′ 38.15260″	18.684	6084594.44	2717357.93	12.5646	6.1194	6.5594
Ran-2	1.58	0.00	0.00	Rangiotu	40° 24′ 42.75029″	175° 25′ 13.03599″	28.330	40° 24′ 42.75017″	175° 25′ 13.02273″	26.998	6085421.95	2715373.18	12.3896	14.6084	15.0484
Whiro-1	1.40	0.05	0.00	Whirokino B	40° 29′ 45.86112″	175° 15′ 31.22968″	14.631	40° 29′ 45.98025″	175° 15′ 31.22784″	12.007	6076437.40	2701422.06	11.9846	0.0224	0.4624
Whiro-2	2.19	1.03	0.00	Whirokino B	40° 30′ 16.57002″	175° 15′ 17.25469″	14.547	40° 30′ 16.68915″	175° 15′ 17.25285″	11.923	6075499.01	2701068.84	12.0154	−0.0924	0.3476
FR-1	2.38	0.21	1.40	LiDAR	–	–	–	–	–	–	6076833.99	2718181.76	–	–	3.8200

Table 7.2: Vibracore GPS survey details. Benchmark names (with the exception of Whirokino A) are the four-character mark codes given in the Land Information New Zealand geodetic database.

Survey	Benchmark	LINZ latitude (NZGD2000)	LINZ longitude (NZGD2000)	LINZ ellipsoidal height (m)	Surveyed latitude (NZGD2000)	Surveyed longitude (NZGD2000)	Surveyed ellipsoidal height (m)	Latitude correction (seconds)	Longitude correction (seconds)	Height correction (m)
Linton	A506	40° 26′ 03.00101″	175° 33′ 15.43253″	49.751	40° 26′ 03.04032″	175° 33′ 15.42140″	53.945	−0.03931	0.01113	−4.194
Rangiotu	BAD7	40° 24′ 56.62162″	175° 24′ 12.25552″	38.040	40° 24′ 56.62174″	175° 24′ 12.26878″	39.372	−0.00012	−0.01326	−1.332
Whirokino A	A4MU	40° 31′ 06.77362″	175° 16′ 35.54799″	37.256	40° 31′ 06.81437″	175° 16′ 35.58327″	37.617	−0.04075	−0.03528	−0.361
Whirokino B	Whirokino A	40° 30′ 35.23015″	175° 15′ 57.64598″	14.753	40° 30′ 35.11102″	175° 15′ 57.64782″	17.377	0.11913	−0.00184	−2.624
Salvie	BAD3	40° 28′ 45.69295″	175° 23′ 46.99729″	17.670	40° 28′ 45.66683″	175° 23′ 47.02393″	19.256	0.02612	−0.02664	−1.586
Himatangi	BAD5	40° 26′ 45.79555″	175° 22′ 41.59324″	33.128	40° 26′ 45.79816″	175° 22′ 41.58049″	29.614	−0.00261	0.01275	3.514
Motua A	B18J	40° 29′ 18.82243″	175° 19′ 54.83582″	44.347	40° 29′ 18.83596″	175° 19′ 54.81381″	45.237	−0.01353	0.02201	−0.890
Motua B	BADP	40° 31′ 18.25752″	175° 23′ 41.80188″	17.087	40° 31′ 18.30092″	175° 23′ 41.77393″	20.716	−0.04340	0.02795	−3.629
Motua C	BADP	40° 31′ 18.25752″	175° 23′ 41.80188″	17.087	40° 31′ 18.26605″	175° 23′ 41.80192″	17.394	−0.00853	−0.00004	−0.307
Cut	BAD3	40° 28′ 45.69295″	175° 23′ 46.99729″	17.670	40° 28′ 45.66080″	175° 23′ 47.03447″	19.333	0.03215	−0.03718	−1.663
Koputaroa	A3MT	40° 32′ 46.36749″	175° 16′ 23.08145″	33.051	40° 32′ 46.37058″	175° 16′ 23.03022″	34.720	−0.00309	0.05123	−1.669

Table 7.3: Summary of radiocarbon ages obtained from samples of shell and wood recovered from vibracores and auger holes in the lower Manawatu valley. Wood CRA calibrated using the the non-marine calibration curve for the Southern Hemisphere (SHCal04; McCormac et al. 2004). *A. stutchburyi* CRAs calibrated using the marine model calibration curve Marine04 (Hughen et al., 2004) with a ΔR value of -7 ± 45 to correct for the marine reservoir effect (see Sections 3.2.2 and 7.2.4).

Source	Radiocarbon sample code	Sample material	Facies	Vibracore/ auger/ borehole	Section sample depth (m)	WVD1953 sample depth (m)	Conventional radiocarbon age (14C years)	Sidereal age range (cal yr BP)
This study	Wk22171	Disarticulated *A. stutchburyi*	ESS	Sh-1	5·66	−2·14	7150±41	7853–8320
	Wk22172	Disarticulated *A. stutchburyi*	ESS	Sh-1	7·07	−3·55	7394±42	7986–8634
	Wk22173	Disarticulated *A. stutchburyi*	ESS	Sh-2	2·20	0·15	5910±37	6501–7144
	Wk22176	Wood	FA	LD-5	2·71	2·28	4974±35	5589–5728
	Wk26357	Articulated *A. stutchburyi*	ESS	E1	4·41	−2·01	5588±30	5883–6153
	Wk26358	Disarticulated *A. stutchburyi*	MTS	Kop-1	5·94	−4·10	5343±30	5594–5857
	Wk26359	Disarticulated *A. stutchburyi*	ESS	Cut-2	5·21	−1·48	6365±30	6699–6988
	Wk26360	Articulated *A. stutchburyi*	ESS	Cut-4	5·31	−1·42	6260±30	6588–6874
	Wk26361	Articulated *A. stutchburyi*	ESS	Cut-7	6·04	−1·72	6733±30	7160–7388
	Wk26362	Articulated *A. stutchburyi*	ESS	Cook-2	5·14	−2·81	5920±30	6237–6468
	Wk26363	Articulated *A. stutchburyi*	ESS	Flood-1	4·40	−3·68	5320±30	5581–5840
	Wk26364	Articulated *A. stutchburyi*	ESS	G	5·63	−3·70	5661±30	5927–6202
	Wk28289	Articulated *A. stutchburyi*	ESS	G	4·77	−2·84	5717±30	5989–6262
	Wk28299	Articulated *A. stutchburyi*	ESS	Cut-7	5·25	−0·94	6386±32	6713–7019
Hesp and Shepherd (1978)	NZ3085	*A. stutchburyi*	ESS	H26[a]	–	1·10	6475±45	6814–7154
Shepherd and Lees (1987)	NZ5218	*A. stutchburyi*	ESS	Murray's Farm[b]	–	−5·60	6613±181	6699–7484
M.J. Shepherd unpublished	NZ7911	Articulated *A. stutchburyi*	ESS	Whiro-1[c]	–	0·02	4525±43	4533–4857

[a] As given by Hesp (1975)
[b] As given by Shepherd and Lees (1987)
[c] In same location as, but not from, this vibracore

using a LiDAR-derived 1 m DEM supplied by Horizons Regional Council. Surface elevations were sampled at 50 m intervals along each profile. Elevations were exaggerated by a factor of 600. The elevations of the vibracores as determined by the GPS surveys were faithfully preserved. The cross-sections also make use of detailed cores recovered by Hesp (1975) and Shepherd and Lees (1987). Details of these cores are presented in Appendix E. Figure 7.7 shows the locations of the vibracore cross-sections. The vibracore cross-sections are included as loose sheets in the rear of the thesis. The vibracore cross-sections use the same lithological symbols as the vibracore stratigraphic logs (see Appendix B, page 327) A key to accompany the vibracore cross-section sheets is included as a loose sheet at the rear of the thesis (Sheet 32). Facies abbreviations on the vibracores cross-sections (e.g., FA or MTS) correspond to the abbreviations used for the facies descriptions below (see Sections 7.3.1 to 7.3.4).

7.3 Lithofacies and interpretation

Five individual facies were identified on the basis of sediment size, texture, and colour, faunal assemblages, organic content, contact relationships and architecture. This is a qualitative rather than quantitative assessment based on the collective evaluation of these six characteristics (e.g., Sloss, 2005; Sloss et al., 2005, 2006b,a, 2007, 2010). A summary of the facies and their individual characteristics is given in Table 7.4, with representative sections ilustrating each of the facies presented in Figure 7.8.

7.3.1 Marine transgressive sands (MTS)

Marine transgressive sands (Figure 7.8) are penetrated in the middle to lower valley at depths below −3 m WVD1953 (Sheets 28 and 30: vibracore cross-sections 5 and 7), at the base of vibracores F (Figure 7.9) and Kop-1 (Figure 7.10). Sedimentological analysis shows that the sands are medium- to coarse-grained, and moderately- to poorly-sorted, suggesting rapid deposition or a mixed energy regime (e.g., Heap and Nichol, 1997; Roy et al., 2001; Sloss, 2005; Sloss et al., 2005, 2010). In both vibracores less than 0.3 m of penetration into the marine transgressive sands was achieved, presumably as the coarse sand retarded penetration of the vibracorer. The sands are free of organic detritus. A single disarticulated *A. stutchburyi* valve was recovered from

Figure 7.7 *(facing page)*: Locations of cross-sections in the lower Manawatu valley constructed using detailed vibracores (1:50,000 scale). The cross-sections are included as loose sheets in the rear of the thesis. The extent of this map is shown on Figure 6.1. Base geological map constructed using data from Kingma (1962), Cowie et al. (1967), Pillans (1990a), Begg and Johnston (2000), Lee and Begg (2002), Townsend et al. (2008), and unpublished data from the QMAP project made available by D. Townsend.

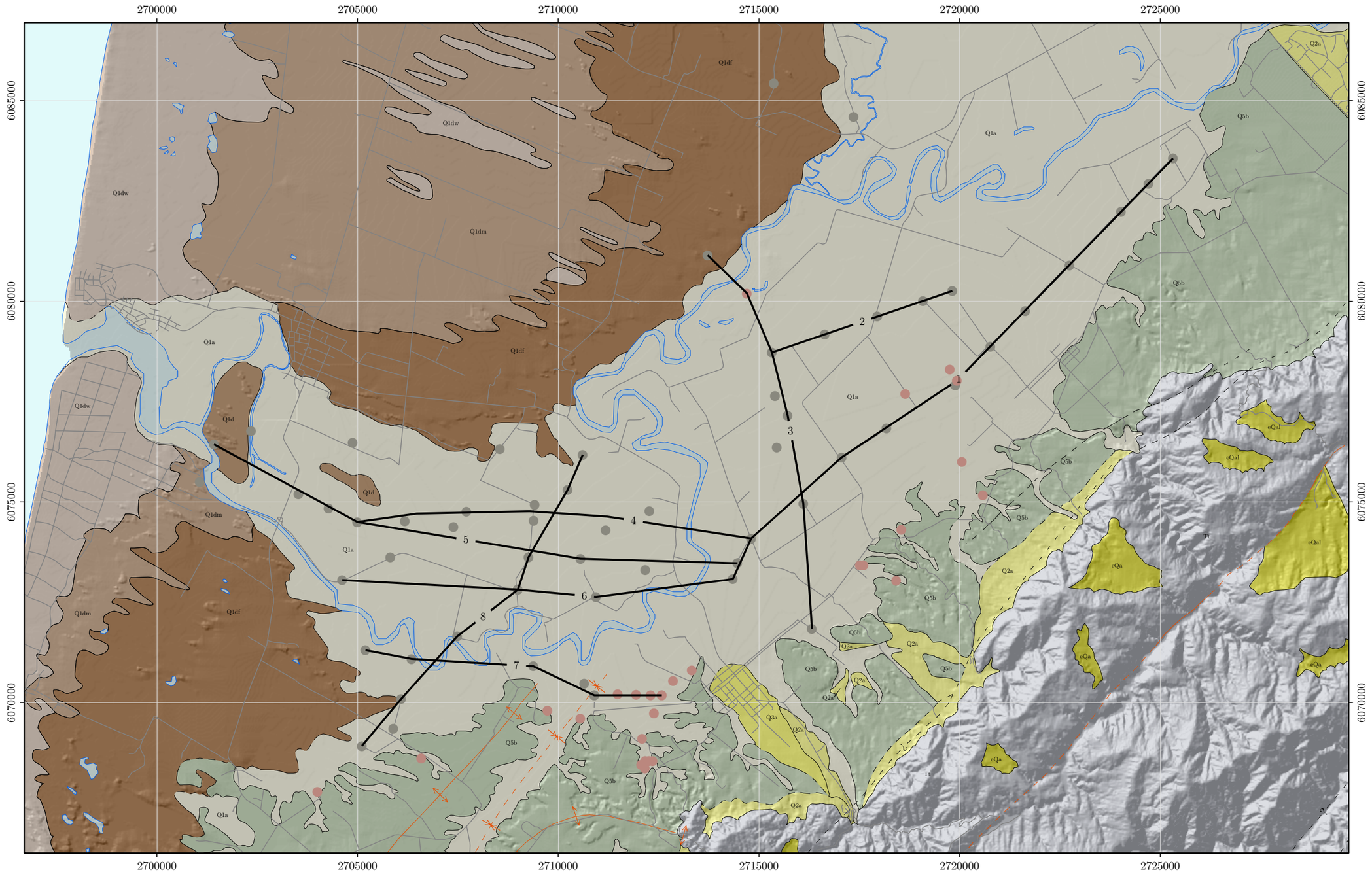
2700000
2705000
2710000
2715000
2720000
2725000
6085000
6080000
6075000
6070000
Q1dw
Q1dm
Q1df
Q1d
Q1a
Q2a
Q3a
Q5b
eQal
eQa
Tr
1
2
3
4
5
6
7
8

Table 7.4: Summary of the defining characteristics of the five facies identified in vibracores recovered from the lower Manawatu valley (approach after Sloss, 2005; Sloss et al., 2005, 2006b,a, 2007, 2010).

Facies	Sediment size, texture, and character	Sediment colour	Faunal assemblages	Organic content
Marine transgressive sands (MTS)	Medium- to coarse-grained, moderately- to poorly-sorted sand	Dark grey	Nil	Nil
Hightstand estuarine silts and sands (ESS)	Fine sand interbedded with silt, both poorly-sorted	Dark grey	Broken and whole *A. stutchburyi* extremely common; *A. crenata* and *Tellina* spp. also common; shell hash extremely common	Nil
Fluvial bay-head delta silts and sands (FBD)	Irregularly mixed fine- to medium-grained sands and silts ('mottled')	Silt: olive brown; sand: dark grey	Nil	Wood, root, and other organic fragments not uncommon
Floodplain alluvium (FA)	Poorly-sorted, near symemtrically skewed silty clay or clayey silt	Grey	Nil	Nil
Fluvial swampy silts (FSS)	Poorly-sorted, near symemtrically skewed silty clay or clayey silt	Greenish grey	Nil	Organic fragments, roots, and wood common

the top of the sands (Figure 7.10) and yielded a radiocarbon age of 5726 ± 132 cal. yr BP (Table 7.3).

7.3.2 Highstand estuarine silts and sands (ESS)

This facies is comprised of fine sands interbedded with silts (Figure 7.8), and was present in almost all the vibracores recovered from the middle and lower valley (see Sheets 24–31: vibracores cross-sections 1–8). Sedimentological analysis shows that both the sands and silts are very poorly sorted. This suggests that the sands and silts were deposited in a moderate energy environment, such as tidal flats, rather than in a low energy central basin (cf., Roy, 1984b; Dalrymple et al., 1992; Allen and Posamentier, 1993, 1994; Heap and Nichol, 1997; Kennedy et al., 2008; Abrahim et al., 2008). The thickness of this facies ranges from 1–5 m, although Shepherd and Lees (1987) penetrated 11 m of estuarine silts and sands at Murray's Farm (Sheet 23: vibracores cross-section 3). *A. stutchburyi* is the dominant fauna, typically encountered as disarticulated valves, though articulated *A. stutchburyi* are not uncommon. The presence of *A. stutchburyi* suggests a low energy, intertidal environment (e.g., Tallis et al., 2004; Hogg et al., 1998; Norkko et al., 2001; Hewitt et al., 1996; Purchase and Fergusson, 1986; Hayward et al., 1997, 2002; Lundquist et al., 2004; Lelieveld et al., 2004; Thrush et al., 1999; Larcombe, 1971; Powell, 1979; Morton and Miller, 1968). Other fossil shells preserved in this facies include the gastropod *Amphibola crenata* and the bivalve *Tellina* spp. Both are encountered only infrequently, and are common to intertidal mudflats and shallow water areas (e.g., Morton and Miller, 1968; Powell, 1979; Juniper, 1981; Pechenik et al., 2003). As filter or deposit feeders neither species is suitable for radiocarbon dating (Higham and Hogg, 1997, A. Hogg, personal communication, F. Petchley, personal communication). Shell fragments and fragmented valves are common. The sedimentological and faunal characteristics of this facies indicate that it was deposited in the estuarine central basin or bordering tidal flats of the middle and lower valley following the culmination of the Holocene marine transgression. Radiocarbon ages from articulated and disarticulated *A. stutchburyi* preserved in the estuarine silts and sands range from 8301 ± 324 cal. yr BP (Figure 7.11) to 5710 ± 130 cal. yr BP (Figure 7.12, Table 7.3; see also Figures 7.13, 7.14, 7.15, and 7.16).

7.3.3 Fluvial bay-head delta silts and sands (FBD)

This facies consists of fine-to-medium grained sands and silts in irregularly mixed but discrete patches (hereafter described as mottling) (Figure 7.8), and is restricted to the centre of the middle and lower valley (Sheets 24, 27–31: vibracores cross-sections 1, 4–8). The silts are typically olive brown, the sands dark grey. Both silts and sands are very poorly sorted. Their mottled nature suggests a mixed fluvial/marine energy regime. Fossil shells are absent; however, wood, root and other organic fragments are not uncommon. Radiocarbon ages from the A. stutchburyi valves within the underlying estuarine

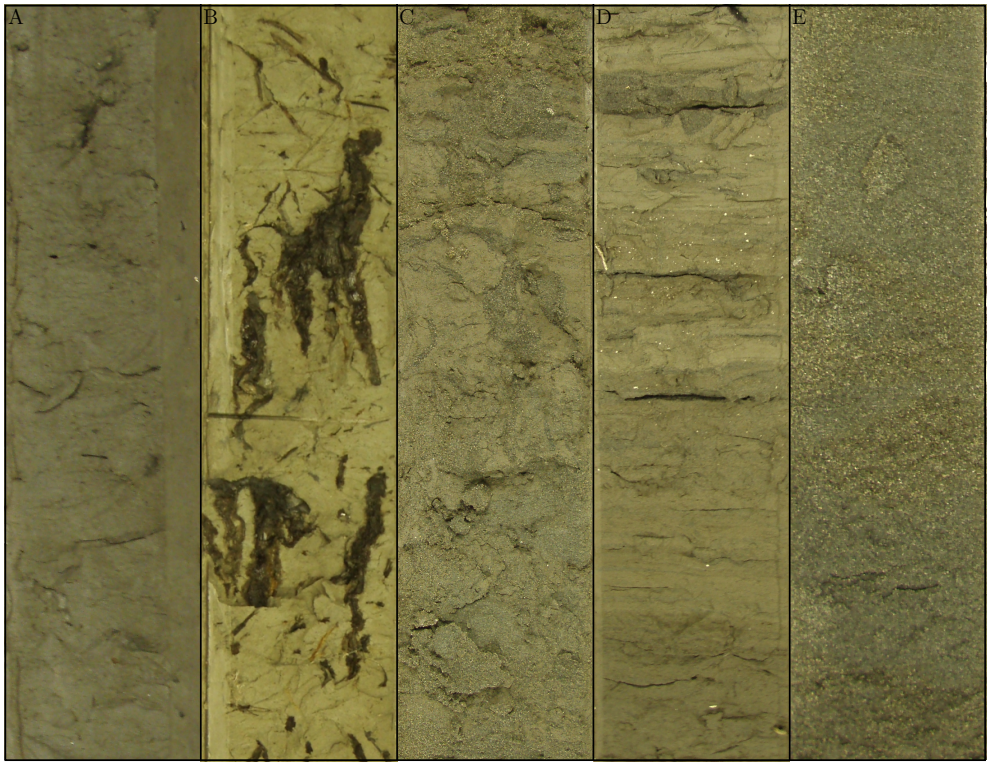

Figure 7.8: Representative sections of each of the five major facies identified in the vibracores recovered from the lower Manawatu valley. From left to right: (A) Floodplain alluvium (FA) recovered in vibracore Kop-5, c. 2.53–2.68 m. (B) Fluvial swampy silts (FSS) recovered in vibracore Kara-1, c. 5.85–5.00 m. (C) Fluvial bay-head delta silts and sands (FBD) (note 'mottled' appearance) recovered in vibracore Flood-4, c. 2.98–3.13 m. (D) Estuarine sands and silts (ESS) recovered in vibracore G, c. 5.30–5.45 m. (E) Marine transgressive sands (MTS) recovered in vibracore F, c. 4.71–4.86 m.

sands and silts indicate that in the middle valley the fluvial bay-head delta deposits are younger than 6,500 cal. yr BP (e.g., Figures 7.15 and 7.17; Sheet 26: vibracores cross-section 3), while in the lower valley the deposits are younger than 6,000–5,500 cal. yr BP (e.g., Figures 7.16 and 7.12; Sheets 28 and 29: vibracores cross-sections 5 and 6).

7.3.4 Floodplain alluvium (FA) and fluvial swampy silts (FSS)

Both floodplain alluvium and fluvial swampy silts are composed of poorly sorted, near symmetrically skewed silty clays or clayey silts. This suggests rapid deposition and/or deposition under mixed energy conditions (cf., Sahu, 1964; Valia and Cameron, 1977; Martins, 2003). The primary discriminating factor between the two facies is the presence or absence of wood, root and other organic fragments. Floodplain alluvium is the uppermost facies recognised in all vibracores recovered from the middle and lower valley, with the exception of vibracores Whiro-1, Whiro-2 and B, which were recovered from Manawatu

River. Floodplain alluvium is typically free of wood, root and other organic fragments. In contrast, fluvial swampy silts are restricted to the margins of the valley, particularly in the box-shaped valleys along the margin of the Tokomaru Marine Terrace (e.g., Sheet 26: vibracores cross-section 3; cf., Hesp, 1975; Hesp and Shepherd, 1978).

7.4 Vibracores cross-sections in the Manawatu valley: results and discussion

7.4.1 Sheet 24: Vibracores cross-section 1

Floodplain alluvium (FA) is penetrated by vibracores and auger holes along the length of vibracores cross-section 1 (Sheet 24), with an average thickness of approximately 3.5 m. North of Tokomaru the floodplain alluvium (FA) is underlain by an indeterminate thickness of fluvial sandy silts (FSS). In the upper valley above Tokomaru the transition from swamp to floodplain appears to have taken place approximately 5,700 cal. yr BP, probably as the result of changing drainage conditions connected to sea-level and the proximity of the estuary at this time. At Tokomaru the fluvial sandy silts (FSS) transition to fluvial bay-head delta silts and sands (FBD). The bay-head delta sediments are spatially restricted to the area around vibracores FR-1 and Cut-9 (Sheet 24), and are only approximately 1.5 m thick. South of vibracore FR-1 estuarine silts and sands (ESS) are penetrated. Notably, in vibracores Cut-5, Cut-6, Cut-7, and Cut-8 the estuarine silts and sands (ESS) are directly overlain by floodplain alluvium (FA), rather than by bay-head delta sediments (cf. models of wave-dominated estuary and incised valley evolution, e.g., Dalrymple et al.,

---

Figure 7.9 *(next two pages)*: Stratigraphic log of drain section and vibracore F.

Figure 7.10 *(pages 206–207)*: Stratigraphic log of drain section and vibracore Kop-1.

Figure 7.11 *(pages 208–209)*: Stratigraphic log of drain section and vibracore Sh-1.

Figure 7.12 *(pages 210–211)*: Stratigraphic log of drain section and vibracore Flood-1.

Figure 7.13 *(pages 212–213)*: Stratigraphic log of drain section and vibracore Sh-2.

Figure 7.14 *(pages 214–215)*: Stratigraphic log of drain section and vibracore Cut-7.

Figure 7.15 *(pages 216–217)*: Stratigraphic log of drain section and vibracore Cut-4.

Figure 7.16 *(pages 218–219)*: Stratigraphic log of drain section and vibracore E-1.

Figure 7.17 *(pages 220–221)*: Stratigraphic log of drain section and vibracore Cut-2.

CORE: F
LOCATION: Kere Kere Road

NZMG COORDINATES: 2709262.28 E, 6073628.84 N PAGE: 1/2
WVD1953 ELEVATION: +1.3328 m

DEPTH (m)	WVD'53 (m)	PHOTO LOG	VISUAL LOG	COLOUR	CHRONOLOGY	SORTING MEAN GRAIN SIZE
				2.5Y4/3		
				10YR4/1		
				5Y5/1		
				Sand: 2.5Y4/0 Clay: 5Y5/1		
				10YR2/1		
				Sand: 2.5Y4/0 Clay: 5Y5/1		

CORE: F
LOCATION: Kere Kere Road

NZMG COORDINATES: 2709262.28 E, 6073628.84 N PAGE: 2/2
WVD1953 ELEVATION: +1.3328 m

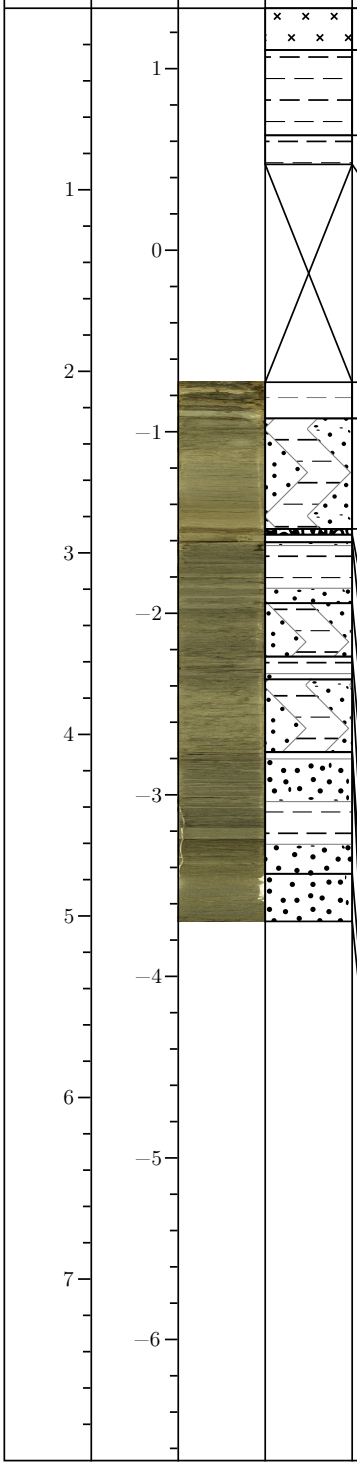

DESCRIPTION	INTERPRETATION
Weathered soil	Floodplain alluvium
Clayey silt	
Clayey silt (colour changes)	
Obscured by water	
Thixotrophic mud	
Fine sand mottled with clayey silt	Fluvial bay-head delta silts and sands
Dense organics	
Fine clayey silt	
Fine sand interbedded with clayey silt	Estuarine sands and silts
Fine sand mottled with clayey silt	
Clayey silt interbedded with fine sand	
Fine sand mottled with clayey silt	
Dense organics	
Medium sand interbedded with clayey silt	
Medium sand	Marine transgressive sand

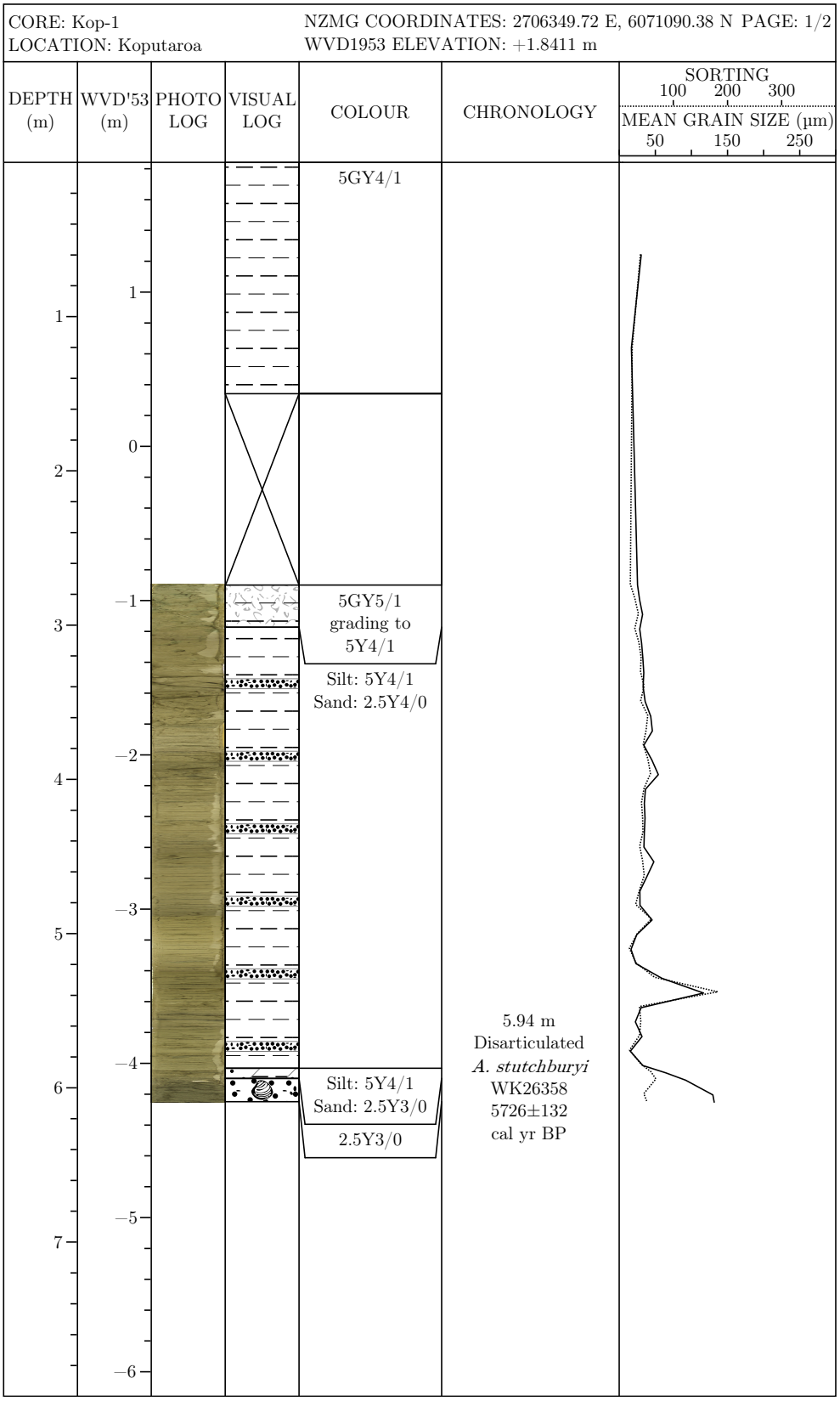
CORE: Kop-1
LOCATION: Koputaroa
NZMG COORDINATES: 2706349.72 E, 6071090.38 N PAGE: 1/2
WVD1953 ELEVATION: +1.8411 m
DEPTH (m)
WVD'53 (m)
PHOTO LOG
VISUAL LOG
COLOUR
CHRONOLOGY
SORTING
100 200 300
MEAN GRAIN SIZE (µm)
50 150 250
5GY4/1
5GY5/1 grading to 5Y4/1
Silt: 5Y4/1
Sand: 2.5Y4/0
Silt: 5Y4/1
Sand: 2.5Y3/0
2.5Y3/0
5.94 m
Disarticulated
A. stutchburyi
WK26358
5726±132
cal yr BP

CORE: Kop-1
LOCATION: Koputaroa

NZMG COORDINATES: 2706349.72 E, 6071090.38 N PAGE: 2/2
WVD1953 ELEVATION: +1.8411 m

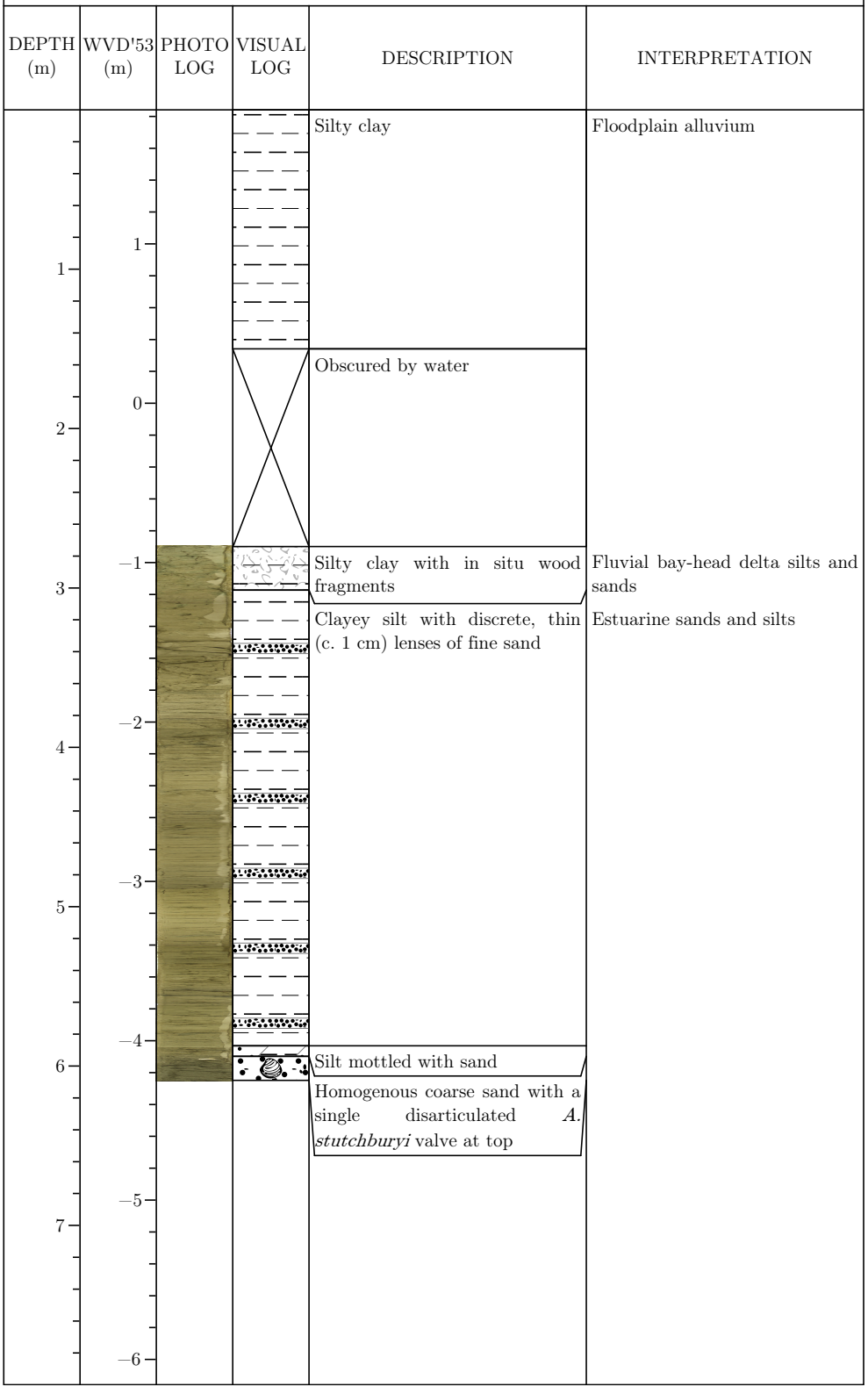

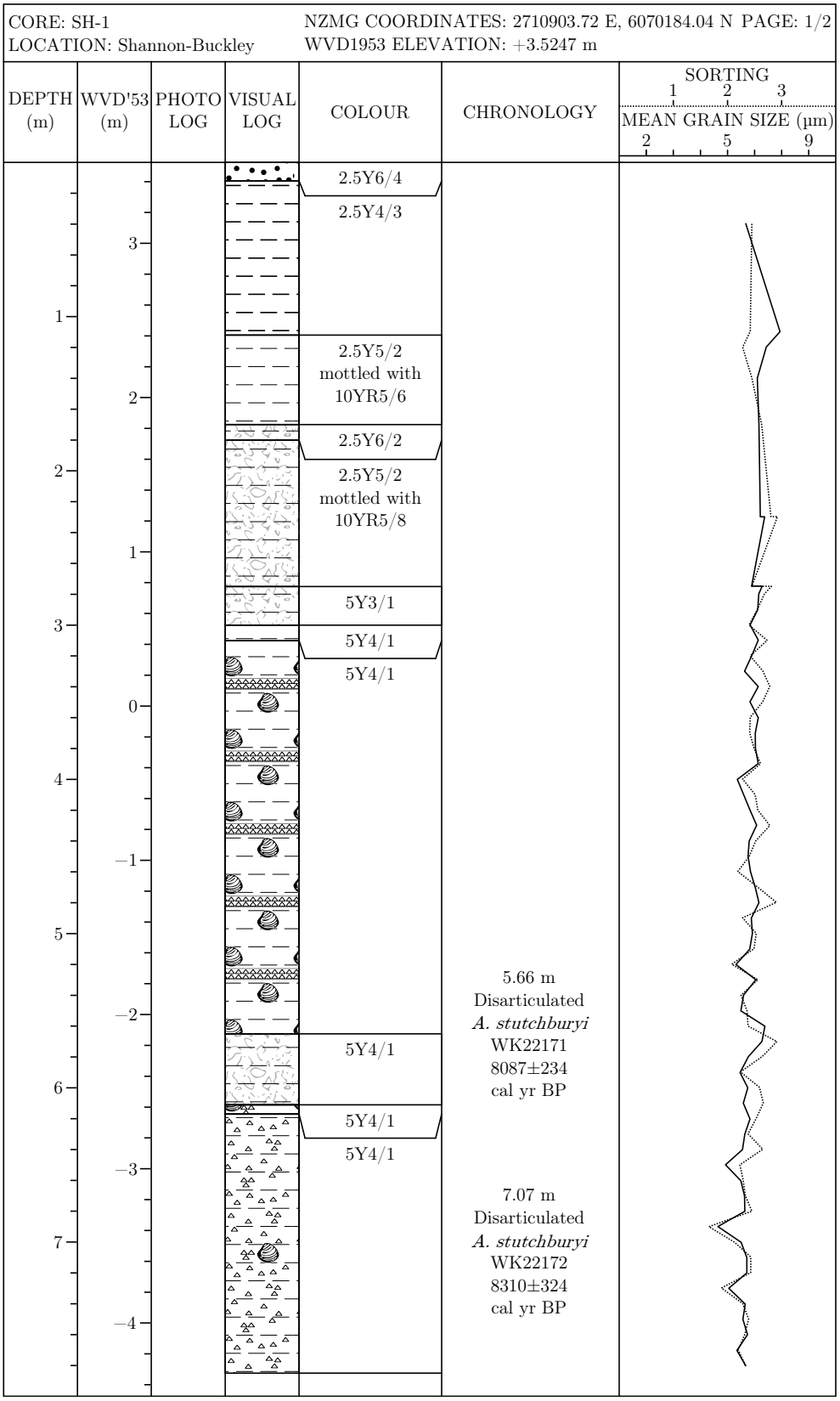
CORE: SH-1
LOCATION: Shannon-Buckley
NZMG COORDINATES: 2710903.72 E, 6070184.04 N PAGE: 1/2
WVD1953 ELEVATION: +3.5247 m
DEPTH (m)
WVD'53 (m)
PHOTO LOG
VISUAL LOG
COLOUR
CHRONOLOGY
SORTING
1 2 3
MEAN GRAIN SIZE (µm)
2 5 9
2.5Y6/4
2.5Y4/3
2.5Y5/2 mottled with 10YR5/6
2.5Y6/2
2.5Y5/2 mottled with 10YR5/8
5Y3/1
5Y4/1
5Y4/1
5Y4/1
5Y4/1
5Y4/1
5.66 m
Disarticulated
A. stutchburyi
WK22171
8087±234
cal yr BP
7.07 m
Disarticulated
A. stutchburyi
WK22172
8310±324
cal yr BP

CORE: SH-1 NZMG COORDINATES: 2710903.72 E, 6070184.04 N PAGE: 2/2
LOCATION: Shannon-Buckley WVD1953 ELEVATION: +3.5247 m

DEPTH (m)	WVD'53 (m)	PHOTO LOG	VISUAL LOG	DESCRIPTION	INTERPRETATION
				Coarse sandy soil	Floodplain alluvium
				Homogenous silt	
1	3				
				Homogenous clay	
	2				
				Clay, densely packed with organic fragments	
2				Clay with random organic fragments	
	1				
				Clay with in situ wood fragments	
3				Transition to fine muddy clay	Alluvial-estuarine transition
				Fine muddy clay with layers of shell hash, isolated random shell fragments, and isolated random disarticulated *A. stutchburyi*	Estuarine sands and silts
	0				
4					
	−1				
5					
	−2				
				Fine silty clay with in situ wood fragments	
6					
				Fine muddy clay with moderate shell hash and random articulated *A. stutchburyi*	
	−3			Fine muddy clay with moderate shell hash and isolated random shell fragments	
7					
	−4				

CORE: Flood-1
LOCATION: Moutoa Floodway

NZMG COORDINATES: 2703528.30 E, 6075193.75 N PAGE: 1/2
WVD1953 ELEVATION: +0.7152 m

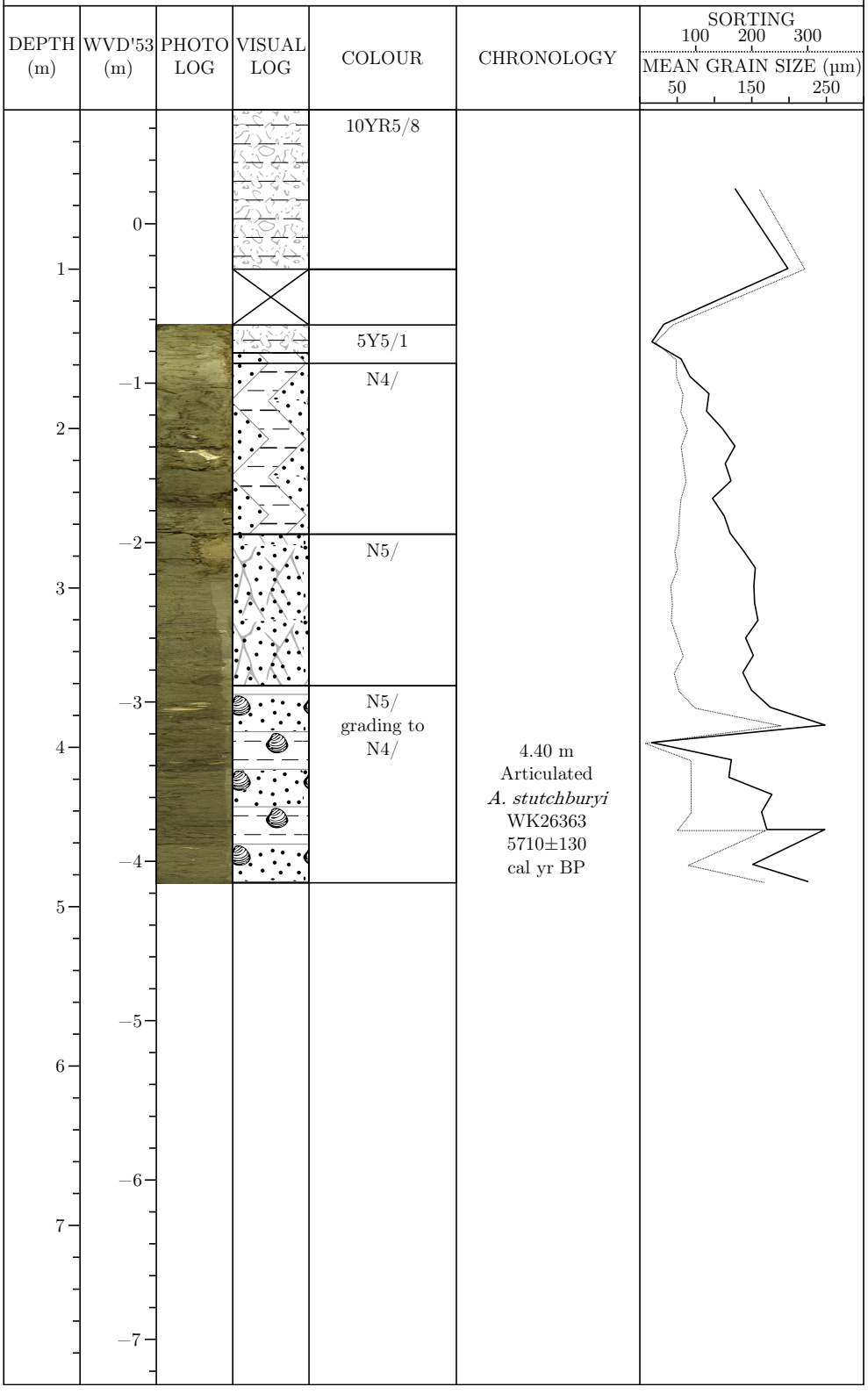

CORE: Flood-1
LOCATION: Moutoa Floodway

NZMG COORDINATES: 2703528.30 E, 6075193.75 N PAGE: 2/2
WVD1953 ELEVATION: +0.7152 m

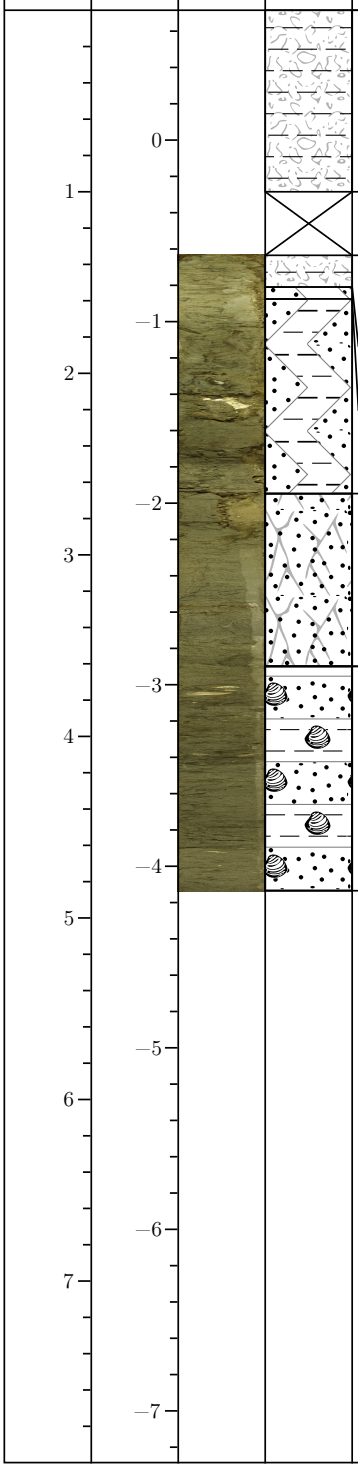

DESCRIPTION	INTERPRETATION
Peaty clay with in situ wood fragments	Floodplain alluvium
Obscured by water	
Clay grading to clayey silt, some infrequent in situ wood fragments	
Grading to fine sand mottled with clayey silt	Fluvial bay-head delta silts and sands
Fine sand mottled with clayey silt	
Homogenous fine sand, some root fargments	Estuarine sands and silts
Fine sand interbedded with silt and discrete layers of organics; many fragmented and whole shells, some articulated	

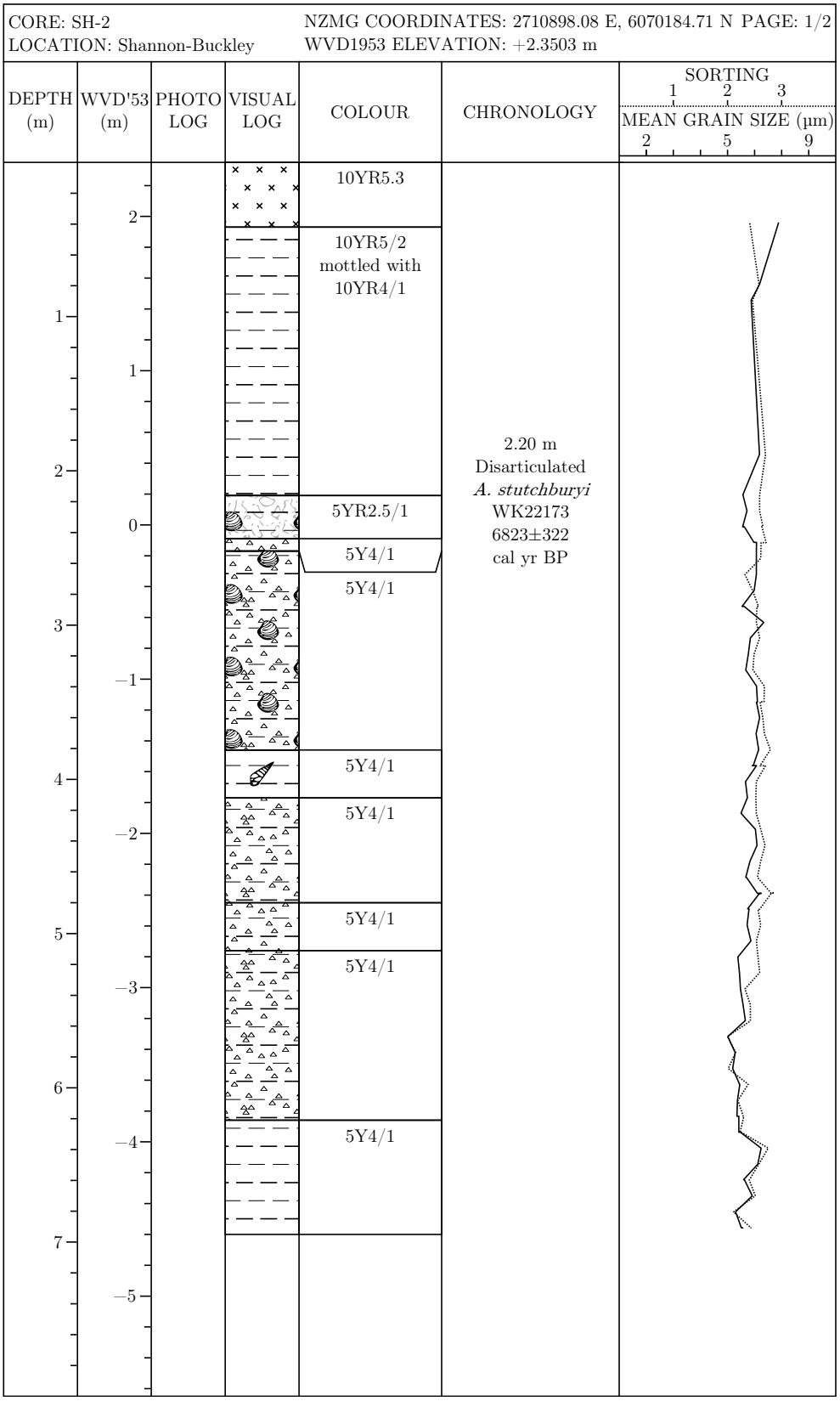
CORE: SH-2
LOCATION: Shannon-Buckley
NZMG COORDINATES: 2710898.08 E, 6070184.71 N PAGE: 1/2
WVD1953 ELEVATION: +2.3503 m
DEPTH (m)
WVD'53 (m)
PHOTO LOG
VISUAL LOG
COLOUR
CHRONOLOGY
SORTING
1 2 3
MEAN GRAIN SIZE (µm)
2 5 9
10YR5.3
10YR5/2 mottled with 10YR4/1
5YR2.5/1
5Y4/1
5Y4/1
5Y4/1
5Y4/1
5Y4/1
5Y4/1
5Y4/1
2.20 m
Disarticulated
A. stutchburyi
WK22173
6823±322
cal yr BP

CORE: SH-2
LOCATION: Shannon-Buckley

NZMG COORDINATES: 2710898.08 E, 6070184.71 N PAGE: 2/2
WVD1953 ELEVATION: +2.3503 m

DEPTH (m)	WVD'53 (m)	PHOTO LOG	VISUAL LOG	DESCRIPTION	INTERPRETATION
0	2			Weathered top soil	Floodplain alluvium
1	1			Homogenous fine clayey silt	
2	0			Fine silty clay with organic fragments and disarticulated *A. stutchburyi*	Estuarine sands and silts
3	−1			Silty clay with densely packed shell hash	
4	−2			Fine silty clay with random infrequent shell fragments and random infrequent disarticulated *A. stutchburyi*	
5	−3			Fine silty clay with random *A. crenata*	
6	−4			Silt clay with infrequent random shell fragments	
7	−5			Fine silty clay with moderate shell hash	
				Fine silty clay with sparse shell hash	
				Fine silty clay	

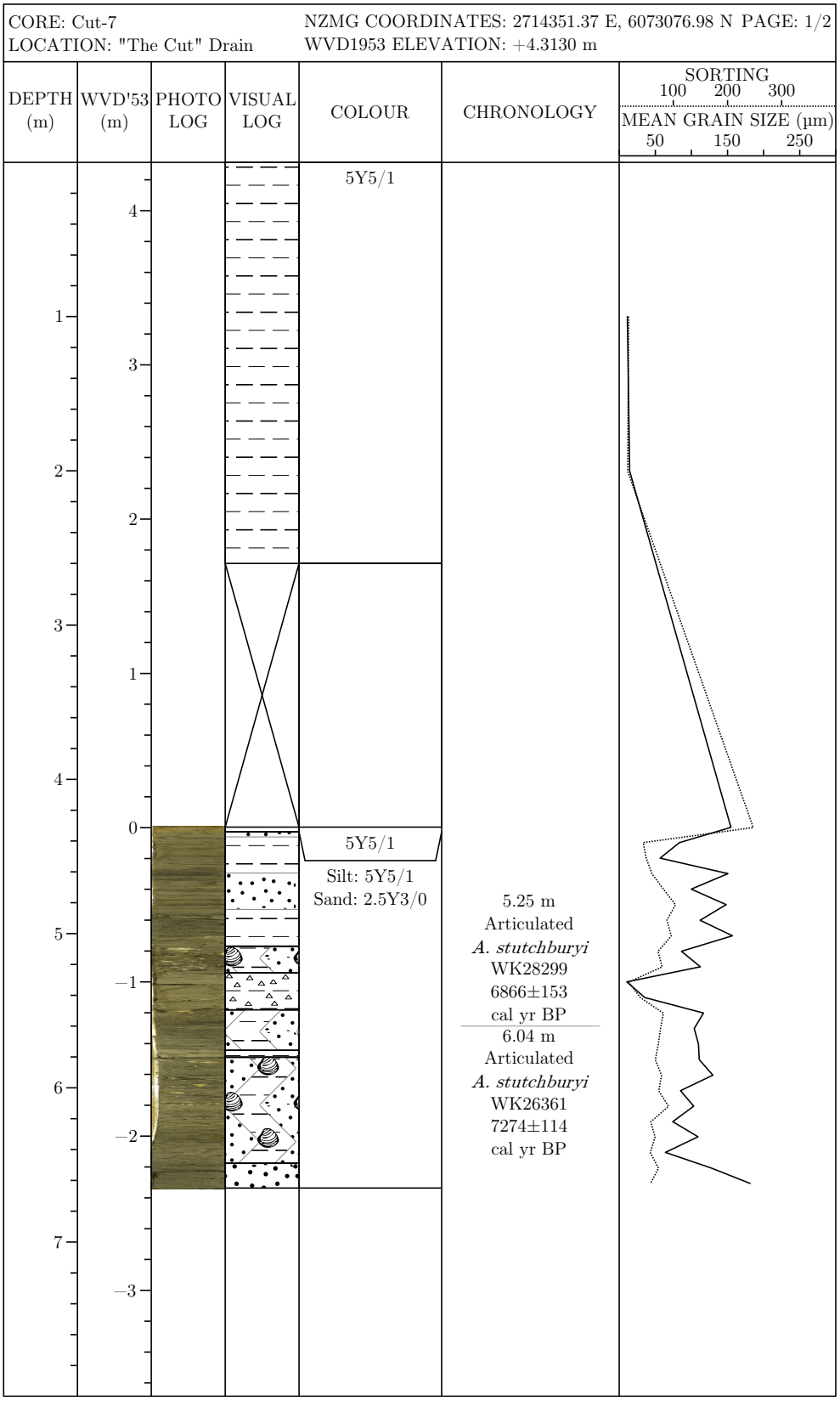
CORE: Cut-7
LOCATION: "The Cut" Drain
NZMG COORDINATES: 2714351.37 E, 6073076.98 N PAGE: 1/2
WVD1953 ELEVATION: +4.3130 m
DEPTH (m)
WVD'53 (m)
PHOTO LOG
VISUAL LOG
COLOUR
CHRONOLOGY
SORTING
100 200 300
MEAN GRAIN SIZE (µm)
50 150 250
5Y5/1
5Y5/1
Silt: 5Y5/1
Sand: 2.5Y3/0
5.25 m
Articulated
A. stutchburyi
WK28299
6866±153
cal yr BP
6.04 m
Articulated
A. stutchburyi
WK26361
7274±114
cal yr BP

CORE: Cut-7
LOCATION: "The Cut" Drain

NZMG COORDINATES: 2714351.37 E, 6073076.98 N PAGE: 2/2
WVD1953 ELEVATION: +4.3130 m

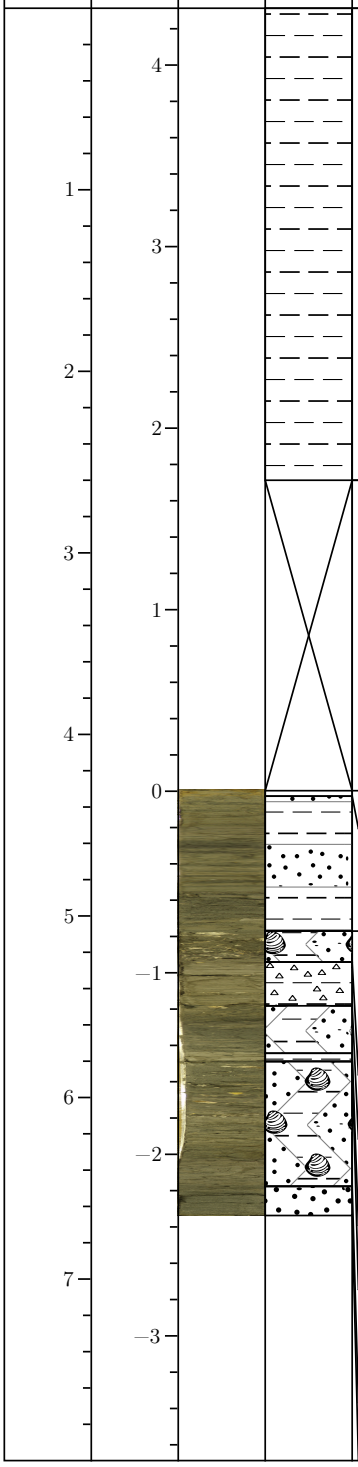

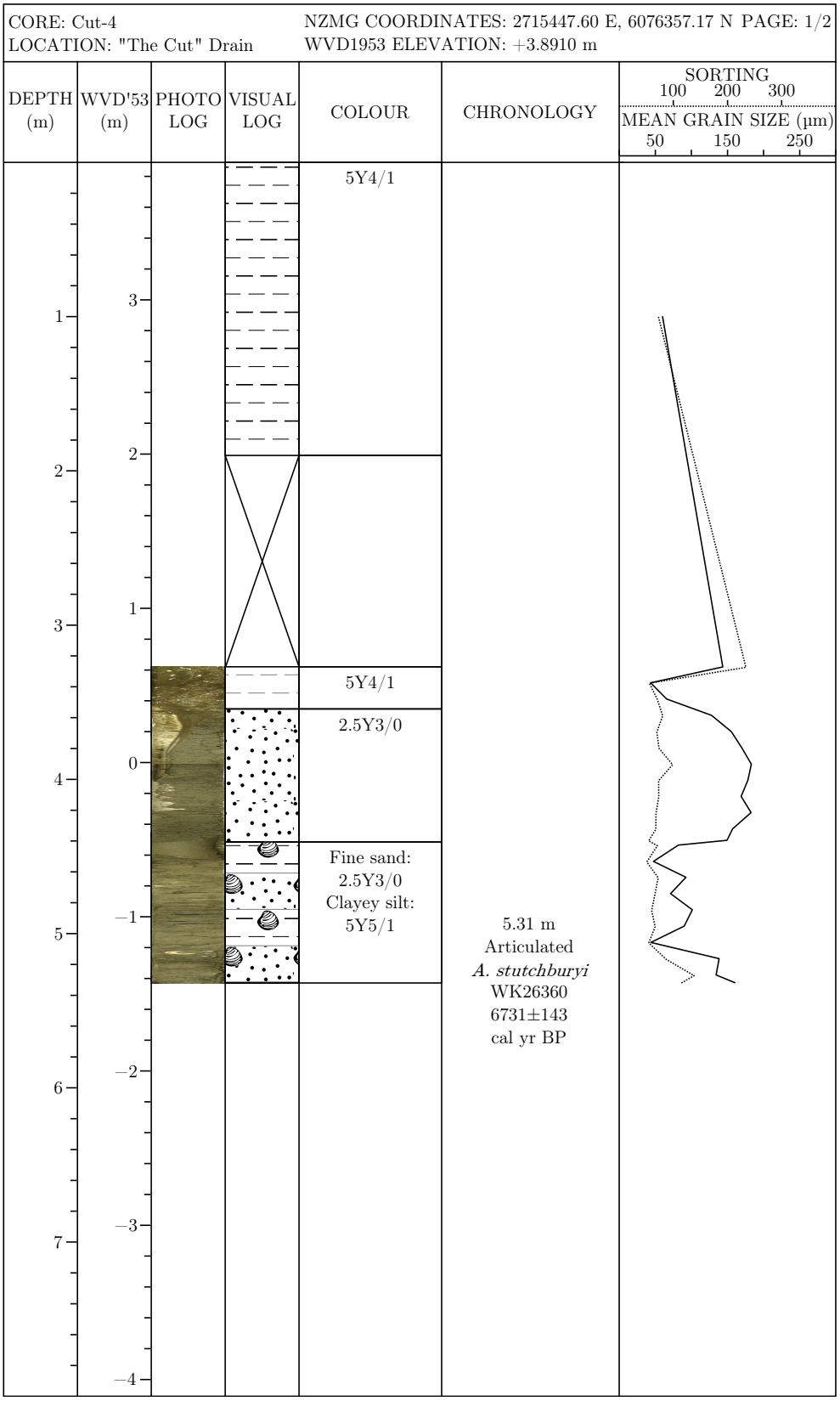
CORE: Cut-4
LOCATION: "The Cut" Drain
NZMG COORDINATES: 2715447.60 E, 6076357.17 N PAGE: 1/2
WVD1953 ELEVATION: +3.8910 m
DEPTH (m)
WVD'53 (m)
PHOTO LOG
VISUAL LOG
COLOUR
CHRONOLOGY
SORTING
100 200 300
MEAN GRAIN SIZE (µm)
50 150 250
5Y4/1
5Y4/1
2.5Y3/0
Fine sand: 2.5Y3/0
Clayey silt: 5Y5/1
5.31 m
Articulated
A. stutchburyi
WK26360
6731±143
cal yr BP

CORE: Cut-4
LOCATION: "The Cut" Drain

NZMG COORDINATES: 2715447.60 E, 6076357.17 N PAGE: 2/2
WVD1953 ELEVATION: +3.8910 m

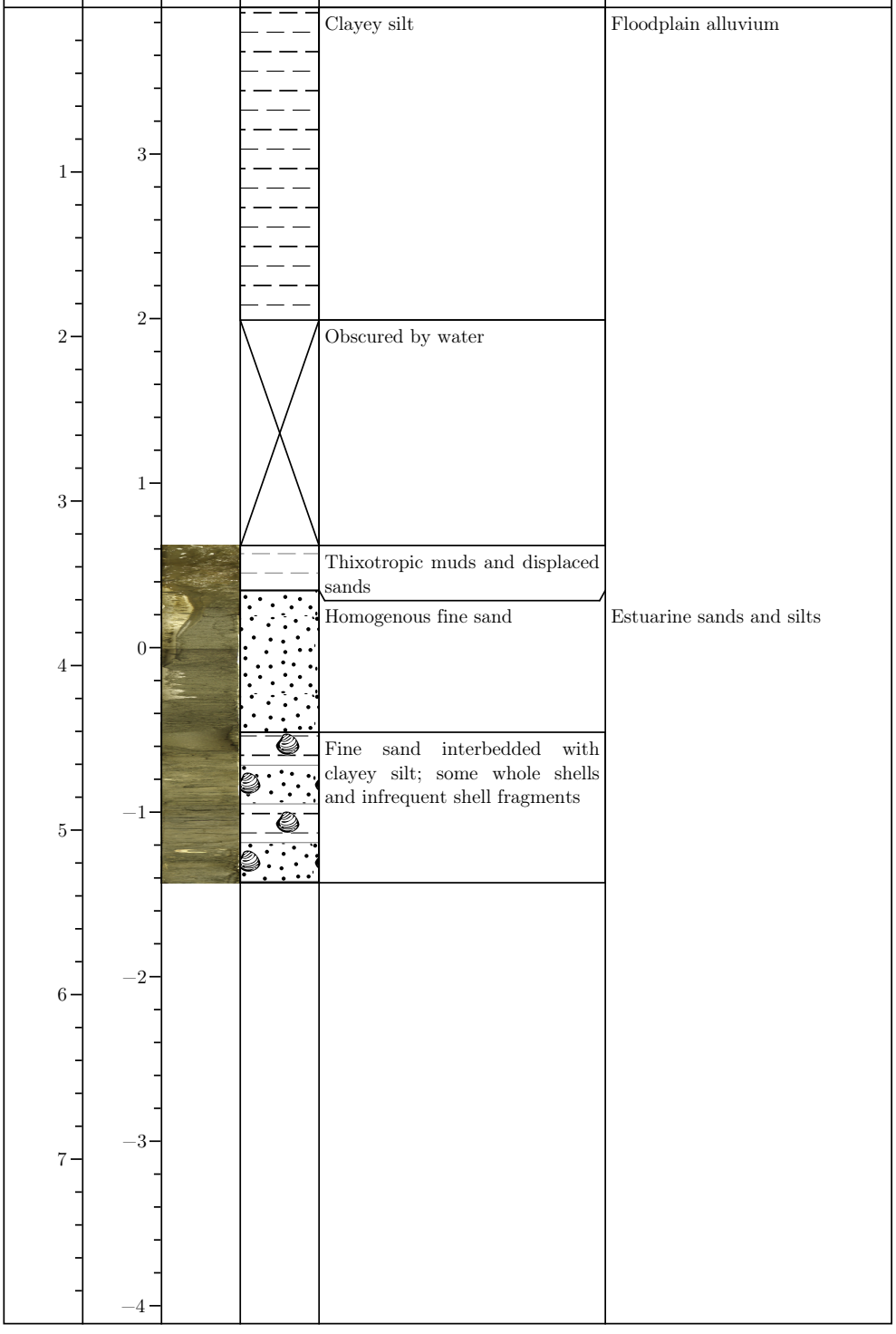

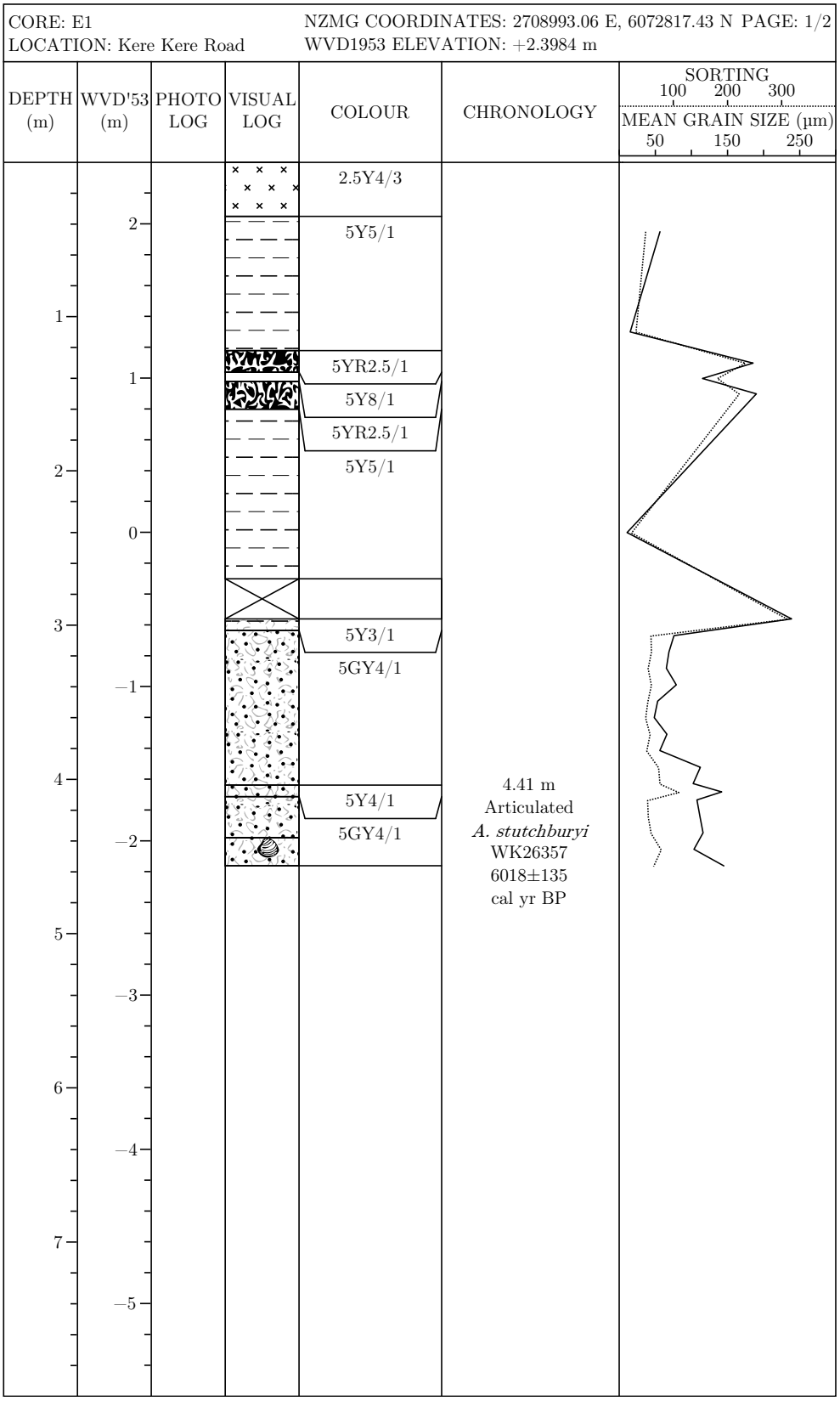
CORE: E1
LOCATION: Kere Kere Road
NZMG COORDINATES: 2708993.06 E, 6072817.43 N PAGE: 1/2
WVD1953 ELEVATION: +2.3984 m
DEPTH (m)
WVD'53 (m)
PHOTO LOG
VISUAL LOG
COLOUR
CHRONOLOGY
SORTING
100 200 300
MEAN GRAIN SIZE (µm)
50 150 250
2.5Y4/3
5Y5/1
5YR2.5/1
5Y8/1
5YR2.5/1
5Y5/1
5Y3/1
5GY4/1
5Y4/1
5GY4/1
4.41 m
Articulated
A. stutchburyi
WK26357
6018±135
cal yr BP

CORE: E1 NZMG COORDINATES: 2708993.06 E, 6072817.43 N PAGE: 2/2
LOCATION: Kere Kere Road WVD1953 ELEVATION: +2.3984 m

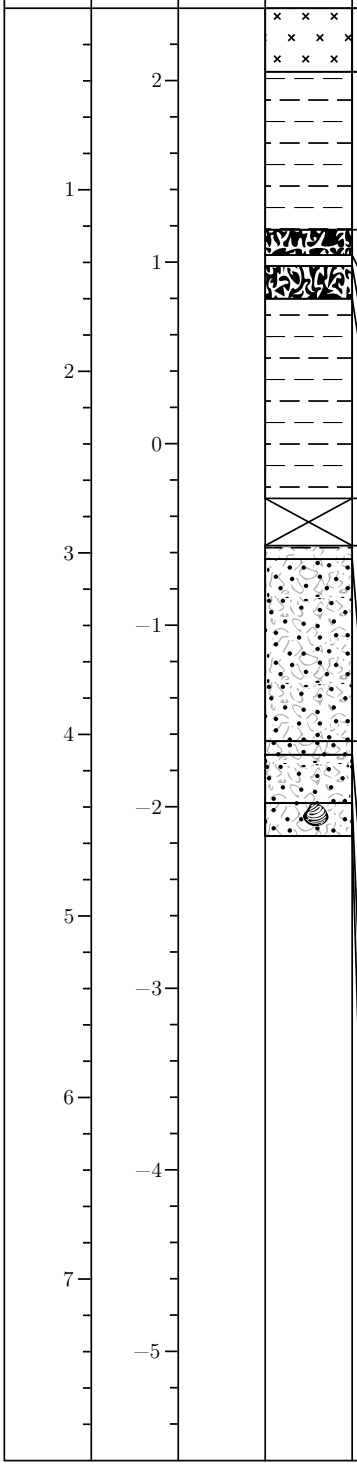

DEPTH (m)	WVD'53 (m)	PHOTO LOG	VISUAL LOG	DESCRIPTION	INTERPRETATION
				Weathered soil	Floodplain alluvium
				Clayey silt	
				Peaty soil	
				Fossil wood?	
				Peaty soil	
				Clayey silt	
				Obscured by water	
				Fine muddy silt with many root fragments and other in situ wood fragments	Fluvial bay-head delta silts and sands
				Fine sand with scattered in situ wood fragments and some scattered organics	
				Fine sand with lighter coloured lenses; some scattered organics and in situ wood fragments	
				Fine sand with a thin (c. 1 cm) layer of dense organics; some scattered in situ wood fragments	
				Fine sand with larger wood fragments (roots?) and large broken/fragmented shells	Estuarine sands and silts

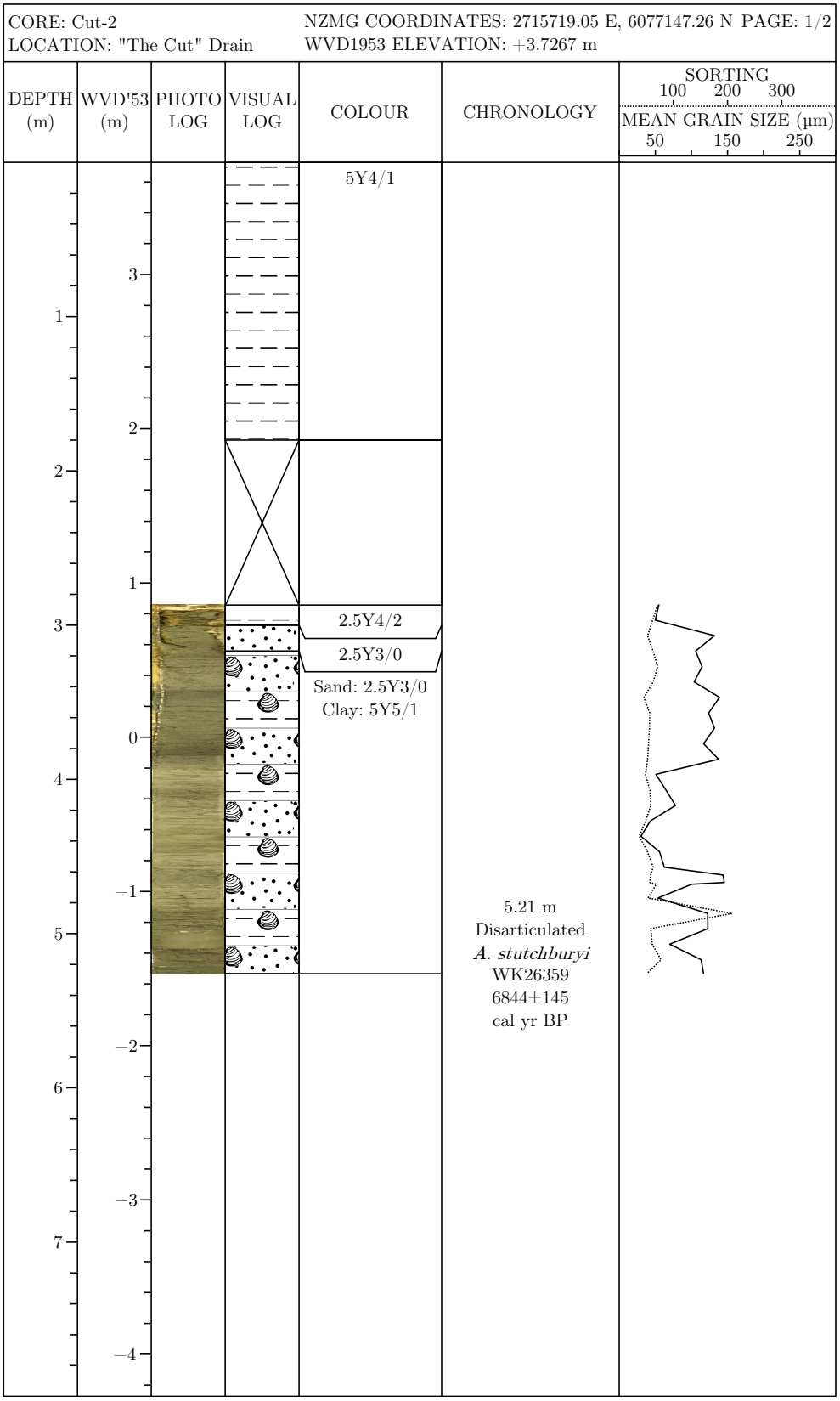
CORE: Cut-2
LOCATION: "The Cut" Drain
NZMG COORDINATES: 2715719.05 E, 6077147.26 N PAGE: 1/2
WVD1953 ELEVATION: +3.7267 m
DEPTH (m)
WVD'53 (m)
PHOTO LOG
VISUAL LOG
COLOUR
CHRONOLOGY
SORTING
100 200 300
MEAN GRAIN SIZE (µm)
50 150 250
5Y4/1
2.5Y4/2
2.5Y3/0
Sand: 2.5Y3/0
Clay: 5Y5/1
5.21 m
Disarticulated
A. stutchburyi
WK26359
6844±145
cal yr BP

CORE: Cut-2
LOCATION: "The Cut" Drain

NZMG COORDINATES: 2715719.05 E, 6077147.26 N PAGE: 2/2
WVD1953 ELEVATION: +3.7267 m

DEPTH (m)	WVD'53 (m)	PHOTO LOG	VISUAL LOG	DESCRIPTION	INTERPRETATION
				Clayey silt	Floodplain alluvium
				Obscured by water	
				Thixotropic mud	
				Homogenous fine sand	Estuarine sands and silts
				Fine sand interbedded with clayey silt; some unbroken disarticulated valves and one articulated bivalve; some shell fragments	

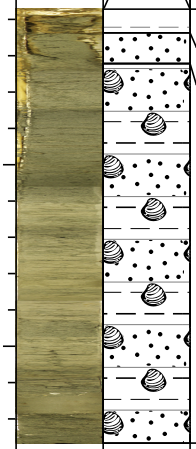

1992; Zaitlin et al., 1994, ; see Chapter 5). The precise thickness of the estuarine silts and sands (ESS) in the area south of Tokomaru is unclear; however, the depth to the reconstructed LGM surface (Figure 6.19) suggests they may be 5–15 m thick.

7.4.2 Sheet 25: Vibracores cross-section 2

Floodplain alluvium (FA) is the uppermost facies penetrated by all five vibracores along the length of vibracores cross-section 2 (Sheet 25). The average thickness of the floodplain alluvium along the length of the cross-section varies from 1.5–2.5 m. Underlying the floodplain alluvium (FA) is 1–2.5 m of fluvial sandy silts (FSS). The fluvial sandy silts (FSS) are in turn underlain by highstand estuarine silts and sands (ESS) of indeterminate thickness. Reference to the reconstructed LGM surface (Figure 6.19) suggests that here the estuarine sandy silts (ESS) may be up to 15 m thick. By comparison with vibracores cross-section 1 (Sheet 24), it appears that the highstand estuarine sandy silts (ESS) probably taper out between Cut-13 and Cut-10b (Sheet 25).

7.4.3 Sheet 26: Vibracores cross-section 3

Vibracores cross-section 3 (Sheet 26) intersects with the western end of vibracores cross-section 2 (sheet 25) at vibracore Cut-14, and with vibracores cross-section 1 (Sheet 24) at vibracore Cut-6. At the northern end of the cross-section, proximal to the Manawatu River, up to 9 m of floodplain alluvium (FA) is penetrated by the Murray's Farm bore drilled by Shepherd and Lees (1987) (Sheet 26). To the south, away from the river, the thickness of floodplain alluvium (FA) decreases to approximately 3 m. Fluvial swampy silts (FSS) between 1–3.5 m thick underlie the floodplain alluvium in vibracores Cut-14, Cut-6, and Kara-1. These fluvial sandy silts are in turn underlain by highstand estuarine silts and sands (ESS) of indeterminate thickness. In the Murray's Farm bore floodplain alluvium (FA) is directly underlain by highstand estuarine silts and sands (ESS), which are penetrated to a depth of c. −12 m below PMSL. A radiocarbon date from an *A. stutchburyi* valve recovered at −5.6 m below PMSL indicates that estuarine conditions prevailed in this area c. 7,100 cal. yr BP (Sheet 26; Table 7.3). In the center of the valley statistically similar radiocarbon ages from *A. stutchburyi* valves recovered in vibracores Cut-2 and Cut-4 indicate that estuarine conditions were maintained here until after 6,800 cal. yr BP. Shepherd and Lees (1987) suggested that the estuarine-alluvial transition took place c. 6,000 years BP. In the central valley fluvial swampy silts (FSS) were therefore probably deposited in the period between 6,500–6,000 cal. yr BP.

7.4.4 Sheet 27: Vibracores cross-section 4

Vibracores cross-section 4 (Sheet 27) intersects with the southwestern end of vibracores cross-section 1 (Sheet 24) at vibracore Cut-5. The western end of

vibracores cross-section 4 (Sheet 27) intersects partway along vibracores cross-section 5 (Sheet 28) which runs c. 1 km south of cross-section 4 (Figure 7.1). Adjacent to the Manawatu River, between vibracores Cut-5 and Cook-3, the thickness of floodplain alluvium (FA) reaches a maximum of approximately 6 m due to the formation of levees by the river. Further down the valley below vibracore Cook-3, floodplain alluvium (FA) penetrated by the vibracores has an average thickness of 1.5–2.5 m. Beneath the floodplain alluvium (FA) the vibracores along the length of the cross-section penetrate c. 1–1.5 m of fluvial bay-head delta silts and sands (FBD). This is comparable with the thickness of fluvial bay-head delta silts and sands (FBD) penetrated by vibracores along the length of vibracores cross-section 5 (Sheet 28), approximately 1 km to the south. Highstand estuarine silts and sands (ESS) are penetrated at the base of all the vibracores along the cross-section (Sheet 27), to a maximum depth of −3.6 m below PMSL.

7.4.5 Sheet 28: Vibracores cross-section 5

Vibracores cross-section 5 (Sheet 28) intersects with the southwestern end of vibracores cross-section 1 (Sheet 24) at vibracore Cut-8, and with the western end of vibracores cross-section 4 (Sheet 27) at vibracore Flood-3. At the eastern end of the cross-section, between vibracores Cut-8 and Cook-5, the thickness of floodplain alluvium (FA) penetrated by the vibracores exceeds 7 m in places, due to the formation of levees by the Manawatu River. However, along the cross-section to the west the thickness of floodplain alluvium (FA) decreases to an average of 1–2 m. Beneath the floodplain alluvium (FA) the vibracores penetrate a thin 0.5–2 m layer of fluvial bay-head delta silts and sands (FBD) that pinches out in the vicinity of the Whirokino Cut (vibracore Whiro-1). Underneath the fluvial bay-head delta sediments (FBD) lie highstand estuarine sands and silts (ESS) of between 2.5–5 m thickness. Radiocarbon ages from *A. stutchburyi* valves recovered in vibracores at the western end of the cross-section indicate that estuarine conditions prevailed in the lower valley between 5,700–4,700 cal. yr BP. The estuarine sands and silts (ESS) are in turn underlain by marine transgressive sands (MTS) of indeterminate thickness.

7.4.6 Sheet 29: Vibracores cross-section 6

Vibracores cross-section 6 (Sheet 29) intersects with the southwestern end of vibracores cross-section 1 (Sheet 24) at vibracore Cut-8, and with vibracores cross-section 8 (Sheet 31) at vibracores E1 and E2 (Figure 7.1). The vibracores along the length of the cross-section penetrate a wedge of highstand estuarine silts and sands (ESS) deposited between 7,300–6,000 cal. yr BP. At the western end of the cross-section the estuarine silts and sands are overlain by fluvial bay-head delta sands and silts (FBD). An articulated *A. stutchburyi* valve recovered in vibracore E1 indicates that the transition for estuarine tidal flats to bay-head delta took place approximately 6,000 cal. yr BP. The fluvial bay-

head delta sediments (FBD) are in turn overlain by floodplain alluvium (FA), while at the eastern end of the cross-section the floodplain alluvium directly overlies the estuarine silts and sands (ESS). Proximal to the Manawatu River the floodplain alluvium has a thickness of up to 6 m, dropping to an average of approximately 2–2.5 m distally.

7.4.7 Sheet 30: Vibracores cross-section 7

Vibracores cross-section 7 (Sheet 30) intersects with vibracores cross-section 8 (Sheet 31) immediately east of vibracore Kop-1. Floodplain alluvium (FA) is penetrated by all vibracores and auger holes along the length of the cross-section with an average thickness of approximately 3 m. West of vibracore Sh-3 the floodplain alluvium (FA) is underlain by a thin layer of fluvial bay-head delta silts and sands (FBD), with an average thickness of 0.2–1.2 m. The fluvial bay-head delta sediments (FBD) are in turn underlain by highstand estuarine silts and sands (ESS), while at the eastern end of the cross-section the estuarine sediments are directly overlain by floodplain alluvium (FA). Radiocarbon ages from articulated *A. stutchburyi* valves recovered in vibracore Sh-1 indicate that estuarine conditions prevailed in the area around Shannon, at the eastern end of the cross-section, from 8,300 cal. yr BP. The estuarine-alluvial transition most probably took place around 6850 cal. yr BP, as indicated by radiocarbon ages from *A. stutchburyi* valves in vibracore Sh-2 and auger hole H26. The estuarine silts and sands (ESS) are underlain by marine transgressive sands (MTS), penetrated at the base of vibracore Kop-1. Shallow estuarine conditions most likely prevailed in the lower part of the valley, around Koputaroa, approximately 5,900 cal. yr BP, as indicated by the radiocarbon age obtained from a disarticulated *A. stutchburyi* valve at the top of the marine transgressive sand (MTS) facies in vibracore Kop-1.

7.4.8 Sheet 31: Vibracores cross-section 8

Vibracores cross-section 8 (Sheet 31) intersects with, from south to north, vibracores cross-section 7 (Sheet 30), cross-section 6 (Sheet 29), cross-section 5 (Sheet 28), and cross-section 4 (Sheet 27). Floodplain alluvium (FA) is the uppermost facies penetrated by all the vibracores along the length of the cross-section. The average thickness of the floodplain alluvium (FA) is 1.5–4 m. North of vibracore Kop-2 the floodplain alluvium (FA) is underlain by fluvial bay-head delta silts and sands (FBD) of between 0.8–1.5 m thick. Beneath the fluvial bay-head delta silts and sands (FBD) lies 2–3.5 m of highstand estuarine sands and silts (ESS). Radiocarbon ages from several *A. stutchburyi* valves recovered in vibracores E1 and G indicate that shallow estuarine conditions prevailed in the middle and lower valley prior to 6,000 cal. yr BP, at which time the estuarine-alluvial transition occurred. The estuarine sands and silts (ESS) are in turn underlain by marine transgressive sands (MTS) of indeterminate thickness.

7.5 Summary

Detailed vibracores recovered from the lower Manawatu valley document the stratigraphic evolution of the valley during and following the Holocene marine transgression. Five distinct lithofacies were identified on the basis of sediment texture and colour, faunal assemblages, organic content, contact relationships and architecture, and were correlated between vibracores through a network of stratigraphic cross-sections. Marine transgressive sands (MTS) are confined to the lowest part of the valley. A highstand estuarine silt and sand facies (ESS) is found throughout the lower valley. Fluvial bay-head delta silts and sands (FBD) are restricted to the centre of the lower valley. Floodplain swampy silts (FSS) are located on the periphery of the valley, adjacent to box-shaped valleys in the Tokomaru Marine Terrace. Floodplain alluvium (FA) is the uppermost facies recognised in all vibracores recovered from the lower Manawatu valley. Shallow estuarine conditions prevailed in the upper valley from 8,300 cal. yr BP, and in the lower valley until 4,700 cal. yr BP. The timing of the estuarine-alluvial transition similarly differs depending upon in-valley location, from 6,800 cal. yr BP at the head of the valley and proximal to the Tokomaru Marine Terrace, to c. 4,700 cal. yr BP near the Whirokino Cut.

Chapter 8

Discussion and synthesis

8.1 Introduction

This synthesis chapter provides a wider context for a discussion of Holocene sea-level change on the Manawatu coast and the geomorphic evolution of the Manawatu incised-valley system (Figure 8.1). The chapter first reviews sea-level changes in the New Zealand region, to provide context for a discussion of sea-level changes on the southwest coast of the North Island. Sea-level index points from the Manawatu valley are then framed within this context. Subsidence mechanisms at a range of spatial and temporal scales are then discussed, to provide an explanation for the variation observed in the record of Holocene sea-level changes in the Manawatu valley. This is followed by a discussion which compares the sedimentary stratigraphy preserved in the lower Manawatu valley with established models of incised-valley infilling. The chapter then considers various aspects of the palaeogeomorphology of the Manawatu coastal plain, before drawing this information together to construct time-series palaeogeographic maps and conceptual models of the evolution of the Manawatu extending from the Last Glacial Maximum to the mid-Holocene.

8.2 Holocene sea-level change on the Manawatu coast

8.2.1 Holocene sea-level fluctuations in the New Zealand archipelago

Local-scale reconstructions of Holocene sea-level changes for areas within the New Zealand archipelago demonstrate a north-south lag in the timing of the attainment of PMSL, and also the timing of subsequent sea-level oscillations (Chapter 3). In the Auckland-Northland region, PMSL was attained c. 7,700 cal. yr BP, c. 1000 cal. yrs earlier than has been suggested for the New Zealand region as a whole (cf. Gibb, 1986). Approximately 200 cal. yrs later c. 7,500 cal. yr BP PMSL was attained in the southwest North Island. PMSL was attained in Pegasus Bay c. 7,100–6,600 cal. yr BP, and in East Otago c. 6,900 cal. yr BP

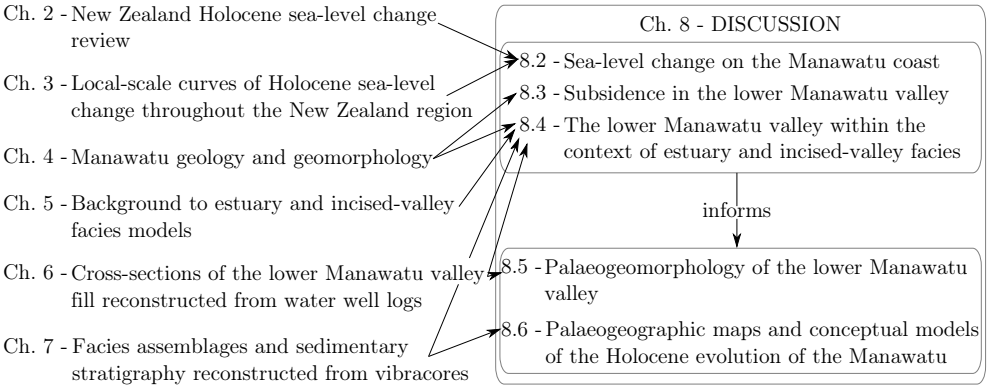

Figure 8.1: Conceptual diagram of the structure of the discussion chapter in relation to previous chapters.

(Figure 3.11). This confirms the suggestion by Clement et al. (2009a,b) that sea-level curves that consider the New Zealand region as a whole (e.g., Carter et al., 1986; Gibb, 1986; Clement et al., 2010) are obscuring local-scale sea-level changes. Local-scale reconstructions of Holocene sea-level fluctuations are therefore crucial for understanding the impact that these changes have had on the geomorphic evolution of landforms at this same scale and below.

8.2.2 Holocene sea-level changes on the south/southwest coast of the North Island

On the south/southwest coast of the North Island sea-level rose quickly from c. −16 m below PMSL c. 9,000 cal. yr BP, to c. −9.3 m below PMSL c. 8,400 cal. yr BP (Figure 8.2). By 8,300 cal. yr BP sea-level had reached c. −3 m below PMSL, rising to −1.5 m below PMSL c. 8,100 cal. yr BP. Present mean sea-level was attained c. 7,500 cal. yr BP, if not shortly before. This is approximately 200 years later than in the Auckland-Northland region, c. 400–900 years earlier than in Pegasus Bay and Christchurch, and c. 500 years earlier than on the East Otago Peninsula (Figure 3.11). Sea-level on the south/southwest coast of the North Island had risen to a maxima of c. +1.2 m above PMSL by 6,800 cal. yr BP. Sea-level then gradually fell from this maxima back to PMSL by c. 5,400 cal. yr BP. Sea-level briefly rose to +0.6 m above PMSL c. 4,700 cal. yr BP, but had fallen back to PMSL by c. 4,200 cal. yr BP. Sea-level on the south/southwest coast probably remained at PMSL until c. 3,700 cal. yr BP, before rising to +0.6 m above PMSL c. 3,350 cal. yr BP.

8.2.3 Indicators of Holocene sea-level change from the lower Manawatu valley

Indicators of Holocene sea-level change from the lower Manawatu valley show some considerable deviation from the sea-level history identified for the south and southwest coast of the North Island (Figure 8.2). It is particularly notable

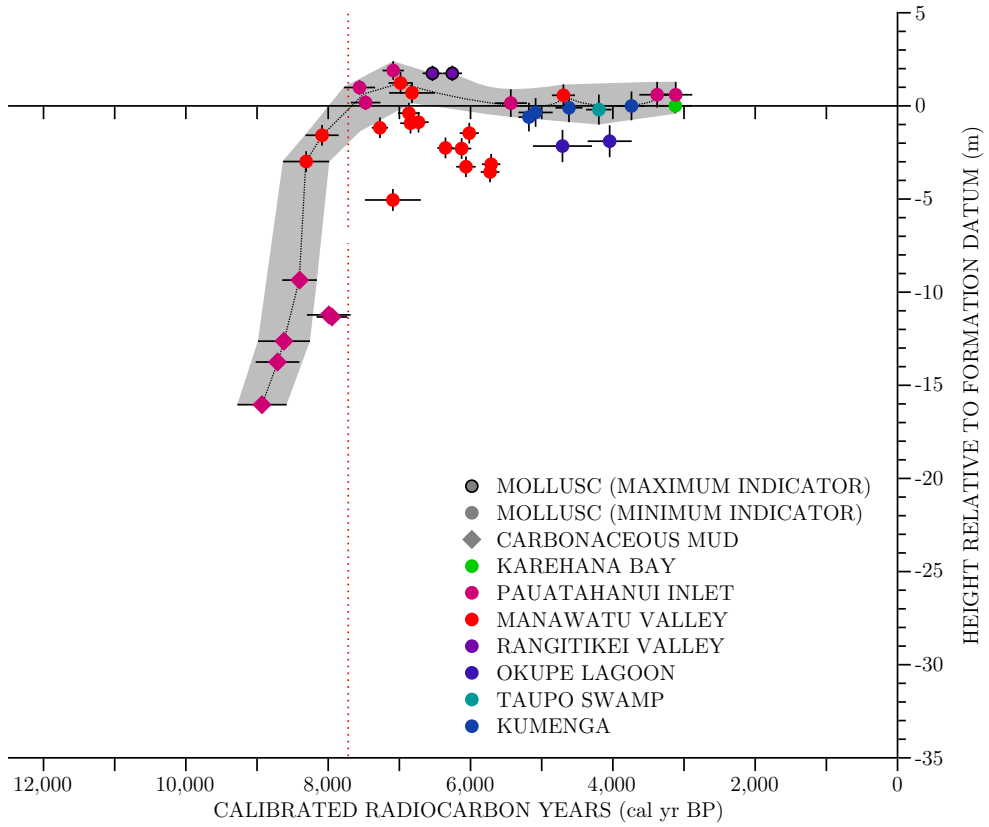

Figure 8.2: Holocene sea-level curve for the south/southwest coast of the North Island, New Zealand (cf. Figure 3.7). Sea-level index points have been colour-coded to indicate the specific location from which they were recovered (see Figure 3.1). The vertical red dotted line indicates 7,700 cal. yr BP, the approximate time PMSL was attained in the Auckland-Northland region.

that there appears to be a trend between 7,000–5,000 cal. yr BP for indicators to record a 'drop' in sea-level elevation with decreasing age. This is coincident with a fall in sea-level in the region from c. +1.2 m PMSL to present mean sea-level during this time period. However, the drop in sea-level elevation recorded by the indicators is nearly five times this amount. In addition, there appears to be a relationship between the elevations of the indicators and their position within the valley (Figure 8.3, Table 8.1). This phenomenon is therefore not being controlled by sea-level change, but is most likely the result of subsidence controlled by a range of mechanisms, and possibly complicated by the effects of local tectonism.

8.3 Subsidence in the lower Manawatu valley

While uplift has been identified in the upper Manawatu valley (e.g., Hesp and Shepherd, 1978; Litchfield and Berryman, 2007), the tectonic regime of the Manawatu coastal plain has been widely suggested to be subsiding due to

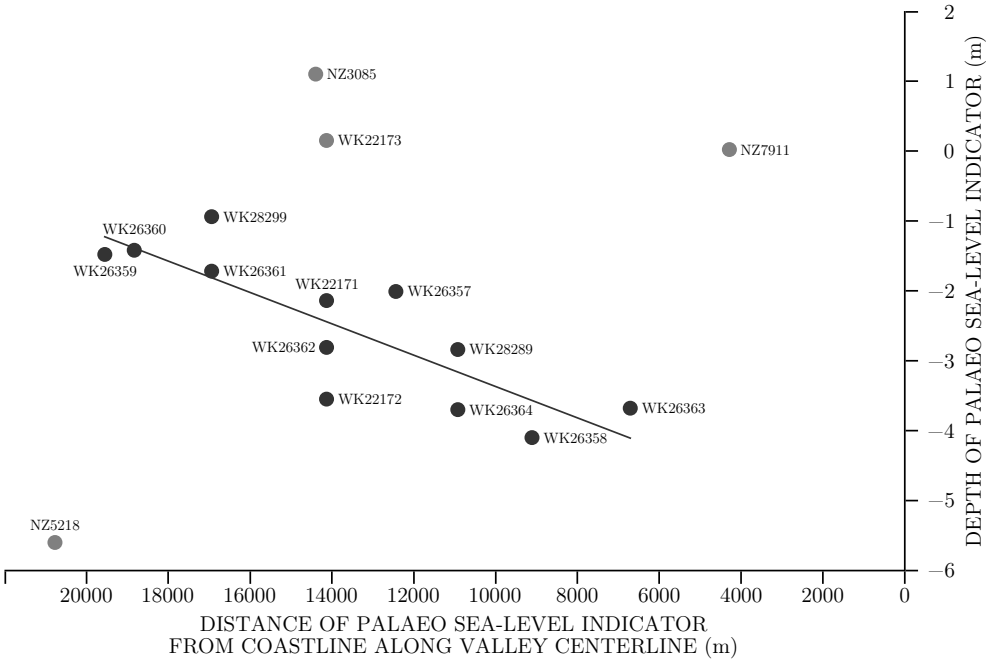

Figure 8.3: Graph illustrating the relationship between the elevations of sea-level index points recovered from the lower Manawatu valley (elevations as recovered, not adjusted to reflect palaeo sea-level) and the distance up valley from the present-day coastline measured against the valley centerline. The values used to construct this graph are presented in Table 8.1.

tectonic processes (e.g., Gibb, 1983; Pillans, 1986; Williams, 1991). However, there are a range of mechanisms beyond the tectonic which may be responsible for subsidence in the lower valley, such as sediment compaction, post-glacial water and sediment loading, the evolution of the Wanganui Basin, the influence of the Kairanga Trough, or any combination of these factors. Additionally, the overall effect of these drivers may be confused by local tectonism.

8.3.1 Sediment compaction

The post-depositional compression of Holocene sediments (sometimes referred to as autocompaction) is a widely observed phenomenon in coastal environments (e.g., Gehrels, 1999; Goodbred and Kuehl, 1999; Tornqvist et al., 2008; Mazzotti et al., 2009; Yuill et al., 2009; Bartholdy et al., 2010). Sediment consolidation can be significant in fine-grained organic rich sediments (e.g., Pizzuto and Schwendt, 1997; Haslett et al., 1998; Allen, 1999, 2000; Gehrels, 1999; Massey et al., 2006), with Holocene compaction ratios of c. 0.2–0.8 reported (e.g., Bloom, 1964; Kaye and Barghoorn, 1964; Belknap, 1975; Pizzuto and Schwendt, 1997; Hayward et al., 2002). Sea-level index points collected from thick sequences of unconsolidated intertidal sediments in estuaries and marshes are therefore likely to require correction to account for autocompaction (Allen, 1995, 2000; Gehrels, 1999; Shennan and Horton, 2002; Massey

Table 8.1: Details of the relationship between the elevations of sea-level index points recovered from the lower Manawatu valley and the distance up valley from the present-day coastline measured against the valley centerline.

Sample	Elevation relative to WVD'53 (m)	Distance from coast along valley centerline (m)
Wk22171	−2·14	14132·85
Wk22172	−3·55	14132·85
Wk22173	0·15	14132·85
Wk26357	−2·01	12438·45
Wk26358	−4·10	9112·10
Wk26359	−1·48	19551·85
Wk26360	−1·42	18830·55
Wk26361	−1·72	16940·62
Wk26362	−2·81	14132·85
Wk26363	−3·68	6711·71
Wk26364	−3·70	10925·67
Wk28289	−2·84	10925·67
Wk28299	−0·94	16940·62
NZ3085	1·10	14396·53
NZ5218	−5·60	20769·50
NZ7911	0·02	4286·59

et al., 2006). However, there is a current lack of applied theory and a shortage of models available to quantify the consolidation of Holocene sediments (e.g., Paul et al., 1995; Pizzuto and Schwendt, 1997; Paul and Barras, 1998; Rybczyk et al., 1998; Allen, 1999, 2000; Tovey and Paul, 2002; Williams, 2003; Bird et al., 2004; Massey et al., 2006).

In the lower Manawatu valley the estuarine/marine sediment overlying the LGM Ashhurst/Ohakea aggradation surface is up to 65 m thick (see Chapter 6). Therefore there is considerable potential for a drop in the elevation of palaeo sea-level indicators in the time since their emplacement. There is possibly a positive relationship between the depth of the estuarine fill and the depth of the palaeo sea level indicators relative to the sea-level history reconstructed for the southwest coast of the North Island (Figure 8.4, Table 8.2). However, this ignores differences in compaction rates due to different sediments or sediment constituents in different parts of the valley, and possible deformation of the LGM surface (see Section 8.3.4, below). A number of dated proxy sea-level indicators present as outliers, the deviation of which may be due to tectonic uplift proximal to the Tokomaru Marine Terrace (Sh-1, Sh-2, and H26; see Section 4.4), or the influence of the Kairanga Trough (Murray's Farm bore; see Section 8.3.4, below). A mechanism for the possible deviation of NZ7911 (M.J. Shepherd, unpublished data) is unclear. Overall, it seems certain that there has been some subsidence in the lower Manawatu valley due to sediment compaction, given how widespread the phenomenon is. However, given the current available data it is not possible to quantify rates of autocompaction. In addition, sediment compaction alone does not appear to account for the deviation in sea-level indicators from the expected sea-level history.

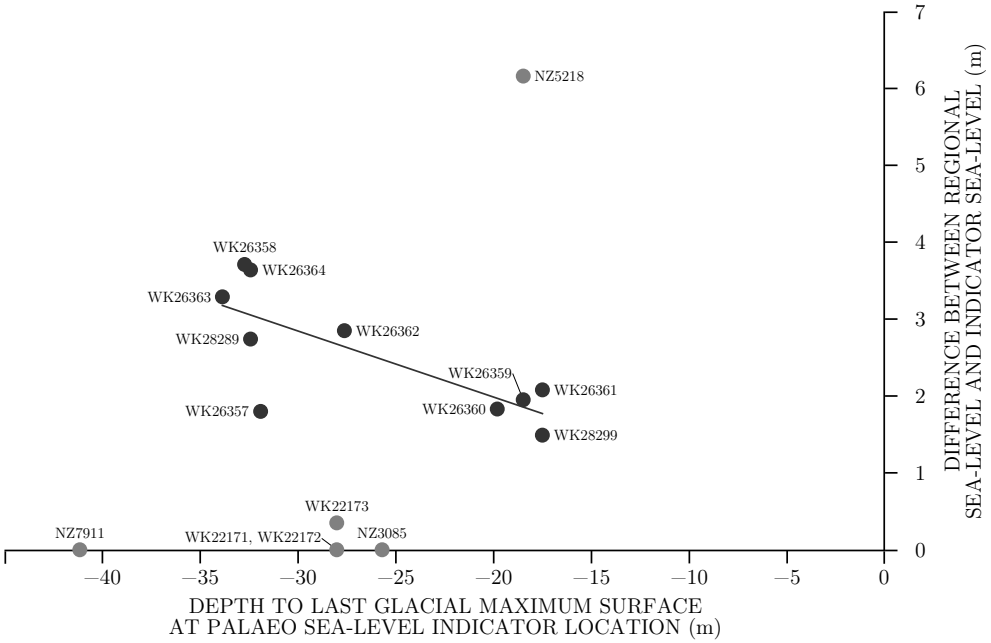

Figure 8.4: Graph illustrating the relationship for each palaeo sea-level indicator recovered form the lower Manawatu valley between the depth to the LGM Ashhurst/ Ohakea aggradation surface (below PMSL) at the location where the indicator was recovered, and the difference between the indicator's inferred palaeo sea-level and the sea-level inferred for the Manawatu region at that time. The values used to construct this graph are presented in Table 8.2.

8.3.2 Post-glacial water and sediment loading

The melting of ice-sheets in Antarctica and the Northern Hemisphere at the end of the LGM resulted in a rise in global sea-level of c. 120 m. This change in ocean volume resulted in hydro-isostatic loading on the continental lithosphere, warping it. The lithospheric response to the loading inundation is commonly investigated through the use of geophysical models that consider variables such as lithospheric thickness and upper and lower mantle rheology and viscosity. No such models have been produced for the New Zealand region.

While the continental shelf surrounding the southern North Island varies in size, it is unclear whether the differences are great enough to create a differential response to the hydro-isostatic loading produced during the Holocene marine transgression, particularly over such a relatively small area. It is more likely that the effect of post-glacial hydro-isostatic loading would be broadly similar across the whole of the southwestern coast of the North Island. Therefore, any effect of hydro-isostatic loading will be "built in" to all the palaeo sea-level indicators used to reconstruct Holocene sea-level on the southwest coast of the North Island. The drop in indicators from the lower Manawatu valley relative to the reconstructed regional sea-level history is accordingly most likely not attributable to hydro-isostatic subsidence.

8.3.3 Evolution of the Wanganui Basin

The Manawatu valley lies on the southeastern edge of the Wanganui Basin, a 200 by 200 km back-arc subsiding sedimentary basin extending from the central volcanic region in the north to the Marlborough Sounds in the south (Figure 4.2 Katz, 1968; Anderton, 1981; Katz and Leask, 1990). The South Wanganui Basin is the surface manifestation of a progressive, southward-travelling, lithospheric-scale downwarp resulting from high friction at the subduction interface between the Australian and Pacific Plates (e.g., Walcott, 1970; Stern and Davey, 1989; Stern et al., 1992, 1993; Wilson and McGuire, 1995). Subsidence of the basin was initiated during the Pliocene when the mass of the leading edge of the subducting Pacific Plate began to exert a net downward pull on the overlying lithosphere in locations where the plate is locked with the Australian Plate (Stern et al., 1992, 1993). The rate of subsidence of the basin since the Pliocene has been estimated at c. 1 m ka^{-1} (e.g., Wilson and McGuire, 1995; Journeaux et al., 1996; Kamp and McIntyre, 1998; Carter et al., 1999; Proust et al., 2005). Through the Plio-Pleistocene gradual movement of the basin depocenter from its position offshore from the Manawatu River mouth (Lewis et al., 1994) to the south and west caused emergence of the basin in the north, and produced a regional 4.5 degree southward tilt of the strata within the basin.

Subsidence in Holocene coastal environments due to the downwarping of the Wanganui Basin has been identified in the Nelson and Marlborough regions of the northern South Island by Hayward et al. (2010a,b). These regions are on the opposite side of the Wanganui Basin from the lower Manawatu valley. Accordingly, the rates of subsidence identified (0.55–1.05 m ka^{-1}) can not be applied in the Manawatu. However, the studies do confirm that subsidence of the Wanganui Basin can have an impact on Holocene sedimentary fill. Given the southwestward-dropping trend of the palaeo sea-level indicators recovered from the lower Manawatu valley (Figure 8.3), some of this drop may be due to the regional southward tilt of the Wanganui Basin strata.

8.3.4 Influence of the Kairanga Trough

The Kairanga Trough is a major structural depression west of Palmerston North City identified by Rich (1959) from analysis of the gravity anomaly pattern of the southern Wanganui Basin (Figure 8.5). Topographically the Kairanga Trough forms an elongate alluvial plain extending from Feilding south to Poroutawhao. The trough therefore bisects the floodplain of the Oroua River, and runs down the true right of the lower Manawatu valley (Figure 4.5). West of Palmerston North City the Kairanga Trough attains a maximum width of c. 16 km. Rich (1959) suggested that sediment at least 2.5 km thick lies at the centre of the downfold (cf. Anderton, 1981). The Kairanga Trough is an essentially unstudied feature of the eastern Wanganui Basin. Hughes (2005a,b) described a borehole drilled into the trough's Plio-Pliestocene fill near Levin. Aharoni (1991) presented the results of a seismic

Table 8.2: Details of the relationship for each palaeo sea-level indicator recovered form the lower Manawatu valley between the depth to the LGM Ashhurst/Ohakea aggradation surface (below PMSL) at the location where the indicator was recovered, and the difference between the indicator's inferred palaeo sea-level and the sea-level inferred for the Manawatu region at that time.

Sample	Sea-level indicator elevation relative to reconstructed sea-level at that time (m)	Depth to the LGM surface below PMSL at indicator location (m)
Wk22171	0·00	−28·02
Wk22172	0·00	−28·02
Wk22173	0·35	−28·02
Wk26357	1·80	−31·91
Wk26358	3·71	−32·74
Wk26359	1·95	−18·49
Wk26360	1·83	−19·81
Wk26361	2·08	−17·51
Wk26362	2·85	−27·63
Wk26363	3·29	−33·87
Wk26364	3·64	−32·43
WK28289	2·74	−32·43
Wk28299	1·49	−17·51
NZ3085	0·00	−25·71
NZ5218	6·16	−18·49
NZ7911	0·00	−41·16

reflection study which crossed the Levin Trough, which was suggested to be southern extension of the Kairanga Trough (Figure 4.6).

The reconstructed Ashhurst/Ohakea aggradation surface (Section 6.6) is generally lower on the western side of the Oroua and Manawatu floodplains, coincident with the axis of the Kairanga Trough (Figure 8.6). As a result the 0 m PMSL contour, which represents the possible maximum extent of estuary if the reconstructed LGM surface was inundated to PMSL, extends a considerable distance north, beyond the boundary of the reconstructed Holocene estuary (Figure 8.6). One possible explanation for this is that the reconstructed Ashhurst/Ohakea surface has been downwarped along the axis of the Kairanga Trough. This may explain why the *A. stutchburyi* valve dated by Shepherd and Lees (1987) from the bore at Murray's Farm is so much lower than the reconstructed sea-level curve (Figures 3.7 and 8.2), despite its position well up the valley (Figure 7.1).

Figure 8.5 *(facing page)*: Residual Bouguer anomaly map of the southern Wanganui Basin (after Rich, 1959). Contour interval is 5 milligals. 2.5 milligal contours interpolated. Base geological map constructed using data from Kingma (1962), Cowie et al. (1967), Pillans (1990a), Begg and Johnston (2000), Lee and Begg (2002), Townsend et al. (2008), and unpublished data from the QMAP project made available by D. Townsend.

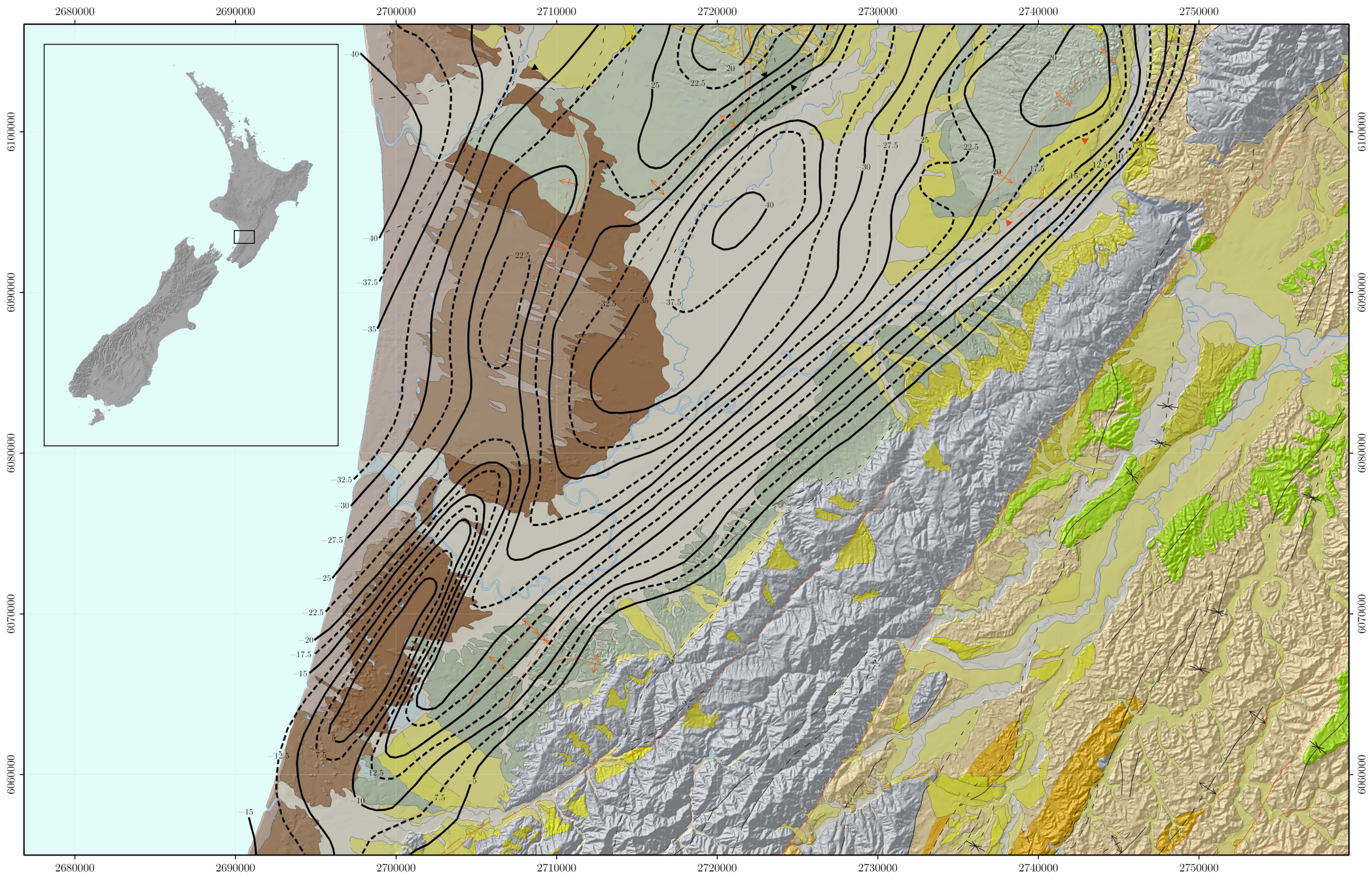
2680000
2690000
2700000
2710000
2720000
2730000
2740000
2750000
6100000
6090000
6080000
6070000
6060000
40
37.5
35
32.5
30
27.5
25
22.5
20
17.5
15
12.5
10
7.5
5

8.3.5 Influence of neotectonics

The effects of subsidence processes operating in the lower Manawatu valley may be confused by tectonic uplift along the margins of the axial ranges. Hesp and Shepherd (1978) suggested that the Tokomaru Marine Terrace, on the southern periphery of the valley, had been uplifted at an average rate of 0.35 mm yr^{-1} since the Last Interglacial. As noted in Chapter 4, the Tokomaru Marine Terrace is tilted along its length, rising from a low of +30 m above PMSL near Levin, to a high of over +90 m above PMSL north of Palmerston North City. Time-averaged uplift of the terrace therefore varies spatially from c. 0.14 mm yr^{-1} in the south, to c. 0.64 mm yr^{-1} in the north (assuming 8 m of cover beds and a Last Interglacial higher sea-level of +5 m above PMSL: see Section 4.4). In the valley upstream of Palmerston North City Litchfield and Berryman (2007) used the elevation of the LGM Ashhurst/Ohakea aggradation surface above the contemporary floodplain to estimate fluvial incision rates as a proxy for rock uplift. On this basis Litchfield and Berryman (2007) inferred an average uplift rate for the upper valley of 0.5 mm yr^{-1} over the past 18,000 years BP.

Uplift in the lower valley may be offsetting or counteracting subduction mechanisms, resulting in confusion of the effects of both processes. In analysis of the depths of palaeo sea-level indicators in the lower Manawatu valley (Figures 8.3 and 8.4), dated indicators proximal to the Tokomaru Marine Terrace are common outliers (Vibracores Sh-1, Sh-2, and auger H26). One possible explanation for the deviation is uplift of the indicators, either operating alone or in conjunction with, and to counteract or moderate, mechanisms of subsidence.

8.3.6 Subsidence in the Manawatu valley: conclusions

The reconstructed Holocene sea-level history for the southwest coast of the North Island clearly reveals that the lower Manawatu valley has subsided. Subsidence accounts for the apparent fall in sea-level of c. 5.6 m during the mid Holocene recorded by palaeo sea-level indicators in the lower Manawatu valley. Subsidence processes also account for the low elevation of mid-to-late Holocene floodplain alluvium deposited in the lower valley as identified on vibracores cross-sections 4–8 (Sheets 27–31).

There are a number of possible subsidence mechanisms that may have operated on and in the lower Manawatu valley. However, it is apparent that no single mechanism accounts for the subsidence seen across the valley. Instead,

Figure 8.6 *(facing page)*: Relationship of the Kairanga Trough to the reconstructed Ashhurst/Ohakea DEM, illustrating the depression of the LGM surface coincident with the axis of the trough. Base geological map constructed using data from Kingma (1962), Cowie et al. (1967), Pillans (1990a), Begg and Johnston (2000), Lee and Begg (2002), Townsend et al. (2008), and unpublished data from the QMAP project made available by D. Townsend.

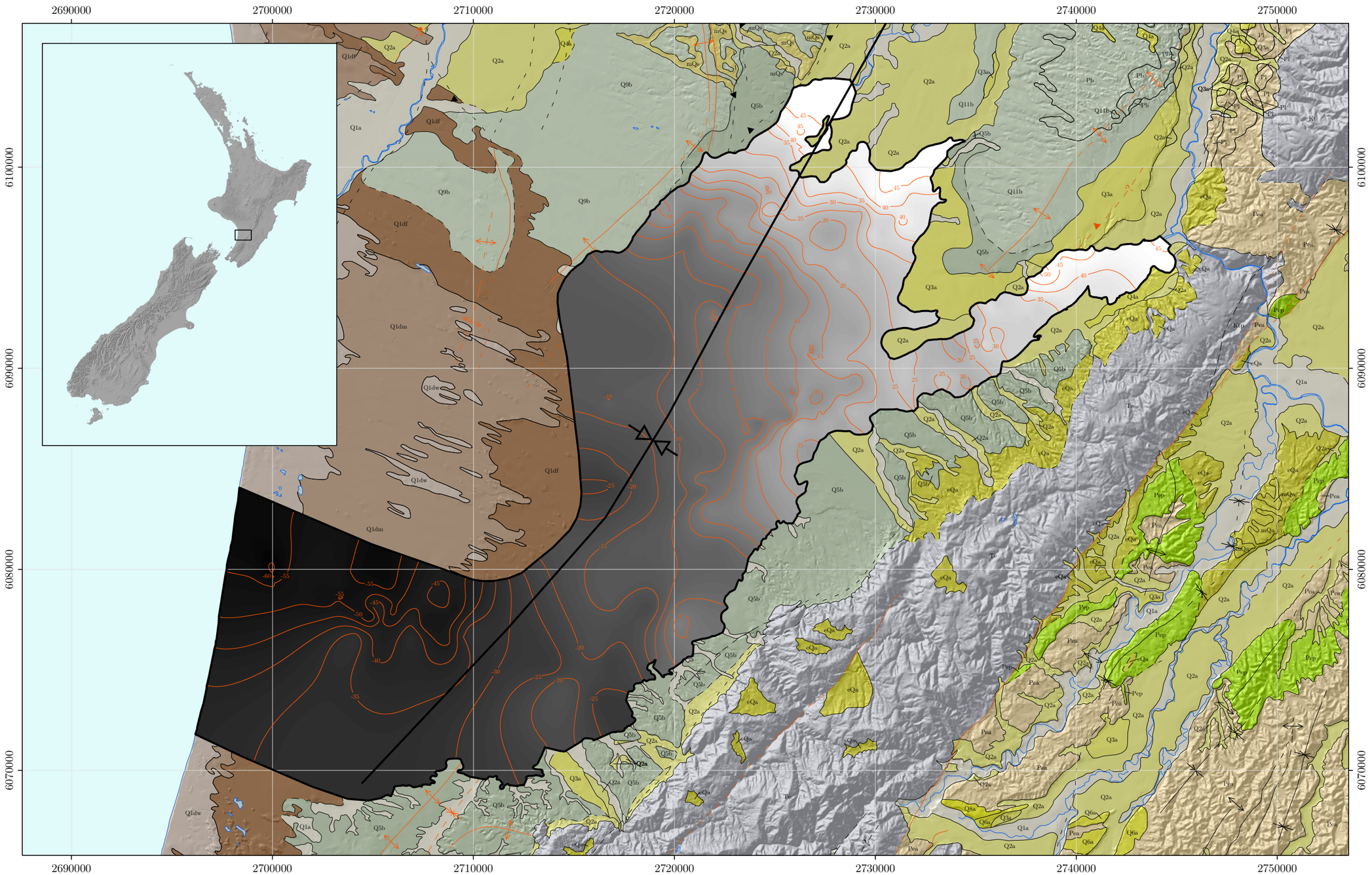
2690000
2700000
2710000
2720000
2730000
2740000
2750000
6100000
6090000
6080000
6070000

it appears that combinations of these mechanisms operating in different timescales, at different spatial scales, and at different rates and magnitudes, are responsible. Further, the individual and/or combined effects of these subsidence mechanisms appear to have been confused by tectonic uplift. Overall, the effect on the lower valley has been ongoing relative sea-level rise through the Holocene, contributing to the formation of accommodation space.

8.4 Comparisons of lower Manawatu valley stratigraphy to tripartite facies models of estuary and incised-valley infilling

8.4.1 Tripartite facies models of estuary and incised-valley infilling

The sedimentary fill of drowned incised-valleys is complex, reflecting the interplay between fluvial and marine processes in the marginal marine environment The application of facies analysis and sequence stratigraphic principles to estuarine deposits has contributed to a number of widely recognized "tripartite" facies models, which broadly differentiate between wave- and tide-dominated estuarine systems (e.g., Roy, 1984a,b; Dalrymple et al., 1992; Allen and Posamentier, 1993, 1994). These models laid the foundation for detailed investigations of the characteristics of the sedimentary infill of incised-valleys associated with transgressive and highstand conditions. Such infill processes manifest distinct bio-lithological facies associations suitable for the reconstruction of palaeo-depositional environments and sea-level histories (e.g., Heap and Nichol, 1997; Sloss et al., 2005, 2006a,b, 2007, 2010; Kennedy et al., 2008; Vis et al., 2008).

These established tripartite facies models recognize three to four broadly similar sedimentary environments. All models identify a fluvial/floodplain depositional environment including deltaic systems prograding into central receiving basins. For example, Dalrymple et al. (1992) recognize a fluvial delta environment at the head of the estuary, while (Allen and Posamentier, 1993, 1994) include a shoreface environment. The central portion of a drowned incised-valley system is occupied by a central basin facies consisting of fine-grained organic-rich silty mud deposited in a low energy back-barrier environment. At the seaward end of the system the tripartite facies models identify marine-influenced sediments, including barrier spit, back-barrier sand-flats, washover deposits, flood-tide delta and tidal inlet channel deposits.

The emphasis tripartite facies models place on the interplay between rising sea levels, sediment supply and the antecedent topography of the lowstand incised-valley is critical. Where the earlier work by Roy, Dalrymple and others has a strong emphasis on geomorphology, more recent work has a much stronger stratigraphic component (e.g., Heap and Nichol, 1997; Sloss et al., 2006a,b, 2007, 2010; Wilson et al., 2007). For example, the stratigraphy of an incised-valley will record the interaction between the rate at which accommo-

dation space is generated and the sedimentation rate. Therefore, transgressive facies will dominate valley fill where the relative sea-level rise exceeds the rate of sediment flux. Regressive facies prevail where the converse occurs (e.g., Curray, 1964; Boyd et al., 1992; Heap and Nichol, 1997; Sloss et al., 2006a,b, 2007, 2010). Under conditions of rising sea-level the tripartite models of valley fill predict that fluvial, estuarine basin and barrier environments will migrate landward, at which point, once the sea-level highstand is attained, the estuary progresses from an immature system with a larger amount of accommodation space to a more mature system that is largely infilled by fluvial sediment (Roy et al., 1980; Roy, 1994; Heap et al., 2004).

8.4.2 Comparisons of lower Manawatu valley stratigraphy with established models of incised-valley evolution

Following the model presented by Roy et al. (1980) the lower Manawatu River valley is anogalous to a drowned river valley estuary: a deeply incised valley with a wide deep-water entrance. Under the Dalrymple et al. (1992) model, the Manawatu valley would classify as a wave-dominated estuary (Chapter 5). As Wilson et al. (2007) noted, the case studies of Holocene incised-valley infill upon which the tripartite facies models are based commonly come from estuaries of extensive size (40–100 km in length) on relatively tectonically stable coastlines, with low river discharges (e.g., Dalrymple et al., 1992) and comparatively limited sediment supplies (e.g., Allen and Posamentier, 1993, 1994). However, the Manawatu valley is sited in a tectonically active landscape and is subject to large river flows and high sediment loads. It is therefore prudent to consider the extent to which the estuary evolution in Manawatu follows the tripartite evolutionary models.

Dalrymple et al. (1992) suggested that the lowstand fluvial deposits at the base of an incised-valleys sedimentary fill will be directly overlain by bay-head delta sediments that transgress up-valley with rising sea levels (see also Roy et al., 1980, 2001; Chapman et al., 1982; Roy, 1984a,b, 1994). In contrast, Sloss et al. (2005, 2006a,b, 2007) identified a transgressive sand sheet as the initial transgressive marine unit overlying the antecedent late-Pleistocene land surface in shallow incised-valleys. These transgressive sand sheets were deposited inside the incised-valleys when rising post-glacial sea levels breached Last Interglacial barriers at the valley mouths. Clement et al. (2010) noted that while the major source of sediment for mid-Holocene dune development adjacent to the lower Manawatu incised-valley is commonly cited as transgressive sands moved onshore by rising sea levels during the early Holocene, neither Hesp (1975) or Hesp and Shepherd (1978) recorded the presence of a sedimentary unit analogous to these transgressive sands in the lower Manawatu valley. The absence of similar sizeable transgressive units within the lower Manawatu valley may be due to the presence of the Poroutawhao High and Himitangi Anticline at the mouth of the valley, restricting marine inundation into the valley during the early stages of sedimentary infill. As a result any transgressive

facies may have been spatially restricted to the mouth of the valley (e.g., Roy et al., 1980, 2001; Chapman et al., 1982; Roy, 1984a,b, 1994; Dalrymple et al., 1992). Stratigraphic analysis of vibracores from the lower valley (Chapter 7) confirms that that marine transgressive sand facies is restricted to the lowest part of the valley. Given the dog-leg configuration of the valley and the prevailing northwesterly wind only this area of the valley would have been directly open to direct marine influences during the Holocene marine transgression. Another factor that may have resulted in restricting the transgressive phase of sedimentation is the high flow regime and sediment load of the Manawatu River (maximum flows of 4,500 m^3 s^{-1}; current sediment yield is 3.4 Mt yr^{-1}; see Chapter 4) which would have removed, reworked or otherwise obscured the transgressive facies by fluvial processes (cf. Wilson et al., 2007), with the infill system essentially operating as a depositional environment experiencing a forced regression.

The estuarine sand and silt facies identified in the Manawatu is similar to the estuarine mud facies detailed by Roy (1984a), the central basin mud facies described by Dalrymple et al. (1992), and the tidal estuarine sand and mud facies defined by Allen and Posamentier (1993, 1994). However, the facies described by Roy (1984a), Dalrymple et al. (1992), and Allen and Posamentier (1993, 1994) are predominantly muds and silts laid down in a deep central basin, while in the Manawatu valley sands are common, and even gravels are present.

Increasingly, studies of incised-valley fill in New Zealand demonstrate that the development and preservation of the central basin facies is affected by the combined effects of the allocentric controls of accommodation space, tectonism, sedimentation rate and sea-level behaviour (e.g., Heap and Nichol, 1997; Wilson et al., 2007; Abrahim et al., 2008; Kennedy et al., 2008). In Tamaki Estuary, Auckland, Abrahim et al. (2008) reported the absence of a central basin facies in a sequence that is otherwise broadly consistent with the idealised case of a wave-dominated incised valley system. This was attributed the restricted form ($\sim$500 m wide) of the incised-valley. In a study of the similarly narrow Pakarae River Estuary ($<$500 m wide), on the tectonically active Raukamarua Peninsula, on the east coast of the North Island, Wilson et al. (2007) documented poor preservation of central basin sediments. This poor preservation was attributed to rapid fluvial progradation into Pakaerae Estuary in direct response to coseismic uplift events, leading to the truncation of central basin deposits in the sedimentary sequence. Both Heap and Nichol (1997) and Kennedy et al. (2008), working in Weiti River Estuary and Whanganui Inlet respectively, reported stratigraphic records where high sedimentation rates, shallow valley form and lack of a seaward barrier have limited the development of a low-energy central basin.

In the Manawatu the deposition of estuarine sediment into the central basin was extremely short lived. Though the lower Manawatu valley is not particularly narrow, or prone to coseismic uplift events, it does possess an extremely high sediment load (although it is to a degree currently anthropogenically en-

hanced), similar to the situation described by Heap and Nichol (1997) and Kennedy et al. (2008). Clement et al. (2010) noted that both Hesp (1975) and Hesp and Shepherd (1978) documented an abrupt transition from estuarine tidal flats (equivalent to the central basin facies) to alluvium; neither described an intermediary bay-head delta sequence. It was therefore posited that the bay-head delta facies may be missing from the lower Manawatu valley, perhaps due to reworking by fluvial processes. Alternatively, Clement et al. (2010) suggested that rapid and high rates of sediment delivery by the Manawatu River may have denied bay-head delta formation, as swift infill of the central basin eliminated the necessary accommodation space, thereafter leading to sediment bypass. However, the vibracores recovered from the lower Manawatu valley (Chapter 7) clearly reveal a bay-head delta prograding down the valley; however it is identified only intermittently. Whether this is a consequence of rapid sedimentation and sediment bypass or the bay-head delta moving about the valley as it prograded is unclear. However, this does not alter the conclusion regarding the impact of rapid sediment delivery by the Manawatu River during the mid to late Holocene. The Manawatu incised-valley infilled extremely quickly, and the estuary's central basin was a very short-lived feature. Tidal flats were therefore the dominant estuarine sedimentary environment in the Manawatu incised-valley after the mid-Holocene sea-level highstand.

Models of incised-valley and wave-dominated estuary infilling identify a number of sedimentary features at their seaward end, such as barriers, flood-tide deltas, and inlet complexes (e.g., Roy et al., 1980; Roy, 1984a,b; Dalrymple et al., 1992; Zaitlin et al., 1994). The existence of such features at the lower end of the Manawatu valley remains unclear, principally because they cannot be reliably identified in the water well logs (see Chapter 6), while the vibracores from the lower valley do not penetrate deep enough into the sedimentary infill to identity such features (Chapter 7). Low energy estuarine conditions were present in the lower valley in the mid-Holocene, as evidenced by the presence of articulated *A. stutchburyi* valves. This would not necessarily be expected, given the configuration of the valley and the dominant northwesterly wind direction. A barrier must have formed at the mouth of the incised-valley following the Holocene sea-level highstand, restricting marine influences in the lower part of the valley. Alternatively, progradation of the coast west of the Himitangi Anticline and Poroutawhao High may have narrowed the estuary entrance, similarly restricting marine incursions into the lower valley.

8.5 Last Glacial Maximum and Holocene palaeogeomorphology of the lower Manawatu valley

8.5.1 Path of the Manawatu River 18,000–15,000 years BP

The path of the Manawatu River during the Last Glacial Maximum, c. 18,000–15,000 years BP, can be identified by the presence of Ashhurst/Ohakea gravels in water wells drilled across the Manawatu coastal plain (Figure 6.16). Such

an interpretation is, however, limited by the issues with well log accuracy and interpretation outlined in Chapter 6. During the LGM the Manawatu and Oroua Rivers occupied the full breadth of available floodplain upstream of their confluence at Rangiotu. Below Rangitotu, the Manawatu River appears to have run to the east of its current channel, from Opiki directly south to Makerua. From Makerua, the gravel signature indicates that the Manawatu River turned to the northeast, running through Moutoa and Marotiri straight to Foxton Beach. This places the path of the Manawatu River during the LGM between 2–6 km north of its present day course.

8.5.2 Role of the Poroutawhao High and the Himitangi Anticline at the height of the Holocene marine transgression

The Poroutawhao High and Himitangi Anticline are widely believed to have restricted major marine incursions into the estuary occupying the lower Manawatu valley at the height of the Holocene marine transgression (e.g., Te Punga, 1953a; Rich, 1959; Hesp, 1975; Hesp and Shepherd, 1978; Heerdegen and Shepherd, 1992). The Poroutawhao High most certainly provided some protection to the lower valley, particularly near Koputaroa (e.g., Sewell, 1991). However, the role of the high must have been limited to this area, as it does not extend north beyond Koputaroa (see Chapter 6, Sheet 20: well logs cross-section 20). Far more important, given the dog-leg configuration of the lower Manawatu valley (Figure 6.17) and the dominant northwesterly wind direction (Figure 4.13), is the role of the barrier in the vicinity of Himitangi.

Hesp (1975) and Hesp and Shepherd (1978) have attributed a barrier here to the Himitangi Anticline. However, the role of a buried reverse-fault structure (cf. Anderton, 1981; Melhuish et al., 1996; Jackson et al., 1998; Lamarche et al., 2005; Clement and Brook, 2008) as the driver behind a barrier is impossible to ascertain without a geophysical study. What is clear from well logs cross-section 9 (Sheet 9, see also Section 6.5.8.1), and the investigations by Rich (1959), Hesp (1975), and Sewell (1991), is that there is a large body of probably Pleistocene-age sand in the vicinity of the Himitangi Anticline. This sandy body may have been deposited during the Last Interglacial, coincident with the formation of the Tokomaru Marine Terrace. Alternatively, the sand body may have been deposited at the same time as the MIS 9 marine terrace a short distance to the north at Carnavon (Figure 4.4). Rich (1959) dug a pit within the dune country 7.2 km northeast of Himitangi. Silts and marine microfauna were documented in the pit, which were considered to be equivalent in age to the Otaki Formation which constitutes the Tokomaru Marine Terrace (Rich, 1959).

The sand barrier at Himitangi influenced the environment in the Manawatu estuary following the culmination of the Holocene marine transgression, by protecting the estuary from the prevailing northwesterly winds and limiting or preventing marine incursions. The vibracores recovered from the lower valley record a low energy estuary environment (Chapter 7), as does the borehole

recorded by Shepherd and Lees (1987) at Murray's Farm. Additionally, both Hesp (1975) and Hesp and Shepherd (1978) identified a low energy estuarine environment at Shannon, which would have been directly open to marine influences if there had not been a barrier in the vicinity of Himitangi.

8.5.3 Extent of the Manawatu estuary at the height of the Holocene marine transgression

The extent of the estuary which occupied the lower Manawatu valley at the height of the Holocene marine transgression on the southwest coast of the North Island, c. 7,500 cal. yr BP, can be identified by the presence of estuarine sedimentary facies in well logs, vibracores and auger holes drilled across the Manawatu coastal plain (Figure 6.22). In the south the estuary abutted the Tokomaru Marine Terrace, while in the north the estuary was restricted by the Plio-Pleistocene sand body in the vicinity of Himitangi. Up-valley the estuary extended to Opiki and across to the Tokomaru Marine Terrace between Tokomaru and Linton.

Hesp and Shepherd (1978) suggested that cutting of the cliffed face of the Tokomaru Marine Terrace in this area took place during the early stages of estuary formation during the Holocene marine transgression. Shepherd and Lees (1987) and Heerdegen and Shepherd (1992) also placed the upper limit of the estuary at Opiki. In contrast Rich (1959), Fair (1968), and Hesp (1975) all placed the limit of the estuary progressively farther and farther up the valley (Figure 4.14). Both Rich (1959) and Fair (1968) placed the limit of the estuary in the vicinity of Tiakitahuna, as they considered the Tokomaru Marine Terrace to represent the shoreline at the height of the most recent marine transgression. Hesp (1975) suggested that the upper limit of the estuary lay at Palmerston North City, due to the misidentification of Pleistocene-age shells found in a bore at Awahuri (Te Punga, 1954a) as being of Holocene age.

The presence of the upper limit of the Holocene estuary at Opiki may explain the change in behaviour of the Manawatu River at this location. Upstream of Opiki the Manawatu River channel has a relatively steep slope (0.0012), is gravel bedded, and has a sinuosity of 1.4 (Page and Heerdegen, 1985). Downstream of Opiki the channel gradient lessens to 0.0002. As a result of the reduction in stream power the river no longer has the competency to transport gravel, and becomes sand-bedded. The change in gradient and resulting change in character is therefore most likely due to the river transitioning from the comparatively high gradient supported by the underlying Ashhurst/Ohakea aggradation surface, and the effectively zero gradient presented by the underlying estuarine sediment.

8.5.4 Manawatu coastline at the height of the Holocene marine transgression

Since the attainment of present mean sea-level on the southwest coast of the North Island, large quantities of sediment sourced from rivers to the north

have been delivered to the Manawatu by southward-dominant littoral drift (Fleming, 1965, 1972; Gibb, 1977, 1979; Muckersie and Shepherd, 1995) enabling progradation of the coast. North of the Manawatu at Tangimoana, Shepherd et al. (1986) and Heerdegen and Shepherd (1992) suggested that the coast had prograded c. 4 km since the culmination of the Holocene marine transgression (Figure 6.2). South of Levin it has been widely posited that the coast has prograded c. 2–3 km (e.g., Fleming, 1965, 1972; Te Punga, 1962; Gibb, 1978; Barnett, 1984; Palmer et al., 1988; Hawke and McConchie, 2005, 2006).

In the Manawatu Heerdegen and Shepherd (1992) and Muckersie and Shepherd (1995) suggested that c. 4 km of coastal progradation occurred following the culmination of the Holocene marine transgression. This is less than the amount suggested by Rich (1959) and Hesp (1975), who inferred that the amount was closer to 5–6 km. Well-log cross-section 9 (Sheet 9), which crosses the Himitangi barrier north of the Manawatu River mouth, supports this greater amount of coastal progradation (see Section 6.5.8.1). A chronology for the progradation of the coast has not yet been forwarded, beyond simple time-averaged rates for the period since the attainment of present mean sea-level.

8.5.5 Infilling of the Manawatu estuary 8,000 cal. yr BP to present

A chronology for the development and infilling of the Manawatu estuary during and following the Holocene marine transgression can be reconstructed from radiocarbon ages from articulated bivalves recovered in vibracores from the lower Manawatu valley (Figures 8.7 and 8.8). During the period of initial sea-level rise, between 9,000–7,000 cal. yr BP (Figures 3.7, 8.2; Chapter 3), a low energy intertidal estuarine environment was established in the vicinity of

Figure 8.7 *(facing page)*: Positions of radiocarbon dated shell and wood samples recovered from the lower Manawatu valley (1:100,000 scale). Sample details are presented in Table 7.3. Elevations given are relative to Wellington Vertical Datum 1953. Vibracores are identified on Figure 7.1. Base geological map constructed using data from Kingma (1962), Cowie et al. (1967), Pillans (1990a), Begg and Johnston (2000), Lee and Begg (2002), Townsend et al. (2008), and unpublished data from the QMAP project made available by D. Townsend.

Figure 8.8 *(page 246)*: Locations of palaeo shorelines in the lower Manawatu valley (a) during the late stages of the Holocene marine transgression prior to the peak in sea levels c. 6,800 cal. yr BP (red dashed lines); (b) following the culmination of the Holocene marine transgression c. 6,800 cal. yr BP (black dashed lines) (1:100,000 scale). Base geological map constructed using data from Kingma (1962), Cowie et al. (1967), Pillans (1990a), Begg and Johnston (2000), Lee and Begg (2002), Townsend et al. (2008), and unpublished data from the QMAP project made available by D. Townsend.

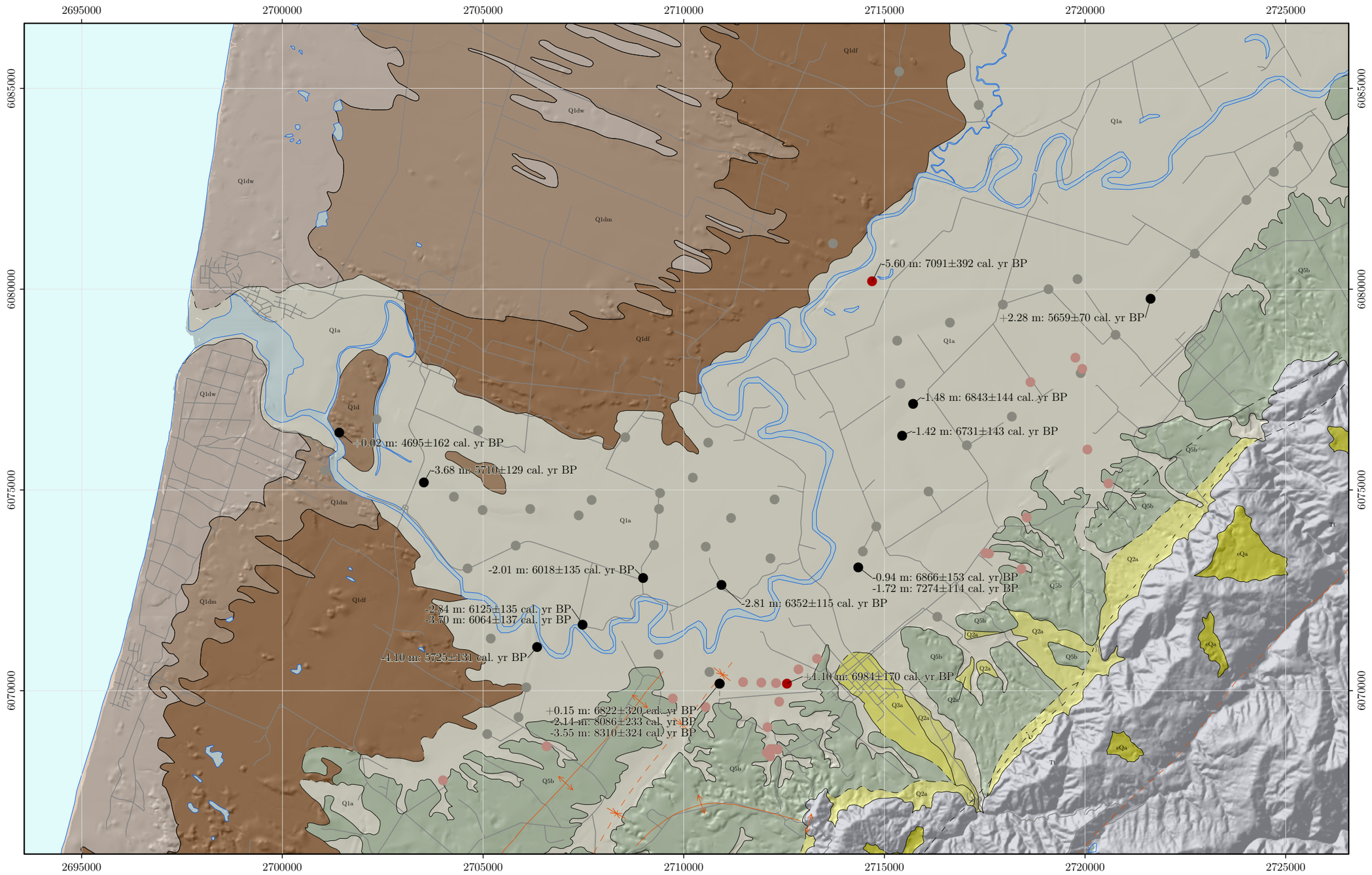
2695000
2700000
2705000
2710000
2715000
2720000
2725000
6085000
6080000
6075000
6070000
Q1dw
Q1dm
Q1df
Q1a
Q1d
Q5b
Q2a
Q3a
eQa
Tr
-5.60 m: 7091±392 cal. yr BP
+2.28 m: 5659±70 cal. yr BP
-1.48 m: 6843±144 cal. yr BP
-1.42 m: 6731±143 cal. yr BP
+0.02 m: 4695±162 cal. yr BP
-3.68 m: 5710±129 cal. yr BP
-2.01 m: 6018±135 cal. yr BP
-0.94 m: 6866±153 cal. yr BP
-1.72 m: 7274±114 cal. yr BP
-2.81 m: 6352±115 cal. yr BP
-2.84 m: 6125±135 cal. yr BP
-3.70 m: 6064±137 cal. yr BP
-4.10 m: 5725±131 cal. yr BP
+4.10 m: 6984±170 cal. yr BP
+0.15 m: 6822±320 cal. yr BP
-2.14 m: 8086±233 cal. yr BP
-3.55 m: 8310±324 cal. yr BP

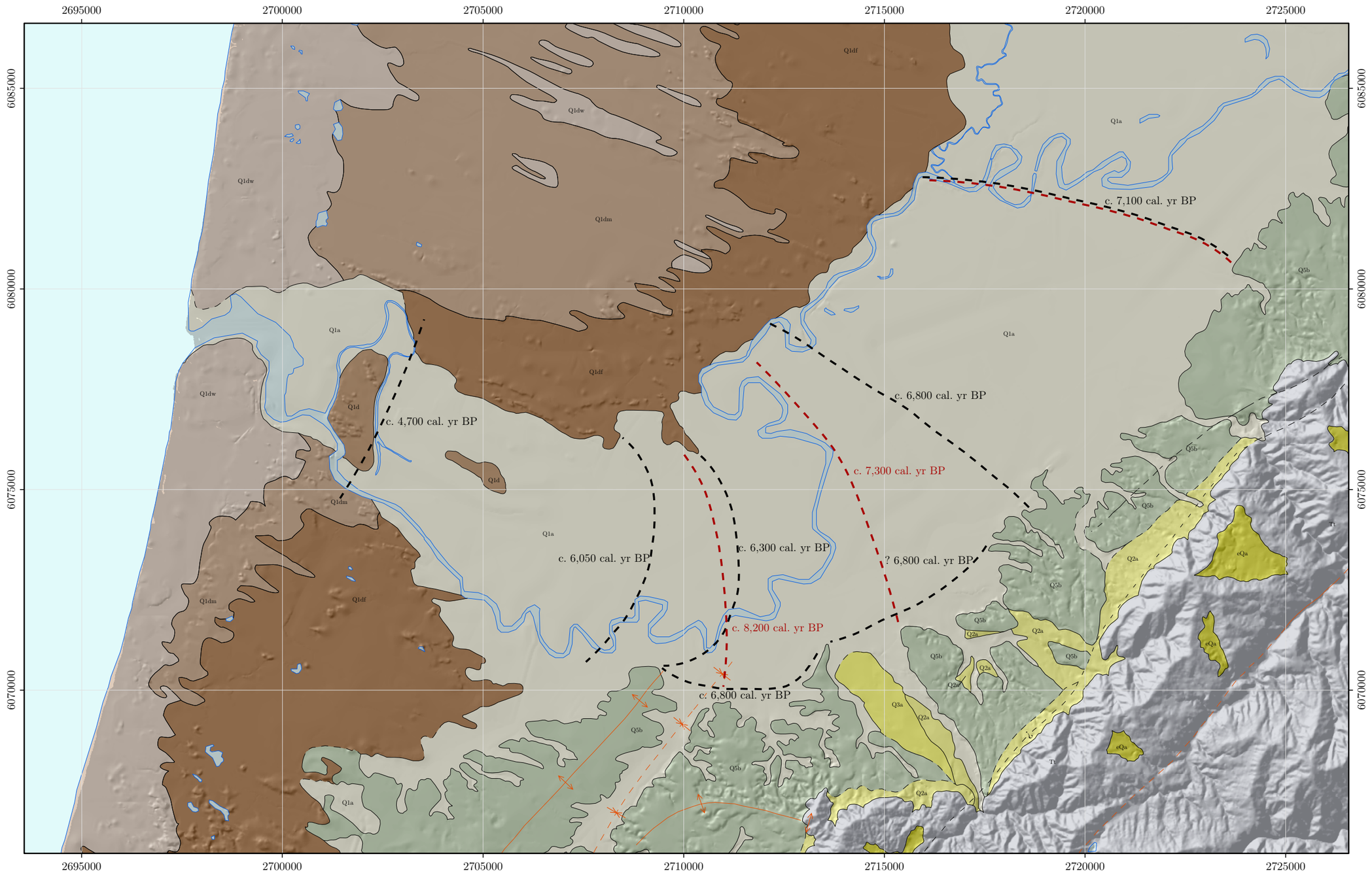
2695000
2700000
2705000
2710000
2715000
2720000
2725000
6085000
6080000
6075000
6070000
Q1dw
Q1dm
Q1df
Q1a
Q1d
Q5b
Q2a
Q3a
eQa
Tr
c. 7,100 cal. yr BP
c. 6,800 cal. yr BP
c. 4,700 cal. yr BP
c. 7,300 cal. yr BP
c. 6,300 cal. yr BP
c. 6,050 cal. yr BP
? 6,800 cal. yr BP
c. 8,200 cal. yr BP
c. 6,800 cal. yr BP

Shannon township c. 8,200 cal. yr BP (Figures 8.7 and 8.8; cf. vibracores Sh-1, Sh-2, Sheet 27: vibracores cross-section 7). As sea levels rose the shoreline migrated up the valley. By 7,300 cal. yr BP sea-level rise had inundated the valley below vibracore Cut-7, southwest of Makerua (WK26361, Table 7.3; Figure 8.7). The valley shoreline at the time PMSL was attained (c. 7,500 cal. yr BP) was therefore somewhere in the vicinity of Shannon and Moutoa. The maximum extent of the estuary was reached c. 7,100 cal. yr BP, c. 300 years before postglacial sea levels peaked at c. +1.2 m above PMSL c. 6,800 cal. yr BP (Figure 8.8). This shoreline lies north of the Murray's Farm bore (Figures 8.7 and 8.8; Shepherd and Lees, 1987). However, the radiocarbon age determination from the *A. stutchburyi* valve recovered at Murray's Farm (NZ5218, Shepherd and Lees, 1987) has a considerable error range of c. ±390 cal. yrs (Table 7.3). The maximum extent of the estuary could therefore coincide with the peak in sea-level c. 6,800 cal. yr BP.

Radiocarbon dated *A. stutchburyi* valves recovered from vibracores Cut-2 and Cut-4 suggest that the Manawatu valley began infilling between 7,100–6,800 cal. yr BP, during the final stages of the Holocene marine transgression (Figures 8.7 and 8.8). This implies that at this time considerable volumes of sediment were being delivered into the estuary by the Manawatu River, sufficient to infill the still increasing accommodation space at the head of the palaeo estuary. As a result, by 6,800 cal. yr BP the valley shoreline would have shifted down valley to lie north of vibracores Cut-2 and Cut-4 (Figures 8.7 and 8.8; cf. Chapter 7, Sheet 23: vibracores cross-section 3). However, it must be recognised that the radiocarbon ages from Cut-2, Cut-4 and the Murray's Farm bore are, as a result of the calibration to sidereal years, statistically similar. This infilling could therefore be an artefact of the sidereal age error.

Coincident with the valley shoreline being shifted down valley to Cut-2 and Cut-4 c. 6,800 cal. yr BP, radiocarbon dates of similar age east of Shannon, c. 8 km farther down the valley (vibracore Sh-1, auger H26; Hesp and Shepherd, 1978) indicate that sediment eroded from the Tokomaru Marine Terrace accelerated infilling of the valley in this area (Figures 8.7 and 8.8). By 6,350 cal. yr BP the centre of the valley had been infilled down to vibracore Cook-2, resulting in one contiguous shoreline east of Shannon (Figures 8.7 and 8.8). Over the next c. 300 years infilling shifted the valley shoreline west, to run approximately north-south from Marotiri to the vicinity of vibracores G, and E1 and E2 c. 6,050 cal. yr BP (Figures 8.7 and 8.8).

Radiocarbon dates from *A. stutchburyi* valves in vibracores Kop-1 and Flood-1 suggest that an estuarine tidal flat environment was established in the vicinity of the Moutoa Floodway from c. 5,700 cal. yr BP (Figures 8.7 and 8.8). The radiocarbon age obtained from an *A. stutchburyi* valve exposed in the Whirokino Cut (NZ7911; Table 7.3; M.J. Shepherd, unpublished data) indicates that infilling of this basin took approximately 1,000 cal. yrs. In contrast, infilling of the valley up until this time had taken only c. 1,100 cal. yr (Figures 8.7 and 8.8). This slower rate of infilling may have been due to relative sea-level rise due to a combination of subsidence mechanisms

(Section 8.3). Alternatively, sediment may have been directly bypassing the basin, as the valley configuration suggests that the basin would have been open to the Tasman Sea. Also, the geomorphology of the Poroutawhao area at this time is unclear. There may have been considerable unfilled accommodation in the vicinity of Poroutawhao, which may have acted as a sink for sediment from the Manawatu River.

The evolution of the valley west of the Whirokino Cut after 4,700 cal. yr BP is unclear. Certainly the coast would have continued to prograde, possibly constricting the mouth of the estuary. Analysis of DEMs of the LGM aggradation surface and the top of the estuarine infill suggests that the total volume of estuarine fill deposited in the lower Manawatu valley since the culmination of the Holocene marine transgression is approximately 8.7 km^3.

8.5.6 Sedimentation rates in the lower Manawatu valley following the culmination of the Holocene marine transgression

Given the estimated volume of marine/estuarine sediment deposited in the lower valley (Section 6.6.3, Table 6.2), and the estimated extent of the palaeo estuary (c. 272 km^2), it is possible to estimate a time and area averaged estuarine sedimentation rate for the lower valley of 4.54 m ka^{-1}. This is quite high, compared to the minimum rates of estuarine sedimentation estimated from radiocarbon dated bivalves recovered in the vibracores (Table 8.3). However, the rates estimated from the vibracores are minimum rates, and are likely to have been significantly underestimated due to the effects of sediment compaction (see Section 8.3.1). Similarly, it is possible to estimate a time and area averaged rate of alluvial sedimentation for the valley of 1.43 m ka^{-1}. This is very similar to the rate of alluvial deposition estimated by Shepherd and Lees (1987) at Murray's Farm (1.5 m ka^{-1}).

8.6 Palaeogeographic maps and conceptual models of the Holocene evolution of the lower Manawatu incised-valley system

8.6.1 18,000–9,000 years BP

During the Last Glacial Maximum sea levels in the New Zealand region were approximately 120 m lower than present (Figure 4.12; e.g., Pinter and Gardner, 1989; Cutler et al., 2003). As a result, the Manawatu shoreline would have shifted well to the south, somewhere in the modern vicinity of Cook Strait (e.g., Te Punga, 1953a; Fleming, 1962; Proctor and Carter, 1989; Mountjoy et al., 2009). At this time the Manawatu River was gravel-bedded and braided (Clement and Fuller, 2007). The Manawatu River flowed from the Manawatu Gorge, southwest across the upper Manawatu floodplain (Figures 8.9 and 8.10). The confluence with the Oroua River was possibly farther east

Table 8.3: Details of estuarine sedimentation rates calculated for vibracores recovered from the lower Manawatu valley. Details of radiocarbon ages are presented in Table 7.3. Vibracore details are presented in Table 7.1.

Vibracore	Upper sample elevation (m)	Lower sample elevation (m)	Upper sample youngest cal. age	Lower sample oldest cal. age	Elevation range (m)	Maximum age range (cal. yrs)	Minimum sedimentation rate (m ka^{-1})
Sh-1	2·14	3·55	7853	8634	1·41	781	1·81
G	2·84	3·70	5989	6206	0·86	217	3·96
Cut-7	0·94	1·72	6713	7388	0·78	675	1·16

than its present location. The Himitangi Anticline was overlain by a large Plio-Pleistocene sand body, which extended from Foxton north to Camarvon, just south of the Rangitikei River (Figures 8.9 and 8.10; e.g., Rich, 1959; Hesp, 1975; Hesp and Shepherd, 1978; Sewell, 1991; Heerdegen and Shepherd, 1992; Hughes, 2005a,b). In the south the Poroutawhao High formed the core of an elongate hill extending from Poroutawhao south to Levin. The Manawatu River flowed south from Opiki in the depression created by the Kairanga Trough, before turning and flowing out onto the continental shelf through the pass between the Himitangi Anticline and the Poroutawhao High (Figures 8.9 and 8.10). The passage of the river in the vicinity of Foxton and Foxton beach was most likely approximately 2–6 km north of its present-day path. South of the river, at Koputaroa, a large area of transgressive dunes formed as sand was mobilised from exposed sand bars of the Manawatu River. Tributaries of the river dissected the relict Tokomaru Marine Terrace (Figures 8.9 and 8.10).

8.6.2 9,000–6,800 cal. yr BP

By 7,100 cal. yr BP sea levels had risen to c. +1 m above PMSL, inundating the lower Manawatu valley. At its maximum extent the estuary that formed extended inland to the vicinity of Opiki. West of the Himitangi Anticline the coastline ran approximately 5–6 km inland from its present day position. South, at Poroutawhao the coastline would have run flush along the western flank of the bedrock high (Figures 8.11 and 8.12). The anticline and bedrock high therefore formed a barrier between the estuary and the Tasman Sea, protecting the lower valley from marine influences. Southwest of Shannon the face of the Tokomaru Marine Terrace was cliffed by waves. Valleys cut into the terrace by tributary streams of the Manawatu River were flooded, initiating the formation of box-shaped valleys (e.g., Cotton, 1918; Hesp, 1975; Hesp and Shepherd, 1978). By 6,800 cal. yr BP the large volumes of sediment delivered to the estuary by the Manawatu River had caused the valley shoreline to have prograded down the valley to Makerua (Figures 8.11, 8.12, and 8.13). At the

Figure 8.9 *(following page)*: Palaeogeographic map of the lower Manawatu valley during the Last Glacial Maximum, c. 18,000–15,000 years BP (1:100,000 scale).

Figure 8.10 *(page 252)*: Conceptual model of the geomorphology of the lower Manawatu valley during the Last Glacial Maximum, c. 18,000–15,000 years BP.

Figure 8.11 *(page 253)*: Palaeogeographic map of the lower Manawatu valley, c. 7,100–6,800 cal. yr BP (1:100,000 scale).

Figure 8.12 *(page 254)*: Conceptual model of the geomorphology of the lower Manawatu valley, c. 7,100 cal. yr BP.

Figure 8.13 *(page 255)*: Conceptual model of the geomorphology of the lower Manawatu valley, c. 6,800 cal. yr BP.

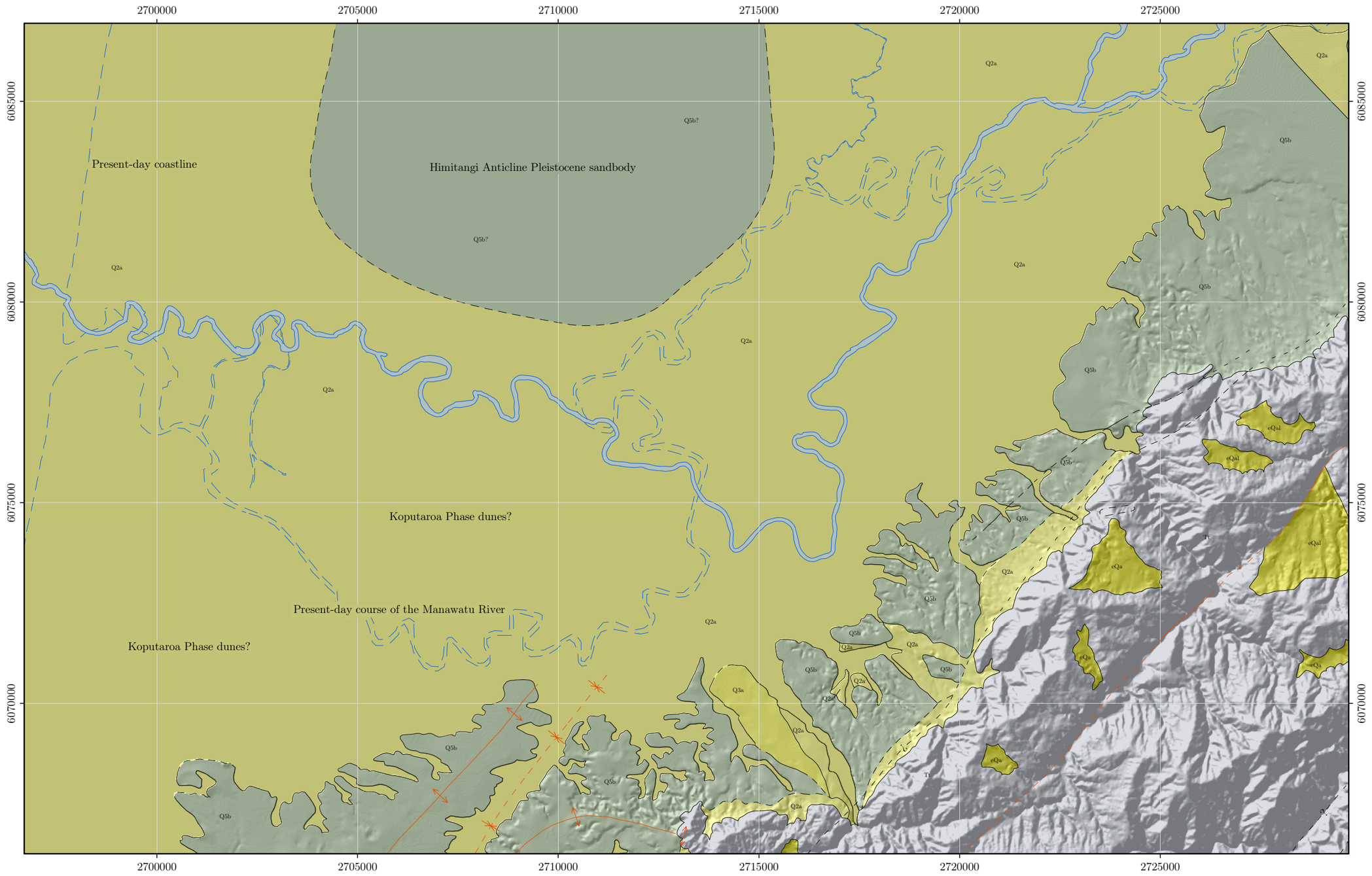
2700000
2705000
2710000
2715000
2720000
2725000
6085000
6080000
6075000
6070000
Present-day coastline
Himitangi Anticline Pleistocene sandbody
Koputaroa Phase dunes?
Present-day course of the Manawatu River
Koputaroa Phase dunes?
Q5b?
Q2a
Q5b
eQa
eQal
Tr
Q3a

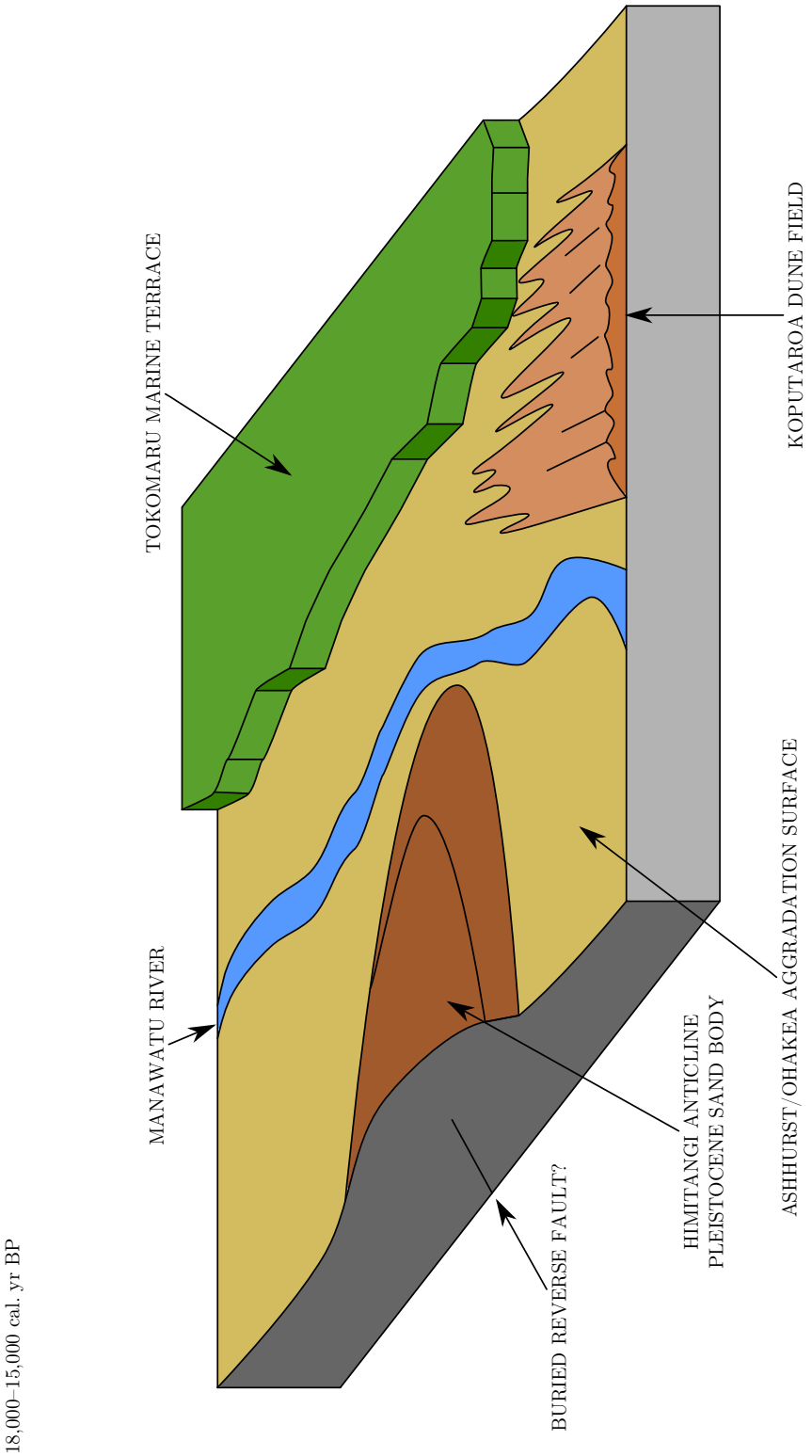
18,000–15,000 cal. yr BP
TOKOMARU MARINE TERRACE
KOPUTAROA DUNE FIELD
MANAWATU RIVER
ASHHURST/OHAKEA AGGRADATION SURFACE
HIMITANGI ANTICLINE
PLEISTOCENE SAND BODY
BURIED REVERSE FAULT?

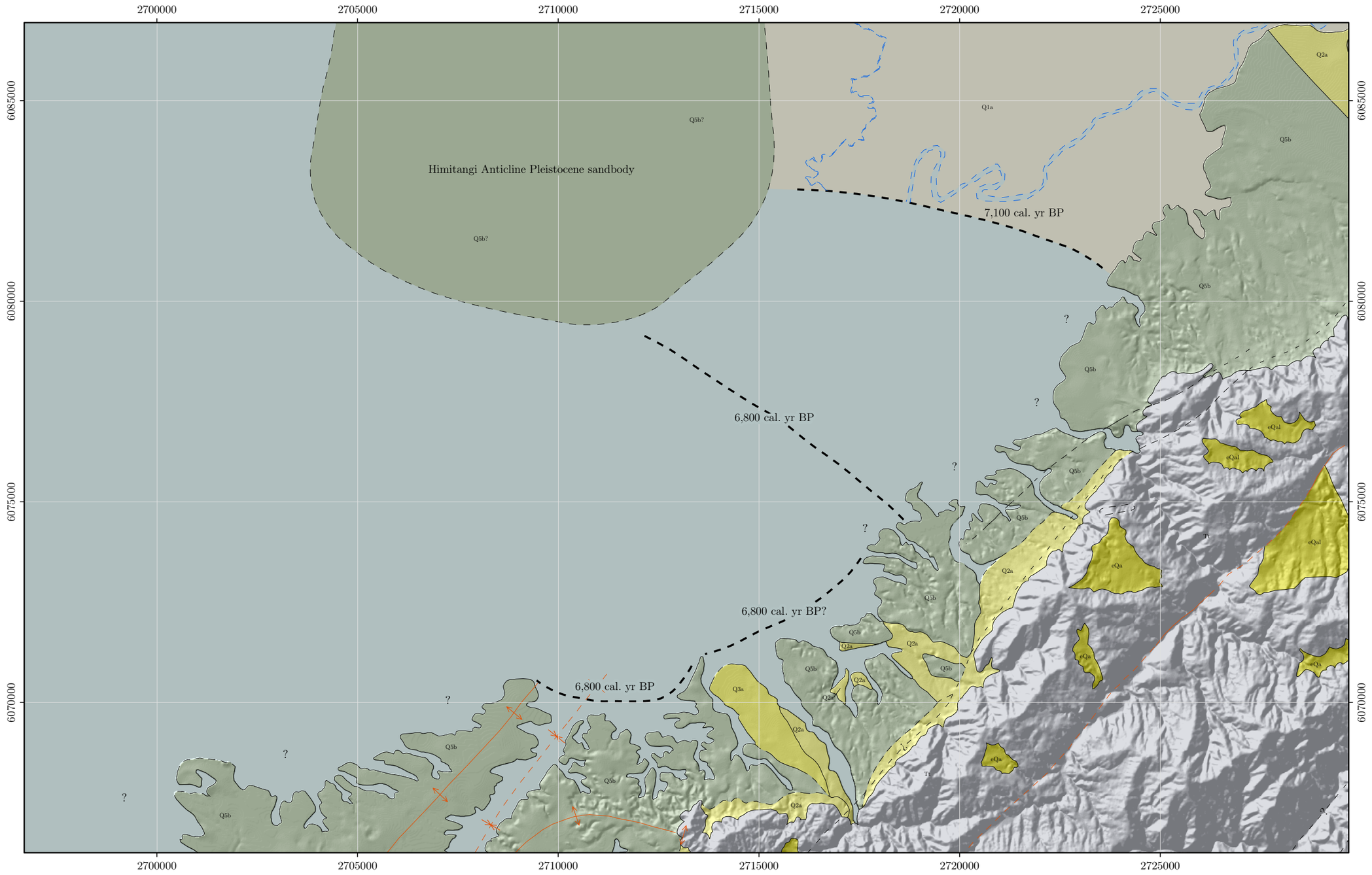
2700000
2705000
2710000
2715000
2720000
2725000
6085000
6080000
6075000
6070000
Himitangi Anticline Pleistocene sandbody
7,100 cal. yr BP
6,800 cal. yr BP
6,800 cal. yr BP?
6,800 cal. yr BP
Q5b?
Q5b?
Q1a
Q2a
Q5b
Q3a
eQa
eQal
Tt
?

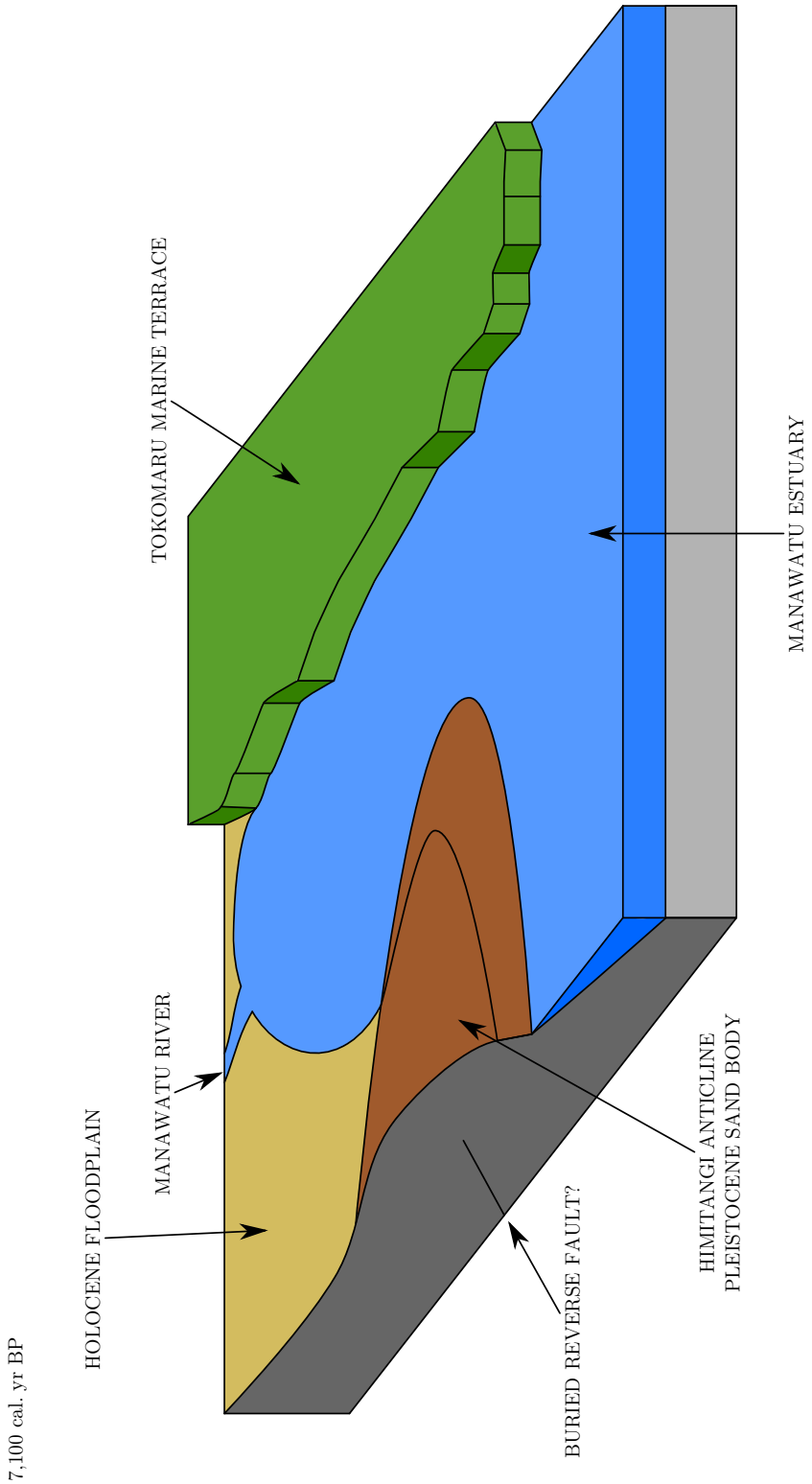
7,100 cal. yr BP
HOLOCENE FLOODPLAIN
MANAWATU RIVER
TOKOMARU MARINE TERRACE
MANAWATU ESTUARY
HIMITANGI ANTICLINE
PLEISTOCENE SAND BODY
BURIED REVERSE FAULT?

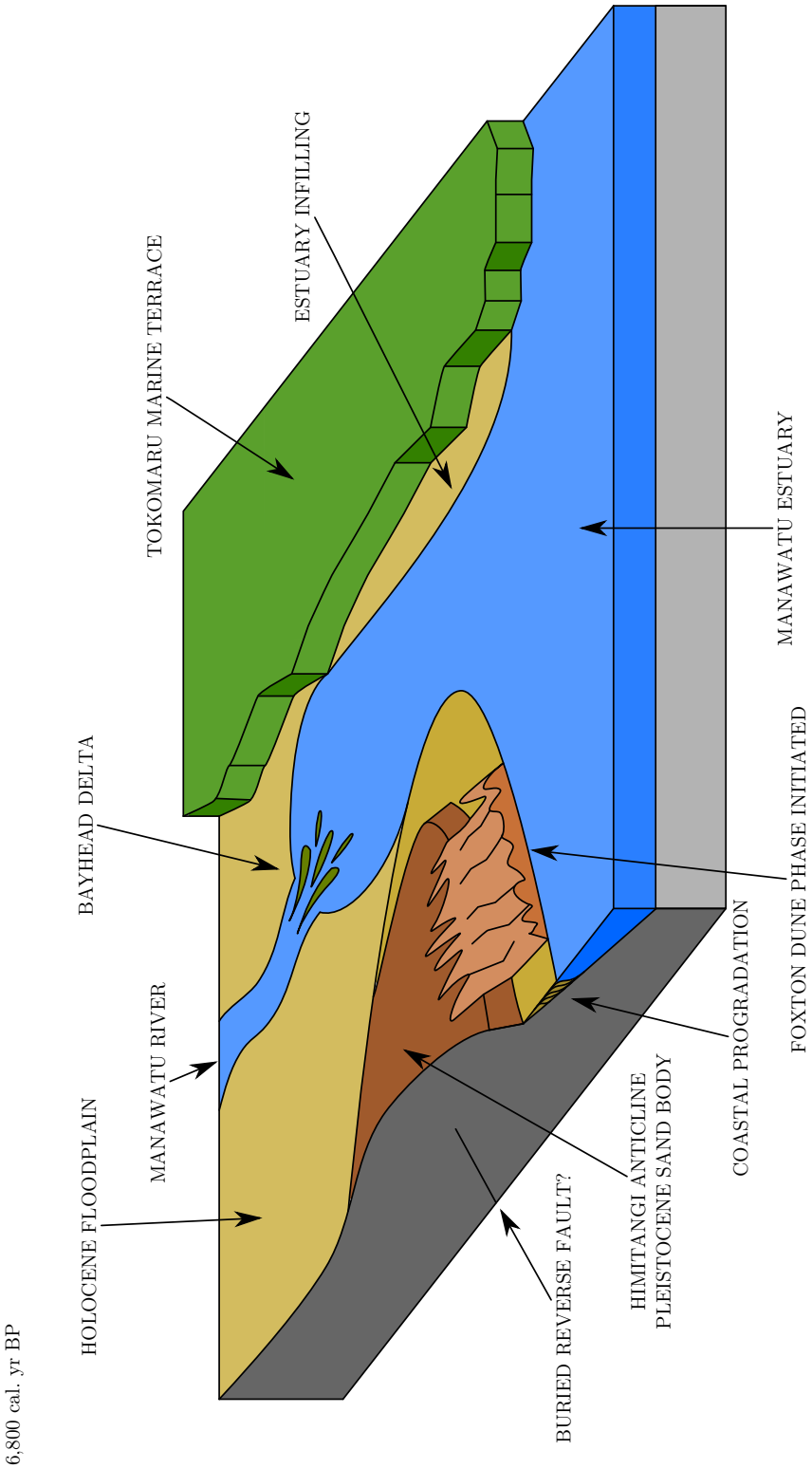
6,800 cal. yr BP
HOLOCENE FLOODPLAIN
MANAWATU RIVER
BAYHEAD DELTA
TOKOMARU MARINE TERRACE
ESTUARY INFILLING
BURIED REVERSE FAULT?
HIMITANGI ANTICLINE
PLEISTOCENE SAND BODY
COASTAL PROGRADATION
FOXTON DUNE PHASE INITIATED
MANAWATU ESTUARY

same time, sediment eroded from the Tokomaru Marine Terrace was infilling the estuary near Shannon. At the coast on the western flank of the Himitangi Anticline, sand which migrated landward with rising sea levels was transported to the nearshore, beach and back-beach environment by the dominant westerly swell, and farther inland by prevailing west-north-westerly winds, initiated the formation of Foxton Phase transgressive dunes (Figures 8.11, 8.12, and 8.13). At Koputaroa those Koputaroa Phase dunes not on top of the Tokomaru Marine Terrace would have been inundated by the estuary, while those dunes on the terrace would have been isolated from their sediment source.

8.6.3 5,700 cal. yr BP

The extent of the Manawatu estuary had shrunk substantially by 5,700 cal. yr BP (Figures 8.14 and 8.15). The coastal plain had prograded to place the shoreline west of Moutoa, and a large estuarine basin had formed in the vicinity of the Moutoa Floodway (Figures 8.14 and 8.15). A barrier-inlet complex may have formed in the vicinity of the Whirokino Cut. Alternatively, progradation of the coast west of the Himitangi Anticline and Poroutawhao High may have narrowed the entrance to the estuary. North of the estuary Foxton Phase transgressive dunes had advanced inland over the Himitangi Anticline (Figures 8.14 and 8.15).

8.6.4 4,700 cal. yr BP

By 4,700 cal. yr BP the estuarine basin in the lower valley had been infilled, while coastal progradation continued to restrict the mouth of the estuary (Figures 8.16 and 8.17). The coastline west of the Himitangi Anticline and Porotowhao High may have prograded several kilometres since the Holocene sea-level maxima; however, the timing of and extent of this progradation is unclear (Figures 8.14 and 8.15; cf. Figure 6.2; Shepherd et al., 1986).

8.6.5 4,700 cal. yr BP to Present

Through the latter half of the Holocene the barrier complex in the Whirokino area would have formed the foundation for coastal progradation fed by sed-

---

Figure 8.14 *(following page)*: Palaeogeographic map of the lower Manawatu valley, c. 5,700 cal. yr BP (1:100,000 scale).

Figure 8.15 *(page 258)*: Conceptual model of the geomorphology of the lower Manawatu valley, c. 5,700 cal. yr BP

Figure 8.16 *(page 259)*: Palaeogeographic map of the lower Manawatu valley, c. 4,700 cal. yr BP (1:100,000 scale).

Figure 8.17 *(page 260)*: Conceptual model of the geomorphology of the lower Manawatu valley, c. 4,700 cal. yr BP

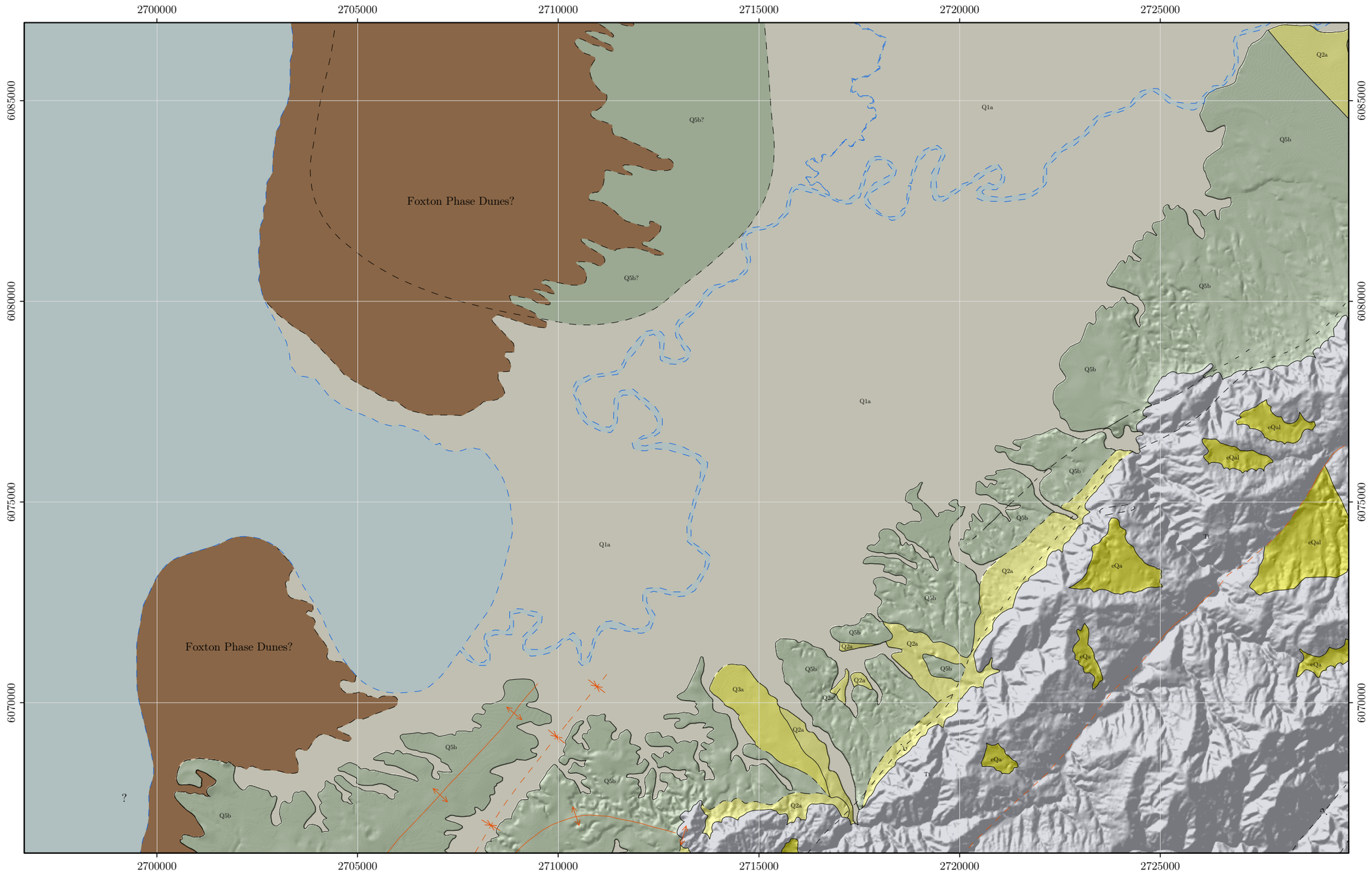
2700000
2705000
2710000
2715000
2720000
2725000
6085000
6080000
6075000
6070000
Foxton Phase Dunes?
Foxton Phase Dunes?
?
Q5b?
Q5b?
Q1a
Q1a
Q1a
Q5b
Q5b
Q5b
Q5b
Q5b
Q5b
Q5b
Q5b
Q5b
Q5b
Q2a
Q2a
Q2a
Q2a
Q2a
Q2a
Q2a
Q3a
eQa
eQa
eQa
eQa
eQa
eQa
eQa
eQa
eQal
eQal
eQal
Tr
Tr
Tr

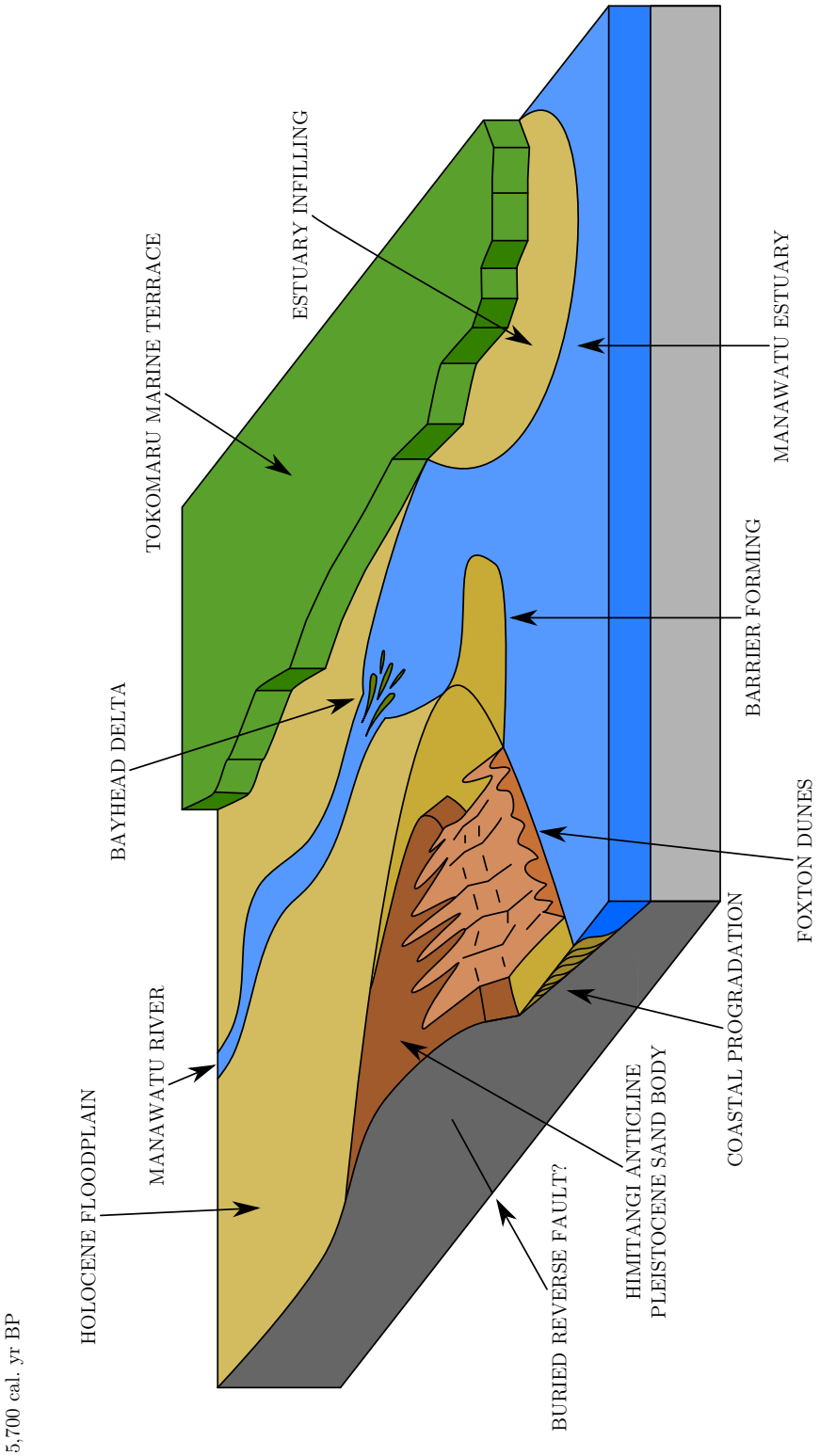
5,700 cal. yr BP
HOLOCENE FLOODPLAIN
MANAWATU RIVER
BAYHEAD DELTA
TOKOMARU MARINE TERRACE
ESTUARY INFILLING
BURIED REVERSE FAULT?
HIMITANGI ANTICLINE
PLEISTOCENE SAND BODY
COASTAL PROGRADATION
FOXTON DUNES
BARRIER FORMING
MANAWATU ESTUARY

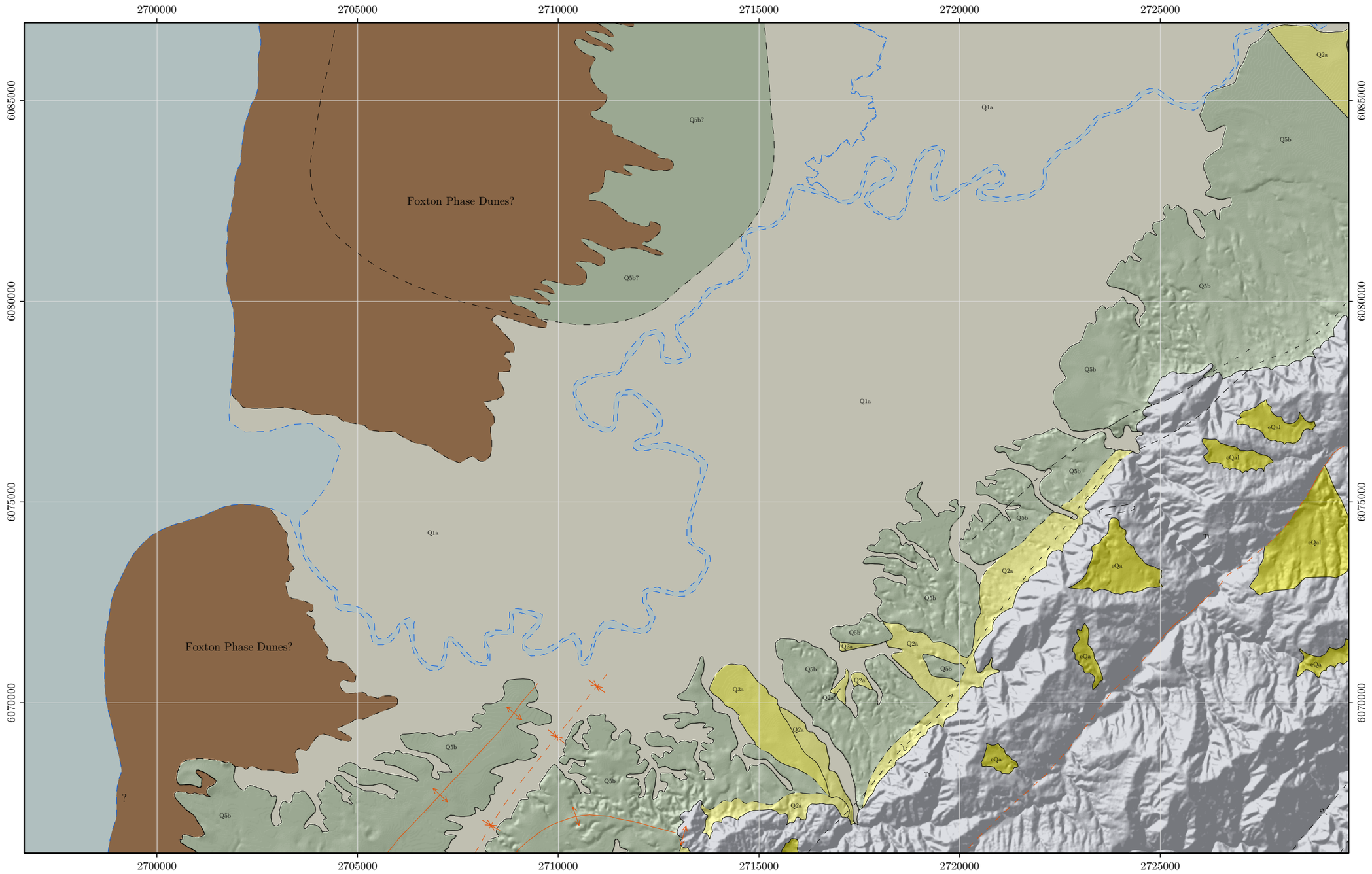
2700000
2705000
2710000
2715000
2720000
2725000
6085000
6080000
6075000
6070000
Foxton Phase Dunes?
Foxton Phase Dunes?
Q5b?
Q5b?
Q1a
Q1a
Q1a
Q5b
Q5b
Q5b
Q5b
Q5b
Q5b
Q5b
Q5b
Q5b
Q2a
Q2a
Q2a
Q2a
Q2a
Q2a
Q2a
Q3a
eQa
eQa
eQa
eQa
eQa
eQal
eQal
Tr
Tr
?
?

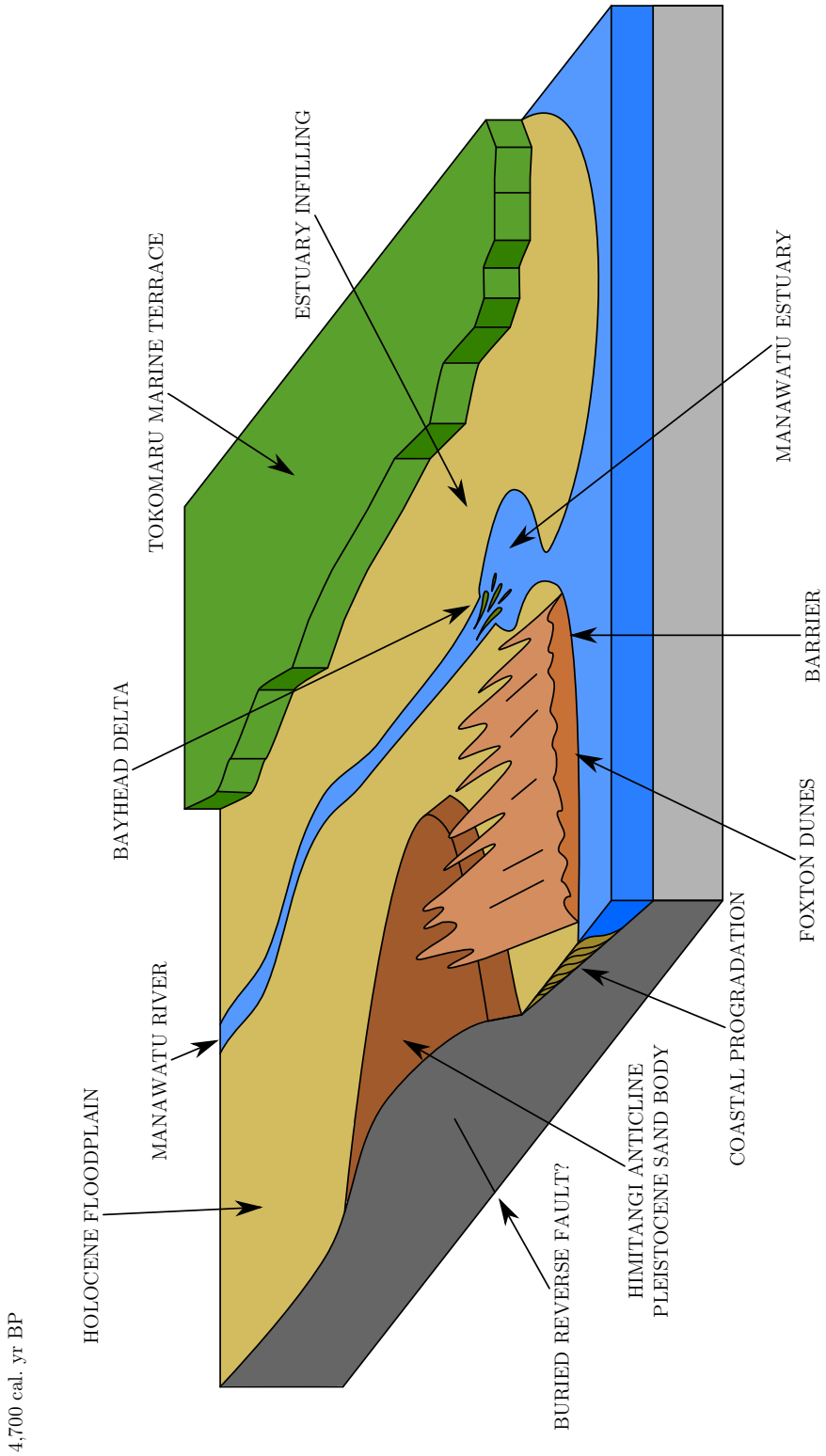
4,700 cal. yr BP
HOLOCENE FLOODPLAIN
MANAWATU RIVER
BAYHEAD DELTA
TOKOMARU MARINE TERRACE
ESTUARY INFILLING
BURIED REVERSE FAULT?
HIMITANGI ANTICLINE
PLEISTOCENE SAND BODY
COASTAL PROGRADATION
FOXTON DUNES
BARRIER
MANAWATU ESTUARY

iment supplied by longshore drift from rivers to the north of the Manawatu region. However, the precise rate of coastal progradation or the position of the coast at any particular time is unclear. The Foxton dune building phase, which had begun c. 7,100 cal. yr BP, continued, with dunes prograding over the top of the Pleistocene sand body on top of the Himitangi Anticline by c. 2,300 cal. yr BP. The Foxton phase of dune building ceased by c. 2,000 cal. yr BP, and was succeeded by the Motuiti and Waitarere phases.

8.7 LGM to Holocene facies evolution of the Manawatu Valley

8.7.1 Lowstand incised-valley system

During the Last Glacial Maximum sea-levels were c. 120 m lower than present. At this time the geomorphology of the Manawatu valley was characterised by fluvial aggradation surfaces in the form of aggradation terraces formed by the Manawatu River, and low angle alluvial fans formed by rivers and streams flowing out of the Tararua Ranges and across the Tokomaru Marine Terrace (Figure 8.18A). This is consistent with other drowned river valley type incised-valley systems in New Zealand that show LGM aggradation surfaces underlying the Holocene sedimentary infill (e.g., Suggate, 1968; Shepherd et al., 1986; Brown, 1995; Bal, 1996; Dravid and Brown, 1997; Heap and Nichol, 1997; Berryman et al., 2000; Litchfield, 2003; Litchfield and Berryman, 2005, 2007; Wolinsky et al., 2010). The incised-valley system was confined between the Last Interglacial deposits of the Tokomaru Marine Terrace and the large body of marine sand preserved in the vicinity of the Himitangi Anticline (Figure 8.18A).

8.7.2 Holocene marine transgression

Between c. 9,000–6,800 cal. yr BP the lowstand incised-valley was inundated by the rising sea levels of the Holocene marine transgression (Chapter 3). During the early stages of this sea-level rise sediment stored on the continental shelf was transported shoreward and into the mouth of the Manawatu valley and deposited on top of the LGM aggradation surface as the marine transgressive sand facies (MTS; Figure 8.18B; Chapter 7). This contrasts with other models of incised-valley fill which identify a transgressive bay-head delta facies at the base of incised valley fill (e.g., Roy et al., 1980, 2001; Chapman et al., 1982; Roy, 1984a,b; Dalrymple et al., 1992; Roy, 1994). On the southeast coast of Australia Sloss et al. (2005, 2006a,b, 2007) have identified transgressive sand sheet deposits similar to the MTS facies identified in the Manawatu. However, a crucial point of difference between the Manawatu and these southeast Australian incised valleys is the spatial extent of the transgressive sand sheet: in southeast Australian examples it extends basin wide (e.g., Sloss et al., 2005, 2006a,b, 2007), while in the Manawatu it is restricted to the mouth of the

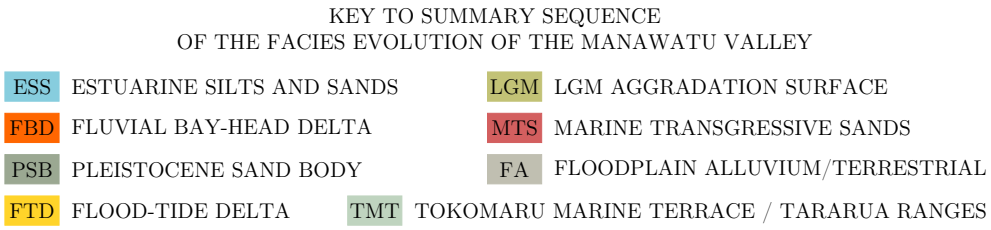

Figure 8.18 *(above and facing page)*: Conceptual summary sequence of the facies evolution of the lower Manawatu valley from the Last Glacial Maximum until present: (A) Last Glacial Maximum; (B) Holocene marine transgression; (C, D) Holocene sea-level highstand; (E, F) Late Holocene barrier development and coastal progradation. Longitudinal profiles approximate the fill along the dashed-line in (A), and are vertically exaggerated.

valley (e.g., Roy et al., 1980, 2001; Chapman et al., 1982; Roy, 1984a,b, 1994; Dalrymple et al., 1992). This may be a result of the geographic configuration of the Manawatu valley. Given the dog-leg configuration of the valley and the prevailing north-westerly wind only the mouth of the valley would have been directly open to direct marine influences during the Holocene marine transgression (Figure 8.18B). An alternative explanation is that the transgressive phase of sedimentation during the early stages of the Holocene marine transgression may have been restricted by the high flow regime and sediment load of the Manawatu river, which may have removed, reworked, or otherwise obscured the transgressive facies by fluvial processes, with the system essentially operating as a depositional environment experiencing a forced regression. Such an effect has been identified in the Pakareae River valley, on the east coast of the North Island (Wilson et al., 2007).

As sea-levels rose an estuarine environment was established in the Manawatu valley, in some locations proximal to the Tokomaru Marine Terrace prior to 8,100 cal. yr BP, a full 1,000 years before the maximum height of the Holocene marine transgression on the southwest coast of the North Island (Figure 8.18B). This is consistent with other estuaries and incised-valleys in New Zealand (e.g., Heap and Nichol, 1997; Wilson et al., 2007; Kennedy et al., 2008; Wolinsky et al., 2010), but predates the establishment of estuarine conditions in narrow incised-valley systems on the southeast coast of Australia, where an estuarine central basin may not have been formed until as late as 5,000 cal. yr BP (e.g., Sloss et al., 2010). There are two key reasons for this difference: (a) the Australian examples are shallower systems, and are therefore higher relative to the LGM low sea-level of -120 m; and (b) the Australian examples are protected by Last Interglacial barriers which must be breached by rising Holocene sea-levels. Therefore, estuarine conditions were only established in these Australian estuaries once sea-level had risen, not as sea-level rose as in the Manawatu.

At the head of the palaeo estuary, in the vicinity of Opiki, estuarine conditions were established c. 7,100 cal. yr BP (Figure 8.18B). At the same time the fluvial bay-head delta (FBD) would have been initiated as the Manawatu

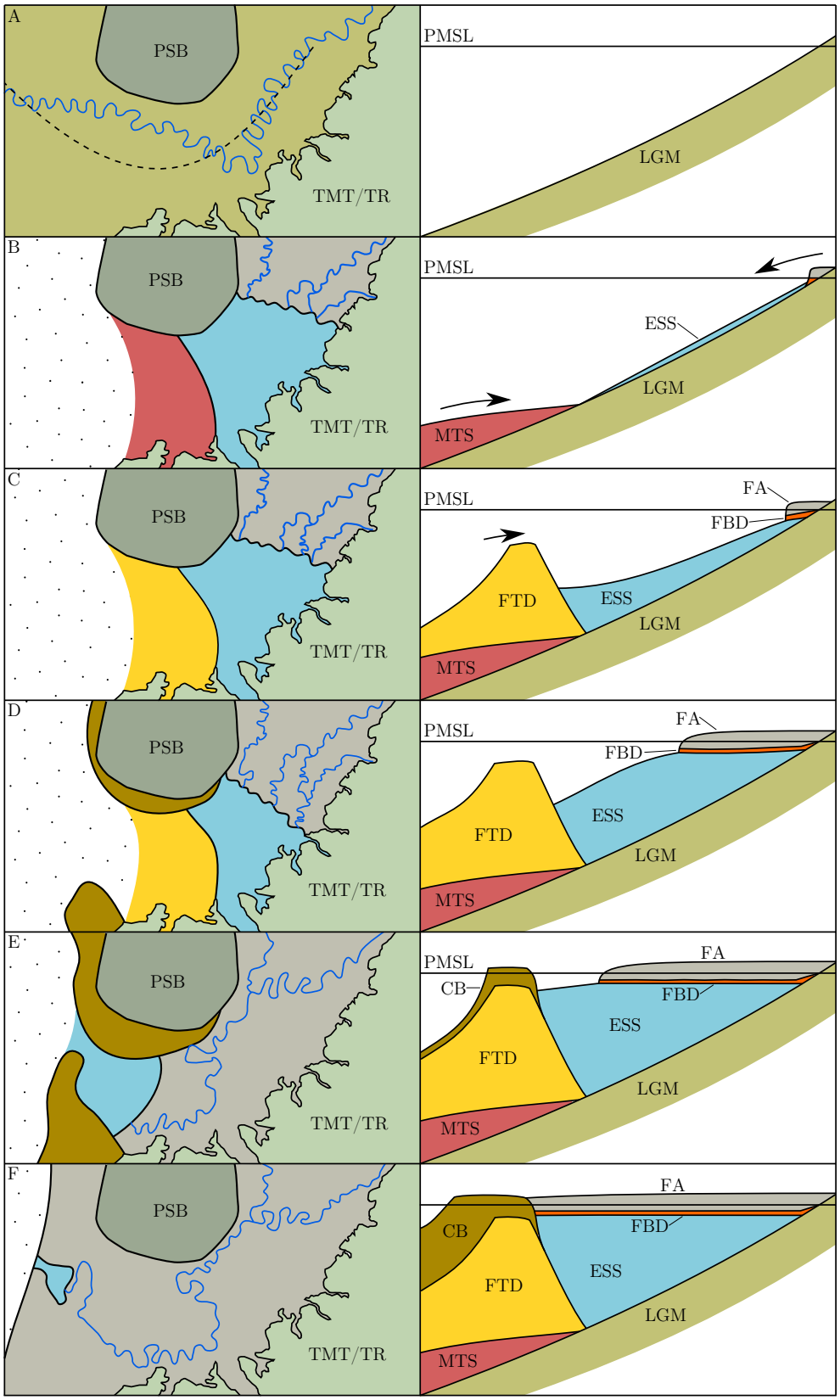
A
PSB
TMT/TR
PMSL
LGM
B
PSB
TMT/TR
PMSL
ESS
LGM
MTS
C
PSB
TMT/TR
PMSL
FA
FBD
FTD
ESS
LGM
MTS
D
PSB
TMT/TR
PMSL
FA
FBD
FTD
ESS
LGM
MTS
E
PSB
TMT/TR
PMSL
CB
FA
FBD
ESS
FTD
LGM
MTS
F
PSB
TMT/TR
FA
CB
FBD
ESS
FTD
LGM
MTS

River delivered significant amounts of sediment to the head of the estuary. A fluvially-dominated swamp environment (FSS) would also have been initiated both at the head of the valley and on the flanks in the proximity of the Tokomaru Marine Terrace as water became impounded behind the delta complex (Figure 8.18B).

8.7.3 Holocene sea-level highstand

Following the culmination of the Holocene marine transgression on the southwest coast of the North Island, c. 6,800 cal. yr BP, estuarine conditions prevailed in the lower Manawatu valley (Figure 8.18C, D). At the head of the valley the fluvial bay-head delta would have expanded extremely swiftly. This is indicated by the thin nature of the preserved bay-head delta facies, which does not exceed 1.5 m thickness (Figure 8.18C, D). This contrasts with the infill of comparatively shallow (up to 10 m deep) Australian incised-valleys where the thickness of bay-head delta facies commonly exceeds that preserved in the Manawatu (e.g., Sloss, 2005; Sloss et al., 2005, 2006a,b, 2010). In incised-valleys of comparable depth to the Manawatu the Holocene bay-head delta may be tens of meters thick (e.g., Roy, 1984a,b; Allen and Posamentier, 1993, 1994; Rodriguez et al., 2008). This difference is attributed to the rapid and high rates of sediment delivery by the Manawatu River to the palaeo estuary, which may have denied the opportunity for expansive bay-head delta formation as swift infilling of the estuarine central basin eliminated the necessary accommodation space, thereafter leading to sediment bypass. In the middle valley the transition from estuarine to alluvial conditions took place approximately 6,000 cal. yr BP, while in the lower valley estuarine conditions persisted until c. 4,700 cal. yr BP (Figure 8.18C, D).

Coincident with the culmination of the Holocene marine transgression a large floodtide delta complex would have formed at the mouth of the valley, between the Poroutawhao High and the Pleistocene marine sand body over the Himitangi Anticline (Figure 8.18C, D). The chronology for the development of the flood-tide delta can only be estimated as it is not penetrated by vibracores, and well logs which do penetrate sufficiently deep lack chronological information.

8.7.4 Barrier development and coastal progradation

By c. 4,700 cal. yr BP the lower Manawatu estuary had almost completely infilled, with the thick estuarine sequence overridden by thin bay-head delta sediments, in turn capped by comparatively thick alluvial sediments (Figure 8.18E, F). At the mouth of the valley, near Whirokino, the floodtide delta evolved into a barrier complex capped by Holocene dunes, presumed to be analogous to the drowned river valley estuary barrier described by Roy (1984a,b) and Roy et al. (1980) (Figure 8.18E, F). The timing of the development of the barrier complex is uncertain, but likely took place between 6,000–5,000 cal. yr BP, in sufficient time to protect the lower estuary from direct marine incur-

sions. This timing of barrier formation is comparable with other estuaries in New Zealand (e.g., Marra, 1997; Roach, 2005; Wilson et al., 2007).

The seaward side of barrier formed the foundation for coastal progradation fed by sediment supplied by longshore drift from rivers to the north of the Manawatu coast (Figure 8.18E, F). As a result the barrier became incorporated within the coastal plain which in the late Holocene would have extended seaward of the barrier. This contrasts with Australian examples where the barrier forms the seaward margin of the coastal plain (e.g., Roy et al., 1980, 2001; Roy, 1984a,b; Nichol, 1991; Sloss, 2005; Sloss et al., 2005, 2006a,b, 2010). This difference is primarily driven by sediment supply, which is sufficiently high at the Manawatu coast to drive late Holocene coastal progradation (Figure 8.18E, F).

Chapter 9

Conclusions

The principal objectives of this investigation have been the accurate delineation of Holocene sea-level fluctuations in the New Zealand archipelago, and the reconstruction of the stratigraphic and geomorphic evolution of the Manawatu incised-valley system. The former has involved a comprehensive, critical review of the state of knowledge of Holocene sea-level fluctuations in the New Zealand region, and the construction of detailed, local-scale Holocene sea-level curves for regions within the New Zealand archipelago. The latter has involved detailed reconstructions of the Holocene sedimentary infill of the lower Manawatu incised-valley from water well logs and detailed vibracores. These reconstructions have been evaluated within the context of Holocene sea-level changes and established models of estuary and incised-valley evolution.

9.1 Findings of this research

9.1.1 State of knowledge of Holocene sea-level fluctuations in the New Zealand region

The most comprehensive, critical review of the state of knowledge of Holocene sea-level fluctuations in the New Zealand region conducted since 1953 reveals a fragmented series of sea-level reconstructions. Many sea-level reconstructions have have been founded on research conducted over 60 years ago; however, the errors and limitations associated with this earlier research are poorly understood. This is typified by the large number of studies which represent sea-level fluctuations as single lines, with no age or elevation errors. Regional sea-level datasets have been widely produced for New Zealand; however, these mask local trends in sea-level fluctuations while blending together an unrealistic picture of regional sea-level movements.

9.1.2 Local-scale reconstructions of Holocene sea-level changes for regions within the New Zealand archipelago

Local-scale reconstructions of the Holocene marine transgression for the regions of Auckland-Northland, the Coromandel Peninsula and the Firth of Thames, the south/southwest coast of the North Island, Christchurch and Pegasus Bay, and the East Otago Peninsula show an apparent north-south trend in sea-level fluctuations:

- In the Auckland-Northland region sea-level had risen to c. −3 m below PMSL by c. 8,000 cal. yr BP. PMSL was attained c. 7,700 cal. yr BP. This was followed by a sea-level rise to +0.9 m above PMSL for the period 6,300–5,600 cal. yr BP. Sea-level gradually declined from +0.9 m above PMSL c. 5,600 cal. yr BP to +0.4 m above PMSL by 3,500 cal. yr BP. By 1,600 cal. yr BP sea-level had fallen to PMSL.
- The extreme variation in sea-level index points recovered from the Coromandel Peninsula and the Firth of Thames prevented the delineation of sea-level trends for this area during the Holocene. Sea levels may have been higher than present in the mid Holocene, falling to PMSL since that time at a rate broadly synchronous with the rate of sea-level fall in the Auckland-Northland region.
- On the south/southwest coast of the North Island sea-level rose swiftly from c. −16 m below PMSL c. 9,000 cal. yr BP to −3 m below PMSL c. 8,300 cal. yr BP. PMSL was attained c. 7,500 cal. yr BP. By 6,800 cal. yr BP sea-level had risen to a maxima of +1.2 m above PMSL. From this high sea-level fell to PMSL c. 5,400 cal. yr BP. Sea-level then rose to c. +0.6 m above PMSL c. 4,700 cal. yr BP, but had fallen back to PMSL by c. 4,200 cal. yr BP. Sea-level remained at PMSL until c. 3,700 cal. yr BP, before rising to c. +0.6 m above PMSL c. 3,350 cal. yr BP. The period of this higher sea-level is unclear due to the absence of sea-level indicators for the period 3,000 cal. yr BP to present.
- In the Christchurch-Pegasus Bay area sea-level rose from c. −34 m below PMSL c. 10,350 cal. yr BP to −23 m below PMSL by 9,500 cal. yr BP. Sea-level reached c. −8.4 m below PMSL c. 8,200 cal. yr BP, rising to −4.5 m below PMSL c. 7,300 cal. yr BP. PMSL may have been attained any time between 7,100–6,600 cal. yr BP. There are not sufficient indicators to enable a sea-level envelope to be delineated for the Christchurch and Pegasus Bay region for the remainder of the Holocene.
- Around the East Otago Peninsula sea-level had reached c. −1 m below PMSL c. 7,600 cal. yr BP. Sea-level rose to c. +0.2 m by c. 6,800 cal. yr BP, remaining at this level until at least 6,300 cal. yr BP. PMSL was therefore attained c. 7,000 cal. yr BP. Sea-level fell from +0.2 m 6,300 cal. yr BP to −0.9 m below PMSL c. 4,800 cal. yr BP. Sea-level then rose to PMSL from 4,800–4,000 cal. yr BP, remaining at this level until 3,500 cal. yr BP. Sea-level then fluctuated between PMSL and −1.0 m below

PMSL between 3,500–900 cal. yr BP. From 900 cal. yr BP to present, sea-level rise sharply from −0.7 m below PMSL to the present level.

These local-scale sea-level histories confirm suggestions that regional sea-level reconstructions mask local trends in sea-level changes. The finding of an earlier attainment of PMSL c. 7,700 cal. yr BP in the New Zealand region is supported by research from the southeast coast of Australia.

9.1.3 Water well log reconstructions of the Holocene sedimentary fill of the lower Manawatu valley

Cross-sections constructed from water well logs across the Manawatu valley reveal the path of the Last Glacial Maximum Ashhurst/Ohakea fluvial aggradation surface beneath the Holocene coastal plain. The surface descends from +40 m above PMSL in the upper part of the coastal plain, to −65 m below PMSL at the coast. Above this surface, the Holocene sedimentary fill can be broadly delineated as marine/estuarine or terrestrial (Holocene alluvium or dune sand). The marine/estuarine wedge extends up-valley to the vicinity of Opiki. Above Opiki, the LGM surface is overlain by 3–25 m of alluvium.

The discrete observations of the LGM aggradation surface presented by the well log cross-sections were interpolated and extrapolated to reconstruct the buried Ashhurst/Ohakea terrace as a continuous digital elevation model (DEM). This is a novel approach, and overcomes limitations of similar reconstructions which have been developed using broadly spaced cross-sections or sediment thickness estimates. This model allowed the volume of accommodation space available to infilling sediment during the Holocene marine transgression to be estimated at c. 9–10 km^3. In addition, the DEM surface reveals that the LGM surface may have been downwarped along the axis of the Kairanga Trough. The reconstruction of the alluvial/estuarine interface suggests that it may have been upwarped at the southern end of the Himitangi Anticline.

9.1.4 Stratigraphy and facies assemblages reconstructed from detailed vibracores

Detailed vibracores recovered from the lower Manawatu valley reveal marine transgressive sands confined to the lowest part of the valley. A highstand estuarine silt and sand facies is found throughout the lower valley. Fluvial bay-head delta silts and sands are restricted to the centre of the lower valley. Floodplain swampy silts are located on the periphery of the valley, adjacent to box-shaped valleys in the Tokomaru Marine Terrace. Floodplain alluvium is the uppermost facies recognised in all vibracores recovered from the lower Manawatu valley. Shallow estuarine conditions prevailed in the upper valley from 8,300 cal. yr BP, and in the lower valley until 4,700 cal. yr BP. The timing of the estuarine-alluvial transition similarly differs depending upon in-valley location, from 6,800 cal. yr BP at the head of the valley and proximal to the Tokomaru Marine Terrace, to c. 4,700 cal. yr BP near the Whirokino Cut.

9.1.5 Subsidence in the Lower Manawatu valley

Palaeo sea-level indicators recovered from the lower Manawatu valley show some divergence from the sea-level reconstruction presented for the southwest coast of the North Island. This divergence may be due to subsidence processes in the Manawatu valley, however no single mechanism accounts for the subsidence seen across the valley. It appears that combinations of mechanisms operating in different time-scales, at different spatial scales, and at different rates and magnitudes, are responsible. Sediment compaction, the evolution of the Wanganui Basin, and the influence of the Kairanga Trough all appear to be responsible for differing degrees of subsidence in the lower Manawatu valley. Hydro-isostatic loading, which may have had an impact on the entire southwestern North Island, is not considered to have had a specific effect on the Manawatu. The individual and/or combined effects of these subsidence mechanisms appear to have been confused by tectonic uplift. Overall, the effect on the lower valley has been ongoing relative sea-level rise through the Holocene, contributing to the formation of accommodation space.

9.1.6 Comparisons of lower Manawatu valley stratigraphy to tripartite facies models of incised-valley infill

The lower Manawatu River valley is analogous to a drowned river valley estuary, or a wave-dominated estuary. Established models of incised-valley infilling are based on estuaries of extensive size (40–100 km in length), on stable coastlines, with comparatively limited sediment supplies and low river discharges. Within this context the Manawatu valley is a novel setting, in which it can be investigated whether these models scale to estuaries an order of magnitude smaller, on actively uplifting coastlines, with high river discharges and sediment loads. The Manawatu valley demonstrates conclusively that in particular river discharge and sediment load can have a significant effect on the preservation of facies in an incised-valley, thereby leading to considerable variation from established models of the sedimentary fill of incised-valleys.

The transgressive sand facies identified in the lower valley is spatially restricted to the valley mouth. This contrasts with recent models of wave-dominated barrier estuary evolution from the southeast coast of Australia. The difference is attributed to the dog-leg configuration of the valley and the prevailing northwesterly wind, which would have restricted direct marine influences during the Holocene marine transgression to the mouth of the Manawatu incised-valley. Another factor that may have resulted in restricting the transgressive phase of sedimentation is the high flow regime and sediment load of the Manawatu River which may have removed, reworked or otherwise obscured the transgressive facies by fluvial processes.

In the Manawatu the deposition of estuarine sediment into the central basin was extremely short lived. In some locations the alluvial-estuarine transition took place as little as 1,000 years after the establishment of estuarine conditions. This contrasts with other examples of wave-dominated estuaries

and incised-valleys, which in some cases still possess a central estuarine basin. This is a product of the extremely high sediment load supplied to the incised-valley by the Manawatu River, which was sufficent to infill the majority of the 14 km^3 volume of of the incised-valley within c. 3,000 years. The earliest date for the establishment of estuarine conditions is 8,300 cal. yr BP, near Shannon. This pre-dates the formation of estuarine conditions in some south-east Australian estuaries by up to 3,000 years, and further illustrates the role antecedent topography has on controlling the spatial and temporal extent of sedimentary facies in incised-valley fill.

In the Manawatu a fluvial bay-head delta facies is identified; however, in contrast to many other incised-valley examples the facies is present only as a very thin layer. This is attributed to the rapid and high rates of sediment delivery by the Manawatu River to the palaeo estuary, which may have denied the opportunity for expansive bay-head delta formation as swift infilling of the estuarine central basin eliminated the necessary accommodation space, thereafter leading to sediment bypass. Indeed, a time and area averaged estuarine sedimentation rate for the Manawatu is estimated at 4.54 m ka^{-1}, with fluvial infilling estimated at 1.43 m ka^{-1}.

These conclusions are reinforced by the development of a summary sequence of the facies evolution of the Manawatu valley from the LGM through the Holocene. This sequence model summaries these similarities and differences with existing models of incised-valley infilling, and presents what may be the first refined model for the evolution of drowned river valley estuaries of this scale under conditions of high sediment load and river flows, on tectonically active coasts.

9.1.7 LGM and Holocene palaeogeomorphology of the lower Manawatu valley

- The path of the Manawatu River during the LGM can be tentatively traced 2–6 km north of its present position.
- The protection offered by the Poroutawhao High against marine incursions into the lower Manawatu valley at the height of the Holocene marine transgression was limited to the area around Koputaroa.
- A large body of Pleistocene-age sand in the vicinity of the Himitangi Anticline acted as the principle protection for the lower Manawatu valley at the height of the Holocene marine transgression.
- The Manawatu coastline at the height of the Holocene marine transgression was approximately 5–6 km inland of its present position.
- The Holocene palaeo estuary that filled the lower Manawatu incised-valley at the height of the Holocene marine transgression extended inland to the area of present-day Opiki.
- Conceptual models and palaeogeographic maps document the geomorphic evolution of the lower Manawatu valley during the Holocene marine transgression.

9.2 Future research

There is considerable scope for studies to target the recovery of palaeo sea-level indicators of high indicative value to fill gaps and deficiencies in the current state of knowledge of palaeo sea-level changes. These gaps are most evident in the Christchurch-Pegasus Bay region through the last 6,700 years BP, and the southwest North Island through the last 3000 years. There is also a deficiency in the Otago Peninsula area through the early Holocene leading up to the attainment of PMSL. In addition, there is a dearth of index points suitable for reconstructing the early Holocene rise in sea-level from all locations except Christchurch-Pegasus Bay. The choice of indicators to fill these gaps and deficiencies is crucial as recent studies illustrate that palaeo sea-level histories assembled using indicators such as fossil molluscs may only reconstruct coarse fluctuations in sea-level.

In the Manawatu, water well logs indicate the broad nature of the sedimentary fill at considerable depths, while vibracores present highly detailed stratigraphic data of the upper part of the sedimentary fill. Future studies could therefore target the recovery of longer cores (>60 m) from the lower part of the valley, particularly in the area around Foxton, which may enable delineation of features of the lower incised-valley, such as a flood-tide delta and mid to late Holocene barrier. There is also considerable scope to further the use of the DEM of the LGM surface, particularly to investigate sediment flux and coastal progradation rates in the Manawatu valley during the Holocene.

References

Abbott, S.T., Carter, R.M., 1994. The sequence architecture of mid-Pleistocene (0.35–0.95 Ma) cyclothems from New Zealand: facies development during a period of known orbital control on sea-level cyclicity. In: De Boer, P.L., Smith, D.G. (Eds.), Orbital forcing and cyclic sequences (IAS Special Publication 19). International Association of Sedimentologists, Oxford, pp. 367–394.

Abrahamson, L., 1987. Aspects of Late Quaternary stratigraphy and evolution of some coastal embayments on the east Coromandel Peninsula, New Zealand. Unpublished MSc Thesis, University of Otago, Hamilton.

Abrahim, G.M.S., 2005. Holocene sediments of Tamaki Estuary: characterisation and impact of recent human activity on an urban estuary in Auckland, New Zealand. Unpublished PhD Thesis, University of Auckland, Auckland.

Abrahim, G.M.S., Nichol, S.L., Parker, R.J., Gregory, M.R., 2008. Facies depositional setting, mineral maturity and sequence stratigraphy of a Holocene drowned valley, Tamaki Estuary, New Zealand. Estuarine, Coastal and Shelf Science 79, 133–142.

Adkin, G.L., 1910. The post-Teritary geological history of the Ohau River and of the adjacent coastal plain, Horowhenua County, North Island. Transactions of the New Zealand Institute 43, 496–520.

Adkin, G.L., 1919. Further notes on the Horowhenua coastal plain and the associated physiographic features. Transactions of the New Zealand Institute 51, 108–118.

Adkin, G.L., 1921. Porirua Harbour: a study of its shore-line and other physiographic features. Transactions of the New Zealand Institute 53, 144–156.

Aharoni, E., 1991. Seismic reflection study across the Horowhenua coastal plain, North Island, New Zealand. Unpublished MSc Thesis, Victoria University of Wellington, Wellington.

Akers, M.J., 1978. From fibre to food: Opiki — the district and its development. Stylex, Palmerston North.

Albrecht, N., Vennell, R., 2007. Tides in two constricted New Zealand lagoons. New Zealand Journal of Marine and Freshwater Research 41, 103–118.

Allen, G.P., 1991. Sedimentary processes and facies in the Gironde estuary: a recent model for macrotidal systems. In: Smith, D.G., Reinson, G.E., Zaitlin, B.A., Rahmani, R.A. (Eds.), Clastic tidal sedimentology (CSPG Memoir 16). Canadian Society of Petroleum Geologists, Calgary, pp. 29–40.

Allen, G.P., Posamentier, H.W., 1993. Sequence stratigraphy and facies model of an incised valley fill: the Gironde Estuary, France. Journal of Sedimentary Petrology 63, 378–391.

Allen, G.P., Posamentier, H.W., 1994. Transgressive facies and sequence architecture in mixed tide- and wave-dominated incised valleys: example from the Gironde Estuary, France. In: Dalrymple, R.W., Boyd, R., Zaitlin, B.A. (Eds.), Incised-valley systems: origin and sedimentary systems (SEPM Special Publication 51). Society for Sedimentary Geology, Tulsa, pp. 225–240.

Allen, G.P., Castaing, P., Feral, A., Klingebiel, A., Vigneaux, M., 1970. Contribution l'etude des facies de comblement et interpretation palogographique de l'evolution des milieux sdimentaires recents et actuels de l'estuaire de la Gironde. Bulletin de l'Institut de Geologie du Bassin d'Aquitaine 8, 99–155.

Allen, J.R.L., 1983. Studies in fluviatile sedimentation: bar complexes and sandstone sheets (low sinuosity braided streams) in the Brownstones (L. Devonian), Welsh Borders. Sedimentary Geology 33, 237–293.

Allen, J.R.L., 1995. Salt-marsh growth and fluctuating sea level: implications of a simulation model for Flandrian coastal stratigraphy and peat-based sea-level curves. Sedimentary Geology 100, 21–45.

Allen, J.R.L., 1999. Geological impacts on coastal wetland landscapes: some general effects of sediment autocompaction in the Holocene of northwest Europe. The Holocene 9, 1–12.

Allen, J.R.L., 2000. Morphodynamics of Holocene salt marshes: a review sketch from the Atlantic and southern North Sea coasts of Europe. Quaternary Science Reviews 19, 1155–1231.

Allmon, W.D., Jones, D., Aiello, R.L., Gowlett-Holmes, K., Probert, P.K., 1994. Observations on the biology of *Maoricolpus roseus* (Quoy and Gaimard) (Prosobranchia: Turritellidae) from New Zealand and Tasmania. Veliger 37, 267–279.

Anderton, P.W., 1981. Structure and evolution of the South Wanganui Basin, New Zealand. New Zealand Journal of Geology and Geophysics 24, 39–63.

Armon, J.W., 1970. Recent shorelines between Banks Peninsula and Coopers Lagoon. Unpublished MA Thesis, University of Canterbury, Christchurch.

Ashley, G.M., Sheridan, R.E., 1994. Depositional model for valley fills on a passive continental margin. In: Dalrymple, R.W., Boyd, R., Zaitlin, B.A. (Eds.), Incised-valley systems: origin and sedimentary sequences (SEPM Special Publication 51). Society for Sedimentary Geology, Tulsa, pp. 285–301.

Baker, R.G.V., Haworth, R.J., 1997. Further evidence from relic shellcrust sequences for a Late Holocene higher sea level for eastern Australia. Marine Geology 141, 1–9.

Baker, R.G.V., Haworth, R.J., 2000a. Smooth or oscillating Late Holocene sea-level curve? Evidence from cross-regional statistical regressions of fixed biological indicators. Marine Geology 163, 353–365.

Baker, R.G.V., Haworth, R.J., 2000b. Smooth or oscillating Late Holocene sea-level curve? Evidence from the palaeo-zoology of fixed biological indicators in east Australia and beyond. Marine Geology 163, 367–386.

Baker, R.G.V., Haworth, R.J., Flood, P.G., 2001a. Inter-tidal fixed indicators of former Holocene sea levels in Australia: a summary of sites and a review of methods and models. Quaternary International 83-85, 257–273.

Baker, R.G.V., Haworth, R.J., Flood, P.G., 2001b. Warmer or cooler Late Holocene marine palaeoenvironments?: interpreting southeast Australian and Brazilian sea-level changes using fixed biological indicators and their δ^{18}O composition. Palaeogeography, Palaeoclimatology, Palaeoecology 168, 249–272.

Bal, A.A., 1996. Valley fills and coastal cliffs buried beneath an alluvial plain: evidence from variation of permeabilities in gravel aquifers, Canterbury plains, New Zealand. Journal of Hydrology (NZ) 35, 1–27.

Barnes, P.M., 1995. High-frequency sequences deposited during Quaternary sea-level cycles on a deforming continental shelf, north Canterbury, New Zealand. Sedimentary Geology 97, 131–156.

Barnett, R., 1984. Upper Quaternary stratigraphy in the Otaki District. Unpublished BSc (Hons) Thesis, Victoria University of Wellington, Wellington.

Barringer, J., Newsome, P., 2006. Digital elevation model applications (Landcare Research SPINFO (SPatial INFOrmation) Workshop 2006). Landcare Research, retreived from `http://www.landcareresearch.co.nz/research/soil/spinfo/2006/SPINFO2006_DEMs.pdf`.

Bartholdy, J., Pedersen, J.B.T., Bartholdy, A.T., 2010. Autocompaction of shallow silt and marsh clay. Sedimentary Geology 223, 310–319.

Baulig, H., 1935. The changing sea level (Institute of British Geographers Publication 3). Institute of British Geographers, London.

Baum, G.R., Vail, P.R., 1988. Sequence stratigraphic concepts applied to Paleogene outcrops, Gulf and Atlantic basins. In: Wilgus, C.K., Hastings, B.K., Posamentier, H., Van Wagoner, J., Ross, C.A., Kendall, C.G.S.C. (Eds.), Sea-level changes: an integrated approach (SEPM Special Publication 42). Society of Economic Paleontologists and Mineralogists, Tulsa, pp. 309–327.

Bax, N.J., McEnnulty, F.R., Gowlett-Holmes, K.L., 2003. Distribution and biology of the introduced gastropod, *Maoricolpus roseus* (Quoy and Gamard, 1834) (Caenogastropoda: Turritellidae) in Australia (Centre for Research on Introduced Marine Pests Technical Report 25). Centre for Research on Introduced Marine Pests, CSIRO Marine Research, Hobart.

Beanland, S., 1995. The North Island dextral fault belt, Hikurangi subduction margin, New Zealand. Unpublished PhD Thesis, Victoria University of Wellington, Wellington.

Beanland, S., Haines, J., 1998. The kinematics of active deformation in the North Island, New Zealand, determined from geological strain rates. New Zealand Journal of Geology and Geophysics 41, 311–323.

Beanland, S., Melhuish, A., Nichol, A., Ravens, J., 1998. Structure and deformational history of the inner forearc region, Hikurangi subduction margin, New Zealand. New Zealand Journal of Geology and Geophysics 41, 325–342.

Beetham, R.D., McSaveney, M., Dellow, G., Rosenberg, M., Johnston, D., Smith, W., 2004. A review of natural hazards information for Northland region (IGNS Science Report 2004/06). Institute of Geological & Nuclear Sciences, Lower Hutt.

Begg, J.G., Johnston, M.R., 2000. Geology of the Wellington area 1:250 000 geological map 10. Institute of Geological & Nuclear Sciences, Lower Hutt.

Begg, J.G., Palmer, A., Gyopari, M., 2005. Geological synopsis of the Manawatu-Horowhenua area for a review of the region's hydrogeology (IGNS Client Report 2005/172). Institute of Geological & Nuclear Sciences, Lower Hutt.

Bekesi, G., 1989. Geophysical studies over the north Horowhenua sedimentary basin. Unpublished MSc Thesis, Victoria University of Wellington, Wellington.

Belknap, D.F., 1975. Dating of late Pleistocene and Holocene relative sea levels in coastal Delaware. Unpublished MSc Thesis, University of Delaware, Newark.

Belknap, D.F., Kraft, J.C., Dunn, R.K., 1994. Transgressive valley-fill lithosomes: Delaware and Maine. In: Dalrymple, R.W., Boyd, R., Zaitlin, B.A. (Eds.), Incised-valley systems: origin and sedimentary sequences (SEPM Special Publication 51). Society for Sedimentary Geology, Tulsa, pp. 303–320.

Berryman, K., Hull, A., 2003. Tectonic controls on Late Quaternary shorelines: a review and prospects for future research. In: Goff, J.R., Nichol, S.L., Rouse, H.L. (Eds.), The New Zealand coast, Te Tai o Aotearoa. Dunmore Press with Whitireia Publishing and Daphne Brasell Associates, Palmerston North.

Berryman, K., Marden, M., Eden, D., 2000. Tectonic and paleoclimatic significance of Quaternary river terraces of the Waipaoa River, east coast, North Island, New Zealand. New Zealand Journal of Geology and Geophysics 43, 229–245.

Biggs, R.B., 1967. The sediments of Chesapeake Bay. In: Lauff, G.H. (Ed.), Estuaries (AAAS Special Publication 83). American Association of the Advancement of Science, Washington, D.C., pp. 239–260.

Biggs, R.B., Howell, B.A., 1984. The estuary as a sediment trap: alternate approaches to estimating its filtering efficency. In: Kennedy, V.S. (Ed.), The estuary as a filter. Academic Press, New York, pp. 107–129.

Bird, E.C.F., 1967. Depositional features in estuaries and lagoons on the south coast of New South Wales, Australia. Geographical Studies 5, 113–124.

Bird, M.I., Fifield, L.K., Chua, S., Goh, B., 2004. Calculating sediment compaction for radiocarbon dating of intertidal sediments. Radiocarbon 46, 421–435.

Bishop, D.G., Turnbull, I.M., 1996. Geology of the Dunedin area 1:250 000 geological map 21. Institute of Geological and Nuclear Sciences, Lower Hitt.

Blackwell, R.G., 1984. Aspects of the population dynamics of *Chione stutchburyi* in Ohiwa Harbour, Bay of Plenty, New Zealand. Unpublished PhD Thesis, University of Auckland, Auckland.

Bloom, A.L., 1964. Peat accumulation and compaction in a Connecticut salt marsh. Journal of Sedimentary Petrology 34, 599–603.

Bloom, A.L., Broecker, W.S., Chappell, J.M.A., Matthews, R.K., Mesolella, K.J., 1974. Quaternary sea level fluctuations on a tectonic coast: new $^{230}\mathrm{Th}/^{234}\mathrm{U}$ dates from the Huon Peninsula, New Guinea. Quaternary Research 4, 185–205.

Blum, M.D., Tornqvist, T.E., 2000. Fluvial responses for climate and sea-level change: a review and look forward. Sedimentology 47, 2–48.

Boyd, R., Dalrymple, R.W., Zaitlin, B.A., 1992. Classification of clastic coastal depositional environments. Sedimentary Geology 80, 139–150.

Boyd, R., Dalrymple, R.W., Zaitlin, B.A., 2006. Estuarine and incised-valley facies models. In: Posamentier, H., Walker, R. (Eds.), Facies models revisited (SEPM Special Publication 84). Society for Sedimentary Geology, Tulsa, pp. 171–235.

Bradshaw, B.E., 1993. Late Quaternary evolution of the St Georges Basin barrier-estuarine system. In: Thoms, M.C. (Ed.), Catchments and coasts in eastern Australia (Research Monograph 5). Department of Geography, University of Sydney, Sydney, pp. 60–71.

Briggs, I.C., 1974. Machine contouring using minimum curvature. Geophysics 39, 39–48.

Broger, E.J.K., Shylonyk, G.E., Zaitlin, B.A., 1997. Glauconitic sandstone exploration: a case study from the Lake Newell Project, southern Alberta. In: Pemberton, S.G., James, D.P. (Eds.), Petroleum geology of the Cretaceous Mannville Group, western Canada (CSPG Memoir 18). Canadian Society of Petroleum Geologists, Calgary, pp. 140–168.

Brook, F.J., 1999. Stratigraphy and landsnail faunas of Late Holocene coastal dunes, Tokerau Beach, northern New Zealand. Journal of the Royal Society of New Zealand 29, 337–359.

Brook, F.J., Thrasher, G.P., 1991. Cretaceous and Cenozoic geology of northernmost New Zealand (New Zealand Geological Survey Record 41). Department of Scientific and Industrial Research, Lower Hutt.

Brothers, R.N., 1954. The relative Pleistocene chronology of the South Kaipara District, New Zealand. Transactions of the Royal Society of New Zealand 82, 677–694.

Brown, L.F., Fisher, W.L., 1977. Seismic-stratigraphic interpretation of depositional systems: examples from Brazilian rift and pull-apart basins. In: Payton, C.E. (Ed.), Seismic stratigraphy — applications to hydrocarbon exploration (AAPG Memoir 26). American Association of Petroleum Geologists, Tulsa, pp. 213–248.

Brown, L.J., 1978. Quaternary geological studies in the Manawatu Region. Manawatu Catchment Board, Palmerston North.

Brown, L.J., 1984. Note on visit to Waitarere District, Horowhenua. Manawatu Catchment Board, Palmerston North.

Brown, L.J., 1990. New Zealand water well drillers' guide to logging water wells (NZGS Report G145). New Zealand Geological Survey, Lower Hutt.

Brown, L.J., 1995. Holocene shoreline depositional processes at Poverty Bay, a tectonically active area, northeastern North Island, New Zealand. Quaternary International 26, 21–33.

Brown, L.J., Gibbs, B.R., 1996. Heretaunga Plains groundwater resource investigations — Awatoto exploratory water well — HBRC No. 3699 (IGNS Client Report 1996/735102). Institute of Geological & Nuclear Sciences, Lower Hutt.

Bryant, E., 1992. Last Interglacial and Holocene trends in sea-level maxima around Australia: implications for modern rates. Marine Geology 108, 209–217.

Bullard, J.E., McTainsh, G.H., 2003. Aeolian-fluvial interactions in dryland environments: examples, concepts and Australia case study. Progress in Physical Geography 27, 471–450.

Burgess, S.M., 1985. The climate and weather of Manawatu and Horowhenua (NZMS Miscellaneous Publication 115[18]). New Zealand Meterological Service, Wellington.

Burrows, C.J., 1979. A chronology for cool-climate episodes in the Southern Hemisphere 12,000-1,000 yrs BP. Palaeogeography, Palaeoclimatology, Palaeoecology 27, 287–347.

Buurman, P., Pape, T., Reijneveld, J.A., de Jong, F., van Gelder, E., 2001. Laser-diffraction and pipette-method grain sizing of Dutch sediments: correlations for fine fractions of marine, fluvial and loess samples. Geologie en Mijnbouw 80, 49–57.

Campbell, J.D., Coombs, D.S., 1966. Murihiku Supergroup (Triassic-Jurassic) of Southland and south Otago. New Zealand Journal of Geology and Geophysics 9, 393–398.

Cann, J.H., Belperio, A.P., Murray-Wallace, C.V., 2000. Late Quaternary paleosealevels and paleoenvironments inferred from Foraminifera, Northern Spencer Gulf, South Australia. Journal of Foraminiferal Research 30, 29–53.

Carrell, J., 2009. Create geologic cross sections — eXacto Section, 9.2 (Arcscript 15806). Illinois State Geological Survey, Champaign, Illinois.

Carrigy, M.A., Fairbridge, R.W., 1954. Recent sedimentation, physiography and structure of the continental shelves of Western Australia. Journal of the Royal Society of Western Australia 38, 65–95.

Carroll, J.L., Wells, R.M.G., 1995. Strategies of anaerobiosis in New Zealand infaunal bivalves: adaptations to environmental and functional hypoxia. New Zealand Journal of Marine and Freshwater Research 29, 137–146.

Carter, L., Carter, R.M., Griggs, G.B., 1982. Sedimentation in the Conway Trough, a deep near-shore marine basin at the junction of the Alpine transform and the Hikurangi subduction plate boundary, New Zealand. Sedimentology 29, 475–497.

Carter, L., Manighetti, B., Elliot, M., Trustrum, N., Gomez, B., 2002. Source, sea level and circulation effect on the sediment flux to the deep ocean over the past 15 ka off eastern New Zealand. Global and Planetary Change 33, 339–355.

Carter, R.M., Johnson, D.P., 1986. Sea-level controls on the post-glacial development of the Great Barrier Reef, Queensland. Marine Geology 71, 137–164.

Carter, R.M., Naish, T.R., 1998. A review of Wanganui Basin, New Zealand: a global reference section for shallow marine, Plio-Pleistocene (0.25–0 Ma) cyclostratigraphy. Sedimentary Geology 122, 37–52.

Carter, R.M., Carter, L., Williams, J.J., Landis, C.A., 1985. Modern and relict sedimentation on the south Otago continental shelf, New Zealand (NZOI Memoir 93). Department of Scientific and Industrial Research, Wellington.

Carter, R.M., Carter, L., Johnson, D.P., 1986. Submergent shorelines in the SW Pacific: evidence for an episodic post-glacial transgression. Sedimentology 33, 629–649.

Carter, R.M., Abbott, S.T., Naish, T.R., 1999. Plio-Pleistocene cyclothems from Wanganui Basin, New Zealand: type locality for an astrochronologic time scale, or template for recognising ancient glacio-eustasy. Philosophical Transactions of the Royal Society of London, Series A 357, 1861–1872.

Cashman, S.M., Kelsey, H.M., Erdman, C.F., Cutten, H.N.C., Berryman, K.R., 1992. Strain partitioning between structural domains in the forearc of the Hikurangi subduction zone, New Zealand. Tectonics 11, 242–257.

Catuneanu, O., 2002. Sequence stratigraphy of clastic systems: concepts, merits, and pitfalls. Journal of African Earth Sciences 35, 1–43.

Catuneanu, O., 2006. Principles of sequence stratigraphy. Elsevier, Amsterdam.

Challands, K.I., 1976. A preliminary investigation of the Pohangina valley river terraces. Unpublished MSc Thesis, Massey University, Palmerston North.

Chapman, D.M., Geary, M., Roy, P.S., Thom, B.G., 1982. Coastal evolution and coastal erosion in New South Wales. Coastal Council of New South Wales, Sydney.

Chapman-Smith, M., Grant-Mackie, J.A., 1971. Geology of the Whangaparaoa area, eastern Bay of Plenty. New Zealand Journal of Geology and Geophysics 14, 3–38.

Chappell, J., 1964. Quaternary geology of south-west Auckland and north Taranaki coast. Unpublished MSc Thesis, University of Auckland, Auckland.

Chappell, J., 1970. Quaternary geology of the south-west Auckland coastal region. Transactions of the Royal Society of New Zealand (Earth Sciences) 8, 133–153.

Chappell, J., 1974. Late Quaternary glacio- and hydro- isostasy, on a layered earth. Quaternary Research 4, 405–428.

Chappell, J., 1975. Upper Quaternary warping and uplift rates in the Bay of Plenty and west coast, North Island, New Zealand. New Zealand Journal of Geology and Geophysics 18, 129–155.

Chappell, J., Omura, A., Esat, T., McCulloch, M., Pandolfi, J., Ota, Y., Pillans, B., 1996. Reconciliation of Late Quaternary sea levels derived from coral terraces at Huon Peninsula with deep sea oxygen isotope records. Earth and Planetary Science Letters 141, 227–236.

Chick, L.M., 1999. Potential tsunami hazard associated with the Kerepehi Fault, Hauraki Gulf, New Zealand. Unpublished MSc Thesis, University of Waikato, Hamilton.

Christensen, G., 2000. Agriculture — strength from the land. In: Saunders, B.G.R. (Ed.), The south of the north: Manawatu and its neighbours. Geography Programme, Massey University, Palmerston North, pp. 57–65.

Claessens, L., Veldkamp, A., ten Broeke, E.M., Vloemans, H., 2009. A Quaternary uplift record for the Auckland region, North Island, New Zealand, based on marine and fluvial terraces. Global and Planetary Change 68, 383–394.

Clark, J.A., Lingle, C.S., 1979. Predicted relative sea-level changes (18,000 years BP to present) caused by late-glacial retreat of the Antarctic Ice Sheet. Quaternary Research 11, 279–298.

Clement, A.J.H., Brook, M.S., 2008. Tilting of active folds and drainage asymmetry on the Manawatu anticlines, New Zealand: a preliminary investigation. Earth Surface Processes and Landforms 33, 1787–1795.

Clement, A.J.H., Fuller, I.C., 2007. Fluvial responses to environmental change in the North Island, New Zealand, during the past c. 30 ka recorded in river terrace sequences: a review and model for river behaviour. New Zealand Journal of Geology and Geophysics 50, 101–116.

Clement, A.J.H., Sloss, C.R., Fuller, I.C., 2008a. Holocene eustatic sea-level change in New Zealand. In: Geosciences '08 programme and abstracts (GSNZ Miscellaneous Publication 124A). Geological Society of New Zealand, Wellington, p. 19.

Clement, A.J.H., Sloss, C.R., Fuller, I.C., 2008b. Holocene sea-level change in New Zealand: a review. In: Boski, T., Duarte, D.N.R. (Eds.), Proceedings, Fifth International Meeting, IGCP 495: Quaternary landocean interactions, Faro, Portugal, 27 October - 1 November 2008. Centre on Marine and Environmental Research, University of the Algarve, Faro, pp. 46–47.

Clement, A.J.H., Sloss, C.R., Fuller, I.C., 2009a. Local-scale reconstructions of Holocene eustatic sea-level in the New Zealand archipelago. In: Proceedings, Sixth International Meeting IGCP 495: Quaternary land-ocean interactions, Myrtle Beach, South Carolina, 25-31 October 2009. Center for Marine and Wetland Studies, Coastal Carolina University, Conway, South Carolina, pp. 36–37.

Clement, A.J.H., Sloss, C.R., Fuller, I.C., 2009b. Reconstructing Holocene eustatic sea-level change in New Zealand . In: Abstracts, 7th International Conference on Geomorphology (ANZIAG), Melbourne, 6-11 July 2009. International Association of Geomorphologists, Melbourne.

Clement, A.J.H., Sloss, C.R., Fuller, I.C., 2010. Late Quaternary geomorphology of the Manawatu coastal plain, North Island, New Zealand. Quaternary International 221, 36–45.

Clifton, H.E., 1983. Discrimination between subtidal and intertidal facies in Pleistocene deposits, Willapa Bay, Washington. Journal of Sedimentary Petrology 53, 353–369.

Coe, A.L., Bosence, D.W.J., Church, K.D., Flint, S.S., Howell, J.A., Wilson, R.C.L., 2003. The sedimentary record of sea-level change. Cambridge University Press, Cambridge.

Cole, J.W., Lewis, K.B., 1981. Evolution of the Taupo-Hikurangi subduction system. Tectonophysics 72, 1–21.

Collinson, J.D., 1969. The sedimentology of the Grindslow Shales and the Kinderscout Grit: a deltaic complex in the Namurian of northern England. Journal of Sedimentary Petrology 39, 194–221.

Coombs, D.S., Landis, C.A., Norris, R., Carter, R.A., Borns, D., Craw, D., 1976. The Dun Mountain ophiolite belt, New Zealand, its tectonic setting, constitution, and origin, with special reference to its southern portion. American Journal of Science 26, 561–603.

Cope, R.N., Reed, J.J., 1967. The Cretaceous palaeogeology of the Taranaki-Cook Strait area. Proceedings of the Australian Institute of Mining and Metallurgy 222, 63–67.

Cotton, C.A., 1918. The geomorphology of the coastal district of south western Wellington. Transactions of the New Zealand Institute 50, 212–222.

Cotton, C.A., 1948. Otago's physiography. In: Garnier, B.J. (Ed.), The Face of Otago. Otago Centennial Historical Committee, Dunedin, pp. 1–17.

Cotton, C.A., 1957a. Pleistocene shorelines on the compound coast of Otago. New Zealand Journal of Science and Technology 38B, 750–762.

Cotton, C.A., 1957b. Tectonic features in a coastal setting at Wellington. Transactions of the Royal Society of New Zealand 84, 761–790.

Cotton, C.A., 1963. The question of high Pleistocene shorelines. Transactions of the Royal Society of New Zealand (Geology) 2, 51–62.

Cotton, C.A., Te Punga, M.T., 1955. Solifluxion and periglacially modified landforms at Wellington, New Zealand. Transactions of the Royal Society of New Zealand 82, 1001–1031.

Cotton, L.A., 1947. The pulse of the Pacific. Journal and Proceedings of the Royal Society of New South Wales 80, 41–76.

Cowie, J.D., 1961. Aokautere ash in the Manawatu district, New Zealand, and its significance to soils and soil formation in the sand country of the Manawatu-Horowhenua district, New Zealand. Unpublished MSc Thesis, Victoria University of Wellington, Wellington.

Cowie, J.D., 1963. Dune-building phases in the Manawatu District, New Zealand. New Zealand Journal of Geology and Geophysics 6, 268–280.

Cowie, J.D., 1964a. Aokautere Ash in the Manawatu District, New Zealand. New Zealand Journal of Geology and Geophysics 7, 67–77.

Cowie, J.D., 1964b. Loess in the Manawatu District, New Zealand. New Zealand Journal of Geology and Geophysics 7, 389–396.

Cowie, J.D., 1978. Soils and agriculture of Kairanga County, North Island, New Zealand (Soil Bureau Bulletin 33). Department of Scientific and Industrial Research, Wellington.

Cowie, J.D., Fitzgerald, P., Owers, W., 1967. Soils of the Manawatu-Rangitikei sand country (Soil Bureau Bulletin 29). Department of Scientific and Industrial Research, Wellington.

Cranfield, H.J., Michael, K.P., 2001a. Growth rates of five species of surf clams on a southern North Island beach, New Zealand. New Zealand Journal of Marine and Freshwater Research 35, 909–924.

Cranfield, H.J., Michael, K.P., 2001b. The surf clam fishery in New Zealand: description of the fishery, its management, and the biology of surf clams (New Zealand Fisheries Assessment Report 2001/62). Ministry of Fisheries, Wellington.

Cranfield, H.J., Michael, K.P., Stotter, D., Doonan, I.J., 1994. Distribution, biomass and yield estimates of surf clams off New Zealand beaches (New Zealand Fisheries Assessment Research Document 94/1). Ministry of Agriculture and Fisheries, Wellington.

Cullen, D.J., 1964. Foveaux bathymetry: New Zealand Oceanographic Institute Chart, Coastal Series; 1:200,000. New Zealand Oceanographic Institute, Wellington.

Cullen, D.J., 1967a. Submarine evidence from New Zealand of a rapid rise in sea-level about 11,000 years BP. Palaeogeography, Palaeoclimatology, Palaeoecology 3, 289–298.

Cullen, D.J., 1967b. The submarine geology of Foveaux Strait (NZOI Memoir 33 / DSIR Bulletin 184). New Zealand Oceanographic Institute, Wellington.

Cummings, V.J., Thrush, S.F., 2004. Behavioural response of juvenile bivalves to terrestrial sediment deposits: implications for post-disturbance recolonisation. Marine Ecology Progress Series 278, 179–191.

Curray, J.R., 1961. Late Quaternary sea-level: a discussion. Geological Society of America Bulletin 72, 1707–1712.

Curray, J.R., 1964. Transgressions and regressions. In: Miller, R.L. (Ed.), Papers in marine geology. Macmillan, New York, pp. 175–203.

Curray, J.R., 1965. Late Quaternary history, continental shelves of the United States. In: Wright, H.E., Frey, D.G. (Eds.), The Quaternary of the United States. Princeton University Press, Princeton, pp. 723–735.

Cutler, K.B., Edwards, R.L., Taylor, F.W., Cheng, H., Adkins, J., Gallup, C.D., Cutler, P.M., Burr, G.S., Bloom, A.L., 2003. Rapid sea-level fall and deep-ocean temperature change since the last interglacial period. Earth and Planetary Science Letters 206, 253–271.

Dalrymple, R.W., 1992. Tidal depositional systems. In: Walker, R.G., James, N.P. (Eds.), Facies models: response to sea level change. Geological Association of Canada, St John's, Newfoundland, pp. 195–218.

Dalrymple, R.W., 2006. Incised valleys in time and space: an introduction to the volume and an examination of the controls on valley formation and filling. In: Dalrymple, R.W., Leckie, D.A., Tillman, R.W. (Eds.), Incised valleys in time and space (SEPM Special Publication 85). Society for Sedimentary Geology, Tulsa, pp. 5–12.

Dalrymple, R.W., Knight, R.J., Zaitlin, B.A., Middleton, G.V., 1990. Dynamics and facies model of a macrotidal sand-bar complex, Cobequid Bay-Salmon River estuary (Bay of Fundy). Sedimentology 37, 577–612.

Dalrymple, R.W., Zaitlin, B.A., Boyd, R., 1992. Estuarine facies models: conceptual basis and stratigraphic implications. Journal of Sedimentary Petrology 62, 1130–1146.

Dalrymple, R.W., Zaitlin, B.A., Boyd, R., 1994. Estuarine facies models, conceptual basis and stratigraphic implications — reply. Journal of Sedimentary Research 64B, 76–77.

Davis, R A, J., Hayes, M.O., 1984. What is a wave-dominated coast? Marine Geology 60, 313–329.

D'Costa, D., Boswijk, G., Ogden, J., 2009. Holocene vegetation and environmental reconstructions from swamp deposits in the Dargaville region of the North Island, New Zealand: implications for the history of kauri (*Agathis australis*). The Holocene 19, 559–574.

de Lange, P.J., Lowe, D.J., 1990. History of vertical displacement of the Kerepehi Fault at Kopouatai bog, Hauraki lowlands, New Zealand, since c. 10,700 years ago. New Zealand Journal of Geology and Geophysics 33, 277–284.

Demarest, J M, I., Kraft, J.C., 1987. Stratigraphic record of Quaternary sea levels: implications for more ancient strata. In: Nummedal, D., Pilkey, O.H., Howard, J.D. (Eds.), Sea-level fluctuation and coastal evolution (SEPM Special Publication 41). Society of Economic Paleontologists and Mineralogists, Tulsa, pp. 223–239.

DeMets, C., Gordon, R.G., Argus, D.F., Stein, S., 1990. Current plate motions. Geophysical Journal International 101, 425–478.

Donaldson, A.C., Martin, R.H., Kanes, W.H., 1970. Holocene Guadalupe delta of Texas Gulf coast. In: Morgan, J.P., Shaver, R.H. (Eds.), Deltaic sedimentation: modern and ancient (SEPM Special Publication 15). Society of Economic Paleontologists and Mineralogists, Tulsa, pp. 107–137.

Donovan, A.D., Baum, G.R., Blechschmidt, G.L., Loutit, T.S., Pflum, C.E., Vail, P.R., 1988. Sequence stratigraphic setting of the Cretaceous-Tertiary boundary in central Alabama. In: Wilgus, C.K., Hastings, B.K., Posamentier, H., Van Wagoner, J., Ross, C.A., Kendall, C.G.S.C. (Eds.), Sea-level changes: an integrated approach (SEPM Special Publication 42). Society of Economic Paleontologists and Mineralogists, Tulsa, pp. 299–307.

Dorjes, J., Howard, J.D., 1975. Estuaries of the Georgia coast, USA: sedimentology and biology. IV. Fluvial-marine transition indicators in an estuarine environment, Ogeechee River-Ossabaw Sound. Senckenbergiana Maritima 7, 137–179.

Dougherty, A.J., Nichol, S.L., 2007. 3-D stratigraphic models of a composite barrier system, northern New Zealand. Journal of Coastal Research SI50.

Dravid, P.N., Brown, L.J., 1997. Heretaunga plains groundwater study: executive summary. Hawke's Bay Regional Council and Institute of Geological & Nuclear Sciences, Napier.

Dreaver, A.J., 1984. Horowhenua County and its people: a centennial history. Dunmore Press and Horowhenua County Council, Levin.

Duchesne, M.J., Pinet, N., Bedard, K., St-Onge, G., Lajeunesse, P., Campbell, D.C., Bolduc, A., 2010. Role of the bedrock topography in the Quaternary filling of a giant estuarine basin: the lower St Lawrence Estuary, eastern Canada. Basin Research 22, 933–951.

Duller, G.A.T., 1992a. Comparison of equivalent doses determined by thermoluminescence and infrered stimulated luminescence for dune sands in New Zealand. Quaternary Science Reviews 11, 39–43.

Duller, G.A.T., 1992b. Luminescence chronology of raised marine terraces , south-west North Island, New Zealand. Unpublished PhD Thesis, University of Wales, Aberystwyth.

Duller, G.A.T., 1994. Luminescence dating using feldspars: a test case from southern North Island, New Zealand. Quaternary Science Reviews 13, 423–427.

Duller, G.A.T., 1996. The age of the Koputaroa dunes, southwest North Island, New Zealand. Palaeogeography, Palaeoclimatology, Palaeoecology 121, 105–114.

Duncan, M.J., 1992. Flow regimes of New Zealand rivers. In: Mosley, M.P. (Ed.), Waters of New Zealand. New Zealand Hydrological Society, Wellington, pp. 13–27.

Edbrooke, S.W., Mazengarb, C., Stephenson, W., 2003. Geology and geological hazards of the Auckland urban area, New Zealand. Quaternary International 103, 3–21.

Eiby, G.A., 1955. The seismicity of Auckland City and Northland. New Zealand Journal of Science and Technology 36B, 488–494.

Eiby, G.A., 1990. Changes in Porirua Harbour in about 1855: historical tradition and geological evidence. Journal of the Royal Society of New Zealand 20, 233–248.

Emery, K.O., Wigley, R.L., Rubin, M., 1965. A submerged peat deposit off the Atlantic coast of the United States. Limnology and Oceanography Supplement 10, R97–R102.

Ensor, M.J., 1986. Sedimentology of Blueskin Bay. Unpublished MSc Thesis, University of Otago, Dunedin.

Esler, A.E., 1962. The Banks Lecture: Forest remnants of the Manawatu lowlands. New Zealand Plants and Gardens 4, 255–268.

Esler, A.E., 1964. The vegetation of early Manawatu. In: Saunders, B.G.R., Anderson, A.G. (Eds.), Introducing Manawatu (The Geography of New Zealand 1). Department of Geography, Massey University, Palmerston North, pp. 39–44.

Esler, A.E., 1978. Botany of the Manawatu District, New Zealand (DSIR Information Series 127). Department of Scientific and Industrial Research, Wellington.

Fair, E.E., 1968. Structural, tectonic and climatic control of the fluvial geomorphology of the Manawatu River west of the Manawatu Gorge. Unpublished MSc Thesis, Massey University, Palmerston North.

Fairbridge, R.W., 1950. Recent and Pleistocene coral reefs of Australia. Journal of Geology 58, 330–401.

Fairbridge, R.W., 1961. Eustatic changes in sea level . Physics and Chemistry of the Earth 4, 99–185.

Fairbridge, R.W., 1962. World sea-level and climatic changes. Quaternaria 6, 111–133.

Feldmeyer, A.E., Jones, B.C., Firth, C.W., Knight, J., 1943. Geology of the Palmerston-Wanganui Basin "west side", North Island, New Zealand (Petroleum Report 171). Superior Oil Company, Wellington.

Fergusson, G.J., Rafter, T.A., 1957. New Zealand 14C age measurements — 3. New Zealand Journal of Science and Technology 38B, 732–749.

Fergusson, G.J., Rafter, T.A., 1959. New Zealand 14C age measurements — 4. New Zealand Journal of Geology and Geophysics 2, 208–241.

Fisher, W.L., McGowen, J.H., 1967. Depositional systems in the Wilcox group of Texas and their relationship to occurrence of oil and gas. Transactions of the Gulf Coast Association Geological Society 17, 105–125.

Fleming, C.A., 1953a. Materials for a recent geochronology of New Zealand. In: Black, M.A. (Ed.), Report of the 7th Science Congress, Christchurch, 1951. Royal Society of New Zealand, Wellington, pp. 114–123.

Fleming, C.A., 1953b. The geology of the Wanganui Subdivision (NZGS Bulletin 52). New Zealand Geological Survey, Wellington.

Fleming, C.A., 1957. The ages of some Quaternary sediments from Wanganui District (N 137, N 138). New Zealand Journal of Science and Technology 38B, 726–731.

Fleming, C.A., 1962. New Zealand biogeography - a paleontologist's approach. Tuatara 10, 53–108.

Fleming, C.A., 1965. Radiocarbon dating from a postglacial beach in western Wellington. New Zealand Journal of Geology and Geophysics 8, 1222–1223.

Fleming, C.A., 1972. The contribution of C14 dates to the Quaternary geology of the 'Golden Coast', western Wellington. Tuatara 19, 61–69.

Froggatt, P.C., Lowe, D.J., 1990. A review of late Quaternary silicic and some other tephra formations from New Zealand: their stratigraphy, nomenclature, distribution, volume, and age. New Zealand Journal of Geology and Geophysics 33, 89–109.

Froggatt, P.C., Nelson, C.S., Carter, L., Griggs, G., Black, K.P., 1986. An exceptionally large Late Quaternary eruption from New Zealand. Nature 319, 578–582.

Fuller, I.C., Passmore, D.G., Heritage, G.L., Large, A.R.G., Milan, D.J., Brewer, P.A., 2002. Annual sediment budgets in an unstable gravel bed river: the River Coquet, northern England. In: Jones, S., E, F.L. (Eds.), Sediment flux to basins: causes, controls and consequences (Geological Society Special Publication 191). The Geological Society, London, pp. 115–131.

Fuller, I.C., Large, A.R.G., Charlton, M.E., Heritage, G.L., Milan, D.J., 2003. Reach-scale sediment transfers: an evaluation of two morphological budgeting approaches. Earth Surface Processes and Landforms 28, 889–903.

Gage, M., 1953. The study of Quaternary strand-lines in New Zealand. Transactions of the Royal Society of New Zealand 81, 27–34.

Galloway, W.E., 1989. Genetic stratigraphic sequences in basin analysis, I. Architecture and genesis of flooding-surface bounded depositional units. American Association of Petroleum Geologists Bulletin 73, 125–142.

Gehrels, W.R., 1999. Middle and Late Holocene sea-level changes in eastern Maine reconstructed from foraminiferal saltmarsh stratigraphy and AMS ^{14}C dates on basal peat. Quaternary Research 52, 350–359.

Gehrels, W.R., Hayward, B.W., Newnham, R.M., Southall, K.E., 2008. A 20th century acceleration of sea-level rise in New Zealand. Geophysical Research Letters 35, L02717.

Ghani, M.A., 1978. Late Cenozoic vertical crust movements in the southern North Island, New Zealand. New Zealand Journal of Geology and Geophysics 21, 117–125.

Gibb, J.G., 1977. Yellow-brown sands. In: Neall, V. (Ed.), Soil groups of New Zealand: part 2, yellow-brown sands. Soil Science Society of New Zealand, Wellington, pp. 77–85.

Gibb, J.G., 1978. The problem of coastal erosion along the 'Golden Coast' western Wellington, New Zealand (Water & Soil Technical Publication 10). Water & Soil Division, Ministry of Works and Development, Wellington.

Gibb, J.G., 1979. Late Quaternary shoreline movements in New Zealand. Unpublished PhD Thesis, Victoria University of Wellington, Wellington.

Gibb, J.G., 1983. Sea levels during the past 10000 years BP from the New Zealand region — South Pacific Ocean. In: Abstracts of International Symposium on Coastal Evolution in the Holocene, August 29-31, Tokyo, Japan. Japan Society for the Promotion of Science, Tokyo, pp. 28–31.

Gibb, J.G., 1986. A New Zealand regional Holocene eustatic sea-level curve and its application to determination of vertical tectonic movements. Royal Society of New Zealand Bulletin 24, 377–395.

Gibb, J.G., Aburn, J.H., 1986. Shoreline fluctuations and an assessment of a coastal hazard zone along Pauanui Beach, eastern Coromandel Peninsula, New Zealand (Water & Soil Technical Publication 27). National Water Soil Conservation Authority and Water and Soil Directorate, Ministry of Works and Development, Wellington.

Gibb, J.G., Cox, G.J., 2009. Patterns and rates of sedimentation within Porirua Harbour (Coastal Management Consultancy Report CR 2009/1). Coastal Management Consultants, Kerikeri.

Glenie, R.C., Schofield, J.C., Ward, W.T., 1968. Tertiary sea levels in Australia and New Zealand. Palaeogeography, Palaeoclimatology, Palaeoecology 5, 141–163.

Glover, D.M.J., 1997. Holocene infill of an incised valley system, Blacksmith's Creek, Whangarei. Unpublished MSc Thesis, University of Auckland, Auckland.

Godwin, H., 1962. Half-life of radiocarbon. Nature 195, 984.

Godwin, H., Suggate, R.P., Willis, E.H., 1958. Radiocarbon dating of the eustatic rise in ocean-level . Nature 181, 1518–1519.

Goff, J.R., Rouse, H.L., Jones, S.L., Hayward, B.W., Cochran, U., McLea, W., Dickinson, W.W., Morley, M.S., 2000. Evidence for an earthquake and tsunami about 3100-3400 yr ago, and other catastrophic saltwater inundations recorded in a coastal lagoon, New Zealand. Marine Geology 170, 231–249.

Goff, J.R., Pearce, S., Nichol, S.L., Chague-Goff, C., Horrocks, M., Strotz, L., 2010. Multi-proxy records of regionally-sourced tsunamis, New Zealand. Geomorphology 118, 369–382.

Goldie, P.J., 1975. The Quaternary geology of an area north of Houhora. Unpublished MSc Thesis, University of Auckland, Auckland.

Goodbred, S.L., Kuehl, S.A., 1999. Holocene and modern sediment budgets for the Ganges-Brahmaputra river system: evidence for highstand dispersal to floodplain, shelf, and deep-sea depocenters. Geology 27, 559–562.

Goodchild, M.F., Mark, D.M., 1987. The fractal nature of geographic phenomena. Annals of the Association of American Geographers 77, 265–278.

Grange, K.R., 1979. Soft-bottom macrobenthic communities of Manukau Harbour, New Zealand. New Zealand Journal of Marine and Freshwater Research 13, 315–329.

Grant, C.M., 1994. Demographics and reproduction of the tuatua — *Paphies subtriangulata*. Unpublished MSc Thesis, University of Auckland, Auckland.

Grant, C.M., Hay, B.E., 2003. A review of issues related to depletion of populations of selected infaunal bivalve species in the Hauraki Gulf marine park. AquaBio Consultants, Auckland.

Grant, P., 1985. Major periods of erosion and alluvial sedimentation in New Zealand during the late Holocene. Journal of the Royal Society of New Zealand 15, 67–121.

Grant-Taylor, T.L., Rafter, T.A., 1962. New Zealand radiocarbon age measurements — 5. New Zealand Journal of Geology and Geophysics 5, 331–359.

Grant-Taylor, T.L., Rafter, T.A., 1971. New Zealand radiocarbon age measurements — 6. New Zealand Journal of Geology and Geophysics 14, 364–402.

Grapes, R., Downes, G., 1997. The 1855 Wairarapa, New Zealand, earthquake — analysis of historical data. New Zealand National Society for Earthquake Engineering Bulletin 30, 272–368.

Haddon, M., Willis, T.J., Wear, R.G., Anderlini, V.C., 1996. Biomass and distribution of five species of surf clam of an exposed west coast North Island beach, New Zealand. Journal of Shellfish Research 15, 331–339.

Handley, S., 2006. An analysis of historical impacts and composition of the benthic environment of Tasman and Golden Bays (NIWA Client Report NEL2006-002). National Institute of Water & Atmospheric Research, Nelson.

Hannigan, J.W., Barnes, K., 1982. History of the Manawatu River and the Manawatu Catchment Board. Manawatu Catchment Board and Regional Water Board, Palmerston North.

Haq, B.U., 1991. Sequence stratigraphy, sea-level change, and significance for the deep sea. In: Macdonald, D.I.M. (Ed.), Sedimentation, tectonics and eustasy: sea-level changes at active margins (IAS Special Publication 12). International Association of Sedimentologists, Oxford, pp. 3–39.

Harrington, H.J., 1958. Geology of the Kaitangata Coalfield (New Zealand Geological Survey Bulletin 59). Department of Scientific and Industrial Research, Wellington.

Haslett, S.K., Davies, P., Curr, R.H.F., Davies, C.F.C., Kennington, K., King, C.P., Margetts, A.J., 1998. Evaluating late Holocene relative sea-level change in the Somerset Levels, southwest Britain. The Holocene 8, 197–207.

Hawke, R.M., McConchie, J.A., 2005. The source, age, and stabilisation of the Koputaroa dunes, Otaki-Te Horo, New Zealand. New Zealand Journal of Geology and Geophysics 48, 517–522.

Hawke, R.M., McConchie, J.A., 2006. Dune phases in the Otaki-Te Horo area (New Zealand): a geomorphic history. Earth Surface Processes and Landforms 31, 633–645.

Haworth, R.J., Baker, R.G.V., Flood, P.G., 2002. Predicted and observed Holocene sea-level in the Australian coast: what do they indicate about hydro-isostatic models in far-field sites? Journal of Quaternary Science 17, 581–591.

Hayes, M.O., 1979. Barrier island morphology as a function of wave and tide regime. In: Leatherman, S.P. (Ed.), Barrier islands from the Gulf of Mexico to the Gulf of St. Lawrence. Academic Press, New York, pp. 1–29.

Hayward, B.W., Stilwell, J.D., 1995. Floating cockle shells *(Austrovenus stutchburyi)* — their significance to paleoenvironmental assessments. Tane 35, 143–148.

Hayward, B.W., Stephenson, A.B., Morley, M., Riley, J.L., Grenfell, H.R., 1997. Faunal changes in Waitemata Harbour sediments, 1930s–1990s. Journal of the Royal Society of New Zealand 27, 1–20.

Hayward, B.W., Grenfell, H.R., Sandiford, A., Shane, P.R., Morley, M.S., Alloway, B.V., 2002. Foraminiferal and molluscan evidence for the Holocene marine history of two breached maar lakes, Auckland, New Zealand. New Zealand Journal of Geology and Geophysics 45, 467–479.

Hayward, B.W., Grenfell, H.R., Sabaa, A.T., Southall, K.E., Gehrels, W.R., 2007. Foraminiferal evidence of Holocene fault displacements in coastal south Otago, New Zealand. Journal of Foraminiferal Research 37, 344–359.

Hayward, B.W., Grenfell, H.R., Sabaa, A.T., Kay, J., 2010a. Using foraminiferal faunas as proxies for low tide level in the estimation of Holocene tectonic subsidence, New Zealand. Marine Micropaleontology 76, 23–36.

Hayward, B.W., Grenfell, H.R., Sabaa, A.T., Kay, J., Daymond-King, R., Cochran, U., 2010b. Holocene subsidence at the transition between strike-slip and subduction on the Pacific-Australian plate boundary, Marlborough Sounds, New Zealand. Quaternary Science Reviews 29, 648–661.

Hayward, B.W., Wilson, K., Morley, M.S., Cochran, U., Grenfell, H.R., Sabaa, A.T., Daymond-King, R., 2010c. Microfossil record of the Holocene evolution of coastal wetlands in a tectonically active region of New Zealand. The Holocene 20, 405–421.

Healy, W.B., 1980. Pauatahanui Inlet — an environmental study (DSIR Information Series 141). Science Information Division, Department of Scientific and Industrial Research, Wellington.

Heap, A.D., 1995. Stratigraphic reconstruction of an incised valley system, Weiti River estuary, New Zealand. Unpublished MSc Thesis, University of Auckland, Auckland.

Heap, A.D., Nichol, S.L., 1997. The influence of limited accommodation space on the stratigraphy of an incised-valley succession: Weiti River estuary, New Zealand. Marine Geology 144, 229–252.

Heap, A.D., Bryce, S., Ryan, D.A., 2004. Facies evolution of Holocene estuaries and deltas: a large-sample statistical study from Australia. Sedimentary Geology 168, 1–17.

Heerdegen, R.G., 1972. Landforms of the Manawatu (Geography of the Manawatu Miscellaneous Paper 2). Department of Geography, Massey University, Palmerston North.

Heerdegen, R.G., Shepherd, M.J., 1992. Manawatu landforms — product of tectonism, climate change and process. In: Soons, J.M., Selby, M.J. (Eds.), Landforms of New Zealand. Longman Paul, Auckland, pp. 308–333.

Heine, R.W., 1982. A new interpretation of the geomorphology of Wellington. Journal of the Royal Society of New Zealand 12, 189–205.

Henderson, J., 1924. The Post-Tertiary history of New Zealand. Transactions of the New Zealand Institute 55, 580–599.

Herzer, R.H., 1977. Late Quaternary geology of the Canterbury continental terrace. Unpublished PhD Thesis, Victoria University of Wellington, Wellington.

Herzer, R.H., 1981. Late Quaternary stratigraphy and sedimentation of the Canterbury continental shelf, New Zealand (NZOI Memoir 89). Department of Scientific and Industrial Research, Wellington.

Hesp, P.A., 1975. The late Quaternary geomorphology of the lower Manawatu. Unpublished MA Thesis, Massey University, Palmerston North.

Hesp, P.A., 2001. The Manawatu dunefield: environmental change and human impacts. New Zealand Geographer 57, 33–40.

Hesp, P.A., Shepherd, M.J., 1978. Some aspects of the late Quaternary geomorphology of the lower Manawatu valley, New Zealand. New Zealand Journal of Geology and Geophysics 21, 403–412.

Hesp, P.A., Shepherd, M.J., Parnell, K., 1999. Coastal geomorphology in New Zealand, 1989-99. Progress in Physical Geography 23, 501–524.

Hesse, P.P., Magee, J.W., van dee Kaars, S., 2004. Late Quaternary climates of the Australian arid zone: a review. Quaternary International 118-119, 87–102.

Hewitt, J.E., Thrush, S.F., Cummings, V.J., Pridmore, R.D., 1996. Matching patterns with processes: predicting the effect of size and mobility on the spatial distributions of the bivalves *Macomona liliana* and *Austrovenus stutchburyi*. Marine Ecology Progress Series 135, 57–67.

Hicks, D.L., 1983. Landscape evolution in consolidated coastal dunesands. Zeitschrift fur Geomorphologie, Supplement 45, 245–250.

Hicks, D.M., Shankar, U., 2003. Sediment from New Zealand rivers (NIWA Miscellaneous Chart 79). National Institute of Water and Atmospheric Research, Wellington.

Hicks, H., Nichol, S.L., 2007. A marine to freshwater sediment succession from Kowhai Beach wetland, Northland: implications for Holocene sea level. Journal of the Royal Society of New Zealand 37, 91–107.

Higham, T.F.G., Hogg, A.G., 1995. Radiocarbon dating of prehistoric shell from New Zealand and calculation of the ΔR value using fish otoliths. Radiocarbon 37, 409–416.

Higham, T.F.G., Hogg, A.G., 1997. Evidence for late Polynesian colonisation of New Zealand: University of Waikato radiocarbon measurements. Radiocarbon 39, 149–192.

Hogg, A.G., Higham, T.F.G., Dahm, J., 1998. ^{14}C dating of modern marine and estuarine shellfish. Radiocarbon 40, 975–984.

Hooker, S.H., Creese, R.G., 1995. The reproductive biology of pipi, *Paphies australis* (Gmelin, 1790) (Bivalvia: Mesodesmatidae). I. Temporal patterns of the reproductive cycle. Journal of Shellfish Research 14, 7–15.

Horrocks, M., Ogden, J., Nichol, S.L., Alloway, B.V., Sutton, D.G., 1999. The palynology and sedimentology of a coastal swamp at Awana, Great Barrier Island, New Zealand, from c. 7000 yr BP to present. Journal of the Royal Society of New Zealand 29, 213–233.

Horrocks, M., Deny, Y., Ogden, J., Sutton, D.G., 2000a. A reconstruction of the history of a Holocene sand dune on Great Barrier Island, northern New Zealand, using pollen and phytolith analyses. Journal of Biogeography 27, 1269–1277.

Horrocks, M., Ogden, J., Nichol, S.L., Alloway, B.V., Sutton, D.G., 2000b. A Late Quaternary palynological and sedimentological record from two coastal swamps at southern Kaitoke, Great Barrier Island, New Zealand. Journal of the Royal Society of New Zealand 30, 49–68.

Horrocks, M., Nichol, S.L., D'Costa, D., Augustinus, P., Jacobi, T., Shane, P.A., Middleton, A., 2007. A Late Quaternary record of natural change and human impact from Rangihoua Bay, Bay of Islands, northern New Zealand. Journal of Coastal Research 23, 592–604.

Horton, B.P., Culver, S.J., Hardbattle, M.I.J., Larcombe, P., Milne, G.A., Morigi, C., Whittaker, J.E., Woodroffe, S.A., 2007. Reconstructing Holocene sea-level change for the central Great Barrier Reef (Australia) using subtidal foraminifera. Journal of Foraminiferal Research 37, 327–343.

Hubbard, C.B., Neall, V.E., 1980. A reconstruction of late Quaternary erosional events in the West Tamaki River catchment, southern Ruahine Range, North Island, New Zealand. New Zealand Journal of Geology and Geophysics 23, 587–593.

Hughen, K.A., Baillie, M.G.L., Bard, E., Beck, J.W., Bertrand, C.J.H., Blackwell, P.G., Buck, C.E., Burr, G.S., Cutler, K.B., Damon, P.E., Edwards, R.L., Fairbanks, R.G., Friedrich, M., Guilderson, T.P., Kromer, B., McCormac, G., Manning, S., Bronk Ramsey, C., Reimer, P.J., Reimer, R.W., Remmele, S., Southon, J.R., Stuiver, M., Talamo, S., Taylor, F.W., van der Plicht, J., Weyhenmeyer, C.E., 2004. Marine04 marine radiocarbon age calibration, 0-26 cal kyr BP. Radiocarbon 46, 1059–1086.

Hughes, G.R., 2005a. Evolution of the north Horowhenua coastal depositional system in response to late Pleistocene sea level changes. Unpublished MSc Thesis, Victoria University of Wellington, Wellington.

Hughes, G.R., 2005b. Paleoenvironmental analysis and chronology of strata encountered within Levin groundwater investigation bore, Main Road South, Levin. School of Earth Sciences, Victoria University of Wellington, Wellington.

Hughes, G.R., Kennedy, D.M., 2009. Late Pleistocene sea-level oscillations (MIS 10–2) recorded in shallow marine and coastal plain sediments of the southern Wanganui Basin, New Zealand. Quaternary Research 71, 477–489.

Hull, A.G., 1985. A possible eustatic sea level rise c. 4500 years BP: evidence from New Zealand coast (note). In: Pillans, B. (Ed.), Proceedings of the second CLIMANZ conference, Harihari, Westland, New Zealand, February 4-8 1985. Geology Department, Victoria University of Wellington, Wellington, pp. 8–12.

Hull, A.G., Berryman, K.R., 1986. Holocene tectonism in the region of the Alpine Fault at Lake McKerrow, Fiordland, New Zealand. Royal Society of New Zealand Bulletin 24, 317–331.

Hull, A.G., Mansergh, G.D., Townsend, T.D., Stagpoole, V.M., 1995. Earthquake hazards in the Auckland region (Auckland Regional Council Technical Publication 57). Auckland Regional Council, Environment Division, Auckland.

Hume, T., 2003. Estuaries and tidal inlets. In: Goff, J.R., Nichol, S.L., Rouse, H.L. (Eds.), The New Zealand coast, Te Tai o Aotearoa. Dunmore Press with Whitireia Publishing and Daphne Brasell Associates, Palmerston North, pp. 191–213.

Hume, T.M., Dahm, J., 1991. An investigation of the effects of Polynesian and European land use on sedimentation in Coromandel estuaries (Water Quality Center, DSIR, Consultancy Report 7106). Water Quality Centre, Department of Scientific and Industrial Research, Hamilton.

Hume, T.M., Herdendorf, C.E., 1988. A geomorphic classification of estuaries and its application to coastal resource management — a New Zealand example‘. Ocean & Shoreline Management 11, 249–274.

Hume, T.M., McGlone, M.S., 1986. Sedimentation patterns and catchment use change recorded in the sediments of a shallow tidal creek, Lucas Creek, upper Waitamata Harbour, New Zealand. New Zealand Journal of Marine and Freshwater Research 20, 677–687.

Hutcheon, R.L., 2006. Evaluation of evidence of mid-Holocene sea-level in the Auckland region. Unpublished MA Thesis, University of Auckland, Auckland.

Jackson, J., Van Dissen, R., Berryman, K., 1998. Tilting of active folds and faults in the Manawatu region, New Zealand: evidence from surface drainage patterns. New Zealand Journal of Geology and Geophysics 41, 377–385.

Jelgersma, S., 1966. Sea-level changes during the last 10,000 years. In: Sawyer, J.S. (Ed.), World climate from 8000 to 0 BC: Proceedings of the International Symposium held at Imperial College, London, 18 and 19 April 1966. Royal Meteorological Society, London, pp. 54–71.

Jervey, M.T., 1988. Quantitative geological modelling of siliciclastic rock sequences and their seismic expression. In: Wilgus, C.K., Hastings, B.K., Kendall, C.G.S.C., Posamentier, H.W., Ross, C.A., Van Wagoner, J.C. (Eds.), Sea-level changes: an integrated approach (SEPM Special Publication 42). Society of Economic Paleontologists and Mineralogists, Tulsa, pp. 47–69.

Jobberns, G., 1926. Raised beaches in the Teviotdale District, North Canterbury. Transactions of the New Zealand Institute 56, 225–226.

Jobberns, G., 1928. The raised beaches of the north east portion of the South Island of New Zealand. Transactions of the New Zealand Institute 59, 508–570.

Johnston, R.M.S., 1984. Sediments and sedimentary processes in Mahurangi Harbour. Unpublished MSc Thesis, University of Waikato, Hamilton.

Jones, C.J., 1979. Anatomy of *Chione cancellata* and some other Chionines (Bivalvia, Veneridae) . Malacologia 19, 157–199.

Journeaux, T.D., Kamp, P.J.J., Naish, T.R., 1996. Middle Pleistocene cyclothems, Mangaweka region, Wanganui Basin, New Zealand: a lithostratigraphic framework. New Zealand Journal of Geology and Geophysics 39, 135–149.

Juniper, S.K., 1981. Stimulation of bacterial activity by a deposit feeder in two New Zealand intertidal inlets. Bulletin of Marine Science 31, 691–701.

Kaewyana, W., 1980. Late Quaternary alluvial terraces and their cover bed stratigraphy, Eketahuna and Pahiatua Districts, New Zealand. Unpublished MSc Thesis, Victoria University of Wellington, Wellington.

Kalish, J.M., 1993. Pre-bomb and post-bomb radiocarbon in fish otoliths. Earth and Planetary Science Letters 114, 549–554.

Kamp, P.J.J., 1992a. Landforms of Hawke's Bay and their origin: a plate tectonic interpretation. In: Soons, J.M., Selby, M.J. (Eds.), Landforms of New Zealand. Longman Paul, Auckland, pp. 344–366.

Kamp, P.J.J., 1992b. Landforms of Wairarapa: a geological perspective. In: Soons, J.M., Selby, M.J. (Eds.), Landforms of New Zealand. Longman Paul, Auckland, pp. 367–381.

Kamp, P.J.J., McIntyre, A.P., 1998. The stratigraphic architecture of Late Pliocene (2.8–2.4 Ma) asymmetrical shelf sequences, western Wanganui Basin, New Zealand. Sedimentary Geology 122, 53–67.

Kampman, I., Caldwell, K.J., 1985. Groundwater resources of the Waitohu, Otaki and Mangone (Report No. 65). Manawatu Catchment Board and Regional Water Board, Palmerston North.

Katz, H.R., 1968. Potential oil formations in New Zealand, and their stratigraphic position as related to basin evolution. New Zealand Journal of Geology and Geophysics 11, 1077–1133.

Katz, R., Leask, B.L., 1990. The South Wanganui Basin — a neglected hydrocarbon prospect. In: Petroleum exploration in New Zealand: proceedings of the 1989 New Zealand oil exploration conference (volume 1). Petroleum and Geothermal Unit, Energy and Resources Division, Ministry of Commerce, Wellington, pp. 71–80.

Kaye, C.A., Barghoorn, E.S., 1964. Late Quaternary sea-level change and crustal rise at Boston, Massachusetts, with notes on the autocompaction of peat. Geological Society of America Bulletin 75, 63–80.

Kear, D., 1957. Stratigraphy of the Kaawa-Ohuka coastal area, west Auckland. New Zealand Journal of Science and Technology 38B, 826–842.

Kear, D., 1959. Geology of the Kamo Mine area. New Zealand Journal of Geology and Geophysics 2, 541–568.

Kear, D., 1962. Geology of ironsand resources of New Zealand (with notes on limestone, silica and bentonite). Department of Scientific and Industrial Research, Wellington.

Kear, D., 1963. Geology of the Te Akau District, west Auckland, New Zealand, and its regional implications. Unpublished PhD Thesis, University of London, London.

Kear, D., 1965. Geology of New Zealand's ironsand resources. In: Buckenham, M.H. (Ed.), Proceedings of New Zealand meeting: Eighth Commonwealth mining and metallurgical Congress, Wellington, 6-8 April 1965. School of Mines and Metallurgy, University of Otago, Dunedin.

Kear, D., Waterhouse, B.C., 1961. Quaternary surfaces and sediments at Waihi Beach. New Zealand Journal of Geology and Geophysics 4, 434–445.

Kear, D., Waterhouse, B.C., 1971. Further comments - Waihi terrace and Hamilton ash ages. Earth Science Journal 5, 114–115.

Kennedy, D.M., 2008. Recent a future higher sea levels in New Zealand: a review. New Zealand Geographer 64, 105–116.

Kennedy, D.M., Paulik, R., Millar, M., 2008. Infill of a structurally controlled estuary: an example from southern Whanganui Inlet, New Zealand. New Zealand Geographer 64, 20–33.

Kershaw, A.P., Strickland, K.M., 1988. A Holocene pollen diagram from Northland, New Zealand. New Zealand Journal of Botany 26, 145–152.

Kidson, C., 1982. Sea level changes in the Holocene. Quaternary Science Reviews 162, 121–151.

King, L.C., 1930. Raised beaches of the south-east coast of the North Island of New Zealand. Transactions of the New Zealand Institute 61, 498–523.

King, L.C., 1932. Notes on the geology and geomorphology of the coast between Napier and Castlepoint. Transactions of the New Zealand Institute 63, 72–79.

King, L.C., Jobberns, G., 1934. Shoreline changes of the New Zealand coast. In: Proceedings of the Fifth Pacific Science Congress, Volume 2: astronomy, geodesy and geography, geology and mineral resources. University of Toronto Press, Toronto, pp. 1285–1295.

Kingma, J.T., 1957. The tectonic setting of the Ruahine-Rimutaka Range. New Zealand Journal of Science and Technology 38B, 858–861.

Kingma, J.T., 1958. Geology of the Wakarara Range: central Hawkes Bay. New Zealand Journal of Geology and Geophysics 1, 76–91.

Kingma, J.T., 1962. Geological map of New Zealand 1:250,000, Sheet 11 Dannevirke. Department of Scientific and Industrial Research, Wellington.

Kingma, J.T., 1967. Geological map of New Zealand 1:250,000, Sheet 12 Wellington. Department of Scientific and Industrial Research, Wellington.

Kirk, R.M., 1977. Rates and forms of erosion on intertidal platforms at Kaikoura Peninsula, South Island, New Zealand. New Zealand Journal of Geology and Geophysics 20, 571–613.

Klum, L.D., Byrne, J.V., 1967. Sediments of Yaquina Bay, Oregon. In: Lauff, G.H. (Ed.), Estuaries (AAAS Special Publication 83). American Association for the Advancement of Science, Washington, D.C., pp. 226–238.

Lamarche, G., Proust, J., Nodder, S.D., 2005. Long-term slip rates and fault interactions under low contractional strain, Wanganui Basin, New Zealand. Tectonics 24, TC4004.

Lamb, S.H., Vella, P., 1987. The last million years of deformation in part of the New Zealand plate-boundary zone. Journal of Structural Geology 9, 877–891.

Lambeck, K., Chappell, J., 2001. Sea level change through the Last Glacial cycle. Science 292, 679–686.

Lambeck, K., Yokoyama, Y., Purcell, T., 2002. Into and out of the Last Glacial Maximum: sea-level change during Oxygen Isotope Stages 3 and 2. Quaternary Science Reviews 21, 343–360.

Landis, C.A., 1988. History of Quaternary sedimentation, erosion and tectonics in a segment of the Otago coast (notes).

Lane, S.N., Chandler, J.H., Richards, K.S., 1994. Developments in monitoring and terrain modelling small-scale river-bed topography. Earth Surface Processes and Landforms 19, 349–368.

Larcombe, M.F., 1971. The ecology, population dynamics, and energetics of some soft shore molluscs. Unpublished PhD Thesis, University of Auckland, Auckland.

Law, M.D., 1987. From bush to swamp: the Centenary of Shannon 1887 – 1987. Dunmore Press, Palmerston North.

Leach, B.F., Anderson, A.J., 1974. The transformation from an estuarine to lacustrine environment in the lower Wairarapa. Journal of the Royal Society of New Zealand 4, 267–275.

Leamy, M.L., 1958. Pleistocene shorelines at Porirua Harbour, near Wellington, New Zealand. New Zealand Journal of Geology and Geophysics 1, 95–102.

Lee, J.M., Begg, J.G., 2002. Geology of the Wairarapa area 1:250 000 geological map 10. Institute of Geological & Nuclear Sciences, Lower Hutt.

Lelieveld, S.D., Pilditch, C.A., Green, M.O., 2004. Effects of deposit-feeding bivalve *(Macomona liliana)* density on intertidal sediment stability. New Zealand Journal of Marine and Freshwater Research 38, 115–128.

Lensen, G.J., 1959. Sheet 10 Wanganui 1:25,000 geological map of New Zealand. Department of Scientific and Industrial Research, Wellington.

Lensen, G.J., 1975. Earth-deformation studies in New Zealand. Tectonophysics 29, 541–551.

Levy, J., Christie-Blick, N., 1994. Neoproterozoic incised valleys of the eastern Great Basin, Utah and Idaho: fluvial response to changes in depositional base level. In: Dalrymple, R.W., Boyd, R., Zaitlin, B.A. (Eds.), Incised-valley systems: origin and sedimentary sequences (SEPM Special Publication 51). Society for Sedimentary Geology, Tulsa, pp. 369–384.

Lewis, K.B., Pettinga, J.R., 1993. The emerging, imbricate frontal wedge of the Hikurangi Margin. In: Ballance, P.F. (Ed.), South Pacific sedimentary basins (Sedimentary Basins of the World, 2). Elsevier, Amsterdam, pp. 225–250.

Lewis, K.B., Carter, L., Davey, F.J., 1994. The opening of Cook Strait: interglacial tidal scour and aligning basins at a subduction to transform plate edge. Marine Geology 116, 293–312.

Lewis, S.E., Wust, R.A.J., Webster, J.M., Sheilds, G.A., 2008. Mid-late Holocene sea-level variability in eastern Australia. Terra Nova 20, 74–81.

Li, B., Li, C., Shen, H., 2003. A preliminary study on sediment flux in the Shangjiang Delta during the postglacial period. Science in China (Series D) 46, 743–752.

Li, C., Wang, P., Fan, D., Yang, S., 2006. Characteristics and formation of Late Quaternary incised-valley-fill sequences in sediment-rich deltas and estuaries: case studies from China. In: Dalrymple, R.W., Leckie, D.A., Tillman, R.W. (Eds.), Incised valleys in time and space (SEPM Special Publication 85). Society for Sedimentary Geology, Tulsa, pp. 141–160.

Lieffering, R.E., 1990. Hydrogeological investigations of the Palmerston North region. Unpublished MSc Thesis, Massey University, Palmerston North.

Lillie, A.R., 1953. The geology of the Dannevirke Subdivision (New Zealand Geological Survey Bulletin 46). Department of Scientific and Industrial Research, Wellington.

Lin, C.M., Gu, L.X., Li, G.Y., Zhao, Y.Y., Jiang, W.S., 2004. Geology and formation mechanism of Late Quaternary shallow biogenic gas reservoirs in the Hangzhou Bay area, eastern China. American Association of Petroleum Geologists Bulletin 98, 613–625.

Lin, C.M., Zhuo, H.C., Gao, S., 2005. Sedimentary facies and evolution in the Aiantang River incised valley, eastern China. Marine Geology 219, 235–259.

Litchfield, N., 2003. Maps, stratigraphic logs and age control data for river terraces in the eastern North Island (IGNS Science Report 2003/31). Institute of Geological & Nuclear Sciences, Lower Hutt.

Litchfield, N., Berryman, K., 2005. Correlation of fluvial terraces within the Hikurangi Margin, New Zealand: implications for climate and base level controls. Geomorphology 68, 291–313.

Litchfield, N., Berryman, K., 2007. Relations between postglacial fluvial incision rates and uplift rates in the North Island, New Zealand. Journal of Geophysical Research 111, F02007.

Litchfield, N., Reiser, U., 2005. Optically stimulated luminescence age constraints for fluvial aggradation terraces and loess in the eastern North Island, New Zealand. New Zealand Journal of Geology and Geophysics 48, 581–589.

Litchfield, N.J., Lian, O.B., 2004. Luminescence age estimates of Pleistocene marine terrace and alluvial fan sediments associated with tectonic activity along coastal Otago, New Zealand. New Zealand Journal of Geology and Geophysics 47, 29–37.

Loizeau, J.L., Arbouille, D., Santiago, S., Vernet, J.P., 1994. Evaluation of a wide range laser diffraction grain size analyser for use with sediments. Sedimentology 41, 353–361.

Loutit, T.S., Hardenbol, J., Vail, P.R., Baum, G.R., 1988. Condensed sections: the key to age dating and correlation of continental margin sequences. In: Wilgus, C.K., Hastings, B.K., Posamentier, H., Van Wagoner, J., Ross, C.A., Kendall, C.G.S.C. (Eds.), Sea-level changes: an integrated approach (SEPM Special Publication 42). Society of Economic Paleontologists and Mineralogists, Tulsa, pp. 183–213.

Lowe, D.J., Newnham, R.M., Ward, C.M., 1999. Stratigraphy and chronology of a 15 ka sequence of multi-sourced silicic tephras in a montane peat bog, eastern North Island, New Zealand. New Zealand Journal of Geology and Geophysics 42, 565–579.

Lowe, D.J., Newnham, R.M., McFadgen, B.G., Higham, T.F.G., 2000. Tephras and New Zealand archaeology. Journal of Archaeological Science 27, 859–870.

Lowe, D.J., Shane, P.A.R., Alloway, B.V., Newnham, R.M., 2008. Fingerprints and age models for widespread New Zealand tephra marker beds erupted since 30,000 years ago: a framework for NZ-INTIMATE. Quaternary Science Reviews 26, 95–126.

Lundquist, C.J., Pilditch, C.A., Cummings, V.J., 2004. Behaviour controls post-settlement dispersal by the juvenile bivalves *Austrovenus stutchburyi* and *Macomona liliana*. Journal of Experimental Marine Biology and Ecology 306, 51–74.

Lyell, C., 1868. Principles of geology, volume 2 (10th edition). John Murray, London.

Manighetti, B., Palmer, A., Eden, D., Elliot, M., 2003. The occuracne of Tuhua Tephra in deep-sea sediments from offshore eastern North Island. New Zealand Journal of Geology and Geophysics 46, 581–590.

Marden, M., 1984. Geology and its relationship to erosion in the southern Ruahine Range, North Island, New Zealand. Unpublished PhD Thesis, Massey University, Palmerston North.

Marden, M., Neall, V., 1990. Dated Ohakean terraces offset by the Wellington Fault near Woodville, New Zealand. New Zealand Journal of Geology and Geophysics 33, 449–453.

Marks, G.P., Nelson, C.S., 1979. Sedimentology and evolution of Omaro Spit, Coromandel Peninsula. New Zealand Journal of Marine and Freshwater Research 13, 347–372.

Marra, M.J., 1997. Holocene evolution of the Waitotahi estuary, Bay of Plenty. Unpublished MSc Thesis, University of Auckland, Auckland.

Marra, M.J., Alloway, B.V., Newnham, R.M., 2006. Paleoenvironmental reconstruction of a well-preserved Stage 7 forest sequence catastrophically buried by basaltic eruptive deposits, northern New Zealand. Quaternary Science Reviews 25, 2143–2161.

Martins, L.R., 2003. Recent sediments and grain size analysis. Gravel 1, 90–105.

Martley, P.R., 2001. Hydrogeology of the Feilding District, Manawatu. MSc Thesis, University of Canterbury, Christchurch.

Marwick, J., 1948. Lower Pliocene mollusca from Otahuhu, Auckland (New Zealand Geological Survey Palaeontological Bulletin 16). Department of Scientific and Industrial Research, New Zealand Geological Survey Branch, Dunedin.

Masatomo, U., Buman, M., Kawase, K., Woodroffe, C.D., 2001. Holocene palaeoecology and formation of the Shoalhaven River deltaic-estuarine plains, southeast Australia. The Holocene 11, 407–418.

Massey, A.C., Paul, M.A., Gehrels, W.R., Charman, D.J., 2006. Autocompaction in Holocene coastal back-barrier sediments from south Devon, southwest England, UK. Marine Geology 226, 225–241.

Mather, N.S., 2004. Coastal sedimentation on the east coast of Auckland: evidence for tsunami. Unpublished MSc Thesis, University of Auckland, Auckland.

Mayo, K.L., 1964. Field drainage. In: Saunders, B.G.R., Anderson, A.G. (Eds.), Introducing Manawatu (The Geography of New Zealand 1). Department of Geography, Massey University, Palmerston North, pp. 51–54.

Mazzotti, S., Lambert, A., Van der Kooij, M., Mainville, A., 2009. Impact of anthropogenic subsidence on relative sea-level rise in the Fraser River Delta. Geology 37, 771–774.

McCormac, F.G., Hogg, A.G., Blackwell, P.G., Buck, C.E., Higham, T.F.G., Reimer, P.J., 2004. SHCal04 Southern Hemisphere calibration, 0-11.0 cal kyr BP. Radiocarbon 46, 1087–1092.

McFadgen, B.G., 1974. Progradation of the Manawatu coast, North Island, New Zealand. In: Geological Society of New Zealand 1974 Conference Abstracts. Geological Society of New Zealand, Wellington.

McFadgen, B.G., 1985. Late Holocene stratigraphy of coastal deposits between Auckland and Dunedin, New Zealand. Journal of the Royal Society of New Zealand 15, 27–65.

McFadgen, B.G., Manning, M.R., 1990. Calibrating New Zealand radiocarbon dates of marine shells. Radiocarbon 32, 229–232.

McGlone, M.S., 1983. Polynesian deforestation of New Zealand: a preliminary synthesis. Archaeology in Oceania 18, 11–25.

McGlone, M.S., Wilmshurst, J.M., 1999. Dating initial Maori environmental impact on New Zealand. Quaternary International 59, 5–16.

McKnight, D.G., 1968. Recent and relict molluscan faunas from off Cape Farewell. New Zealand Journal of Marine and Freshwater Research 2, 708–711.

McKnight, D.G., 1969. Infaunal benthic communities of the New Zealand continental shelf. New Zealand Journal of Marine and Freshwater Research 3, 409–444.

McLachlan, A., Jaramillo, E., Defeo, O., Dugan, J., de Ruyck, A., Coetzee, P., 1995. Adaptations of bivalves to different beach types. Journal of Experimental Marine Biology and Ecology 187, 147–160.

Meade, R.H., 1972. Transport and deposition of sediments in estuaries. In: Nelson, B.W. (Ed.), Environmental framework of coastal plain estuaries (GSA Memoir 133). Geological Society of America, Boulder, Colorado, pp. 91–120.

Melhuish, A., Van Dissen, R., Berryman, K., 1996. Mount Stewart-Halcombe anticline: a look inside a growing fold in the Manawatu region, New Zealand. New Zealand Journal of Geology and Geophysics 39, 123–133.

Middleton, G.V., 1973. Johannes Walther's Law of the correlation of facies. Geological Society of America Bulletin 84, 979–988.

Middleton, G.V., 1978. Facies. In: Fairbridge, R.W., Bourgeois, J. (Eds.), Encyclopedia of sedimentology. Dowden, Hutchinson & Ross, Stroudsburg, Pennsylvania, pp. 323–325.

Mildenhall, D.C., Brown, L.J., 1987. An early Holocene occurrence of the mangrove *Avicennia marina* in Poverty Bay, North Island, New Zealand: its climatic and geological implications. New Zealand Journal of Botany 25, 281–294.

Millener, P.R., 1981. The Quaternary avifauna of the North Island, New Zealand (2 volumes). Unpublished PhD Thesis, University of Auckland, Auckland.

Milliman, J.D., Emery, K.O., 1968. Sea levels during the past 35,000 years. Science 162, 1121–1123.

Milne, J.D.G., 1968. The geology and soils of the Apiti District. Unpublished MSc Thesis, Victoria University of Wellington, Wellington.

Milne, J.D.G., 1973. Upper Quaternary geology of the Rangitikei drainage basin, North Island, New Zealand. Unpublished PhD Thesis, Victoria University of Wellington, Wellington.

Milne, J.D.G., Smalley, I.J., 1979. Loess deposits in the southern part of the North Island of New Zealand: an outline stratigraphy. Acta Geologica Academiae Scientiarum Hungaricae, Tomus 22, 197–204.

Mitchum, R.M., 1977. Seismic stratigraphy and global changes of sea level, part 1: glossary of terms used in seismic stratigraphy. In: Payton, C.E. (Ed.), Seismic stratigraphy — applications to hydrocarbon exploration (AAPG Memoir 26). American Association of Petroleum Geologists, Tulsa, pp. 205–212.

Morner, N.A., 1971. Eustatic changes during the last 20,000 years and a method of separating the isostatic and eustatic factors in an uplifted area. Palaeogeography, Palaeoclimatology, Palaeoecology 9, 153–181.

Morner, N.A., 1976. Eustasy and geoid changes. Journal of Geology 84, 123–151.

Morrisey, D., Beard, C., Morrison, M., Craggs, R., Lowe, M., 2007. The New Zealand mangrove: review of the current state of knowledge (NIWA Client Report HAM2007-052; Auckland Regional Council Technical Publication 325). National Institute of Water & Atmospheric Research, Hamilton.

Morrison, M., Drury, J., Shankar, U., Middleton, C., Smith, M., 2003. A broad scale, soft sediment habitat assessment of the Hauraki Gulf (NIWA Client Report AKL2003-64). National Institute of Water and Atmospheric Research, Auckland.

Mortimer, N., 1994. Origin of the Torlesse Terrane and coeval rocks, North Island, New Zealand. International Geology Review 36, 891–910.

Morton, J.E., Miller, M.C., 1968. The New Zealand sea shore. Collins, Auckland.

Mountjoy, J.J., Barnes, P.M., Pettinga, J.R., 2009. Morphostructure and evolution of submarine canyons across an active margin: Cook Strait sector of the Hikurangi Margin, New Zealand. Marine Geology 260, 45–68.

Muckersie, C., Shepherd, M.J., 1993. Chronology of the Manawatu dunefield. In: Froggatt, P. (Ed.), Geological Society of New Zealand 1993 Annual Conference Programme and Abstracts (GSNZ Miscellaneous Publication 79A). Geological Society of New Zealand, Wellington, p. 119.

Muckersie, C., Shepherd, M.J., 1995. Dune phases as time transgressive phenomena, Manawatu, New Zealand. Quaternary International 26, 61–67.

Murray-Wallace, C.V., 2002. Pleistocene coastal stratigraphy, sea-level highstands and neotectonism of the southern Australian passive continental margin — a review. Journal of Quaternary Science 17, 469–489.

Naden, P., Brayshaw, A.C., 1987. Bedforms in gravel-bed rivers. In: Richards, K.S. (Ed.), River channels: environment and process (IBG Special Publication 18). Blackwell, Oxford, pp. 249–271.

Naish, T.R., 1990. Late Holocene mud sedimentation and diagenesis in the Firth of Thames: bentonites in the making. Unpublished MSc Thesis, University of Waikato, Hamilton.

Naish, T.R., 1997. Constraints on the amplitude of late Pliocene eustatic sea-level fluctuations: new evidence from the New Zealand shallow-marine sediment record. Geology 25, 1139–1142.

Naish, T.R., Kamp, P.J.J., 1995. Pliocene-Pleistocene marine cyclothems, Wanganui Basin, New Zealand: a lithostratigraphic framework. New Zealand Journal of Geology and Geophysics 38, 223–243.

Naish, T.R., Kamp, P.J.J., 1997a. Foraminiferal depth palaeoecology of Late Pliocene shelf sequences and systems tracts, Wanganui Basin, New Zealand. Sedimentary Geology 110, 237–255.

Naish, T.R., Kamp, P.J.J., 1997b. Sequence stratigraphy of 6th order (41 k.y.) Pliocene-Pleistocene cyclothems, Wanganui Basin, New Zealand: a case for the regressive systems tract. Geological Society of America Bulletin 109, 978–999.

Naish, T.R., Beu, A.G., Carter, R.M., Edwards, A.R., Kamp, P.J.J., Pillans, B., Saul, G., Woolfe, K., 1998. Astronomical calibration of a southern hemisphere PlioPleistocene reference section, Wanganui Basin, New Zealand. Quaternary Science Reviews 17, 695–710.

Naish, T.R., Field, B.D., Zhu, H., Melhuish, A., Carter, R.M., Abbott, S.T., Edwards, S., Alloway, B.V., Wilson, G.S., Niessen, F., Barker, A., Browne, G.H., Maslen, G., 2005. Integrated outcrop, drill core, borehole and seismic stratigraphic architecture of a cyclothemic, shallow-marine depositional system, Wanganui Basin, New Zealand. Journal of the Royal Society of New Zealand 35, 91–122.

Nakada, M., Lambeck, K., 1989. Late Pleistocene and Holocene sea-level change in the Australian region and mantle rheology. Geophysical Journal 96, 497–517.

Nanson, G.C., Croke, J.C., 1992. A genetic classification of floodplains. Geomorphology 4, 459–486.

Nelson, H.F., Bray, E.E., 1970. Stratigraphy and history of the Holocene sediments in the Sabine-High Island area, Gulf of Mexico. In: Morgan, J.P., Shaver, R.H. (Eds.), Deltaic sedimentation: modern and ancient (SEPM Special Publication 15). Society of Economic Paleontologists and Mineralogists, Tulsa, pp. 48–77.

Newnham, R.M., Lowe, D.J., Green, J.D., Turner, G.M., Harper, M.A., McGlone, M.S., Stout, S.L., Horie, S., Froggatt, P.C., 2004. A discontinuous ca. 80 ka record of Late Quaternary environmental change from Lake Omapere, Northland, New Zealand. Palaeogeography, Palaeoclimatology, Palaeoecology 207, 165–198.

Nichol, S.L., 1991. Zonation and sedimentology of estuarine facies in an incised valley, wave-dominated, microtidal setting. In: Smith, D.G., Zaitlin, B.A., Reinson, G.E. (Eds.), Clastic tidal sedimentology (CSPG Memoir 16). Canadian Society of Petroleum Geologists, Calgary, pp. 41–58.

Nichol, S.L., 2002. Morphology, stratigraphy and origin of Last Interglacial beach ridges at Bream Bay, New Zealand. Journal of Coastal Research 18, 149–159.

Nichol, S.L., Boyd, R., Penland, S., 1994. Stratigraphic response of wave-dominated estuaries to different relative sea-level and sediment supply histories: Quaternary case studies from Nova Scotia, Louisiana and eastern Australia. In: Dalrymple, R.W., Boyd, R., Zaitlin, B.A. (Eds.), Incised-valley systems: origin and sedimentary sequences (SEPM Special Publication 51). Society for Sedimentary Geology, Tulsa, pp. 265–283.

Nichol, S.L., Deny, Y., Horrocks, M., Zhou, W., Hume, T.M., 2009. Preservation of a Late Glacial terrestrial and Holocene estuarine record on the margins of Kaipara Harbour, Northland, New Zealand. Journal of the Royal Society of New Zealand 39, 1–14.

Nichols, M.M., Johnson, G.H., Peebles, P.C., 1991. Modern sediment and facies model for a macrotidal coastal plain estuary, the James estuary, Virginia. Journal of Sedimentary Petrology 61, 883–899.

Nipper, M.G., Roper, D.S., 1995. Growth of an amphipod and a bivalve in uncontaminated sediments: implications for chronic toxicity assessments. Marine Pollution Bulletin 31, 424–430.

Norkko, A., Cummings, V.J., Thrush, S.F., Hewitt, J.E., Hume, T., 2001. Local dispersal of juvenile bivalves: implications for sandflat ecology. Marine Ecology Progress Series 212, 131–144.

Norris, R.M., 1972. Shell and gravel layers, western continental shelf, New Zealand. New Zealand Journal of Geology and Geophysics 15, 572–589.

Nott, J.F., Price, D.M., 1991. Late Pleistocene to early Holocene aeolian activity in the upper and middle Shoalhaven catchment, New South Wales. Australian Geographer 22, 168–177.

Nunn, P.D., 1995. Holocene sea-level changes in the south and west Pacific. Journal of Coastal Research SI17, 311–319.

Nunn, P.D., 1998. Sea-level changes over the past 1,000 years in the Pacific. Journal of Coastal Research 14, 23–30.

Oil, B., 1970. Wanganui and South Canterbury reflection seismic survey final report (Petroleum Report 275). Bounty Oil, Wellington.

Oldman, J.W., Black, K.P., Swales, A., Stroud, M.J., 2009. Prediction of annual average sedimentation rates in an estuary using numerical models with verification against core data — Mahurangi Estuary, New Zealand. Estuarine, Coastal and Shelf Science 84, 483–492.

Oliver, R.L., 1948. The Otaki Sandstone and its geological history (New Zealand Geological Memoir 7). Department of Scientific and Industrial Research, Wellington.

Oomkens, E., Terwindt, J.H.T., 1960. Inshore estuarine sediments of Haringvleit (Netherlands). Geologie end Mijnbouw 39, 701–710.

Osborne, N.M., 1983. Holocene coastal depositional landforms: Bream Bay, Northland. Unpublished MA Thesis, University of Auckland, Auckland.

Osborne, N.M., Nichol, S.L., 2006. Geomorphology and evolution of Te Aupouri Peninsula and Karikari Peninsula: a summary. Mid-conference field trip guide, 12th Australia and New Zealand Geomorphology Group Conference, Taipa Bay, Northland, 12-17 February 2006. University of Auckland, Auckland.

Osborne, N.M., Enright, N.J., Parnell, K.E., 1991. The age and stratigraphic significance of sea-rafted Loisels Pumice in northern New Zealand. Journal of the Royal Society of New Zealand 21, 357–371.

Ota, Y., Brown, L.J., Berryman, K.R., Fujimori, T., Miyauchi, T., 1995. Vertical tectonic movement in northeastern Marlborough: stratigraphic, radiocarbon, and paleoecological data from Holocene estuaries. New Zealand Journal of Geology and Geophysics 38, 269–282.

Page, K., Nanson, G., Price, D., 1996. Chronology of Murrumbidgee River palaeochannels on the Riverine Plain, southeastern Australia. Journal of Quaternary Science 11, 311–326.

Page, K.J., Heerdegen, R.G., 1985. Channel change on the lower Manawatu River. New Zealand Geographer 41, 35–38.

Palmer, A.S., Barnett, R., Pillans, B.J., Wilde, R.H., 1988. Loess, river aggradation terraces and marine benches at Otaki, southern North Island, New Zealand. In: Eden, D.N., Furkert, R.J. (Eds.), Loess: its distribution, geology and soils. Balkema, Rotterdam, pp. 163–174.

Pattison, S.A.J., 1992. Recognition and interpretation of estuarine mudstones (central basin mudstones) in the tripartite valley-fill deposits of the Viking Formation, central Alberta. In: Pemberton, S.G. (Ed.), Applications of ichnology to petroleum exploration (SEPM Core Workshop 17). Society for Sedimentary Geology, Tulsa, pp. 223–250.

Paul, M.A., Barras, B.F., 1998. A geotechnical correction for post-depositional sediment compression: examples from the Forth Valley, Scotland. Journal of Quaternary Science 13, 171–176.

Paul, M.A., Barras, B.F., Peacock, J.D., 1995. Flandrian stratigraphy and sedimentation in the Bothkennar-Grangemouth area. Quaternary Newsletter 75, 22–35.

Payton, C.E., 1977. Seismic stratigraphy — applications to hydrocarbon exploration (AAPG Memoir 26). American Association of Petroleum Geologists, Tulsa.

Pechenik, J.A., Marsden, I.D., Pechenik, O., 2003. Effects of temperature, salinity , and air exposure on development of the estuarine pulmonate gastropod *Amphibola crenata*. Journal of Experimental Marine Biology and Ecology 292, 159–176.

Peltier, W.R., 1988. Lithospheric thickness, Antarctic deglaciation history, and ocean basin descretization effects in a global model of postglacial sea level change: a summary of some sources of nonuniqueness. Quaternary Research 29, 93–112.

Petersen, K.S., 1986. Marine molluscs as indicators of former sea-level stands. In: van de Plassche, O. (Ed.), Sea-level research: a manual for the collection and evaluation of data. Geo Books, Norwich.

Pillans, B., 1983. Upper Quaternary marine terrace chronology and deformation, south Taranaki, New Zealand. Geology 11, 292–297.

Pillans, B., 1985. Southwest North Island palaeoenvironments 150,000 years BP to present. In: Pillans, B. (Ed.), Proceedings of the second CLIMANZ

conference, Harihari, Westland, New Zealand, February 4-8 1985. Geology Department, Victoria University of Wellington, Wellington, pp. 37–43.

Pillans, B., 1986. A late Quaternary uplift map for the North Island, New Zealand. Royal Society of New Zealand Bulletin 24, 409–417.

Pillans, B., 1990a. Late Quaternary marine terraces, south Taranaki - Wanganui (New Zealand Geological Survey miscellaneous series map 18) (Map and notes). Department of Scientific and Industrial Research, Wellington.

Pillans, B., 1990b. Pleistocene marine terraces in New Zealand: a review. New Zealand Journal of Geology and Geophysics 33, 219–232.

Pillans, B., Huber, P., 1995. Interpreting coseismic deformation using Holocene coastal deposits, Wellington, New Zealand. Quaternary International 26, 87–95.

Pillans, B., McGlone, M., Palmer, A., Mildenhall, D., Alloway, B., Berger, G., 1993. The Last Glacial Maximum in central and southern North Island, New Zealand: a palaeoenvironmental reconstruction using the Kawakawa Tephra Formation as a chronostratigraphic marker. Palaeogeography, Palaeoclimatology, Palaeoecology 101, 283–304.

Pillans, B., Kohn, B.P., Berger, G., Froggatt, P., Duller, G., Alloway, B., Hesse, P., 1996. Multi-method dating comparison for mid-Pleistocene Rangitawa Tephra, New Zealand. Quaternary Science Reviews 15, 641–653.

Pinter, N., Gardner, T.W., 1989. Construction of a polynomial model of glacioeustatic fluctuation: estimating palaeo-sea levels continuously through time. Geology 17, 295–298.

Pirazzoli, P.A., 1991. World atlas of Holocene sea-level changes. Elsevier, Amsterdam.

Pizzuto, J.E., Schwendt, A.E., 1997. Mathematical modelling of autocompaction of a Holocene transgressive valley-fill deposit, Wolfe Glade, Delaware. Geology 25, 57–60.

Pocknall, D.T., Gregory, M.R., Greig, D.A., 1989. Palynology of core 80/20 and its implications for understanding Holocene sea level changes in the Firth of Thames, New Zealand. Journal of the Royal Society of New Zealand 19, 171–179.

Posamentier, H., Allen, G.P., 1999. Siliciclastic sequence stratigraphy: concepts and applications (SEPM Concepts in Sedimentology and Paleontology 7). Society for Sedimentary Geology, Tulsa.

Posamentier, H.W., Vail, P.R., 1988. Eustatic controls on clastic deposition II — sequence and systems tract models. In: Wilgus, C.K., Hastings, B.K., Kendall, C.G.S.C., Posamentier, H.W., Ross, C.A., Van Wagoner,

J.C. (Eds.), Sea-level changes: an integrated approach (SEPM Special Publication 42). Society of Economic Paleontologists and Mineralogists, Tulsa, pp. 125–154.

Posamentier, H.W., Jervey, M.T., Vail, P.R., 1988. Eustatic controls on clastic deposition I — conceptual framework. In: Wilgus, C.K., Hastings, B.K., Kendall, C.G.S.C., Posamentier, H.W., Ross, C.A., Van Wagoner, J.C. (Eds.), Sea-level changes: an integrated approach (SEPM Special Publication 42). Society of Economic Paleontologists and Mineralogists, Tulsa, pp. 110–124.

Powell, A.W.B., 1979. New Zealand mollusca — marine, land and freshwater shells. Collins, Auckland.

Pritchard, D.W., 1967. What is an estuary: physical viewpoint. In: Lauff, G.H. (Ed.), Estuaries (AAAS Special Publication 83). American Association for the Advancement of Science, Washington D.C., pp. 3–5.

Probst, T.A., Crawford, C.M., 2008. Population characteristics and planktonic larval stage of the New Zealand screwshell *Maoricolpus roseus*. Journal of Molluscan Studies 74, 191–197.

Proctor, R., Carter, L., 1989. Tidal and sedimentary response to the late Quaternary closure and opening of Cook Strait, New Zealand: results from numerical modelling. Paleooceanography 4, 167–180.

Proust, J.N., Lamarche, G., Nodder, S.D., Kamp, P.J.J., 2005. Sedimentary architecture of a Plio-Pleistocene proto-back-arc basin: Wanganui Basin, New Zealand. Sedimentary Geology 181, 107–145.

Purchase, N.G., Fergusson, J.E., 1986. *Chione (Austrovenus) stutchburyi*, a New Zealand cockle, as a bio-indicator for lead pollution. Environmental Pollution (Series B) 11, 137–151.

Purser, B.H., 1961. Geology of the Port Waikato Region (New Zealand Geological Survey Bulletin 69). Department of Scientific and Industrial Research, Wellington.

Rafter, T.A., Jansen, H.S., Lockerbie, L., Trotter, M.M., 1972. New Zealand reference standards. In: Rafter, T.A., Grant-Taylor, T.L. (Eds.), Proceedings of the 8th International Conference on 14C dating. Royal Society of New Zealand, Wellington, pp. H29–H79.

Rahmani, R.A., 1988. Estuarine tidal channel and nearshore sedimentation of a Late Cretaceous epicontinental sea, Drumheller, Alberta, Canada. In: de Boer, P.L., van Gelder, A., Nio, S.D. (Eds.), Tide-influenced sedimentary environments and facies. D. Reidel Publishing, Boston, pp. 433–481.

Rayns, N.D., 1985. Sedimentation in Hoopers and Papanui Inlets. Unpublished MSc Thesis, University of Otago, Dunedin.

Reading, H.G., Levell, B.K., 1996. Controls on the sedimentary rock record. In: Reading, H.G. (Ed.), Sedimentary environments: processes, facies and stratigraphy. Blackwell Science, Oxford, pp. 5–36.

Reinson, G.E., 1977. Hydrology and sediments of a temperate estuary — Mallacoota Inlet, Victoria (Australian Bureau of Mineral Resources, Geology and Geophysics Bulletin 178). Australian Government Publishing Service, Canberra.

Reinson, G.E., 1992. Transgressive barrier island and estuarine systems. In: Walker, R.G., James, N.P. (Eds.), Faices models: response to sea level change. Geological Association of Canada, St John's, Newfoundland, pp. 179–194.

Reinson, G.E., Clark, J.E., Foscolos, A.E., 1988. Reservoir geology of Crystal Viking field, Lower Cretaceous estuarine tidal channel-bay complex, south-central Alberta. American Association of Petroleum Geologists Bulletin 72, 1270–1294.

Rhea, K.P., 1968. Aokautere Ash, loess, and river terraces in the Dannevirke District, New Zealand. New Zealand Journal of Geology and Geophysics 11, 685–692.

Rich, C.C., 1959. Late Cenozoic geology of the lower Manawatu valley, New Zealand. Unpublished PhD Thesis, Harvard University, Cambridge.

Richards, H.G., 1970. Annotated bibliography of Quaternary shorelines: supplement 1965-1969 (Academy of Natural Sciences Special Publication 10). Academy of Natural Sciences, Philadelphia.

Richards, H.G., 1974. Annotated bibliography of Quaternary shorelines: second supplement 1970-1973 (Academy of Natural Sciences Special Publication 11). Academy of Natural Sciences, Philadelphia.

Richards, H.G., Fairbridge, R.W., 1965. Annotated bibliography of Quaternary shorelines (1945-1964) (Academy of Natural Sciences Special Publication 6). Academy of Natural Sciences, Philadelphia.

Richards, H.G., Shapiro, E.A., 1979. Annotated bibliography of Quaternary shorelines: third supplement 1974-1977 (Geo Abstracts Bibliography 5). Geo Abstracts, Norwich.

Richards, H.G., Gallagher, W.B., Colquhoun, D.J., 1986. Annotated bibliography of Quaternary shorelines: fourth supplement 1978-1983 (Journal of Coastal Research Special Issue 2). Coastal Education and Research Foundation (CERF), Charlottesville, Virginia.

Richardson, R.J.H., 1985. Quaternary geology of the North Kaipara Barrier, Northland, New Zealand. New Zealand Journal of Geology and Geophysics 28, 111–127.

Ricketts, B.D., 1975. Quaternary geology of the Parengarenga Harbour — Te Kao District. Unpublished MSc Thesis, University of Auckland, Auckland.

Roach, D., 2005. Evolution of an estuary and barrier system in a volcanic and tectonically active setting: Maketu, Bay of Plenty. Unpublished MSc Thesis, University of Auckland, Auckland.

Roberts, E., 1855. Memorandum on the earthquake in the islands of New Zealand, January 23, 1855. In: Taylor, R. (Ed.), Te Ika a Maui, or New Zealand and its habitants. Wertheim and MacIntosh, London, pp. 471–472.

Robinson, R., 1987. Seismicity, structure and tectonics of the Wellington region, New Zealand. Geophysical Journal of the Royal Astronomical Society 87, 379–409.

Roche, M.M., 2000. Taming the land — a complete transformation. In: Saunders, B.G.R. (Ed.), The south of the north: the Manawatu and its neighbours. Geography Programme, Massey University, Palmerston North, pp. 9–13.

Rodriguez, A.B., Greene, D.L., Anderson, J.B., Simms, A.R., 2008. Response of Mobile Bay and Mississippi Sound, Alabama, to changes in sediment accomodation and accumulation. In: Anderson, J.B., Rodriguez, A.B. (Eds.), Response of Upper Gulf Coast estuaries to Holocene climate change and sea-level rise (GSA Special Paper 443). Geological Society of America, Boulder, pp. 13–29.

Roper, D.S., 1990. Benthos associated with an estuarine outfall, Tauranga Harbour, New Zealand. New Zealand Journal of Marine and Freshwater Research 24, 487–498.

Roper, D.S., Pridmore, R.D., Thrush, S.F., 1992. Recruitment to the macrobenthos of *Macomona liliana* (Bivalvia: Tellinidae) in Manakau Harbour, New Zealand. New Zealand Journal of Marine and Freshwater Research 26, 385–392.

Roy, P.S., 1984a. Holocene sedimentation histories of estuaries in southeastern Australia. In: Hodgkins, E.P. (Ed.), Estuarine environments of the Southern Hemisphere (WADCE Bulletin 161). Western Australia Department of Conservation and Environment, Perth, pp. 23–60.

Roy, P.S., 1984b. New South Wales estuaries: their origin and evolution. In: Thom, B.G. (Ed.), Coastal geomorphology in Australia. Academic Press, Sydney, pp. 99–121.

Roy, P.S., 1994. Holocene estuary evolution — stratigraphic studies from southeastern Australia. In: Dalrymple, R.W., Boyd, R., Zaitlin, B.A. (Eds.), Incised-valley systems: origin and sedimentary sequences (SEPM Special Publication 51). Society for Sedimentary Geology, Tulsa, pp. 241–263.

Roy, P.S., Boyd, R., 1996. Quaternary geology of southeast Australia: a tectonically stable, wave-dominated, sediment deficient margin (IGCP 367 Field Guide). IGCP Project 367, Sydney.

Roy, P.S., Thom, B.G., Wright, L.D., 1980. Holocene sequences on an embayed high-energy coast: an evolutionary model. Sedimentary Geology 26, 1–19.

Roy, P.S., Cowell, P.J., Ferland, M.A., Thom, B.G., 1994. Wave-dominated coasts. In: Carter, R.W.G., Woodroffe, C.D. (Eds.), Coastal evolution: Late Quaternary shoreline morphodynamics. Cambridge University Press, Cambridge, pp. 121–186.

Roy, P.S., Williams, R.J., Jones, A.R., Yassini, I., Gibbs, P.J., Coates, B., West, R.J., Scanes, P.R., Hudson, J.P., Nichol, S.L., 2001. Structure and function of south-east Australian estuaries. Estuarine, Coastal and Shelf Science 53, 351–384.

Rybczyk, J.M., Callaway, J., Day Jr, J.W., 1998. A relative elevation model (REM) for a subsiding coastal forested wetland receiving wastewater effluent. Ecological Modelling 112, 23–44.

Sahu, B.K., 1964. Depositional mechanisms from the size analysis of clastic sediments. Journal of Sedimentary Petrology 34, 73–83.

Saul, G., Naish, T.R., Abbott, S.T., Carter, R.M., 1999. Sedimentary cyclicity in the marine Plio-Pleistocene: sequence stratigraphic motifs characteristic of the last 2.5 Ma. Geological Society of America Bulletin 111, 524–537.

Saunders, B.G.R., 1964. Climate. In: Saunders, B.G.R., Anderson, A.G. (Eds.), Introducing Manawatu (The Geography of New Zealand 1). Department of Geography, Massey University, Palmerston North, pp. 45–50.

Schofield, J.C., 1958. Notes on volcanism and structure in Franklin County. New Zealand Journal of Geology and Geophysics 1, 541–559.

Schofield, J.C., 1960a. Sea level fluctuations during the last 4000 years as recorded by a chenier plain, Firth of Thames, New Zealand. New Zealand Journal of Geology and Geophysics 3, 467–485.

Schofield, J.C., 1960b. Sea-level fluctuations during the past four thousand years. Nature 185, 836.

Schofield, J.C., 1962. Post-glacial sea-levels. Nature 195, 1191.

Schofield, J.C., 1964. Postglacial sea levels and isostatic uplift. New Zealand Journal of Geology and Geophysics 7, 359–370.

Schofield, J.C., 1968. Dating of recent low sea level and Maori rock carvings, Ongari Point. Earth Science Journal 2, 167–174.

Schofield, J.C., 1973. Post-glacial sea levels of Northland and Auckland. New Zealand Journal of Geology and Geophysics 16, 359–366.

Schofield, J.C., 1975. Sea-level fluctuations cause periodic, post-glacial progradation, South Kaipara Barrier, North Island, New Zealand. New Zealand Journal of Geology and Geophysics 18, 295–316.

Schumacher, J., 1999. Groundwater in the lower Manawatu valley (Palmerston North area), New Zealand. Unpublished MSc Thesis, University of Waikato, Hamilton.

Schumm, S.A., 1993. River response to baselevel change: implications for sequence stratigraphy. Journal of Geology 101, 279–294.

Searle, E.J., 1956. Aspects of the Pleistocene and recent history of the Auckland Isthmus. New Zealand Geographer 12, 75–88.

Selby, M.J., Pullar, W.A., McCraw, J.D., 1971. The age of Quaternary surfaces at Waihi Beach. Earth Science Journal 5, 106–113.

Sewell, A.H., 1991. Paleoenvironmental analysis of Quaternary strata in the Levin area. Unpublished MSc Thesis, Massey University, Palmerston North.

Shackleton, N.J., Opdyke, N.D., 1973. Oxygen isotope and palaeomagnetic stratigraphy of equatorial Pacific core V28-238: oxygen isotope temperatures and ice volumes on a 10^5 year and 10^6 year scale. Quaternary Research 3, 39–55.

Shand, R.D., Bailey, D.G., Shepherd, M.J., 2001. Longshore realignment of shore-parallel sand-bars at Wanganui, New Zealand. Marine Geology 179, 147–161.

Shane, P., 1994. A widespread, early Pleistocene tephra (Potaka Tephra, 1 Ma) in New Zealand: character, distribution and implications. New Zealand Journal of Geology and Geophysics 37, 25–35.

Shane, P., 2000. Tephrochronology: a New Zealand case study. Earth-Science Reviews 49, 223–259.

Shane, P., Sandiford, A., 2003. Paleovegetation of Marine Isotope Stages 4 and 3 in northern New Zealand and the age of the widespread Rotoehu Tephra. Quaternary Research 59, 420–429.

Shane, P., Black, T.M., Alloway, B.V., Westgate, J., 1996. Early to middle Pleistocene tephrochronology of North Island, New Zealand: implications for volcanism, tectonism, and paleoenvironments. Geological Society of America Bulletin 108, 915–925.

Shanley, K.W., McCabe, P.J., Hettinger, R.D., 1992. Tidal influences in Cretaceous fluvial strata from Utah, USA: a key to sequence stratigraphic interpretation. Sedimentology 39, 905–930.

Shennan, I., Horton, B.P., 2002. Holocene land- and sea-level changes in Great Britain. Journal of Quaternary Science 17, 511–526.

Shepard, F.P., 1963. Thirty-five thousand years of sea level. In: Clements, T. (Ed.), Essays in marine geology in honor of K.O. Emery. University of Southern California Press, Los Angeles, pp. 1–10.

Shepard, F.P., 1964. Sea level changes in the past 6000 years: possible archaeological significance. Science 143, 574–576.

Shepherd, M.J., 1985. The origin of the Koputaroa dunes, Horowhenua, New Zealand. New Zealand Journal of Geology and Geophysics 28, 323–327.

Shepherd, M.J., Lees, C.M., 1987. Holocene alluviation and transgressive dune activity in the lower Manawatu Valley, New Zealand. New Zealand Journal of Geology and Geophysics 30, 175–187.

Shepherd, M.J., Price, D.M., 1990. Thermoluminescence dating of late Quaternary dune sand, Manawatu/Horowhenua area, New Zealand: a comparison with ^{14}C age determinations. New Zealand Journal of Geology and Geophysics 33, 535–539.

Shepherd, M.J., Gibb, J.G., Johnson, M., 1986. Geological Society of New Zealand 16th annual conference field excursions guide book (GSNZ Miscellaneous Publication 35B). Geological Society of New Zealand, Wellington.

Shulmeister, J., Kirk, R.M., 1993. Evolution of a mixed sand and gravel barrier system in North Canterbury, New Zealand, during Holocene sea-level rise and still-stand. Sedimentary Geology 87, 215–235.

Shulmeister, J., Kirk, R.M., 1997. Holocene fluvial-coastal interactions on a mixed sand and sand and gravel beach system, North Canterbury, New Zealand. Catena 30, 337–355.

Sikes, E.L., Samso, C.R., Guilderson, T.P., Howard, W.R., 2000. Old radiocarbon ages in the southwest Pacific Ocean during the last glacial period and deglaciation. Nature 405, 555–559.

Skuja, K.A., 2006. The stratigraphy of the upper Tairua estuary. Unpublished MSc Thesis, University of Auckland, Auckland.

Sloss, C.R., 2005. Holocene sea-level change and the aminostratigraphy of wave-dominated barrier estuaries on the southeast coast of Australia. Unpublished PhD Thesis, University of Wollongong, Wollongong.

Sloss, C.R., Jones, B.G., Murray-Wallace, C.V., 2004a. Litho- and chrono-stratigraphy of Holocene sedimentary successions preserved in Lake Illawarra, NSW south coast, Australia. Wetlands (Australia) 21, 61–72.

Sloss, C.R., Murray-Wallace, C.V., Jones, B.G., Walin, T., 2004b. Aspartic acid racemisation dating of mid-Holocene to recent estuarine sedimentation in New South Wales, Australia: a pilot study. Marine Geology 212.

Sloss, C.R., Jones, B.G., Murray-Wallace, C.V., McClennen, C.E., 2005. Holocene sea level fluctuations and the sedimentary evolution of a barrier estuary: Lake Illawarra, New South Wales, Australia. Journal of Coastal Research 21.

Sloss, C.R., Jones, B.G., McClennen, C.E., de Carli, J., Price, D.M., 2006a. The geomorphological evolution of a wave-dominated barrier estuary: Burrill Lake, New South Wales, Australia. Sedimentary Geology 187, 229–249.

Sloss, C.R., Murray-Wallace, C.V., Jones, B.G., 2006b. Aminostratigraphy of two Holocene wave-dominated barrier estuaries in southeastern Australia. Journal of Coastal Research 22, 113–136.

Sloss, C.R., Murray-Wallace, C.V., Jones, B.G., 2007. Holocene sea-level change on the southeast coast of Australia: a review. The Holocene 17, 999–1014.

Sloss, C.R., Jones, B.G., Switzer, A.D., Nichol, S.L., Clement, A.J.H., Nicholas, A.W., 2010. The Holocene infill of Lake Conjola, a narrow incised valley system on the southeast coast of Australia. Quaternary International 221, 23–35.

Smith, E.G.C., Stern, T.A., Reyners, M.E., 1989. Subduction and back-arc activity at the Hikurangi convergent margin, New Zealand. Pure and Applied Geophysics 129, 203–231.

Smith, W.H.F., Wessel, P., 1990. Gridding with continuous curvature splines in tension. Geophysics 55, 293–305.

Soons, J.M., Shulmeister, J., Holt, S., 1997. The Holocene evolution of a well nourished gravelly barrier and lagoon complex, Kaitorete "Spit", Canterbury, New Zealand. Marine Geology 138, 69–90.

Sperazza, M., Moore, J.N., Hendrix, M.S., 2004. High-resolution particle size analysis of naturally occurring very fine-grained sediment through laser diffractometry. Journal of Sedimentary Research 75, 736–743.

Stern, T.A., Davey, F.J., 1989. Crustal structure and origin for basins formed behind the Hikurangi subduction zone of New Zealand. In: Price, R.A. (Ed.), Origin and evolution of sedimentary basins and their energy and mineral resources (AGU Geophysical Monograph 48). American Geophysical Union, Washington D.C., pp. 73–86.

Stern, T.A., Quinlan, G.M., Holt, W.E., 1992. Basin formation behind an active subduction zone: 3D flexural modelling of Wanganui Basin. Basin Research 4, 197–214.

Stern, T.A., Quinlan, G.M., Holt, W.E., 1993. Crustal dynamics associated with the formation of Wanganui Basin, New Zealand. In: Ballance, P.F. (Ed.), South Pacific sedimentary basins (Sedimentary Basins of the World, 2). Elsevier, Amsterdam, pp. 213–223.

Stevens, G.R., 1956a. Earth movements in the Wellington area. New Zealand Geographer 12, 189–194.

Stevens, G.R., 1956b. Stratigraphy of the Hutt Valley, New Zealand. New Zealand Journal of Science and Technology 38B, 201–235.

Stevens, G.R., 1957. Geomorphology of the Hutt Valley, New Zealand. New Zealand Journal of Science and Technology 38B, 297–327.

Stevens, G.R., 1990. Rugged landscape: the geology of central New Zealand, including Wellington, Wairarapa, Manawatu and the Marlborough Sounds. DSIR Publishing, Wellington.

Stevens, K.F., Palmer, A.S., 1986. Geological Society of New Zealand 1986 annual conference field trip guide. Geological Society of New Zealand, Palmerston North.

Stuiver, M., Braziunas, T.F., 1993. Modelling atmospheric ^{14}C influences and ^{14}C ages of marine samples to 10,000 BC. Radiocarbon 35, 137–189.

Stuiver, M., Polach, H.A., 1977. Reporting of ^{14}C data. Radiocarbon 19, 355–363.

Stuiver, M., Reimer, P.J., 1993. Extended ^{14}C database and revised CALIB radiocarbon calibration program. Radiocarbon 35, 215–230.

Suess, H.E., 1955. Radiocarbon concentration in modern wood. Science 122, 415–417.

Suggate, R.P., 1958. Late Quaternary deposits of the Christchurch metropolitan area. New Zealand Journal of Geology and Geophysics 1, 103–122.

Suggate, R.P., 1960. Time-stratigraphic subdivision of the Quaternary as viewed from New Zealand. Quaternaria 5, 1–12.

Suggate, R.P., 1965. Late Pleistocene geology of the northern part of the South Island, New Zealand (New Zealand Geological Survey Bulletin 77). Department of Scientific and Industrial Research, Wellington.

Suggate, R.P., 1968. Post glacial sea-level rise in the Christchurch metropolitan area, New Zealand. Geologie en Mijnbouw 47, 291–297.

Swales, A., Hume, T.M., Oldman, J.W., Green, M.O., 1997. Mahurangi Estuary: sedimentation history and recent human impacts (NIWA Client Report ARC60210). National Institute of Water and Atmospheric Research, Hamilton.

Swales, A., Bentley, S.J., McGlone, M.S., Ovenden, R., Hermanspahn, N., Budd, R., Hill, A., Pickmere, S., Haskew, R., Okey, M.J., 2005. Pauatahanui Inlet: effects of historical catchment landcover changes on inlet sedimentation (NIWA Client Report HAM2004-149). National Institute of Water and Atmospheric Research, Hamilton.

Swift, D.J.P., 1968. Coastal erosion and transgressive stratigraphy. Journal of Geology 76, 444–456.

Tallis, H.M., Wing, S.R., Frew, R.D., 2004. Historical evidence for habitat conversion and local population decline in a New Zealand fjord. Ecological Applications 14, 546–554.

Tans, P.P., de Jong, A.F.M., Mook, W.G., 1979. Natural atmospheric ^{14}C variation and the Suess effect. Nature 280, 826–828.

Taylor, C.B., Trompetter, V.J., Brown, L.J., Bekesi, G., 2001. The Manawatu aquifers, North Island, New Zealand: clarification of hydrogeology using a multidisciplinary environmental tracer approach. Hydrological Processes 15, 3269–3286.

Te Punga, M.T., 1953a. A late Pleistocene land bridge across Cook Strait, New Zealand. New Zealand Journal of Science and Technology 35B, 161–192.

Te Punga, M.T., 1953b. Radiocarbon dating of a Rangitikei River terrace. New Zealand Journal of Science and Technology 35B, 45–48.

Te Punga, M.T., 1954a. Fossiliferous late-Pleistocene beds in a well at Awahuri, near Palmerston North. New Zealand Journal of Science and Technology 36B, 82–92.

Te Punga, M.T., 1954b. Late Pleistocene buckshot from western Wellington. New Zealand Journal of Science and Technology 36B, 1–13.

Te Punga, M.T., 1954c. The Late Tertiary and Quaternary geological history of western Wellington. Unpublished PhD Thesis, Victoria University of Wellington.

Te Punga, M.T., 1957. Live anticlines in western Wellington. New Zealand Journal of Science and Technology 38B, 433–446.

Te Punga, M.T., 1958. Evidence for a low sea-level 9900 years ago. New Zealand Journal of Geology and Geophysics 1, 92–94.

Te Punga, M.T., 1962. Some geological features of the Otaki-Waikanae District. New Zealand Journal of Geology and Geophysics 5, 517–530.

Terzopoulos, D., 1988. The computation of visible surface representations. IEEE Transactions on Pattern Analysis and Machine Intelligence 10, 417–438.

Thom, B.G., Chappell, J., 1975. Holocene sea levels relative to Australia. Search 6, 90–93.

Thomas, D., 1998. Late Holocene radiocarbon ages from Blueskin Bay Estuary: relevance to local eustatic sea-level during the last 7000 years. In: Bassett, K.N., Nobes, D.C. (Eds.), Geological Society of New Zealand and New Zealand Geophysical Society 1998 joint annual conference, 30 November - 3 December: programme and abstracts. University of Canterbury, Christchurch, p. 226.

Thomas, D., 2000. Holocene stratigraphy and sequence architecture of the Blueskin Bay estuary, East Otago (2 volumes). Unpublished MSc Thesis, University of Otago, Dunedin.

Thomas, M.A., Anderson, J.B., 1994. Sea-level controls on the facies architecture of the Trinity/Sabine incised-valley system, Texas continental shelf. In: Dalrymple, R.W., Boyd, R., Zaitlin, B.A. (Eds.), Incised-valley systems: origin and sedimentary sequences (SEPM Special Publication 51). Society for Sedimentary Geology, Tulsa, pp. 63–82.

Thrush, S.F., Lawrie, S.M., Hewitt, J.E., Cummings, V.J., 1999. The problem of scale: uncertainties and implications for soft-bottom marine communities and the assessment of human impacts. In: Gray, J.S., Ambrose, W.G., Szaniawska, A. (Eds.), Biogeochemical cycling and sediment ecology. Kluwer Academic Publishers, Dordrecht, pp. 195–210.

Thrush, S.F., Hewitt, J.E., Cummings, V.J., Green, M.O., Funnell, G.A., Wilkinson, M.R., 2000. The generality of field experiments: interactions between local and broad-scale processes. Ecology 81, 399–415.

Tornqvist, T.E., Wallace, D.J., Storms, J.E.A., Wallinga, J., van Dam, R.L., Blaauw, M., Derksen, M.S., Klerks, C.J.W., Miejneken, C., Snijders, E.M.A., 2008. Mississippi Delta subsidence primarily caused by compaction of Holocene strata. Nature Geoscience 1, 173–176.

Tovey, N.K., Paul, M.A., 2002. Modelling self-weight consolidation in Holocene sediments. Bulletin of the International Association of Engineering Geologists 61, 21–33.

Townsend, D., Vonk, A., Kamp, P.J.J., 2008. Geology of the Taranaki area. Institute of Geological & Nuclear Sciences, Lower Hutt.

Trentesaux, A., Recourt, P., Bout-Roumazeilles, V., Tribovillard, N., 2001. Carbonate grain-size distribution in hemipelagic sediments from a laser particle sizer. Journal of Sedimentary Research 71, 858–862.

Uemura, Y., Shepherd, M.J., 2006. Marine terrace and Quaternary tectonic movement of the eastern Palmerston North area, North Island, New Zealand. Geographical Review of Japan 79, 769–785.

Vail, P.R., 1975. Eustatic cycles from seismic data for global stratigraphic analysis (abstract). American Association of Petroleum Geologists Bulletin 59, 2198–2199.

Vail, P.R., 1987. Seismic stratigraphy interpretation using sequence stratigraphy, part 1: seismic stratigraphy interpretation procedure. In: Bally, A.W. (Ed.), Atlas of seismic stratigraphy, vol. 1 (AAPG Studies in Geology 27). American Association of Petroleum Geologists, Tulsa, pp. 1–10.

Vail, P.R., Mitchum, R.M., 1977. Seismic stratigraphy and global changes of sea level, part 1: overview. In: Payton, C.E. (Ed.), Seismic stratigraphy — applications to hydrocarbon exploration (AAPG Memoir 26). American Association of Petroleum Geologists, Tulsa, pp. 51–52.

Vail, P.R., Mitchum, R.M., Thompson, S, I., 1977. Seismic stratigraphy and global changes of sea level, part 3: relative changes of sea level from coastal onlap. In: Payton, C.E. (Ed.), Seismic stratigraphy — applications to hydrocarbon exploration (AAPG Memoir 26). American Association of Petroleum Geologists, Tulsa, pp. 63–97.

Vail, P.R., Mitchum, R.M., Shipley, T.H., Buffler, R.T., 1980. Unconformities in the North Atlantic. Philosophical Transactions of the Royal Society of London, Series A 294, 137–155.

Valia, H.S., Cameron, B., 1977. Skewness as a paleoenvironmental indicator. Journal of Sedimentary Petrology 47, 784–793.

Van der Linden, W.J.M., Norris, R.M., 1974. Structure and Quaternary history of Karamea Bight, South Island, New Zealand. New Zealand Journal of Geology and Geophysics 17, 375–388.

Van Wagoner, J.C., 1995. Overview of sequence stratigraphy of foreland basin deposits: terminology, summary of papers, and glossary of sequence stratigraphy. In: Van Wagoner, J.C., Bertram, G.T. (Eds.), Sequence stratigraphy of foreland basin deposits (AAPG Memoir 64). American Association of Petroleum Geologists, Tulsa, pp. ix–xxi.

Van Wagoner, J.C., Posamentier, H.W., Mitchum, R.M., Vail, P.R., Sarg, J.F., Loutit, T.S., Hardenbol, J., 1988. An overview of sequence stratigraphy and key definitions. In: Wilgus, C.K., Hastings, B.K., Kendall, C.G.S.C., Posamentier, H.W., Ross, C.A., Van Wagoner, J.C. (Eds.), Sea-level changes: an integrated approach (SEPM Special Publication 42). Society of Economic Palaeontologists and Mineralogists, Tulsa, pp. 39–45.

Van Wagoner, J.C., Mitchum, R.M., Campion, K.M., Rahmanian, V.D., 1990. Siliciclastic sequence stratigraphy in well logs, cores, and outcrops: concepts for high-resolution correlation of time and facies (AAPG Methods in Exploration 7). American Association of Petroleum Geologists, Tulsa.

Vella, P., Kaewyana, W., Vucetich, C.G., 1988. Late Quaternary terraces and their cover beds, north-western Wairarapa, New Zealand, and provisional correlations with oxygen isotope stages. Journal of the Royal Society of New Zealand 18, 309–324.

Vis, G.J., Kasse, C., Vandenberghe, J., 2008. Late Pleistocene and Holocene palaeogeography of the lower Tagus Valley (Portugal): effects of relative sea level, valley morphology and sediment supply. Quaternary Science Reviews 27, 1682–1709.

Walcott, R.I., 1970. Flexural rigidity, thickness, and viscosity of the lithosphere. Journal of Geophysical Research 75, 3941–3954.

Walcott, R.I., 1978. Present tectonics and late Cenozoic evolution of New Zealand. Geophysical Journal of the Royal Astronomical Society 52, 137–164.

Walcott, R.I., 1984. The kinematics of the plate boundary zone through New Zealand: a comparison of short and long term deformation. Geophysical Journal of the Royal Astronomical Society 79, 613–633.

Walcott, R.I., 1987. Geodetic strain and the deformational history of the North Island of New Zealand during the late Cainozoic. Philosophical Transactions of the Royal Society of London, Series A 321, 163–183.

Walker, R.G., 1984. Facies, facies sequences and facies models. In: Walker, R.G. (Ed.), Facies models. Geological Association of Canada, Toronto.

Walker, R.G., 1990. Perspectives: facies modelling and sequence stratigraphy. Journal of Sedimentary Petrology 60, 777–786.

Walker, R.G., 1992. Facies, facies models and modern stratigraphic concepts. In: Walker, R.G., James, N.P. (Eds.), Facies models: response to sea level change. Geological Association of Canada, St John's, Newfoundland, pp. 1–14.

Walther, J., 1894. Lithogenesis der Gegenwart (Einleitung in die Geologie als historische Wissenschaft, 3). Verlag von Gustav Fischer, Jena.

Ward, W.T., 1960. Geology of the Glen Murray and Rotongaro districts with particular reference to the volcanic ash beds. Unpublished MSc Thesis, University of Auckland, Auckland.

Ward, W.T., 1965. Eustatic and climatic history of the Adelaide area, South Australia. Journal of Geology 73, 592–602.

Ward, W.T., 1966. Geology, geomorphology and soils of the south-western part of County Adelaide, South Australia (CSIRO Soil Bulletin 23). Commonwealth Scientific and Industrial Research Organization, Melbourne.

Ward, W.T., 1967. Volcanic ash beds of the lower Waikato Basin, North Island, New Zealand. New Zealand Journal of Geology and Geophysics 10, 1109–1135.

Ward, W.T., 1972. Pleistocene ash in the Waikato Basin: ages implied by changes in sea level (note). New Zealand Journal of Geology and Geophysics 15, 678–685.

Ward, W.T., Ross, P.J., Colquhoun, D.J., 1971. Interglacial high sea levels - an absolute chronology derived from shoreline elevations. Palaeogeography, Palaeoclimatology, Palaeoecology 9, 77–99.

Warr, E.C.R., 1964. The rise of the pastoral industries. In: Saunders, B.G.R., Anderson, A.G. (Eds.), Introducing Manawatu (The Geography of New Zealand 1). Department of Geography, Massey University, Palmerston North, pp. 148–180.

Washington, P.A., Chisick, S.A., 1994. Estuarine facies model, conceptual basis and stratigraphic implications — discussion. Journal of Sedimentary Research 64B, 74–75.

Waterhouse, B.C., 1978. Sheet N51 Onewhero - Geological map of New Zealand 1:63360. Department of Scientific and Industrial Research, Wellington.

Wellman, H.W., 1962. Holocene of the North Island of New Zealand: a coastal reconnaissance. Transactions of the Royal Society of New Zealand (Geology) 1, 29–99.

Wellman, H.W., 1972. Rate of horizontal fault displacement in New Zealand. Nature 237, 275–277.

Wellman, H.W., 1979. An uplift map for the South Island of New Zealand, and a model for uplift of the Southern Alps. Royal Society of New Zealand Bulletin 18, 13–20.

Westcott, W.A., 1993. Geomorphic thresholds and complex response of fluvial systems — some implications for sequence stratigraphy. American Association of Petroleum Geologists Bulletin 77, 1208–1218.

Whitehouse, I.E., Pearce, A.J., 1992. Shaping the mountains of New Zealand. In: Soons, J.M., Selby, M.J. (Eds.), Landforms of New Zealand. Longman Paul, Auckland, pp. 144–160.

Wilgus, C.K., Hastings, B.K., Kendall, C.G.S.C., Posamentier, H.W., Ross, C.A., Van Wagoner, J.C., 1988. Sea-level changes: an integrated approach (SEPM Special Publication 42). Society of Economic Palaeontologists and Mineralogists, Tulsa.

Williams, H., 2003. Modelling shallow autocompaction in coastal marshes using Cesium-137 fallout: preliminary results from the Trinity River Estuary, Texas. Journal of Coastal Research 19, 180–188.

Williams, P.W., 1991. Tectonic geomorphology, uplift rates and geomorphic response in New Zealand. Catena 18, 439–452.

Wilson, G.S., McGuire, D.M., 1995. Distributed deformation due to coupling across a subduction thrust: mechanism of young tectonic rotation within the south Wanganui Basin, New Zealand. Geology 23, 645–648.

Wilson, K., Berryman, K., Cochran, U., Little, T., 2007. A Holocene incised valley infill sequence developed on a tectonically active coast: Pakarae River, New Zealand. Sedimentary Geology 197, 333–354.

Witman, J.D., 1974. Sedimentological and ecological studies of Blueskin Bay Estuary. Unpublished Independent Study (Geology) Thesis, University of Otago, Dunedin.

Wolinsky, M.A., Swenson, J.B., Litchfield, N., McNinch, J.E., 2010. Coastal progradation and sediment partitioning in the Holocene Waipaoa Sedimentary System, New Zealand. Marine Geology 270, 94–107.

Wood, J.M., Hopkins, J.C., 1989. Reservoir sandstone bodies in estuarine valley fill: Lower Cretaceous Glauconitic Member, Little Bow Field, Alberta, Canada. American Association of Petroleum Geologists Bulletin 73, 1361–1382.

Woodroffe, C.D., Curtis, R.J., McLean, R.F., 1983. Development of a chenier plain, Firth of Thames, New Zealand. Marine Geology 53, 1–22.

Woodroffe, C.D., Murray-Wallace, C.V., Bryant, E.A., Brooke, B., Heijnis, H., Price, D.M., 1995. Late Quaternary sea-level highstands in the Tasman Sea: evidence from Lord Howe Island. Marine Geology 125, 61–72.

Woodroffe, S.A., 2009. Testing models of mid to late Holocene sea-level change, north Queensland, Australia. Quaternary Science Reviews 28, 2474–2488.

Wratt, C.R.L., 1999. Stratigraphic reconstruction of a cross section in the upper Puhoi River Estuary, Northland. Unpublished MSc Thesis, University of Auckland, Auckland.

Wright, V.P., Marriott, S.B., 1993. The sequence stratigraphy of fluvial depositional systems: the role of floodplain sediment storage. Sedimentary Geology 86, 203–210.

Wynne, K.E., 1981. Porirua Harbour Authority harbour investigation May 1981. Unpublished Consulting Report prepared for the Porirua Harbour Authority.

Yassini, I., Jones, B.G., 1995. Foraminifera and ostracoda from estuarine and shelf environments on the southeastern coast of Australia. University of Wollongong Press, Wollongong.

Yeats, R.S., 1986. Faults related to folding with examples from New Zealand. Royal Society of New Zealand Bulletin 24, 273–292.

Yuill, B., Lavoie, D., Reed, D.J., 2009. Understanding subsidence processes in coastal Louisiana. Journal of Coastal Research 54, 23–36.

Zaitlin, B.A., Shultz, B.C., 1984. An estuarine-embayment fill model from the Lower Cretaceous Mannville Group, west-central Saskatchewan. In: Scott, D.F., Glass, D.J. (Eds.), Mesozoic of middle North America (CSPG Memoir 9). Canadian Society of Petroleum Geologists, Calgary, pp. 455–469.

Zaitlin, B.A., Shultz, B.C., 1990. Wave-influenced estuarine sand body, Senlac heavy oil pool, Saskatchewan, Canada. In: Barwis, J.H., McPherson, J.G., Studlick, J.R.J. (Eds.), Sandstone petroleum reservoirs. Springer-Verlag, New York, pp. 363–387.

Zaitlin, B.A., Dalrymple, R.W., Boyd, R., 1994. The stratigraphic organisation of incised-valley systems associated with relative sea-level change. In: Dalrymple, R.W., Boyd, R., Zaitlin, B.A. (Eds.), Incised-valley systems: origin and sedimentary sequences (SEPM Special Publication 51). Society for Sedimentary Geology, Tulsa, pp. 45–60.

Zeuner, F.E., 1945. The Pleistocene Period. Ray Society, London.

Zeuner, F.E., 1950. Dating the past. Methuen, London.

Zeuner, F.E., 1954. Pleistocene geology of Great Britain. Nature 173, 1178–1180.

Zeuner, F.E., 1959. The Pleistocene Period. Hutchinson Scientific & Technical, London.

Zhang, G., Li, C., 1998. Sources of sediment filling the Qiantangjiang estuary incised valley since the Last Glaciation. Chinese Science Bulletin 43, 1280–1284.

Zoraster, S., 2003. A surface modeling algorithm designed for speed and ease of use with all petroleum industry data. Computers & Geosciences 29, 175–182.

Appendix A

Contents of the DVD

A DVD accompanies this thesis, and is stored in a pocket at the rear. The DVD contains a PDF copy of the thesis, as well as PDF copies of the loose sheets stored in the pocket at the rear. The DVD also contains GIS files used/generated during the construction of the well logs and vibracores cross-sections (Sheets 1–31). These are ESRI shapefiles generated using ArcGIS Desktop 9.2. These files have not been tidied or cleaned up, and are provided "as is". Any use of these files should be acknowledged with reference to the thesis.

A typical cross-section contains a number of folders and files:

Cross-section `root folder`: contains shapefiles required to run the cross-section tool (Carrell, 2009), including:

`XS00_bores`	Well log positions.
`XS00_geology`	QMAP geology for the length of the cross-section.
`XS00_line`	The cross-section line.

The `root folder` also contains a number of other shapefiles used to assemble the cross-section sheets. These are included for completeness but are not detailed here.

Folder `bores_output_1`: contains files generated during the first run-through with the cross-section tool. For details of these files refer to Carrell (2009).

Folder `bores_output_2`: contains files generated during the second run-through with the cross-section tool. For details of these files refer to Carrell (2009). Other files found in this folder include:

`...wellln_buffer`	`wellln` lines buffered to create the well symbols.
`...wellln_dem_q2a`	`wellln` units identified as LGM gravel, extracted from `wellln` to construct the DEM.

`...wellln_points` Center points for `wellln`, used for displaying lithological information.

Folder `extra_bores_output`: Contains files generated with the cross-section tool on "extra" bores, either to the left or right of the cross-section, to provide wider context. For details of these files refer to Carrell (2009), and the summary for folder `bores_output_2`.

Folder `lidar_profile`: Surface profile along the cross-section line generated from the LiDAR DEM of the lower Manawatu valley.

Folder `3D_lines`: conversion from points to 3D lines for all the lithological units (ie. `wellln`). Shapefiles for use in ArcScene.

Folder `3D_cross-sections`: conversion from 2D to 3D for the cross-sections (see Sheets 1–20) as either 3D polylines or 3D polygons. Shapefiles for use in ArcScene.

The DVD also contains the digital elevation models of the LGM surface and estuarine-alluvial interface used for estimating accommodation space in the lower valley. Also included are the various contour shapefiles generated from the DEM.

The DVD does not contain GIS data not created as part of this research. Therefore, the ECOSAT DEM subset and the LiDAR DEM made avalible by Landcare Research and Horizons Regional Council, respectively, are not included.

Appendix B

Vibracore lithological logs

Retrieved vibracores were opened and visually logged for colour, sediment texture, lithological composition, the presence of macrofossils, and significant facies changes. Compiled data was plotted as stratigraphic sections using Inkscape 0.47. Logs for vibracores F, Kop-1, Sh-1, Sh-2, Flood-1, Cut-2, Cut-4, Cut-7, and E1 are presented in Chapter 7. All other logs are presented in this appendix. A key to the stratigraphic symbols used in the logs is given below.

KEY FOR STRATIGRAPHIC LOGS

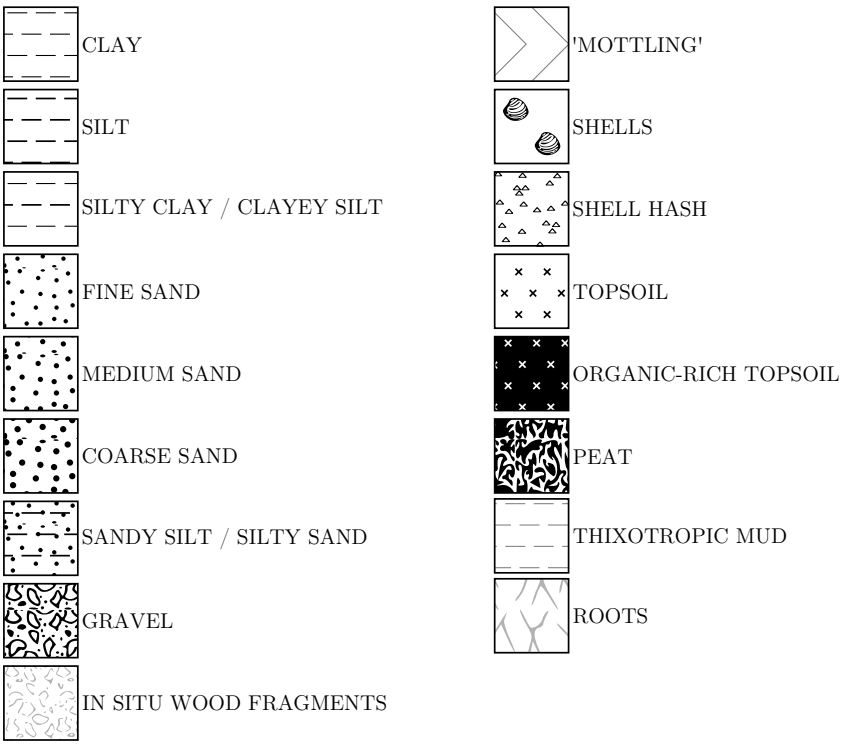

CORE: LD-1 NZMG COORDINATES: 2725319.17 E, 6083559.52 N PAGE: 1/2
LOCATION: Linton Main Drain WVD1953 ELEVATION: +15.4876 m

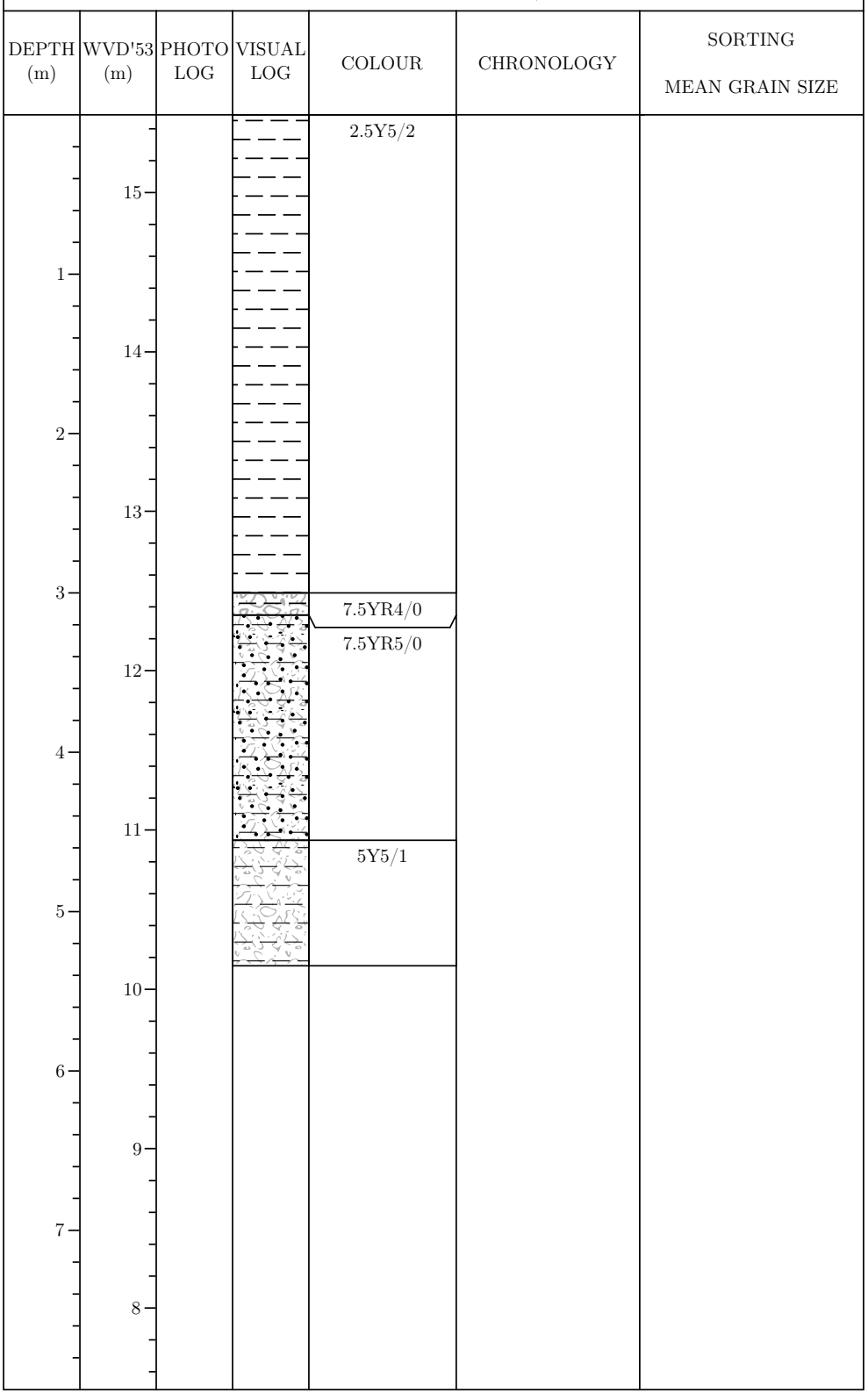

CORE: LD-1 NZMG COORDINATES: 2725319.17 E, 6083559.52 N PAGE: 2/2
LOCATION: Linton Main Drain WVD1953 ELEVATION: +15.4876 m

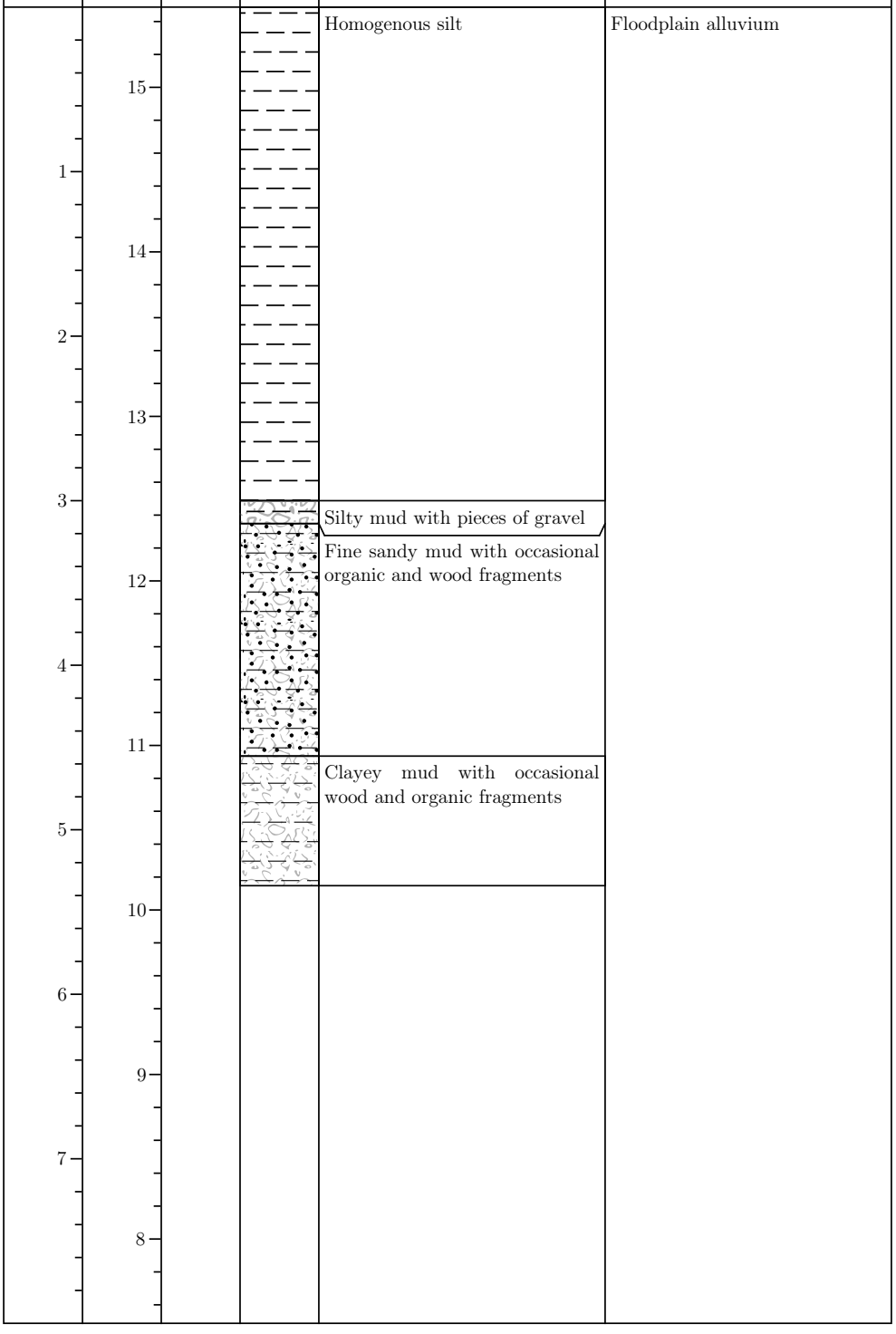

CORE: LD-2
LOCATION: Linton Main Drain

NZMG COORDINATES: 2724710.99 E, 6082928.31 N PAGE: 1/2
WVD1953 ELEVATION: +13.9240 m

DEPTH (m)	WVD'53 (m)	PHOTO LOG	VISUAL LOG	COLOUR	CHRONOLOGY	SORTING MEAN GRAIN SIZE
				5Y5/1		
1	13					
2	12					
3	11					
4	10					
5	9			7.5YR5/6 mottled with 2.5Y5/2		
				5GY5/1		
6	8					
7	7					
	6					

CORE: LD-2 NZMG COORDINATES: 2724710.99 E, 6082928.31 N PAGE: 2/2
LOCATION: Linton Main Drain WVD1953 ELEVATION: +13.9240 m

DEPTH (m)	WVD'53 (m)	PHOTO LOG	VISUAL LOG	DESCRIPTION	INTERPRETATION
				Homogenous silt	Floodplain alluvium
1	13				
2	12				
3	11				
4	10				
5	9			Coarse sandy gravel with bunched root material	
				Fine silty mud	
6	8				
7	7				
	6				

CORE: LD-3 NZMG COORDINATES: 2724025.40 E, 6082229.74 N PAGE: 1/2
LOCATION: Linton Main Drain WVD1953 ELEVATION: +9.7377 m

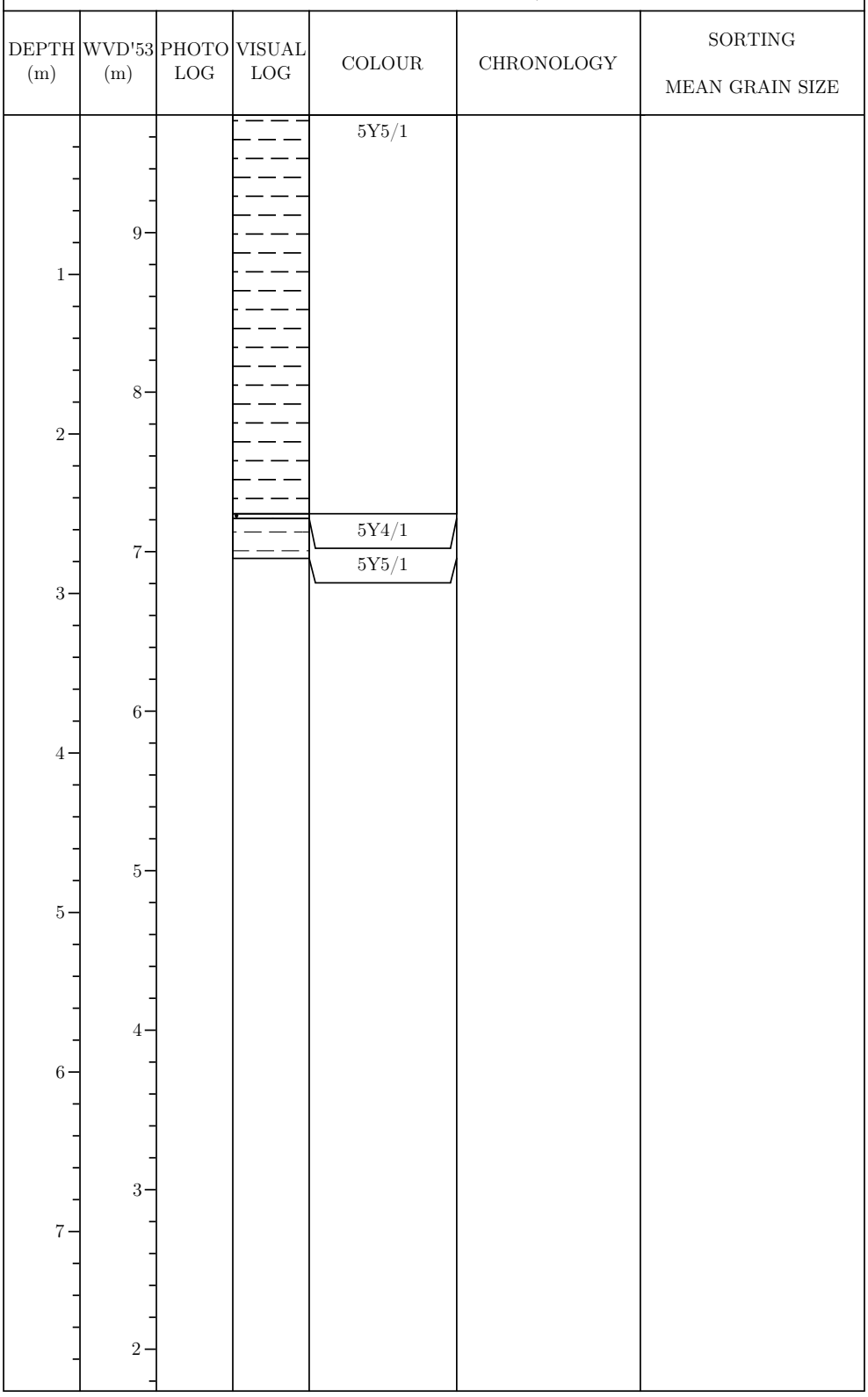

CORE: LD-3 NZMG COORDINATES: 2724025.40 E, 6082229.74 N PAGE: 2/2
LOCATION: Linton Main Drain WVD1953 ELEVATION: +9.7377 m

DEPTH (m)	WVD'53 (m)	PHOTO LOG	VISUAL LOG	DESCRIPTION	INTERPRETATION
				Homogenous silt	Floodplain alluvium
				Fine sandy mud	
				Fine clayey mud with a single insitu wood fragment	

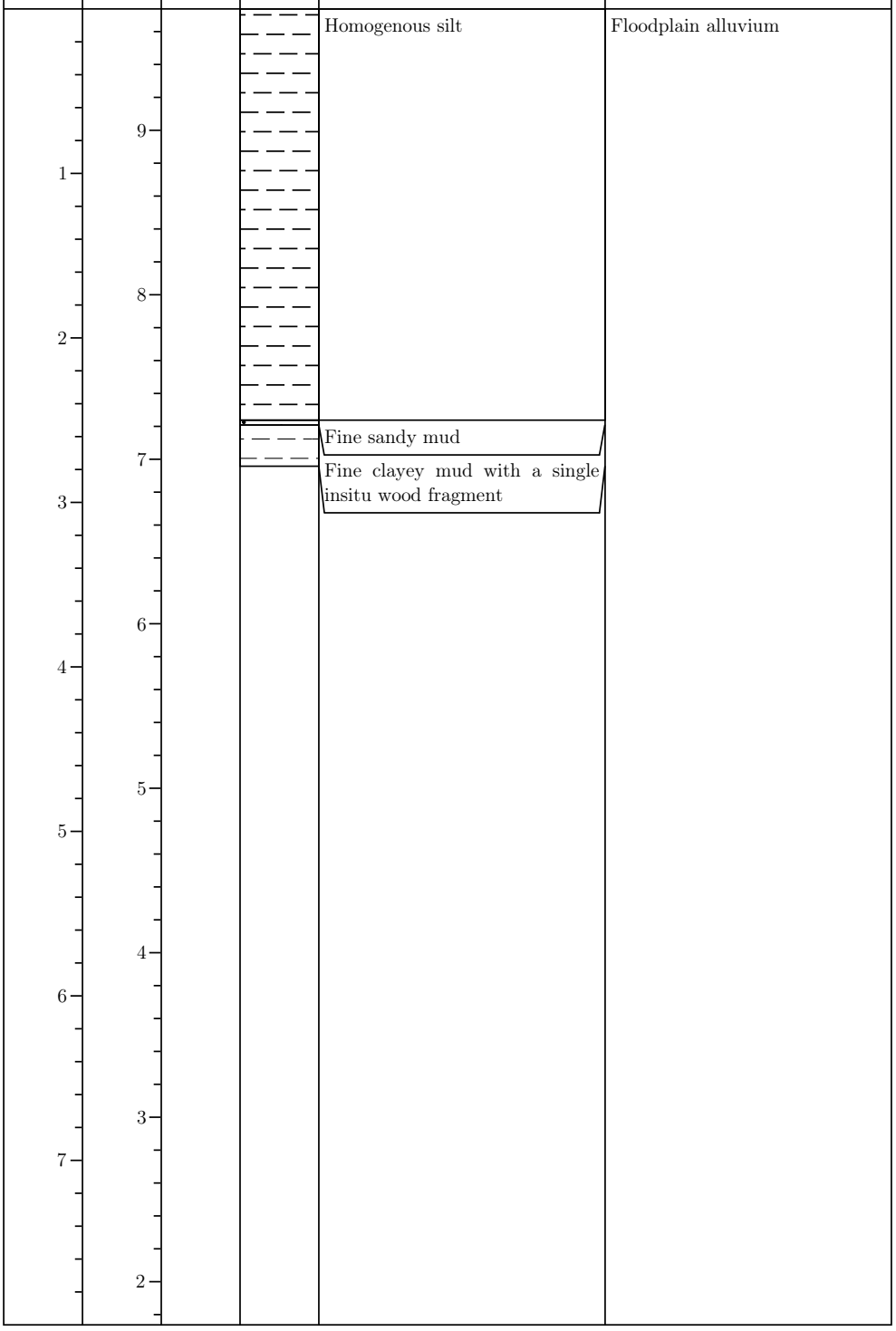

CORE: LD-4 NZMG COORDINATES: 2722739.66 E, 6080895.21 N PAGE: 1/2
LOCATION: Linton Main Drain WVD1953 ELEVATION: +7.9912 m

DEPTH (m)	WVD'53 (m)	PHOTO LOG	VISUAL LOG	COLOUR	CHRONOLOGY	SORTING MEAN GRAIN SIZE
1	7			5Y5/1		
2	6					
3	5					
				5GY4/1		
				5BG5/1		
4	4					
				5BG5/1		
5	3					
6	2					
7	1					

CORE: LD-4 NZMG COORDINATES: 2722739.66 E, 6080895.21 N PAGE: 2/2
LOCATION: Linton Main Drain WVD1953 ELEVATION: +7.9912 m

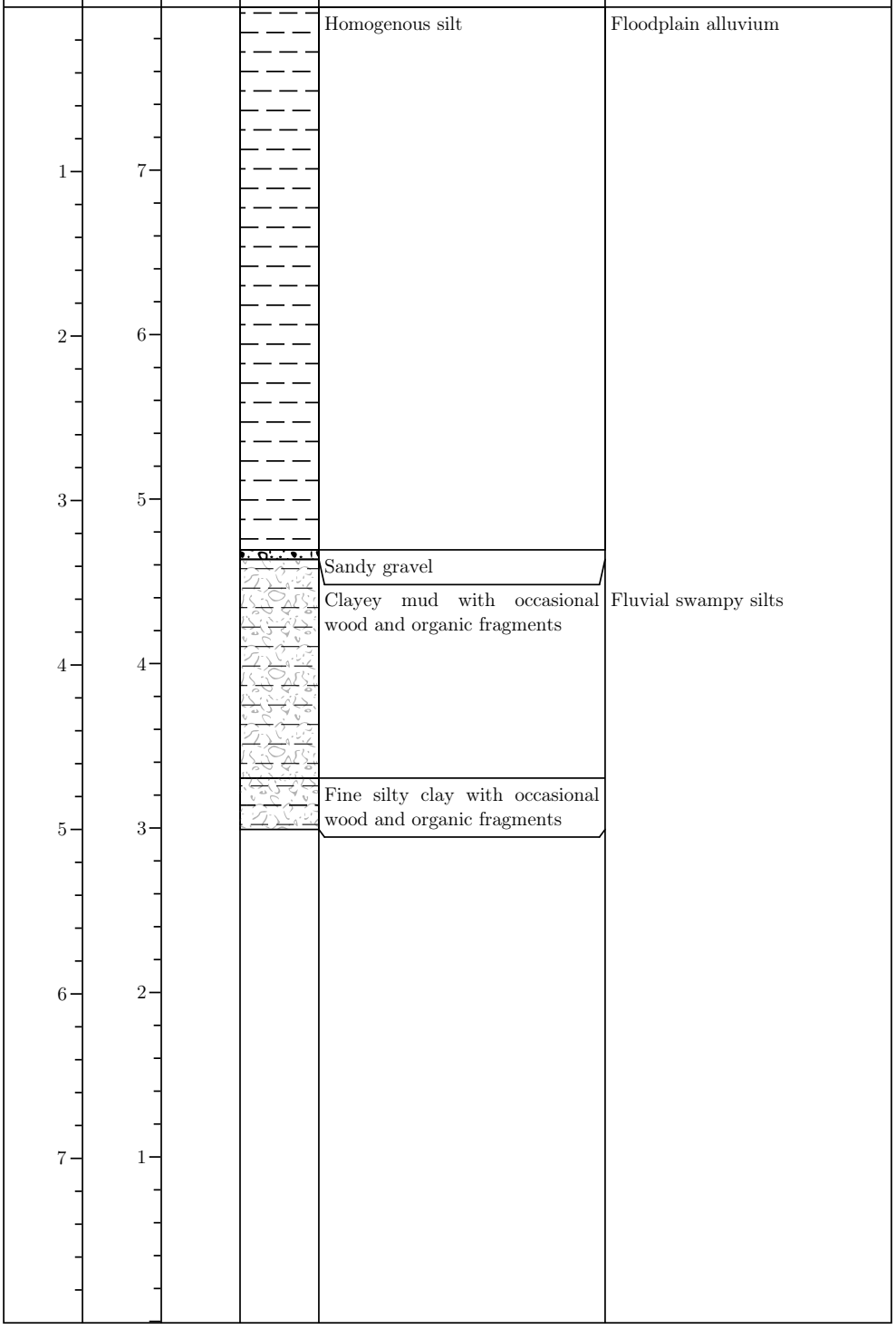

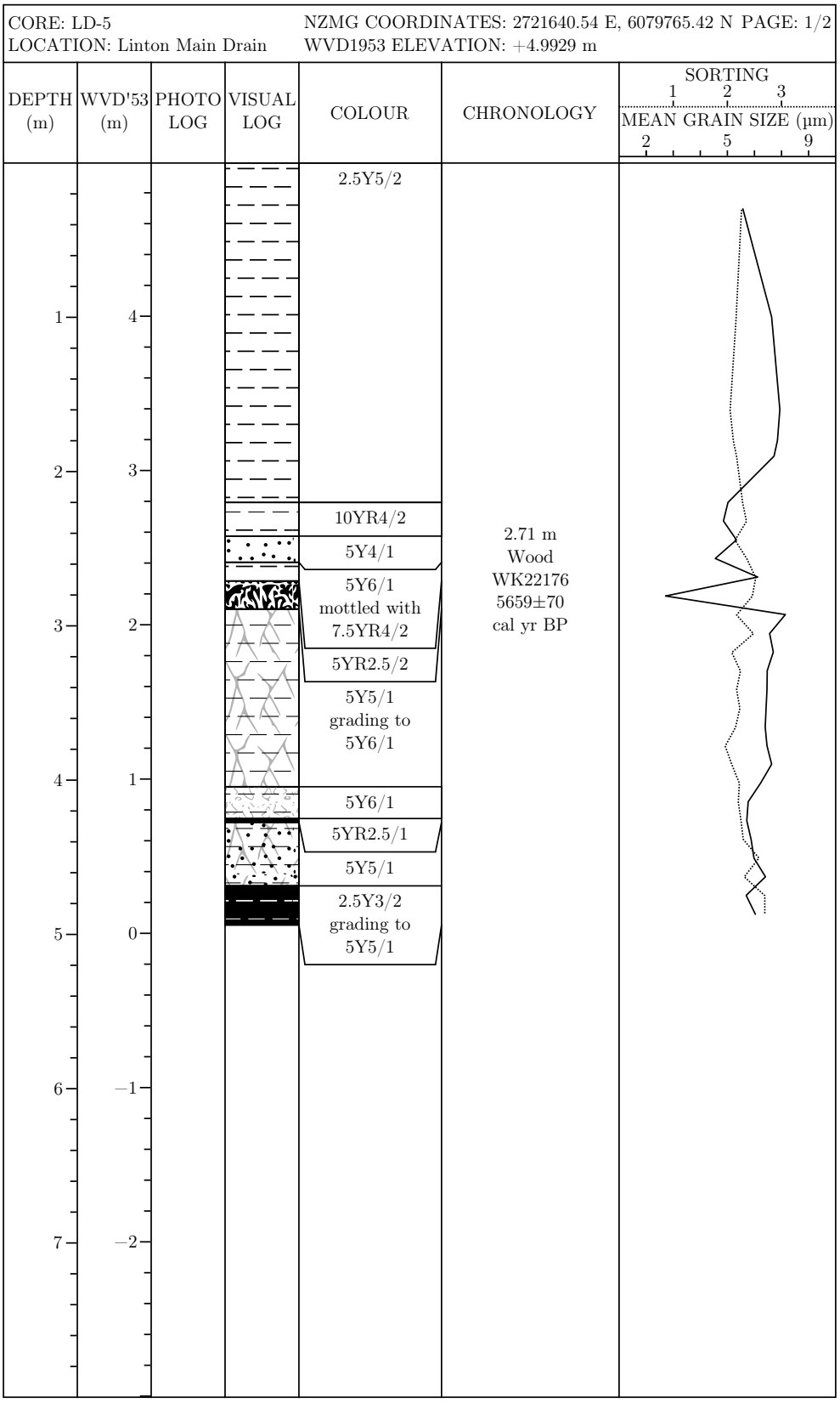
CORE: LD-5
LOCATION: Linton Main Drain
NZMG COORDINATES: 2721640.54 E, 6079765.42 N PAGE: 1/2
WVD1953 ELEVATION: +4.9929 m
DEPTH (m)
WVD'53 (m)
PHOTO LOG
VISUAL LOG
COLOUR
CHRONOLOGY
SORTING
1 2 3
MEAN GRAIN SIZE (µm)
2 5 9
2.5Y5/2
10YR4/2
5Y4/1
5Y6/1 mottled with 7.5YR4/2
5YR2.5/2
5Y5/1 grading to 5Y6/1
5Y6/1
5YR2.5/1
5Y5/1
2.5Y3/2 grading to 5Y5/1
2.71 m
Wood
WK22176
5659±70
cal yr BP

CORE: LD-5 NZMG COORDINATES: 2721640.54 E, 6079765.42 N PAGE: 2/2
LOCATION: Linton Main Drain WVD1953 ELEVATION: +4.9929 m

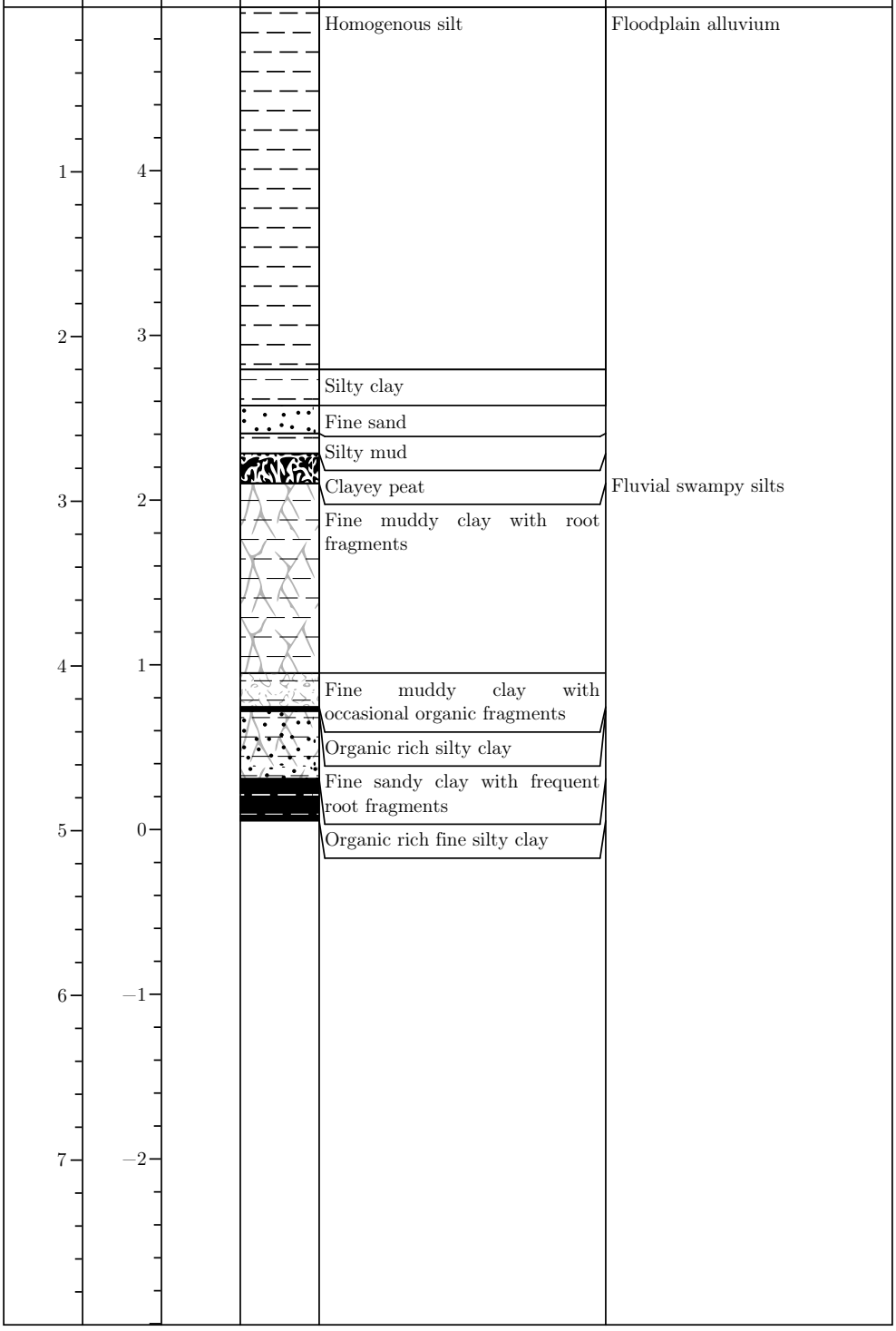

CORE: LD-6 NZMG COORDINATES: 2720767.44 E, 6078867.74 N PAGE: 1/2
LOCATION: Linton Main Drain WVD1953 ELEVATION: +5.4851 m

DEPTH (m)	WVD'53 (m)	PHOTO LOG	VISUAL LOG	COLOUR	CHRONOLOGY	SORTING / MEAN GRAIN SIZE
				2.5Y5/2		
				5Y4/1		
				5Y4/1		
				5Y5/1		
				5Y4/1		
				5GY5/1 grading to 5Y4/1		
				10YR4/1		
				5GY5/1 mottled with 10YR5/2		
				10YR2/1 grading to 5Y4/1		
				5Y5/1		
				5Y3/1		
				5Y5/1		

CORE: LD-6 NZMG COORDINATES: 2720767.44 E, 6078867.74 N PAGE: 2/2
LOCATION: Linton Main Drain WVD1953 ELEVATION: +5.4851 m

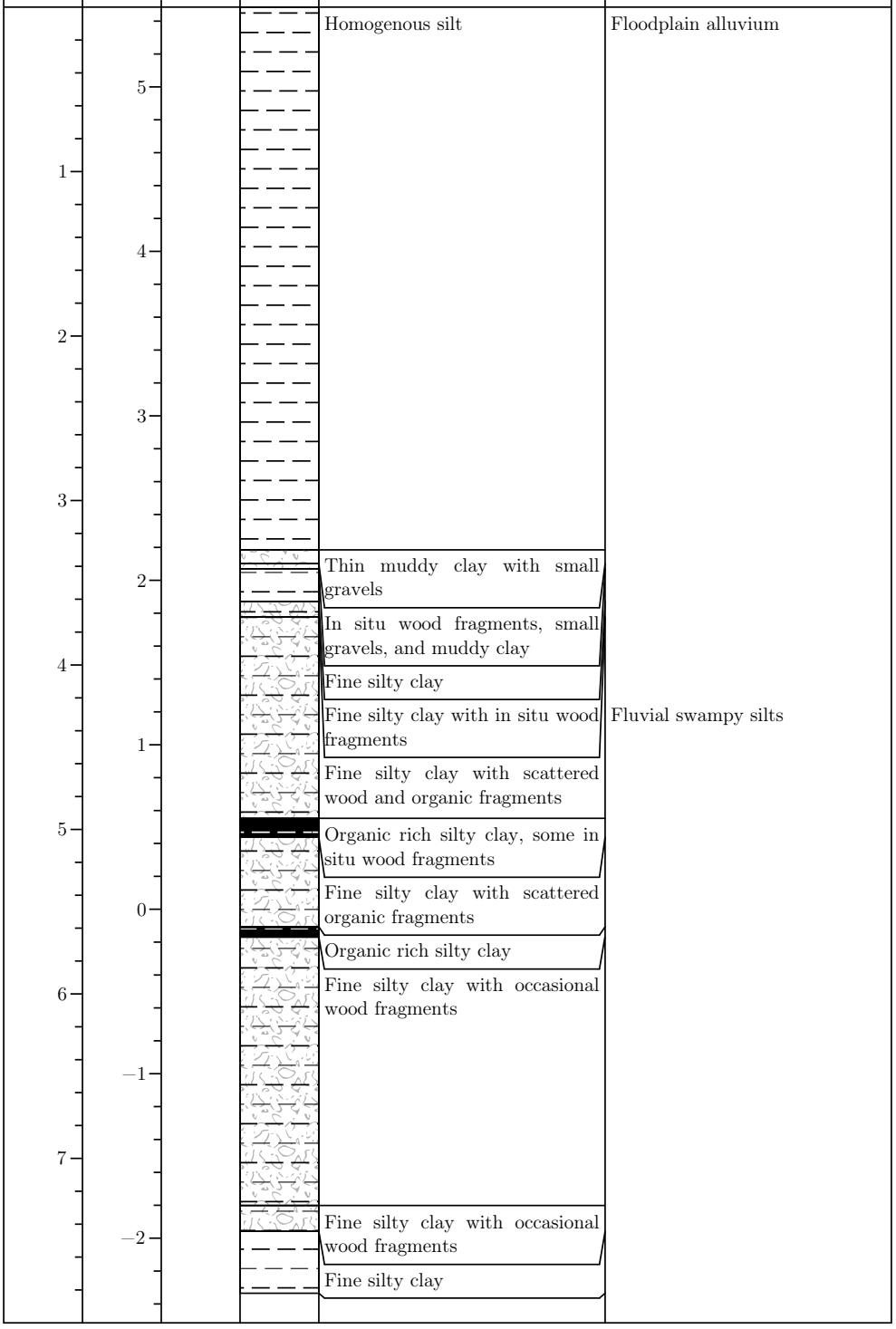

CORE: AK-2
LOCATION: Temukanui Road

NZMG COORDINATES: 2719819.92 E, 6080259.52 N PAGE: 1/2
WVD1953 ELEVATION: +6.7422 m

DEPTH (m)	WVD'53 (m)	PHOTO LOG	VISUAL LOG	COLOUR	CHRONOLOGY	SORTING MEAN GRAIN SIZE
1 6 5 2 4 3 3 4 2 5 1 6 0 7 −1				2.5Y3/2 5Y5/1		

CORE: AK-2
LOCATION: Temukanui Road

NZMG COORDINATES: 2719819.92 E, 6080259.52 N PAGE: 2/2
WVD1953 ELEVATION: +6.7422 m

DEPTH (m)	WVD'53 (m)	PHOTO LOG	VISUAL LOG	DESCRIPTION	INTERPRETATION
1 6	6			Weathered soil	Floodplain alluvium
2	5			Clayey silt with in situ wood fragments	
3 4	4 3			Clayey silt	
4 5 6 7	3 2 1 0 −1				

CORE: Cut-3 NZMG COORDINATES: 2715404.98 E, 6077645.86 N PAGE: 1/2
LOCATION: "The Cut" Drain WVD1953 ELEVATION: +3.4010 m

DEPTH (m)	WVD'53 (m)	PHOTO LOG	VISUAL LOG	COLOUR	CHRONOLOGY	SORTING MEAN GRAIN SIZE
1 2 3 4 5 6 7	3 2 1 0 −1 −2 −3 −4		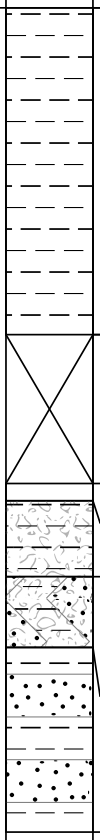	5Y4/1 5Y5/1 5Y5/1 Clayey silt: 5Y5/1 Fine sand: 2.5Y4/0 Clayey silt: 5Y5/1 Fine sand: 2.5Y3/0		

CORE: Cut-3
LOCATION: "The Cut" Drain

NZMG COORDINATES: 2715404.98 E, 6077645.86 N PAGE: 2/2
WVD1953 ELEVATION: +3.4010 m

DEPTH (m)	WVD'53 (m)	PHOTO LOG	VISUAL LOG	DESCRIPTION	INTERPRETATION
0	3			Clayey silt	Floodplain alluvium
1	2				
2	1			Obscured by water	
3	0			Thixotrophic mud	
				Clayey silt with scattered in situ wood fragments	Fluvial swampy silts
				Grading to fine sand mottled with clayey silt; some organic fragments	
4	−1			Fine sand interbedded with clayey silt	Estuarine sands and silts
5	−2				
6	−3				
7	−4				

CORE: Cut-5 NZMG COORDINATES: 2714806.80 E, 6074091.16 N PAGE: 1/2
LOCATION: "The Cut" Drain WVD1953 ELEVATION: +4.6953 m

DEPTH (m)	WVD'53 (m)	PHOTO LOG	VISUAL LOG	COLOUR	CHRONOLOGY	SORTING MEAN GRAIN SIZE
				5Y4/1		
				Clay: 5Y5/1 Sand: 2.5Y4/0		

CORE: Cut-5 NZMG COORDINATES: 2714806.80 E, 6074091.16 N PAGE: 2/2
LOCATION: "The Cut" Drain WVD1953 ELEVATION: +4.6953 m

DEPTH (m)	WVD'53 (m)	PHOTO LOG	VISUAL LOG	DESCRIPTION	INTERPRETATION
				Sandy silt grading to clayey silt	Floodplain alluvium
				Obscured by water	
				Fine sand interbedded with silty clay	Estuarine sands and silts

CORE: Cut-6 NZMG COORDINATES: 2716107.53 E, 6074960.00 N PAGE: 1/2
LOCATION: "The Cut" Drain WVD1953 ELEVATION: +3.6313 m

DEPTH (m)	WVD'53 (m)	PHOTO LOG	VISUAL LOG	COLOUR	CHRONOLOGY	SORTING MEAN GRAIN SIZE
				5Y5/1		
				2.5Y3/0		
				Sand: 2.5Y4/0 Clay: 5Y5/1		

CORE: Cut-6 NZMG COORDINATES: 2716107.53 E, 6074960.00 N PAGE: 2/2
LOCATION: "The Cut" Drain WVD1953 ELEVATION: +3.6313 m

DEPTH (m)	WVD'53 (m)	PHOTO LOG	VISUAL LOG	DESCRIPTION	INTERPRETATION
1 2 2 3 3 4 4 5 5 6 6 7	3 2 1 0 −1 −2 −3 −4		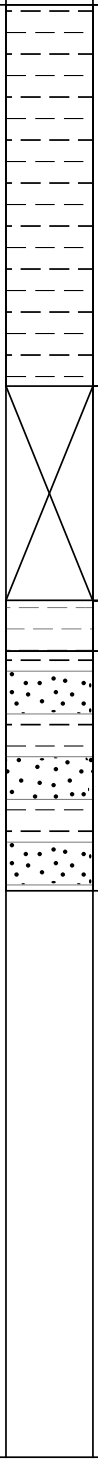	Clayey silt Obscured by water Thixotrophic mud Fine sand interbedded with silty clay	Floodplain alluvium Estuarine sands and silts

CORE: Cut-8
LOCATION: "The Cut" Drain

NZMG COORDINATES: 2714465.83 E, 6073472.63 N PAGE: 1/2
WVD1953 ELEVATION: +3.5013 m

DEPTH (m)	WVD'53 (m)	PHOTO LOG	VISUAL LOG	COLOUR	CHRONOLOGY	SORTING MEAN GRAIN SIZE
				5Y4/1		
				5Y5/1		
				Sand: 2.5Y3/0 Clay: 5Y5/1		

CORE: Cut-8 NZMG COORDINATES: 2714465.83 E, 6073472.63 N PAGE: 2/2
LOCATION: "The Cut" Drain WVD1953 ELEVATION: +3.5013 m

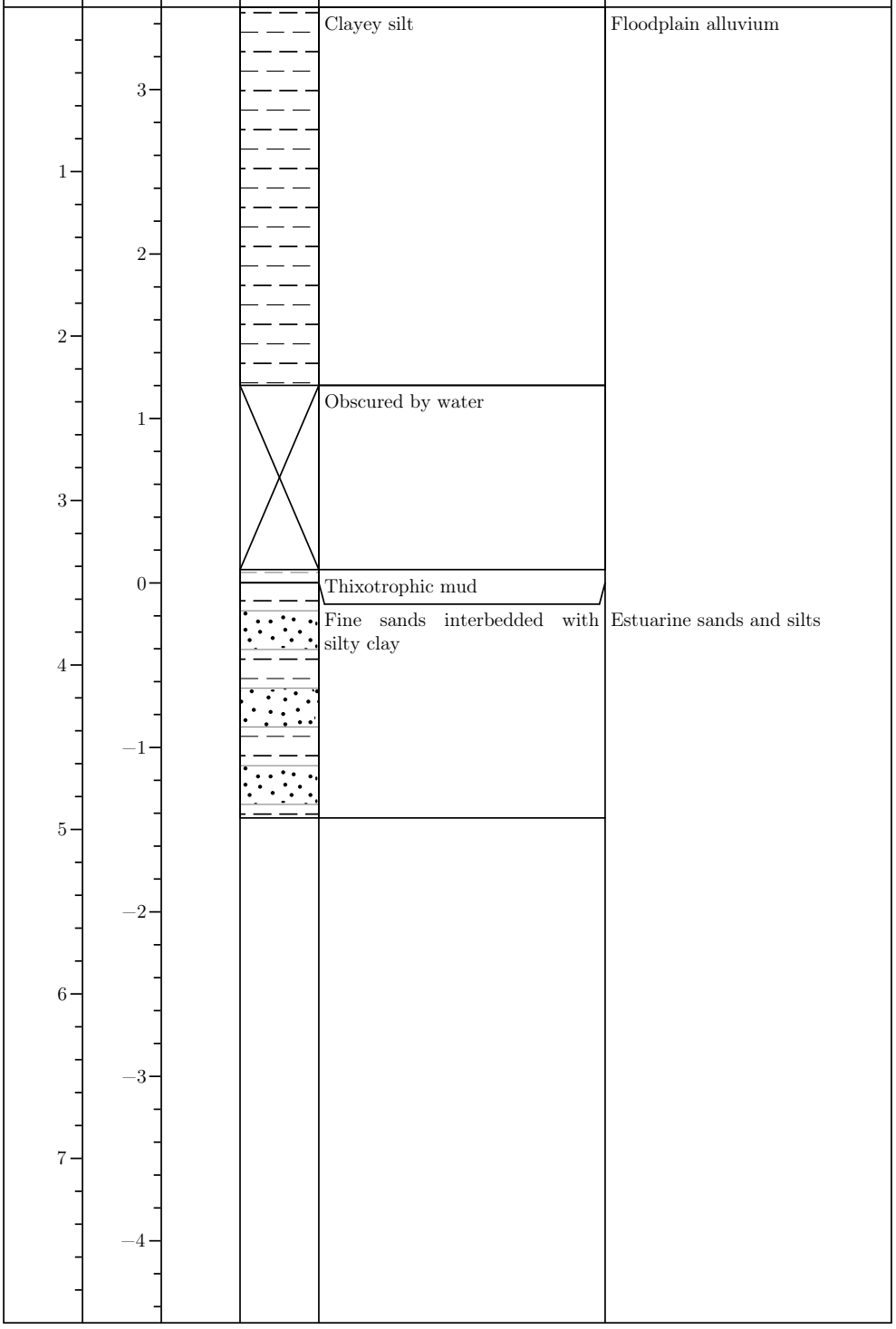

CORE: Cut-9 NZMG COORDINATES: 2717063.93 E, 6076115.54 N PAGE: 1/2
LOCATION: Te Rewa Road WVD1953 ELEVATION: +3.4035 m

DEPTH (m)	WVD'53 (m)	PHOTO LOG	VISUAL LOG	COLOUR	CHRONOLOGY	SORTING MEAN GRAIN SIZE
				5Y4/1		
				2.5Y3/0		
				Sand: 2.5Y4/0 Clay: 5Y5/1		
				2.5Y3/0		

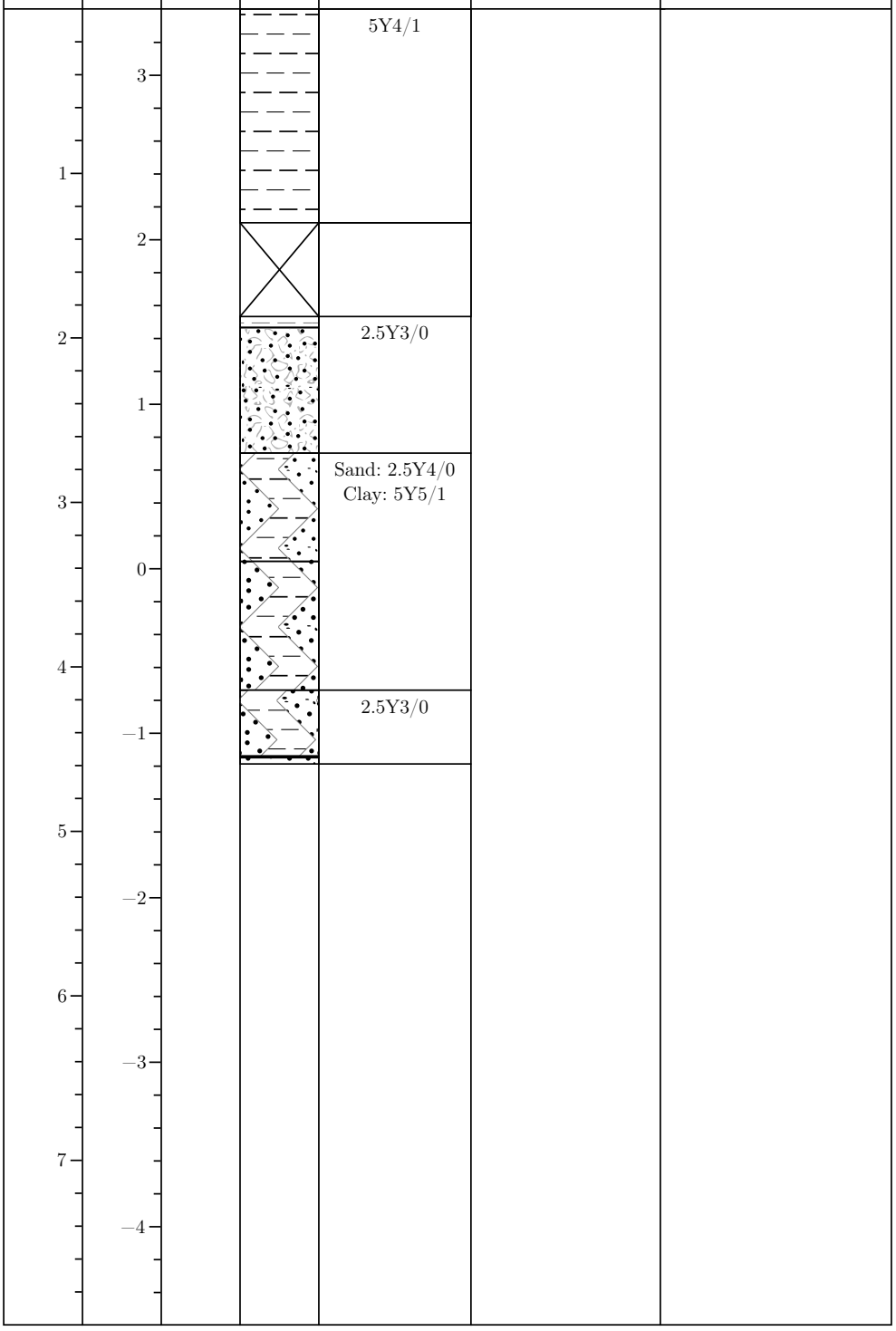

CORE: Cut-9
LOCATION: Te Rewa Road

NZMG COORDINATES: 2717063.93 E, 6076115.54 N PAGE: 2/2
WVD1953 ELEVATION: +3.4035 m

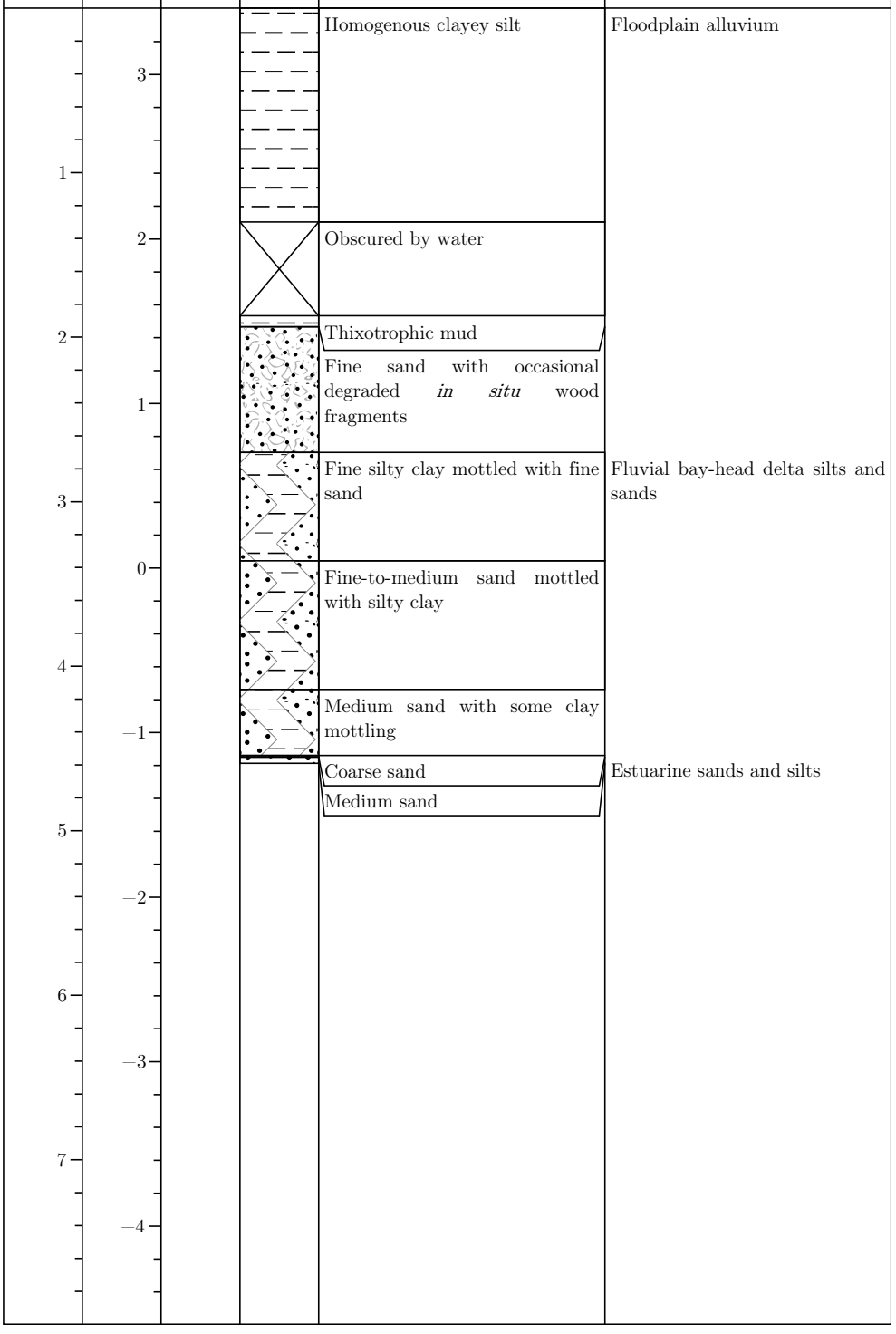

CORE: Cut-10B
LOCATION: Ashela Road

NZMG COORDINATES: 2717954.06 E, 6079622.49 N PAGE: 1/2
WVD1953 ELEVATION: +4.3117 m

DEPTH (m)	WVD'53 (m)	PHOTO LOG	VISUAL LOG	COLOUR	CHRONOLOGY	SORTING MEAN GRAIN SIZE
				5Y5/1		
				2.5Y5/6		
				5Y5/1 grading to 5GY5/1		

CORE: Cut-10B
LOCATION: Ashela Road

NZMG COORDINATES: 2717954.06 E, 6079622.49 N PAGE: 2/2
WVD1953 ELEVATION: +4.3117 m

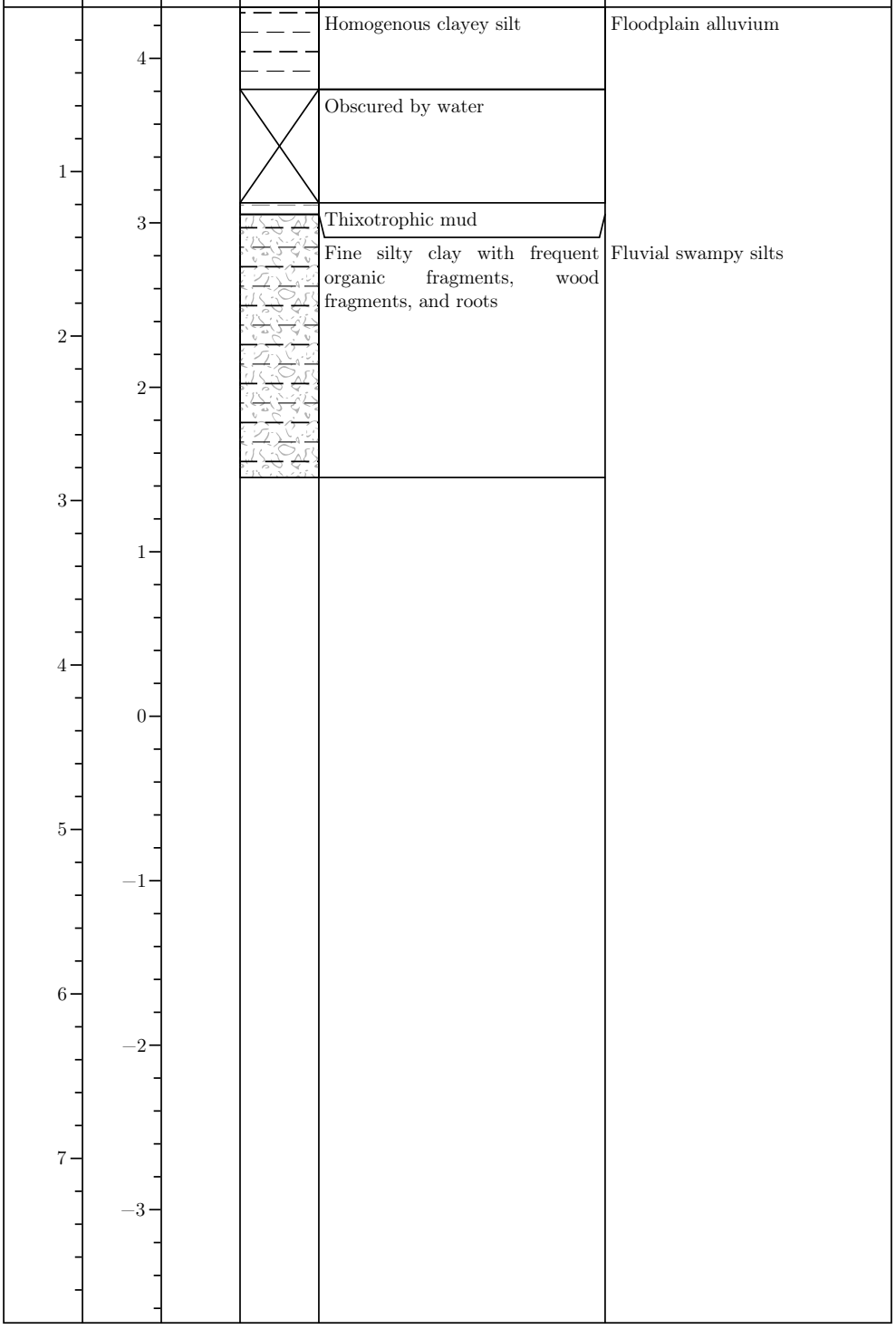

CORE: Cut-11
LOCATION: Ashlea Road

NZMG COORDINATES: 2719093.38 E, 6080009.84 N PAGE: 1/2
WVD1953 ELEVATION: +4.2758 m

DEPTH (m)	WVD'53 (m)	PHOTO LOG	VISUAL LOG	COLOUR	CHRONOLOGY	SORTING MEAN GRAIN SIZE
1 2 3 4 5 6 7	4 3 2 1 0 −1 −2 −3		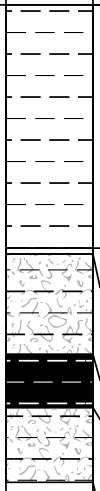	2.5Y3/2 grading to N5/ 5Y5/1 5Y5/1 grading to 2.5Y4/2 2.5Y4/2 5GY5/1 grading to 5Y5/1		

CORE: Cut-11
LOCATION: Ashlea Road

NZMG COORDINATES: 2719093.38 E, 6080009.84 N PAGE: 2/2
WVD1953 ELEVATION: +4.2758 m

DEPTH (m)	WVD'53 (m)	PHOTO LOG	VISUAL LOG	DESCRIPTION	INTERPRETATION
				Clayey silt	Floodplain alluvium
				Thixotrophic mud	
				Silty clay with frequent root fragments and organics, and some in situ wood fragments	Fluvial swampy silts
				Organic-rich silty clay	
				Silty clay with frequent root fragments and organics, and some in situ wood fragments	

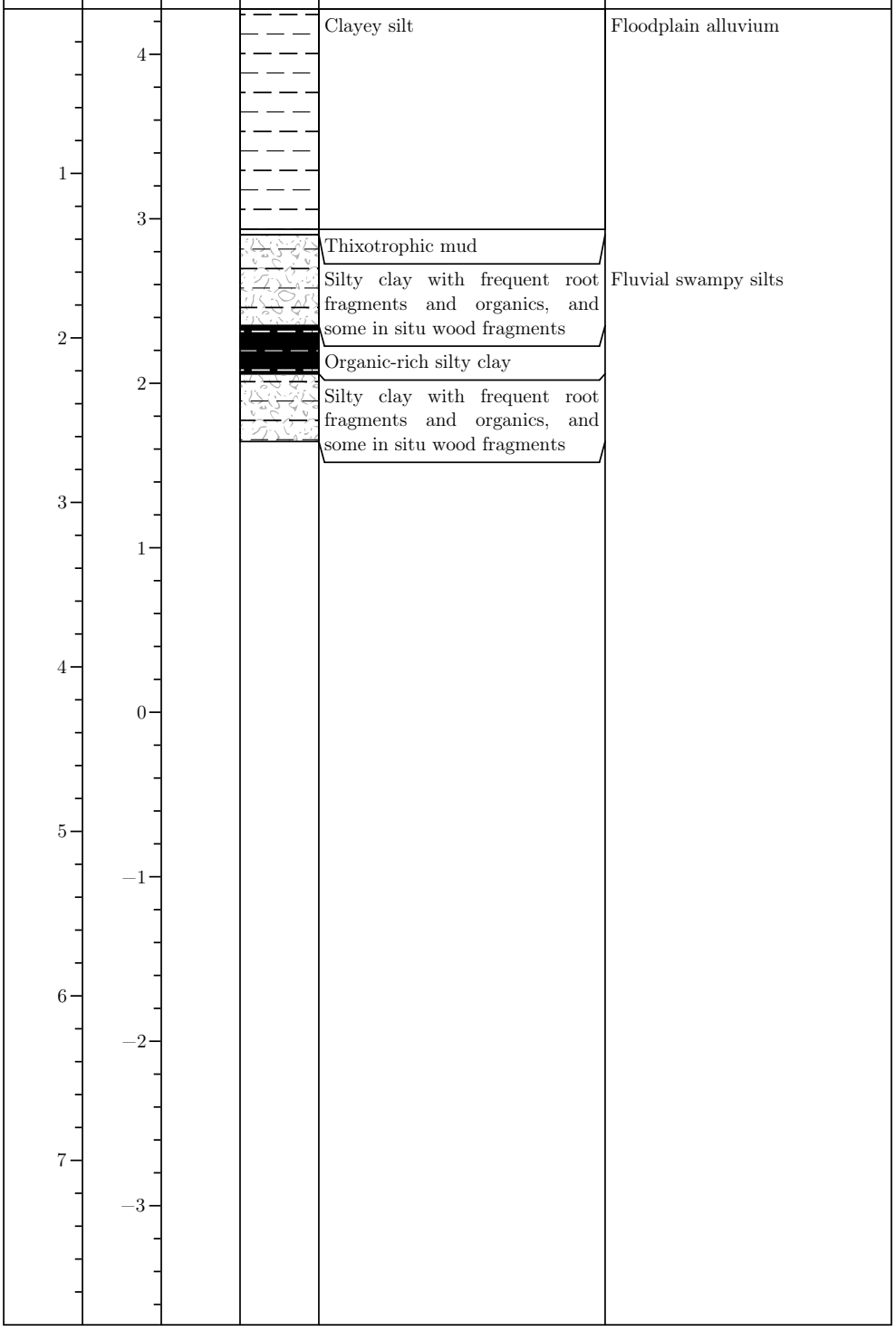

CORE: Cut-12 NZMG COORDINATES: 2719897.93 E, 6077907.19 N PAGE: 1/2
LOCATION: Boundary Drain WVD1953 ELEVATION: +5.2965 m

DEPTH (m)	WVD'53 (m)	PHOTO LOG	VISUAL LOG	COLOUR	CHRONOLOGY	SORTING MEAN GRAIN SIZE
				10YR3/4 grading to 10YR2/2		
				5Y5/1		
				5GY5/1		
				5Y5/1		
				5Y4/1		
				2.5Y4/2 grading to 5Y4/1		

CORE: Cut-12
LOCATION: Boundary Drain

NZMG COORDINATES: 2719897.93 E, 6077907.19 N PAGE: 2/2
WVD1953 ELEVATION: +5.2965 m

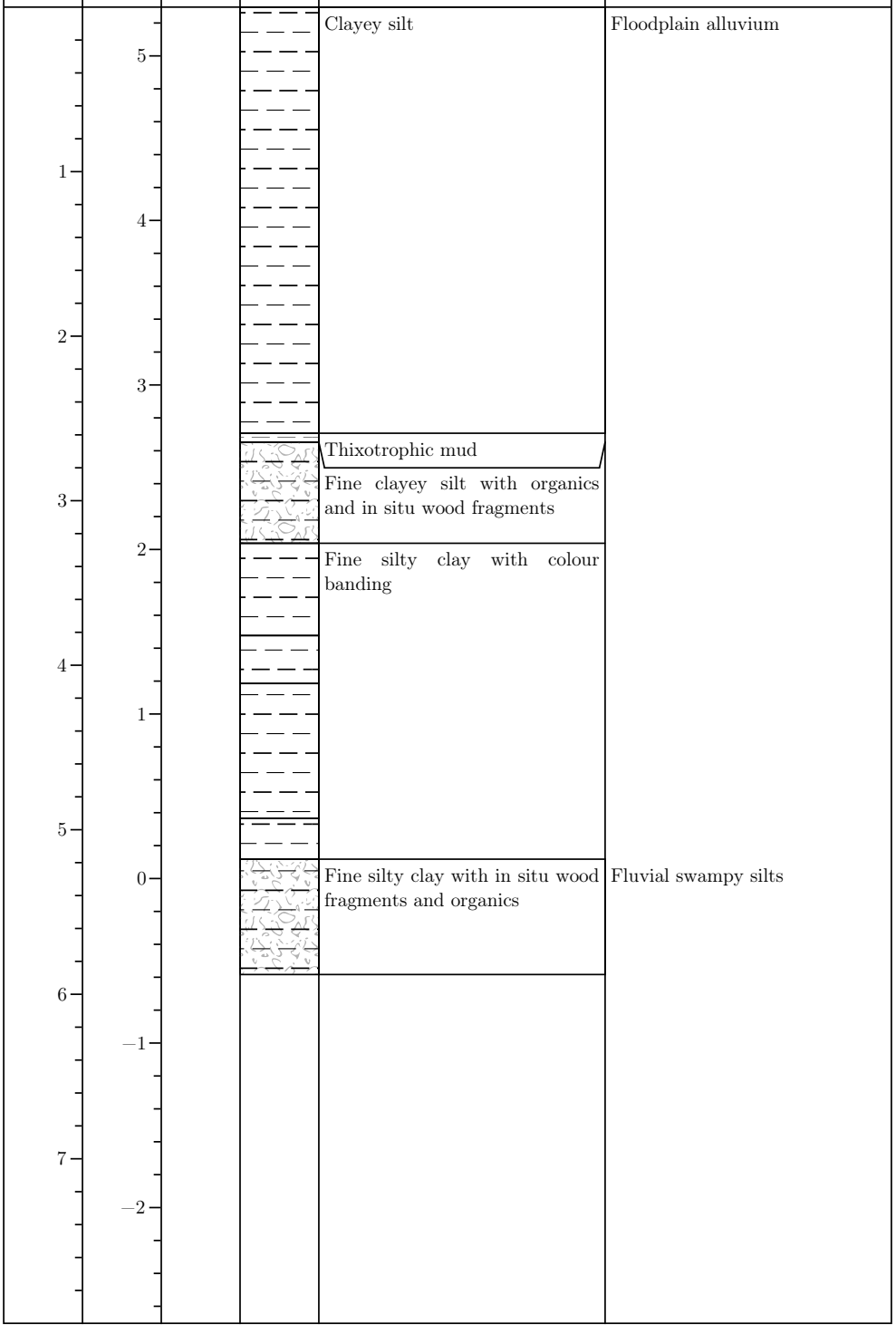

CORE: Cut-13
LOCATION: Salvie's Farm

NZMG COORDINATES: 2716640.94 E, 6079175.79 N PAGE: 1/2
WVD1953 ELEVATION: +4.4583 m

DEPTH (m)	WVD'53 (m)	PHOTO LOG	VISUAL LOG	COLOUR	CHRONOLOGY	SORTING MEAN GRAIN SIZE
				5YR4/6		
				7.5YR2/6		
				5Y5/1		
				2.5Y5/6		
				5Y5/1 grading to 5GY5/1		
				Sand: 2.5Y4/0 Clay: 5Y5/1		

CORE: Cut-13
LOCATION: Salvie's Farm

NZMG COORDINATES: 2716640.94 E, 6079175.79 N PAGE: 2/2
WVD1953 ELEVATION: +4.4583 m

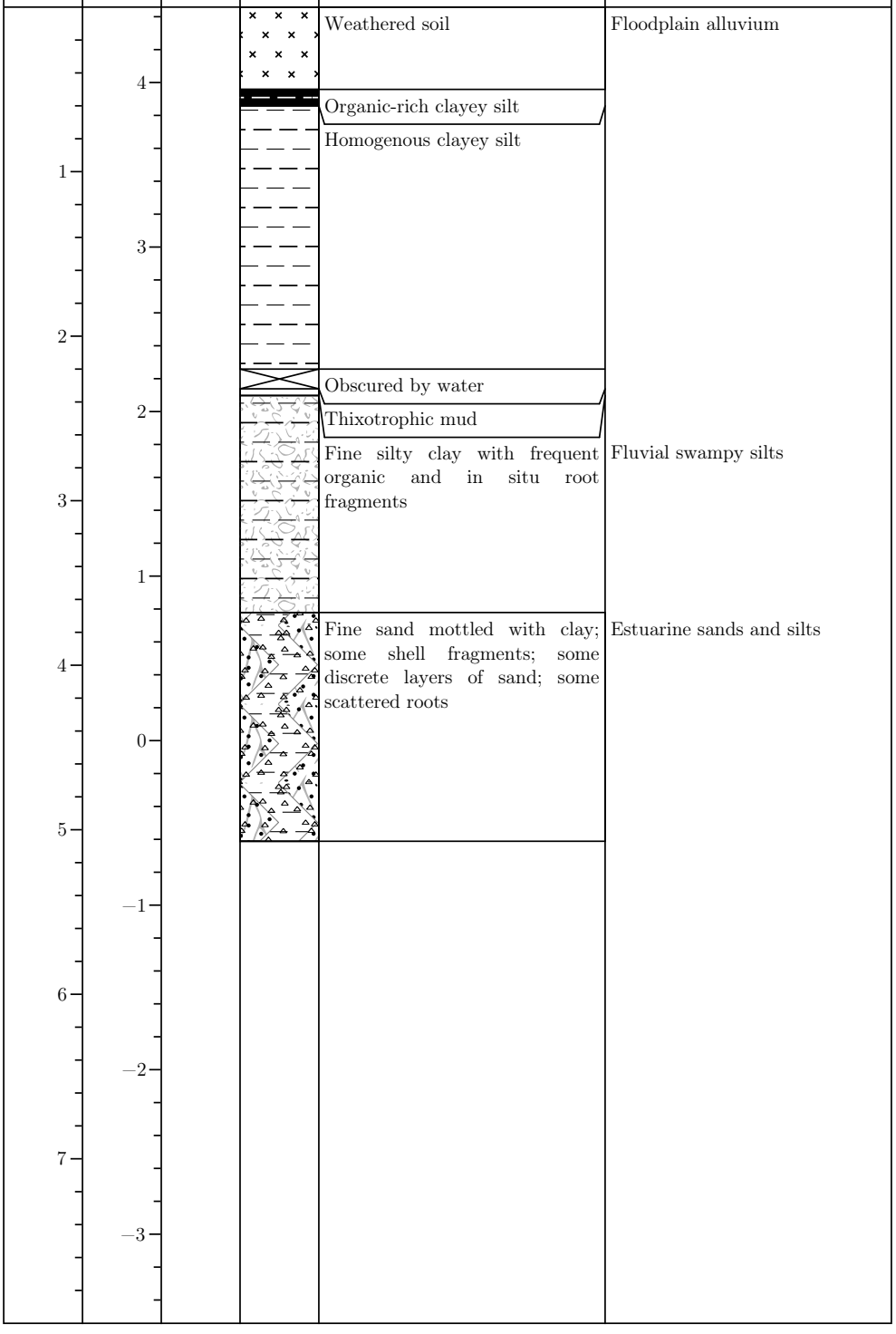

CORE: Cut-14
LOCATION: Salvie's Farm

NZMG COORDINATES: 2715324.93 E, 6078725.92 N PAGE: 1/2
WVD1953 ELEVATION: +4.5674 m

DEPTH (m)	WVD'53 (m)	PHOTO LOG	VISUAL LOG	COLOUR	CHRONOLOGY	SORTING MEAN GRAIN SIZE
0 1 2 3 4 5 6 7	4 3 2 1 0 −1 −2 −3		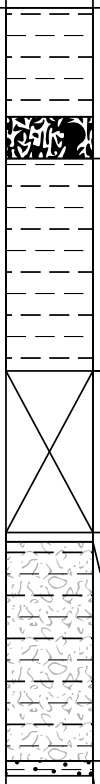	10YR4/3 5Y6/1 2.5Y5/4 5Y5/1 grading to 2.5Y4/2 Sand: 2.5Y4/0 Clay: 5Y5/1		

CORE: Cut-14
LOCATION: Salvie's Farm

NZMG COORDINATES: 2715324.93 E, 6078725.92 N PAGE: 2/2
WVD1953 ELEVATION: +4.5674 m

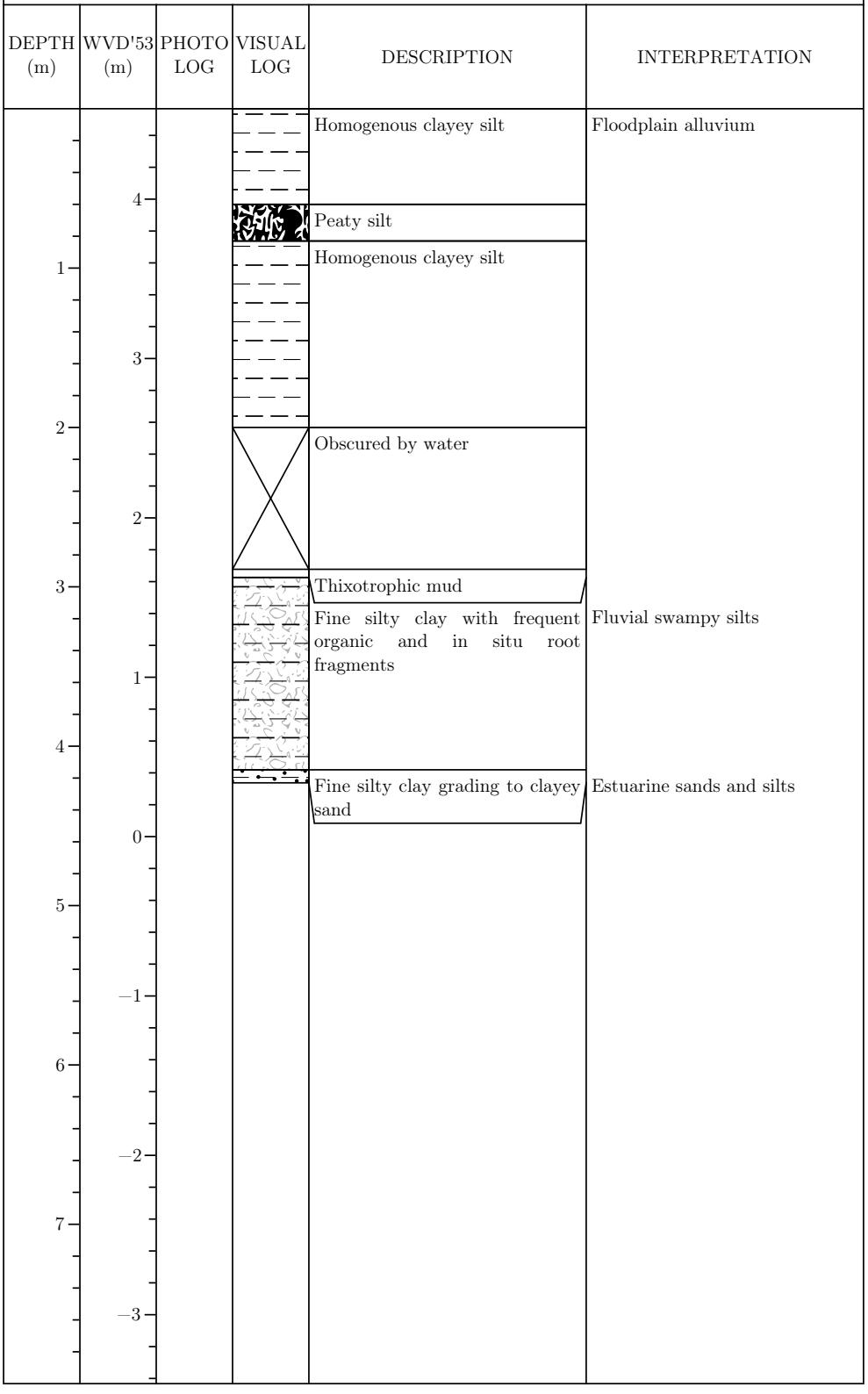

CORE: Kop-2 NZMG COORDINATES: 2706085.75 E, 6070091.90 N PAGE: 1/2
LOCATION: Koputaroa WVD1953 ELEVATION: +1.0068 m

DEPTH (m)	WVD'53 (m)	PHOTO LOG	VISUAL LOG	COLOUR	CHRONOLOGY	SORTING / MEAN GRAIN SIZE
1	0		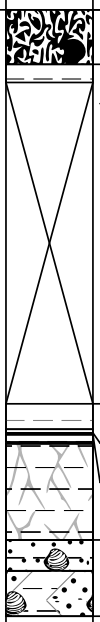	10YR2/1 5Y5/1		
2	−1					
3	−2			5Y5/1 10YR3/3 5Y4/1 2.5Y3/0		
4	−3					
5	−4					
6	−5					
7	−6					

CORE: Kop-2
LOCATION: Koputaroa

NZMG COORDINATES: 2706085.75 E, 6070091.90 N PAGE: 2/2
WVD1953 ELEVATION: +1.0068 m

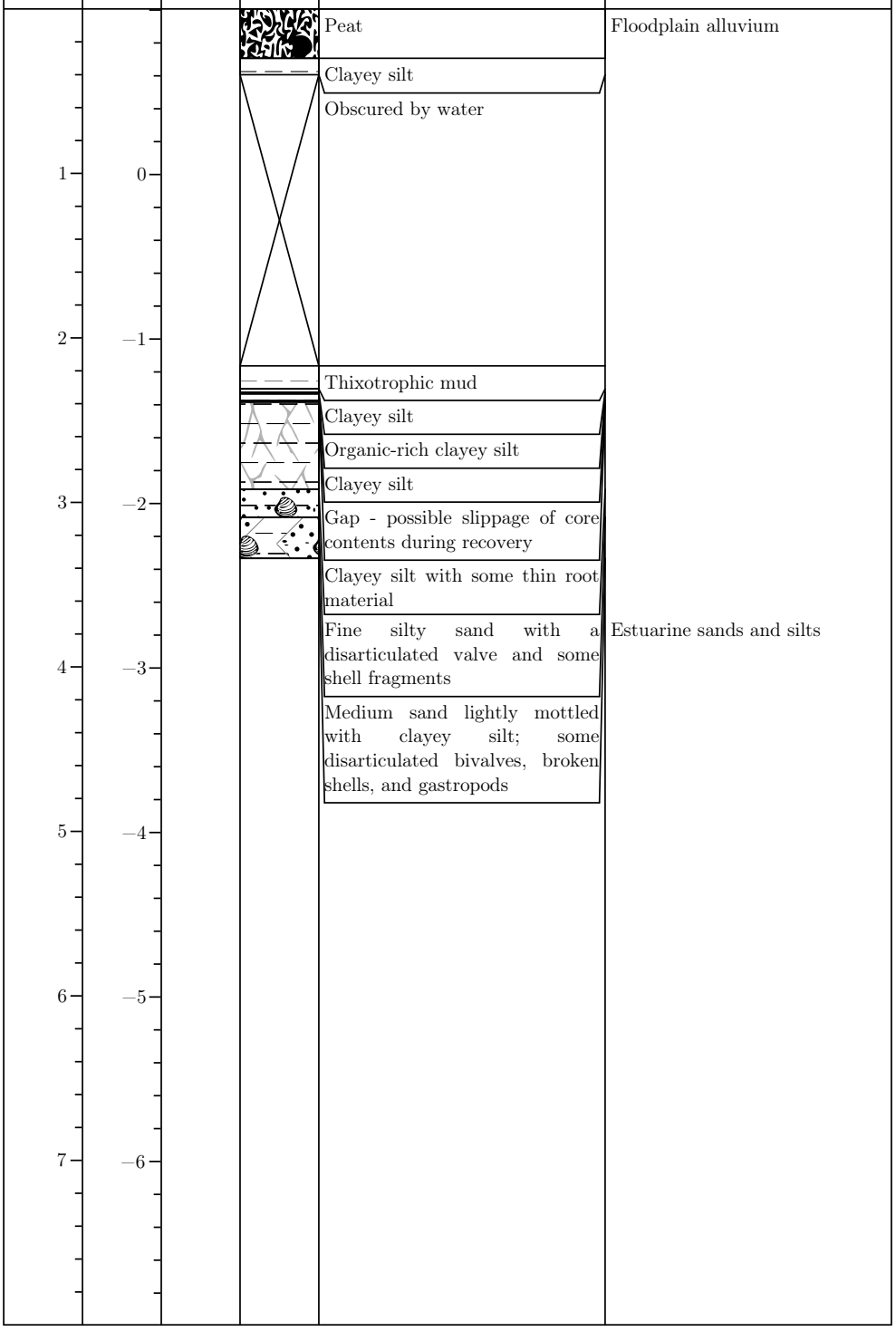

CORE: Kop-3
LOCATION: Koputaroa

NZMG COORDINATES: 2705888.81 E, 6069346.75 N PAGE: 1/2
WVD1953 ELEVATION: +0.9017 m

DEPTH (m)	WVD'53 (m)	PHOTO LOG	VISUAL LOG	COLOUR	CHRONOLOGY	SORTING MEAN GRAIN SIZE
1 2 3 4 5 6 7	0 −1 −2 −3 −4 −5 −6 −7		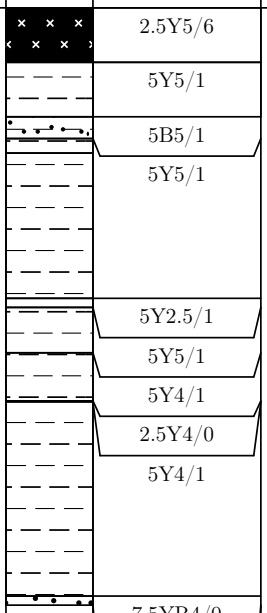	2.5Y5/6 5Y5/1 5B5/1 5Y5/1 5Y2.5/1 5Y5/1 5Y4/1 2.5Y4/0 5Y4/1 7.5YR4/0 mottled with 2.5Y6/8		

CORE: Kop-3
LOCATION: Koputaroa

NZMG COORDINATES: 2705888.81 E, 6069346.75 N PAGE: 2/2
WVD1953 ELEVATION: +0.9017 m

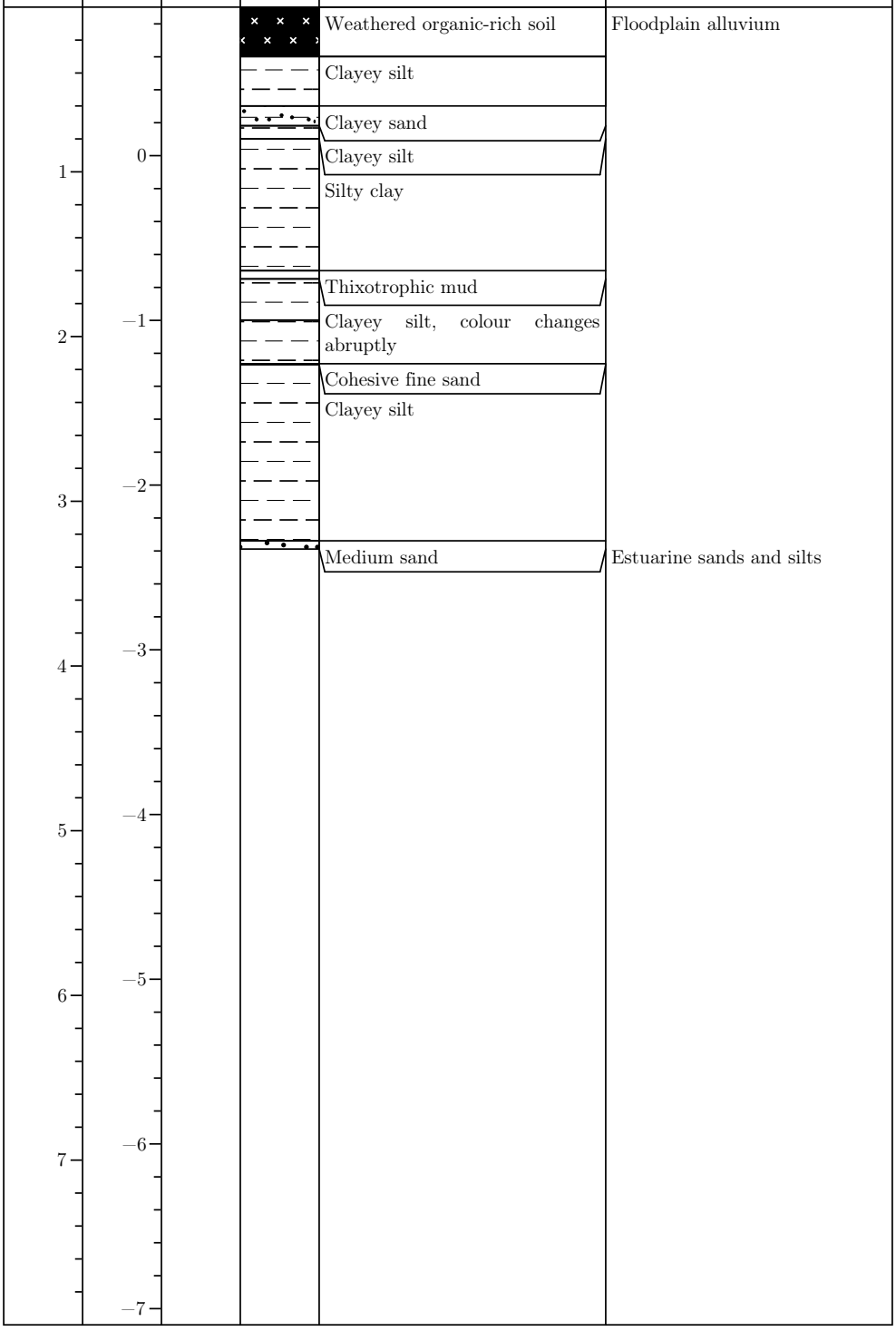

CORE: Kop-4
LOCATION: Koputaroa

NZMG COORDINATES: 2705197.18 E, 6071305.35 N PAGE: 1/2
WVD1953 ELEVATION: +0.7440 m

DEPTH (m)	WVD'53 (m)	PHOTO LOG	VISUAL LOG	COLOUR	CHRONOLOGY	SORTING MEAN GRAIN SIZE
1	0			2.5Y7/3 10YR3/3 grading to 10YR2/1		
2	−1			10YR2/1 5Y5/1 5Y5/1 5G5/1 5G5/1 grading to 5Y4/1		
3	−2			5Y4/1		
4	−3					
5	−4					
6	−5					
7	−6					
	−7					

CORE: Kop-4
LOCATION: Koputaroa

NZMG COORDINATES: 2705197.18 E, 6071305.35 N PAGE: 2/2
WVD1953 ELEVATION: +0.7440 m

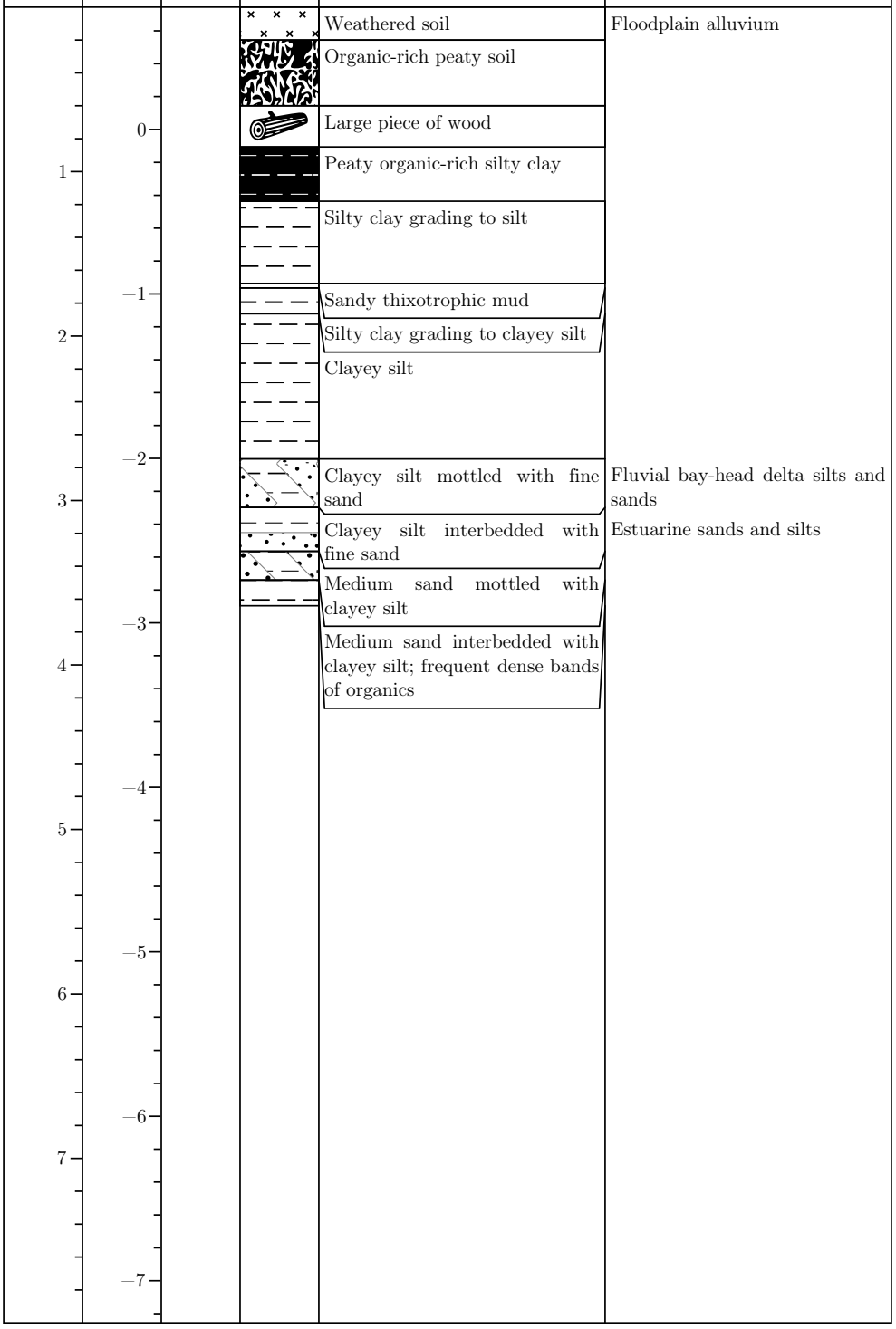

CORE: Kop-5
LOCATION: Koputaroa

NZMG COORDINATES: 2705107.08 E, 6068920.31 N PAGE: 1/2
WVD1953 ELEVATION: +1.5678 m

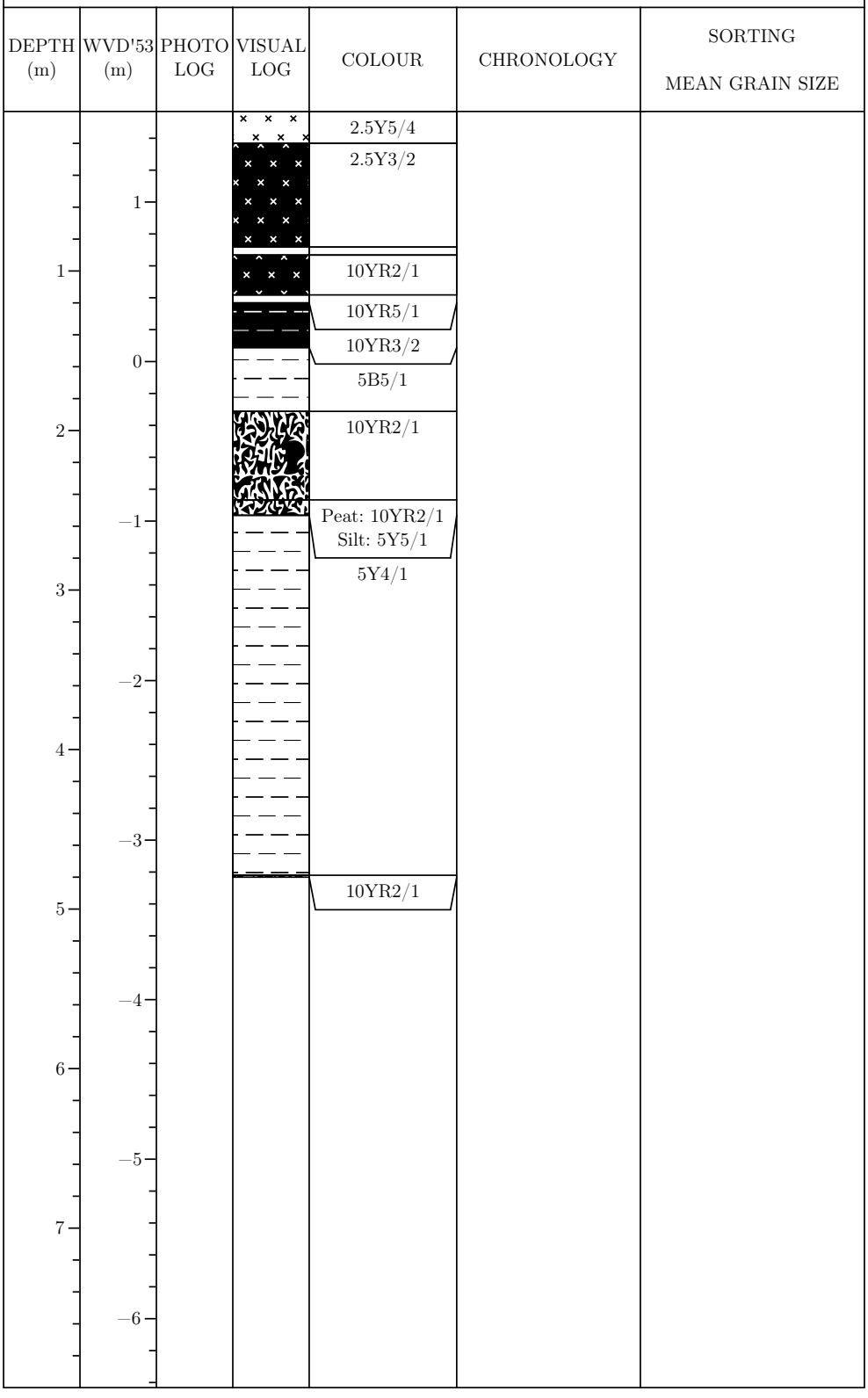

CORE: Kop-5
LOCATION: Koputaroa

NZMG COORDINATES: 2705107.08 E, 6068920.31 N PAGE: 2/2
WVD1953 ELEVATION: +1.5678 m

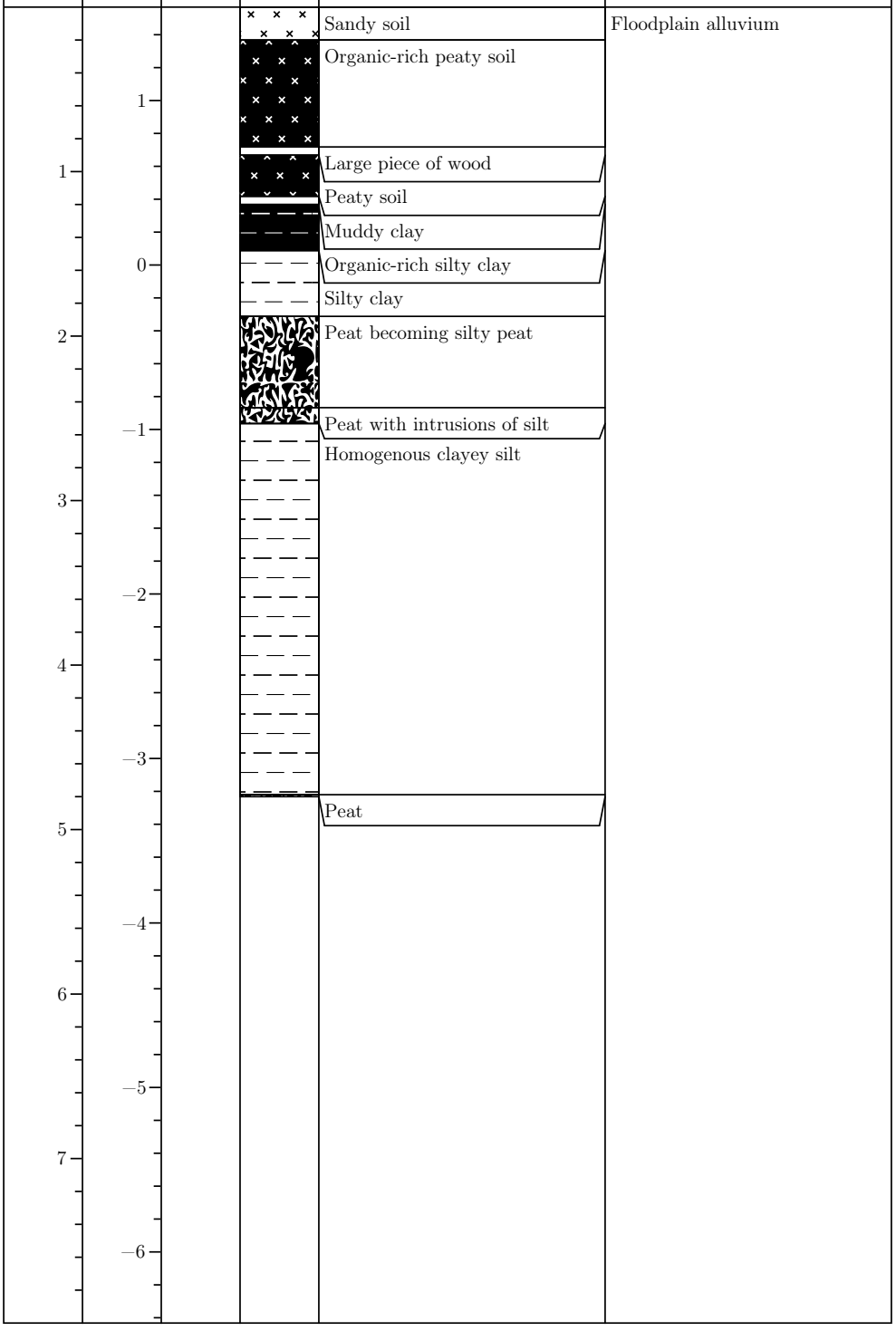

CORE: Kop-6 NZMG COORDINATES: 2709377.97 E, 6070904.71 N PAGE: 1/2
LOCATION: Koputaroa WVD1953 ELEVATION: +4.4041 m

DEPTH (m)	WVD'53 (m)	PHOTO LOG	VISUAL LOG	COLOUR	CHRONOLOGY	SORTING / MEAN GRAIN SIZE
				2.5Y7/3		
	4			2.5Y5/4		
1						
	3					
2						
	2					
				5Y6/1		
3						
	1			N5/		
				5Y5/1		
4				5Y4/1		
				N4/		
	0			5Y4/1		
				10YR2/1		
				5Y4/1		
5				10YR2/1		
	−1			5Y4/1		
6						
				10YR2/1		
	−2			5Y4/1		
7						
	−3					

CORE: Kop-6
LOCATION: Koputaroa

NZMG COORDINATES: 2709377.97 E, 6070904.71 N PAGE: 2/2
WVD1953 ELEVATION: +4.4041 m

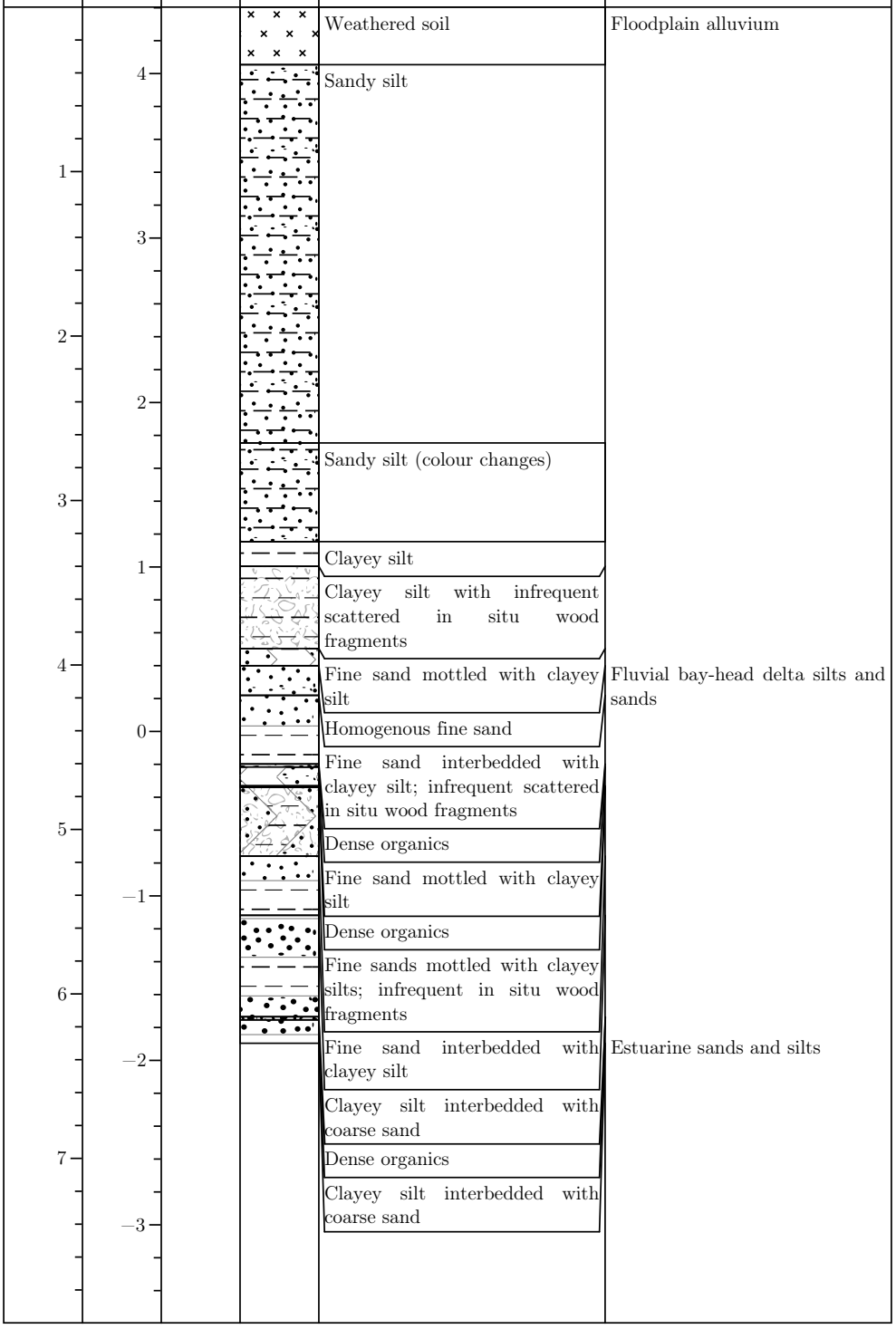

CORE: A1
LOCATION: Whirokino Road

NZMG COORDINATES: 2704618.17 E, 6073053.55 N PAGE: 1/2
WVD1953 ELEVATION: +0.8418 m

DEPTH (m)	WVD'53 (m)	PHOTO LOG	VISUAL LOG	COLOUR	CHRONOLOGY	SORTING MEAN GRAIN SIZE
1 2 3 4 5 6 7	0 −1 −2 −3 −4 −5 −6 −7			2.5Y4/3 5Y5/1 Clay: 5Y5/1 Sand: 2.5Y4/0		

CORE: A1
LOCATION: Whirokino Road

NZMG COORDINATES: 2704618.17 E, 6073053.55 N PAGE: 2/2
WVD1953 ELEVATION: +0.8418 m

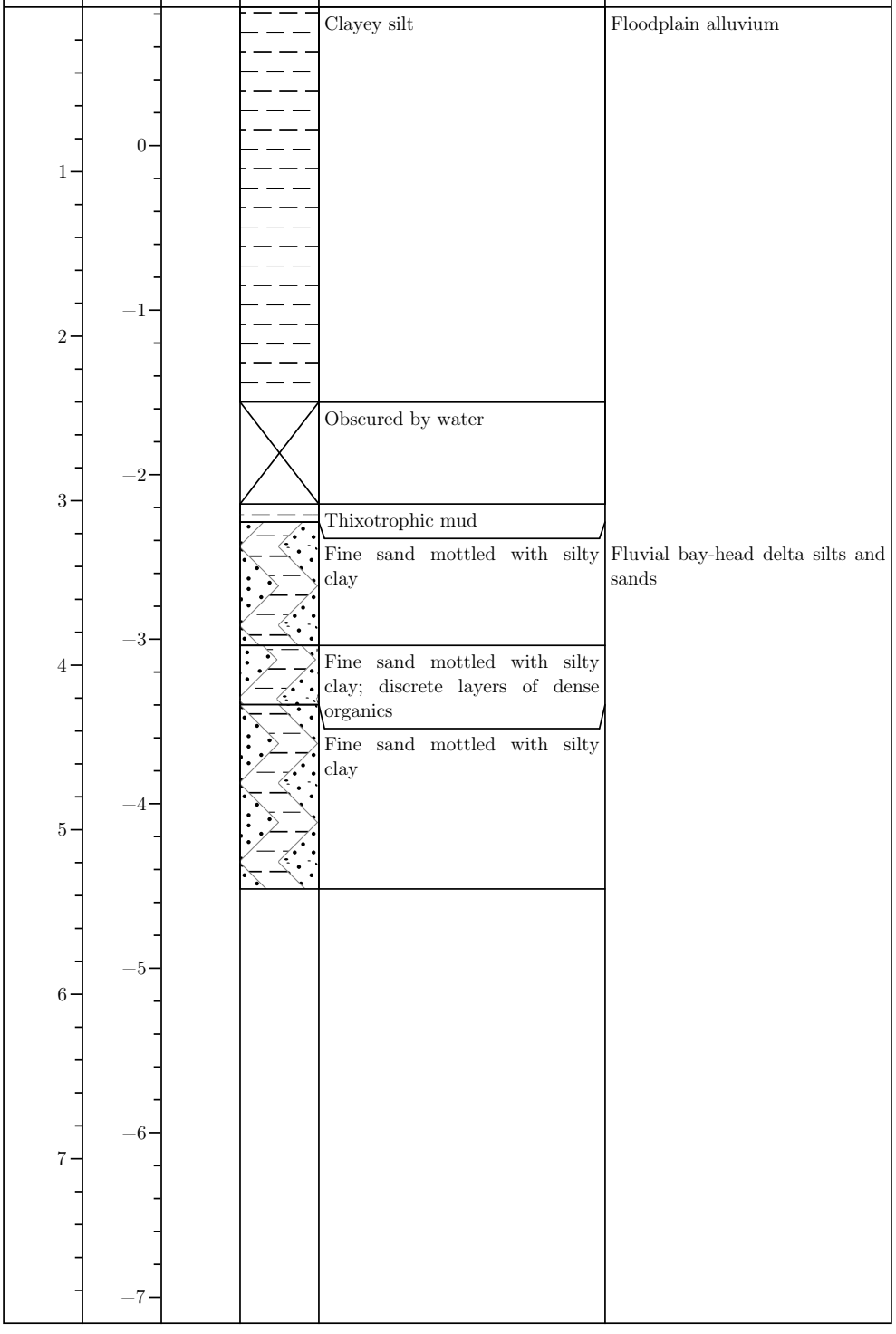

CORE: B
LOCATION: River cutoff, Foxton

NZMG COORDINATES: 2702348.47 E, 6076768.38 N PAGE: 1/2
WVD1953 ELEVATION: −0.7756 m

DEPTH (m)	WVD'53 (m)	PHOTO LOG	VISUAL LOG	COLOUR	CHRONOLOGY	SORTING MEAN GRAIN SIZE
0	−1			5Y5/1		
1	−2			5Y5/1 mottled with 2.5Y3/0		
2	−3			5Y5/1 2.5Y4/0 5Y5/1		
3	−4			Clay: 5Y5/1 Sand: 2.5Y3/0		
4	−5			2.5Y3/0 with bands of 2.5Y4/4		
5	−6					
6	−7					
7	−8					

CORE: B
LOCATION: River cutoff, Foxton

NZMG COORDINATES: 2702348.47 E, 6076768.38 N PAGE: 2/2
WVD1953 ELEVATION: −0.7756 m

DEPTH (m)	WVD'53 (m)	PHOTO LOG	VISUAL LOG	DESCRIPTION	INTERPRETATION
0	−1			Thixotrophic mud	Estuarine sands and silts
				Fine muddy clay	
1	−2			Fine muddy clay with many small (c. 0.25 cm) gastropds	
				Fine muddy clay	
				Fine sand, mottled colour	
				Fine sand with many small (c. 0.25 cm) gastropods	
2	−3			Fine sand, mottled colour	
				Fine muddy clay	
				Fine sand	
				Fine muddy clay	
3	−4			Fine muddy clay interbedded with fine sand	
				Medium sand, some colour banding	
4	−5				
5	−6				
6	−7				
7	−8				

CORE: C
LOCATION: Moutoa

NZMG COORDINATES: 2707389.50 E, 6074377.12 N PAGE: 1/2
WVD1953 ELEVATION: +0.5569 m

DEPTH (m)	WVD'53 (m)	PHOTO LOG	VISUAL LOG	COLOUR	CHRONOLOGY	SORTING MEAN GRAIN SIZE
0 1 2 3 4 5 6 7	0 −1 −2 −3 −4 −5 −6 −7		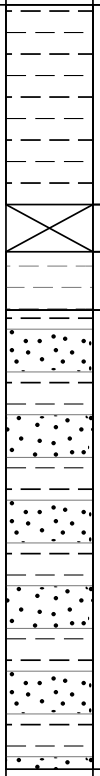	5Y4/1 5Y5/1 Silt: 5Y5/1 Sand: 2.5Y3/0		

CORE: C
LOCATION: Moutoa

NZMG COORDINATES: 2707389.50 E, 6074377.12 N PAGE: 2/2
WVD1953 ELEVATION: +0.5569 m

DEPTH (m)	WVD'53 (m)	PHOTO LOG	VISUAL LOG	DESCRIPTION	INTERPRETATION
1	0			Clayey silt	Floodplain alluvium
				Obscured by water	
	−1			Thixotrophic mud	
2				Fine sand interbedded with clayey silt	Estuarine sands and silts
3	−2				
4	−3				
5	−4				
6	−5				
7	−6				
	−7				

CORE: D
LOCATION: Whirokino Road

NZMG COORDINATES: 2705816.91 E, 6073623.55 N PAGE: 1/2
WVD1953 ELEVATION: +0.5179 m

DEPTH (m)	WVD'53 (m)	PHOTO LOG	VISUAL LOG	COLOUR	CHRONOLOGY	SORTING MEAN GRAIN SIZE
1 2 3 4 5 6 7	0 −1 −2 −3 −4 −5 −6 −7		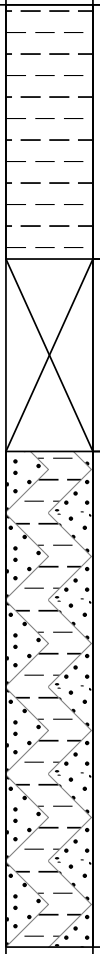	2.5Y3/3 Silt: 5Y5/1 Sand: 2.5Y3/0		

CORE: D
LOCATION: Whirokino Road

NZMG COORDINATES: 2705816.91 E, 6073623.55 N PAGE: 2/2
WVD1953 ELEVATION: +0.5179 m

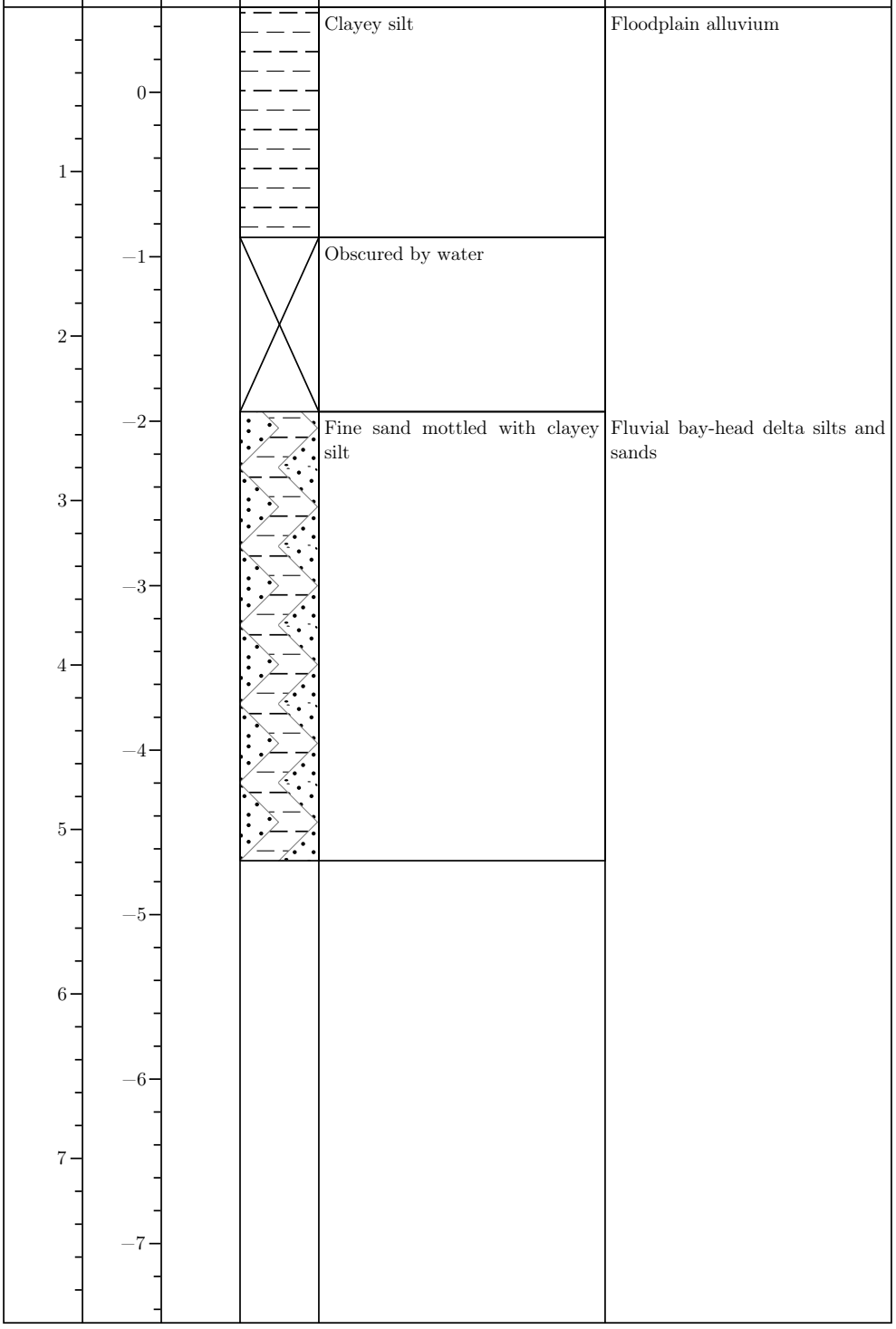

CORE: E2
LOCATION: Kere Kere Road

NZMG COORDINATES: 2708993.06 E, 6072817.43 N PAGE: 1/2
WVD1953 ELEVATION: +2.3984 m

DEPTH (m)	WVD'53 (m)	PHOTO LOG	VISUAL LOG	COLOUR	CHRONOLOGY	SORTING MEAN GRAIN SIZE
				2.5Y4/3		
				5Y5/1		
				5YR2.5/1		
				5Y8/1		
				5YR2.5/1		
				5Y5/1		
				5GY4/1		

CORE: E2
LOCATION: Kere Kere Road

NZMG COORDINATES: 2708993.06 E, 6072817.43 N PAGE: 2/2
WVD1953 ELEVATION: +2.3984 m

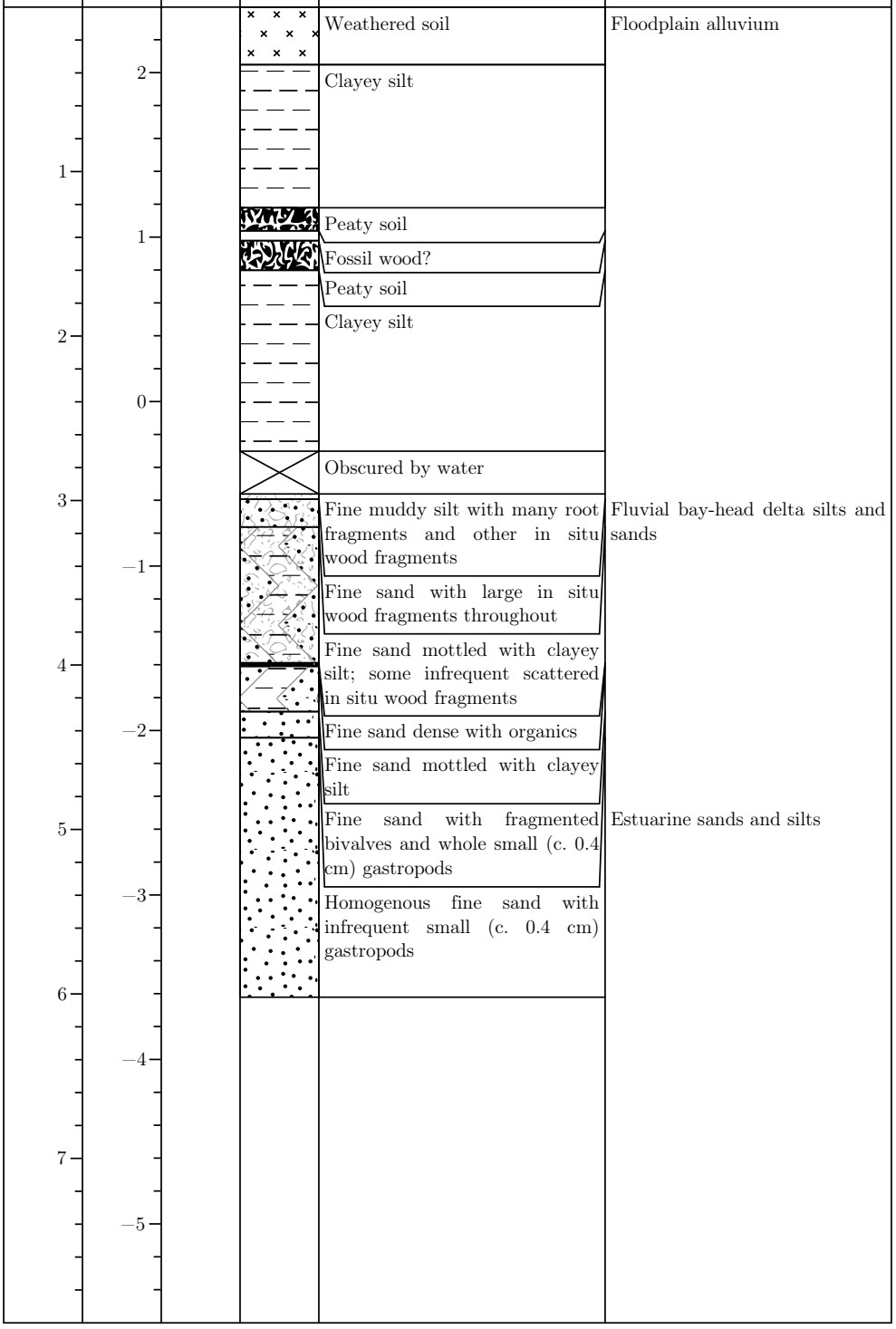

CORE: G
LOCATION: Vickerman Road

NZMG COORDINATES: 2707484.27 E, 6071651.57 N PAGE: 1/2
WVD1953 ELEVATION: +1.9330 m

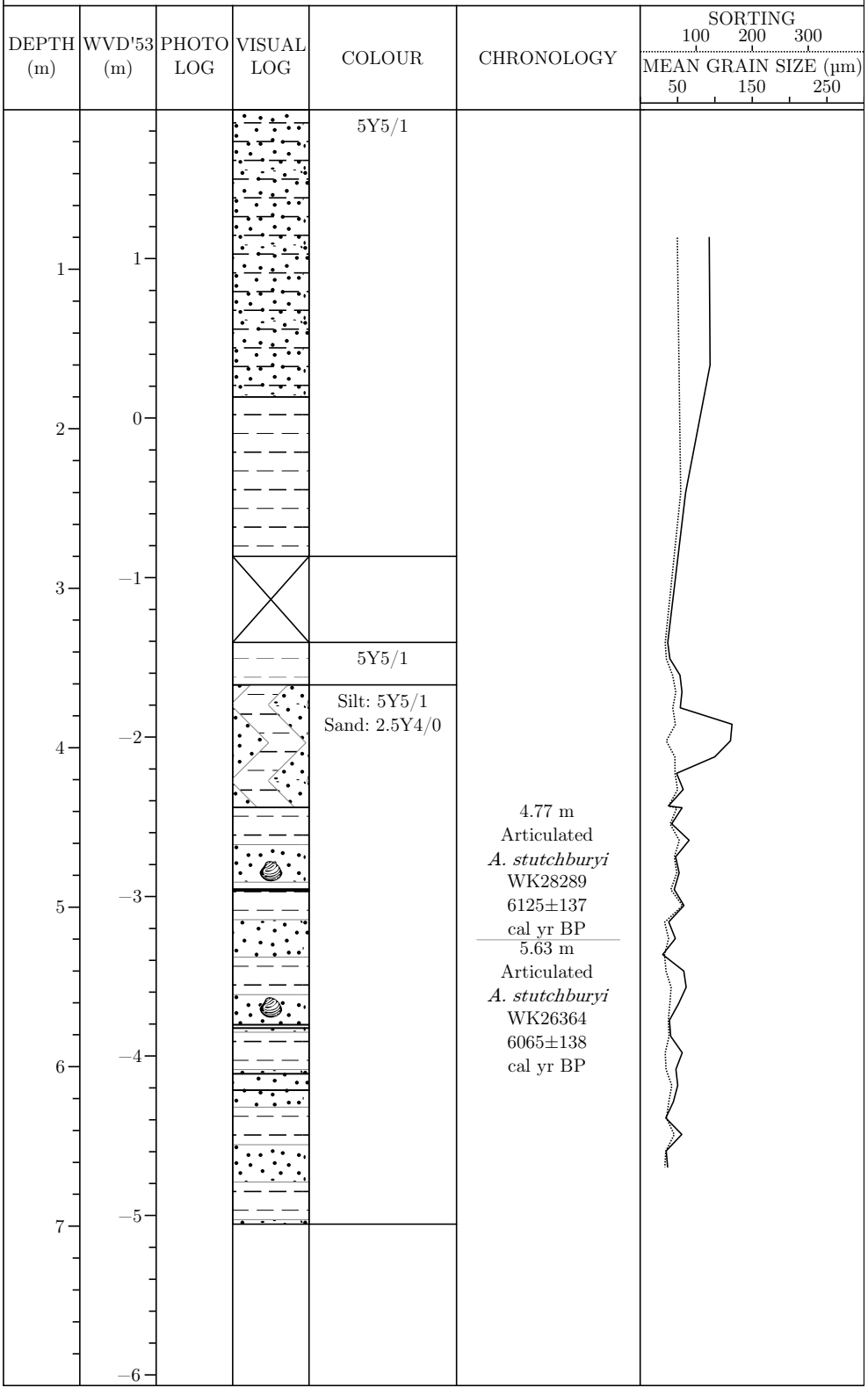

CORE: G
LOCATION: Vickerman Road

NZMG COORDINATES: 2707484.27 E, 6071651.57 N PAGE: 2/2
WVD1953 ELEVATION: +1.9330 m

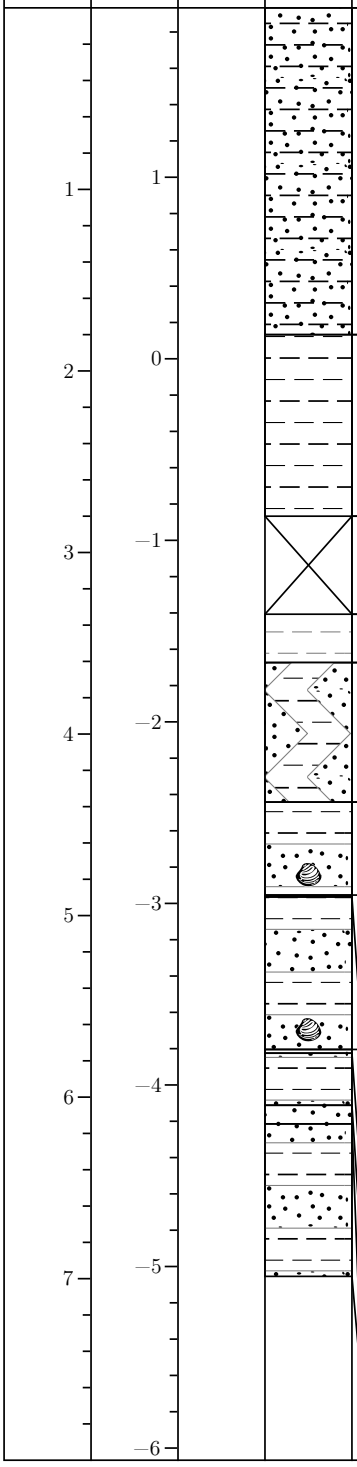

DEPTH (m)	WVD'53 (m)	PHOTO LOG	VISUAL LOG	DESCRIPTION	INTERPRETATION
1	1			Sandy silt	Floodplain alluvium
2	0			Clayey silt	
3	−1			Obscured by water	
				Thixotrophic mud	
4	−2			Fine sand mottled with clayey silt	Fluvial bay-head delta silts and sands
				Calyey silt interbedded with fine sand	Estuarine sands and silts
5	−3			Calyey silt interbedded with fine sand; six disarticulated valves, one articulated bivalve	
				Calyey silt interbedded with fine sand	
6	−4			Clayey silt interbedded with fine sand; six disarticulated valves, one articulated bivalve	
				Calyey silt interbedded with fine sand	
7	−5			Clayey silt interbedded with fine sand; four disarticulated valves	
				Clayey silt interbedded with fine sand	
	−6				

CORE: Flood-2
LOCATION: Moutoa Floodway

NZMG COORDINATES: 2704279.81 E, 6074840.78 N PAGE: 1/2
WVD1953 ELEVATION: +0.3734 m

DEPTH (m)	WVD'53 (m)	PHOTO LOG	VISUAL LOG	COLOUR	CHRONOLOGY	SORTING MEAN GRAIN SIZE
0	0					
1	−1			5Y5/1 Sand: 5GY5/1 Silt: 5Y5/1 5Y4/1 Sand: 2.5Y4/0 Clay: 5Y4/1		
2	−2					
3	−3					
4	−4					
5	−5					
6	−6					
7	−7					

CORE: Flood-2
LOCATION: Moutoa Floodway

NZMG COORDINATES: 2704279.81 E, 6074840.78 N PAGE: 2/2
WVD1953 ELEVATION: +0.3734 m

DEPTH (m)	WVD'53 (m)	PHOTO LOG	VISUAL LOG	DESCRIPTION	INTERPRETATION
0	0			Obscured by water	Fluvial bay-head delta silts and sands
				Thixotrophic mud	
1	−1			Fine sand mottled with clayey silt; frequent woody fragments throughout	
				Clayey silt	
2	−2		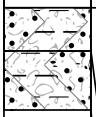	Medium sand mottled with clayey silt; some in situ wood fragments	
				Clayey silt mottled with medium sand; some insitu wood fragments	
3	−3				
4	−4				
5	−5				
6	−6				
7	−7				

CORE: Flood-3
LOCATION: Moutoa Floodway

NZMG COORDINATES: 2704993.36 E, 6074502.04 N PAGE: 1/2
WVD1953 ELEVATION: +0.5871 m

DEPTH (m)	WVD'53 (m)	PHOTO LOG	VISUAL LOG	COLOUR	CHRONOLOGY	SORTING MEAN GRAIN SIZE
1 2 3 4 5 6 7	0 −1 −2 −3 −4 −5 −6 −7		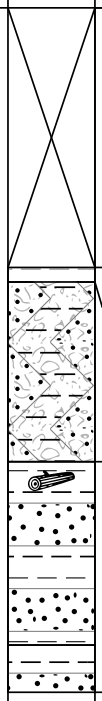	2.5Y4/3 Sand: N4/ Clayey silt: 5Y5/1 Sand: N4/ Clayey silt: 5Y6/1		

CORE: Flood-3 NZMG COORDINATES: 2704993.36 E, 6074502.04 N PAGE: 2/2
LOCATION: Moutoa Floodway WVD1953 ELEVATION: +0.5871 m

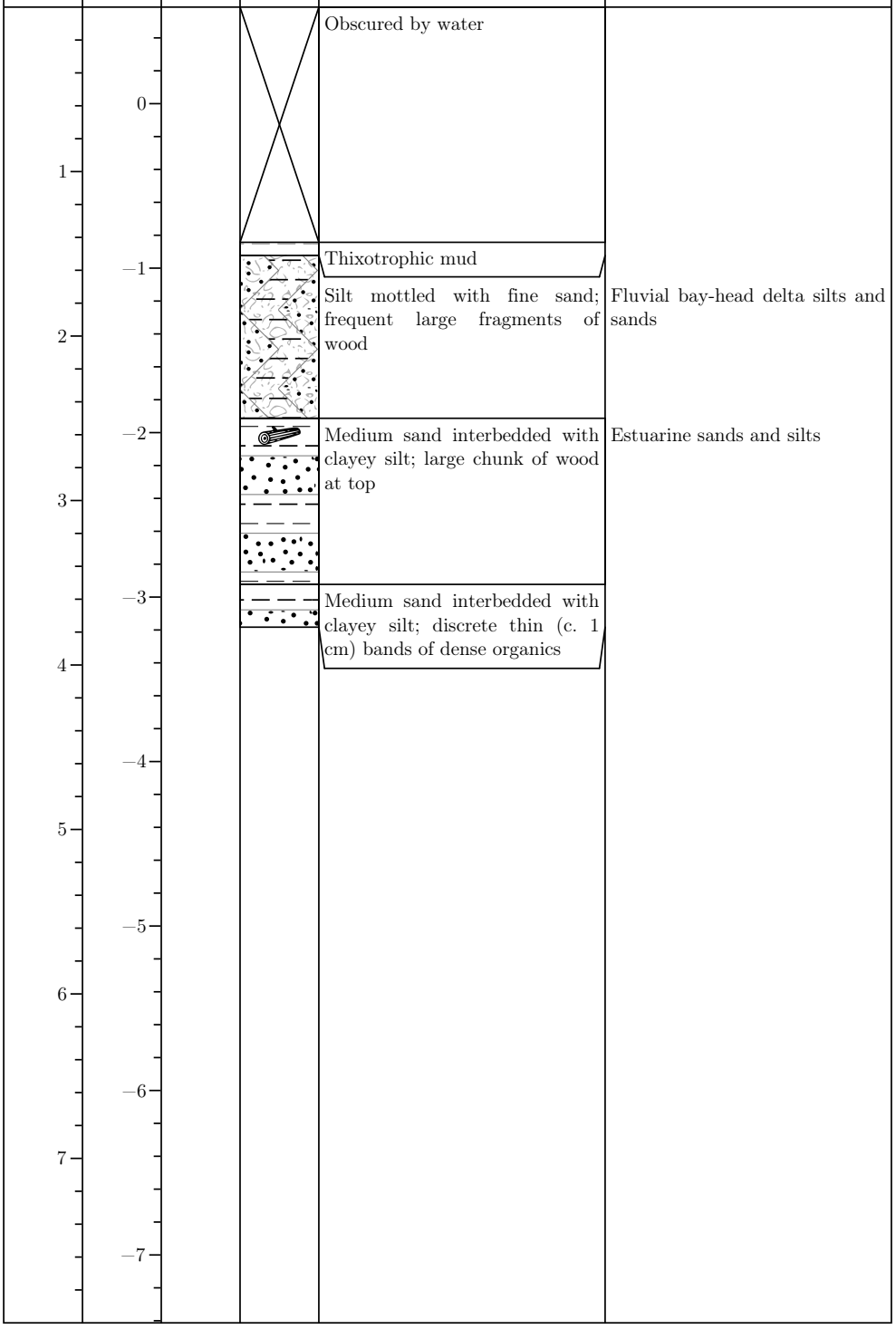

CORE: Flood-4
LOCATION: Moutoa Floodway

NZMG COORDINATES: 2706177.07 E, 6074528.29 N PAGE: 1/2
WVD1953 ELEVATION: +0.7055 m

DEPTH (m)	WVD'53 (m)	PHOTO LOG	VISUAL LOG	COLOUR	CHRONOLOGY	SORTING MEAN GRAIN SIZE
				5Y5/1		
				Sand: N4/ Silt: 5Y5/1		
				N4/		
				10YR2/1		
				Sand: N4/ Silt: 5Y5/1		
				N4/		
				Sand: N4/ Silt: 5Y5/1		

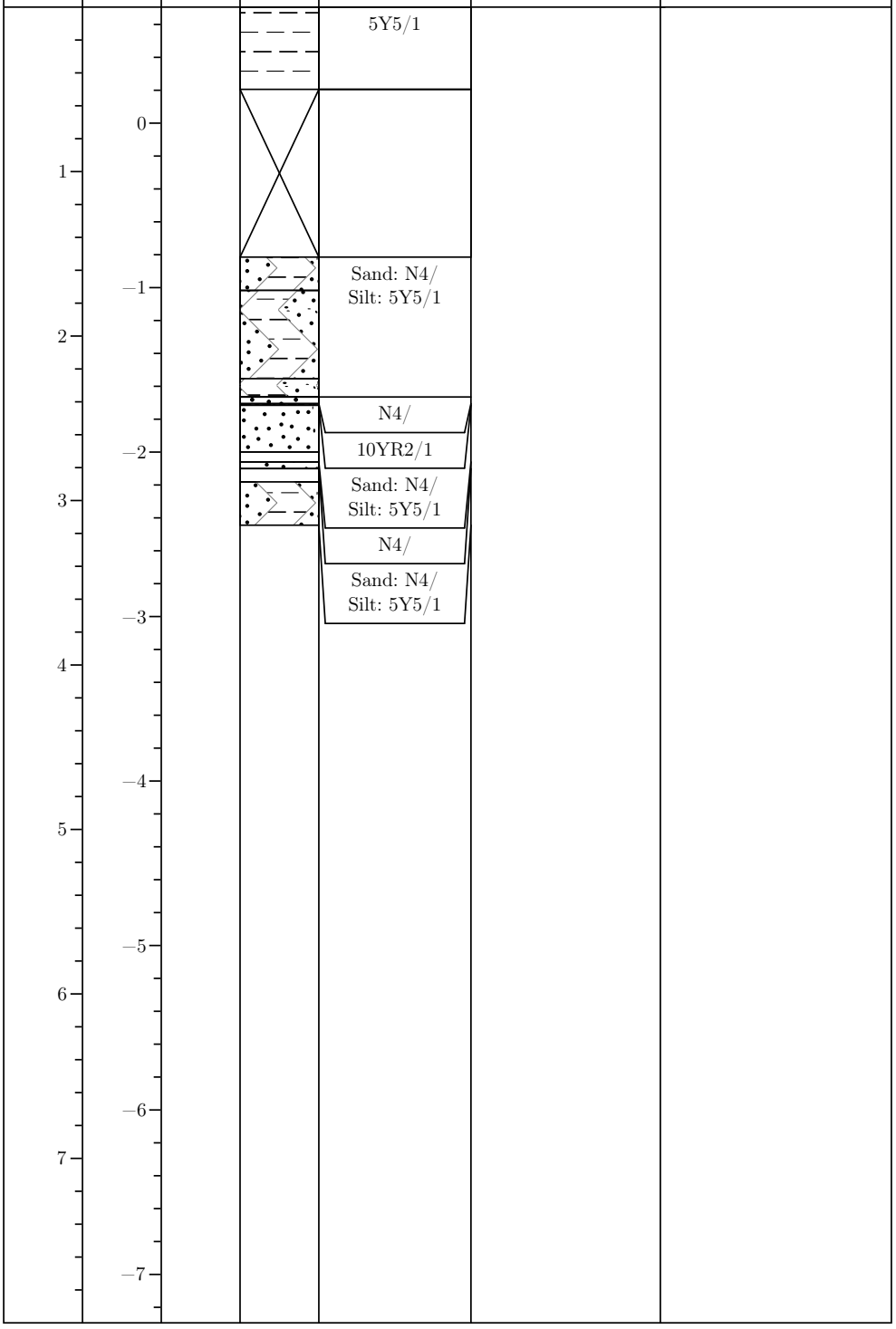

CORE: Flood-4
LOCATION: Moutoa Floodway

NZMG COORDINATES: 2706177.07 E, 6074528.29 N PAGE: 2/2
WVD1953 ELEVATION: +0.7055 m

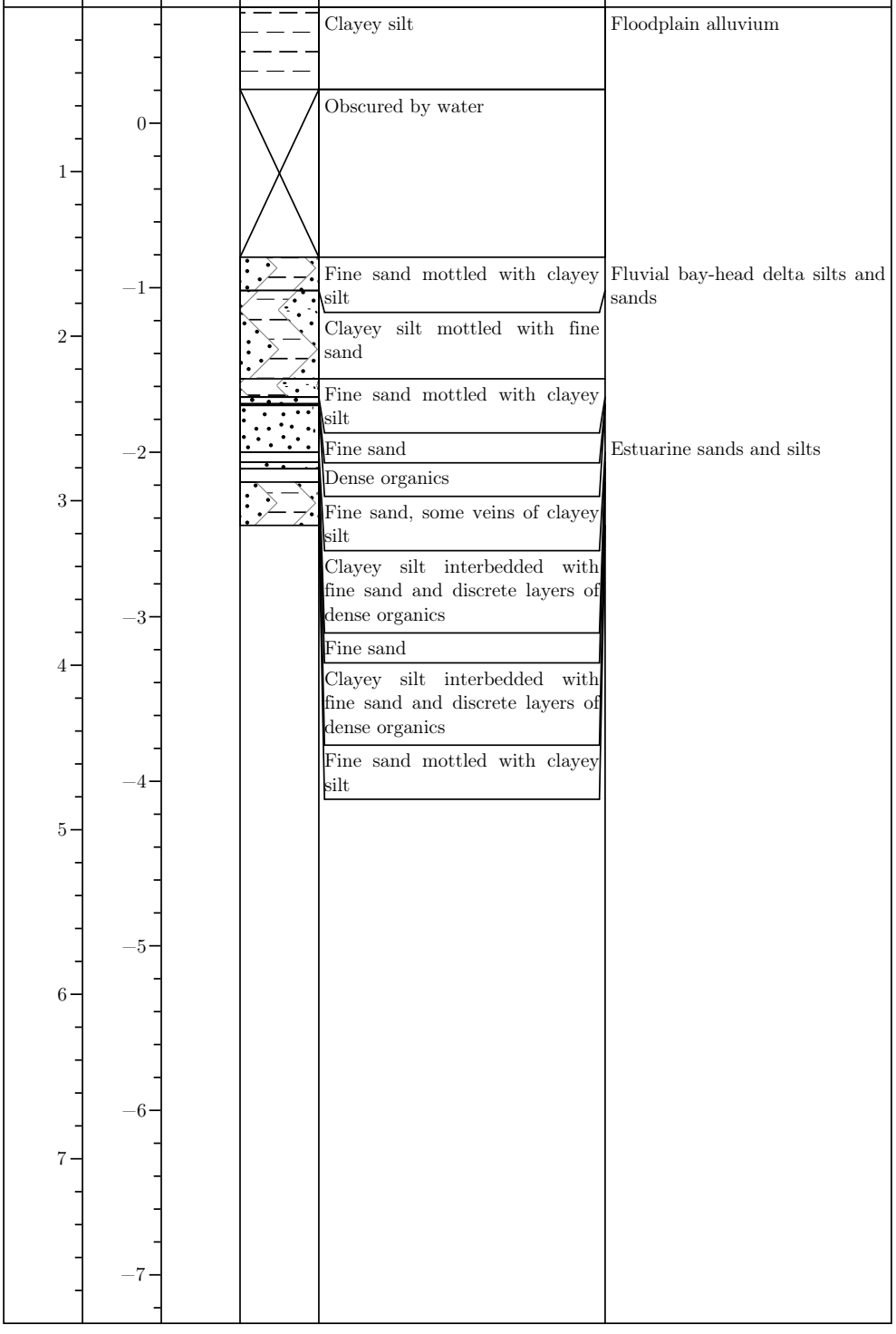

CORE: Flood-5
LOCATION: Moutoa Floodway

NZMG COORDINATES: 2710612.68 E, 6076179.47 N PAGE: 1/2
WVD1953 ELEVATION: +3.6880 m

DEPTH (m)	WVD'53 (m)	PHOTO LOG	VISUAL LOG	COLOUR	CHRONOLOGY	SORTING MEAN GRAIN SIZE
1 2 3 4 5 6 7	3 2 1 0 −1 −2 −3 −4			2.5Y4/3 Sand: 2.5Y3/0 Silt: 5Y5/1 10YR3/2 grading to 5Y5/1 2.5Y4/0 10YR2/1 5Y4/1		

CORE: Flood-5 NZMG COORDINATES: 2710612.68 E, 6076179.47 N PAGE: 2/2
LOCATION: Moutoa Floodway WVD1953 ELEVATION: +3.6880 m

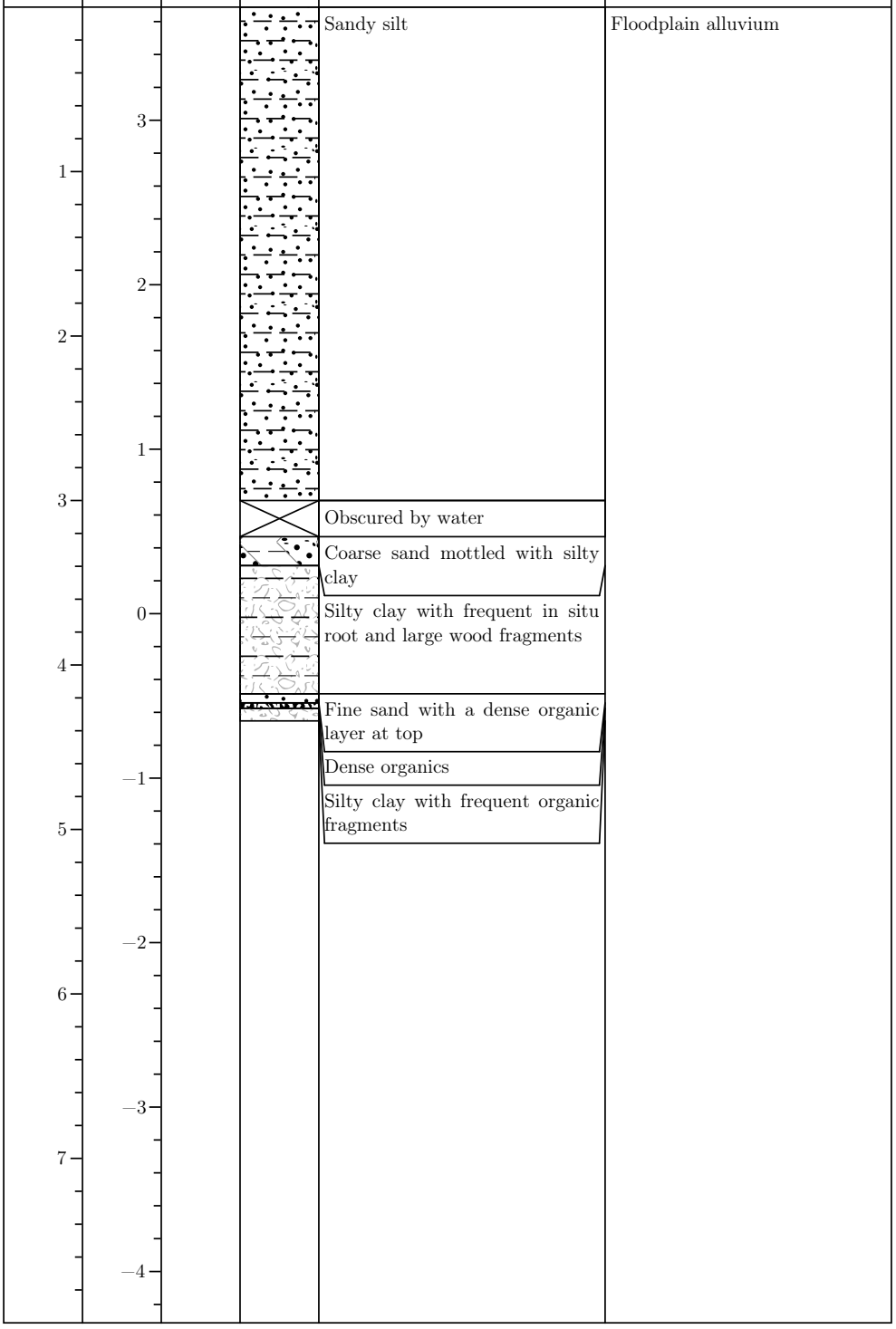

CORE: Flood-6 NZMG COORDINATES: 2710235.42 E, 6075304.56 N PAGE: 1/2
LOCATION: Moutoa Floodway WVD1953 ELEVATION: +2.4091 m

DEPTH (m)	WVD'53 (m)	PHOTO LOG	VISUAL LOG	COLOUR	CHRONOLOGY	SORTING MEAN GRAIN SIZE
				2.5Y4/3		
				5Y5/1		
				2.5Y4/0		

CORE: Flood-6 NZMG COORDINATES: 2710235.42 E, 6075304.56 N PAGE: 2/2
LOCATION: Moutoa Floodway WVD1953 ELEVATION: +2.4091 m

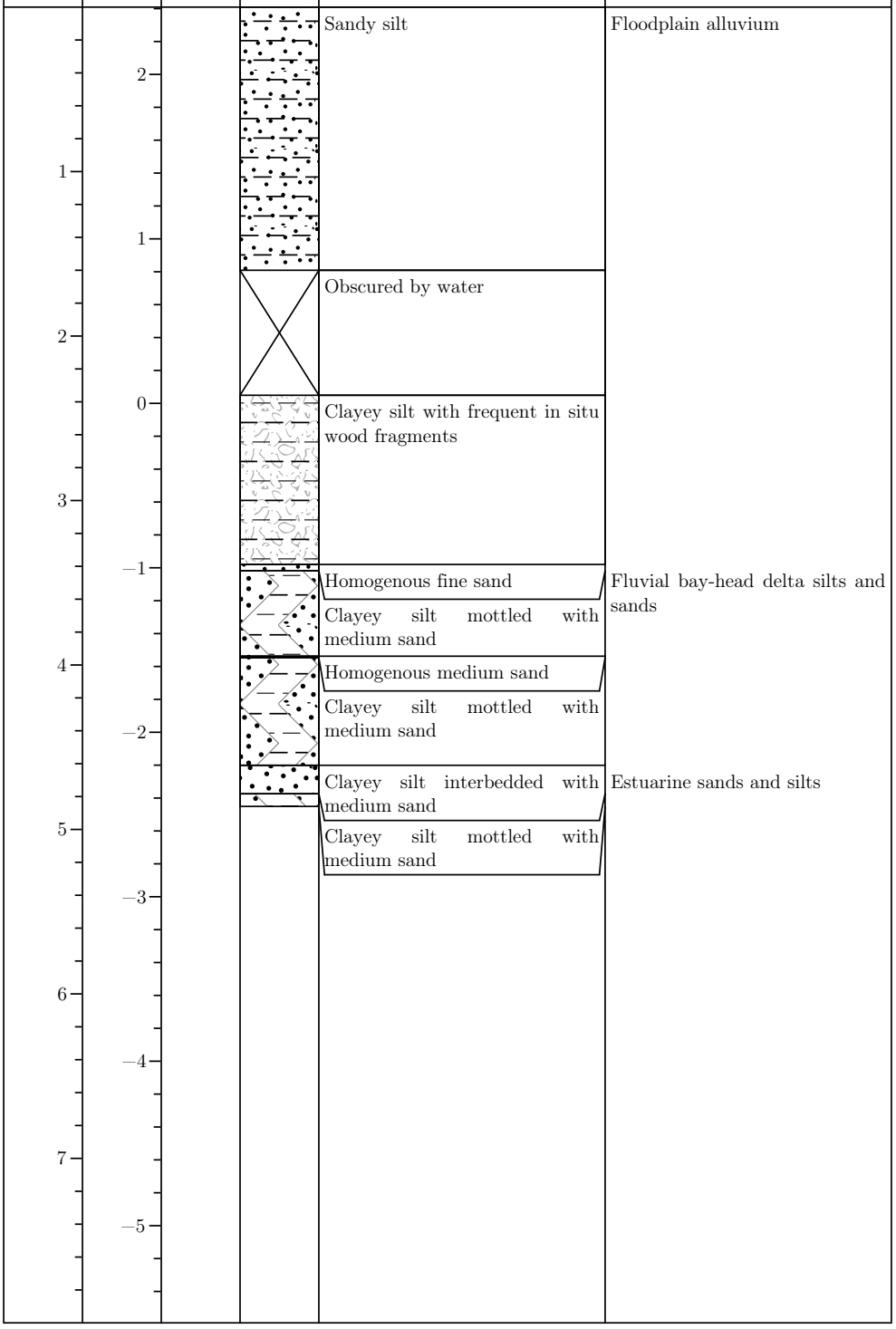

CORE: Flood-7
LOCATION: Moutoa Floodway

NZMG COORDINATES: 2707710.61 E, 6074758.29 N PAGE: 1/2
WVD1953 ELEVATION: +1.2281 m

DEPTH (m)	WVD'53 (m)	PHOTO LOG	VISUAL LOG	COLOUR	CHRONOLOGY	SORTING MEAN GRAIN SIZE
1	1			2.5Y4/3		
	0					
2	−1			5Y5/1		
				Sand: 2.5Y4/0 Silt: 5Y5/1		
3	−2			5Y5/1 2.5Y4/0 5Y5/1		
4	−3			Sand: 2.5Y4/0 Silt: 5Y5/1		
5	−4					
6	−5					
7	−6					

CORE: Flood-7
LOCATION: Moutoa Floodway

NZMG COORDINATES: 2707710.61 E, 6074758.29 N PAGE: 2/2
WVD1953 ELEVATION: +1.2281 m

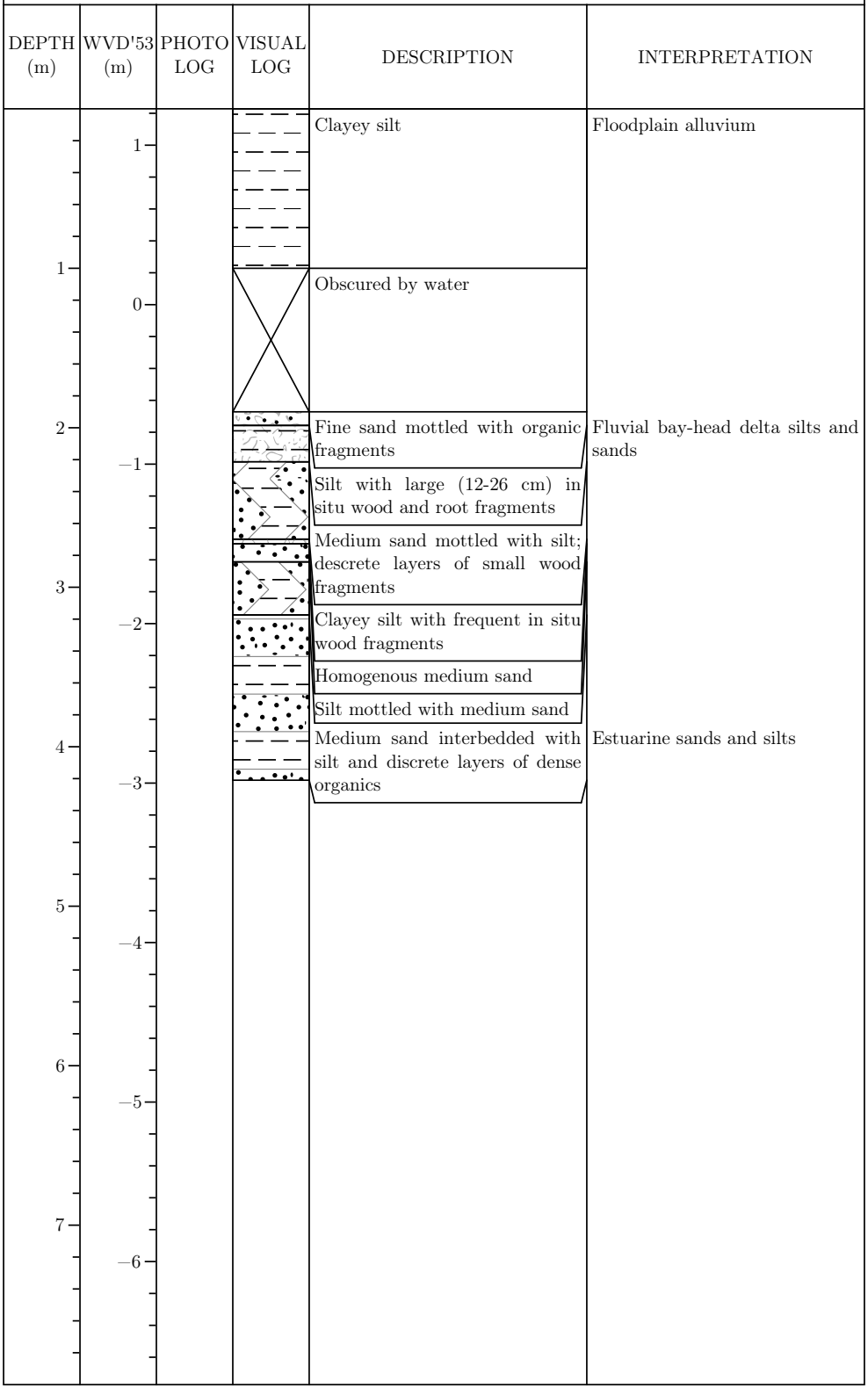

CORE: Flood-8
LOCATION: Moutoa Floodway

NZMG COORDINATES: 2709415.93 E, 6074933.90 N PAGE: 1/2
WVD1953 ELEVATION: +1.6833 m

DEPTH (m)	WVD'53 (m)	PHOTO LOG	VISUAL LOG	COLOUR	CHRONOLOGY	SORTING MEAN GRAIN SIZE
1 2 3 4 5 6 7	1 0 −1 −2 −3 −4 −5 −6			5Y5/1 Sand: N4/ Clayey silt: 5Y5/1 5Y5/1 Sand: N4/ Silt: 5Y5/1 Sand: N4/ Clayey silt: 5Y5/1 Sand: 2.5Y3/0 Clayey silt: 5Y5/1		

CORE: Flood-8
LOCATION: Moutoa Floodway

NZMG COORDINATES: 2709415.93 E, 6074933.90 N PAGE: 2/2
WVD1953 ELEVATION: +1.6833 m

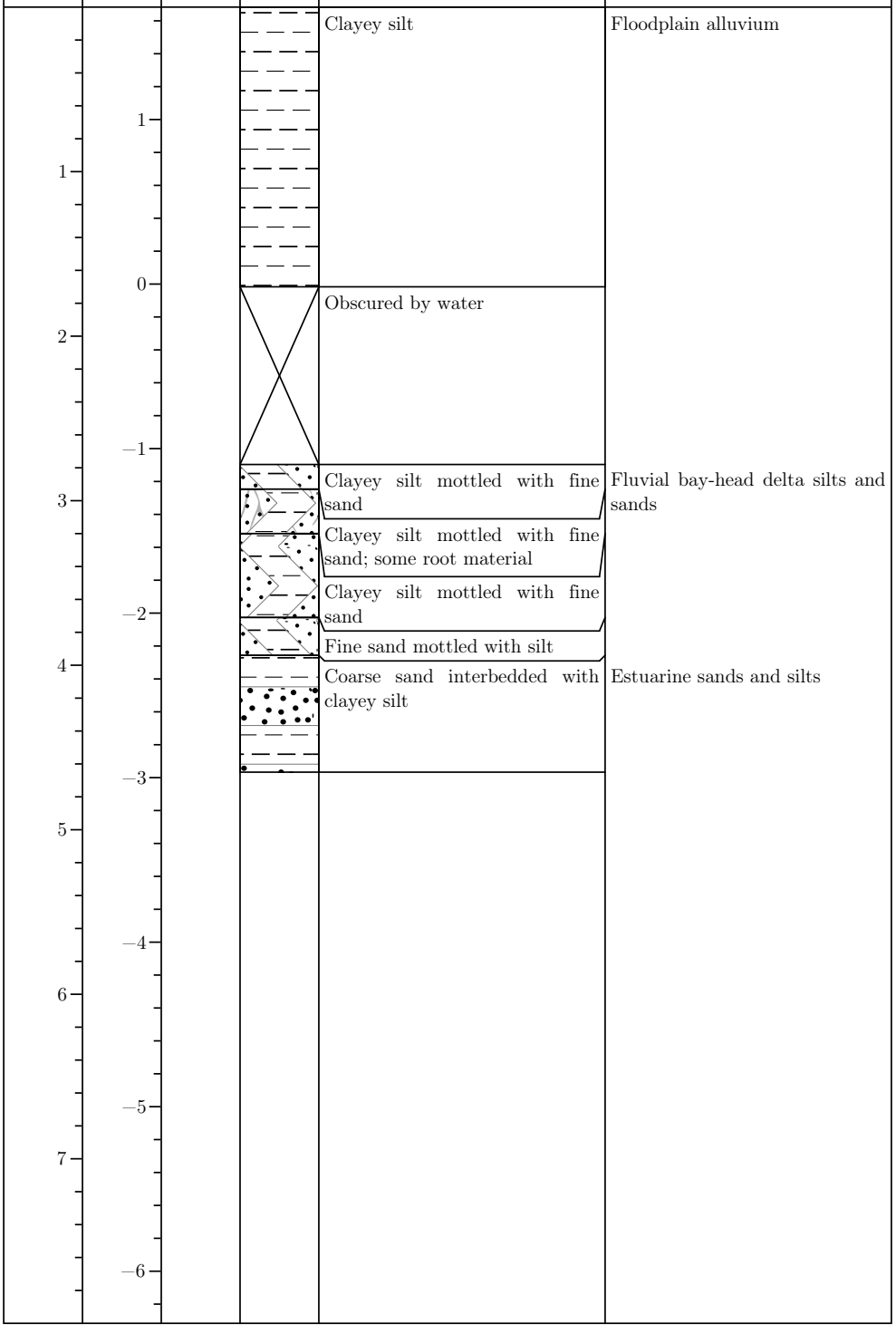

CORE: Flood-9
LOCATION: Kere Kere Road

NZMG COORDINATES: 2709389.05 E, 6074531.54 N PAGE: 1/2
WVD1953 ELEVATION: +0.7533 m

DEPTH (m)	WVD'53 (m)	PHOTO LOG	VISUAL LOG	COLOUR	CHRONOLOGY	SORTING MEAN GRAIN SIZE
				2.5Y4/3		
				5Y5/1		
1	0					
	−1			5Y5/1		
2						
				Sand: N4/ Silt: 5Y5/1		
3	−2					
	−3					
4						
	−4					
5						
	−5					
6						
	−6					
7						
	−7					

CORE: Flood-9
LOCATION: Kere Kere Road

NZMG COORDINATES: 2709389.05 E, 6074531.54 N PAGE: 2/2
WVD1953 ELEVATION: +0.7533 m

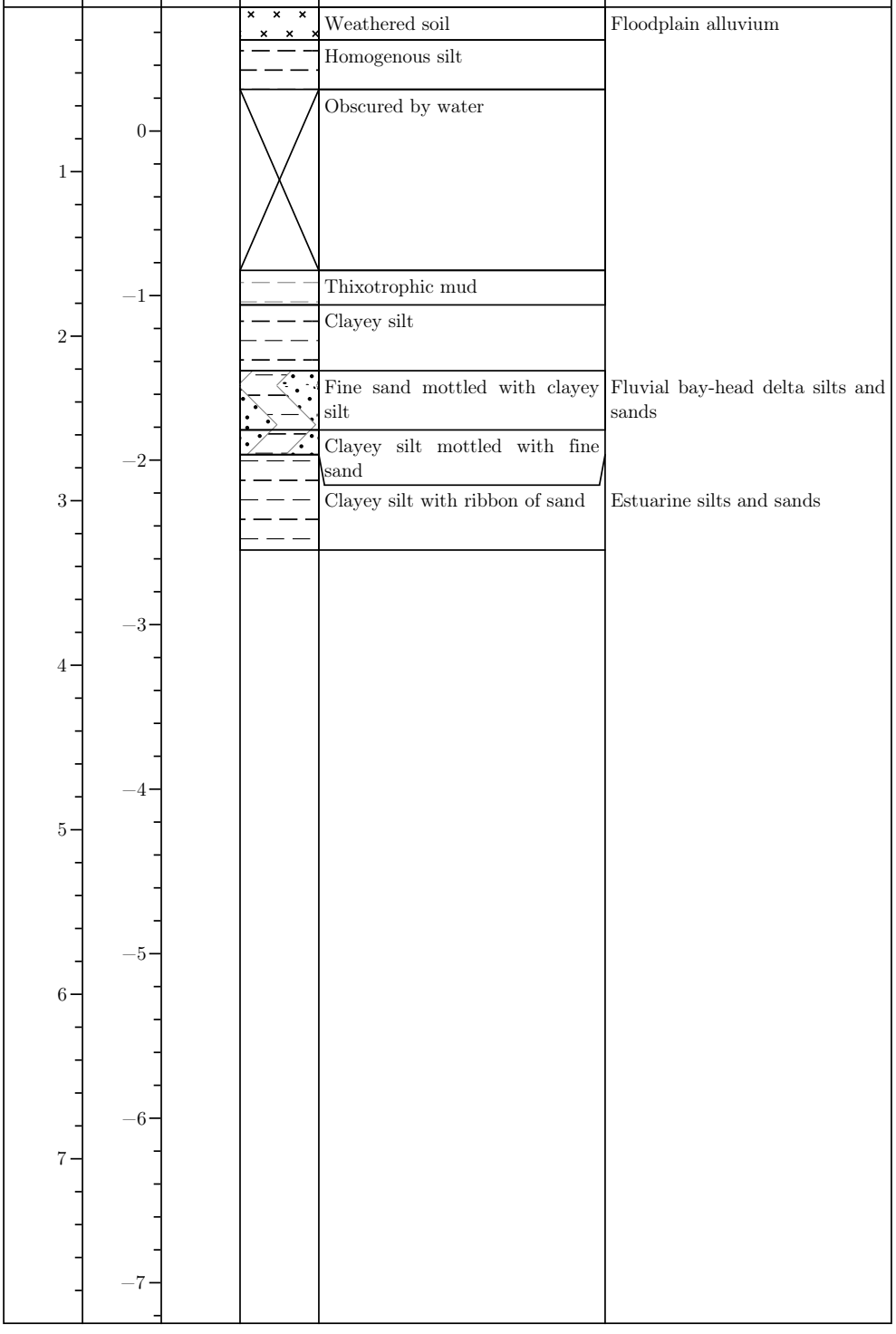

CORE: Cook-1
LOCATION: Cook's Drain

NZMG COORDINATES: 2710556.42 E, 6073587.00 N PAGE: 1/2
WVD1953 ELEVATION: +1.7157 m

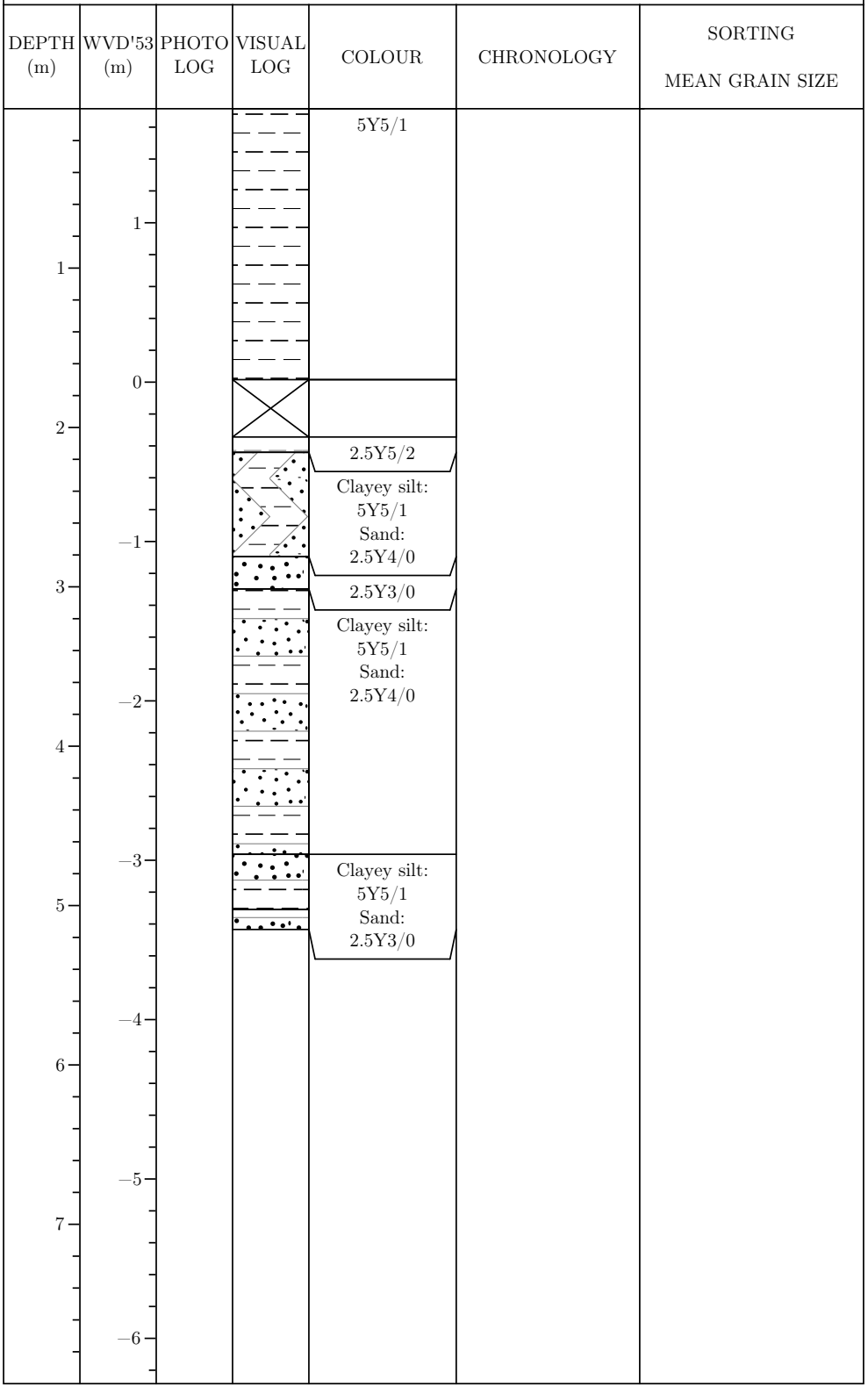

CORE: Cook-1
LOCATION: Cook's Drain

NZMG COORDINATES: 2710556.42 E, 6073587.00 N PAGE: 2/2
WVD1953 ELEVATION: +1.7157 m

DEPTH (m)	WVD'53 (m)	PHOTO LOG	VISUAL LOG	DESCRIPTION	INTERPRETATION
1	1			Clayey silt	Floodplain alluvium
1	0			Obscured by water	
2				Thixotrophic mud	
				Clayey silt mottled with fine sand	Fluvial bay-head delta silts and sands
	−1			Homogenous medium sand	Estuarine sands and silts
3				Clayey silt interbedded with fine sand	
4	−2				
5	−3			Clayey silt interbedded with medium sand	
				Clayey silt interbedded with medium sand; infrequent shell fragments	
6	−4				
7	−5				
	−6				

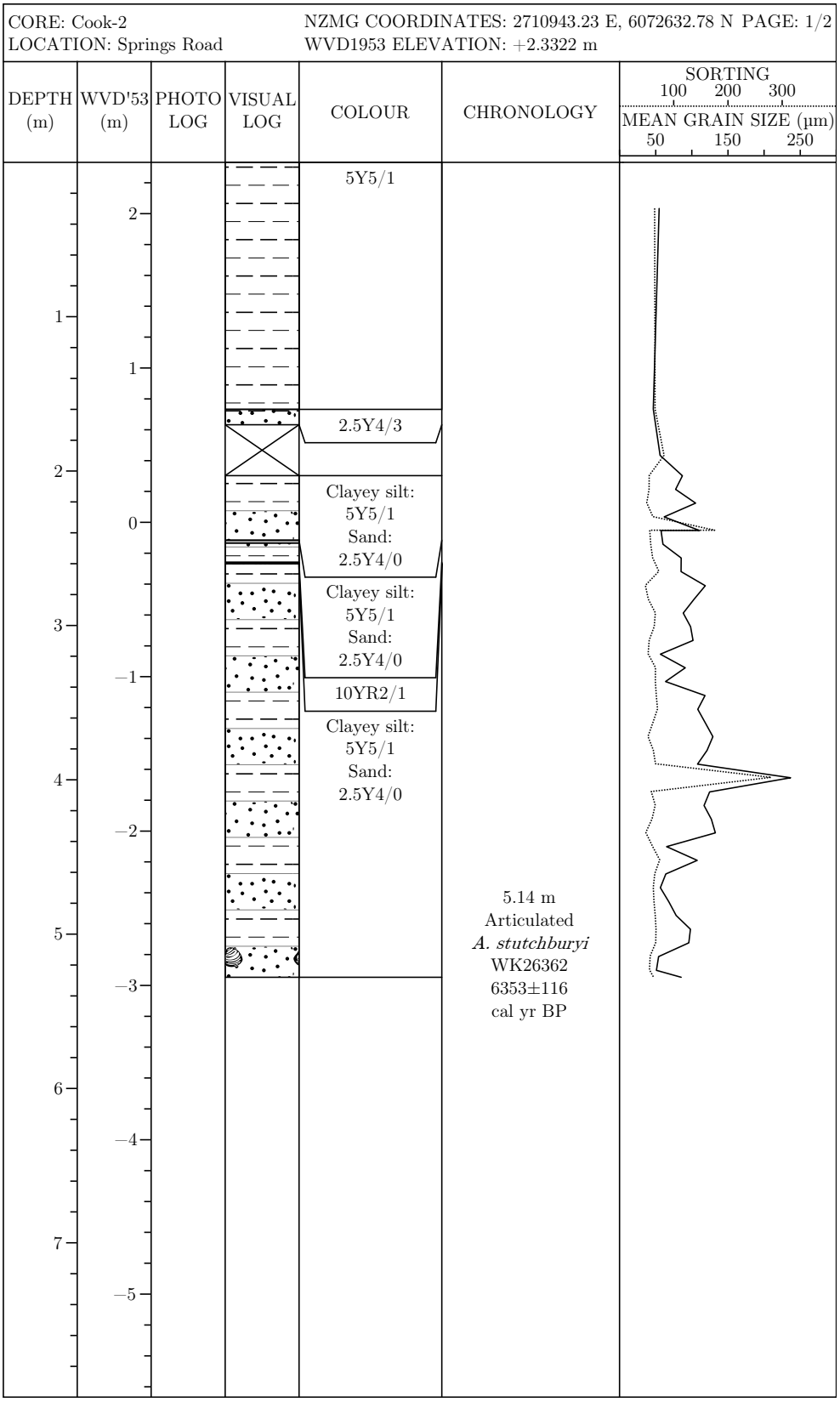
CORE: Cook-2
LOCATION: Springs Road
NZMG COORDINATES: 2710943.23 E, 6072632.78 N PAGE: 1/2
WVD1953 ELEVATION: +2.3322 m
DEPTH (m)
WVD'53 (m)
PHOTO LOG
VISUAL LOG
COLOUR
CHRONOLOGY
SORTING
100 200 300
MEAN GRAIN SIZE (µm)
50 150 250
5Y5/1
2.5Y4/3
Clayey silt:
5Y5/1
Sand:
2.5Y4/0
Clayey silt:
5Y5/1
Sand:
2.5Y4/0
10YR2/1
Clayey silt:
5Y5/1
Sand:
2.5Y4/0
5.14 m
Articulated
A. stutchburyi
WK26362
6353±116
cal yr BP

CORE: Cook-2
LOCATION: Springs Road

NZMG COORDINATES: 2710943.23 E, 6072632.78 N PAGE: 2/2
WVD1953 ELEVATION: +2.3322 m

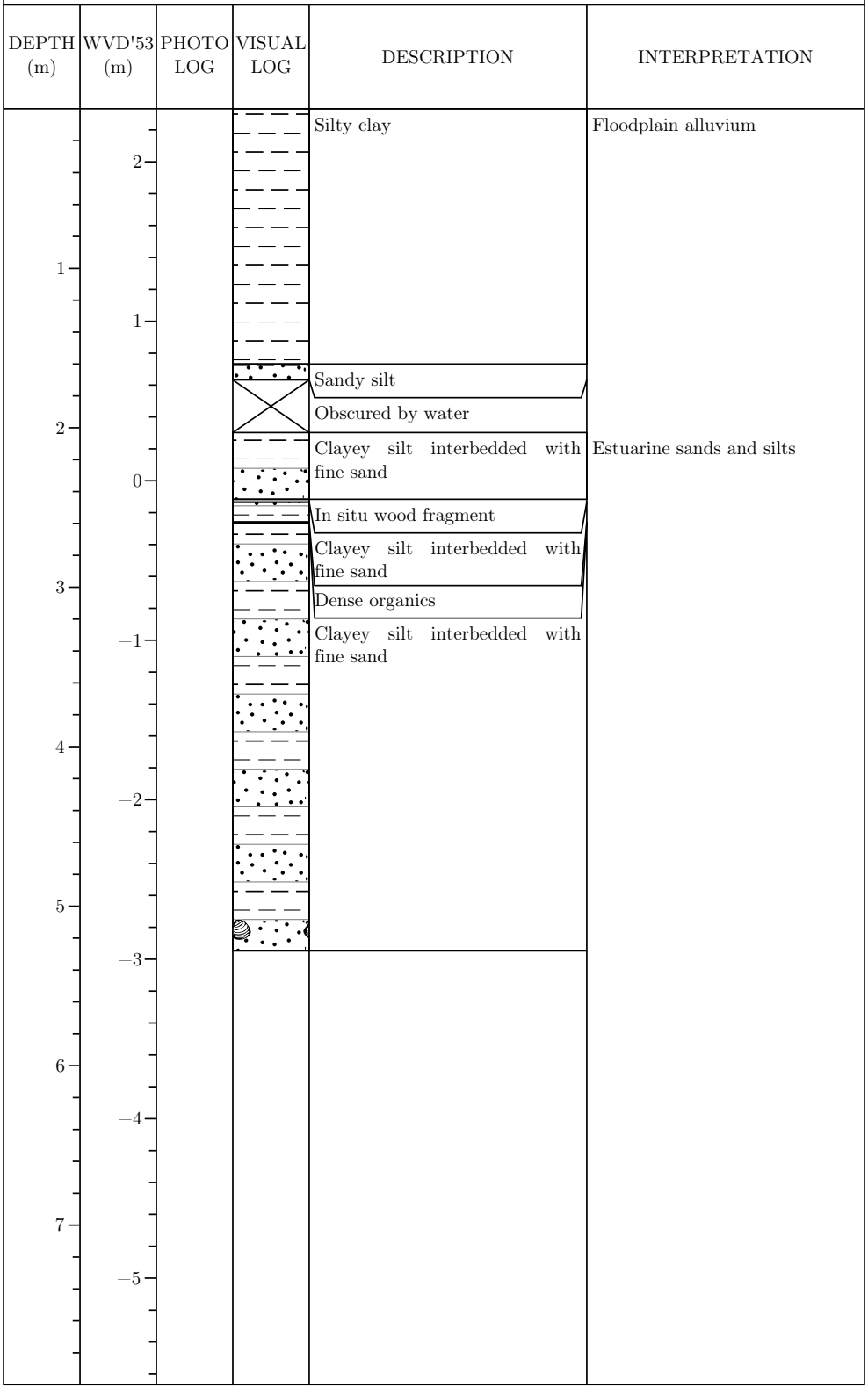

CORE: Cook-3
LOCATION: Carter Road

NZMG COORDINATES: 2712269.14 E, 6074768.75 N PAGE: 1/2
WVD1953 ELEVATION: +2.0665 m

DEPTH (m)	WVD'53 (m)	PHOTO LOG	VISUAL LOG	COLOUR	CHRONOLOGY	SORTING MEAN GRAIN SIZE
1 2 3 4 5 6 7	2 1 0 −1 −2 −3 −4 −5		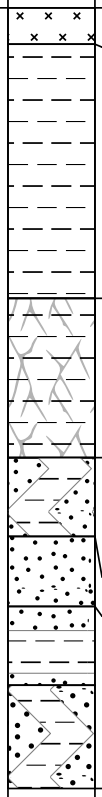	2.5Y4/3 5Y5/1 5GY5/1 grading to 5Y5/1 Clayey silt: 5Y5/1 Sand: 2.5Y4/0 2.5Y4/0 Sand: 2.5Y4/0 Clayey silt: 5Y5/1		

CORE: Cook-3
LOCATION: Carter Road

NZMG COORDINATES: 2712269.14 E, 6074768.75 N PAGE: 2/2
WVD1953 ELEVATION: +2.0665 m

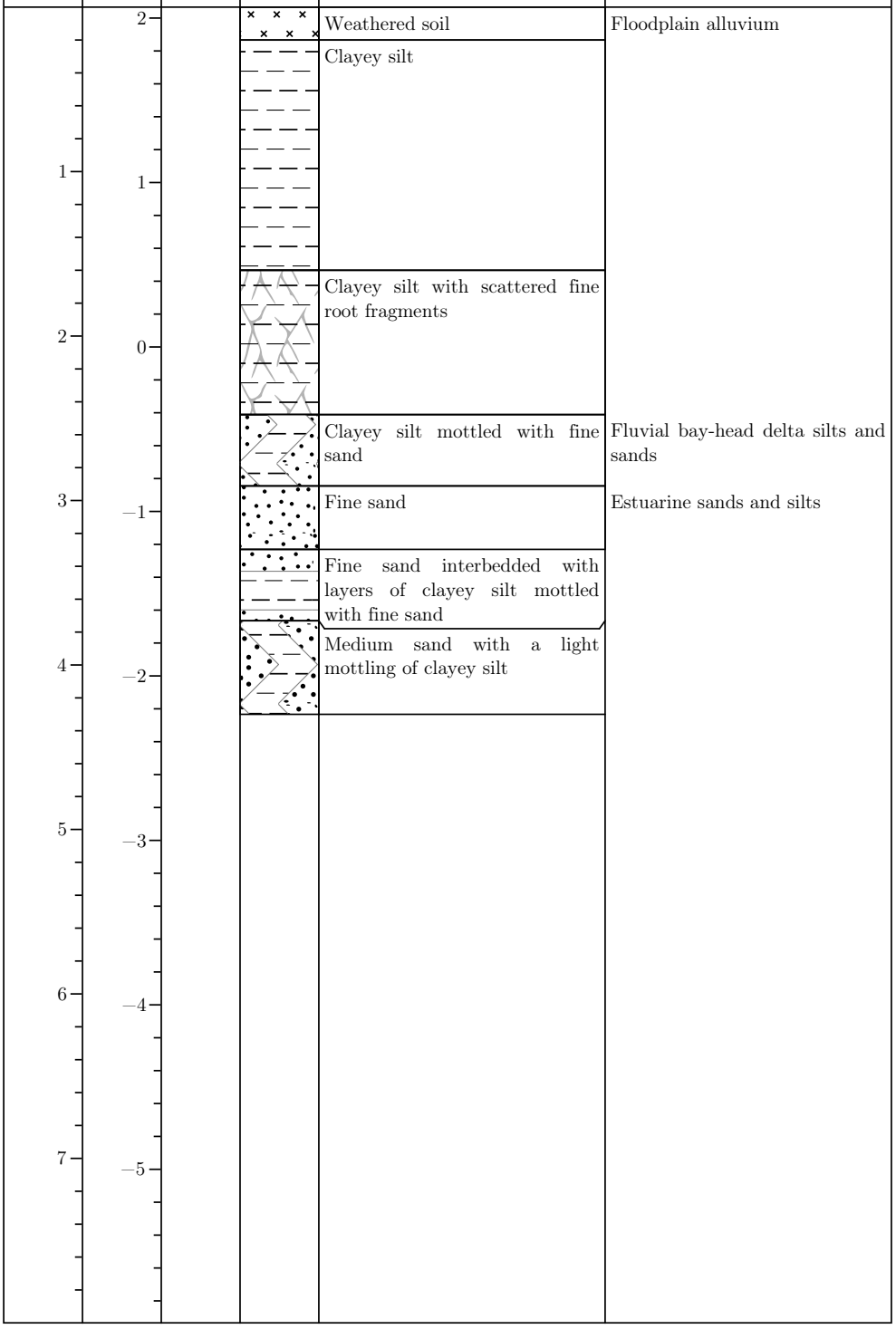

CORE: Cook-4
LOCATION: Moutoa

NZMG COORDINATES: 2711184.81 E, 6074302.03 N PAGE: 1/2
WVD1953 ELEVATION: +1.1503 m

DEPTH (m)	WVD'53 (m)	PHOTO LOG	VISUAL LOG	COLOUR	CHRONOLOGY	SORTING MEAN GRAIN SIZE
1 2 3 4 5 6 7	1 0 −1 −2 −3 −4 −5 −6		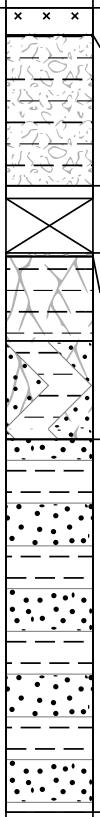	2.5Y4/3 10YR5.2 grading to 10YR3/2 5GBG5/1 10YR3/3 5Y5/1 Silt: 5Y5/1 Sand: N4/		

CORE: Cook-4
LOCATION: Moutoa

NZMG COORDINATES: 2711184.81 E, 6074302.03 N PAGE: 2/2
WVD1953 ELEVATION: +1.1503 m

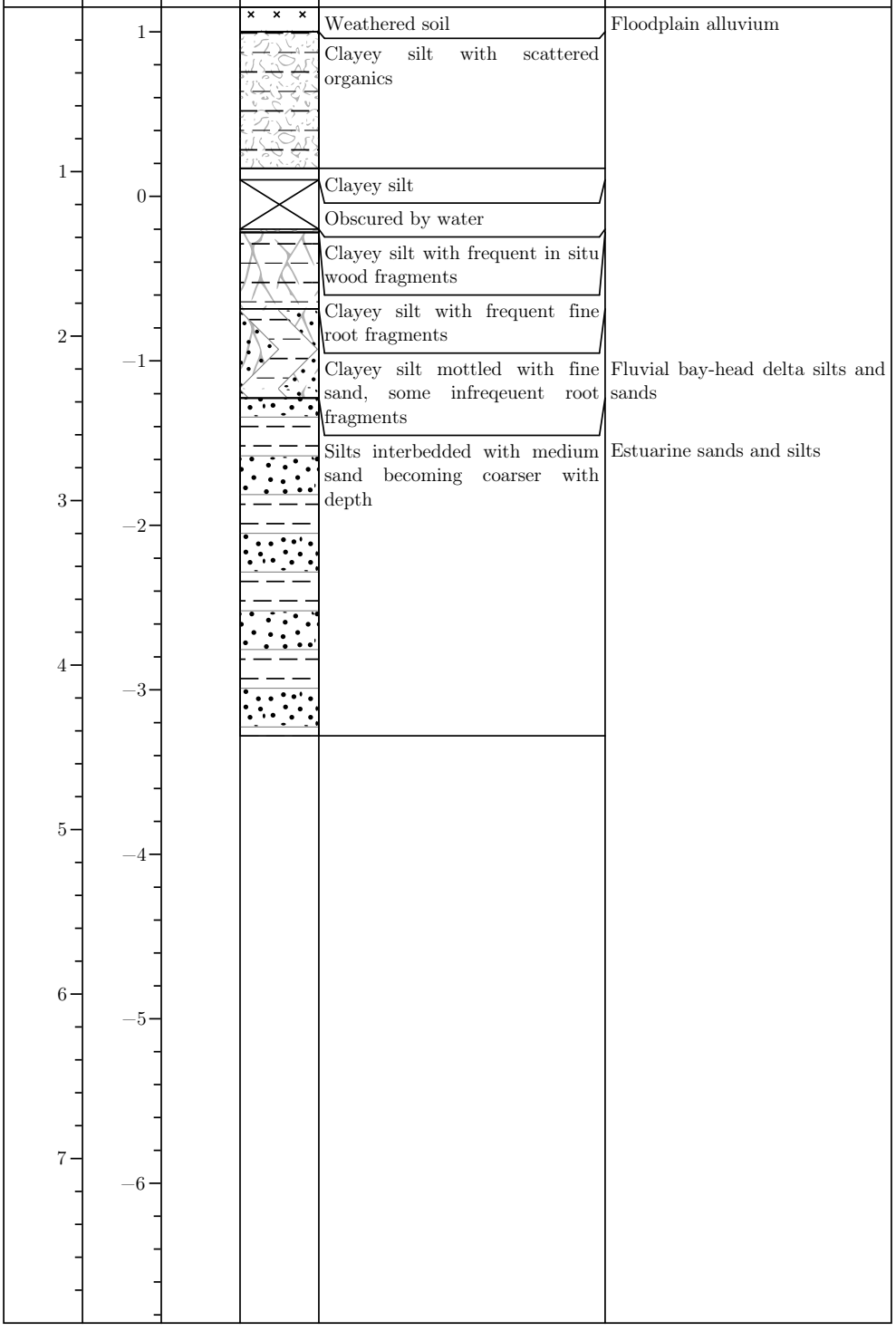

CORE: Core-5
LOCATION: Springs Road

NZMG COORDINATES: 2712167.90 E, 6073302.48 N PAGE: 1/2
WVD1953 ELEVATION: +2.5523 m

DEPTH (m)	WVD'53 (m)	PHOTO LOG	VISUAL LOG	COLOUR	CHRONOLOGY	SORTING MEAN GRAIN SIZE
				10YR4/1		
				5Y5/1		
				2.5Y4/3		
				5Y5/1		
				5Y4/1		

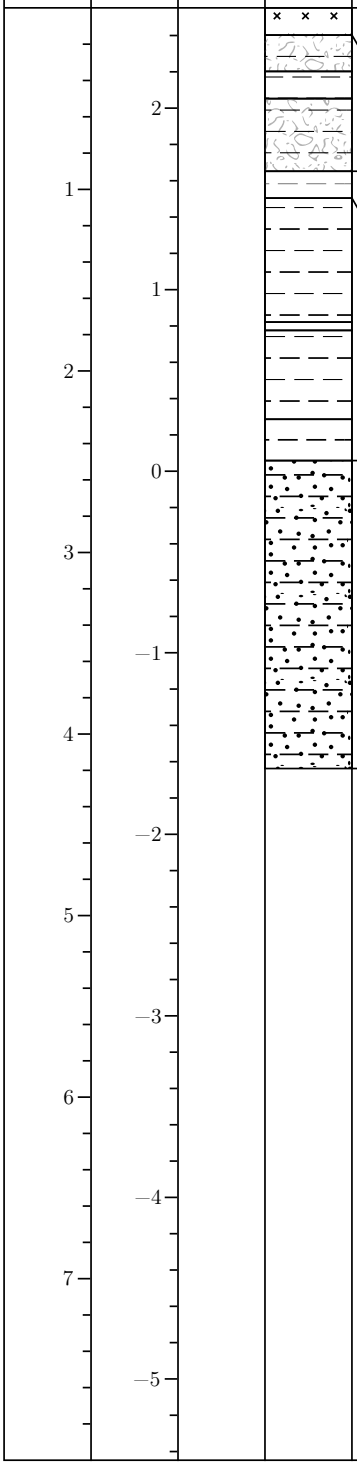

CORE: Core-5
LOCATION: Springs Road

NZMG COORDINATES: 2712167.90 E, 6073302.48 N PAGE: 2/2
WVD1953 ELEVATION: +2.5523 m

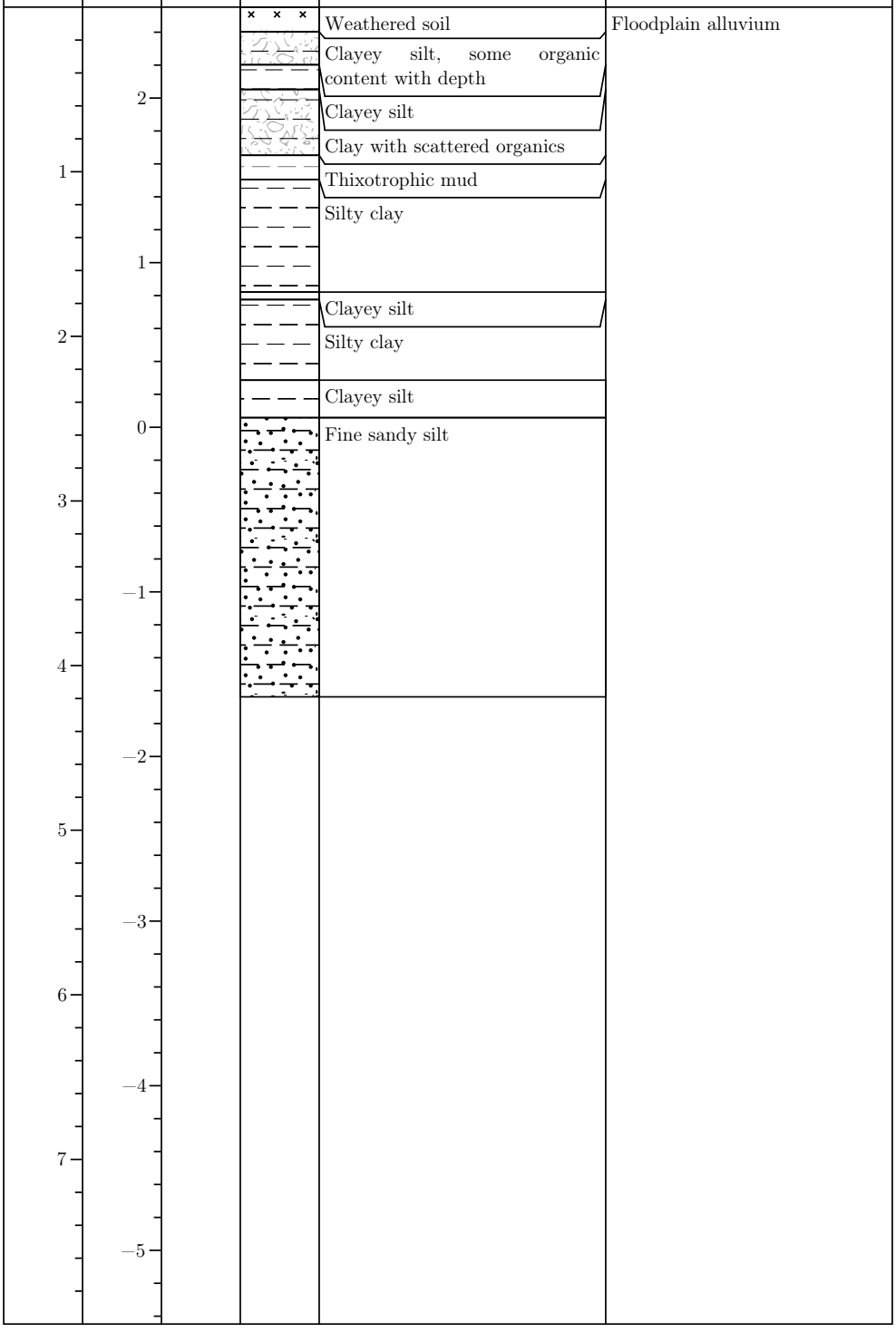

CORE: Kere-1
LOCATION: Kere Kere Road

NZMG COORDINATES: 2708547.50 E, 6076320.91 N PAGE: 1/2
WVD1953 ELEVATION: +3.2679 m

DEPTH (m)	WVD'53 (m)	PHOTO LOG	VISUAL LOG	COLOUR	CHRONOLOGY	SORTING MEAN GRAIN SIZE
				10YR3/3		
				N5/		

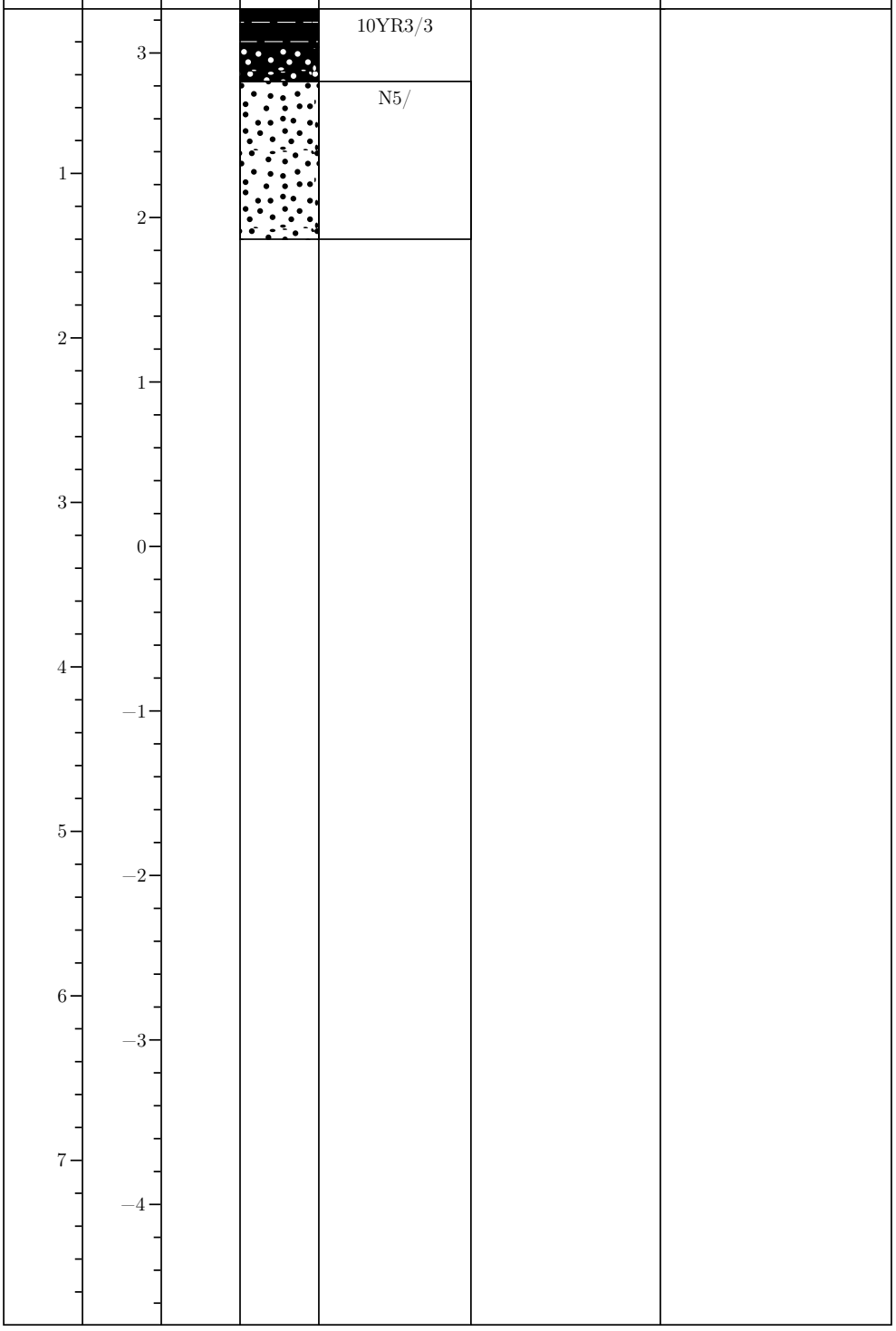

CORE: Kere-1
LOCATION: Kere Kere Road

NZMG COORDINATES: 2708547.50 E, 6076320.91 N PAGE: 2/2
WVD1953 ELEVATION: +3.2679 m

DEPTH (m)	WVD'53 (m)	PHOTO LOG	VISUAL LOG	DESCRIPTION	INTERPRETATION
1	3		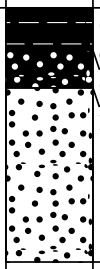	Organic rich mud grading to coarse sand Organic rich coarse sand Homogenous coarse sand	Reworked dune sands (modern)
2	2				
3	1				
4	0				
5	−1				
6	−2				
7	−3				
	−4				

CORE: New-1
LOCATION: Newth Road

NZMG COORDINATES: 2704879.61 E, 6076480.75 N PAGE: 1/2
WVD1953 ELEVATION: +3.0538 m

DEPTH (m)	WVD'53 (m)	PHOTO LOG	VISUAL LOG	COLOUR	CHRONOLOGY	SORTING MEAN GRAIN SIZE
1 2 3 4 5 6 7	3 2 1 0 −1 −2 −3 −4		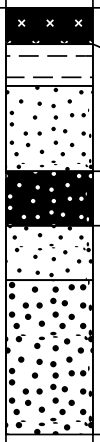	5YR2.5/1 N5/ 5YR2.5/1 N5/		

CORE: New-1
LOCATION: Newth Road

NZMG COORDINATES: 2704879.61 E, 6076480.75 N PAGE: 2/2
WVD1953 ELEVATION: +3.0538 m

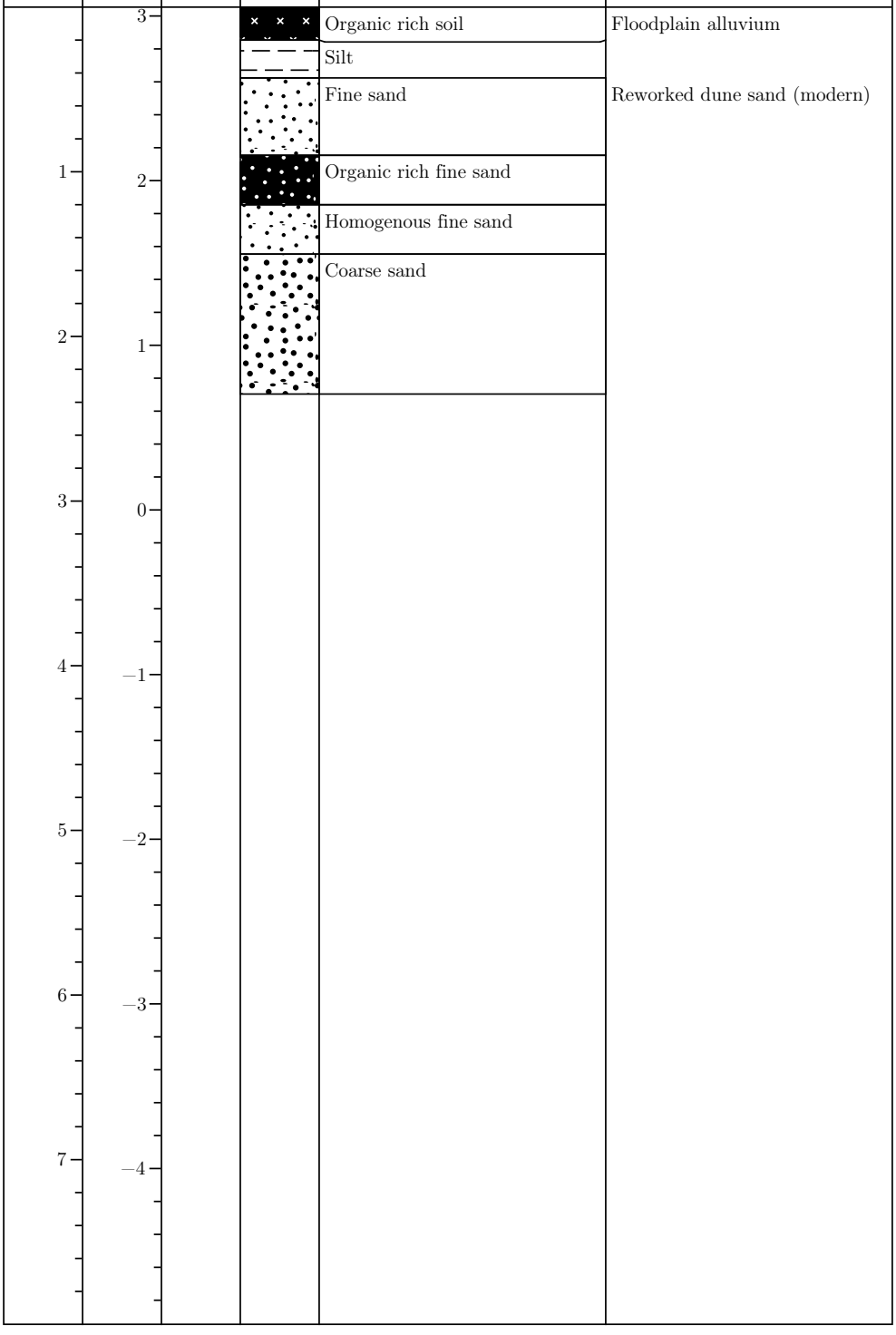

CORE: Kara-1
LOCATION: Kara Road

NZMG COORDINATES: 2716324.50 E, 6071841.96 N PAGE: 1/2
WVD1953 ELEVATION: +4.9468 m

DEPTH (m)	WVD'53 (m)	PHOTO LOG	VISUAL LOG	COLOUR	CHRONOLOGY	SORTING MEAN GRAIN SIZE
1	4			5Y6/1		
2	3			2.5Y4/3 N4/		
3	2			5GY6/1 with bands of 5Y5/1		
4	1					
5	0					
6	−1					
7	−2					
	−3					

CORE: Kara-1
LOCATION: Kara Road

NZMG COORDINATES: 2716324.50 E, 6071841.96 N PAGE: 2/2
WVD1953 ELEVATION: +4.9468 m

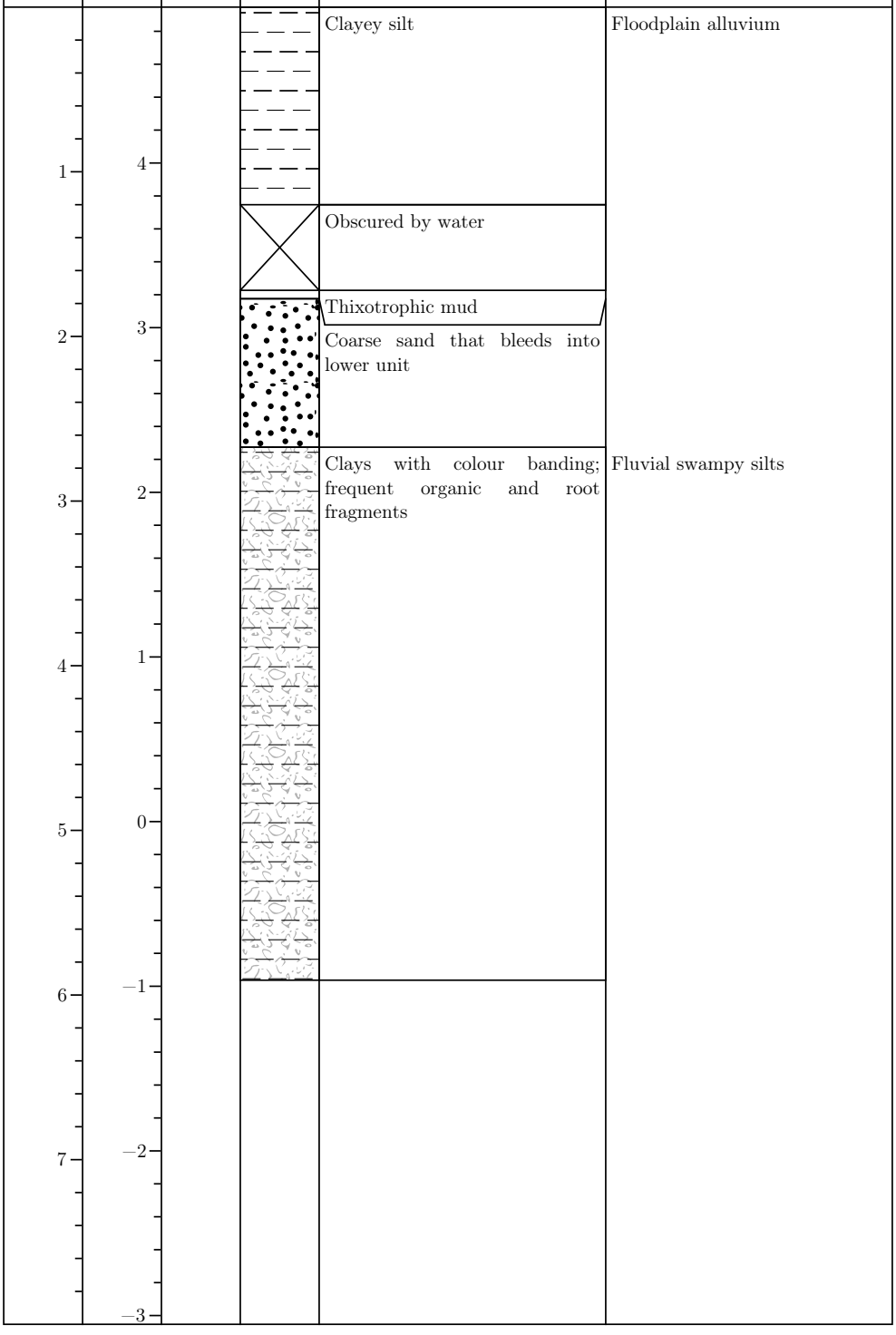

CORE: SH-3 NZMG COORDINATES: 2710648.39 E, 6070470.75 N PAGE: 1/4
LOCATION: Shannon-Buckley WVD1953 ELEVATION: +4.8389 m

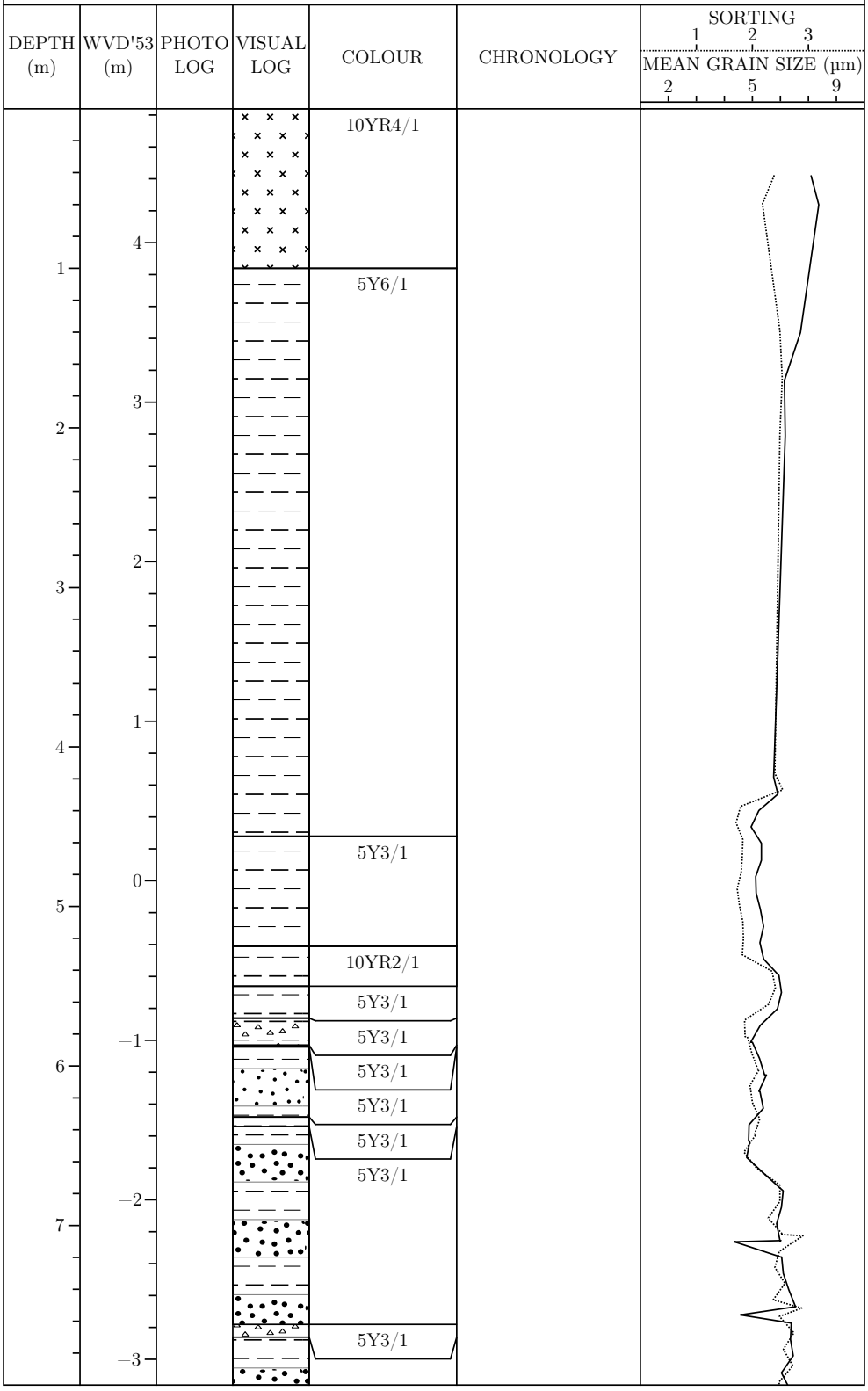

CORE: SH-3 NZMG COORDINATES: 2710648.39 E, 6070470.75 N PAGE: 2/4
LOCATION: Shannon-Buckley WVD1953 ELEVATION: +4.8389 m

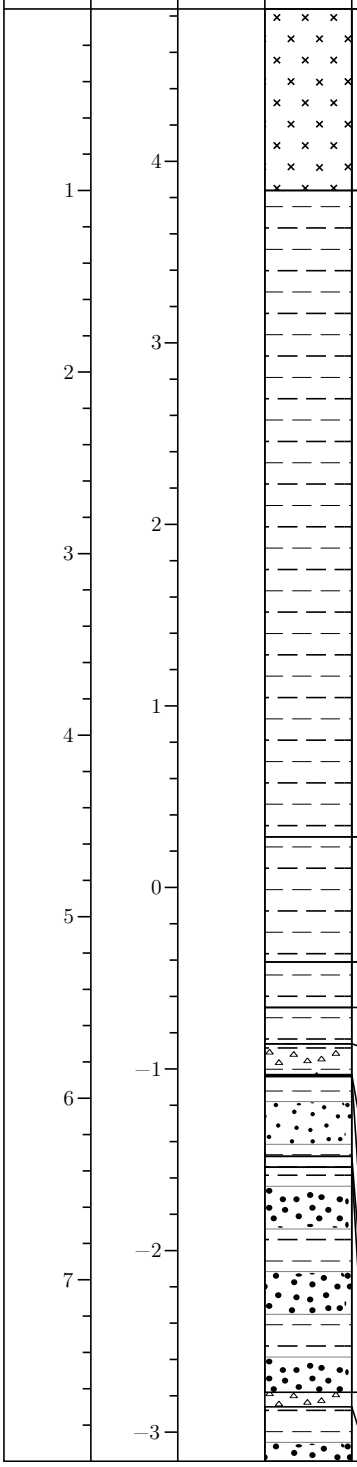

DEPTH (m)	WVD'53 (m)	PHOTO LOG	VISUAL LOG	DESCRIPTION	INTERPRETATION
1	4			Weathered top soil	Floodplain alluvium
2	3			Homogenous fine clayey silt	
3	2				
4	1				
5	0			Fine silty clay	Estuarine sands and silts
				Fine silty clay with bioturbation	
				Fine silty clay	
6	−1			Fine silty clay with random infrequent shell fragments	
				Fine silty clay with rich organic matter	
				Fine sand interbedded with cohesive fine silty clay	
7	−2			Fine silty clay with bioturbation	
				Cohesive fine silty clay interbedded with coarse sand	
	−3			Burrow filled with shell hash	
				Continued on page 4	

CORE: SH-3 NZMG COORDINATES: 2710648.39 E, 6070470.75 N PAGE: 3/4
LOCATION: Shannon-Buckley WVD1953 ELEVATION: +4.8389 m

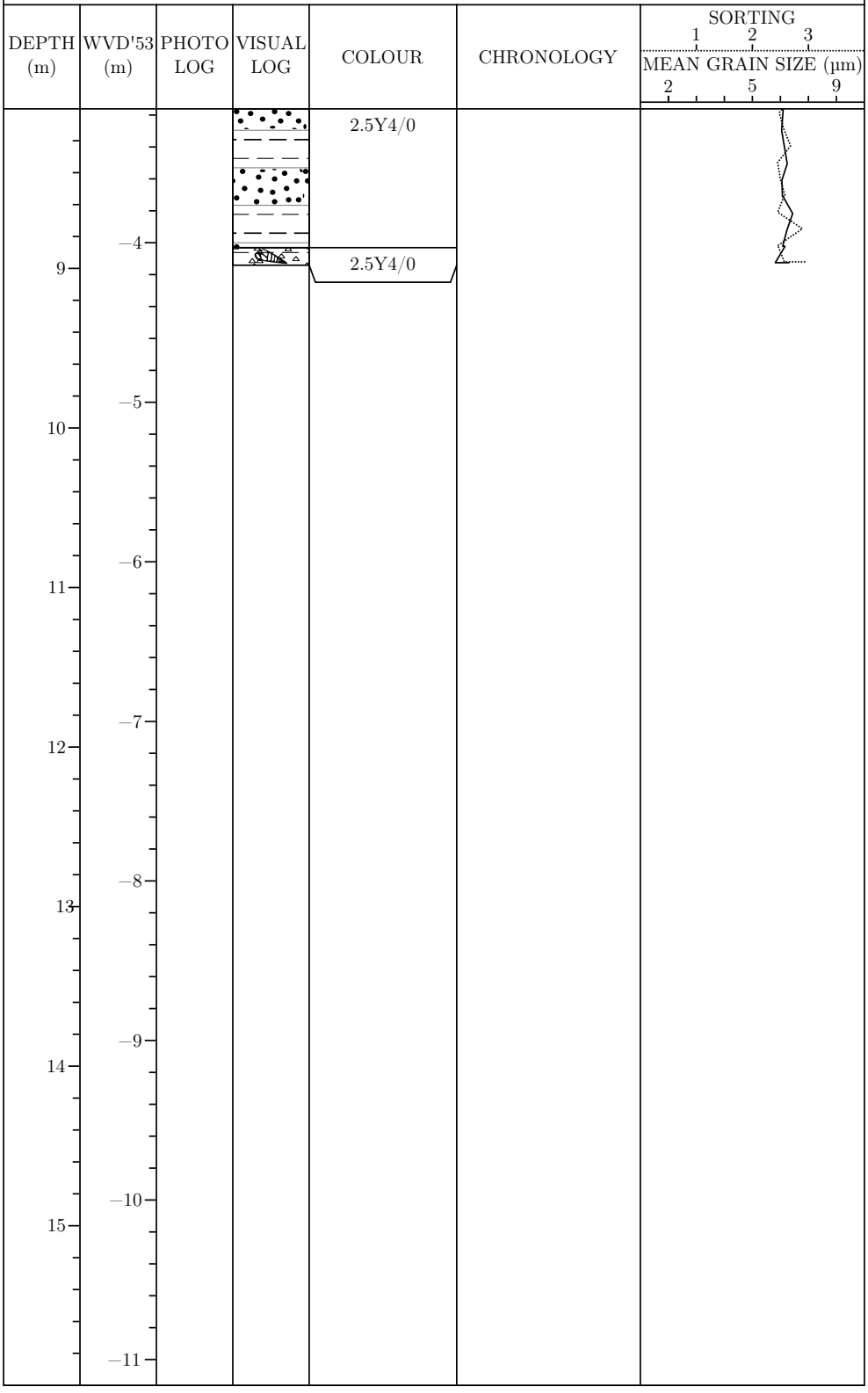

CORE: SH-3 NZMG COORDINATES: 2710648.39 E, 6070470.75 N PAGE: 4/4
LOCATION: Shannon-Buckley WVD1953 ELEVATION: +4.8389 m

DEPTH (m)	WVD'53 (m)	PHOTO LOG	VISUAL LOG	DESCRIPTION	INTERPRETATION
9	−4		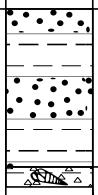	Cohesive fine silty clay interbedded with coarse sand, with random isolated fossil crabs	Estuarine sands and silts
				Thin (c. 1 cm) layers of shell hash, silty clay, and dense organics; single *in situ A. crenata*	
10	−5				
11	−6				
12	−7				
13	−8				
14	−9				
15	−10				
	−11				

CORE: Him-1 NZMG COORDINATES: 2713722.07 E, 6081148.74 N PAGE: 1/2
LOCATION: Himatangi Block Road WVD1953 ELEVATION: +7.5862 m

DEPTH (m)	WVD'53 (m)	PHOTO LOG	VISUAL LOG	COLOUR	CHRONOLOGY	SORTING MEAN GRAIN SIZE
				5Y5/1		
1	7					
				N5/		
	6			10YR3/3		
2				10YR5/8		
				5Y5/1		
	5					
3						
	4					
4						
	3			N5/		
5				5Y5/1		
	2					
6						
	1					
7						
	0					

CORE: Him-1 NZMG COORDINATES: 2713722.07 E, 6081148.74 N PAGE: 2/2
LOCATION: Himatangi Block Road WVD1953 ELEVATION: +7.5862 m

DEPTH (m)	WVD'53 (m)	PHOTO LOG	VISUAL LOG	DESCRIPTION	INTERPRETATION
				Clayey silt	Floodplain alluvium with some reworked dune sand
1	7			Obscured by water	
				Coarse sand	
	6			Heavily degraded wood, almost peat	
2				Sandy peat	
				Clayey silt	
	5				
3					
	4				
4					
	3			Coarse sand	
5				Sandy silt	
	2				
6					
	1				
7					
	0				

CORE: Ran-1
LOCATION: Main Drain Road

NZMG COORDINATES: 2717357.93 E, 6084594.44 N PAGE: 1/2
WVD1953 ELEVATION: +6.5594 m

DEPTH (m)	WVD'53 (m)	PHOTO LOG	VISUAL LOG	COLOUR	CHRONOLOGY	SORTING MEAN GRAIN SIZE
				7.5YR2/0 5BG5/1		

CORE: Ran-1 NZMG COORDINATES: 2717357.93 E, 6084594.44 N PAGE: 2/2
LOCATION: Main Drain Road WVD1953 ELEVATION: +6.5594 m

DEPTH (m)	WVD'53 (m)	PHOTO LOG	VISUAL LOG	DESCRIPTION	INTERPRETATION
1 2 3 4 5 6 7	6 5 4 3 2 1 0 −1		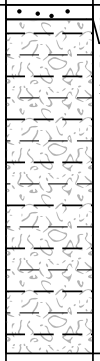	Sandy mud Silty clay with infrequent large root fragments	Floodplain alluvium

CORE: Ran-2
LOCATION: Pyke Road

NZMG COORDINATES: 2715373.18 E, 6085421.95 N PAGE: 1/2
WVD1953 ELEVATION: +15.0484 m

DEPTH (m)	WVD'53 (m)	PHOTO LOG	VISUAL LOG	COLOUR	CHRONOLOGY	SORTING MEAN GRAIN SIZE
0	15			2.5YR2.5/0		
1	14			2.5YR2.5/0 grading to 10YR2/2		
				10YR2/2 grading to N4/		
2	13					
3	12					
4	11					
5	10					
6	9					
7	8					

CORE: Ran-2 NZMG COORDINATES: 2715373.18 E, 6085421.95 N PAGE: 2/2
LOCATION: Pyke Road WVD1953 ELEVATION: +15.0484 m

DEPTH (m)	WVD'53 (m)	PHOTO LOG	VISUAL LOG	DESCRIPTION	INTERPRETATION
0	15			Medium sand	Reworked dune sands (modern)
				Dense organics	
				Medium sand	
				Medium sand with pieces of gravel	
1	14			Medium sand	
2	13				
3	12				
4	11				
5	10				
6	9				
7	8				

CORE: Whiro-1 NZMG COORDINATES: 2701422.06 E, 6076437.40 N PAGE: 1/2
LOCATION: Whirokino Cut WVD1953 ELEVATION: +0.4624 m

DEPTH (m)	WVD'53 (m)	PHOTO LOG	VISUAL LOG	COLOUR	CHRONOLOGY	SORTING MEAN GRAIN SIZE
				N5/		
				Sand: N4/ Silty clay: 5Y5/1		

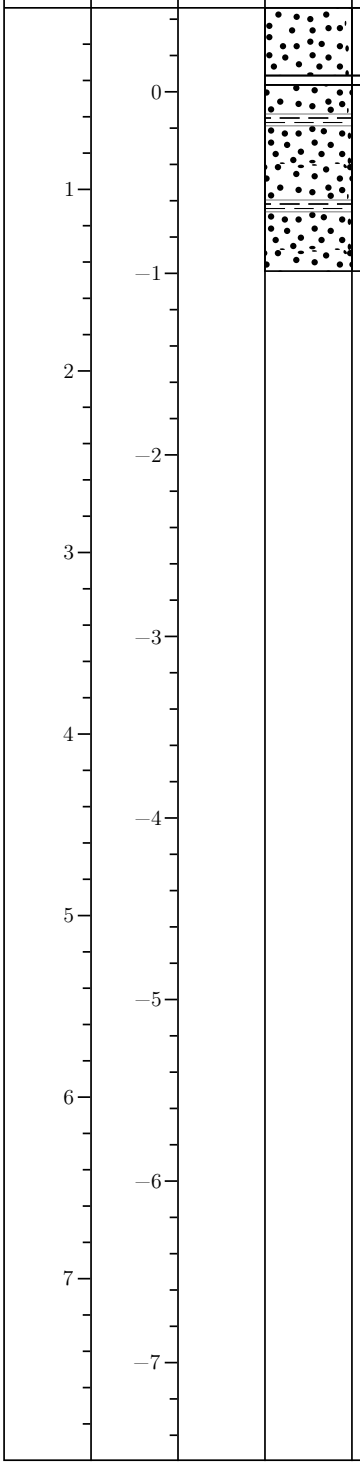

CORE: Whiro-1 NZMG COORDINATES: 2701422.06 E, 6076437.40 N PAGE: 2/2
LOCATION: Whirokino Cut WVD1953 ELEVATION: +0.4624 m

DEPTH (m)	WVD'53 (m)	PHOTO LOG	VISUAL LOG	DESCRIPTION	INTERPRETATION
0	0		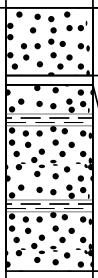	Homogenous coarse sand	Estuarine sands and silts
1	−1			Fossilised wood	
2	−2			Coarse sand interbedded with thin (< 1 cm) lenses of silty clay	
3	−3				
4	−4				
5	−5				
6	−6				
7	−7				

CORE: Whiro-2 NZMG COORDINATES: 2701068.84 E, 6075499.01 N PAGE: 1/2
LOCATION: Whirokino Cut WVD1953 ELEVATION: +0.3476 m

DEPTH (m)	WVD'53 (m)	PHOTO LOG	VISUAL LOG	COLOUR	CHRONOLOGY	SORTING / MEAN GRAIN SIZE
0–7	+0 to −7		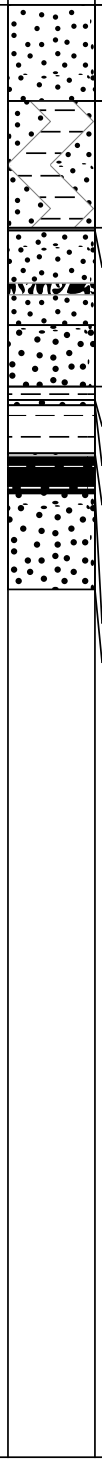	N4/ Sand: N4/ Silt: 5Y5/1 5Y5/1 N4/ 5Y5/1 N5/ 5Y5/1 Silty clay: 5YR2.5/1 Sand: N5/ N4/		

CORE: Whiro-2
LOCATION: Whirokino Cut

NZMG COORDINATES: 2701068.84 E, 6075499.01 N PAGE: 2/2
WVD1953 ELEVATION: +0.3476 m

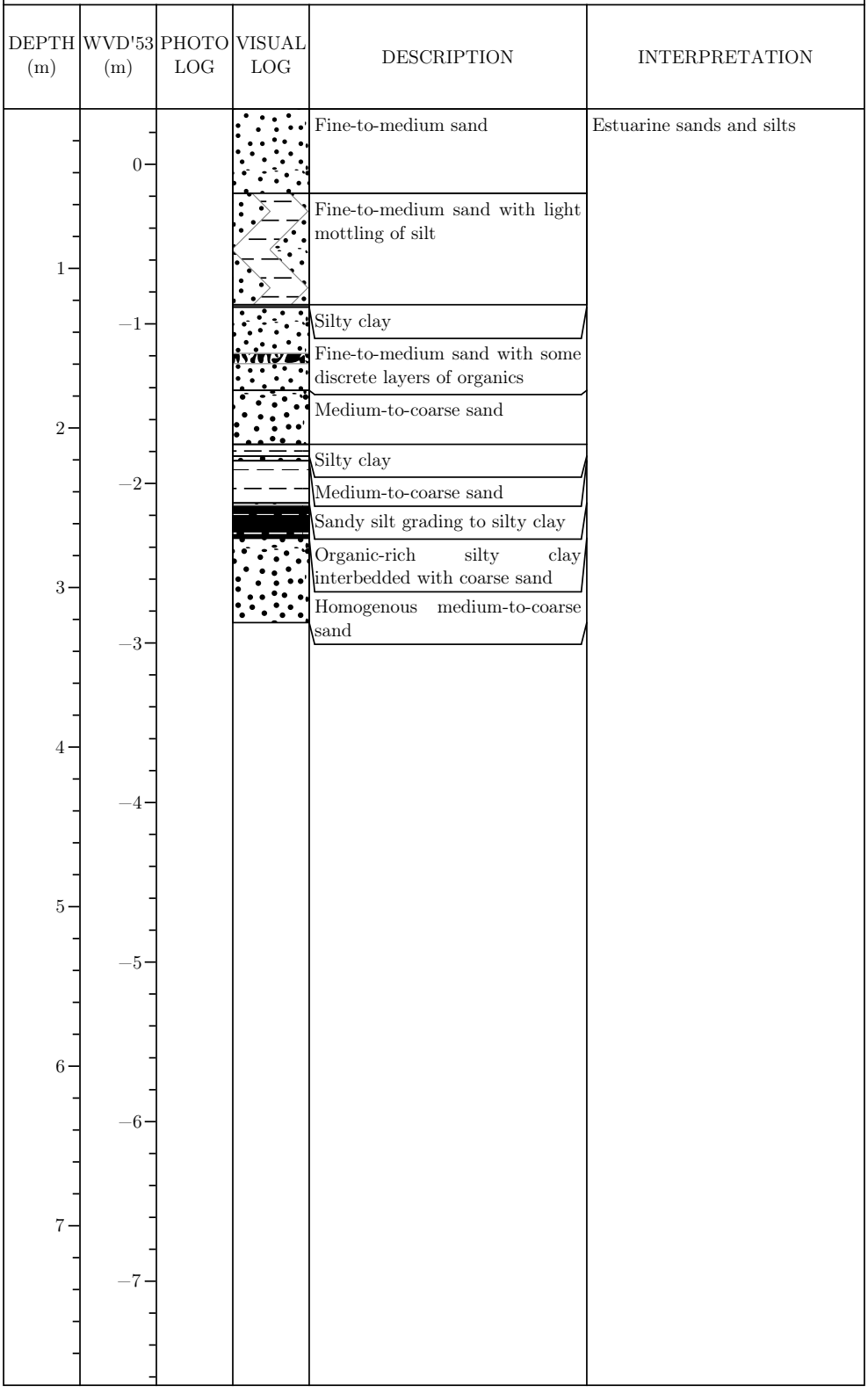

CORE: FR-1
LOCATION: Te Rewa Road

NZMG COORDINATES: 2718181.76 E, 6076833.99 N PAGE: 1/2
WVD1953 ELEVATION: +3.8200 m

DEPTH (m)	WVD'53 (m)	PHOTO LOG	VISUAL LOG	COLOUR	CHRONOLOGY	SORTING MEAN GRAIN SIZE
				2.5Y3/2 N4/		

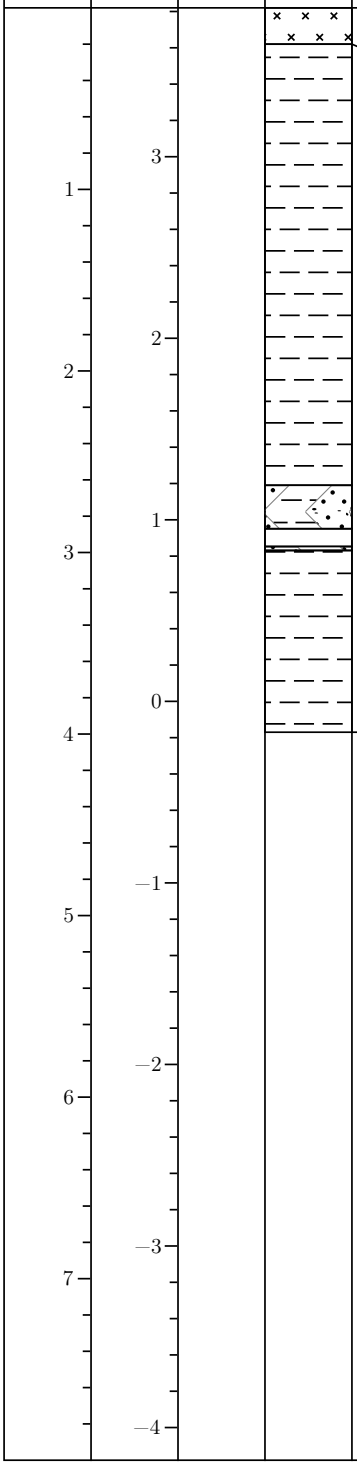

CORE: FR-1 NZMG COORDINATES: 2718181.76 E, 6076833.99 N PAGE: 2/2
LOCATION: Te Rewa Road WVD1953 ELEVATION: +3.8200 m

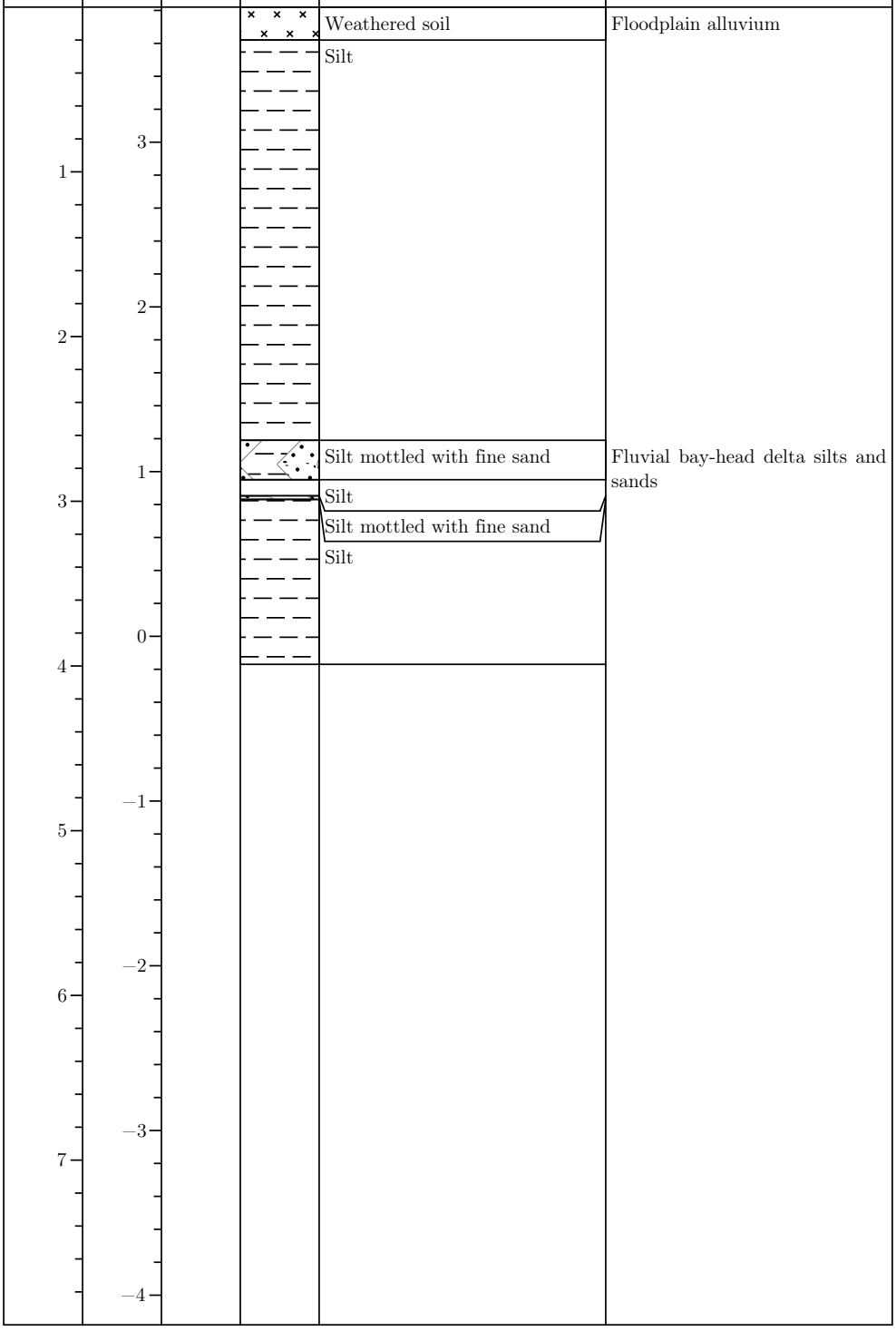

Appendix C

Sediment analysis results

In selected vibracores approximately 50 g (wet weight) of sediment was collected every 10 cm, as well as at locations of significant facies changes, for sediment analysis to determine sediment constituents, textural characteristics and to distinguish between sediments from different depositional environments. Given financial and time constraints sediment analysis was only performed on sediment samples from locations where radiocarbon ages had been obtained. Samples from vibracores Sh-1, Sh-2, Sh-3 and LD-5 were analysed using a Malvern Mastersizer 2000 laser particle size analyser at the University of Wollongong. Samples from vibracores Cut-2, Cut-4, Cut-7, E1, Flood-1, G, and Kop-1 were analysed using a Horiba Partica LA-950V2 laser particle size analyser at the Institute of Natural Resources, Massey University. The Malvern Mastersizer 2000 was used initially for sediment analysis, prior to the Institute of Natural Resources acquiring the Horiba Partica LA-950V2, at which time financial considerations precluded returning to Wollongong to complete the analyses. The Horiba Partica LA-950V2 requires that the refractive index of the suspension medium and sample material be specified at the time of measurement. Measurements were taken using refractive index values of 1.33 for the deionised water suspension medium and 1.56 for the sample material. The latter value is valid for quartz, clay minerals and feldspars (e.g., Loizeau et al., 1994; Buurman et al., 2001; Trentesaux et al., 2001; Sperazza et al., 2004). Such settings are not required for the operation of the Malvern Mastersizer 2000. Unfortunately the sediment size results from each analyser differ such that they are not directly comparable, but are useful as relative measures of sediment constituents and textural characteristics.

Appendix C. Sediment analysis results

Grain size results for vibracore E1

Depth (m)	Adjusted depth (m)	Mean grain size (μm)	Sorting value
0·45	0·45	56·64	48·84
1·10	1·10	15·41	31·20
1·30	1·30	185·63	232·07
1·40	1·40	115·52	181·03
1·50	1·50	190·23	220·72
2·40	2·40	10·97	23·03
0·00	2·96	239·12	309·33
0·10	3·07	76·16	58·74
0·20	3·17	69·09	59·54
0·30	3·28	65·33	53·30
0·40	3·39	79·12	59·45
0·50	3·49	53·38	52·80
0·60	3·60	48·71	48·74
0·70	3·71	66·28	56·86
0·80	3·81	56·37	51·02
0·90	3·92	112·62	72·76
1·00	4·03	102·47	75·04
1·05	4·08	142·25	109·86
1·10	4·13	107·72	52·49
1·20	4·24	112·02	53·55
1·30	4·35	116·32	58·89
1·40	4·45	103·80	77·31
1·50	4·56	145·07	63·29

Appendix C. Sediment analysis results

Grain size results for vibracore Cook-2

Depth (m)	Adjusted depth (m)	Mean grain size (μm)	Sorting value
0·30	0·30	54·64	64·83
1·60	1·60	46·48	65·42
1·90	1·90	56·03	82·22
0·00	2·03	86·99	54·49
0·10	2·12	77·53	54·46
0·20	2·21	104·99	50·31
0·30	2·30	61·62	61·24
0·40	2·39	57·33	55·64
0·50	2·48	59·92	57·55
0·60	2·56	85·10	60·84
0·70	2·65	84·88	72·52
0·80	2·74	118·44	47·63
0·90	2·83	102·95	52·85
1·00	2·92	88·01	65·91
1·10	3·01	98·22	64·05
1·20	3·10	101·58	54·61
1·30	3·19	56·26	52·57
1·40	3·28	90·80	66·23
1·50	3·37	63·58	65·91
1·60	3·45	118·03	67·56
1·70	3·54	108·14	70·11
1·80	3·63	118·64	61·40
1·90	3·72	129·07	52·32
2·00	3·81	120·95	62·33
2·10	3·90	107·85	66·14
2·20	3·99	236·58	280·06
2·30	4·08	124·44	58·36
2·40	4·17	116·93	65·60
2·50	4·26	127·03	59·84
2·60	4·35	132·38	48·20
2·70	4·43	64·99	60·69
2·80	4·52	107·44	74·02
2·90	4·61	63·88	64·94
3·00	4·70	56·29	62·03
3·10	4·79	68·06	63·52
3·20	4·88	78·24	65·72
3·30	4·97	97·97	67·13
3·40	5·06	95·56	66·60
3·50	5·15	53·98	56·60
3·60	5·24	50·98	54·97
3·65	5·28	85·18	62·03

Appendix C. Sediment analysis results

Grain size results for vibracore Cut-2

Depth (m)	Adjusted depth (m)	Mean grain size (μm)	Sorting value
0·00	2·87	54·86	71·37
0·10	2·97	49·82	62·08
0·20	3·07	131·70	53·01
0·30	3·17	105·66	63·37
0·40	3·27	114·67	71·61
0·50	3·37	103·70	63·20
0·60	3·47	138·70	46·23
0·70	3·57	123·68	57·07
0·80	3·67	131·63	56·64
0·90	3·77	116·70	54·58
1·00	3·87	137·41	52·89
1·10	3·97	50·80	48·68
1·20	4·07	64·60	57·24
1·30	4·17	77·78	58·83
1·40	4·27	42·98	49·09
1·50	4·37	30·13	37·32
1·60	4·47	55·78	52·63
1·70	4·57	62·39	63·29
1·75	4·62	143·68	58·53
1·80	4·67	145·29	56·89
1·81	4·68	100·23	69·09
1·90	4·77	53·61	53·68
2·00	4·87	122·34	208·90
2·10	4·97	122·44	58·60
2·20	5·07	69·80	61·34
2·30	5·17	113·41	77·67
2·39	5·26	116·44	52·07

Grain size results for vibracore Cut-4

Depth (m)	Adjusted depth (m)	Mean grain size (μm)	Sorting value
1·00	1·00	59·92	72·96
0·00	3·27	143·42	234·68
0·10	3·38	43·53	55·99
0·20	3·48	65·79	70·94
0·30	3·59	127·86	80·76
0·40	3·69	155·24	69·93
0·50	3·80	169·77	74·00
0·60	3·90	182·88	98·95
0·70	4·01	178·17	73·28
0·80	4·11	168·93	73·55
0·90	4·22	182·65	68·24
1·00	4·32	157·05	67·85
1·07	4·39	149·24	54·78
1·10	4·43	82·06	70·90
1·20	4·53	47·41	51·15
1·30	4·64	92·48	72·40
1·40	4·74	71·15	66·45
1·50	4·85	101·31	60·32
1·60	4·95	90·04	66·61
1·70	5·06	43·89	55·08
1·80	5·16	138·46	87·06
1·90	5·27	134·21	138·80
1·95	5·32	160·2	114·17

Appendix C. Sediment analysis results

Grain size results for vibracore Cut-7

Depth (m)	Adjusted depth (m)	Mean grain size (μm)	Sorting value
1·00	1·00	11·83	17·89
2·00	2·00	14·83	15·84
0·00	4·31	155·23	247·60
0·10	4·41	83·86	44·74
0·20	4·51	57·01	50·15
0·30	4·61	151·00	60·90
0·40	4·71	100·19	82·13
0·50	4·81	148·80	104·15
0·60	4·91	112·51	88·49
0·70	5·01	157·33	96·30
0·80	5·11	86·73	72·21
0·90	5·21	112·98	79·66
1·00	5·31	11·05	17·98
1·10	5·41	35·70	39·46
1·20	5·52	117·30	81·81
1·30	5·62	104·36	76·51
1·40	5·72	110·22	72·67
1·50	5·82	111·42	67·06
1·60	5·92	130·11	78·32
1·70	6·02	85·23	73·47
1·80	6·12	103·73	91·39
1·90	6·22	74·70	58·41
2·00	6·32	109·7	66·62
2·10	6·42	64·42	57·84
2·20	6·52	127·74	72·97
2·30	6·62	181·86	57·97

Appendix C. Sediment analysis results

Grain size results for vibracore G

Depth (m)	Adjusted depth (m)	Mean grain size (μm)	Sorting value
0·80	0·80	92·44	66·48
1·60	1·60	93·40	69·22
2·40	2·40	60·64	72·42
0·00	3·34	36·83	44·72
0·10	3·44	39·68	46·93
0·20	3·54	53·28	58·00
0·30	3·65	55·80	63·62
0·40	3·75	53·71	58·19
0·50	3·85	122·81	62·79
0·60	3·95	120·75	46·98
0·70	4·06	99·81	62·11
0·80	4·16	48·76	62·41
0·90	4·26	57·65	67·00
1·00	4·36	37·91	50·68
0·00	4·37	55·90	65·56
0·10	4·48	42·12	53·54
0·20	4·58	65·42	69·69
0·30	4·68	47·42	61·20
0·40	4·78	52·08	65·55
0·50	4·89	45·42	54·78
0·60	4·99	58·48	75·51
0·70	5·09	38·28	43·62
0·80	5·19	47·10	50·75
0·90	5·30	30·13	43·40
1·00	5·40	58·28	46·28
1·10	5·50	61·53	55·39
1·20	5·60	51·52	53·07
1·30	5·71	39·21	50·35
1·40	5·81	40·67	51·38
1·50	5·91	56·35	44·60
1·60	6·01	47·81	46·45
1·70	6·12	50·10	56·50
1·80	6·22	44·34	51·03
1·90	6·32	34·25	47·03
2·00	6·42	55·61	60·95
2·10	6·53	34·72	45·88
2·20	6·63	36·59	43·91

Appendix C. Sediment analysis results

Grain size results for vibracore Flood-1

Depth (m)	Adjusted depth (m)	Mean grain size (μm)	Sorting value
0·50	0·50	127·84	213·2
1·00	1·00	198·56	294·03
0·00	1·35	32·05	58·30
0·10	1·46	16·10	27·06
0·20	1·57	55·28	64·25
0·30	1·68	67·12	65·17
0·40	1·79	92·53	76·82
0·50	1·90	89·43	72·98
0·60	2·01	111·11	84·80
0·70	2·12	127·54	73·47
0·80	2·23	114·55	77·88
0·90	2·33	122·09	82·04
1·00	2·44	97·25	73·19
1·10	2·55	113·31	70·05
1·20	2·66	120·97	69·44
1·30	2·77	139·02	62·08
1·40	2·88	154·71	67·18
1·50	2·99	152·97	54·84
1·60	3·10	153·79	57·68
1·70	3·21	158·29	55·78
1·80	3·32	141·84	66·61
1·90	3·43	152·13	76·97
2·00	3·54	138·02	61·13
2·10	3·65	149·69	69·38
2·20	3·76	175·06	98·62
2·30	3·87	248·27	251·54
2·40	3·98	15·73	9·09
2·50	4·08	122·67	90·72
2·60	4·19	119·30	91·13
2·70	4·30	176·99	90·95
2·80	4·41	163·27	91·18
2·90	4·52	248·06	224·36
3·10	4·74	151·52	86·21
3·20	4·85	225·41	221·72

Appendix C. Sediment analysis results

Grain size results for vibracore LD-5

Depth (m)	Adjusted depth (m)	Mean grain size (μm)	Sorting value
0·30	0·30	6·18	2·27
1·00	1·00	7·42	2·17
1·60	1·60	7·77	2·06
1·80	1·80	7·67	2·12
1·90	1·90	7·52	2·18
0·00	2·20	5·54	2·29
0·10	2·32	5·34	2·36
0·20	2·44	5·90	2·15
0·30	2·56	4·99	2·37
0·40	2·68	6·82	2·53
0·50	2·81	2·85	2·47
0·60	2·93	8·01	2·18
0·70	3·05	7·33	2·49
0·80	3·17	7·49	2·09
0·90	3·29	7·23	2·25
1·00	3·41	7·22	2·18
1·10	3·53	7·18	2·24
1·20	3·65	7·14	2·16
1·30	3·78	7·22	1·97
1·40	3·90	7·42	2·09
1·50	4·02	6·94	2·23
1·60	4·14	6·41	2·21
1·70	4·26	6·35	2·26
1·80	4·38	6·53	2·30
1·90	4·50	6·66	2·59
2·00	4·62	7·15	2·32
2·10	4·75	6·32	2·70
2·20	4·87	6·72	2·70

Appendix C. Sediment analysis results

Grain size results for vibracore Kop-1

Depth (m)	Adjusted depth (m)	Mean grain size (μm)	Sorting value
0·60	0·60	30·13	39·38
1·20	1·20	16·40	24·47
0·00	2·74	24·92	20·65
0·10	2·83	27·87	29·21
0·20	2·93	31·88	35·47
0·30	3·02	28·03	29·01
0·40	3·12	30·68	36·52
0·50	3·21	32·32	40·57
0·60	3·31	33·65	39·51
0·70	3·40	32·78	46·25
0·80	3·49	35·57	39·74
0·90	3·59	43·36	53·02
1·00	3·68	45·54	49·88
1·10	3·78	33·71	44·76
1·20	3·87	44·81	53·15
1·30	3·97	53·89	57·96
1·40	4·06	35·93	46·10
1·50	4·16	34·47	41·36
1·60	4·25	35·34	43·36
1·70	4·34	34·43	44·11
1·80	4·44	33·88	38·11
1·90	4·53	47·72	43·51
2·00	4·63	38·01	46·30
2·10	4·72	28·20	37·60
2·20	4·82	28·35	30·58
2·30	4·91	45·13	59·61
2·40	5·00	23·86	33·48
2·50	5·10	16·01	19·19
2·60	5·19	22·58	30·85
2·70	5·29	58·95	65·56
2·80	5·38	116·44	182·22
2·90	5·48	29·87	37·66
3·00	5·57	22·00	40·01
3·10	5·67	31·07	37·75
3·20	5·76	15·08	19·26
3·30	5·85	32·28	40·94
3·35	5·90	64·23	58·63
3·40	5·95	91·86	67·83
3·50	6·04	129·44	45·60
3·55	6·09	131·51	50·97

Appendix C. Sediment analysis results

Grain size results for vibracore Sh-1

Depth (m)	Adjusted depth (m)	Mean grain size (μm)	Sorting value
0·40	0·40	6·28	2·44
1·10	1·10	7·76	2·41
1·20	1·20	7·17	2·27
1·40	1·40	6·78	2·44
1·70	1·70	6·85	2·62
2·30	2·30	6·91	2·79
2·75	2·75	6·99	2·80
2·80	2·80	6·84	2·67
2·90	2·90	6·80	2·54
3·00	3·00	6·47	2·39
0·00	3·10	6·82	2·72
0·10	3·20	6·53	2·41
0·20	3·30	6·23	2·64
0·30	3·40	6·82	2·77
0·40	3·50	6·46	2·64
0·50	3·60	6·82	2·41
0·60	3·70	6·69	2·40
0·70	3·80	6·70	2·48
0·80	3·90	6·82	2·60
0·90	4·00	5·92	2·27
1·00	4·10	6·19	2·50
1·10	4·20	6·46	2·55
1·20	4·30	6·75	2·77
1·30	4·40	6·43	2·51
1·40	4·50	6·38	2·39
1·50	4·60	6·49	2·18
1·60	4·70	6·69	2·54
1·70	4·80	6·85	2·89
1·80	4·90	6·52	2·27
1·90	5·00	6·57	2·52
2·00	5·10	6·45	2·48
2·10	5·20	5·86	2·07
2·20	5·30	6·72	2·55
2·30	5·40	6·19	2·24
2·40	5·50	6·07	2·35
2·50	5·60	7·11	2·37
2·60	5·70	6·98	2·90
2·70	5·80	6·39	2·63
2·80	5·90	6·04	2·23
2·90	6·00	6·37	2·58
3·00	6·10	6·18	2·65
3·10	6·20	6·46	2·52
3·20	6·30	6·24	2·37
3·30	6·40	6·14	2·64
3·40	6·50	5·41	2·22
3·50	6·60	6·07	2·28
3·60	6·70	6·23	2·32
3·70	6·80	6·24	2·44
3·80	6·90	5·08	1·65
3·90	7·00	6·08	2·12
4·00	7·10	6·33	2·42
4·10	7·20	6·33	2·42
4·20	7·30	5·55	1·88
4·30	7·40	6·26	2·27
4·40	7·50	6·16	2·38
4·50	7·60	6·36	2·31
4·60	7·70	5·90	2·19
4·70	7·80	6·28	2·32

Appendix C. Sediment analysis results

Grain size results for vibracore Sh-2

Depth (m)	Adjusted depth (m)	Mean grain size (μm)	Sorting value
0·40	0·40	7·70	2·41
0·80	0·80	6·88	2·58
0·90	0·90	6·52	2·46
1·90	1·90	6·88	2·70
0·00	2·16	6·16	2·59
0·10	2·26	6·34	2·59
0·20	2·37	6·23	2·63
0·30	2·47	6·75	2·62
0·40	2·57	6·74	2·61
0·50	2·68	6·74	2·32
0·60	2·78	6·65	2·46
0·70	2·88	6·22	2·54
0·80	2·99	7·06	2·53
0·90	3·09	6·49	2·59
1·00	3·19	6·40	2·49
1·10	3·30	6·29	2·47
1·20	3·40	6·75	2·68
1·30	3·50	6·75	2·60
1·40	3·61	6·89	2·65
1·50	3·71	6·73	2·68
1·60	3·81	6·85	2·79
1·70	3·91	6·75	2·70
1·80	4·02	6·28	2·53
1·90	4·12	6·36	2·52
2·00	4·22	6·08	2·53
2·10	4·33	6·70	2·61
2·20	4·43	6·77	2·69
2·30	4·53	6·47	2·61
2·40	4·64	6·32	2·55
2·50	4·74	6·88	2·81
2·60	4·84	6·43	2·56
2·70	4·95	6·35	2·61
2·80	5·05	6·51	2·53
2·90	5·15	5·95	2·56
3·00	5·26	6·02	2·59
3·10	5·36	6·06	2·32
3·20	5·46	6·17	2·42
3·30	5·57	6·27	2·42
3·40	5·67	5·51	2·00
3·50	5·77	5·83	2·15
3·60	5·88	5·73	2·01
3·70	5·98	6·03	2·38
3·80	6·08	5·93	2·19
3·90	6·19	5·99	2·30
4·00	6·29	6·05	2·26
4·10	6·39	6·95	2·75
4·20	6·50	6·80	2·58
4·30	6·60	6·23	2·40
4·40	6·70	6·57	2·51
4·50	6·81	5·85	2·11
4·60	6·91	6·16	2·42

Appendix C. Sediment analysis results

Grain size results for vibracore Sh-3

Depth (m)	Adjusted depth (m)	Mean grain size (μm)	Sorting value
0·42	0·42	7·79	2·39
0·60	0·60	8·15	2·18
1·40	1·40	7·28	2·49
1·70	1·70	6·52	2·53
2·05	2·05	6·56	2·49
0·00	4·19	6·01	2·40
0·10	4·29	6·21	2·54
0·20	4·40	5·31	1·79
0·30	4·50	4·94	1·71
0·40	4·60	5·43	1·83
0·50	4·71	5·43	1·82
0·60	4·81	5·16	1·80
0·70	4·92	5·18	1·73
0·80	5·02	5·38	1·77
0·90	5·12	5·53	1·83
1·00	5·23	5·36	1·84
1·10	5·33	5·54	1·82
1·20	5·43	6·26	2·35
1·30	5·54	6·38	2·41
1·40	5·64	6·19	2·29
1·50	5·75	5·38	1·86
1·60	5·85	4·92	1·87
1·60	5·85	5·00	1·91
1·70	5·95	5·34	1·99
1·80	6·06	5·67	2·12
1·90	6·16	5·36	1·96
2·00	6·26	5·52	2·00
2·10	6·37	4·84	2·13
2·20	6·47	4·88	2·05
2·30	6·57	4·73	1·85
2·40	6·68	5·60	2·08
2·50	6·78	6·46	2·49
2·60	6·89	6·38	2·49
2·70	6·99	6·15	2·28
2·80	7·09	6·36	2·52
2·81	7·10	4·15	2·90
2·90	7·20	6·39	2·48
3·00	7·30	6·47	2·40
3·10	7·40	6·73	2·58
3·20	7·51	7·05	2·37
3·25	7·56	4·43	2·88
3·30	7·61	6·85	2·48
3·40	7·72	6·81	2·74
3·50	7·82	6·94	2·55
3·60	7·92	6·38	2·72
3·70	8·03	6·78	2·47
3·80	8·13	6·73	2·55
3·90	8·23	6·85	2·67
4·00	8·34	6·96	2·44
4·10	8·44	6·74	2·49
4·20	8·54	6·79	2·56
4·30	8·65	7·19	2·44
4·40	8·75	6·95	2·88
4·50	8·86	6·87	2·44
4·60	8·96	7·04	2·94

Appendix D

Radiocarbon results

Results of radiocarbon age determinations undertaken by the Waikato University Radiocarbon Laboratory on wood and shell samples recovered from the lower Manawatu valley during the course of this study.

The University of Waikato
Radiocarbon Dating Laboratory

Private Bag 3105
Hamilton,
New Zealand.
Fax +64 7 838 4192
Ph +64 7 838 4278
email c14@waikato.ac.nz
Head: Dr Alan Hogg

Report on Radiocarbon Age Determination for Wk- 22171

(AMS measurement)

Submitter	C R Sloss
Submitter's Code	SH1-S-255
Site & Location	Manawatu Coastal Plain, New Zealand
Sample Material	A. stutchburyi
Physical Pretreatment	Surfaces cleaned. Washed in an ultrasonic bath. Tested for recrystallization: aragonite.
Chemical Pretreatment	Sample acid washed using 0.1N HCl, rinsed and dried.

$\delta^{13}C$	-1.0 ± 0.2	‰
$D^{14}C$	-589.4 ± 2.1	‰
$F^{14}C\%$	41.1 ± 0.2	%
Result	**7150 ± 41 BP**	

Comments

A G Hogg
10/10/07

- Result is *Conventional Age or % Modern* as per Stuiver and Polach, 1977, Radiocarbon 19, 355-363. This is based on the Libby half-life of 5568 yr with correction for isotopic fractionation applied. This age is normally quoted in publications and must include the appropriate error term and Wk number.
- Quoted errors are 1 standard deviation due to counting statistics multiplied by an experimentally determined Laboratory Error Multiplier.
- The isotopic fractionation, $\delta^{13}C$, is expressed as ‰ wrt PDB.
- $F^{14}C\%$ is also known as pMC (percent modern carbon).

The University of Waikato
Radiocarbon Dating Laboratory

Private Bag 3105
Hamilton,
New Zealand.
Fax +64 7 838 4192
Ph +64 7 838 4278
email c14@waikato.ac.nz
Head: Dr Alan Hogg

Report on Radiocarbon Age Determination for Wk- 22172

(AMS measurement)

Submitter	C R Sloss
Submitter's Code	SH1-S 396
Site & Location	Manawatu Coastal Plain, New Zealand
Sample Material	A. stutchburyi
Physical Pretreatment	Surfaces cleaned. Washed in an ultrasonic bath. Tested for recrystallization: aragonite.
Chemical Pretreatment	Sample acid washed using 0.1N HCl, rinsed and dried.

$\delta^{13}C$	-0.5 ± 0.2	‰
$D^{14}C$	-601.7 ± 2.1	‰
$F^{14}C\%$	39.8 ± 0.2	%
Result	**7394 ± 42 BP**	

Comments

A G Hogg
10/10/07

- Result is *Conventional Age or % Modern* as per Stuiver and Polach, 1977, Radiocarbon 19, 355-363. This is based on the Libby half-life of 5568 yr with correction for isotopic fractionation applied. This age is normally quoted in publications and must include the appropriate error term and Wk number.
- Quoted errors are 1 standard deviation due to counting statistics multiplied by an experimentally determined Laboratory Error Multiplier.
- The isotopic fractionation, $\delta^{13}C$, is expressed as ‰ wrt PDB.
- $F^{14}C\%$ is also known as pMC (percent modern carbon).

The University of Waikato
Radiocarbon Dating Laboratory

Private Bag 3105
Hamilton,
New Zealand.
Fax +64 7 838 4192
Ph +64 7 838 4278
email c14@waikato.ac.nz
Head: Dr Alan Hogg

Report on Radiocarbon Age Determination for Wk- 22173

(AMS measurement)

Submitter	C R Sloss
Submitter's Code	SH2-S-4
Site & Location	Manawatu Coastal Plain, New Zealand
Sample Material	A. stutchburyi
Physical Pretreatment	Surfaces cleaned. Washed in an ultrasonic bath. Tested for recrystallization: aragonite.
Chemical Pretreatment	Sample acid washed using 0.1N HCl, rinsed and dried.

$\delta^{13}C$	-1.6 ± 0.2	‰
$D^{14}C$	-520.8 ± 2.2	‰
$F^{14}C\%$	47.9 ± 0.2	%
Result	**5910 ± 37 BP**	

Comments

A G Hogg
10/10/07

- Result is *Conventional Age or % Modern* as per Stuiver and Polach, 1977, Radiocarbon 19, 355-363. This is based on the Libby half-life of 5568 yr with correction for isotopic fractionation applied. This age is normally quoted in publications and must include the appropriate error term and Wk number.
- Quoted errors are 1 standard deviation due to counting statistics multiplied by an experimentally determined Laboratory Error Multiplier.
- The isotopic fractionation, $\delta^{13}C$, is expressed as ‰ wrt PDB.
- $F^{14}C\%$ is also known as pMC (percent modern carbon).

The University of Waikato
Radiocarbon Dating Laboratory

Private Bag 3105
Hamilton,
New Zealand.
Fax +64 7 838 4192
Ph +64 7 838 4278
email c14@waikato.ac.nz
Head: Dr Alan Hogg

Report on Radiocarbon Age Determination for Wk- 22176

(AMS measurement)

Submitter	C R Sloss
Submitter's Code	LD5-W-42
Site & Location	Manawatu Coastal Plain, New Zealand
Sample Material	Wood from alluvium above estuarine muds
Physical Pretreatment	Sample cleaned and ground.
Chemical Pretreatment	Sample washed in hot HCl, rinsed and treated with multiple hot NaOH washes. The NaOH insoluble fraction was treated with hot HCl, filtered, rinsed and dried.

$\delta^{13}C$	-26.6 ± 0.2	‰
$D^{14}C$	-461.6 ± 2.4	‰
$F^{14}C\%$	53.8 ± 0.2	%
Result	**4974 ± 35 BP**	

Comments

AG Hogg

10/10/07

- Result is *Conventional Age or % Modern* as per Stuiver and Polach, 1977, Radiocarbon 19, 355-363. This is based on the Libby half-life of 5568 yr with correction for isotopic fractionation applied. This age is normally quoted in publications and must include the appropriate error term and Wk number.
- Quoted errors are 1 standard deviation due to counting statistics multiplied by an experimentally determined Laboratory Error Multiplier.
- The isotopic fractionation, $\delta^{13}C$, is expressed as ‰ wrt PDB.
- $F^{14}C\%$ is also known as pMC (percent modern carbon).

The University of Waikato
Radiocarbon Dating Laboratory

Private Bag 3105
Hamilton,
New Zealand.
Fax +64 7 838 4192
Ph +64 7 838 4278
email c14@waikato.ac.nz
Head: Dr Alan Hogg

Report on Radiocarbon Age Determination for Wk- 26357

(AMS measurement)

Submitter	A Clement
Submitter's Code	E1
Site & Location	Lower Manawatu Valley, New Zealand
Sample Material	A. stutchburyi
Physical Pretreatment	Surfaces cleaned. Washed in an ultrasonic bath. Tested for recrystallization: aragonite.
Chemical Pretreatment	Sample acid washed using 0.1N HCl, rinsed and dried.

$\delta^{13}C$	-4.3 ±	0.2 ‰
$D^{14}C$	-501.3 ±	1.0 ‰
$F^{14}C\%$	49.9 ±	0.1 %
Result	**5588 ± 30 BP**	

Comments

9/11/09

- Result is *Conventional Age or Percent Modern Carbon (pMC)* following Stuiver and Polach, 1977, Radiocarbon 19, 355-363. This is based on the Libby half-life of 5568 yr with correction for isotopic fractionation applied. This age is normally quoted in publications and must include the appropriate error term and Wk number.
- Quoted errors are 1 standard deviation due to counting statistics multiplied by an experimentally determined Laboratory Error Multiplier.
- The isotopic fractionation, $\delta^{13}C$, is expressed as ‰ wrt PDB.
- $F^{14}C\%$ is also known as *Percent Modern Carbon (pMC)* .

The University of Waikato
Radiocarbon Dating Laboratory

Private Bag 3105
Hamilton,
New Zealand.
Fax +64 7 838 4192
Ph +64 7 838 4278
email c14@waikato.ac.nz
Head: Dr Alan Hogg

Report on Radiocarbon Age Determination for Wk- 26358

(AMS measurement)

Submitter	A Clement
Submitter's Code	Kop 1
Site & Location	Lower Manawatu Valley, New Zealand
Sample Material	A. stutchburyi
Physical Pretreatment	Surfaces cleaned. Washed in an ultrasonic bath. Tested for recrystallization: aragonite.
Chemical Pretreatment	Sample acid washed using 0.1N HCl, rinsed and dried.

$\delta^{13}C$	-1.8 ±	0.2 ‰
$D^{14}C$	-485.8 ±	1.0 ‰
$F^{14}C\%$	51.4 ±	0.1 %
Result	**5343 ± 30 BP**	

Comments

9/11/09

- Result is *Conventional Age or Percent Modern Carbon (pMC)* following Stuiver and Polach, 1977, Radiocarbon 19, 355-363. This is based on the Libby half-life of 5568 yr with correction for isotopic fractionation applied. This age is normally quoted in publications and must include the appropriate error term and Wk number.
- Quoted errors are 1 standard deviation due to counting statistics multiplied by an experimentally determined Laboratory Error Multiplier.
- The isotopic fractionation, $\delta^{13}C$, is expressed as ‰ wrt PDB.
- $F^{14}C\%$ is also known as *Percent Modern Carbon (pMC)* .

The University of Waikato
Radiocarbon Dating Laboratory

Private Bag 3105
Hamilton,
New Zealand.
Fax +64 7 838 4192
Ph +64 7 838 4278
email c14@waikato.ac.nz
Head: Dr Alan Hogg

Report on Radiocarbon Age Determination for Wk- 26359

(AMS measurement)

Submitter	A Clement
Submitter's Code	Cut 2
Site & Location	Lower Manawatu Valley, New Zealand
Sample Material	A. stutchburyi
Physical Pretreatment	Surfaces cleaned. Washed in an ultrasonic bath. Tested for recrystallization: aragonite.
Chemical Pretreatment	Sample acid washed using 0.1N HCl, rinsed and dried.

$\delta^{13}C$	-1.7 ±	0.2 ‰
$D^{14}C$	-547.2 ±	0.9 ‰
$F^{14}C\%$	45.3 ±	0.1 %
Result	**6365 ± 30 BP**	

Comments

9/11/09

- Result is *Conventional Age or Percent Modern Carbon (pMC)* following Stuiver and Polach, 1977, Radiocarbon 19, 355-363. This is based on the Libby half-life of 5568 yr with correction for isotopic fractionation applied. This age is normally quoted in publications and must include the appropriate error term and Wk number.
- Quoted errors are 1 standard deviation due to counting statistics multiplied by an experimentally determined Laboratory Error Multiplier.
- The isotopic fractionation, $\delta^{13}C$, is expressed as ‰ wrt PDB.
- $F^{14}C\%$ is also known *Percent Modern Carbon (pMC)* .

The University of Waikato
Radiocarbon Dating Laboratory

Private Bag 3105
Hamilton,
New Zealand.
Fax +64 7 838 4192
Ph +64 7 838 4278
email c14@waikato.ac.nz
Head: Dr Alan Hogg

Report on Radiocarbon Age Determination for Wk- 26360

(AMS measurement)

Submitter	A Clement
Submitter's Code	Cut 4
Site & Location	Lower Manawatu Valley, New Zealand
Sample Material	A. stutchburyi
Physical Pretreatment	Surfaces cleaned. Washed in an ultrasonic bath. Tested for recrystallization: aragonite.
Chemical Pretreatment	Sample acid washed using 0.1N HCl, rinsed and dried.

$\delta^{13}C$	-1.8 ±	0.2 ‰
$D^{14}C$	-541.3 ±	1.2 ‰
$F^{14}C\%$	45.9 ±	0.1 %
Result	**6260 ± 30 BP**	

Comments

9/11/09

- Result is *Conventional Age or Percent Modern Carbon (pMC)* following Stuiver and Polach, 1977, Radiocarbon 19, 355-363. This is based on the Libby half-life of 5568 yr with correction for isotopic fractionation applied. This age is normally quoted in publications and must include the appropriate error term and Wk number.
- Quoted errors are 1 standard deviation due to counting statistics multiplied by an experimentally determined Laboratory Error Multiplier.
- The isotopic fractionation, $\delta^{13}C$, is expressed as ‰ wrt PDB.
- $F^{14}C\%$ is also known *Percent Modern Carbon (pMC)* .

The University of Waikato
Radiocarbon Dating Laboratory

Private Bag 3105
Hamilton,
New Zealand.
Fax +64 7 838 4192
Ph +64 7 838 4278
email c14@waikato.ac.nz
Head: Dr Alan Hogg

Report on Radiocarbon Age Determination for Wk- 26361

(AMS measurement)

Submitter	A Clement
Submitter's Code	Cut 7
Site & Location	Lower Manawatu Valley, New Zealand
Sample Material	A. stutchburyi
Physical Pretreatment	Surfaces cleaned. Washed in an ultrasonic bath. Tested for recrystallization: aragonite.
Chemical Pretreatment	Sample acid washed using 0.1N HCl, rinsed and dried.

$\delta^{13}C$	-1.8 ±	0.2 ‰
$D^{14}C$	-567.5 ±	1.3 ‰
$F^{14}C\%$	43.3 ±	0.1 %
Result	**6733 ± 30 BP**	

Comments

9/11/09

- Result is *Conventional Age or Percent Modern Carbon (pMC)* following Stuiver and Polach, 1977, Radiocarbon 19, 355-363. This is based on the Libby half-life of 5568 yr with correction for isotopic fractionation applied. This age is normally quoted in publications and must include the appropriate error term and Wk number.
- Quoted errors are 1 standard deviation due to counting statistics multiplied by an experimentally determined Laboratory Error Multiplier.
- The isotopic fractionation, $\delta^{13}C$, is expressed as ‰ wrt PDB.
- $F^{14}C\%$ is also known *Percent Modern Carbon (pMC)* .

The University of Waikato
Radiocarbon Dating Laboratory

Private Bag 3105
Hamilton,
New Zealand.
Fax +64 7 838 4192
Ph +64 7 838 4278
email c14@waikato.ac.nz
Head: Dr Alan Hogg

Report on Radiocarbon Age Determination for Wk- 26362

(AMS measurement)

Submitter	A Clement
Submitter's Code	Cook 2
Site & Location	Lower Manawatu Valley, New Zealand
Sample Material	A. stutchburyi
Physical Pretreatment	Surfaces cleaned. Washed in an ultrasonic bath. Tested for recrystallization: aragonite.
Chemical Pretreatment	Sample acid washed using 0.1N HCl, rinsed and dried.

$\delta^{13}C$	-1.6 ±	0.2 ‰
$D^{14}C$	-521.4 ±	1.3 ‰
$F^{14}C\%$	47.9 ±	0.1 %
Result	**5920 ± 30 BP**	

Comments

9/11/09

- Result is *Conventional Age or Percent Modern Carbon (pMC)* following Stuiver and Polach, 1977, Radiocarbon 19, 355-363. This is based on the Libby half-life of 5568 yr with correction for isotopic fractionation applied. This age is normally quoted in publications and must include the appropriate error term and Wk number.
- Quoted errors are 1 standard deviation due to counting statistics multiplied by an experimentally determined Laboratory Error Multiplier.
- The isotopic fractionation, $\delta^{13}C$, is expressed as ‰ wrt PDB.
- $F^{14}C\%$ is also known *Percent Modern Carbon (pMC)* .

The University of Waikato
Radiocarbon Dating Laboratory

Private Bag 3105
Hamilton,
New Zealand.
Fax +64 7 838 4192
Ph +64 7 838 4278
email c14@waikato.ac.nz
Head: Dr Alan Hogg

Report on Radiocarbon Age Determination for Wk- 26363

(AMS measurement)

Submitter	A Clement
Submitter's Code	Flood 1
Site & Location	Lower Manawatu Valley, New Zealand
Sample Material	A. stutchburyi
Physical Pretreatment	Surfaces cleaned. Washed in an ultrasonic bath. Tested for recrystallization: aragonite.
Chemical Pretreatment	Sample acid washed using 0.1N HCl, rinsed and dried.

$\delta^{13}C$	0.0 ±	0.2 ‰
$D^{14}C$	-484.3 ±	1.4 ‰
$F^{14}C\%$	51.6 ±	0.1 %
Result	**5320 ± 30 BP**	

Comments

9/11/09

- Result is *Conventional Age or Percent Modern Carbon (pMC)* following Stuiver and Polach, 1977, Radiocarbon 19, 355-363. This is based on the Libby half-life of 5568 yr with correction for isotopic fractionation applied. This age is normally quoted in publications and must include the appropriate error term and Wk number.
- Quoted errors are 1 standard deviation due to counting statistics multiplied by an experimentally determined Laboratory Error Multiplier.
- The isotopic fractionation, $\delta^{13}C$, is expressed as ‰ wrt PDB.
- $F^{14}C\%$ is also known as *Percent Modern Carbon (pMC)* .

The University of Waikato
Radiocarbon Dating Laboratory

Private Bag 3105
Hamilton,
New Zealand.
Fax +64 7 838 4192
Ph +64 7 838 4278
email c14@waikato.ac.nz
Head: Dr Alan Hogg

Report on Radiocarbon Age Determination for Wk- 26364

(AMS measurement)

Submitter	A Clement
Submitter's Code	G
Site & Location	Lower Manawatu Valley, New Zealand
Sample Material	A. stutchburyi
Physical Pretreatment	Surfaces cleaned. Washed in an ultrasonic bath. Tested for recrystallization: aragonite.
Chemical Pretreatment	Sample acid washed using 0.1N HCl, rinsed and dried.

$\delta^{13}C$	-1.7 ±	0.2 ‰
$D^{14}C$	-505.8 ±	1.3 ‰
$F^{14}C\%$	49.4 ±	0.1 %
Result	**5661 ± 30 BP**	

Comments

9/11/09

- Result is *Conventional Age or Percent Modern Carbon (pMC)* following Stuiver and Polach, 1977, Radiocarbon 19, 355-363. This is based on the Libby half-life of 5568 yr with correction for isotopic fractionation applied. This age is normally quoted in publications and must include the appropriate error term and Wk number.
- Quoted errors are 1 standard deviation due to counting statistics multiplied by an experimentally determined Laboratory Error Multiplier.
- The isotopic fractionation, $\delta^{13}C$, is expressed as ‰ wrt PDB.
- $F^{14}C\%$ is also known as *Percent Modern Carbon (pMC)* .

Appendix D. Radiocarbon results

Appendix E

Other detailed bores from the lower Manawatu valley

H- bore and auger holes were drilled by Hesp (1975). Murray's Farm was drilled by Shepherd and Lees (1987). The following details come from Hesp (1975), unpublished records made available to M.J. Shepherd by P.A. Hesp, and Shepherd and Lees (1987).

Details of other bore and auger holes drilled in the lower Manawatu valley.

Bore/auger	Elevation (m)	NZMG north	NZMG east
H1	3·66	6068549·70	2712167·40
H3	6·80	6075170·53	2720587·79
H4	16·60	6076008·66	2720062·79
H5	0·00	6073428·33	2717519·81
H6	0·00	6067775·70	2704004·71
H7	3·19	6070184·41	2712579·75
H8	3·40	6070192·20	2712305·57
H9	3·05	6070202·60	2711939·99
H10	3·04	6070215·59	2711483·02
H11	3·91	6073425·73	2717611·20
H12	3·91	6073036·77	2718423·37
H14	3·70	6069100·66	2712091·59
H15	4·06	6070803·39	2713329·10
H16	3·50	6070542·19	2712864·33
H17	4·11	6069732·63	2712383·97
H19	3·70	6068547·10	2712258·79
H20	0·00	6074313·71	2718551·13
H21	3·96	6068460·90	2712073·40
H22	4·24	6068544·50	2712350·19
H23	4·26	6068366·91	2712162·20
H24	4·80	6077695·32	2718647·21
H25	0·00	6069601·82	2710550·88
H26	3·19	6070184·41	2712579·75
H27	0·00	6069808·00	2709733·53
H28	4·80	6078303·92	2719762·12
H29	4·80	6078024·55	2719937·12
H30	1·32	6068616·85	2706589·74
Shepherd and Lees (1987) - Murray's Farm	8·00	6080200·00	2714700·00

Appendix E. Other Manawatu bores

Lithological details of other bore and auger holes drilled in the lower Manawatu valley.

Bore	Top	Bottom	Lithology
H1	0·00	0·30	Topsoil
	0·30	4·50	Mud
H3	0·00	0·28	Topsoil
	0·28	1·50	Sandy clay
	1·50	1·90	Muddy sand
	1·90	3·05	Blue mud
H4	0·00	0·15	Topsoil
	0·15	1·52	Clay, wood
	1·52	4·00	Blue mud
	4·00	4·70	Brown sandy mud
H5	0·00	0·51	Topsoil
	0·51	0·74	Clay/soil/bits of wood
	0·74	1·35	Sand, roots
	1·35	1·52	Speckled: grey sand/rust brown
	1·52	2·24	Rust brown sand (oxidised)
	2·24	2·64	Sand getting coarser; oxidised lumps of orange sand/charcoal
	2·64	3·37	Sand grading back into orange
	3·37	3·49	Grading into pale grey mud
	3·49	3·51	Charcoal oxidised wood 0.5in
	3·51	6·10	Light brown sand
H6	0·00	3·04	Peat, roots
H8	0·00	2·58	Grey mud
	2·58	3·00	Sand, shell
H9	0·00	2·70	Blue/grey sandy mud
	2·70	2·80	Blue/grey sandy mud, shell onwards from 2.7 m
H10	0·00	1·80	Grey sand
	1·80	2·13	Mud
	2·13	3·04	Mud, shells
H11	0·00	0·61	Topsoil
	0·61	0·76	Clay, wood
	0·76	1·52	Sandy clay
	1·52	2·28	Blue/grey sand
	2·28	2·43	Clay, wood
	2·43	2·90	Peaty clay
	2·90	7·60	Clay, plant fragments
H12	0·00	0·31	Topsoil
	0·31	0·70	Silt/clay
	0·70	3·60	Clay, plant fragments
	3·60	3·90	Peaty clay
	3·90	7·60	Blue/grey clay
H14	0·00	0·10	Topsoil
	0·10	0·70	Silt
	0·70	1·80	Sandy mud, vegetation
	1·80	5·28	Sand
	5·28	6·50	Sand, shell
H15	0·00	0·10	Topsoil
	0·10	0·45	Brown mud
	0·45	3·35	Oxidised grey sand
H16	0·00	0·15	Topsoil
	0·15	3·04	Mud, vegetation
	3·04	3·05	Sand
	3·05	3·50	Mud
	3·50	6·10	Blue sand
H17	0·00	0·17	Topsoil
	0·17	1·36	Mud
	1·36	4·26	Sand
H19	0·00	0·25	Topsoil
	0·25	0·45	Grey-brown mud
	0·45	0·90	Grey mud, wood

Continued on next page

Lithological details (continued).

Bore	Top	Bottom	Lithology
	0·90	1·90	Sandy grey mud, wood and sand lenses
	1·90	5·80	Grey/blue sandy mud, sand lenses, shells, wood
	5·80	6·10	Grey blue sandy mud
H20	0·00	0·45	Topsoil
	0·45	1·36	Brown mud
	1·36	4·57	Blue mud
H21	0·00	0·40	Topsoil
	0·40	0·62	Muddy peat
	0·62	2·20	Mud
	2·20	7·30	Mud, shell and wood fragments
	7·30	9·10	Mud, wood
H22	0·00	0·50	Topsoil/silt
	0·50	1·21	Brown oxidised mud
	1·21	1·97	Grey mud, rootlets
	1·97	2·28	Dark grey peaty mud
	2·28	5·48	Grey sandy mud, sand lenses
	5·48	6·09	Muddy sand
	6·09	6·41	Sand, green mottling (Otaki sandstone)
H23	0·00	0·28	Topsoil
	0·28	1·06	Grey oxidised mud
	1·06	1·36	Grey peaty mud
	1·36	1·50	Grey mud, roots
	1·50	2·28	Grey peaty mud
	2·28	2·35	Peat
	2·35	2·58	Grey mud
	2·58	3·90	Blue mud
	3·90	4·20	Dry sand, green mottling (Otaki sandstone)
H24	0·00	0·76	Topsoil
	0·76	1·20	Grey brown clay
	1·20	2·70	Blue grey clay
	2·70	2·90	Grey mud
	2·90	3·10	Peaty mud
	3·10	3·30	Blue mud
H25	0·00	0·31	Topsoil
	0·31	0·85	Dry grey clay, wood
	0·85	1·50	Grey/brown muddy sand
	1·50	3·04	Grey/blue muddy sand, shells begin at 1.8m
H26	0·00	0·27	Topsoil
	0·27	2·00	Brown mud
	2·00	2·13	Mud, vegetation
	2·13	6·09	Sand, shells, sandy muddier at times, lenses of fine and coarse grained sand
H27	0·00	3·04	Mud, plant remains
H28	0·00	0·55	Peaty topsoil
	0·55	1·60	Grey mud, wood
	1·60	4·90	Blue mud
H29	0·00	0·10	Topsoil
	0·10	1·50	Sandy mud
	1·50	1·60	Sand/fine rock fragments
	1·60	1·70	Sandy mud
	1·70	1·80	Peaty mud, wood
	1·85	6·10	Grey plastic mud
H30	0·00	1·52	Peat
	1·52	3·40	Grey/blue mud, few roots and wood after 6', at 9'3" few shell fragments, 10' shells (*Chione*), snails and mud
Murray's Farm	0·00	9·00	Fine alluvium
	9·00	20·00	Thinly interbedded silty sand and clay, *A. stutchburyi* shells